NASA CR-72224
AEROJET 3422

GLASS-FIBER-REINFORCED METALLIC TANKS FOR CRYOGENIC SERVICE

by

E. E. Morris

prepared for

NATIONAL AERONAUTICS AND SPACE ADMINISTRATION

CONTRACT NAS 3-6292

GPO PRICE $ _____

CFSTI PRICE(S) $ _____

Hard copy (HC) 3.00

Microfiche (MF) _____

ff 653 July 65

N68-12088 (ACCESSION NUMBER) (THRU)
314 (PAGES) 1 (CODE)
CR-72224 (NASA CR OR TMX OR AD NUMBER) 32 (CATEGORY)
FF No. 602(C)
AVAILABLE TO U.S. GOVERNMENT AGENCIES ONLY

AEROJET-GENERAL CORPORATION
VON KARMAN CENTER
AZUSA, CALIFORNIA

NASA CR-72224
Aerojet 3422

FINAL REPORT

GLASS-FIBER-REINFORCED METALLIC TANKS FOR CRYOGENIC SERVICE

by

E. E. Morris

prepared for

NATIONAL AERONAUTICS AND SPACE ADMINISTRATION

June 1967

Contract NAS 3-6292

Technical Management
NASA Lewis Research Center
Cleveland, Ohio
Liquid Rocket Technology Branch
James R. Barber

AEROJET-GENERAL CORPORATION
Von Karman Center
Azusa, California

FOREWORD

This report is submitted by Aerojet-General Corporation in fulfillment of the contract and covers the period from 16 June 1965 to 15 April 1967.

The work was done by the Structural Products Division, Von Karman Center, Azusa, California. E. E. Morris was the Aerojet Program Manager and principal investigator. F. J. Darms and Dr. J. W. Lambert developed the structural analysis for glass-fiber-reinforced metal tanks and formulated the computer-program logic sequences. R. E. Landes conducted the parametric study, assisted in the preparation of the structural analysis and the computer program, and assisted in the analysis of test results. J. W. Campbell, metallurgist for this program, analyzed the candidate metal-shell materials.

Pressure-vessel fabrication was accomplished in the Structural Products Division. Contributors were R. L. Jensen, D. E. Barnett, J. A. Abatecola, A. W. Leland, and J. J. Dawson for the metal shell, and W. D. Bowers, A. A. Madrigal, and P. A. McDonald for the glass-filament-wound shell.

Tank testing was conducted by the Test Operations Division under the direction of J. C. Shafer and J. R. Barr. A. I. Taoyama and P. B. Guhl conducted the tests and G. L. Ramos and J. L. Hostetter were responsible for the instrumentation-engineering aspects.

Special acknowledgement is due to R. G. Fiedler, who edited the report manuscript, and to R. J. Hilgaertner, who prepared the technical illustrations.

Guidance and many helpful suggestions were provided throughout the program by the NASA Project Manager, J. R. Barber of the Liquid Rocket Technology Branch, Lewis Research Center.

Approved by:

W. T. Cox, Manager
Structural Products Division

GLASS-FIBER-REINFORCED METALLIC TANKS FOR CRYOGENIC SERVICE

by

E. E. Morris

ABSTRACT

Advantages of and design requirements for a load-bearing metal shell with an overwrapped glass-filament shell for high-pressure-fluid storage at 75 to -423°F were investigated analytically and experimentally. Proper design permits utilization of the maximum load-bearing capabilities of both shells and makes possible tanks of significantly lighter weight than the best cylindrical and spherical homogeneous metal pressure vessels.

Glass-fiber-reinforced metal tanks were fabricated and tested; they successfully met design objectives in cyclic fatigue, creep, and burst tests in the 75 to -423°F range, and should be considered for application to aerospace systems. The testing (1) confirmed the results of a parametric study of the vessels, (2) revealed that no degradation in tank strength resulted from cyclic-fatigue and sustained-loading tests at 75, -320, and -423°F, and (3) established that vessel strength increased about 25% at cryogenic temperatures.

PRECEDING PAGE BLANK NOT FILMED.

CONTENTS

		Page
SUMMARY		xv
I.	INTRODUCTION	1
	A. Background	1
	B. Program Plan	2
II.	DESCRIPTION OF GFR METAL TANKS	3
	A. Filament-Wound-Composite Material	3
	B. Sealant-Liner Requirements	3
	C. Liner Materials	4
	D. Metal-Liner Design Concepts	4
	E. GFR Metal Tanks	5
III.	TASK I - PARAMETRIC STUDY	9
	A. Compressive Properties and Buckling Strengths of Overwrapped Metal Shells	9
	B. Study Results	10
IV.	TASK II - PRESSURE-VESSEL DESIGN	14
	A. Selection of Configuration	14
	B. Service-Cycle Requirement	15
	C. Analysis of Material Properties	15
	D. Preliminary Sizing and Design	16
	E. Structural Design and Analysis	17
V.	TASK II - PRESSURE-VESSEL FABRICATION	20
	A. Procedure	20
	B. Specifications	21
	C. Development of Weld Schedule	21
	D. Detailed Fabrication Sequence	21
	E. Material-Verification Tests	24
	F. Comments on Fabricated Tanks	25
VI.	TASK III - TEST PROGRAM FOR STRUCTURAL EVALUATION OF PRESSURE VESSELS	28
	A. Test Plan, Facility, and Instrumentation	28
	1. Test Plan	28
	2. Facility for Cryogenic Tests	29
	3. Instrumentation	29

CONTENTS (cont.)

		Page
B.	Test Results	31
1.	Room-Temperature Tests (75°F)	31
2.	LN_2 Tests (-320°F)	35
3.	LH_2 Tests (-423°F)	38
4.	Wall-Temperature-Gradient Tests	40
VII.	EVALUATION OF STRENGTH AND PERFORMANCE LEVELS, PRESSURE-STRAIN CHARACTERISTICS, AND PARAMETRIC-STUDY FINDINGS	43
A.	Strength and Performance Levels	43
B.	Pressure-Strain Characteristics	45
C.	Head-Reinforcement Design and Boss-to-Metal-Shell Transition	46
D.	Parametric-Study Report	48
VIII.	CONCLUSIONS AND RECOMMENDATIONS	50
References		53

	Table
Typical Inconel X-750 (STA) Properties for Design Use	1
Material Properties Used for Design Analysis, 18-Inch-Diameter GFR Inconel X-750 Tank	2
Design Parameters for 18-in.-dia GFR Inconel X-750 Oblate-Spheroid Pressure Vessel	3
Tensile Properties of Welded and Unwelded Specimens of Inconel X-750 (STA)	4
Characteristics of Metal Shells, Glass-FWC Shells, and GFR Inconel X-750 (STA) Tanks	5
Average Dimensional, Weight, and Volume Parameters for 18-in.-dia GFR Inconel X-750 Pressure Vessels	6
Performance Data for 18-in.-dia GFR Inconel X-750 Pressure Vessels	7
Vessel-Failure Modes	8

	Figure
Photomicrographs of Glass-Filament-Wound and Boron-Filament-Wound Composites	1
Stress-Strain Characteristics of Component Materials	2

CONTENTS (cont.)

	Figure
Liner-Design Concepts	3
Stress-Strain Diagram for Glass-Filament-Reinforced (GFR) Metal Shell	4
Comparison of Constrictive-Wrap Buckling Strengths for Cylindrical Tubes with Design Allowable Used for Parametric Study	5
Additional Data on Constrictive-Wrap Buckling Strengths for Cylindrical Tubes	6
Summary Comparison, GFR-Metal and Homogeneous-Metal Pressure-Vessel Performance Levels	7
Relationship of Room-Temperature Proof Pressure to Operating Pressures at 75, -320, and -423°F	8
GFR Inconel X-750 (STA) Tanks, Optimum Diameter-to-Liner-Thickness Ratio (T_D = 75°F)	9
GFR Inconel X-750 (STA) Tanks, Optimum Liner-to-Longitudinal-Composite-Thickness Ratio (T_D = 75°F)	10
Optimum Efficiency, GFR Inconel X-750 (STA) Tanks (T_D = 75°F)	11
Optimum Efficiency, GFR Inconel X-750 (STA) Tanks (Optimum Room-Temperature Design Operated at -320 and -423°F)	12
Factors of Safety for GFR Inconel X-750 (STA) Tanks	13
Boss, 18-in.-dia GFR Inconel X-750 (STA) Tank	14
Metal Shell, 18-in.-dia GFR Inconel X-750 (STA) Tank	15
Initial and Final Designs, 18-in.-dia GFR Inconel X-750 (STA) Tank Assembly	16
Head Reinforcement, 18-in.-dia GFR Inconel X-750 (STA) Tank	17
Test Assembly, 18-in.-dia GFR Inconel X-750 (STA) Tank	18
Room-Temperature Stress-Strain Relationships (2220-psi Proof Pressure and 2000-psi Operating Pressure)	19
-320°F Stress-Strain Relationships (2220-psi Proof Pressure at 75°F and 2300-psi Operating Pressure at -320°F)	20
-423°F Stress-Strain Relationships (2220-psi Proof Pressure at 75°F and 2350-psi Operating Pressure at -423°F)	21
Head Stresses at 2220-psi Proof Pressure	22
Head Stresses at Operating Pressure (2220-psi Proof Pressure and 2000-psi Operating Pressure at 75°F)	23
Head Stresses at Zero Pressure (2220-psi Proof Pressure at 75°F)	24
Tank Pressure vs Strain (75°F)	25

CONTENTS (cont.)

	Figure
Tank Pressure vs Strain (-320°F)	26
Tank Pressure vs Strain (-423°F)	27
Manufacturing Flow Diagram for Tank	28
Polar Boss	29
18-in.-dia Formed Head	30
Electron-Beam-Welding Machine	31
Half Shell in Welding Chamber	32
Assembly of Formed Head and Polar Boss with Electron Gun in Position for Welding	33
Completed Half Shell, Exterior View	34
Boss-to-Head Weld, Exterior View	35
Completed Half Shell, Interior View	36
Boss-to-Head Weld, Interior View	37
Assembly of Two Half Sections in Welding Chamber with Electron Gun in Position for Welding	38
Complete Metal-Shell Assembly	39
Metal-Shell Assembly in Filament-Winding Machine	40
Application of Longitudinal Filament Winding to Metal Shell	41
Overwinding of Metal Shell, Showing Head Reinforcement	42
Completed Tank Instrumented for Testing	43
Acceptable, Unacceptable, and Repaired Welds	44
75°F Stress-Strain Curve for Inconel X-750 (STA)	45
GFR Inconel X-750 Tanks	46
Liquid-Cryogen Pressurization System	47
Cryogenic-Test Control Facility	48
Extensometer Instrumentation	49
Bow-Tie Installation on Tank	50
Tank 2 After Test, Top View	51
Tank 2 Pressure vs Strain for Proof and Burst-Test Phases at 75°F	52
Strain-Gage Instrumentation, Top View	53
Tank 3 After Test	54

CONTENTS (cont.)

	Figure
Tank 3 Pressure vs Strain for Proof and Burst-Test Phases at 75°F	55
Tank 3 Hoop Strain Near Polar Boss for Proof and Burst-Test Phases at 75°F	56
Tank 3 Longitudinal Strain Near Polar Boss for Proof and Burst-Test Phases at 75°F	57
Tank 5 After Test	58
Tank 5 Pressure vs Strain for Proof and Burst-Test Phases at 75°F	59
Tank 5 Hoop Strain Near Polar Boss for Proof and Burst-Test Phases at 75°F	60
Tank 5 Longitudinal Strain Near Polar Boss for Proof and Burst-Test Phases at 75°F	61
Tank 7 After Test	62
Tank 7 Pressure vs Strain for Proof and Burst-Test Phases at 75°F	63
Tank 7 Pressure vs Strain During Pressure Cycling at 75°F	64
Tank 8 After Test	65
Tank 8 Pressure vs Strain for Proof-Test Phase at 75°F	66
Tank 8 Pressure vs Strain During Pressure Cycling at 75°F	67
Tank 4 After Test	68
Tank 4 Pressure vs Strain for Proof and Burst-Test Phases at 75°F	69
Tank 4 Strain During Creep Test at 75°F	70
Tank 4 Creep Test, Start and End Transients at 75°F	71
Tank 6 After Test	72
Tank 6 Pressure vs Strain for Proof and Burst-Test Phases at 75°F	73
Tank 6 Strain During Creep Test at 75°F	74
Tank 6 Creep Test, Start and End Transients at 75°F	75
Tank 13 After Test	76
Tank 13 Pressure vs Strain During Burst Test at -320°F	77
Tank 14 After Test	78
Tank 16 After Test	79
Tank 16 Pressure vs Strain During Burst-Test Phase at -320°F	80

CONTENTS (cont.)

	Figure
Tank 20 After Test	81
Tank 20 Pressure vs Strain for Initial-Pressurization and Burst-Test Phases at -320°F	82
Tank 20 Pressure vs Strain During Pressure Cycling at -320°F	83
Tank 21 After Test	84
Tank 21 Pressure vs Strain for Initial-Pressurization and Burst-Test Phases at -320°F	85
Tank 21 Pressure vs Strain During Pressure Cycling at -320°F	86
Tank 15 After Test	87
Tank 15 Pressure vs Strain for Initial-Pressurization and Burst-Test Phases at -320°F	88
Tank 15 Pressure vs Strain During Creep Test at -320°F	89
Tank 17 After Test	90
Tank 17 Pressure vs Strain for Initial-Pressurization and Burst-Test Phases at -320°F	91
Tank 17 Pressure vs Strain During Creep Test at -320°F	92
Tank 11 After Test	93
Tank 11 Pressure vs Strain for Burst Test at -423°F	94
Tank 19 After Test	95
Tank 19 Pressure vs Strain for Burst Test at -423°F	96
Tank 9 After Test	97
Tank 9 Pressure vs Strain for Initial-Pressurization and Burst-Test Phases at -423°F	98
Tank 9 Pressure vs Strain During Pressure Cycling at -423°F	99
Tank 10 After Test	100
Tank 10 Pressure vs Strain for Initial-Pressurization and Burst-Test Phases at -423°F	101
Tank 10 Pressure vs Strain During Pressure Cycling at -423°F	102
Tank 12 After Test	103
Tank 12 Pressure vs Strain for Initial-Pressurization and Burst-Test Phases at -423°F	104
Tank 12 Pressure vs Strain During Creep Test at -423°F	105
Tank 22 After Test	106
Tank 22 Pressure vs Strain for Initial-Pressurization and Burst-Test Phases at -423°F	107

CONTENTS (cont.)

	Figure
Tank 22 Pressure vs Strain During Creep Test at -423°F	108
Sensor Locations for Temperature-Evaluation Test	109
Pressure vs Temperature, Cycle 1	110
Pressure vs Temperature, Cycle 5	111
Pressure vs Temperature, Burst Cycle	112
Tank After Temperature-Evaluation Test	113
Pressure-Vessel Performance Factors for 18-in.-dia GFR Inconel X-750 (STA) Tanks	114
S-HTS Glass-Filament Tensile Stress at Burst Pressure for 18-in.-dia GFR Inconel X-750 (STA) Tanks	115
Ultimate S-HTS Glass-Filament Strength at Burst Pressure in 18-in.-dia GFR Inconel X-750 (STA) Tanks	116
Predicted and Measured Pressure-vs-Strain Characteristics, 75°F Proof and Burst Tests of 18-in.-dia GFR Inconel X-750 Tank (Serial No. 3)	117
Comparison of Calculated and Measured Longitudinal-Filament Strains for 75°F Burst Tests of 18-in.-dia GFR Inconel X-750 (STA) Tanks	118
Strain Distribution in Metal Structure	119
GFR Inconel X-750 (STA) Tanks, Optimum Diameter-to-Liner-Thickness Ratio	120
GFR Inconel X-750 (STA) Tanks, Optimum Liner-to-Longitudinal-Composite-Thickness Ratio	121
Operating-Pressure Performance Factors Demonstrated by 18-in.-dia GFR Inconel X-750 (STA) Tanks	122
Factors of Safety Demonstrated by 18-in.-dia GFR Inconel X-750 (STA) Tanks	123

	Page
APPENDIX A - EXPERIMENTAL EVALUATION OF COMPRESSIVE-STRESS-STRAIN CHARACTERISTICS AND BUCKLING STRENGTH OF FILAMENT-OVERWRAPPED METAL CYLINDERS	A-1

	Table
Compressive Properties for Metal-Cylinder Materials	A-1
Metal-Cylinder Description	A-2
Overwrapped-Metal-Cylinder Data	A-3

CONTENTS (cont.)

	Figure
Range of Cylinder Geometries Used in Calculation of Buckling of Circular Cylinders Under External Pressure	A-1
Cylinders for Buckling Study	A-2
Strain-Gage Locations	A-3
Strain-Gage Instrumentation	A-4
Cylinder Assembly to End Plate	A-5
Cylinder and Tooling Assembly in Winding Machine	A-6
Buckled Cylinders	A-7
Buckled Cylinder with Portion of Windings Removed	A-8
Aluminum Cylinder 2	A-9
Aluminum Cylinder 3	A-10
Inconel Cylinder 1	A-11
Inconel Cylinder 2	A-12
Titanium Cylinder 1	A-13
Titanium Cylinder 2	A-14
Aluminum Cylinder 2, Compression vs Pressure	A-15
Aluminum Cylinder 3, Compression vs Pressure	A-16
Inconel Cylinder 1, Compression vs Pressure	A-17
Inconel Cylinder 2, Compression vs Pressure	A-18
Titanium Cylinder 1, Compression vs Pressure	A-19
Titanium Cylinder 2, Compression vs Pressure	A-20
Compressive Stress-Strain Curve for Aluminum Cylinder 2, Buckling Test	A-21
Compressive Stress-Strain Curve for Aluminum Cylinder 3, Buckling Test	A-22
Compressive Stress-Strain Curve for Inconel Cylinder 1, Buckling Test	A-23
Compressive Stress-Strain Curve for Inconel Cylinder 2, Buckling Test	A-24
Compressive Stress-Strain Curves for Titanium Cylinder 1, Buckling Test	A-25
	Page
APPENDIX B - COMPUTER PROGRAM FOR ANALYSIS OF FILAMENT-REINFORCED METAL-SHELL PRESSURE VESSELS	B-1

CONTENTS (cont.)

	Page
APPENDIX C - METAL-BOSS ANALYSIS	C-1
APPENDIX D - FILAMENT-WINDING PATTERN AND HEAD-REINFORCEMENT DESIGN	D-1

	Figure
Tank Geometry	D-1
Stress-Strain Diagram for Various Points on Head (Design Without Head Reinforcement)	D-2
Pressure-Vessel Membrane and Meridional Loads	D-3
Geometry of Head Reinforcement	D-4
Stress-Strain Diagram for Z = 0.264 for Tank with Head Reinforcement	D-5

	Page
APPENDIX E - METAL-SHELL ASSEMBLY SPECIFICATION	E-1
APPENDIX F - FABRICATION PROCEDURE FOR GLASS-FWC SHELL	F-1

	Table
Winding Data (Form)	F-1

	Figure
Inspection of Metal-Shell Assembly (Form)	F-1

	Page
APPENDIX G - CALIBRATION OF BOW-TIE, STRAIN-GAGE, DISPLACEMENT TRANSDUCERS	G-1

	Figure
Calibration-Test Data to Demonstrate Linearity of Strain-Gage Displacement Transducers	G-1

	Page
APPENDIX H - METALLURGICAL ANALYSIS OF INCONEL X-750 TANK LINER	H-1

	Figure
Fracture Surface Between Boss and Tank Liner	H-1
Microstructure of Boss-to-Liner Weld	H-2
Microstructure of Tank Weld Adjacent to Fracture	H-3
Microstructure of Weld Nugget and Location of Fracture in Tank	H-4
Microstructure of Metal Liner	H-5
Macrophotographs of Tensile Specimen No. L-6	H-6
Microstructure Along Length of Weld	H-7

	Page
DISTRIBUTION LIST	I-1

PRECEDING PAGE BLANK NOT FILMED.

GLASS-FIBER-REINFORCED METALLIC TANKS FOR CRYOGENIC SERVICE

by

E. E. Morris

SUMMARY

The advantages of combining a load-bearing metal shell with an overwrapped glass-filament shell for high-pressure-fluid storage in the 75 to -423°F range were investigated analytically and experimentally, as were the design requirements. The research was concentrated on a parametric study of glass-fiber-reinforced (GFR) metal tanks, followed by design, fabrication, and structural evaluation of GFR metal tanks at 75, -320, and -423°F in burst, cyclic-fatigue-plus-burst, and sustained-loading-plus-burst tests. The results demonstrated that GFR metal tanks utilize the maximum load-bearing capabilities of both the liner and the filament shell, and are significantly lighter in weight than the highest-performance, cylindrical and spherical, homogeneous metal tanks.

The parametric study involved characterization of candidate metal-liner materials; definition of design-allowable strength levels for S-HTS glass-filament-wound composites; development of analytical procedures for tank design and evaluation; development of curves characterizing design features of GFR Ti-5Al-2.5Sn, GFR Inconel X-750, GFR 2219-T62 aluminum, and GFR 301 stainless steel tanks with operating pressures in the 1000 to 4000-psi range; and comparative rating of GFR-metal-tank performance with homogeneous metal tankage made from the Ti-6Al-4V, Type 301 stainless steel, 2219-T87 aluminum, and Inconel 718 alloys.

The design criteria used included requirements that the compressive buckling and yield strengths of the liner were not to be exceeded at a zero internal pressure (when the liner is in maximum compression due to external forces produced by the overwrapped filaments). Consequently, the designs that were developed do not require an adhesive bond between the two shells to keep the liner from buckling, as do glass-filament-wound tanks with very thin metal liners. Adhesive-bond integrity during the service life of GFR metal tanks is therefore not an area of concern. The tanks were also designed to minimize liner hysteresis effects during cyclic operating-pressure application by requiring that the liner-stress range between zero and the operating pressure be within the offset biaxial compressive and tensile elastic limits, after an initial prestress-pressure load (which plastically deforms the liner beyond its biaxial-yield stress).

The parametric-study results were verified by the fabrication and testing of twenty 18-in.-dia GFR Inconel X-750 tanks that had an operating pressure of 2000 psi and a burst pressure of 3000 psi at 75°F. The metal shell had sufficient biaxial ductility over the 75 to -423°F range to perform satisfactorily up to the failure stress of the filament-wound shell. The

average tankage burst strength at 75°F was within 0.67% of the design value, and the variation was only 4.30% of the average. The average increase in tank performance between 75°F and cryogenic temperatures was 22 to 25% at -320°F and 23 to 27% at -423°F for vessels subjected to single-cycle burst tests, 100-cycle-fatigue plus burst tests, or 72-hour sustained-pressurization plus burst tests. There was no significant difference between the burst-strength levels attained in the fatigue-cycling or sustained-loading tests (at 60 to 70% of the single-cycle burst strength) and in direct pressurization to the burst point without such prior exposure.

As compared with existing tankage, considerable weight savings can be obtained with GFR Inconel X-750 tanks, which merit serious consideration for application to aerospace systems. Improved efficiency and greater weight savings over the 75 to -423°F range will be provided by GFR Ti-5Al-2.5Sn vessels; investigations are warranted to evaluate their performance advantages, as well as to provide the data required by system designers for advanced applications.

I. INTRODUCTION

A. BACKGROUND

Successful application of glass-filament-wound construction to the design of pressure vessels, particularly in solid-propellant rocket-motor cases, has suggested its use for the containment of cryogenic fluids. The high strength-to-density ratio, dimensional stability, structural reliability, low thermal conductivity, and ease and low cost of fabrication of glass/resin composite structures are characteristics inherently attractive for cryogenic applications, including efficient tankage.

The use of such structures for cryogenic pressure vessels will result in considerable weight savings because the filament-wound-composite (FWC) material has a much higher strength for its weight than do metal-tankage materials. Although the composite is light in weight, it is permeable to pressurized fluids and requires an inner sealant liner when used for cryogenic vessels.

Suitable liner materials are available for room-temperature service. Liners for cryogenic use, however, have presented difficult developmental problems. They must respond repeatedly, without failure, to very large biaxial strains in order to be compatible with the filament-wound composite at its operating-stress level, and must then strain biaxially to the failure stress of the filaments.

Metals have the required cryogenic-liner properties, but the high strength and relatively low modulus of glass fibers currently used produce elastic strains 3 to 10 times the biaxial elastic strain of metals at efficient operating and burst stresses, and the liners must work well beyond their initial yield point. Considerable effort is being devoted to the development of relatively thin strain-compatible liners that can work in their plastic region for a number of cycles. These thin liners must be bonded to the tank wall to keep from buckling on depressurization, and attempts to use high-elongation foils and to strain-cycle liners in their plastic range at cryogenic temperatures have had only moderate success. This was because of (1) liner buckling on vessel depressurization when the liner-to-composite bond failed, and (2) subsequent fatigue failure in the buckled area.

Another sealing approach for cryogenic service is to combine the glass-filament-wound composite with a load-bearing, nonbuckling, metal shell that need not be adhesively bonded to the wall to keep from buckling. This shell provides the necessary liner and permits exploitation of the strength potential of glass fibers. For high-pressure-fluid storage containers, a metal shell can be combined with a glass-fiber overwrap to achieve a vessel of less total weight for a given operating pressure and volume than is possible with an all-metal vessel. For the inner and outer shells to operate at their optimum efficiencies, however, a proper preload or strain relationship must be achieved when the vessel is unpressurized.

The work reported here was undertaken to determine analytically and experimentally the advantages and design requirements of combining a

load-bearing metal shell with an overwrapped glass-filament shell for high-pressure gas or liquid storage in the range from 75 to -423°F. A topical report, entitled Parametric Study of Glass-Filament-Reinforced Metal Pressure Vessels (Reference 1), was issued to cover the characterization of liner materials, definition of design-allowable strengths for glass-filament-wound composites, analytical procedures for use in the design and evaluation of glass-fiber-reinforced (GFR) metal tanks, parametric investigations, and comparative ratings of pressure vessels. This report provides a detailed summary of all work performed during the program (including a summary of Reference 1), with emphasis on the design, fabrication, and structural evaluation of GFR metal tanks at +75, -320 and -423°F in burst, fatigue, and creep tests.

B. PROGRAM PLAN

The objective of this work was to determine analytically and experimentally the advantages of and design requirements for combining a load-bearing metal shell with an overwrapped glass-filament shell for high-pressure gas or liquid storage in the 75 to -423°F range.

The program consisted of a three-task, 22-month technical effort. Task I included an analytical design study and parametric evaluation of the glass-shell/metal-shell combination. The task was completed with an investigation of the buckling characteristics of open-ended metal cylinders overwrapped circumferentially with layers of tensioned filaments.

Twenty 18-in.-dia GFR metal tanks designed in accordance with the requirements established in Task I were fabricated during Task II.

These vessels were evaluated in a Task III structural-test program. They were subjected to burst, cyclic-fatigue-plus-burst, and creep-plus-burst tests at 75, -320 and -423°F. The results were analyzed and evaluated, and were then compared with the predictions made for GFR metal tanks in Task I.

II. DESCRIPTION OF GFR METAL TANKS

The most significant property of glass-filament-wound composites for pressure vessels is the high composite-wall strength-to-density ratio attainable - of the order of 2.0×10^6 in. for the cylinder and 3.20×10^6 in. for the heads at 75°F. The large fiber strains associated with this performance create extremely difficult design problems when the requirement for a sealant liner is introduced. These problems, and the design approaches used to overcome them, are reviewed below.

A. FILAMENT-WOUND-COMPOSITE MATERIAL

A filament-wound reinforced-plastic structure contains many continuous, small-diameter, high-strength fibers imbedded in a matrix of organic or inorganic material. The constituents of typical glass-filament and boron-filament composites are shown photomicrographically in Figure 1.

These composites are fabricated by winding a specifically oriented pattern of pretensioned, matrix-impregnated, continuous filaments onto a mandrel. The fibers, which in most applications have been glass, constitute the primary load-carrying element. The maximum structural efficiency is obtained by orienting them to provide the strength components required to meet the applied loads. In pressure vessels and other structures, where the directions and relative magnitudes of forces are fixed, the resin matrix has the secondary role of controlling fiber efficiency by transferring loads from broken fibers, hardening the structure in terms of shape and fiber orientation, and protecting fibers from each other and from degrading environments.

The filament content of a glass-FWC structure for pressure-vessel application is generally about 67 vol% (or 82 wt%), with the resin matrix constituting the remainder. This construction, with a density of 0.088 $lb/in.^3$ for S-HTS glass* and an epoxy-resin density of 0.042 $lb/in.^3$, results in a composite density of 0.073 $lb/in.^3$, which is about one-quarter the density of steel and less than one-half the density of titanium. This low weight and a high FWC strength (e.g., a 150,000-psi wall-hoop stress for a pressure-vessel cylinder) characterize a highly efficient structural material.

B. SEALANT-LINER REQUIREMENTS

The filament-wound composite, while light in weight, is permeable to gases and liquids under pressure. Furthermore, the filament and/or resin may be subject to chemical corrosion by contained fluids, such as propellants. Permeability and corrosion can be overcome by using a thin interior liner to prevent or minimize fluid contact or transmission through the wall. Because pressure-vessel performance is based on the total weight, operating pressure, and volume, a minimum-weight liner is desirable.

---

*Also designated S-901 glass by the manufacturer, Owens-Corning Fiberglas Corporation.

The functional requirements for sealant liners include

- Impermeability to gases and liquids under pressure
- Resistance to corrosion by contained fluids
- Strain compatibility between the liner and the composite structure up to the composite-failure stress
- Resistance to fatigue when subjected to repetitive loading to the operating stress level
- Toleration of tank expansion and contraction during temperature cycling.

C. LINER MATERIALS

Molded elastomers, polymeric films, metal coatings, metal foil, and thin metal sheet have been used for liners. The polymeric materials have been suitable when the service life is short and when some permeation through the structure is tolerable. Elastomeric liners have thus far been restricted to temperatures greater than -65°F because they lose extensibility as the glass-transition temperature is reached.

When a polymeric liner is functionally adequate, the designing of the filament-wound vessel is relatively straightforward. When stringent limitations are imposed on fluid leakage or when the operating temperatures are below -65°F, metal liners must be used because elastomers and polymers cannot now provide the necessary properties.

D. METAL-LINER DESIGN CONCEPTS

The high strength and relatively low modulus of glass filaments create a requirement for large biaxial strains in the metal liner, and are the most significant factors influencing material selection and design. The liner membrane must strain under a 1-to-1 biaxial field past its yield point to the operating and ultimate stresses of the filaments without failure or fluid permeation under pressure. At 75°F, S-HTS filaments have an elastic modulus of 12.4×10^6 psi and a representative ultimate filament strength in pressure vessels of 330,000 psi, yielding a biaxial-failure strain of about 2.7%. At cryogenic temperatures, the filament strength may increase as much as 50% to 495,000 psi, while the modulus increases about 10% to 13.6×10^6 psi, producing a biaxial-failure strain of about 3.6%. Stress-strain relationships for S-glass filaments and three possible metal-liner materials at 75°F are shown in Figure 2. As indicated, the strains at the operating stress will cause the liner to exceed its yield point and to deform plastically. In general, this will occur even if the design makes use of the complete compression-to-tension elastic-strain range of the liner.

When the liner is permitted to work beyond the proportional limit into its plastic zone upon application of the zero-to-maximum use or limit

pressures, it will spring back along its offset, biaxial, elastic, stress-strain curve as the pressure is relieved and will be pushed into compression by external pressure from the overwrapped filaments until load equilibrium is reached. An adhesive bond must be retained between the liner and the filaments to prevent buckling, or the liner must be strong enough not to buckle and thereby suffer fatigue failure.

Metal-liner design concepts have been categorized into four groups, (defined below), based on their zero-to-operating-to-zero-pressure strain characteristics. Figure 3 presents their associated schematic stress-strain curves; for simplicity, the plots assume no liner prestress in compression during fabrication and a common origin for the liner and FWC stress-strain curves.

1. Elastic Liner (Concept A)

This is a very thin, smooth liner that is strained only in the tensile elastic zone or the compressive and tensile elastic zones. It may or may not require tank-wall bonding to prevent buckling under compression loading.

2. Smooth, Bonded Liner (Concept B)

This is a very thin, smooth liner that is strained in the tensile and compressive elastic and plastic zones and requires a bond to the tank wall to prevent buckling under compressive stress.

3. Corrugated Liner (Concept C)

This very thin, corrugated-metal liner is designed so that pleats considerably increase its elastic-strain capability as compared with the smooth parent material of construction. It is strained only in its elastic zone.

4. Plastic-Elastic, Load-Bearing Liner (Concept D)

This is a thicker, smooth, load-bearing liner that is strained only in the tensile and compressive elastic zones after an initial prestress into the plastic zone. It is strong enough to resist buckling under compressive loading.

The first three concepts are referred to as metal-lined glass-filament-wound pressure vessels, and the fourth as the GFR-metal pressure-vessel concept. This program analytically and experimentally investigated the design requirements and advantages of GFR metal tanks.

E. GFR METAL TANKS

When design requirements dictate the use of a metal liner to meet performance specifications, thick liners that share loads with the FWC shell offer an excellent approach to workable, low-weight, high-pressure-fluid, storage vessels.

This concept provide a tank formed by combining a load-bearing metal shell with an overwrapped glass-filament shell. Metal-tank fabrication procedures are used in constructing the liner. The glass shell is fabricated by winding a specifically oriented pattern of pretensioned, resin-impregnated, continuous filaments over the metal shell.

1. Stress-Strain Conditions

A schematic stress-strain diagram for a pressure vessel so constructed is presented in Figure 4. With reference to that figure, a "load-bearing metal shell" is defined as one capable of resisting buckling at the compressive-stress level (E) shown there (produced by external pressure from the overwrapped shell), when no bond exists between the two shells. The two shells are designed to minimize the hysteresis loop of the liner in the operational-pressure-cycle stress range (E) to (J) to (E) [i.e., (E) to (J) is an elastic stress-strain curve].

Significantly different stress-strain conditions are imposed on GFR metal tanks during application of the internal pressures associated with tank fabrication, proof testing, burst testing, and operation. Figure 4 depicts these states for both shells during fabrication, after mandrel removal, and at the proof-pressure prestress, zero pressure, operating pressure, and burst pressure. It provides a basis for the ensuing discussion, which repeatedly refers to points depicted there.

The metal shell may be held in a stress-free (strain-free) state by a rigid mandrel while being overwrapped with tensioned filaments [point (M)]. Upon mandrel removal, however, it will spring back into a compressive state, due to the overwrap pressure [point (O)]. The magnitude of compression at zero-internal-pressure equilibrium depends on the relative thicknesses and moduli of the overwrapped filaments and the liner, as well as the biaxial stress-strain characteristics of the liner and the filament-winding tension used during FWC fabrication.

When the first pressure load (p_p) is applied, the GFR metal tank is strained to point (A), which is fixed by material properties and thicknesses and by the load. For factors of safety associated with aerospace tankage and with the glass-filament and metallic materials now available, point (A) will be beyond the metal-shell yield point and considerable plastic deformation may occur. In general, it can be said that the biaxial tensile strain produced in the liner by the initial prestress load will exceed 1% and may be greater than 2%.

When that initial load is removed, the liner will spring back along the offset, biaxial, elastic, stress-strain curve (A)-(E) and will be pushed into high compression by external pressure from the overwrapped filaments until load equilibrium is reached at point (E) [strain (G)]. The GFR metal tanks are designed so that point (E) does not exceed (a) the critical buckling-stress level of the liner in the absence of a bond between the two shells, or (b) the compressive elastic limit of the liner.

The operating-pressure level (p_o) will always be less than or equal to p_p. During the application of cyclic operating-pressure loads, therefore, the metal-liner strain range is between points (G) and (K), and the value of (K) may be as large as (B).

Specific stress and strain values fixing the range between (G) and (K) depend on design details, but maximum values for that range can be estimated from candidate-material properties by assuming that the minimum value of (G) occurs at the biaxial-compressive-yield stress of the metal shell and that the maximum value of (K) is equal to the strain (B) and occurs when $p_o = p_p$. Associated with the minimum value of strain (G) is the stress σ_E and with the maximum value of strain (K) the stress σ_J. As an approximation, and in the absence of the Bauschinger effect,* it may be assumed that $-\sigma_E = \sigma_J$ = material tensile-yield point, in accordance with the foregoing assumptions. This strain range between σ_E and σ_J is the maximum-permissible operating-strain range for GFR metal tanks.

2. Unique Design Criteria

Designs of GFR metal tanks must be based on both internal-pressure requirements and zero-pressure stress states in the liner. In addition to the usual requirements, the following conditions are imposed on the liner design:

a. An adhesive bond between the two shells is not required to prevent buckling when the liner is loaded in compression. The unbonded liner must have sufficient buckling strength and load-carrying capability to sustain external forces from the overwrapped filaments.

b. The compressive-stress level in the liner will not exceed the compressive elastic limit, to minimize hysteresis effects and thereby improve the cyclic-fatigue endurance.

c. The stress level in the liner at the operating pressure will not exceed the tensile elastic limit, to minimize hysteresis effects during cyclic applications of the operating pressure.

In GFR metal tanks, efficient use of filament strength requires that the parent metal and weldments of the liner have sufficient ductility to permit biaxial straining to (a) the maximum design-allowable filament stress at p_o, and (b) the ultimate elongation of the filaments at their ultimate stress. Metal shells without the required strain capability [due to cryogenic-temperature effects, heat-treatment level, low weld-joint ductility, or propagating defects in the welds (cracks, incomplete fusion, lack of penetration, excessive porosity, excessive inclusions, etc.)] will fail prematurely by local fracture of weldments or the parent metal, followed by leakage. Candidate materials must therefore have suitable elongation capability to be strain-compatible with the glass filaments.

---

*Reduced deformation resistance in one loading direction following initial prestraining in the opposite direction.

Under the 1-to-1 biaxial-stress-field conditions, such as exist in FWC pressure vessels and GFR metal tanks, metals have a significantly reduced strain capability as compared with their uniaxial (1-to-0) ductility. As shown in Reference 1 (pp. B-1 to B-3), the allowable elongation under such conditions in the +75 to -423°F range is less than 50% (and closer to 25%) of the uniaxial ductility. On this basis, the design rule is used that the allowable biaxial elongation of a metal under 1-to-1 stress-field conditions is 25% of the uniaxial value. With such a design allowable, the liner materials, in the parent metal and weldments, must have a uniaxial ductility capability about 4 times the ultimate filament strain, or 10.8% uniaxial elongation at +75°F and 14.4% at -423°F, to be able to strain as a liner to achieve the full strength potential of the glass-FWC shell.

III. TASK I - PARAMETRIC STUDY

The design, fabrication, and testing of GFR metal tanks were preceded by an investigation of overwrapped-metal-shell buckling strengths, and a comprehensive characterization analysis and parametric study of these tanks. The results, reported in Reference 1, are summarized below.

A. COMPRESSIVE PROPERTIES AND BUCKLING STRENGTHS OF OVERWRAPPED METAL SHELLS

An important design innovation associated with this configuration is extension of the elastic range of the metal by operating from compression to tension rather than in just the tension range. This is accomplished by imposing on the unpressurized filament shell a positive tension load that is reacted by a compressive load in the metal shell. Compressive liner stress at a zero chamber pressure can be set up by a number of techniques: using tension during filament winding, subjecting the fabricated tank to a prestress pressure that produces plastic yielding of the liner, or combinations of these two techniques.

To design the load-bearing component, it is necessary to know the compressive-stress level at which (1) liner buckling occurs, or (2) the elastic limit of the liner is exceeded. Present methods of analysis do not permit the calculation of compressive-buckling-stress design limits; however, this information has been established by experimental evaluation, and Reference 1 summarizes data available in the literature. As described there, R. H. Johns and A. Kaufman of the NASA Lewis Research Center tested the buckling of metal cylinders due to overwrapping in the circumferential direction with layers of tensioned filaments.

They conducted 29 tests on mild steel, stainless steel, nickel, titanium, and aluminum specimens with diameter-to-thickness (D/t) ratios ranging from 175 to 3000, and obtained another five data points (with D/t ratios in the range from 320 to 600) from the literature. Their analysis of all these results indicates that a straight-line correlation exists in logarithmic coordinates between D/t and σ_c/E_s, where σ_c is the critical stress from overwrapping at buckling failure and E_s is the metal-cylinder secant modulus at failure taken from the stress-strain curve, as shown in Figure 5. The σ_c/E_s parameter is thus the compressive strain at which buckling occurs. This correlation was used for the parametric study covered in Reference 1.

Additional work was done to determine the 75°F compressive properties and buckling strengths of filament-overwrapped, open-ended, metal cylinders. A detailed report on the experimental evaluation is presented in Appendix A. In summary, compressive-stress-strain curves and the point at which buckling failure occurred were determined for 12-in.-dia cylinders made from 2219-T62 aluminum alloy, nickel-base-alloy Inconel X-750 in the solution-treated and aged (STA) condition, and 5Al-2.5Sn titanium alloy (Ti-5Al-2.5Sn). Data from these experiments were evaluated and compared with other available data to provide a means for estimating compressive-stress limits as a function of the controlling parameters. The buckling characteristics

were in excellent agreement with the predicted behavior (determined from Figure 5) and correlations used for the parametric study. This agreement is shown in Figure 6, where data from the six cylinders tested are compared with other available data.

In all six cylinders, buckling failure occurred in the longitudinal seam weld at high stress levels. All failed in a cusp buckle. Compressive stress-strain curves were developed from the data recorded during the buckling tests.

B. STUDY RESULTS

This section summarizes the results of the parametric study (Reference 1), in which the advantages of and requirements for combining a metal shell with a glass-filament shell for high-pressure-fluid storage in the +75 to -423°F range were investigated. The research was concentrated on characterization of candidate metallic materials, definition of design-allowable strength levels for S-HTS glass-FWC structures, development of analytical procedures for the design and evaluation of GFR metal tanks, parametric study of the tanks, and rating of tank performance in comparison with homogeneous metal tankage made from Ti-6Al-4V, Type 301 stainless steel (SS), Inconel 718 (a nickel-base alloy), and the 2219-T87 aluminum alloy. The service requirement included sustained loading and 100 pressure cycles to the operating pressure.

To minimize hysteresis effects in the metal shell during cyclic operation, the tanks were designed so that, after the application of an initial prestress-pressure load (which plastically deforms the liner beyond its biaxial-yield stress), the stress range between zero pressure and the operating pressure was within the offset biaxial compressive and tensile elastic limits. In the parametric study, the liner stress at the operating pressure was required not to exceed 90% of the offset biaxial-yield stress.

Analyses of material properties revealed that several available alloys provide sufficient ductility and strength to meet the design requirements. The alloys studied were Ti-5Al-2.5Sn [annealed, extra-low-interstitial (ELI) grade], Type 301 SS (half-hard temper), the 2219-T62 aluminum alloy, and the Inconel X-750 (STA) nickel-base alloy. Because of cyclic-pressurization effects on FWC strength, it was estimated that the operating-pressure filament-stress level had to be maintained at 60% or less of the single-pressure-cycle burst stress to sustain the 100-cycle requirement for the tanks. An operating-pressure design-allowable filament-stress level of 200,000 psi at 75°F, compared with a representative single-cycle tank-burst-pressure filament-stress level of 330,000 psi, was necessary. At -320 and -423°F, these allowable levels were expected to increase by 50% to a 300,000-psi operating stress and a 495,000-psi burst stress.

A structural analysis and computer program were developed for use in designing and analyzing complete tanks, wound with either geodesic or in-plane patterns along the cylinder and over the end domes and complemented by circumferential windings in the cylinder. Optimum head contours were developed, and the following were computed for more than 1000 different configurations of

GFR metal tanks: filament- and metal-shell stresses and strains at zero pressure and the design pressure; hoop-wrap thickness required for the cylindrical portion; and weight, volume, and filament-path lengths for the components and complete vessel. For these designs, the computer program also determined the stresses and strains in both shells throughout service cycling from a series of input pressures, composite temperatures, and metal-liner temperatures.

Tanks were designed for room-temperature service so that the compressive-yield stress of the liner is not exceeded at any point on the head and in the cylinder, and so that the critical buckling-stress level is not exceeded in the cylinder or at the equator of the head when the liner is in maximum compression due to the overwrap. Thus, the designs developed in the study do not require an adhesive bond between the glass-fiber and metal shells to prevent buckling.

The optimum room-temperature designs were found to be optimum also for cryogenic temperatures if the tank is warmed at some time during its service life. The reason is that such designs have the maximum-permissible compressive stress in the metal shell at zero pressure after the proof test, and additional plastic deformation at any temperature results in too high compressive stresses at room temperature. At cryogenic temperatures, these designs can operate at an increased pressure to improve the performance if use is made of the change in metal-shell tensile-yield strength produced by the temperature change.

The necessary head contours are intermediate between that for the FWC pressure vessel and the spherical shape optimum for homogeneous metal heads. In GFR-metal-tank heads with the optimum contour, stresses are constant in the filaments up the contour, and a 1-to-1 stress field is produced in the liner at the design pressure and temperature, thus satisfying the requirements for optimum closure design. Completely wrapped GFR metal tanks with optimum head contours have higher performance than spherical GFR metal tanks or circumferentially reinforced, cylindrical tanks with hemispherical end closures. The performance level for completely wrapped oblate spheroids is comparable to that of completely wrapped cylinders.

Proper design of GFR metal tanks permits exploitation of the maximum load-bearing capabilities of the metal and filament shells. It makes possible operating pressures in the range from 1000 to 4000 psi and higher, with performances significantly greater than those of the highest-performance, cylindrical and spherical, homogeneous metal tanks. Figure 7 presents a summary comparison of operating-pressure performance factors $(p_oV/W)^*$ for GFR metal tanks, homogeneous metal tanks, and high-pressure glass-FWC tanks with very thin metal liners at 75°F and cryogenic operating temperatures. The design stress of the homogeneous tanks was 67% of the

*Where p = design pressure, psi [e.g., operating pressure (p_o) or burst pressure (p_b)]; V = internal volume, $in.^3$; and W = pressure-vessel weight, lb (not including fittings).

ultimate tensile strength or 77% of the yield strength, whichever gave the lower operating-stress level (a factor of safety of 1.5 based on ultimate strength or 1.3 based on yield strength). The GFR metal tanks and FWC vessels were assumed to operate at filament-stress levels of 200,000 psi at 75°F and 300,000 psi or less at -320 and -423°F. The low-temperature performances are maximum values based on full use of material properties at those temperatures. The GFR metal tanks are designed, however, so that after they are worked at their operating pressure at cryogenic temperatures, they may be warmed to room temperature without exceeding the maximum-permissible compressive stress. If the vessel warms during use or there are other reasons for not employing the properties of the structural material at the operating temperature, the performance factors given for each type of vessel as a function of temperature must be adjusted correspondingly.

Maximum performance for cryogenic service will be provided by high-pressure FWC tanks with very thin metal liners, provided that a reliable liner design can be developed. For this reason, the comments that follow pertain only to comparison of GFR metal tanks and homogeneous metal vessels.

Maximum efficiency over the 75 to -423°F range is provided by GFR Ti-5Al-2.5Sn vessels. Their performance is considerably greater than that of the other GFR metal tanks and all candidate homogeneous vessels. At room temperature, it is 35% higher than that of Ti-6Al-4V (annealed) spheres and 70% higher than that of Ti-6Al-4V (annealed) cylinders. When compared with the performance of the highest-strength homogeneous vessels made from 301 SS, Inconel 718 (STA), and 2219-T87 aluminum (see Figure 7), the improvement ranges from 40 to 130%, depending on the shape and the alloy used.

The GFR titanium tanks have a minimum safety factor of 1.40 to 1.57 at 75°F, which is comparable to that of the homogeneous tanks. At -320 and -423°F, burst-strength performance is believed to be limited by the biaxial-strain capability of the liner weldments, and the full glass-filament potential cannot be realized. When the cryogenic properties are used to maximize p_oV/W, the safety factors are 1.16 to 1.30 at -320°F and 1.08 at -423°F. However, if the cryogenic-strength properties of both shells are not employed to increase the p_o level, the safety factors increase to about 1.70 to 1.80 at -320°F and 1.60 to 1.70 at -423°F. In designing these tanks for cryogenic service, a compromise must therefore be reached between the safety factor and the resulting p_oV/W value.

The second highest performance at 75°F is provided by GFR 2219-T62 aluminum tanks. Compared with Ti-6Al-4V (annealed), it is as much as 15% higher than that of spheres and 25 to 45% higher than that of cylinders. The safety factors are 1.43 to 1.57 at 75°F, depending on shape and pressure. At -320°F, these values are close to 1.40 at the maximum operating-pressure level. At -423°F, however, low weldment ductility decreases the estimated factor to only 1.08 at the maximum operating pressure. As was the case for titanium, safe operation at -423°therefore requires a compromise between adequate safety and high p_oV/W. As an example, if the 75°F p_oV/W of 355,000 to 405,000 in. is acceptable at -320 and -423°F, the operating pressure could be held at the 75°F value in cryogenic use. If this is done, the 75°F safety factor of 1.43 to 1.57 changes to about 1.50 at -320°F but drops to 1.20 at -423°F.

The performance of GFR 301 SS (half-hard) oblate-spheroid vessels is slightly below that of GFR aluminum tanks and of homogeneous Ti-6Al-4V (annealed) spheres, but is above that of all the other homogeneous vessels. The factors of safety at the maximum operating pressure are about 1.50 at 75°F and 1.70 at -320°F; at -423°F, the value is reduced to only 1.08, due to the low estimated strain capability of metal-shell weldments.

The GFR Inconel X-750 (STA) tanks have a number of unique features. In the 75 to -423°F range, the liner has sufficient ductility to strain to the ultimate filament strength, thereby achieving the maximum performance obtainable with this material combination and the design requirements imposed on GFR metal tanks. The factors of safety based on the maximum-permissible p_o increase as the operating temperature decreases; except for cylindrical vessels at 75°F, they range from 1.50 to 1.85 at 75 to -423°F. Because of the good liner performance (large biaxial-strain capability and 100% weld-joint efficiency) it appears feasible (and is recommended, if optimum performance is to be attained) to operate at levels that produce liner stresses equal to the proof-pressure stress at 75°F or at the offset-yield stress as the temperature is reduced from 75 to -423°F. This p_o increase results in an improvement of about 10% in p_oV/W.

If GFR Inconel tanks are operated at 90% of the offset-yield stress, the 75°F performance is about 20% greater than that for homogeneous Ti-6Al-4V (annealed) cylinders, and about 30% greater than for 301 SS (extra-full-hard temper) cylinders. The performance advantage is maintained at these and higher values in comparison with spherical and cylindrical homogeneous tanks fabricated from Inconel 718 (STA) and 2219-T87 aluminum. The GFR Inconel X-750 (STA) tanks can have equivalent or slightly higher performance factors than Ti-6Al-4V and 301 SS spheres. If the low-temperature mechanical properties are employed, their rate of performance increase at cryogenic temperatures is less than that for homogeneous titanium and stainless steel vessels, which develop superior p_oV/W values in cryogenic use.

If the GFR Inconel tanks are operated at 100% of the offset-yield stress, the 75 to -423°F performance is equivalent to that of GFR aluminum and GFR stainless steel tanks, as shown in Figure 7. At 75°F, they are superior to all configurations of homogeneous vessels made from the representative stainless steel and titanium-, aluminum-, and nickel-base alloys. When cryogenic-temperature properties are used to increase the p_oV/W, homogeneous titanium spheres and cylinders and homogeneous stainless steel spheres have higher values than GFR Inconel tanks. Creep of homogeneous titanium-alloy vessels, when subjected to the operating-stress levels assumed in this analysis, may create a problem in the 75 to -423°F range. If the problem is shown to be serious, the performance advantages offered by GFR Inconel tanks will be greatly amplified.

IV. TASK II - PRESSURE-VESSEL DESIGN

A. SELECTION OF CONFIGURATION

Using the Task I results, a GFR metal vessel was selected for design, fabrication, and testing. The parametric study showed that tanks of GFR Ti-5Al-2.5Sn (annealed, ELI grade) were the most efficient. However, the study also revealed that, with the exception of Inconel X-750, the titanium-alloy and other candidate materials [2219-T62 aluminum and 301 (half-hard) stainless steel] might have insufficient biaxial ductilities in weldments at cryogenic temperatures for satisfactory performance. The burst-strength performance of vessels made with these liner materials could be limited by the biaxial-strain capability of the weldments, and the full strength potential of the glass filaments would not be realized. Nickel-base alloy Inconel X-750 (STA) was thus selected, because it offered a higher probability of success for exploitation of the full potential of fiber glass at all temperatures than did Ti-5Al-2.5Sn, 2219-T62 aluminum, or 301 SS (half-hard). S-glass filament roving with the HTS finish was selected for the filament-wound-shell component on the basis of high strength, experience in its use, and commercial availability. Aerojet work under Contract NAS 3-6287 led to the development of a resin matrix with higher elongation at cryogenic temperature than commonly used resins. This resin [Epon 828/DSA/Empol 1040/BDMA (100/115.9/20/1 parts by weight)]* has been shown to improve the $p_o V/W$ for filament-wound vessels at cryogenic temperatures while giving a performance equivalent to that of standard epoxies at ambient temperatures (Reference 2), and was therefore selected as the FWC resin matrix.

A review of optimum designs for GFR Inconel X-750 tanks showed that an oblate spheroid would provide the best combination of operating- and burst-pressure performance factors (pV/W), factors of safety for 75, -320, and -423°F service temperatures, and fabrication practicality. The highest pV/W for such tanks is obtained with a 75°F p_o value of about 1800 psi or greater. For vessel design, 2000 psi was selected; the parametric-design curves show that the related 75°F factor of safety is 1.50 and the design burst pressure is 3000 psi.

To minimize hysteresis effects during cyclic pressurization, the tank was designed so that, after an initial prestress-pressure load that plastically deforms the metal shell beyond its biaxial-yield stress, the stress range in the liner between zero and the operating pressure (p_o) was within the offset biaxial compressive and tensile elastic limits. In the parametric study and for vessel design, the liner stress at p_o was required not to exceed 90% of the offset biaxial-yield stress. This was implemented by using a 2220-psig proof pressure (p_p) at 75°F in conjunction with the 2000-psi p_o to establish the required margin between proof and operating stresses in the liner.

---

*Epon 828 is a bisphenol A epoxy; DSA is dodecenyl succinic anhydride, a flexibilizing curing agent; Empol 1040 is a high-molecular-weight tri-carboxy acid; and BDMA is benzyldimethylamine, a cure catalyst.

The selected dimensions for the oblate spheroid were a diameter of 18 in. and a length of 14 in. The axial-port size at each end was fixed at 2.70 in., or 15% of the vessel diameter.

B. SERVICE-CYCLE REQUIREMENT

The service requirement used for the design included a minimum fatigue life of 100 pressure cycles and 72 hours of sustained loading at the 75, -320, and -423°F operating pressures.

C. ANALYSIS OF MATERIAL PROPERTIES

1. Metal Shell

Detailed characterization analyses of Inconel X-750 over the 75 to -423°F range were reported in detail in Reference 1. Properties used for the design and computer analyses of the metal shell are shown in Tables 1 and 2.

2. Glass-Filament Shell

An analysis was undertaken to determine the minimum, maximum, and typical values of room-temperature, single-pressure-cycle, allowable, S-HTS glass-filament, strength levels in vessels having p_o values from 1000 to 4000 psi, diameters in the 12 to 40-in. range, and length-to-diameter (L/D) ratios ranging from 0.62 to 5. Reference 1 covers this analysis in detail and reviews other filament-shell properties. It shows that representative strengths ranged from 314,000 to 368,000 psi for hoop filaments and from 272,000 to 370,000 psi for longitudinal filaments. A typical value suitable for calculations was found to be 330,000 psi; it was used for the pressure-vessel design analysis.

Adjustments were made in the single-cycle design allowables to account for the effects of cyclic and sustained loading (assumed to be 100 pressure cycles and 72 hours of sustained loading at the operating-stress level). The typical single-cycle strength of 330,000 psi was reduced, by multiplication with a factor of 0.60, to 200,000 psi to provide for the service-life requirement, based on Aerojet Independent Research and Development (IR&D) data on the effects of pressure loading at ambient temperature on the strength of glass-FWC vessels. The outer shell was thus designed to have a filament stress of 200,000 psi at the 75°F p_o of 2000 psi.

Data on glass-fiber and glass-FWC properties at cryogenic temperatures were compiled and developed. They provided the basis for the following estimates for S-HTS glass filaments with a design-temperature decrease from 75°F to -320 or -423°F: a design-allowable filament-strength increase of 50% and a tensile-modulus increase of 10%. With these estimates, the filament strengths increased from the typical 330,000 psi at 75°F to 495,000 psi at -320 and -423°F; the tensile modulus increased from 12.4×10^6 to 13.6×10^6 psi; and the ultimate filament tensile strain increased from about 2.68% to about 3.64%.

Material properties used for the design and computer analyses of the glass shell are given in Table 2, along with other design data.

D. PRELIMINARY SIZING AND DESIGN

Preliminary tank-design parameters were established with the design curves of Reference 1, reproduced here as Figures 8 to 13. The only information needed to establish the preliminary design was the following:

Operating pressure at 75°F	2000 psi
Diameter	18 in.
Shape	Oblate spheroid
Filament stress at 75°F p_o	200,000 psi
Metal-shell stress at operating pressure and temperature	0.90 of offset yield stress at temperature
Winding pattern	Longitudinal in-plane
Metal-shell material	Inconel X-750 (STA)
Overwrap material	S-HTS glass filaments

It was assumed that the boss diameter is 20% of the vessel diameter, and that a rigid mandrel and filament-winding stress of 47,000 psi are used. (In the subsequent detailed analysis, these parameters are altered, as described in paragraph IV,E,2.)

The relationship given in Figure 8 for p_o vs room-temperature p_p shows that for p_o = 2000 psi at 75°F in a GFR Inconel X-750 (STA) tank, p_p = 2220 psi. The use of a higher value for p_p will cause an overly high compressive stress in the liner at zero pressure and room temperature. Figure 8 also shows that the -320 and -423°F $p_o \approx$ 2300 psi.

With this information, the design curves of Figures 9 to 13 can be used to establish other tank parameters. Figure 9 shows that a liner diameter-to-thickness ratio (D/T_L) of 383 is required when p_p = 2220 psi and the shape is an oblate spheroid. For D = 18 in. and D/T_L = 383, T_L = 0.047 in. The optimum liner-to-glass-shell thickness ratio (T_L/T_O) is found from Figure 10 to be 1.66 for p_p = 2220 psi. Thus, with T_L = 0.047 in. and T_L/T_O = 1.66, the longitudinal FWC thickness at the equator of the head (T_O) is 0.028 in. From Figure 11, p_oV/W for the design at 75°F is 327,000 in. From Figure 12, p_oV/W at -320 and -423°F is 365,000 in. if the operating pressure develops 90% of the liner offset-yield stress at that temperature.

The factor of safety for the design is 1.50 at 75°F and 1.85 at -320 and -423°F, from Figure 13.

E. STRUCTURAL DESIGN AND ANALYSIS

1. Method of Analysis

The shape and component thicknesses were established with the computer program for analysis of GFR metal tanks developed under this contract (detailed in Reference 3 and summarized in Appendix B). The program was used to investigate the filament shell by means of a netting analysis, which assumes constant stresses along the filament path and that the resin matrix makes a negligible structural contribution. The filament and metal shells are combined by equating strains in the longitudinal and hoop directions and by adjusting the shell radii of curvature to match the combined material strengths at the design pressure.

The program established the optimum head contour and defined the component thicknesses and other dimensional coordinates, as well as the shell stresses and strains at zero pressure and the design pressure, the filament-path length, and the weight and volume of the components and complete vessel. It was also used to determine the stresses and strains in the two shells during vessel operation through the use of a series of pressures, composite temperatures, and metal-shell temperatures as inputs. This permitted analyses of pressure and temperature cycles taking into account previous strains and loads.

2. Design Parameters and Drawings

Table 2 presents input variables used for the computer analysis, and other pressure, dimensional, and material parameters.

Designs were prepared for the Inconel X-750 polar boss (Part No. 178089), Inconel X-750 metal-shell assembly (Part No. 178090), GFR Inconel X-750 pressure vessel (Part No. 178091 initial design, and Part No. 1268928, final design), the head reinforcements (Part Nos. 178163 and 1268927), and the GFR Inconel X-750 test assembly (Part No. 178134). They are shown in Figures 14 to 18.

The 18-in.-dia test vessel was an oblate spheroid with p_p = 2220 psi at 75°F, and design p_o values of 2000 psi at 75°F, 2300 psi at -320°F, and 2350 psi at -423°F. The design burst pressure (p_b) at 75°F was 3010 psi; at -320°F it was 4263 psi and at -423°F was 4300 psi, based on a 50% increase in design-allowable filament stresses at those temperatures. Table 3 gives the vessel-design parameters.

The tank consists of a 0.047-in.-thick Inconel X-750 (STA) metal liner overwrapped with an S-HTS glass-FWC thickness of 0.030 in. at the equator of the heads. The FWC resin matrix is a highly modified, highly flexibilized, epoxy resin of the following formulation: Epon 828/DSA/Empol 1040/BDMA (100/115.9/20/1 pbw) (Resin System 2 developed by Aerojet under Contract NAS 3-6287). The polar bosses at each end of the vessel are 15% of the vessel diameter.

Reinforcement consisting of unidirectional, resin-impregnated, glass-filament tapes laid tangentially to the polar boss and extending along each head to a normalized radial distance (Z) of 0.50 is required for each head. It is designed to provide sufficient strength so that plastic deformation of the metal shell at p_p = 2220 psi is reduced between $0.50 \leq Z \leq 0.15$ (polar boss) to ensure that, on post-proofing depressurization, the compressive-springback stress does not exceed the liner's proportional limit at any point on the head.

The pressure-vessel membrane is analyzed in detail below. The polar-boss design is analyzed in Appendix C, and filament-winding-pattern calculations and head-reinforcement design are covered in Appendix D.

3. Detailed Analysis of Pressure-Vessel Stress-Strain and Pressure-Strain Relationships

Computer output was used in analyzing the metal- and glass-shell stress-strain and pressure-strain relationships.

Figure 19 presents 75°F stress-strain relationships for the hoop and longitudinal directions at the equator of the heads (Z = 1.0) and at Z = 0.5. It shows conditions in the component materials at winding, after mandrel removal, at the liner-yield point, at p_p = 2220 psi, at zero pressure after proofing, at p_o = 2000 psi (at 75°F), and at p_b = 3010 psi.

Observations of interest are (a) at zero pressure after proofing, a longitudinal compressive stress of -108,000 psi [the design-allowable compressive-yield stress for Inconel X-750 (STA)] occurs in the liner heads at Z = 0.5; (b) the maximum tensile stress in the liner at p_o after proofing occurs in the longitudinal direction of the heads at the equator and equals 90% of the offset-yield stress; (c) the filament stress at the equator of the heads at p_o is the required 200,000 psi; and (d) the design-allowable filament stress of 330,000 psi is developed in the longitudinal filaments at 3010 psig.

Figures 20 and 21 show the -320 and -423°F stress-strain conditions. The curves assume that vessels are proofed at 75°F and depressurized before cooldown to the cryogenic temperature; the curve shifts due to temperature changes are indicated. The maximum tensile stress in the liner at p_o occurs in the longitudinal direction of the heads and equals 90% of the offset-yield stress at the operating temperature. The filament stresses reach a maximum of 495,000 psi at pressures of 4263 psi (-320°F) and 4300 psi (-423°F).

At 75°F, the longitudinal and hoop strains at the design p_b of 3010 psi are the same (see Figure 19). However, when the vessel is pressurized to the burst point at -320 and -423°F, the hoop strain at the design p_b is considerably greater than the longitudinal strain, inducing large biaxial-strain requirements for the liner.

Stress conditions in the tank heads at 75°F as a function of Z are given in Figure 22 for p_p = 2220 psi. The liner stresses are essentially constant up the contour.

Figure 23 shows stresses at p_o = 2000, 2300, and 2350 psig at 75, -320, and -423°F, respectively. The p_o filament stress at 75°F at the equator of the heads is the required 200,000 psi. The maximum liner stress at p_o occurs in the longitudinal direction of the heads (at the equator at 75°F, and up the head at -320 and -423°F) and equals approximately 90% of the liner's offset-yield stress.

Stresses at zero pressure after proofing are shown in Figure 24 for 75, -320, and -423°F exposure temperatures. The compressive stresses in the liner heads at that pressure controlled the tank design. They increased from relatively low values at the equator (Z = 1.0) to very large values where the thicker axial-port boss was welded to the shell at about Z = 0.25. A decrease from 75°F to -320 and -423°F produced only slight stress changes in the unpressurized tank.

In review, the tank-design criteria with regard to compressive stresses in the liner were (a) the critical-buckling stress must not be exceeded at the equator of the head, and (b) the head stresses must not exceed the compressive-yield stress. In this case, the liner values did not exceed the -65,000-psi buckling stress allowable at the equator, but did exceed the compressive-yield stress of -108,000 psi at $Z \leq 0.50$. Therefore, either the liner thickness or the composite thickness at $\overline{Z} \leq 0.50$ had to be increased to reduce the stresses to acceptable values in the depressurized tank after proofing. The latter approach was selected, and patterns of glass/resin-composite reinforcements (design shown in Figure 17) were added locally (as indicated in Figure 16), to increase the composite thickness, decrease the liner deformation at $Z \leq 0.50$, and thereby reduce the compressive stresses at zero pressure to acceptable levels. These local reinforcements also reduce FWC radial deflection adjacent to the rigid center boss, and thereby minimize abrupt increases in liner strain adjacent to the boss.

At the 75° design p_b of 3010 psi, the filament stresses were constant up the contour and a 1-to-1 stress field was produced in the liner (see Figure 19), thus satisfying the requirement for optimum closure design.

The computer output was used to construct pressure-strain curves for 75, -320 and -423°F test conditions, to be used to compare the measured pressure-strain characteristics with the predicted behavior. The predicted curves are presented in Figures 25 to 27.

V. TASK II - PRESSURE-VESSEL FABRICATION

Twenty 18-in.-dia GFR Inconel X-750 (STA) tanks were fabricated as described below for structural evaluation at 75 to -423°F.

A. PROCEDURE

Tank fabrication was accomplished in accordance with the design drawings, a metal-shell fabrication specification, an FWC-shell fabrication procedure, and the general sequence shown in Figure 28, a manufacturing flow diagram.

Inconel X-750 forgings were machined to provide the required polar bosses (Figure 29). Heads were formed from Inconel X-750 sheet (Figure 30); they had an opening at the apex of the dome to accept the polar bosses, and were matched into sets ready to weld with a maximum gap between butt edges of 0.002 to 0.004 in. and a diameter tolerance of ±0.002 in. at the butt edges. Each boss was match-fitted to the opening, and the joint areas were cleaned before welding.

A Sciaky 30-kw electron-beam-welding machine with a 68 by 46 by 68-in. vacuum chamber was used (Figures 31 and 32). It permits movement in the x, y, and z directions. The relative movements of the electron beam and the work were programed in advance, and all welding was automatic.

This approach differs from fusion welding in that it does not depend on heat conduction from an external source to achieve coalescence. Basically, a small hole is "vaporized" through the joint by a narrow beam of electrons. As the beam travels along the joint, the molten metal solidifies behind the traveling hole, thus forming the weld in a vacuum environment and eliminating atmospheric contamination.

The setup used for welding a boss to a formed head is shown in Figures 31 to 33, and a typical completed half shell in Figures 34 to 37.

The half shells were inspected and mated on the basis of fit at the girth weld. After the joint areas were cleaned, each set of half shells was assembled in the vacuum chamber (as illustrated in Figure 38) and welded together. A typical completed assembly is shown in Figure 39.

All welds were subjected to 100% radiographic inspection to the required specification (AGC-13860, Class 11), which permits no weld cracks, parent-metal cracks, incomplete penetration, incomplete fusion, aligned porosity, linear porosity, undercut, sharp weld edges, etc. that might propagate or become sites of stress concentrations. The specification permits scattered porosities no greater than 0.010 in. in diameter if they are no closer to each other than three diameters (or a 0.020-in. minimum) and there are no more than three pores per inch. The weldments also were subjected to 100% dye-penetrant inspection.

After acceptance, the units were solution-treated and aged in dry hydrogen to develop their full mechanical properties.

Glass roving, resin, unidirectional glass-filament tape, and other materials needed for overwinding and curing were procured. Layup molds for the head reinforcements were fabricated. The filament-winding machine, roving-tension devices, resin-impregnation system, and payoff rollers were installed and thoroughly checked before the initiation of overwinding. Several trial windings were made on a liner assembly to verify the procedures and the pattern.

After preparations were completed, the liners were wound and cured. Figure 40 shows the positioning of an assembly in the winding machine, Figures 41 and 42 show overwinding with resin-impregnated glass, and Figure 43 shows a typical, completed, GFR Inconel X-750 tank instrumented for testing.

B. SPECIFICATIONS

Detailed fabrication specifications and procedures were written to facilitate planning, data collection, and all allied phases of work. The liner specification is presented in Appendix E, and the FWC procedure in Appendix F.

C. DEVELOPMENT OF WELD SCHEDULE

The importance of joint integrity led to the initiation of a weld-schedule and weld-joint verification program prior to fabrication. Simulated circular boss-to-head welds and circumferential half-shell to half-shell welds were made and evaluated to define and optimize the schedule required for each operation.

Simulated boss-weld specimens were machined from Inconel X-750 to the same dimensions as in the weld-joint design. After cleaning, they were mounted on fixtures in the welder, and the optimum schedule was developed. The specimens were evaluated radiographically and by the dye-penetrant method and were inspected for weld bead and dropthrough.

The simulated-girth-weld specimens were rings fabricated in accordance with the joint design. After cleaning, they were mounted in the welder, the optimum schedule was developed, and the specimens were inspected.

D. DETAILED FABRICATION SEQUENCE

The detailed manufacturing sequence for each tank included the operations summarized below.

1. Metal-Shell Fabrication

a. Closed-die pancake forgings for the bosses and formed half shells were procured and accepted on the basis of certification and quality-assurance inspection of the base-material chemical and physical properties, heat-treat number, tensile coupons, and compliance with dimensional requirements.

b. Heat numbers were logged and serial numbers were marked on all parts throughout machining.

c. Each boss forging was rough-machined and finish-machined with the aid of contour templates, drill jigs, and forming tools.

d. Formed half shells were dimensionally inspected for inside diameter, wall thickness, contour, and length.

e. If required, forward and aft formed-shell halves were machined to generate square edges for the joint at the outside diameter of the boss.

f. The shell halves and bosses were cleaned and enclosed in individual polyethylene bags.

g. The boss-to-head-weld fixture was assembled in the welding chamber.

h. The forward boss and the forward shell half were mounted on the fixture.

i. These parts were inspected for weld-joint fit and were repositioned as required to minimize gap and mismatch.

j. The forward boss was welded to the forward shell half in accordance with the weld schedule.

k. This assembly was visually inspected for weld crown, penetration, undercut, and surface condition.

l. The weld joint was radiographically inspected and fluorescent-penetrant-inspected.

m. It was blended as required for the desired surface condition, and all penetrant-inspection indications were removed.

n. If required, the weld was repaired in accordance with radiographic-inspection records and the fabrication specification, and was reinspected as in Operations l and m, above. Figure 44 shows typical acceptable, unacceptable, and repaired weld joints.

o. Operations h through n were repeated for the aft boss and the mating aft shell half.

p. Pairs of forward and aft half-shell subassemblies were mated and identified to assure a minimum of midsection weld-joint mismatch.

q. Half-shell pairs were cleaned and each half shell was enclosed in a polyethylene bag.

r. Forward and aft half shells were mounted on the girth-weld fixture.

s. The assembly was inspected for mismatch and weld-joint gap.

t. It was checked for runout condition, and was repositioned and corrected as required to minimize runout.

u. The half shells were tack-welded together.

v. The circumferential joint was completely welded in accordance with the qualified schedule.

w. The weld was visually inspected and was reworked as required to satisfy tolerances on the crown, undercut, and finish.

x. The assembly was radiographically inspected and fluorescent-penetrant-inspected.

y. It was reworked, if required, in accordance with the fabrication specification and was reinspected. Figure 44 shows typical acceptable, unacceptable, and repaired weld joints.

z. The shell assembly was solution-treated and aged in dry hydrogen as required by the fabrication specification.

2. GFR-Metal-Tank Fabrication

a. Glass-filament roving and resin constituents were procured and accepted on the basis of certifications and quality-assurance inspection for the required chemical and physical properties.

b. The roving and resin were stored and were preconditioned as required.

c. The exterior of the metal shell was powder-blasted, and the shell was enclosed in a polyethylene bag.

d. The shell was mounted on the winding shaft.

e. The shell/shaft assembly was positioned in the filament-winding machine.

f. The polyethylene bag was removed and the shell was wiped with methyl ethyl ketone solvent and allowed to air-dry.

g. The resin was mixed, and the shell was brush-coated.

h. Rolls of glass roving were positioned on the winding machine, and the roving tension, wrapping angle, and machine turn/rpm ratio were set.

i. Mixed resin was placed in the resin-impregnation device.

j. The longitudinal filament layers were wound to the required number of turns; head reinforcements were applied and positioned during winding.

k. The wound unit was wiped to remove excess resin.

l. The filament-wound composite was covered with a bleeder cloth.

m. The entire, wrapped, shell assembly was vacuum-bagged, and a vacuum was applied (minimum, 22 in. Hg).

n. The unit was oven-cured for 2 hours at 150°F and 4 hours at 300°F.

o. It was removed from the oven, and the vacuum bag and bleeder cloth were stripped off.

p. The filament-wound shell assembly was removed from the winding shaft.

q. The vessel was solvent-cleaned and allowed to air-dry.

r. The complete tank was identified with a part number and a serial number, and was enclosed in a sealed polyethylene bag.

After this operation, tanks were sent to the test facility for structural testing.

E. MATERIAL-VERIFICATION TESTS

1. Inconel X-750 (STA)

Uniaxial tensile tests were conducted at ambient temperature on parent-metal, transverse-welded, and longitudinally welded specimens of Inconel X-750 (STA). The specimens were of standard configuration: 8 in. long by 3/4 in. wide, with a reduced section 1/2 in. wide machined for a gage length of 2 in. The parent-metal specimens were taken from (a) the sheet of material used to form the heads for Tank 2 (0.065 in. thick), and (b) another sheet of approximately the same thickness as the finished heads (0.053 in.) and used for the fabrication of weld-schedule-development specimens. Welded specimens were fabricated by electron-beam welding to simulate the metal-shell joint. The transverse specimens were welded at the midpoint of the gage length. The longitudinal specimens were welded along the entire long axis. All specimens were solution-treated and aged with the first group of metal-shell assemblies.

Table 4 summarizes the test results. Typical properties of formed-head parent-metal specimens (87,700-psi proportional limit, 110,500-psi yield strength, 171,870-psi ultimate strength, and 26.9% elongation) were lower than the properties used for the parametric study (Reference 1: 108,000-psi

proportional limit, 120,000-psi yield strength, 174,000-psi ultimate strength, and 25% elongation). When the stress-strain curve used for the parametric study was plotted and compared with typical measured values for the Inconel specimens, very close correspondence was found (see Figure 45). By changing the plastic modulus of the parametric study (796,000 psi) to the measured value (440,000 psi), the stress-strain curves were essentially the same, within the two-straight-line* approximation of the design analysis.

Parent-metal specimens made from the same sheet as the welded specimens yielded test results very similar to those from the formed-head parent-metal coupons. As shown in Table 4, the longitudinally and transverse-welded specimens had higher proportional limits, yield strengths, and ultimate strengths than for the parent metal, because of the weld bead (left on the specimens and not included in the calculated stress). The average elongation of 21.7 to 22.5% was only 90% of the parent-metal values, but was more than adequate to meet the biaxial-ductility design requirements for the liner.

The test results confirmed the information compiled for Inconel X-750 (STA) and indicated the adequacy of the properties used for liner design.

2. S-HTS Glass Roving

The 20-end S-HTS glass roving employed was tested to ensure conformance with the procurement specification. The average strand strength was 466,570 psi (standard deviation of 22,940 psi), compared with a specified minimum tensile strength of 400,000 psi. The roving weight was 0.6019 g/yard, compared with specified limits of 0.5600 (minimum) to 0.6480 (maximum) g/yard.

F. COMMENTS ON FABRICATED TANKS

1. Metal Shells

Twenty-three 18-in.-dia, 14-in.-long, oblate-spheroid, Inconel X-750 shells were fabricated to obtain the 20 needed for the program. Two of them were damaged beyond repair when the automatic welder malfunctioned, and Table 5 summarizes the characteristics of the remaining 21, including average wall thicknesses, weights, volumes, remarks on fabrication deviations, and test assignments.

Fourteen of the shells (Serial Nos. 2 through 12, 19, 20, and 22) conformed to all design-drawing and fabrication-specification requirements.

Three (Serial Nos. 13, 15, and 21) conformed to all design requirements except that the girth-weld-joint mismatch exceeded the objective of a 0.004-in. maximum. This excessive mismatch (0.007-in. maximum) was a local condition extending over 1 to 4 in. of circumference. One shell (Serial No. 17) had a local 0.007-in. girth-weld-joint mismatch and a single

*One for elastic modulus and one for plastic modulus.

0.015-in.-dia spherical pore in the weld.* These four shells were approved for use in the test program, with the stipulation that the vessel with the 0.015-in.-dia weld pore be used for -320°F burst or creep testing.

Two other shells (Serial Nos. 14 and 16) had more serious weld-joint mismatches. Their worst conditions were 0.010 and 0.014-in. mismatches, respectively. They were assigned to the -320°F burst tests.

The twenty-first shell (Serial No. 23, 0.018-in. mismatch) was not required for the contractual test program. It was subsequently used to evaluate cryogenic-temperature-measurement instrumentation, and was burst-tested at -320°F.

Average dimensional, weight, and volume characteristics are summarized and compared with design values in Table 6.

The design wall thickness for the 18-in.-dia liner was 0.047 in., +0.010 and -0.000 in. The actual wall thicknesses were within tolerances and averaged 0.053 in., or 11.3% above the nominal 0.047-in. design value.

The design weight of the liner assembly based on the 0.047-in. thickness was 12.148 lb, not including bosses. The shells without bosses actually weighed an average of 13.123 lb, or an increase of 8%. The excess was the consequence of an average wall thickness greater than the nominal design value. The bosses averaged 1.500 lb each. The complete liner assemblies averaged 16.149 lb, compared with the 15.148-lb design value.

The original internal volumes averaged 2330 cu in., compared with a design value of 2370 cu in. (After proof testing, the average measured volume was 2374 cu in.)

2. GFR Metal Tanks

The 21 liner assemblies were overwrapped with resin-impregnated S-HTS glass-filament roving and were cured to produce GFR Inconel X-750 (STA) pressure vessels. Four of them are shown in Figure 46.

The tank design originally incorporated an epoxy-polyurethane adhesive layer (Narmco 7343/7139) between the liner and the filament overwrap, and a single local glass-filament reinforcement on each head. The changes described below were made after the first two tanks were fabricated and tested.

Problems were encountered in the curing** of the first two vessels fabricated (Serial Nos. 2 and 3). During the Tank 2 cure an oven malfunction caused the temperature to hold at 300°F for 15 hours rather than the scheduled 4 hours. Surveillance was intensified to eliminate recurrence.

---

*The fabrication specification permits scattered porosities no greater than 0.010 in. in diameter, if they are no closer than three diameters (or a 0.020-in. minimum) and there are no more than three pores per inch.

**The resin-cure schedule for the filament-wound composite and metal-shell-to-composite adhesive was 2 hours at 150°F and 4 hours at 300°F.

After Tank 3 was cured, the filament-wound composite appeared discolored. Examination after burst testing revealed that the adhesive layer between the liner and the FWC shell was uncured. Additionally, the adhesive coating (about 0.003 to 0.005 in. thick when applied to the liner) appeared to have migrated into the resin of the first of four overwrap layers; this portion was also uncured. It was concluded that the probable cause was improper mixing of the resin-adhesive constituents. Because the design criteria are not based on a bond between the two shells to keep the liner from buckling, it was decided to eliminate this adhesive layer to minimize potential fabrication problems. Instead, a thin coat of the FWC resin matrix was applied to the liner before overwinding. This procedure was used for all tanks fabricated after the first two.

The test results for the first two tanks indicated a need for additional liner reinforcement at the boss-to-head weld to reduce strains there. It was decided to incorporate another glass-filament reinforcement on each head (for a total of two). This was done for all tanks fabricated after the first two.

Characteristics of the 21 tanks are summarized in Table 5, which includes wall thicknesses, weights, resin contents, volumes, and remarks on fabrication deviations.

The average dimensional, weight, and volume characteristics of the 20 tanks used in the contractual test program are summarized in Table 6. The average FWC thickness of 0.028 in. and equivalent filament thickness of 0.020 in. at the equator of the vessels were within 0.002 in. of the design values. The 72-vol% filament content in the composite was greater than the 67.3% expected and is attributed to the vacuum-bag cure used to consolidate the structure and remove excess resin. The FWC weight of 2.974 lb was slightly below the 3.041-lb design value, primarily because of the low resin content. The average tank weight of 19.525 lb was greater than the 18.630-lb design value because the 0.053-in. liner-wall thickness was greater than the 0.047-in. design value.

3. Assignment of Vessels for Testing

Detailed review and evaluation of fabrication records, and of the relative severity of the tests planned, led to the assignment of vessels for testing as shown in Table 5.

VI. TASK III - TEST PROGRAM FOR STRUCTURAL EVALUATION OF PRESSURE VESSELS

A. TEST PLAN, FACILITY, AND INSTRUMENTATION

1. Test Plan

Tests were conducted in conformance with a NASA-approved test plan, which defined the test facility and the methods for vessel instrumentation and pressurization. Structural evaluations of the 20 18-in.-dia GFR Inconel X-750 (STA) tanks were made in the following burst, fatigue-plus-burst, and creep-plus-burst tests:

Type of Test	No. of Test Vessels		
	At 75°F	At -320°F	At -423°F
Pressurization to the burst point	3	3	2
100 pressure cycles to the operating pressure, followed by pressurization to the burst point	2	2	2
72 hours of sustained pressurization at the operating pressure, followed by pressurization to the burst point	2	2	2
Total	7	7	6

In addition, a test was conducted at -320°F to determine the temperature gradients across the wall during cyclic pressurization and pressurization to burst, and to evaluate cryogenic-temperature-measurement instrumentation for FWC pressure vessels.

The serial numbers of tanks assigned the various tests are shown in Table 5. Vessels were pressurized at rates producing approximately 1% strain/min (1200 psi/min at 75°F and 1700 psi/min at -320 and -423°F).

a. Proof Tests

It was planned to proof-test all the tanks to 2220 psig at room temperature to establish the proper preload between the inner and outer shells. These tests were conducted by increasing the pressure to 2220 psig, holding it for 1 min, and then returning it to zero. All vessels tested at room temperature as well as the initial units tested at cryogenic temperatures were proof-tested, but this procedure was deleted in most of the cryogenic testing for reasons discussed below.

b. Burst Tests

Burst tests were conducted by increasing the internal pressure until failure occurred.

c. Fatigue-Plus-Burst Tests

Fatigue tests were conducted by increasing the internal pressure to the design operating value and then reducing it to zero (for room-temperature tests) or to about 100 psi (for cryogenic tests). This was repeated for 100 cycles, after which the vessels were pressurized to the burst point.

d. Creep-Plus-Burst Tests

Creep tests were conducted by increasing the internal pressure to the design operating value and holding it for 72 hours, after which the vessels were pressurized to the burst point.

2. Facility for Cryogenic Tests

The facility used is shown schematically in Figure 47. The vessels were pressurized with inhibited water for room-temperature tests, with liquid nitrogen (LN_2) for -320°F tests, and with liquid hydrogen (LH_2) for -423°F tests. For the cryogenic tests, gas-controlled valves were used to regulate the pressurization rate. The cryogenic-test fixture (Figure 48) consisted of a vacuum chamber with provisions for instrument leads and vacuum-jacketed pressurization lines.

For the cryogenic testing, vessels were installed in the vacuum chamber, which was pumped down to 10 mm Hg to assure the required temperatures. The tank temperatures were maintained as low as possible, and thermal equilibrium was obtained before the tests were initiated. When LN_2 was used, thermal equilibrium was defined as a vessel flange or skin temperature of -300°F or less, and attainment of -310°F or below at the vessel-outlet vent line. For LH_2 tests, it was defined as -405°F or less as measured at the vessel-outlet line, with flange and skin temperatures of -400°F or less.

For most of these tests, a cryogenically cooled shroud covered with layers of low-emissivity aluminum foil was installed over the tank to reduce heat inputs due to radiation and residual gas conduction. Glass marbles were used inside the LH_2-test tanks to reduce the quantity of hydrogen needed.

3. Instrumentation

Instruments were used to monitor the specimen temperature (for cryogenic tests), longitudinal and circumferential strain, and internal pressure throughout the pressurization cycle. Figure 49 shows the strain-instrument locations.

Temperature was monitored with copper-constantan thermocouples in the -320°F tests. Because thermocouple accuracy was questionable below -320°F, platinum resistance-thermometers were used for the -423°F tests. Two temperature measurements were made on the tank exterior (90° apart circumferentially) near the equator. In addition, the temperatures of the cryogenic fluids inside and outside the tank were measured and recorded.

Strain measurements were obtained with Aerojet-developed "bow-tie" extensometers. This device consists of a piece of beryllium-copper sheet in a configuration that provides two cantilever beams, which are fitted with bonded strain gages. Metal-foil strip, approximately 0.25 in. wide, was used to link the beam ends to the gage ends. Both the extensometer and the foil strip were positioned against the test-vessel surface.

For girth (hoop) measurements, the thin metal strip was placed around the tank equator and secured to opposite ends of the beam; circumferential deflection resulted in a proportional output of the gages on the bow-tie cantilever beams. For longitudinal-deflection measurements, metal strips were affixed to terminals wound into the tank near the polar bosses and run along the heads longitudinally toward the equator; the cantilever-beam ends of the bow tie were connected to the ends of the strips at the midsection of the tank. A longitudinal deflection produced a proportional strain-gage output. Figure 50 shows one girth and two longitudinal bow-tie extensometers installed on a GFR Inconel X-750 tank.

The accuracy of the extensometer strain gages depends on the gage factor, which is extremely sensitive to cryogenic-temperature variations. To provide the required accuracy, the concept of controlled-temperature strain transduction was employed: Heaters were provided to maintain the gages at temperatures within their compensation range and a sensor was added to record the vessel-surface temperature in the vicinity of the extensometer. This sensor was used to verify that the heat input to the bow tie did not warm the tank surface in the region of the transducer. Thermal insulation was used under the heated extensometers to minimize heat transfer to the vessel. Data taken during the tests showed that no significant vessel warming was produced by the heated bow ties.

Each extensometer was calibrated before testing, as described in Appendix G. The bow ties were installed on the vessel and calibrated end-to-end under ambient conditions. The gage factors did not vary under cryogenic conditions because heaters at the gage locations kept their temperature at essentially the ambient value; monitoring during cryogenic testing revealed that the bow ties were usually maintained at 70 $\pm 20^{\circ}$F. Because the strain reading varies only 1% per 100°F change in the 70°F range due to gage-factor variation, there was negligible loss in accuracy due to temperature effects.

To calibrate for longitudinal displacements, the distance between the bow-tie attachment points or terminals (L_1) was measured with an engineering scale. The bow tie and its metal-strip extensions were then stretched to the maximum expected deflection, using accurately determined positions (ΔL_1). The strain was calculated as $\Delta L_1/L_1$ to indicate the total between the two attachment points. To calibrate the girth extensometer, the tank circumference (L_2) was measured and the bow-tie attachment band was moved to produce the maximum expected deflection (ΔL_2). The girth strain was calculated as $\Delta L_2/L_2$. Calibration was done under ambient conditions, and a zero shift occurred due to thermal contraction when the tank was cooled to cryogenic temperatures. However, because the bow-tie repeatibility under ambient conditions was essentially linear and the heaters maintained ambient temperatures, it was only necessary to reset the recorder to zero to correct for thermal contraction.

B. TEST RESULTS

The test results at 75, -320, and -423°F are individually discussed in this section and summarized in Table 7.

1. Room-Temperature Tests (75°F)

Ambient-temperature proof, fatigue, creep, and burst tests were conducted on seven vessels. The vessels were designed for a 2000-psig operating pressure, a 2220-psig proof pressure, and a 3010-psig burst pressure at ambient temperature. All tanks were subjected to the 2220-psig proof test at 75°F before the fatigue, creep, and/or burst tests. Prior to testing. all were instrumented with one girth and two longitudinal extensometers as shown in Figure 49.

a. Proof and Burst Tests

Proof and burst tests were conducted on three vessels. All passed the proof test. The average burst pressure was 2990 psig, 0.67% less than the nominal design p_b; the minimum and maximum were within 4.30% of the average. Continuous strain-vs-pressure records were obtained, and the tests are discussed below.

(1) Serial No. 2

Tank 2 was taken to the proof pressure at a 1% strain rate, was held there for 1 min, and was depressurized and inspected. Only minor FWC crazing had occurred. FWC delamination from the metal shell was noted in the region of the polar boss, extending no more than 1 in. past the edge of the head reinforcement.

The tank was hydrostatically pressurized to the burst point (2960 psig). Failure occurred in the liner at the boss-to-head weld. When the internal pressure dropped to zero, due to water leakage through the fracture, both liner heads buckled under compressive forces produced by the filament shell (see Figure 51).

The hoop- and longitudinal-strain data obtained (at locations shown in Figure 49) were excellent (see Figure 52). At the burst, the maximum stress in the liner was 134,000 psi and in the filament shell was 313,000 psi. The strains at burst were about 2.40% in the longitudinal direction and 1.98% in the hoop direction.

No weld-joint defects were shown in X-rays of the boss-to-head welds made before the test. Radiographic inspection of the tank after testing revealed no degradation of the girth weld or the boss-to-head welds other than at the fracture site, but buckling in the region of the boss-to-head welds at both ends prevented satisfactory X-ray resolution.

A metallurgical analysis of the fracture area was conducted (Appendix H). The conclusions were as follows:

(a) Fracture occurred at the interface between the heat-affected zone of the formed head and the weld nugget joining the head to the boss.

(b) The grains in the Y-shaped nugget were relatively coarse and had directional orientation. The narrow heat-affected zone had coarser grains than the parent metal away from the weld.

(c) No defects were found in the undamaged portion of the fracture surface. The possibility of localized weld undercut could not be evaluated because of plastic deformation and necking.

(d) The probable cause of failure was an abrupt change in microstructure at the interface between the parent-metal heat-affected zone and the weld.

To investigate the Tank 2 failure mode, the other two tanks in this series were instrumented with hoop and longitudinal strain gages in the vicinity of a polar boss.

(2) Serial No. 3

Before testing, three hoop and three longitudinal strain gages were mounted in the vicinity of one polar boss on Tank 3, in addition to the hoop and longitudinal extensometers used for all tests. The locations and orientations are shown in Figure 53.

Pressure was increased until FWC failure occurred (at 2940 psig) adjacent to a polar boss (Figure 54). The metal shell did not fracture; it plastically deformed at filament failure, and reduced the water pressure in the tank to 800 psig. The maximum burst-pressure stresses were 134,100 psi for the liner and 317,200 psi for the filaments.

As reported in Section V,F,2, examination revealed that the adhesive layer between the two shells was not cured and had migrated into the inner one-fourth of the overwrap, which was also uncured.

Excellent hoop- and longitudinal-strain data were obtained (Figure 55). The strains at burst were about 2.18 and 2.70%, respectively. Data from gages in the vicinity of the polar boss (as shown in Figure 53) are presented in Figures 56 and 57. These strains were greater than expected, both in tension and compression, and increased up the head as the boss was approached. As an example, filament strains adjacent to the polar boss were 1.10% at the proof pressure, -0.24% at 0 psig after proofing, and 2.20% at the 2940-psig burst pressure. The high tensile strain at the proof pressure and the high compressive strain after proofing indicate that the plastic deformation and springback were greater than predicted by the design analysis.

The high strains recorded in the boss region led to a decision to incorporate an additional reinforcement on each head (for a

total of two) to reduce strains at the boss. All tanks were subsequently fabricated with the additional reinforcements.

Radiographic inspection of the liner after testing showed that a small crack had propagated from a 0.008-in.-dia porosity in the girth weld. No other weld-joint degradation was found.

(3) Serial No. 5

Tank 5 passed the proof test with a small amount of FWC crazing and no apparent delamination between the two shells.

After depressurization, the vessel was taken to a burst pressure of 3070 psig. A very energetic FWC failure occurred adjacent to the polar boss and caused all filaments to separate from the liner (see Figure 58). The liner did not fracture or leak under a pressure of several hundred psig. The burst-pressure stresses were 136,000 psi for the liner and 322,500 psi for the filaments.

Excellent hoop- and longitudinal-strain data were again obtained (Figure 59). Significantly greater hoop strains at the proof pressure were noted as compared with the Tank 2 and 3 data. The burst-pressure strains were about 2.80% (longitudinal) and 2.92% (hoop).

High strains were again recorded in the FWC gages adjacent to the polar boss (Figures 60 and 61). Filament strains immediately beside the polar boss were 1.00% at the proof pressure, -0.40% at 0 psig after proofing, and 3.48% at the burst. The polar-boss region sustained much greater tensile and compressive springback strains than predicted by the design analysis. On the basis of Tank 3 and 5 data, it was concluded that the local head reinforcements (one set in Tank 3 and two sets in Tank 5) were not reducing plastic deformation around the boss.

b. Proof, Fatigue, and Burst Tests

Ambient-temperature fatigue tests were conducted on two vessels by proofing at 2220 psig, cyclically applying the 2000-psig operating pressure (p_o), and pressurizing to the burst point if the tank achieved 100 p_o cycles.

Both tanks passed the proof test. One sustained 100 cycles between zero and p_o and then was burst-tested to 2910 psig (97% of the average original burst strength). The other failed after approximately 50 p_o cycles in a compressive-buckling mode when the internal pressure was reduced to zero. Strain-vs-pressure records were obtained for the proof test; for pressure cycles 1, 2, 3, 4, 5, 10, 20, 30, 40, 50, 60, 70, 80, 90, and 100; and for the burst test.

(1) Serial No. 7

After successful proofing and depressurization for inspection, Tank 7 was pressure-cycled between 0 and 2000 psig 100 times.

Inspection revealed no visible degradation. Slight FWC crazing was found after proofing, but its magnitude did not seem to have increased after cycling.

The tank was pressurized to failure (at 2910 psig, or 97% of the average original vessel strength), which occurred in the FWC shell next to the boss (Figure 62). Apparently as a result, the liner developed two longitudinal splits joined by a hoopwise fracture along the heat-affected zone of one boss-to-head weld. Hoop- and longitudinal-strain data for the proof and burst phases are shown in Figure 63, and for the 1st, 50th, and 100th pressure cycle in Figure 64. The pressure-cycling hysteresis loops were small, as was the permanent set.

The burst-pressure stresses were 133,700 psi for the liner and 309,500 psi for the filaments.

(2) Serial No. 8

Tank 8 was proofed, depressurized, and pressure-cycled between 0 and 2000 psig. Leakage around a polar boss was noted after 50 cycles, and the tank was depressurized and inspected. The head had buckled as shown in Figure 65. The tank interior revealed a fracture line extending approximately 3 in. along the boss-to-head weld. It is believed that the head buckled under external FWC forces during fatigue-test depressurization, after which the application of a few pressure cycles fatigued and fractured the metal at the weld joint.

The other head was unchanged at the end of the test but buckled within the next 2 days. Pressure-vs-strain data for the proof test are presented in Figure 66, and for the 1st and 50th pressure cycles in Figure 67. The pressure-cycling hysteresis loops were small.

c. Proof, Creep, and Burst Tests

Ambient-temperature creep tests were conducted on two vessels, by proofing at 2220 psig, holding them at p_o = 2000 psig for 3 days (72 hours), and then pressurizing to the burst point.

Both passed the proof and sustained-pressurization tests. One achieved a p_b of 3000 psig (100% of the original average strength). The other had a p_b of 2630 psig (88% of the original average strength); during the test, however, the pressure was held for 1 min at 2400 psig (80% of the original average strength) because of incorrect pressurizing-system operation, which may have contributed to the relatively low p_b. Pressure-strain data were obtained for the proof tests, for the creep tests at 4-hour intervals, and for the burst tests.

(1) Serial No. 4

After proofing and depressurization, Tank 4 was held at p_o for 72 hours. Inspection showed no visible degradation, and the burst test was initiated. The vessel was loaded to 2400 psig, the test

engineer found he could not increase the pressure, and the tank was held at that level for 1 min before the test could proceed. Failure occurred at 2630 psig (88% of the original strength) in the form of a fracture at the boss-to-head weld. Both heads buckled after internal pressure was lost (see Figure 68).

Pressure-vs-strain data are presented in Figure 69 for the proof and burst phases, and in Figure 70 for the creep test (whose start and end transients are shown in Figure 71). Negligible creep was detected during sustained loading.

(2) Serial No. 6

Tank 6 was proofed, depressurized, creep-tested for 72 hours, and burst-tested at 3000 psig (100% of the original average strength). FWC failure occurred adjacent to the polar boss. As in the case of Tank 7, the liner had two longitudinal splits joined by a hoopwise fracture along the heat-affected zone of a boss-to-head weld. A post-test view is shown in Figure 72.

The pressure-strain data were excellent. Hoop- and longitudinal-strain data are presented in Figure 73 for the proof and burst phases, and in Figure 74 for the creep test (whose start and end transients are shown in Figure 75). Negligible creep occurred during sustained pressurization. The burst-pressure stresses were 137,800 psi for the liner and 331,700 psi for the filaments. Longitudinal strains of 2.59% and hoop strains of 2.49% were obtained at the burst.

2. LN_2 Tests (-320°F)

Liquid-nitrogen fatigue, creep, and burst tests were conducted on seven vessels. The proof pressure at 75°F was established as 2220 psig and the operating pressure at -320°F as 2300 psi. Prior to cryogenic testing, the tanks were to be proofed at ambient temperature. All the vessels were instrumented with one girth and two longitudinal extensometers, as well as copper-constantan thermocouples on the exterior (Figure 49).

a. Ambient-Temperature Proofing

Tank 16 was the first to be proof-tested. There was concern over the possibility of buckling after proofing (due to high FWC compressive stresses) and the tank was examined periodically; no buckling occurred.

Tank 14 was then proofed; on depressurization one liner head buckled (but the metal did not fracture). The other head buckled by the next day. After discussion with the NASA Project Manager, it was decided to reduce the proof pressure to 2000 psig to decrease the liner-springback stresses. Tank 11 was then proofed at 2000 psig, and one head buckled on depressurization (to a less severe degree than Tank 14). Additional discussions with NASA resulted in a decision not to proof-test the remaining tanks and to

amend procedures so that, if liner yielding occurred in subsequent testing, the internal pressure level would not be reduced below 100 psi (which would stabilize the liner and give it no opportunity to buckle).

b. Burst Tests

Three tanks were LN_2 burst-tested. All had girth-weld-joint mismatches in excess of the specified 0.004 in. (see Table 5). The average p_b was 3544 psi, 18% higher than the ambient-temperature p_b. The minimum and maximum p_b values varied 7% from the average.

(1) Serial No. 13

Tank 13 was assembled in the vacuum chamber and filled with LN_2. After steady-state conditions were attained, it was taken to a p_b of 3588 psi. The failure appeared to originate in the FWC shell at the polar boss, with subsequent liner fracture. The 0.007-in. weld mismatch noted after fabrication did not appear to contribute to the failure. A post-test view is shown in Figure 76. Excellent hoop- and longitudinal-strain data were obtained (Figure 77), and the strains at failure were in excess of 4%. The burst-pressure stresses were 162,500 psi for the liner and 384,200 psi for the filaments.

(2) Serial No. 14

Both heads of Tank 14 had buckled after proofing at 2220 psig. The tank was filled, cooled with LN_2, and taken to a p_b of 3400 psi.

Both shells failed, apparently as a result of liner girth-weld failure, which in turn was probably caused by the excessive mismatch of 0.014 in. noted after fabrication. This was the only vessel in which failure appeared to originate in the girth weld; a post-test view is shown in Figure 78.

The burst-pressure stresses were 157,800 psi for the liner and 357,400 psi for the filaments.

(3) Serial No. 16

Tank 16 had been proofed (2220 psi) and depressurized without buckling. It was then taken to a p_b of 3645 psi. As for Tank 13, the failure appeared to have originated in the FWC shell at the polar boss; the liner was broken into several pieces, as shown in Figure 79. The weld mismatch of 0.010 in. did not influence the test results.

Excellent hoop- and longitudinal-strain data were obtained (Figure 80). Because they do not include the initial proofing data, they appear to indicate a higher yield strength and reduced strain at fracture as compared with Tank 13. Data for other tanks indicate that the permanent set after the proof test amounted to about 0.2% in hoop strain

and 0.6% in longitudinal strain; when these values are added to the strain data in Figure 80 to get the approximate total vessel strain at failure, the indicated ultimate strains are 4.55% (hoop) and 3.90% (longitudinal). These values are comparable to the results obtained in the Tank 13 burst test. The burst-pressure stresses were 163,700 psi for the liner and 391,100 psi for the filaments.

c. Fatigue-Plus-Burst Tests

Fatigue tests were conducted on two vessels by cyclically applying a 2300-psi p_o 100 times, and then pressurizing to the burst point. Both tanks sustained 100 cycles; one subsequently failed at 3169 psi in the boss-to-head weld and the other at 3554 psi (100% of the original average strength) in the membrane structure.

(1) Serial No. 20

On the first pressure cycle, Tank 20 was inadvertently overpressurized to 2555 psi rather than 2300 psi. It was then successfully cycled to 2300 psi 100 times, followed by pressurization to failure at 3169 psi. A liner leak developed in one boss-to-head-weld area; the pressure was maintained at 3100 psi and LN_2 flowed profusely through the FWC shell in the vicinity of the liner fracture. The tank pressure was relieved, and both liner heads buckled as shown in Figure 81.

Hoop- and longitudinal-strain data for the first pressure cycle and the burst test are shown in Figure 82, and for the 2nd, 50th, and 100th cycles in Figure 83. There was negligible permanent set due to pressure cycling. The hysteresis loops were larger than noted in room-temperature tests.

(2) Serial No. 21

Tank 21 underwent three fill, cooldown, and warmup cycles before testing. After the fourth cooldown, it was successfully subjected to 100 p_o cycles. It was then taken to a p_b of 3554 psi (identical to the average original single-cycle -320°F burst strength). The failure was very energetic; both shells were blown into many pieces (some shown in Figure 84). The 0.007-in. girth-weld mismatch (Table 5) did not appear to contribute to the failure.

Strain-vs-pressure data for the first cycle and the burst test are presented in Figure 85. A longitudinal strain of 3.86% and a high hoop strain of 5.00% were obtained at the burst point. Pressure-strain curves for the 2nd, 50th, and 100th pressure cycles are given in Figure 86; the results are similar to those for Tank 20.

The burst-pressure stresses were 162,700 psi for the liner and 385,500 psi for the filaments.

d. Creep-Plus-Burst-Tests

Creep tests were conducted on two vessels that had 0.007-in. weld-joint mismatches; this condition did not affect the test results, nor did a 0.015-in.-dia spherical porosity noted in one of the girth welds. The testing consisted of sustained pressurization at 2300 psi for 72 hours followed by pressurization to failure. Both tanks passed the sustained-loading tests; they achieved p_b values of 3538 and 3797 psi - i.e., within 7% of each other and higher than those attained in single-cycle burst tests.

(1) Serial No. 15

Tank 15 was maintained at the operating pressure for 72 hours, and was then taken to a p_b of 3797 psi, the highest obtained in the program. Failure occurred at the polar-boss region in both shells (see Figure 87). Pressure-vs-strain data are shown in Figure 88 for the initial pressurization to p_o and for the burst test after sustained loading. Pressure and strain fluctuations during the creep-test loading are shown in Figure 89. Although the recorded data did not indicate overpressurization, Figure 88 indicates that an increase in vessel yield to about 2500 psi occurred during sustained loading.

The burst-pressure strains were 3.68 and 4.44% in the longitudinal and hoop directions, respectively. The burst-pressure stresses were 172,600 psi for the liner and 423,800 psi for the filaments.

(2) Serial No. 17

After creep testing, Tank 17 was taken to a p_b of 3538 psi. FWC failure occurred near the polar boss, causing subsequent liner fracture (see Figure 90).

Pressure-strain data shown in Figures 91 and 92 indicate that creep apparently occurred. The burst-pressure strains were about 3.70% (longitudinal) and 4.50% (hoop), which were very similar to those for Tank 15. The burst-pressure stresses were 161,800 psi for the liner and 380,700 psi for the filaments.

3. LH_2 Tests (-423°F)

Liquid-hydrogen fatigue, creep, and burst tests were conducted on six vessels. The design p_o at -423°F was 2350 psi. All vessels were instrumented with one girth and two longitudinal extensometers, plus platinum resistance-thermometers bonded to the outer surface.

a. Burst Tests

Single-cycle, LH_2 burst tests were conducted on two vessels. One failed at 3185 psi in the boss-to-head weld of the liner and the other failed at 3685 psi in the filament-wound composite.

(1) Serial No. 11

Tank 11 had been proof-tested at 2000 psig at ambient temperature, after which one head buckled (see paragraph VI,B,2,a, foregoing). It was assembled in the vacuum chamber, was filled with LH_2 and cooled down, and was then taken to a p_b of 3185 psi. Failure apparently occurred in the liner at the boss weld of the head that had not previously buckled. Both heads buckled after the burst. A post-test view is shown in Figure 93.

The hoop- and longitudinal-strain data presented in Figure 94 do not include data for the 2000-psi proofing, which raised the yield pressure. If a permanent set of 0.2%-hoop and 0.6%-longitudinal strain is assumed for the proof test and these values are used in Figure 94, the failure strains would be 3.0% (hoop) and 2.8% (longitudinal).

(2) Serial No. 19

After cooldown, Tank 19 was taken to a p_b of 3685 psi. The failure apparently occurred in the filament shell, which was blown to pieces. The liner was broken into several portions, as shown in Figure 95.

Very good pressure-vs-strain data were obtained (Figure 96). The burst-pressure longitudinal strain was 3.75%, hoop strain 4.22%, liner stress 167,600 psi, and filament stress 390,100 psi.

b. Fatigue-Plus-Burst Tests

Fatigue tests were conducted on two vessels through the application of a 2350-psi p_o for 100 cycles, followed by pressurization to the burst point. Both vessels passed the LH_2 cycling test. One tank had a p_b of only 2535 psi while the other burst at 3700 psi, the highest value in the LH_2 tests.

(1) Serial No. 9

After cooling, Tank 9 was successfully subjected to 100 p_o cycles and was taken to a p_b of 2535 psi. Failure apparently originated in the liner at the boss-to-head weld; the filament shell was severely damaged (see Figure 97).

Figure 98 gives longitudinal- and hoop-strain data for the initial pressurization and the burst phase, and Figure 99 provides pressure-strain data for the 2nd, 50th, and 100th cycles. The pressure-cycling hysteresis loops were small, and only negligible permanent set was found.

(2) Serial No. 10

Tank 10 also passed the 100-cycle test and was then taken to a p_b of 3700 psia. Failure occurred in the filament shell, and the liner was severely fractured (see Figure 100).

Figure 101 gives strain-vs-pressure data for the initial pressure cycle and the burst phase, when a longitudinal strain of 4.10% and a hoop strain of 4.76% were obtained. The burst-pressure stresses were 168,400 psi for the liner and 395,100 psi for the filaments. Figure 102 provides pressure-strain curves for the 2nd, 50th, and 100th cycles.

c. Creep-Plus-Burst Tests

Creep tests were conducted on two vessels, which survived sustained pressurization at 2350 psi for 72 hours, and then achieved burst pressures of 3615 and 3700 psi - values within 2.5% of each other and higher than the average in the LH_2 single-cycle burst tests.

(1) Serial No. 12

After cooldown, Tank 12 was taken to the design p_o and held there for 72 hours (except for a short depressurization to approximately 500 psi after 12 and 36 hours to permit recharging of the liquid- and gaseous-hydrogen trailers). It was then taken to a p_b of 3700 psia. Failure apparently originated at the polar boss in the filament shell, which was blown to pieces. The metal shell was broken into a few portions, as shown in Figure 103.

Figures 104 and 105 present pressure-vs-strain data; overpressurization to 2450 psi caused additional plastic deformation, as indicated there. The burst-pressure strains were about 3.6% (longitudinal) and 3.5% (hoop). The failure stresses were 168,000 psi in the liner and 382,600 psi in the filaments.

(2) Serial No. 22

Tank 22 was also successfully creep-tested. After about 22 hours of sustained loading, the pressure was inadvertently increased to 2600 psia and caused considerable plastic deformation of the liner and permanent set in the tank. The pressure was reduced to 2350 psia, and the test was continued (except for a short depressurization to approximately 500 psi after 24 and 48 hours) until the loading period totaled 72 hours. The tank was then taken to a p_b of 3615 psia. Again, failure apparently originated in the filament shell, which was severely damaged. The metal shell was also blown into several pieces, as shown in Figure 106.

Figures 107 and 108 give the pressure-vs-strain data. The burst-pressure strains were 3.62% (longitudinal) and 3.80% (hoop). The failure stresses were 166,200 psi in the liner and 382,400 psi in the filaments.

4. Wall-Temperature-Gradient Tests

A considerable increase in measured cryogenic temperatures on the outer skin of the composite was encountered during pressurization to the p_o value (in fatigue and creep tests) and to the burst pressure. The instruments used were platinum resistance-thermometers for the LH_2 and LN_2

tests, with copper-constantan thermocouples added for the LN_2 tests. They were bonded to the tank exterior after fabrication.

When the problems were encountered, it was believed that measurement inaccuracy was being caused by unbonding of the instruments as the vessels were pressurized to high strain levels. This was verified in a special -320°F test conducted on an 18-in.-dia GFR Inconel X-750 tank that had been fabricated with both types of instrument wrapped against the liner and into the FWC shell.

The objectives of this LN_2 evaluation were (a) to investigate installation techniques and the reliability of placement within the FWC wall, and (b) to measure actual temperatures on the liner, at various distances from the liner in the FWC wall, and on the outer surface of the FWC wall.

a. Procedure

Platinum resistance-thermometers and copper-constantan thermometers were installed on the test vessel (Serial No. E-1) in the positions depicted in Figure 109. The liner was a rejected part having a girth-weld-joint mismatch of 0.018 in. The following tests were performed, with all temperatures recorded continuously:

(1) Two pressure cycles were conducted in which the tank was pressurized to 1800 psi and was vented to zero at approximately 1700 psi/min. Initial LN_2 equilibrium-temperature conditions were obtained before the first pressure cycle, and an LN_2-cooled shroud was used over the vessel during the test.

(2) Three additional pressure cycles identical to the foregoing were performed, except that the LN_2-cooled shroud was not used.

(3) A final test was performed, without the shroud, in which the vessel was pressurized to failure.

b. Results

Two platinum resistance-thermometers (T-E and T-D) did not function during testing; the sensing elements shorted to the liner. The T-3 copper-constantan thermocouple apparently partially open-circuited, and its data were inaccurate.

Figure 110 shows the transient-temperature data from the other instruments plotted against pressure for the first cycle of Test (1). Similar data plotted for Tests (2) and (3) are shown in Figures 111 and 112, respectively. Failure during Test (3) occurred at 3232 psi, and a post-test view is shown in Figure 113.

The plot for the tank exterior shows progressively higher values for the initial temperature measurements in the three cycles of Test (2) and in Test (3). External instrument-wall bond degradation was

found that apparently was caused by thermal cycling and pressure cycling and gave rise to invalid readings. All other thermometers, however, indicated only a slight increase in temperature during test-cycle pressurization, as shown by their plots.

c. Conclusions

This investigation verified that the vessels tested in the tank-evaluation program were essentially at the nominal cryogenic temperature required. It demonstrated also that thermometers can be practically and reliably placed within the glass-FWC wall to provide accurate readings at cryogenic temperatures.

VII. EVALUATION OF STRENGTH AND PERFORMANCE LEVELS, PRESSURE-STRAIN CHARACTERISTICS, AND PARAMETRIC-STUDY FINDINGS

A. STRENGTH AND PERFORMANCE LEVELS

GFR Inconel X-750 (STA) tanks successfully sustained burst, fatigue, and creep tests at 75 to -423°F. The test results are compared on the basis of the pressure-vessel performance factor (p_bV/W) in Figure 114 and on the basis of glass-filament stress at the burst pressure in Figure 115. The results are evaluated below, following an analysis of modes of failure.

1. Failure Modes

The apparent failure modes, summarized in Table 8, include glass-FWC failures near the polar boss, liner fractures at the boss-to-head weld, a liner fracture at the girth weld, and a liner failure in compressive buckling during fatigue testing.

There are important implications in the fact that 18 of 20 vessels failed during burst testing near the polar bosses. The boss area was the most highly strained portion (see paragraphs VI,B,1,a,(2) and (3), and Figures 56, 57, 60, and 61) and also the most sensitive to fabrication imperfections because local head reinforcements were incorporated there.

Five of the 18 failed in the liner at the boss-to-head weld. Of these, Tank 11 underwent head buckling after an ambient-temperature proof test, Tank 20 experienced overpressurization and excessive plastic deformation on the first of 100 pressure cycles during fatigue testing, and Tank 4 was taken to a high stress level that was held for about 1 min before pressurization was continued to the burst point. It is believed that these factors, coupled with strain magnification in the liner at the boss-to-head weld due to head-reinforcement ineffectiveness and high polar-boss rigidity, precipitated liner failures at that weld. This subject is discussed further in Section VII,C, below.

The remaining 13 boss-area failures occurred in the FWC shell at rather consistent filament-stress levels (see Figure 115). The local high FWC strains at the boss (see Figures 56, 57, 60 and 61) indicate a stress concentration that restricted potential FWC performance; if this is the case, higher ultimate-glass-filament-strength levels than indicated in Figure 115 may be obtainable over the 75 to -423°F range.

One vessel, Tank 14, failed in the liner at the girth weld. This premature failure was attributed to an excessive weld-joint mismatch of 0.014 in.

Tank 8, the only one that did not sustain the intended service-cycle testing, failed during pressure cycling by liner-head buckling. This was attributed to the ineffective head reinforcement, which had been designed to ensure that compressive stresses in the metal heads would not exceed the buckling strength. Strains measured during proof testing and depressurization to zero showed greater-than-expected values for (a) plasti-

deformation of the liner in the boss vicinity, and (b) compressive stresses in the liner at zero pressure after proofing.

2. Burst Tests

As shown in Figures 114 and 115, the p_b performance was consistent at each temperature for tanks not failing in the liner. Based on the p_bV/W factor, performance increased 22% at -320°F and 25% at -423°F over the room-temperature values. On the basis of ultimate-glass-filament-stress levels, performance increased 21% at -320°F and 23% at -423°F.

3. Cyclic-Fatigue-Plus-Burst Tests

A significant finding was that the tanks were able to sustain the 100-cycle fatigue test to the operating pressure at all temperatures, and then to develop high-burst-strength levels. Although one vessel tested at 75°F failed to achieve the 100 p_o cycles (due to compressive-buckling failure), all others passed this test. As shown in Figures 114 and 115, the p_b performance was very close to the single-cycle burst-strength levels, except for (a) one -320°F test vessel that failed prematurely in the liner during the burst-test phase (probably as a result of significant over-pressurization on the first fatigue-pressure cycle that set up a severe pre-load between the two shells), and (b) one -423°F test vessel that failed prematurely in the liner during the burst-test phase for reasons that could not be established. Data for vessels failing in the glass-FWC shell show that both the p_bV/W performance and ultimate glass-filament stresses increased 25% at -320°F and 27% at -423°F as compared with 75°F.

No significant difference between strength levels was found for vessels subjected to cyclic fatigue before burst testing and those pressurized directly to the burst point without fatigue cycling. This characteristic of the GFR Inconel X-750 (STA) tanks is attributed to the fact that the pressure cycling did not subject the filaments to a full zero-stress to operating-stress range (such as occurs in FWC tanks that have non-load-carrying liners), but instead represented a small stress (strain) amplitude superimposed on a much larger residual filament tensile stress at zero pressure after the liner was plastically deformed by the initial load.

The filament-stress conditions under cyclic fatigue are shown in Figures 19, 20, and 21. The longitudinal-glass-filament stresses at zero pressure after proofing amounted to about 140,000 to 150,000 psi, and at the operating pressure to about 200,000 to 220,000 psi. Thus, pressure cycling superimposed a cyclic stress of about 50,000 psi on the zero-pressure filament stress of 140,000 to 150,000 psi.

The strength degradation characteristic of glass-FWC vessels subjected repeatedly to large strain cycles thus does not apply to GFR metal tanks.

4. Sustained-Loading-Plus-Burst Tests

No degradation in vessel strength occurred as the result of 72-hour sustained pressurization at the p_o value over the entire temperature

range. As shown in Figures 114 and 115, the burst strengths after such pressurization were just as high as for tanks taken to the burst point without exposure to sustained loading. Based on the $p_b V/W$ rating factor, the performance increased 25% at -320°F and 23% at -423°F as compared with 75°F. The ultimate-glass-filament-strength levels were 21% higher at -320°F and 15% higher at -423°F.

5. Glass-Filament Strength Levels

Figure 116 shows the average values for and range in ultimate S-HTS glass-filament-strength levels obtained in all tests of 18-in.-dia GFR Inconel X-750 (STA) tanks in which filament failures occurred.

The average level at ambient conditions (75°F) was 320,200 psi, which is 97% of the 330,000 psi used for design and analysis. At -320°F, the average strength was 393,100 psi, or a 23% improvement over the 75°F value. At -423°F, the average strength was 387,600 psi, or 21% greater than the 75°F value.

The strengths demonstrated at cryogenic temperatures were 79% of the 495,000 psi previously estimated for design and analysis.

B. PRESSURE-STRAIN CHARACTERISTICS

This section compares predicted behavior (computer design analysis) and measured behavior with regard to stress-strain and pressure-strain characteristics of the GFR Inconel X-750 (STA) tank. (Paragraph IV,E,3 discusses these characteristics, and Section VI,B presents the test data.)

Figure 117 provides predicted and measured pressure-strain curves for a 75°F proof test to 2220 psig, depressurization to zero, and loading to a burst pressure of 2940 psig (Tank 3). Generally good correspondence was obtained. The analysis predicted that longitudinal strains would lead hoop strains until the design p_b of 3010 psi was approached, when they would approach each other until they reached identical values at the design p_b. The measured pressure-strain curve displayed this characteristic.

Yielding in the hoop direction occurred at a lower pressure than estimated, probably because the analysis assumed the metal stress-strain curve could be represented by two straight lines when in fact the curve bends as the liner yields. At the proof pressure, the vessel yielded in the hoop direction. On depressurization to zero from this point, the tank relaxed down an offset, biaxial, elastic, pressure-strain curve having the predicted slope. On repressurization, the hoop-strain curve almost exactly retraced the springback curve up to the offset-yield point, where additional plastic deformation occurred. As the vessel-yield point was exceeded, the measured hoop-strain curve rose to the predicted curve and followed it up to the burst point.

Yield in the longitudinal direction occurred at about the estimated pressure, and the predicted and measured pressure-strain curves up to the proof pressure were fairly close. The measured longitudinal strains were less than expected at the proof pressure. On depressurization

to zero from this point, the tank relaxed down an offset curve with the expected slope to about 400 psi, where excessive springback was noted. This springback could have been caused by (1) compressive liner yield, or (2) local high compression in the liner near the polar bosses that caused excessive inward deflection of the boss region, which in turn relaxed the longitudinal extensometers sufficiently to produce the readings indicated at zero pressure in Figure 117. The test-data review for Tank 3 in paragraph VI,B,1,a, (2) tends to support the latter interpretation. On repressurization, the longitudinal-strain curve paralleled the springback curve until the offset-yield pressure was reached; from there it essentially followed the predicted curve up to the burst point.

Computed ultimate vessel strains were compared with the measured values to evaluate the design analysis. Figure 118 shows this comparison, for all tanks tested at ambient conditions (75°F) that failed in the glass-FWC shell, as a plot of calculated ultimate filament stress vs calculated strains and measured strains. The calculated and measured values corresponded closely, indicating that the analysis and the ambient-temperature material properties used in analysis yielded results very close to the actual test measurements.

When the same comparison was made for -320 and -423°F test results, it was found that the correlation was not as close. The measured strains were greater than the computed strains. Possible explanations are that (1) the plastic modulus and yield strength of Inconel X-750 were not as well characterized at cryogenic temperatures as under ambient conditions, and (2) the FWC coefficient of thermal contraction, with the filaments oriented as in the GFR Inconel X-750 tanks, is not accurately known.

C. HEAD-REINFORCEMENT DESIGN AND BOSS-TO-METAL-SHELL TRANSITION

The test data revealed that the head reinforcements incorporated in the continuous windings of the FWC shell were not reducing strain there as expected. It is believed that a contributing factor was the difficulty, in fabrication, of positioning reinforcements tightly against the continuous windings and consequent failure of the reinforcements to take their design load until after some composite straining had occurred, and not at the beginning of pressurization. This would result in higher-than-design strains in the liner and higher compressive stresses at zero pressure after proofing. In future designs, it is concluded, the metal shell should be designed to fulfill the role assigned to the glass-filament head reinforcement in this program.

Several vessels failed in the liner at the boss-to-head weld. This can be attributed in part to head-reinforcement ineffectiveness, but another very important consideration is that of boss rigidity as compared with the extensibility of the filament-wound composite on top of the boss. In the membrane away from the boss, both shells strain uniformly; at the transition from the liner to the boss, however, the filaments remain essentially isotensoid (with their high strains), while rigidity does not permit the thick boss to strain with the filaments. This leads to a strain mismatch and relative movement between the boss and the overwrap. Localized strain magnification will occur in the transition area in order to maintain the overall strain compatibility.

Test-data analysis has shown that the length over which this strain magnification occurs is between 15 and 20 times the liner thickness. On the basis of this length and a typical boss, specific strain regions may be defined and a theoretical strain curve can be drawn (see Figure 119). The calculation of a strain-magnification value is based on the matching of filament- and metal-shell extensions (δ_f and δ_m, respectively), which requires that

$$\delta_m = \delta_f$$

where the filament extension is

$$\delta_f = \epsilon_f L$$

with

$$L = (D_w/2) + 20\ t_L$$

and the metal-shell extension is

$$\delta_m = \int_0^{R=L} \epsilon_m\ dR$$

where ϵ_m is some function of the radial distance (R) as shown in Figure 119, which defines the symbols.

Assuming that the strain magnification is constant and limited to the region of length 20 t_L, the metal-shell extension is

$$\delta_m = \epsilon_{m,max}\ (20\ t_L)$$

By combining equations, the strain magnification is found to be

$$\frac{\epsilon_{m,max}}{\epsilon_f} = 1 + \frac{D_w}{40\ t_L}$$

For the 18-in.-dia GFR Inconel X-750 (STA) tank,

$$t_L = 0.047 \text{ in.}$$

$$D_w = 3.602 \text{ in.}$$

and

$$\frac{\epsilon_{m,max}}{\epsilon_f} = 2.9$$

Based on this information, several general conclusions can be drawn: (1) The magnitude of the strain magnification is considerable and should not be neglected, (2) smaller bosses tend to reduce the magnitude of the strain magnification, and (3) thin liners amplify the strain magnification, which indicates that strain damping might be accomplished by a more gradual liner taper in future designs of GFR metal tanks.

For maximum compatibility with the high strains in the end domes, the metal boss should be designed to have low rigidity and be as small as possible (i.e., the liner should have the minimum possible dimensions that do not plastically deform to the same strains as the isotensoid filaments of the end domes). In practice, this would be accomplished by reducing the body of the boss to the smallest practical dimensions in width and thickness. By keeping the width small, the magnitude of the mismatch between FWC and boss deflections can be reduced and the strain absorbed by the liner membrane at the edge of the boss flange can be minimized. By keeping the thickness small, the boss flange can be blended into the liner membrane over a short distance to reduce the effective width of the boss.

D. PARAMETRIC-STUDY REPORT

An important objective of the test program was evaluation of the analytical methods and parametric investigation reported in Reference 1. Test data confirmed that the parametric-study methods, results, and conclusions were essentially valid. Modifications are noted below.

Figures 120 to 123 compare the parametric-study predictions with detailed-vessel-design values and the values measured in fabrication and testing. As shown in Figure 120, the liner D/T_L design ratio was the same as predicted and the measured value was lower because of fabrication tolerances. For the T_L/T_O ratio, shown in Figure 121, the detailed computer analysis gave a value close to but less than the parametric-study value (because the boss-diameter/vessel-diameter ratio was 0.20 for the parametric study and 0.15 for the fabricated 18-in.-dia tank), and the measured T_L/T_O was larger than the design value, due to fabrication tolerances. Similar comments apply to the performance-factor data shown in Figure 122. Figure 123 presents factor-of-safety data for the tanks. The safety factor predicted by the parametric study and design analysis was achieved at 75°F, but not at -320 and -423°F for reasons discussed below.

Glass-FWC strength degradation expected to result from cyclic pressurization led to selection of the operating-pressure filament-stress level as 60% of the single-cycle burst stress, so that the 100-pressure-cycle requirement could be sustained. An operating-pressure design-allowable filament-stress level of 200,000 psi at 75°F, compared with an expected burst-pressure filament-stress level of 330,000 psi was used in the parametric study.

At -320 and -423°F, these levels were expected to increase by 50% to an operating-stress level of 300,000 psi and a burst-stress level of 495,000 psi.

The cyclic-pressurization tests at all temperatures produced no detectable filament-strength degradation, so that the operating stress assumed for the parametric study (200,000 psi at 75°F and a 300,000-psi maximum at cryogenic temperatures) was conservative. On this basis, all parametric-design curves of Reference 1, except those giving safety factors for GFR Inconel X-750 and GFR 301 stainless steel (half-hard) tanks (in Figures 44 and 53 of Reference 1), may be considered accurate for use in preliminary design of GFR metal tanks.

The room-temperature burst-pressure glass-FWC stress level of 330,000 psi used for the parametric study was substantiated by the test results. The ultimate-glass-filament-strength levels at -320 and -423°F, however, were about 20 to 25% higher than at room temperature, rather than the 50% increase assumed in the parametric study. This result affected only two parametric-design curves of Reference 1: (1) Figure 44, which presented -320 and -423°F safety-factor curves for GFR Inconel X-750 based on an ultimate filament stress of 495,000 psi rather than the demonstrated 20 to 25% increase (from 330,000 psi to about 410,000 psi), and (2) Figure 53, which presented the -320°F safety-factor curve [for GFR 301 SS (half-hard)], for the same reason. These curves should be displaced to show the lower safety factors associated with an ultimate filament stress of 410,000 psi. It is estimated that the safety-factor curves based on this value will be 80 to 90% of the values shown for a stress of 495,000 psi.

The other parametric-design curves for the GFR metal tanks remain unaffected because either (1) they were based on the design operating-pressure conditions selected in the parametric study, which were verified by the test program, or (2) the safety-factor curves for GFR titanium (5Al-2.5Sn, ELI grade), GFR 2219-T62 aluminum, and GFR 301 SS (half-hard) tanks [Reference 1 Figures 39, 49, and 53 (except the -320°F values)] were independent of the allowable ultimate-glass-filament-strength level at cryogenic temperatures because the allowable liner-biaxial-strain capability controlled the design burst pressure.

The structural analysis of and computer program for GFR metal tanks developed during the parametric study were essentially verified. Test data substantiated that the new head contours developed for these tanks have a 1-to-1 stress field in the liner and nearly constant stresses in the filaments up the head at the design temperature and pressure, thus satisfying the requirements for optimum closure design. Analysis improvements that can be made include provisions for (1) a more accurate stress-strain curve for the liner (rounding during the yield), and (2) the input of a variable Poisson's ratio as the metal shell yields past the elastic limit.

VIII. CONCLUSIONS AND RECOMMENDATIONS

A. The principal objective of this program - analytical and experimental evaluation of GFR metal tanks for service at 75 to -423°F - was accomplished.

B. Analysis, design, fabrication, and testing demonstrated the feasibility and potential of GFR metal tanks. Their performance is intermediate between that of thin-metal-lined glass-FWC and homogeneous metal pressure vessels. Adhesive-bond integrity during service is not an area of concern, however, because the GFR metal tanks do not require a liner-overwrap bond to keep the liner from buckling (as do thin-metal-lined tanks).

C. Proper design permits exploitation of the maximum load-bearing capabilities of both the liner and the glass-FWC shell and makes possible tanks whose performance is significantly greater than the highest-performance, cylindrical and spherical, homogeneous metal tanks.

D. The parametric-study results and conclusions (reported in Reference 1) were essentially verified by the fabrication of GFR metal tanks and evaluation in burst, fatigue-plus-burst, and creep-plus-burst tests at 75, -320, and -423°F.

E. The parametric study may be used to accurately determine preliminary designs of GFR metal tanks for which the allowable glass-filament stress at the 75°F operating pressure is 200,000 psi. A change in this design criterion will change the liner and glass-FWC-shell design details from those given there, but new designs can readily be determined with the computerized analysis developed under this contract.

F. The 18-in.-dia GFR Inconel X-750 (STA) tanks that were fabricated and tested demonstrated most of the characteristics predicted by the parametric study. An exception was that the ultimate-glass-filament-strength level attained in cryogenic-temperature tests was less than the increase over room-temperature strength predicted on the basis of glass-monofilament and simple-composite-specimen tests. The following conclusions were drawn from the vessel-test results:

1. Inconel X-750 (STA) has sufficient biaxial ductility in the parent metal and electron-beam-welded joints over the 75 to -423°F range to perform satisfactorily as the liner for the glass-FWC shell.

2. The average pressure-vessel burst strength at ambient temperature (75°F) was within 0.67% of the design burst pressure and varied only 4.30% from the average. The average ultimate glass-filament strength of 320,200 psi was 97% of the 330,000-psi value used for design and analysis.

3. The average increase in performance between ambient and cryogenic temperatures for vessels failing in the FWC shell was 22 to 25% at -320°F and 23 to 27% at -423°F, based on the $p_b V/W$ values for single-cycle burst tests, 100-cycle-fatigue plus burst tests, or 72-hour-sustained-pressurization plus burst tests. Based on average ultimate-filament-stress levels, the performance increased 23% at -320°F and 21% at -423°F.

4. There was no significant difference between the strength levels attained by (a) vessels subjected to 100-pressure-cycle fatigue or 72-hour sustained loading before burst testing, and (b) vessels pressurized directly to the burst point without exposure to a simulated service cycle. For these tests the ratio of burst pressure to operating pressure was about 1.50, and the operating pressure was about 60 to 70% of the burst pressure.

5. The tank design was controlled by compressive stresses in the liner heads at zero pressure after proofing at 75°F. As designed on the basis of the computer analysis, the compressive stresses did not exceed the buckling stress allowable at the equator but did exceed the compressive-yield stress up the head near the boss, which gave rise to the incorporation of local glass-filament reinforcements there to decrease plastic deformation at the proof pressure and subsequent compressive stresses at zero pressure. The test data revealed that high strains occurred near the polar bosses despite the local reinforcements.

6. In burst tests, 18 of 20 vessels failed near the polar bosses - 13 in the FWC shell and 5 in the metal shell. It is believed that strain magnification occurred at the boss-to-head juncture, due to head-reinforcement ineffectiveness and high polar-boss rigidity, and caused the five liner failures. The other 13 vessels failed at rather consistent filament-stress levels, but the high local strains measured in the FWC shell indicated a stress concentration that may have restricted the potential performance of the filaments over the 75 to -423°F range.

7. Generally good correspondence was obtained between the expected and the measured pressure-strain characteristics. As predicted, longitudinal strains led hoop strains until the design burst pressure was approached, when the hoop strains caught up with and then exceeded the longitudinal strains.

8. The tanks could be operated at 100% of the liner's offset-yield strength (rather than the 90% assumed in the parametric study) and at about 60 to 70% of the burst pressure in the cyclic-fatigue and sustained-loading tests at all temperatures without apparent degradation in performance. Liner operation at 100% rather than 90% of the offset-yield stress, if applied to the results of the parametric study, will increase the p_oV/W factors given there by about 10%.

9. Although most of the tanks were fabricated without design deviations, a few liners had girth-weld-joint mismatches in excess of the requirements. Testing revealed that the mismatch apparently did not contribute to failure until it exceeded 25% of the liner thickness.

G. The buckling strengths determined for Ti-5Al-2.5Sn, 2219-T62 aluminum, and Inconel X-750 cylinders overwrapped circumferentially with layers of tensioned filaments were in agreement with the values used for the parametric study.

H. GFR Inconel X-750 tanks offer weight savings as compared with existing tankage. The successful results obtained indicate that they are worthy of serious consideration for application in aerospace systems.

I. Improved efficiency for GFR metal tanks over the 75 to -423°F range will be provided by GFR Inconel 718 and GFR Ti-5Al-2.5Sn vessels. Their projected performance is considerably greater than that of GFR Inconel X-750 tanks and homogeneous metal tanks. Additional studies and evaluations are warranted to establish performance data for GFR metal tanks having higher-performance liners than used in this program. The investigations should include the use of higher-modulus filaments in the FWC shell to lower liner strains and thereby improve performance.

J. Future GFR metal tanks should be designed so that the metal boss is as small as possible and of low rigidity. The liner component should be designed to fulfill the role assigned to the glass-filament head reinforcements in this program, by appropriately increasing the liner thickness in the polar-boss region.

K. Continued research and development work incorporating the new technology being developed for advanced composite materials, as well as lighter-weight high-strength metal-shell materials having adequate biaxial ductility, will lead to tankage optimization and advanced aerospace applications.

REFERENCES

1. E. E. Morris, F. J. Darms, R. E. Landes, and J. W. Campbell, Parametric Study of Glass-Filament-Reinforced Metal Pressure Vessels, NASA CR 54-855 (prepared by Aerojet-General under Contract NAS 3-6292), April 1966.

2. L. M. Soffer and R. Molho, Cryogenic Resins for Glass-Filament-Wound Composites, NASA CR-72114 (prepared by Aerojet-General under Contract NAS 3-6287), January 1967.

3. F. J. Darms and R. E. Landes, Computer Program for the Analysis of Filament-Reinforced Metal-Shell Pressure Vessels, NASA CR-72124 (prepared by Aerojet-General under Contract NAS 3-6292), May 1966.

TABLE 1

TYPICAL INCONEL X-750 (STA) PROPERTIES FOR DESIGN USE*

	Specimen Direction	Uniaxial			1-to-1 Biaxial-Stress State		
		75°F	-320°F	-423°F	75°F	-320°F	-423°F
		Proportional Limit, psi					
Tension	L	108,000	122,000	126,000	Same as uniaxial		
	T	108,000	124,000	128,000	↓		
Compression	L	108,000	122,000	126,000	↓		
	T	108,000	124,000	128,000	Same as uniaxial		
		Ratio of Proportional Limit to Density (0.300 lb/in.^{3}), in.					
Compression	L	360,000	407,000	420,000	Same as uniaxial		
	T	360,000	413,000	427,000	↓		
		Yield Strength, psi			↓		
Tension	L	120,000	136,000	140,000	↓		
	T	120,000	138,000	142,000	↓		
Compression	L	120,000	136,000	140,000	↓		
	T	120,000	138,000	142,000	↓		
		Tensile Strength, psi			↓		
Tension	L	174,000	214,000	234,000	↓		
	T	174,000	216,000	234,000	Same as uniaxial		
		Elongation, % in 2 in.**					
Tension	L	25	31	28	6.25	7.75	7.0
	T	25.5	30	31	6.4	7.5	7.75

*L = longitudinal direction, T = transverse. Dashes in last six columns indicate data not available.

**Biaxial elongation assumed to be 25% of uniaxial value.

Table 1, Sheet 1 of 3

TABLE 1 (cont.)

	Specimen Direction	Uniaxial 75°F	Uniaxial -320°F	Uniaxial -423°F	1-tc-1 Biaxial-Stress State 75°F	1-tc-1 Biaxial-Stress State -320°F	1-tc-1 Biaxial-Stress State -423°F
Modulus of Elasticity, psi							
Tension	L	31	31.5	32	41	41.5	42
	T	31	31.5	32	41	41.5	42
Compression	L	31	31.5	32	41	41.5	42
	T	31	31.5	32	41	41.5	42
Fracture Toughness, Notch-to-Unnotch Strength Ratio							
Parent Metal*							
K_T=6.3	L	0.97	0.86	0.85	-	-	-
K_T=6.3	T	0.97	0.87	0.86	-	-	-
K_T=7.2	L	0.99	0.88	0.80	-	-	-
K_T=8	L	1.00	0.86	0.86	-	-	-
K_T=8	T	0.97	0.86	0.85	-	-	-
K_T=10	L	0.90	0.79	0.82	-	-	-
Welded	-	-	-	-	-	-	-
Fracture Toughness, Notched-Strength to Unnotched-Yield-Strength Ratio							
Parent Metal							
K_T=6.3	L	1.42	1.41	1.48	-	-	-
K_T=6.3	T	1.42	1.41	1.44	-	-	-
K_T=7.2	L	1.44	1.42	1.50	-	-	-
K_T=8	L	1.40	1.32	1.41	-	-	-
K_T=8	T	1.40	1.38	1.36	-	-	-
K_T=10	L	1.28	1.25	1.33	-	-	-
Welded	-	-	-	-	-	-	-

*K_T, the notch-concentration factor, is an expression of the sharpness or acuity of the notch in test specimens. Its value increase as the notch radius decreases. For edge-notched flat specimens, it is determined as follows: $K_T = \sqrt{a/r}$, where a is half the width between the notches and r is the notch radius.

TABLE 1 (cont.)

	Specimen Direction	Uniaxial 75°F	Uniaxial -320°F	Uniaxial -423°F	1-to-1 Biaxial-Stress State 75°F	1-to-1 Biaxial-Stress State -320°F	1-to-1 Biaxial-Stress State -423°F
Weld-Joint Properties							
Joint efficiency, %	-	105	119	116	Same as uniaxial		
Elongation, % in 2-in.	-	20.5	21	24	5.1	5.25	6.0
Poisson's Ratio							
-	-	0.29	0.29	0.29	Same as uniaxial		
Low-Cycle, High-Strain Fatigue - Reversed Cycle							
Parent Metal							
No. of cycles to failure at max operating strain range	-	3500	7000	10,000	Insufficient data available		
Magnitude of elastic-strain range for failure at 100 cycles (max $\Delta\epsilon_e$), in./in.	-	0.0120	0.0145	0.0150			
Factor of safety based on 100-cycle requirement	-	35	70	100			
Factor of safety based on max $\Delta\epsilon_e$	-	1.50	1.67	1.74	Insufficient data available		
Welded	-	-	-	-	-	-	-

Table 1, Sheet 3 of 3

TABLE 2

MATERIAL PROPERTIES USED FOR DESIGN ANALYSIS
OF 18-INCH-DIAMETER GFR INCONEL X-750 TANK

Property	Inconel X-750 (STA)	Glass-Filament-Wound Composite
Density, $lb/in.^3$	0.300	0.072
Coefficient of thermal expansion, $in./in.-^oF$ at +75 to -423^oF	4.990×10^{-6}	2.010×10^{-6}
Tensile-yield strength, psi	118,000	-
Derivative of yield strength with respect to temperature, $psi/^oF$	-60.1	-
Proportional limit, psi	108,000	-
Derivative of proportional limit with respect to temperature, $psi/^oF$	-54.2	-
Elastic modulus, psi	31.0×10^6	12.4×10^6
Derivative of elastic modulus with respect to temperature, $psi/^oF$	-2010	-2410
Plastic modulus, psi	440,000	-
Derivative of plastic modulus with respect to temperature, $psi/^oF$	-0.1	-
Poisson's ratio	0.290	-
Derivative of Poisson's ratio with respect to temperature, $1/^oF$	0.0	-
Maximum metal-shell biaxial longitudinal strain at design condition, in./in.		
At $+75^oF$	0.0625	-
At -320^oF	0.0750	-
At -423^oF	0.0700	-
Volume fraction of filament in composite	-	0.673
Filament, design-allowable stress, psi		
At $+75^oF$	-	330,000
At -320^oF	-	495,000
At -423^oF	-	495,000

TABLE 3

DESIGN PARAMETERS FOR 18-INCH-DIAMETER
GFR INCONEL X-750 OBLATE-SPHEROID PRESSURE VESSEL

Parameter	Value
Major diameter, in.	18.00
Polar-boss diameter, in.	2.70
Operating pressure (p_o), psi	
At +75°F	2000
At -320°F	2300
At -423°F	2350
Burst pressure (p_b), psi	
At +75°F	3010
At -320°F	4263
At -423°F	4300
Metal-shell thickness, in.	0.047
FWC thickness at equator, in.	0.030
Internal volume (V), $in.^3$	2370
Total vessel weight (without bosses or head reinforcements), (W), lb	15.200
Performance factor (pV/W), in.	
Based on operating pressure (p_o)	
At +75°F	312,000
At -320°F	358,000
At -423°F	364,000
Based on burst pressure (p_b)	
At +75°F	469,300
At -320°F	664,000
At -423°F	670,000

TABLE 4

TENSILE PROPERTIES OF WELDED AND UNWELDED SPECIMENS OF INCONEL X-750 (STA)*

Specimen No.	Description	Thickness In.		Proportional Limit psi	0.2% Yield Strength psi	Ultimate Tensile Strength psi	Elongation in 2 in. %	Failure Location
				Parent Metal				
1	Specimens from sheet used	0.0658		96,600	113,500	173,200	27.0	Center of GL**
2	to fabricate formed heads	0.0653		83,100	107,700	169,200	26.5	Center of GL
3	for Tank 2***	0.0645		-	114,800	172,900	28.0	Grip; retested, failed at center of GL
4		0.0653		87,700	106,200	172,200	26.1	GL
			Av	89,130	110,550	171,870	26.9	-
13	Specimens of parent metal	0.0534		90,800	106,000	173,000	26.2	Center of GL
14	used for weldment-test	0.0534		90,600	116,600	174,200	24.6	Center of GL
15	specimens	0.0534		102,000	114,700	172,200	24.4	Center of GL
			Av	94,500	112,400	173,100	25.1	-
				Longitudinal Weld				
5	Specimens electron-beam-	0.0535		110,100	125,000	178,000	24.9	Center of GL
6	welded along entire longi-	0.0535		104,100	119,000	173,600	20.0	Center of GL at weld defect
	tudinal axis (center line)		Av	107,100	122,000	175,800	22.5	-
	Efficiency, %****			113	108	101	90	-
				Transverse Weld				
7	Specimens electron-beam-	0.0535		98,500	116,000	173,000	23.6	GL parent metal
8	welded transverse to	0.0535		84,000	111,000	174,100	21.7	GL parent metal
9	longitudinal direction at	0.0537		103,300	119,700	172,700	20.1	Weld
10	center of gage length	0.0528		88,300	111,100	170,900	22.1	GL parent metal
11		0.0534		95,100	112,900	175,700	23.9	Grip; retested GL parent metal
12		0.0528		103,800	116,000	171,100	18.6	Weld
			Av	95,500	114,450	172,900	21.7	-
	Efficiency, %****			101	112	100	86.5	-

*All specimens solution-treated at 1900°F in hydrogen for 30 min, air-cooled, age-hardened at 1300°F in hydrogen for 20 hours, and air-cooled. All specimens conformed to FTMS 151a, Type F2. Weld bead left on welded specimens.

**GL = gage length.

***Specimens 1 and 2 represented one shell head and 3 and 4 the other.

****Efficiencies based on comparison with average parent-metal results.

TABLE 5

CHARACTERISTICS OF METAL SHELLS, GLASS-FWC SHELLS, AND GFR INCONEL X-750 (STA) TANKS

Serial No.	Test Temp °F	Type of Test	Inconel X-750 (STA) Shell: Average Thickness at Equator in.	Inconel X-750 (STA) Shell: Weight, lb With Bosses	Inconel X-750 (STA) Shell: Weight, lb Without Bosses	Inconel X-750 (STA) Shell: Girth-Weld-Joint Remarks	Glass-FWC Shell: Thickness at Equator, in. Filament (Equivalent)	Glass-FWC Shell: Thickness at Equator, in. Composite	Glass-FWC Shell: Weight, lb Glass	Glass-FWC Shell: Weight, lb Resin	Glass-FWC Shell: Weight, lb Port Reinforcement	Glass-FWC Shell: Weight, lb Total Composite	Glass-FWC Shell: Glass Content vol%	Glass-FWC Shell: Remarks	GFR Metal Tank: Weight, lb With Bosses	GFR Metal Tank: Weight, lb Without Bosses	GFR Metal Tank: Volume, $in.^3$ Original	GFR Metal Tank: Volume, $in.^3$ After Proof Test
2	75	Burst	0.0526	16.600	13.575	-	0.0207	0.0314	2.550	0.520	0.214	3.070	66	Resin overcured by 11 hours at 300°F	19.850	16.825	2335	2380
3	75	Burst	0.0519	16.387	13.362	-	0.0208	0.0293	2.608	0.448	0.225	3.056	71	Liner-to-overwrap adhesive layer and approx 1/4 of inner windings uncured	19.667	16.642	2322	2380
4	75	Creep	0.0537	16.332	13.307	-	0.0200	0.0283	2.500	0.459	0.442	2,959	70.5	Adhesive layer removed, one additional set of head reinforcements used	19.733	16.708	2300	2350
5	75	Burst	0.0552	16.325	13.300	-	0.0203	0.0278	2.544	0.387	0.451	2.931	73		19.707	16.682	2330	2375
6	75	Creep	0.0513	16.224	13.199	-	0.0202	0.0285	2.542	0.438	0.438	2.931	71		19.643	16.618	2335	2380
7	75	Fatigue	0.0527	16.270	13.245	-	0.0203	0.0278	2.548	0.383	0.441	2.932	73		19.643	16.618	2340	2380
8	75	Fatigue	0.0542	16.440	13.415	-	0.0203	0.0286	2.553	0.427	0.441	2.981	71		19.861	16.836	2340	2373
9	-423	Fatigue	0.0532	16.276	13.252	-	0.0202	0.0285	2.540	0.459	0.441	2.998	71		19.716	16.691	-	-
10	-423	Fatigue	0.0530	16.257	13.232	-	0.0203	0.0278	2.546	0.432	0.441	2.978	73		19.676	16.651	-	-
11	-423	Burst	0.0534	16.138	13.112	-	0.0204	0.0280	2.565	0.421	0.441	2.986	73		19.565	16.540	-	-
12	-423	Creep	0.0535	16.263	13.239	-	0.0207	0.0281	2.604	0.381	0.441	2.985	74		19.689	16.664	-	-
13	-320	Burst	0.0530	16.270	13.244	Mismatch: 0.006 in. max	0.0204	0.0280	2.561	0.419	0.441	2.980	73		19.691	16.666	-	-
14	-320	Burst	0.0524	15.946	12.920	Mismatch: 0.014 in. max	0.0205	0.0273	2.570	0.375	0.441	2.944	75		19.331	16.306	-	-
15	-320	Creep	0.0518	15.648	12.622	Mismatch: 0.007 in. max	0.0204	0.0280	2.558	0.225	0.441	2.960	73		19.049	16.024	-	-
16	-320	Burst	0.0535	15.974	12.948	Mismatch: 0.010 in. max	0.0203	0.0271	2.554	0.359	0.441	2.913	75		19.329	16.304	-	-
17	-320	Creep	0.0524	15.895	12.869	Mismatch: 0.007 in. max (Also, one 0.015-in.-dia spherical pore in girth-weld joint)	0.0203	0.0278	2.556	0.419	0.441	2.975	73		19.311	16.286	-	-
19	-423	Burst	0.0533	15.992	12.966	-	0.0204	0.0279	2.572	0.415	0.437	2.985	73		19.415	16.390	-	-
20	-320	Fatigue	0.0532	15.913	12.887	-	0.0202	0.0302	2.532	0.569	0.437	3.101	67		19.450	16.425	-	-
21	-320	Fatigue	0.0520	15.761	12.735	Mismatch: 0.007 in. max	0.0203	0.0282	2.552	0.427	0.441	2.980	72		19.181	16.156	-	-
22	-423	Creep	0.0529	16.056	13.030	-	0.0203	0.0278	2.556	0.401	0.441	2.958	73	Adhesive layer removed, one additional set of head reinforcements used	19.455	16.430	-	-
E-1	-320	**	0.0532	-	-	Mismatch: 0.018 in. max	0.0203	0.0282	-	-	-	-	72	-	-	-	-	-
Averages for S/N 2-22			0.0530	16.149	13.123	-	0.0203	0.0283	2.556	0.418	0.441***	2.974***	72	-	19.525***	16.500***	-	-

*Not including port reinforcement.

**Used for evaluation of cryogenic-temperature-measurement instrumentation at -320°F.

***Not including Serial Nos. 2 and 3.

TABLE 6

AVERAGE DIMENSIONAL, WEIGHT, AND VOLUME PARAMETERS FOR 18-IN.-DIA, GFR INCONEL X-750, PRESSURE VESSELS

Parameter	Value	
	Design	Actual
Inconel X-750 Shell Assembly		
Outside diameter, in.	17.970	17.937
Overall length, in.	14.138	14.170
Wall thickness, in.	0.047 (+0.010,-0.000)	0.0530
Boss weight (2), lb	3.000	3.000
Formed-head weight (2), lb	12.148	13.123
Total weight, lb	15.148	16.149
Internal volume, $in.^3$		
Before proof test	2370	2330*
After proof test	-	2374*
GFR Inconel X-750 Pressure Vessel		
Outside diameter, in.	18.030	18.009
Overall length, in.	14.138	14.161
FWC thickness at equator, in.	0.030	0.028
Equivalent glass-filament thickness at equator, in.	0.019	0.020
FWC glass content, vol%	67.3	72
FWC weight, lb	3.041	2.974
Head-reinforcement weight (2 sets), lb	0.441	0.441
Total vessel weight, lb	18.630	19.525
Total vessel weight (without bosses), lb	15.630	16.500

*Average for first seven vessels.

TABLE 7

PERFORMANCE DATA FOR 18-IN.-DIA GFR INCONEL X-750 PRESSURE VESSELS

Serial No.	Test Temp °F	Type	Pressure, psig			Burst-Pressure Stresses, psi			Performance Factor (pV/W),* in.			Failure Mode	Remarks
			Proof	Operating	Burst	Glass Filament	Liner Longitudinal	Liner Hoop	At Proof Pressure	At Operating Pressure	At Burst Pressure		
2	75	Proof, burst	2220	-	2960	313,100	134,000	132,000	314,000	-	418,000	Liner at boss-to-head weld; filaments did not fail; subsequent head buckling on depressurization.	-
3	75	Proof, burst	2220	-	2940	317,200	134,100	133,800	317,000	-	420,000	Filaments at boss; liner did not fail.	-
4	75	Proof, creep, burst	2220	2000	2630	270,100	126,300	119,400	312,000	281,000	370,000	Liner at boss-to-head weld; filaments did not fail; subsequent head buckling on depressurization.	During burst test, pressure inadvertently held at 2400 psi for 1 min.
5	75	Proof, burst	2220	-	3070	322,500	136,000	135,200	316,000	-	437,000	Filaments at boss; liner did not fail.	-
6	75	Proof, creep, burst	2220	2000	3000	331,700	137,700	137,800	318,000	286,000	430,000	Filaments at boss; longitudinal liner fractures.	-
7	75	Proof, cyclic fatigue, burst	2220	2000	2910	309,500	133,700	131,500	318,000	287,000	417,000	Filaments at boss; longitudinal liner fractures.	-
8	75	Proof, cyclic fatigue, burst	2220	2000	-	-	-	-	313,000	282,000	-	Buckling of liner head at boss, 50th pressure cycle; fluid leakage through liner at boss-to-head weld.	-
9	-423	Cyclic fatigue, burst	-	2350	2535	215,200	153,100	118,500	-	334,000	360,000	Liner at boss-to-head weld, with subsequent filament fracture.	-
10	-423	Cyclic fatigue, burst	-	2350	3700	395,100	168,400	166,600	-	335,000	527,000	Filaments at boss; extensive liner fractures.	-
11	-423	Proof, burst	2000	NA	3185	318,400	156,600	144,100	287,000	-	457,000	Liner at boss-to-head weld; subsequent head buckling on depressurization.	Buckled in one head only after depressurization following 2000-psi proof test; during subsequent burst test, vessel failed at 3185 psi.
12	-423	Creep, burst	-	2350**	3700	382,600	168,000	164,500	-	335,000	527,000	Filaments at boss; liner fracture.	-
13	-320	Burst	-	-	3588	384,200	162,500	161,300	-	-	512,000	Filaments at boss; liner fracture.	-
14	-320	Proof, burst	2220	-	3400	357,400	157,800	153,600	323,000	-	495,000	Liner at girth weld; subsequent filament fracture.	Buckled in both heads after depressurization following 2220-psi proof test.
15	-320	Creep, burst	-	2300	3797	423,800	169,400	172,600	-	341,000	562,000	Filaments at boss; liner fracture.	-
16	-320	Proof, burst	2220	-	3645	391,100	163,700	163,300	324,000	-	531,000	Filaments at boss; liner fracture.	-
17	-320	Creep, burst	-	2300	3538	380,700	161,800	160,300	-	336,000	516,000	Filaments at boss; liner fracture.	-
19	-423	Burst	-	-	3685	390,100	167,600	165,200	-	-	534,000	Filaments at boss; extensive liner fractures.	-
20	-320	Cyclic fatigue, burst	-	2300***	3169	326,100	151,800	143,800	-	332,000	458,000	Leak in liner at boss-to-head weld; subsequent head buckling on depressurization.	-
21	-320	Cyclic fatigue, burst	-	2300	3554	385,500	162,700	161,700	-	338,000	521,000	Filament and liner fracture.	-
22	-423	Creep, burst	-	2350****	3615	382,400	166,200	163,000	-	339,000	525,000	Filament failure, with extensive liner fractures.	-

*Where p = pressure (psi), V = internal volume after proof test ($in.^3$), and W = pressure-vessel weight, without bosses (lb).

**Inadvertent overpressurization to 2450 psi during creep test.

***Inadvertent overpressurization to 2555 psi on first fatigue cycle.

****Inadvertent overpressurization to 2600 psi during creep test.

TABLE 8

VESSEL-FAILURE MODES

Test Temp °F	Tank Serial No.			
	Filament Failure at Boss	Liner Fracture At Boss Weld	Liner Fracture At Girth Weld	Liner Failure in Compressive Buckling
75	3, 5, 6, 7,	2, 4*	-	8
-320	13, 15, 16, 17, 21	20*	14**	-
-423	10, 12, 19, 22	9, 11***	-	-
Total at each location	(13)	(5)	(1)	(1)

*Overpressurization during test.

**Excessive girth-weld-joint mismatch of 0.014 in. and head buckling after ambient-temperature proof test.

***Head buckling after ambient-temperature proof test.

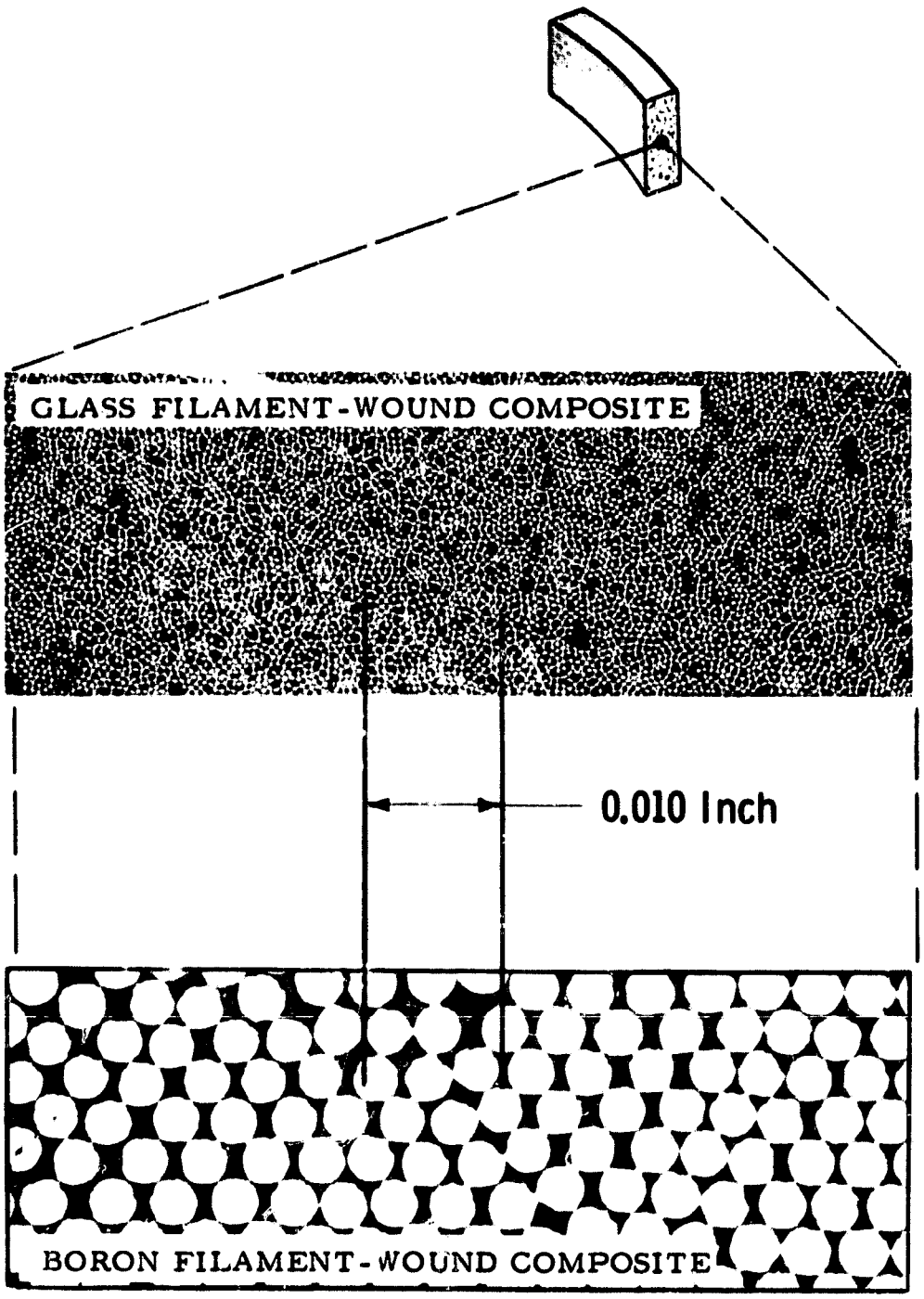

Photomicrographs of Glass-Filament-Wound and Boron-Filament-Wound Composites

Figure 1

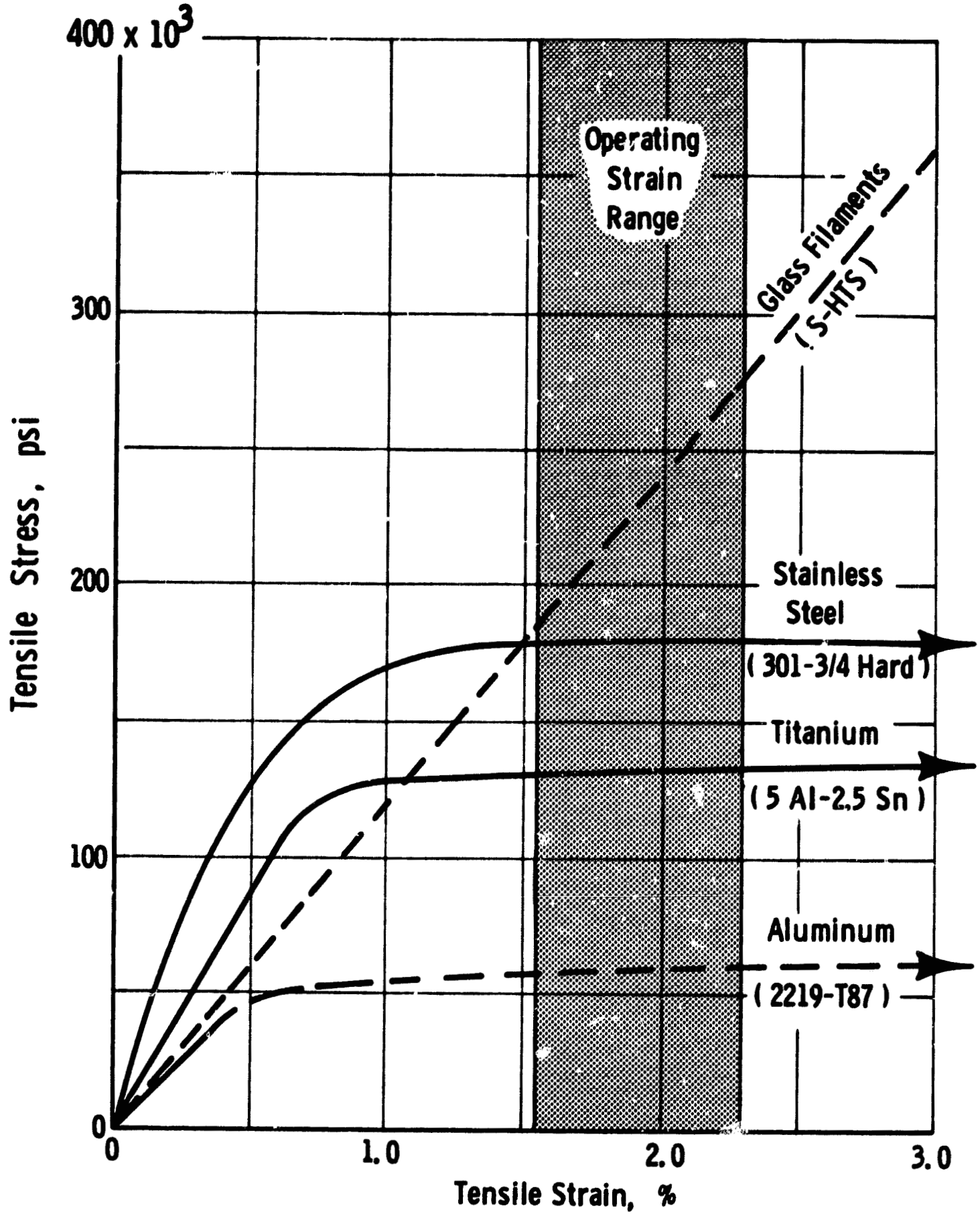

Stress-Strain Characteristics of Component Materials

Figure 2

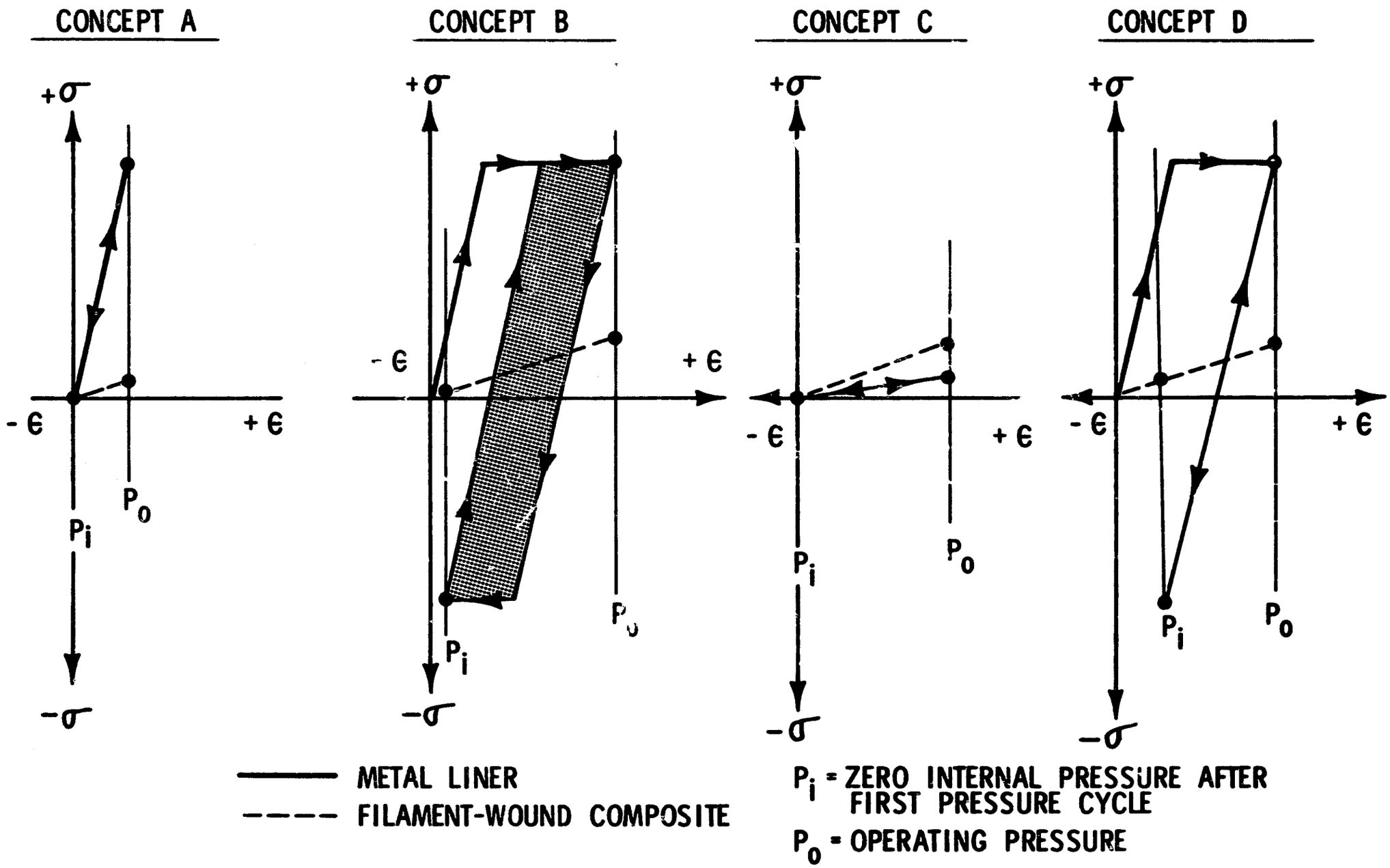

Figure 3

Liner-Design Concepts

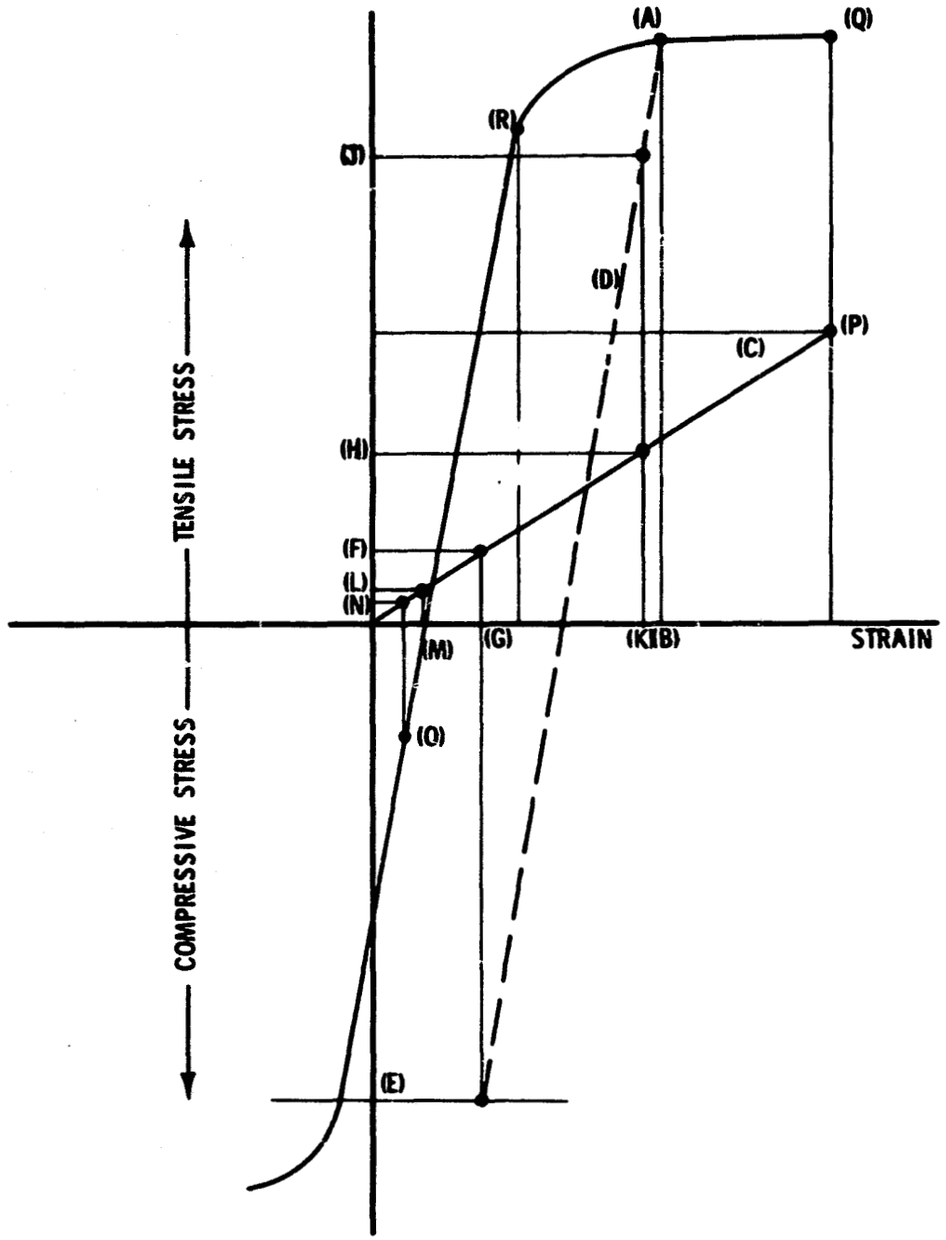

(A) STRESS-STRAIN CURVE FOR METAL SHELL - FIRST CYCLE
(B) MAXIMUM STRAIN REQUIRED OF COMPLETE SHELL - FIRST CYCLE
(C) STRESS-STRAIN CURVE FOR GLASS-FIBER SHELL - ALL CYCLES
(D) STRESS-STRAIN CURVE FOR METAL SHELL-UNLOADING FROM FIRST CYCLE
(E) COMPRESSIVE STRESS ACHIEVED IN METAL SHELL WHEN VESSEL PRESSURE IS ZERO AFTER STRAIN TO (A)
(F) TENSION STRESS IN GLASS FIBER SHELL THAT BALANCES COMPRESSION STRESS (E) IN METAL SHELL
(G) RESIDUAL STRAIN IN GLASS FIBER AND METAL SHELLS WHEN VESSEL PRESSURE IS ZERO AFTER STRAIN TO (A)
(H) OPERATING STRESS IN GLASS FIBER SHELL - ALL CYCLES SUBSEQUENT TO THE FIRST
(J) OPERATING STRESS IN METAL SHELL - ALL CYCLES SUBSEQUENT TO FIRST
(K) OPERATING STRAIN IN GLASS-FIBER AND METAL SHELLS - ALL CYCLES SUBSEQUENT TO FIRST
(L) STRESS IN GLASS FIBER SHELL FROM WINDING ON RIGID MANDREL
(M) STRAIN IN GLASS FIBER SHELL FROM WINDING ON A RIGID MANDREL; ZERO STRAIN POINT OF METAL SHELL BEFORE WINDING
(N) STRESS IN GLASS FIBER SHELL AFTER MANDREL REMOVAL WHEN VESSEL PRESSURE IS ZERO
(O) STRAIN IN METAL AND GLASS FIBER SHELLS AFTER MANDREL REMOVAL WHEN VESSEL PRESSURE IS ZERO
(P) ULTIMATE STRESS OR STRAIN OF GLASS FIBER SHELL
(Q) ULTIMATE STRESS OR STRAIN OF METAL SHELL WHEN FILAMENTS FRACTURE
(R) ARBITRARY STRAIN POINT IN METAL SHELL AND GLASS FIBER SHELL BELOW METAL SHELL PROPORTIONAL LIMIT

Figure 4

Stress-Strain Diagram for Glass-Filament-Reinforced (GFR)
Metal Shell

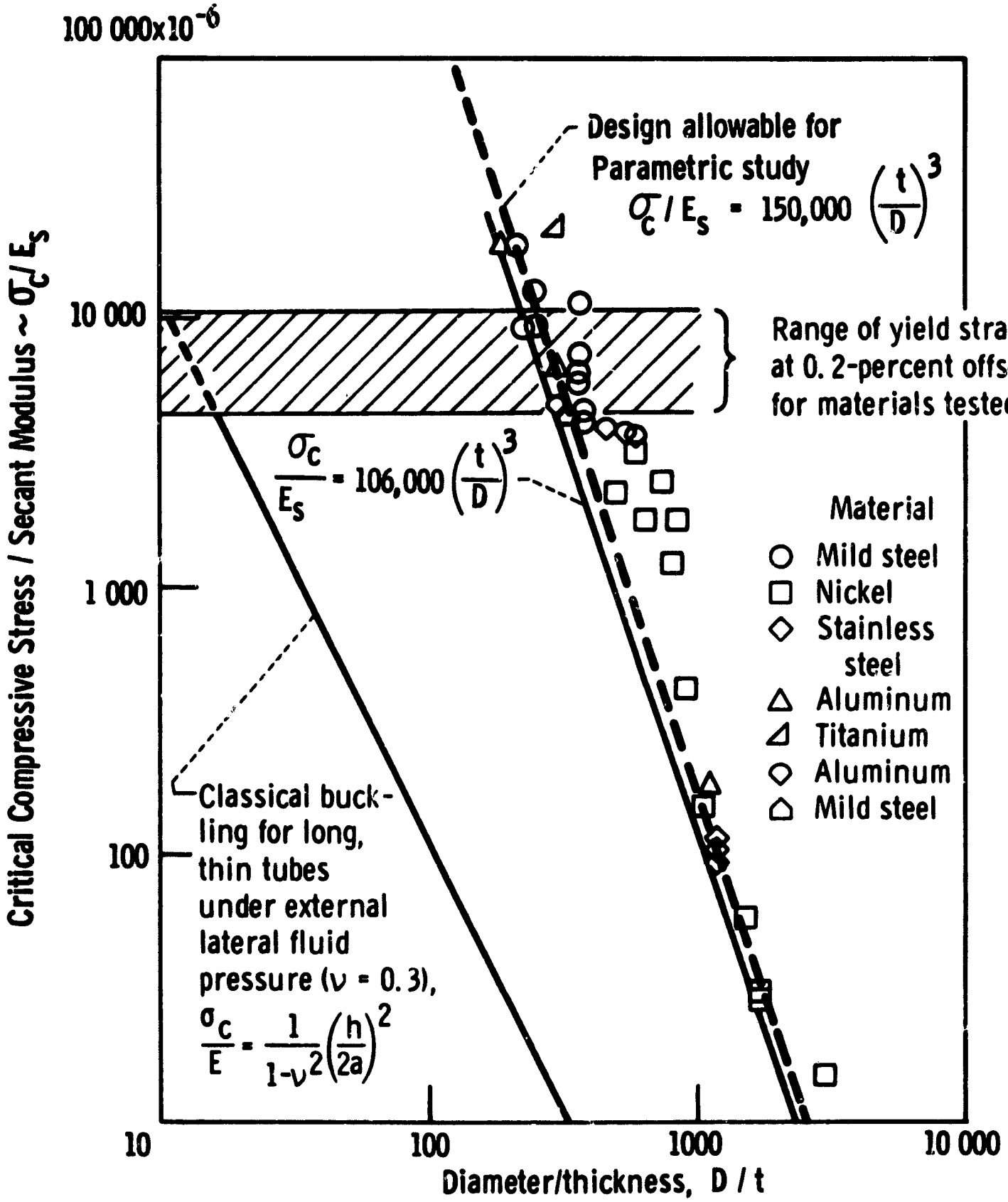

Comparison of Constrictive-Wrap Buckling Strengths for Cylindrical Tubes with Design Allowable Used for Parametric Study

Figure 5

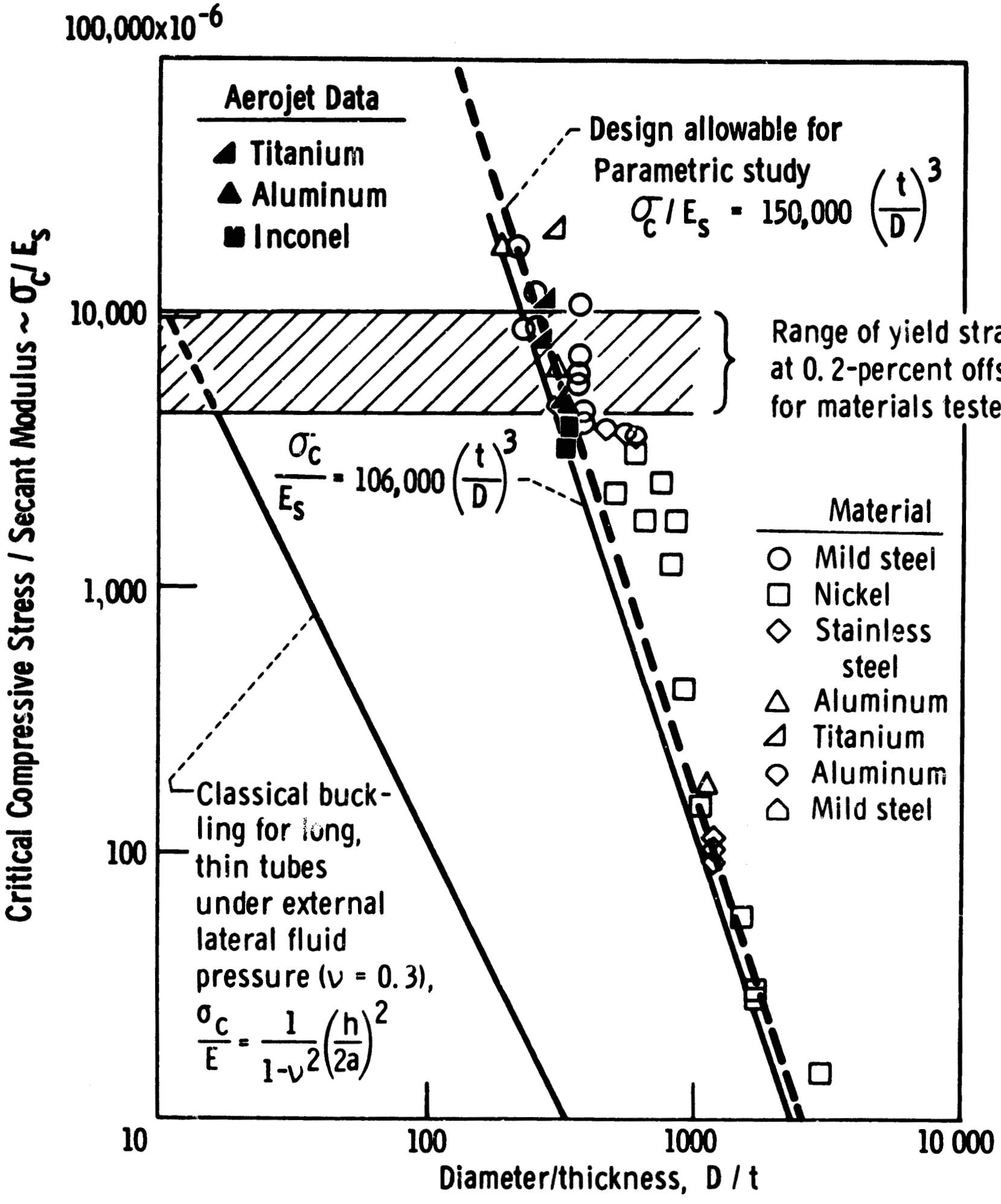

Additional Data on Constrictive-Wrap Buckling Strengths for Cylindrical Tubes

Figure 6

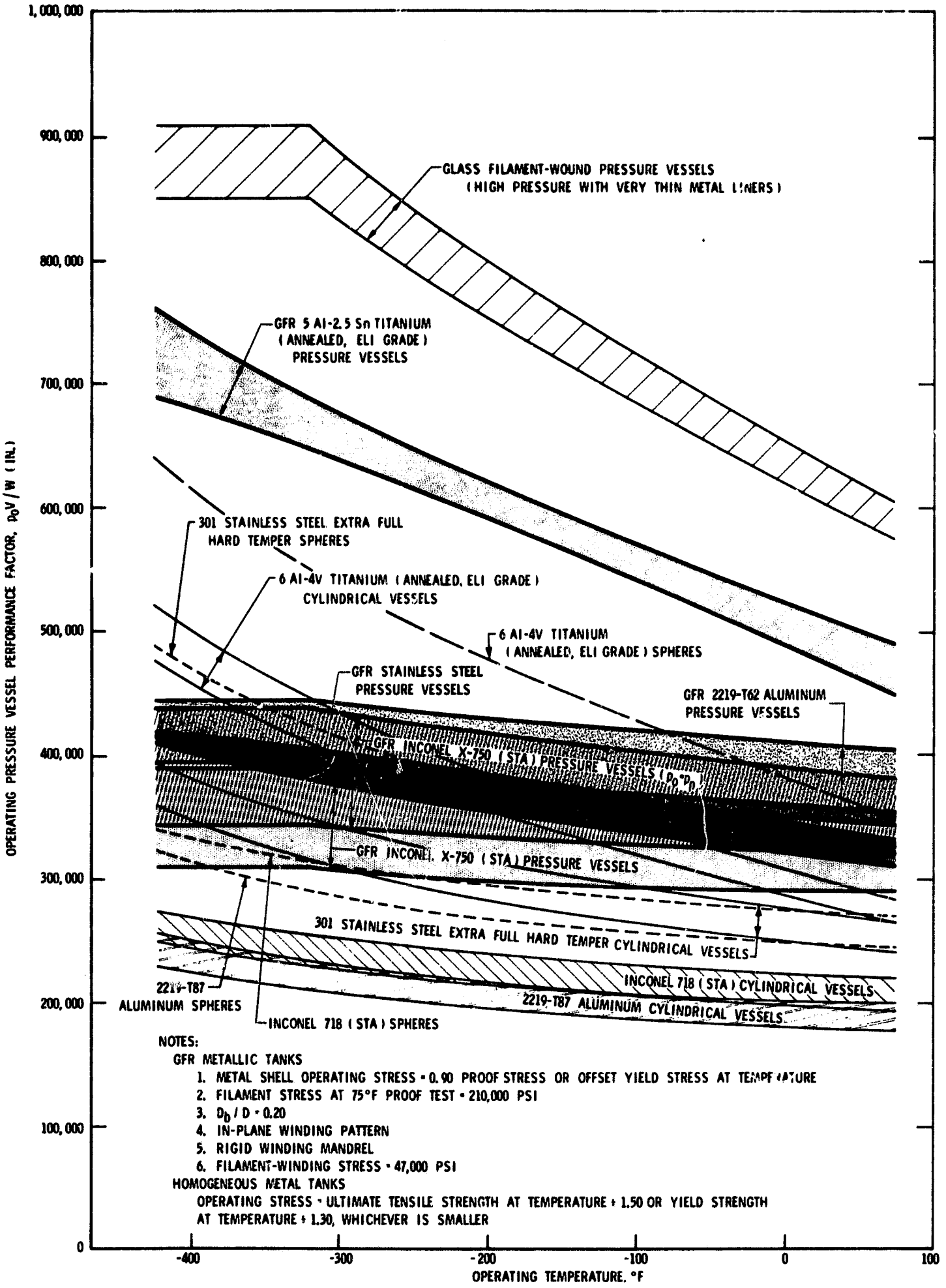

Summary Comparison, GFR-Metal and Homogeneous-Metal Pressure-Vessel Performance Levels

Figure 7

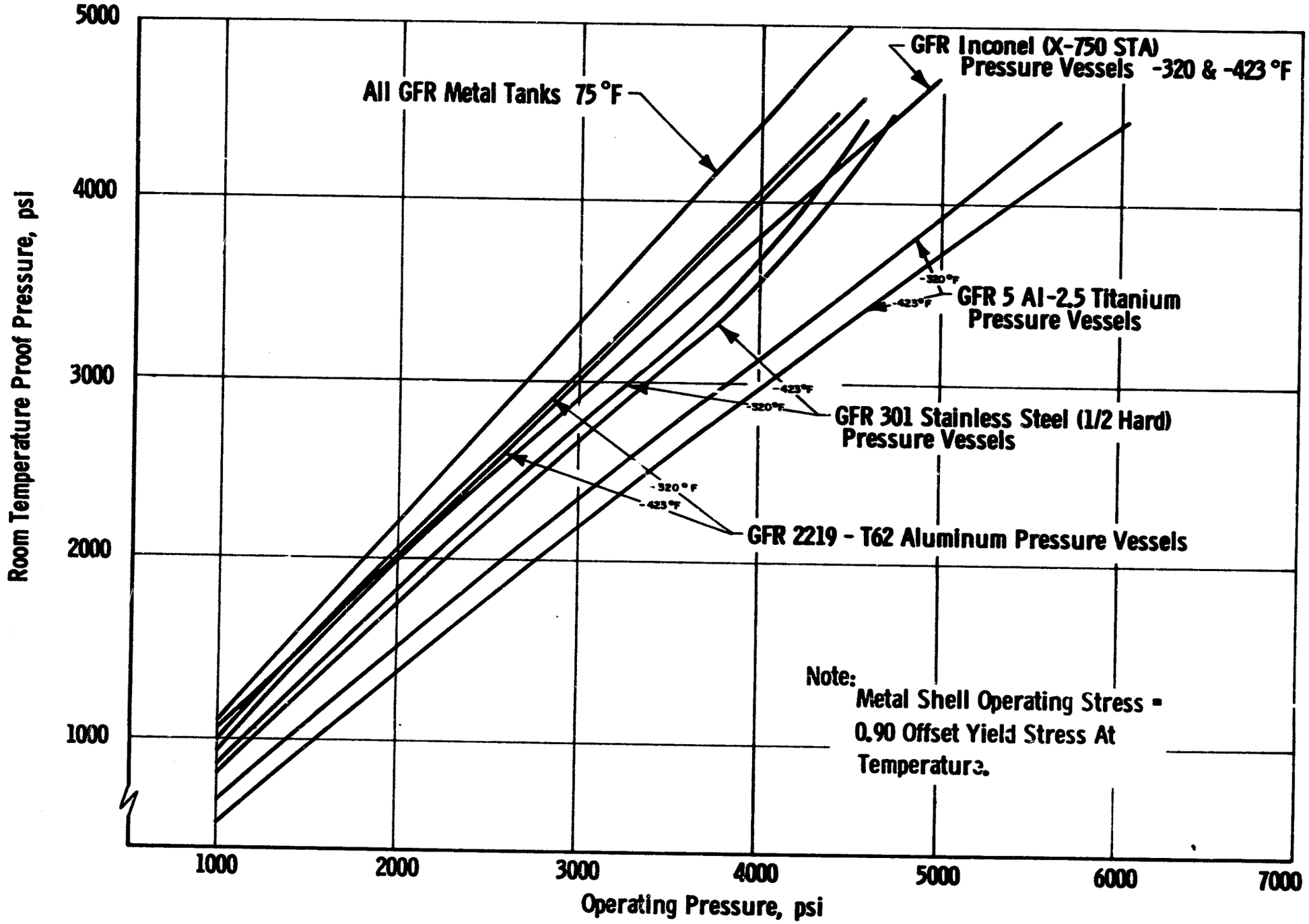

Figure 8

Relationship of Room-Temperature Proof Pressure to Operating Pressures at 75, -320, and -423°F

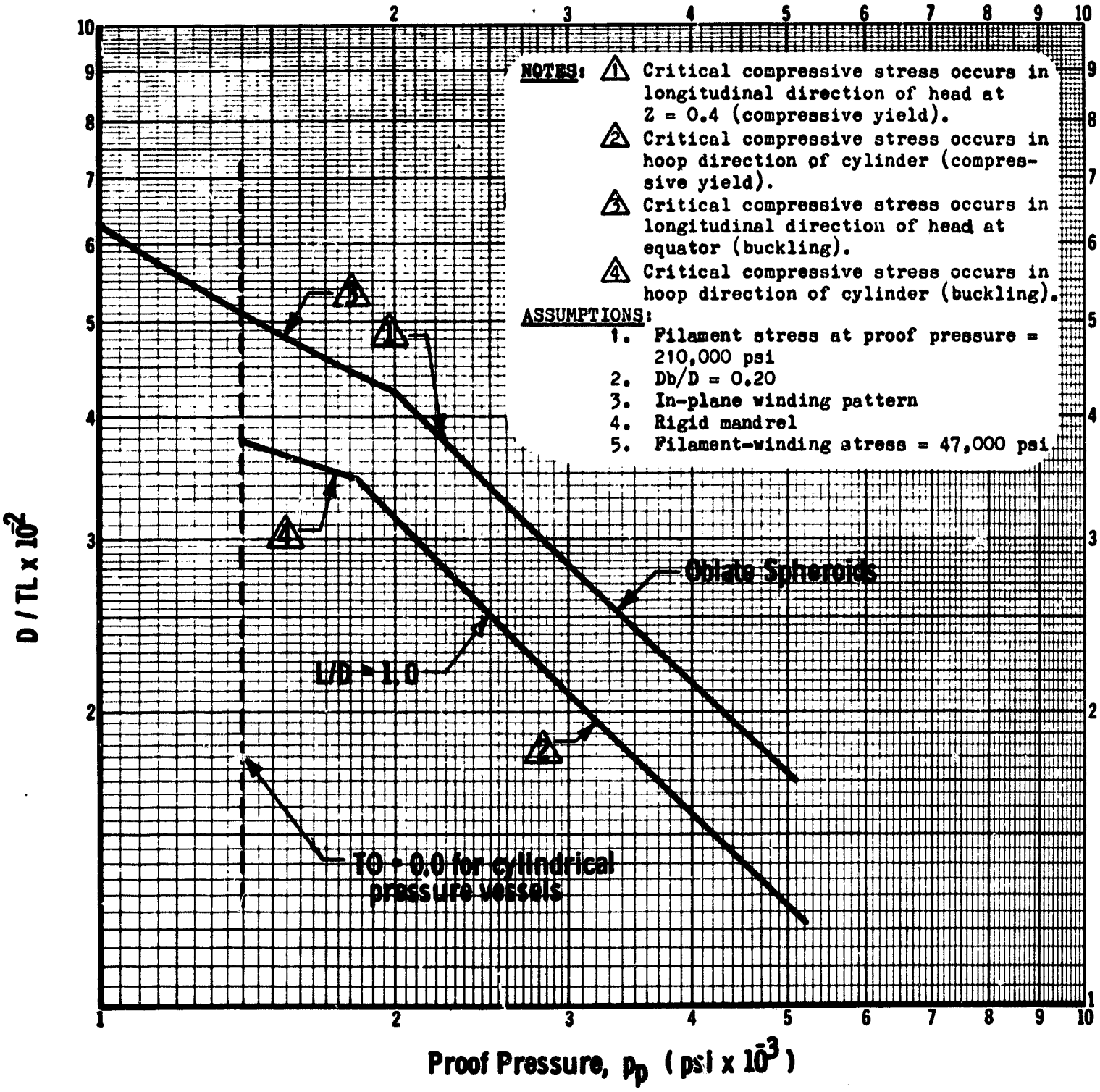

GFR Inconel X-750 (STA) Tanks, Optimum Diameter-to-Liner-Thickness Ratio (T_D = 75°F)

Figure 9

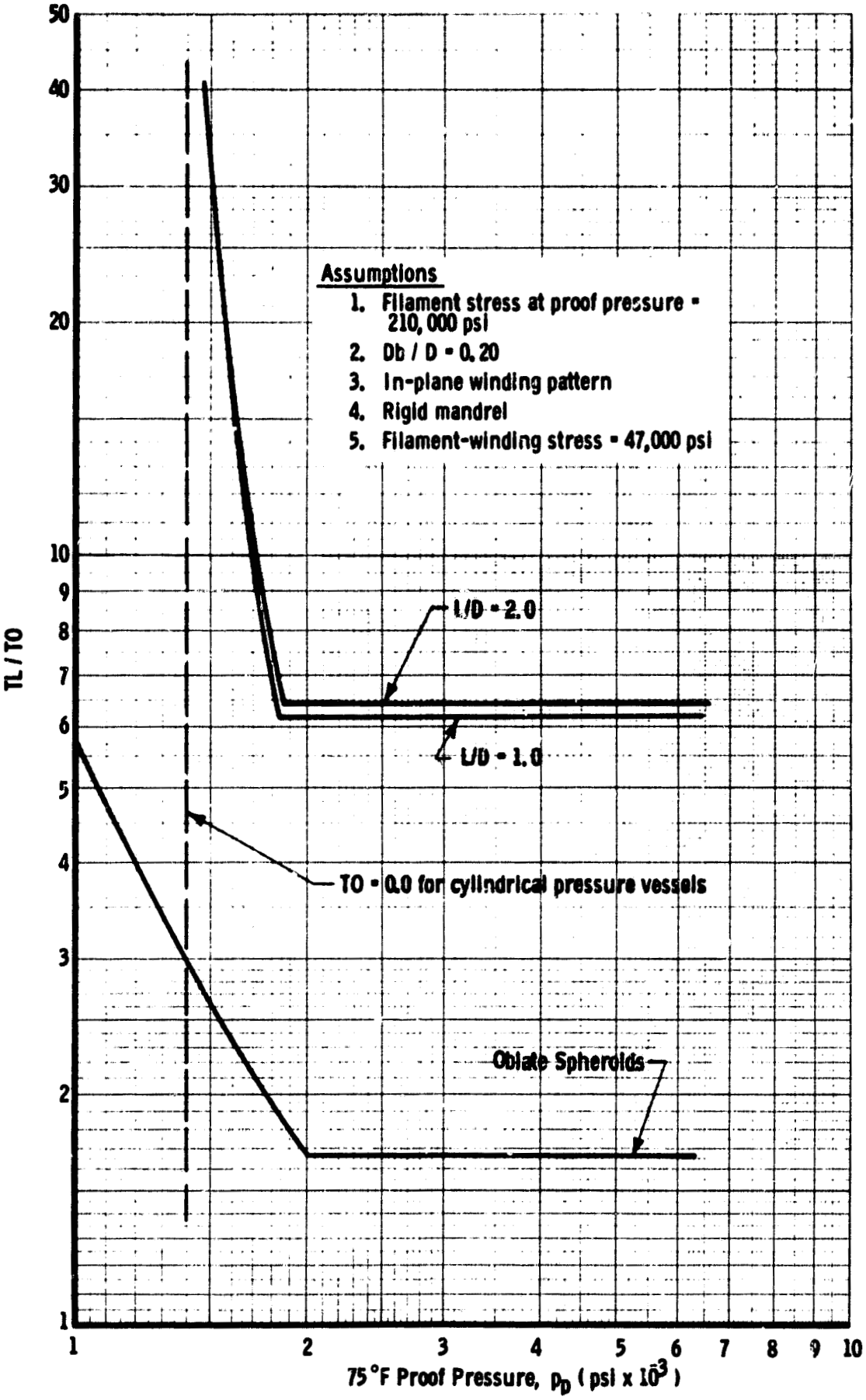

GFR Inconel X-750 (STA) Tanks, Optimum Liner-to-Longitudinal-Composite-Thickness Ratio (T_D = 75°F)

Figure 10

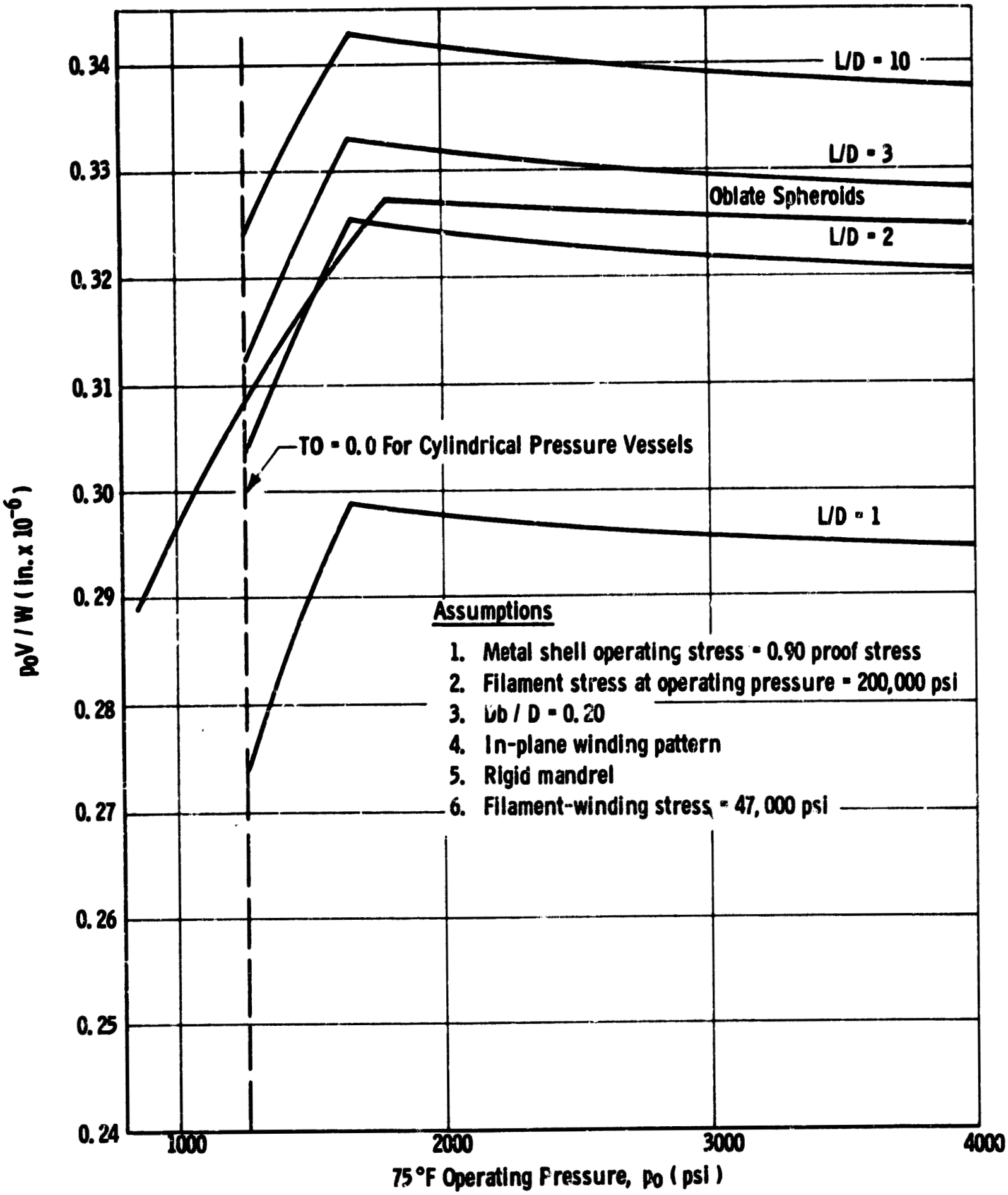

Optimum Efficiency, GFR Inconel X-750 (STA) Tanks
(T_D = 75°F)

Figure 11

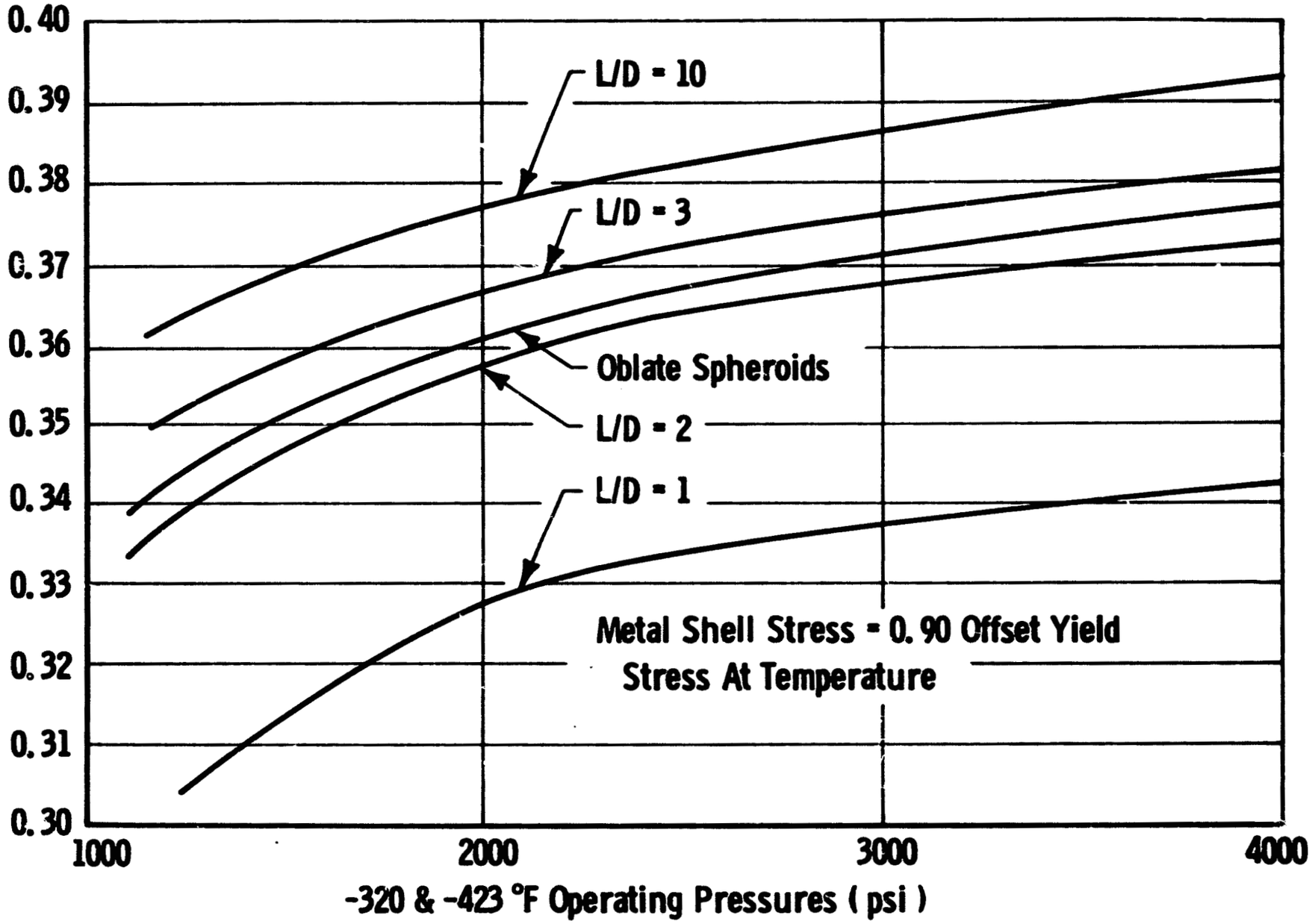

Figure 12

Optimum Efficiency, GFR Inconel X-750 (STA) Tanks
(Optimum Room-Temperature Design Operated at -320 and -423°F)

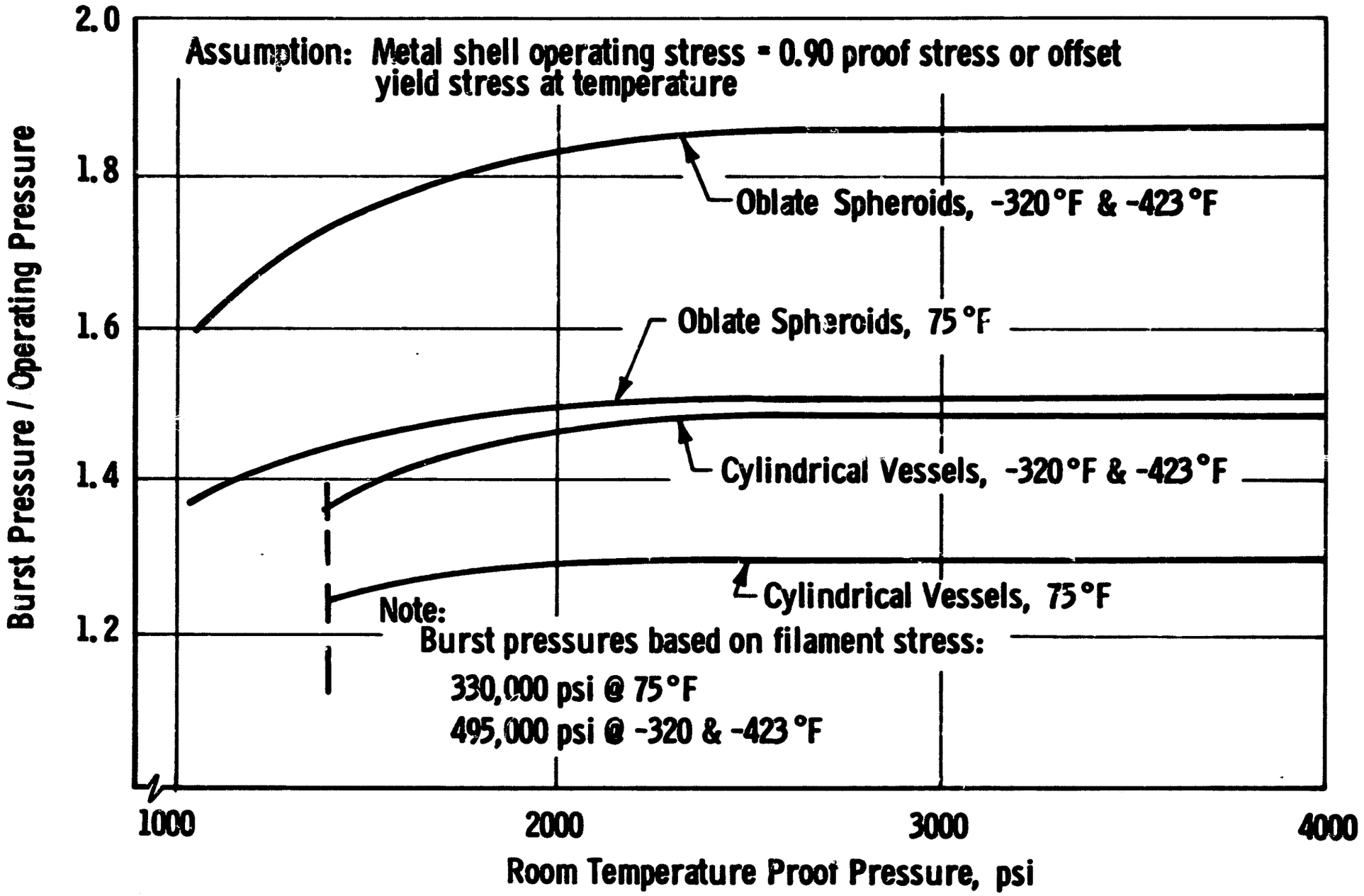

Figure 13

Factors of Safety for GFR Inconel X-750 (STA) Tanks

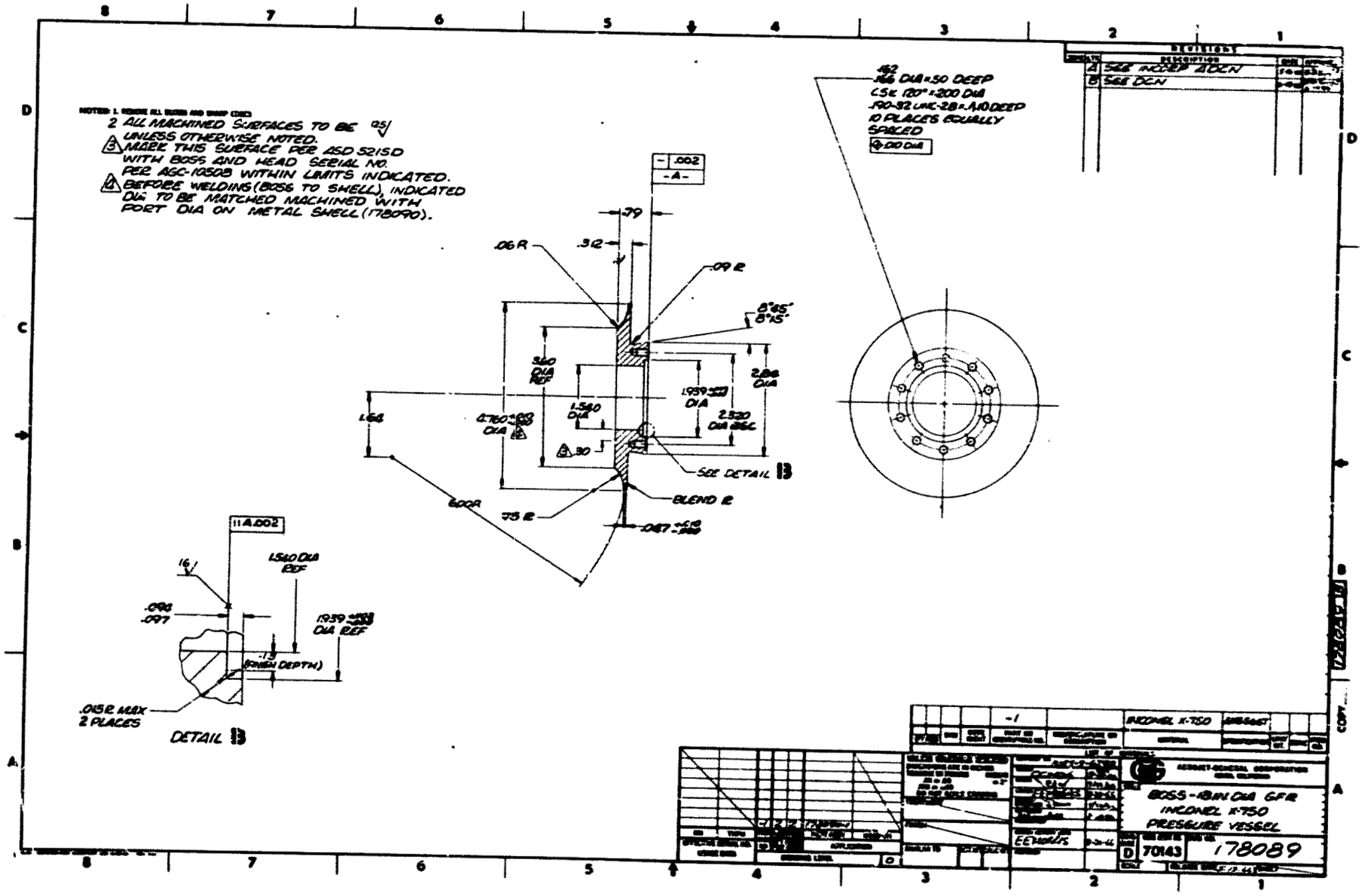

Figure 14.

Boss, 18-in.-dia GFR Inconel X-750 (STA) Tank

NOTES:
1. REMOVE ALL BURRS AND SHARP EDGES
2. FABRICATE METAL SHELL IN ACCORDANCE WITH AGC 10503.
3. CARE SHALL BE EXERCISED TO MINIMIZE SHELL DISTORTION.
4. WELD JOINT MISMATCH SHALL NOT EXCEED .008 WHEN MEASURED FROM NEUTRAL AXES OF MATING PARTS AS SHOWN.
5. INTERNAL WELD BEAD ON INDICATED SURFACE TO BE AS FLUSH AS POSSIBLE, AND NOT TO EXCEED A HEIGHT OF 0.010
6. MARK THIS SURFACE PER ASD521SC WITH ASSY SERIAL NO. PER AGC 10503.
7. ALL SURFACES TO BE 125 UNLESS OTHERWISE SPECIFIED.
8. MATERIAL THICKNESS TO BE DETERMINED AT FABRICATION.

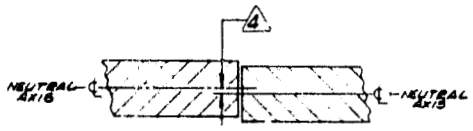

FABRICATION GUIDE
SCALE: NONE

OUTSIDE SURFACE REF		INSIDE SURFACE	
X_A	Y	M_A +.010 -.000	N ±.010
8.985	.000	8.938	.000
8.983	.180	8.936	.178
8.975	.359	8.928	.356
8.962	.539	8.915	.535
8.932	.808	8.886	.802
8.856	1.257	8.810	1.247
8.745	1.706	8.700	1.693
8.598	2.155	8.554	2.138
8.412	2.603	8.370	2.584
8.184	3.052	8.143	3.029
7.907	3.501	7.868	3.474
7.575	3.949	7.539	3.919
7.178	4.397	7.144	4.364
6.699	4.845	6.668	4.809
6.109	5.292	6.082	5.253
5.356	5.787	5.334	6.696
4.310	6.180	4.295	6.135
3.559	6.396	3.547	6.361
3.168	6.480	3.152	6.434
2.680	6.559	2.673	6.513
2.376	6.594	2.370±.006	6.547

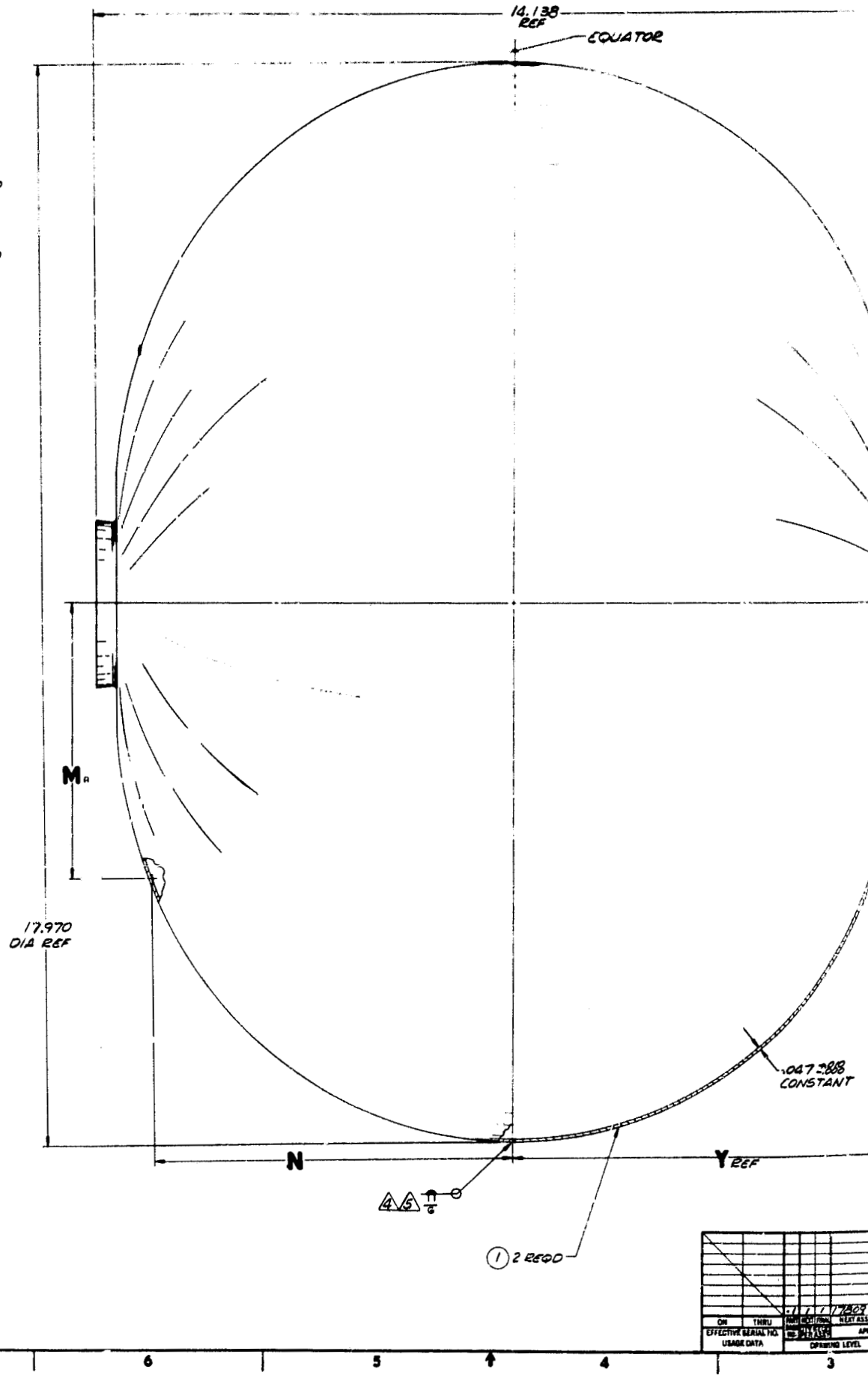

Metal Shell, 18-in.-dia GFR Inconel X-750 (STA) Tar

Fig 15-1

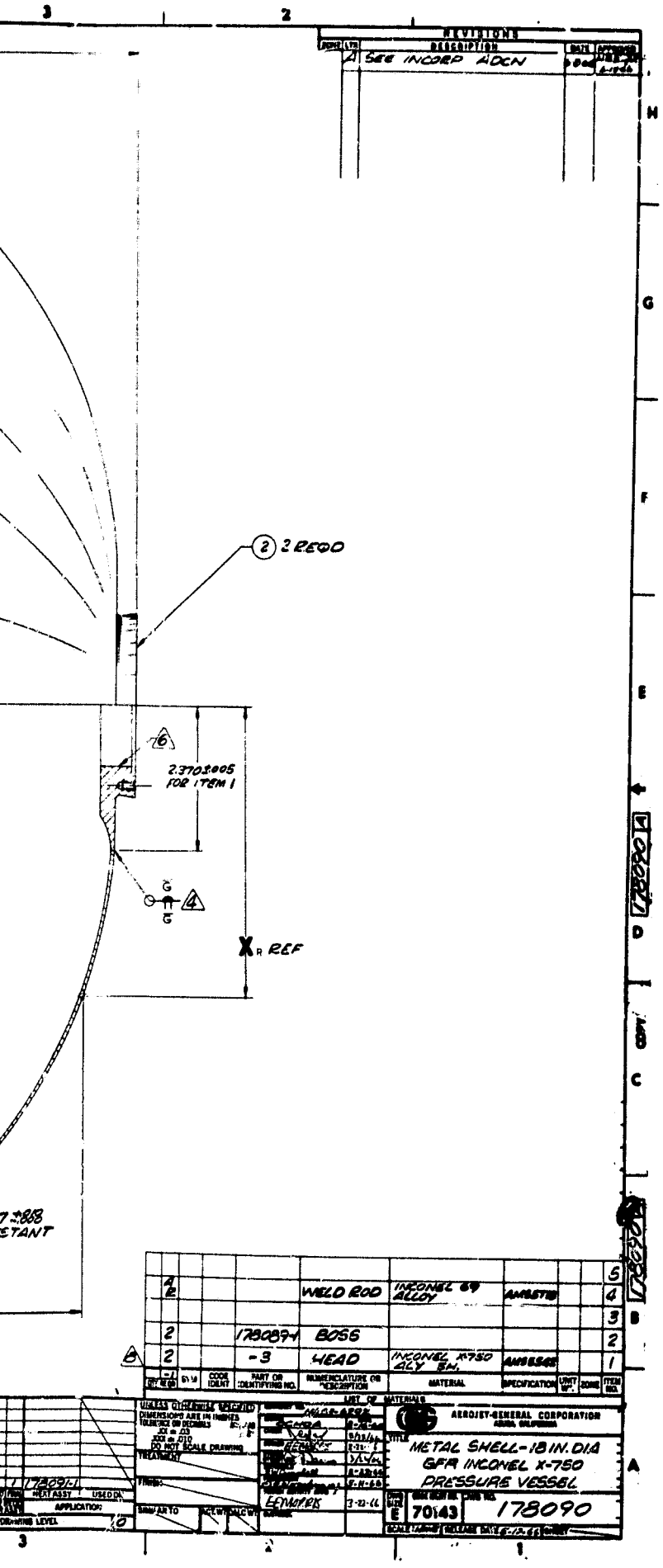

) Tank

Fig 15-2

Figure 15

NOTES:
1. REMOVE ALL BURRS AND SHARP EDGES
2. OVERWRAP METAL SHELL ASSY (ITEM 1) AS SPECIFIED IN ENGINEERING MANUFACTURING INSTRUCTIONS.
3. COAT ENTIRE SURFACE OF METAL SHELL ASSY (EXCEPT BOSSES) WITH .008 THICKNESS OF ITEM 7
4. GLASS FILAMENT MATERIAL SHALL BE S/WTS 20-END ROVING PURCHASED TO SPEC WS 1126B NOTICE 2 AND IMPREGNATED WITH EPOXY RESIN:
   EPON 828/DSA/EMPOL 1040/BDMA
   (100 / 1159 / 20 / 1)
   PER COGNIZANT ENGINEER.
5. WINDING PATTERN:
   A. ROVINGS PER TAPE: FOUR 20-END ROVINGS LOCATED SIDE BY SIDE TO GIVE 0.338 IN. TAPE WIDTH.
   B. LAYERS: 4 LAYERS UNIFORMLY DISTRIBUTED.
   C. NUMBER OF MANDREL REVOLUTIONS: 2
   D. WINDING ARM TURNS PER MANDREL REVOLUTION: 166 ± 5.
   E. TOTAL NUMBER OF WINDING ARM TURNS: 332 ± 10.
   F. TENSION: 10 ± 1 OZ. PER 20-END ROVING.
6. POSITION OF BOSS REINFORCEMENT (ITEM 2): POSITION ITEM 2 AT COMPLETION OF FIRST MANDREL REVOLUTION (166 ± 5 TURNS).
7. RESIN CURE: 2 HRS AT 150°F
   4 HRS AT 300°F
8. SOURCE OF SUPPLY:
   WHITTAKER CORPORATION
   NARMCO RESEARCH & DEVELOPMENT DIVISION
   SAN DIEGO, CALIFORNIA.
9. MARK IN ACCORDANCE WITH ASD 5215 H WITH 178091-1.
10. SUGGESTED SOURCE OF SUPPLY:
    EMERY INDUSTRIES, LOS ANGELES, CALIF.
11. SUGGESTED SOURCE OF SUPPLY:
    GREAT WESTERN CHEMICAL CO.,
    LOS ANGELES, CALIF.
12. IN LIST OF MATERIALS "B" IN SYMBOL COLUMN DENOTES BULK ITEMS.

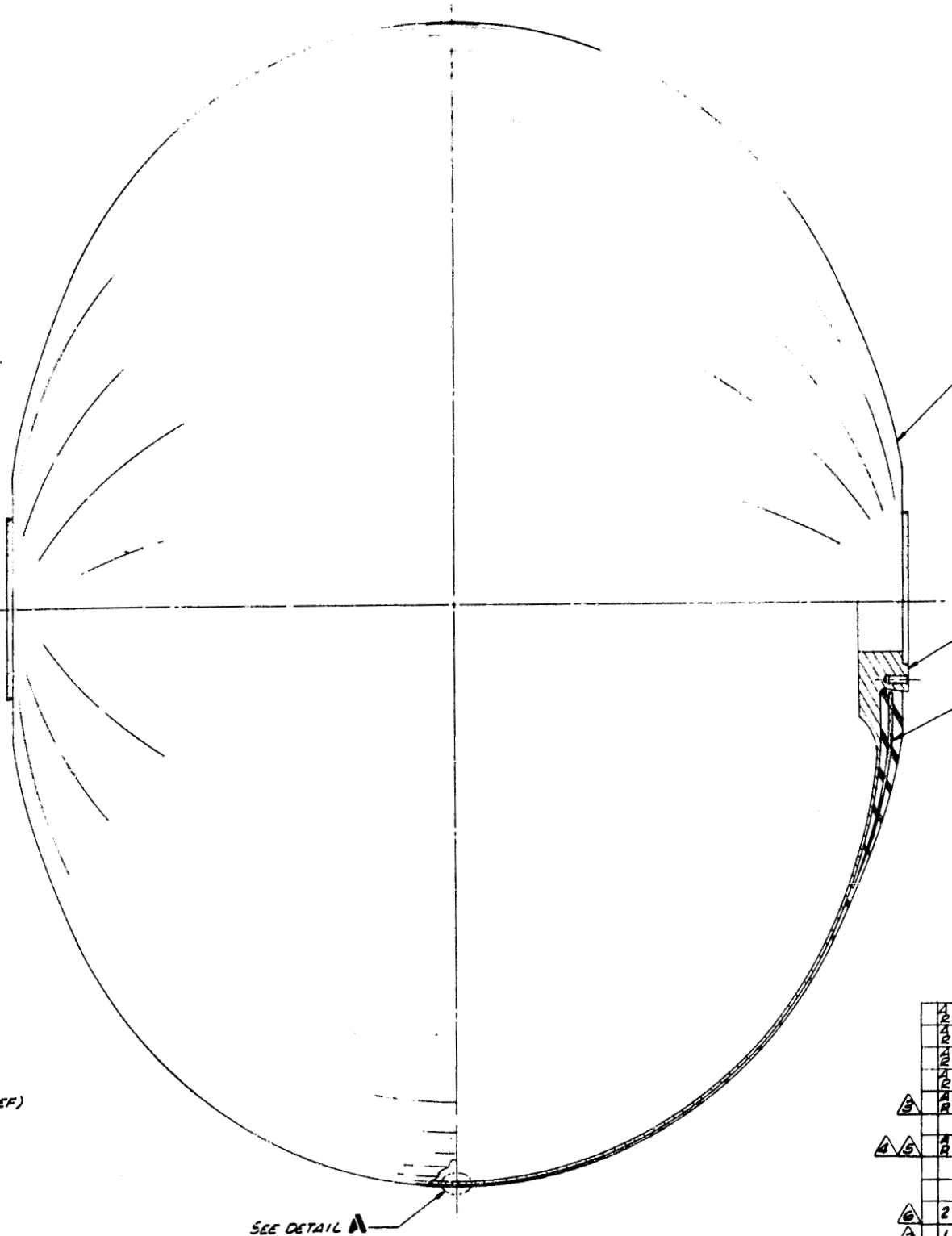

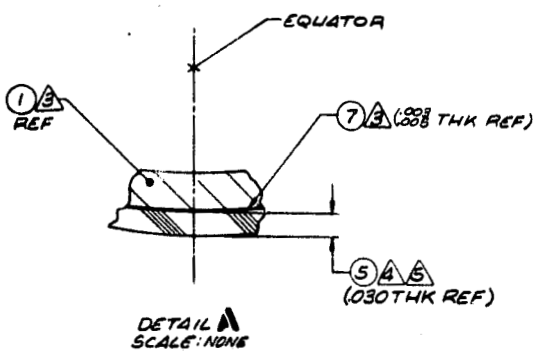

DETAIL A
SCALE: NONE

Initial Design, 18-in.-dia GFR Inconel X-750 (STA) Tank Assembly

Figure 16, Sheet 1

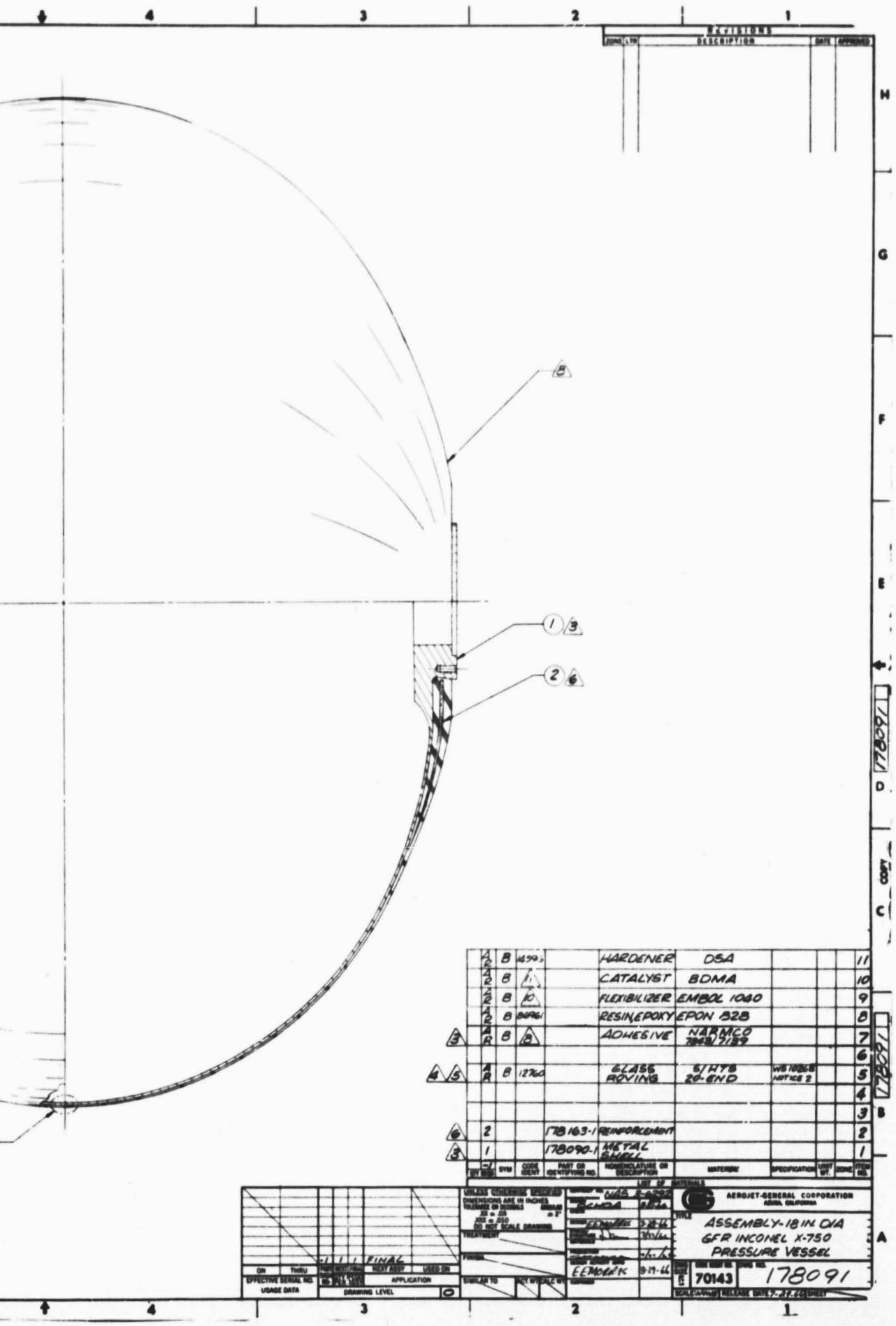

Inconel X-750 (STA) Tank Assembly

Figure 16, Sheet 1 of 2

NOTES:
1. REMOVE ALL BURRS AND SHARP EDGES

2 OVERWRAP METAL SHELL ASSY (ITEM 1) AS SPECIFIED IN ENGINEERING MANUFACTURING INSTRUCTIONS.

3 COAT ENTIRE SURFACE OF METAL SHELL ASSY (EXCEPT BOSSES) WITH UNIFORM THICKNESS OF RESIN SPECIFIED IN 4

4 GLASS FILAMENT MATERIAL SHALL BE S/HTS 20-END ROVING PURCHASED TO SPEC MIL 1126B NOTICE 2 AND IMPREGNATED WITH EPOXY RESIN:
EPON 828/DSA/EMPOL 1020/BDMA
(100 / 1159 / 20 / 1)
PER COGNIZANT ENGINEER.

5 WINDING PATTERN:
- A. ROVINGS PER TAPE: FOUR 20-END ROVINGS LOCATED SIDE BY SIDE TO GIVE 0.338 IN. TAPE WIDTH.
- B. LAYERS: 4 LAYERS UNIFORMLY DISTRIBUTED
- C. NUMBER OF MANDREL REVOLUTIONS: 2
- D. WINDING ARM TURNS PER MANDREL REVOLUTION: 166 ± 5.
- E. TOTAL NUMBER OF WINDING ARM TURNS: 332 ± 10.
- F. TENSION: 10 ± 1 LB. PER 20-END ROVING.

6 POSITION OF BOSS REINFORCEMENTS (ITEMS 2 & 3):
POSITION ITEM 3 AGAINST METAL LINER @ POSITION ITEM 2 AT COMPLETION OF FIRST MANDREL REVOLUTION (166 ± 5 TURNS)

7 RESIN CURE: 2 HRS AT 150°F
4 HRS AT 300°F

8 IN LIST OF MATERIALS "B" IN SYMBOLS COLUMN DENOTES BULK ITEMS.

9 MARK IN ACCORDANCE WITH ASD 5215 H WITH 178091-1.

10 SUGGESTED SOURCE OF SUPPLY:
EMBEY INDUSTRIES, LOS ANGELES, CALIF.

11 SUGGESTED SOURCE OF SUPPLY:
GREAT WESTERN CHEMICAL CO.
LOS ANGELES, CALIF.

DETAIL A
SCALE: NONE

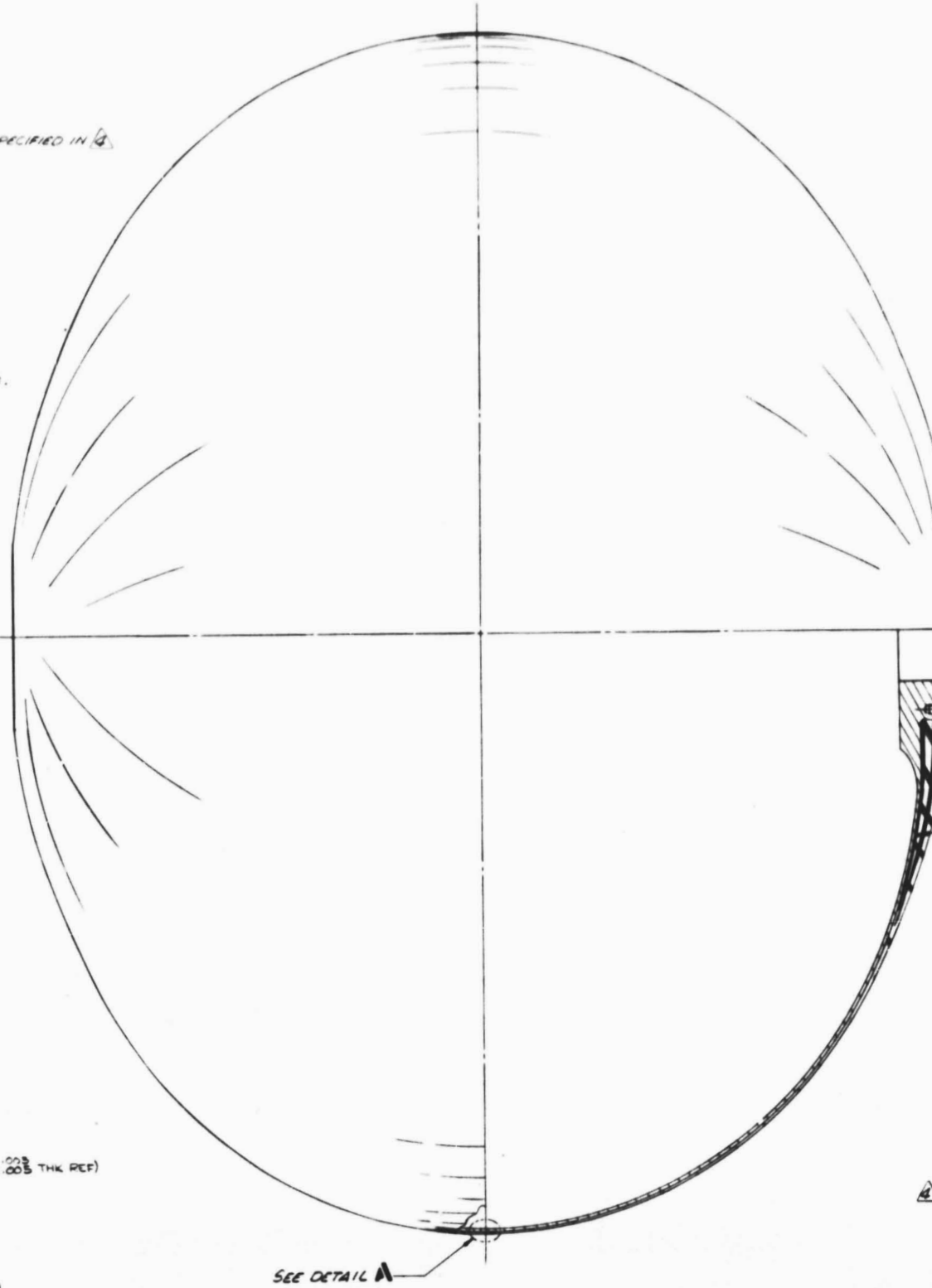

Final Design, 18-in.-dia GFR Inconel X-750 (STA) Tank Ass

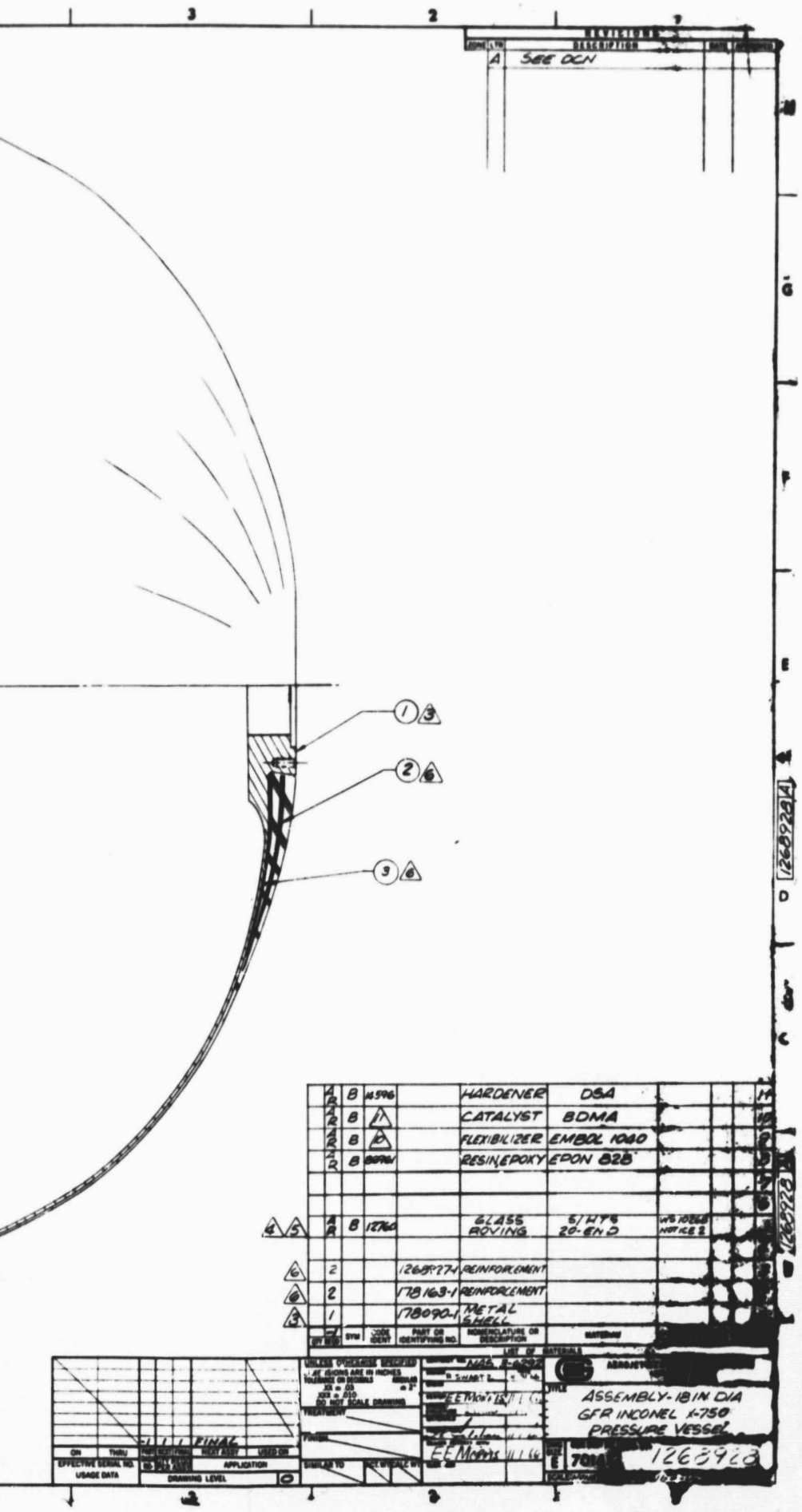

750 (STA) Tank Assembly

Figure 16, Sheet

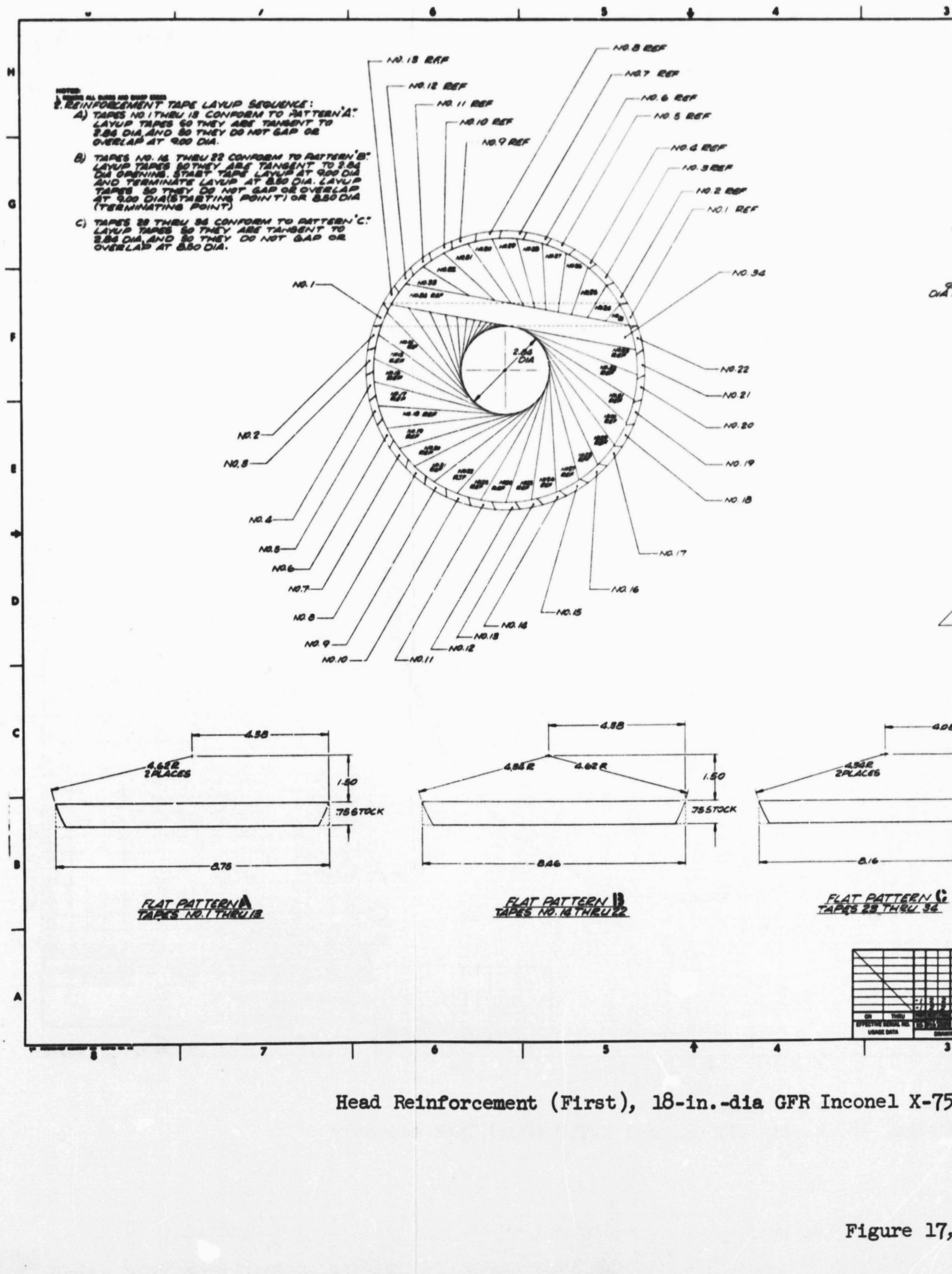

Head Reinforcement (First), 18-in.-dia GFR Inconel X-75

Figure 17,

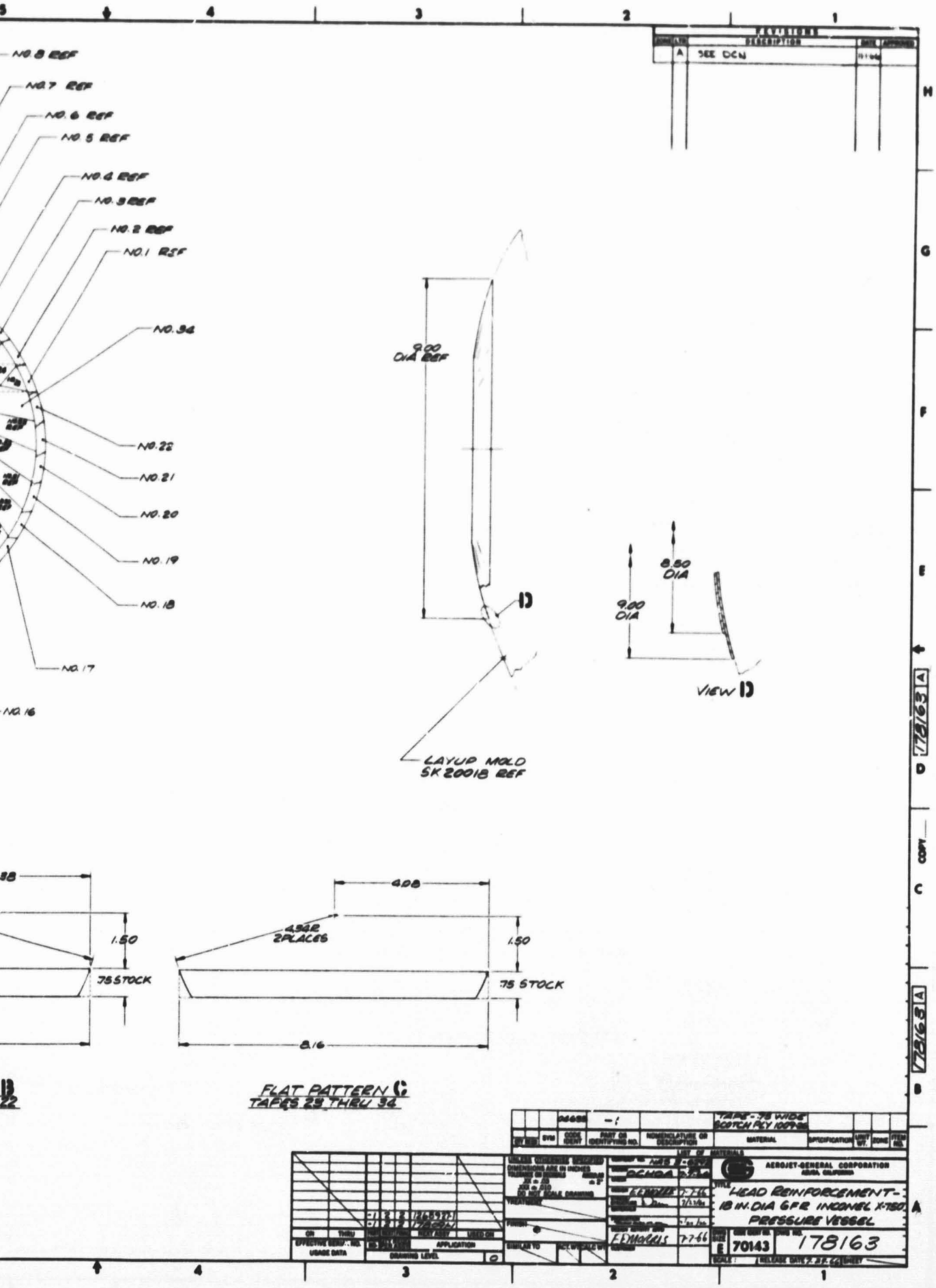

), 18-in.-dia GFR Inconel X-750 (STA) Tank

Figure 17, Sheet 1 of 2

NOTES:
1. REMOVE ALL BURRS AND SHARP EDGES
2. REINFORCEMENT TAPE LAYUP SEQUENCE:
   A) TAPES NO. 1 THRU 13 CONFORM TO PATTERN "A". LAYUP TAPES SO THEY ARE TANGENT TO 2.84 DIA. AND SO THEY DO NOT GAP OR OVERLAP AT 9.00 DIA.
   B) TAPES NO. 14 THRU 22 CONFORM TO PATTERN "B". LAYUP TAPES SO THEY ARE TANGENT TO 2.84 DIA. OPENING. START TAPE LAYUP AT 9.00 DIA. AND TERMINATE LAYUP AT 8.50 DIA. LAYUP TAPES SO THEY DO NOT GAP OR OVERLAP AT 9.00 DIA (STARTING POINT) OR 8.50 DIA. (TERMINATING POINT).
   C) TAPES 28 THRU 34 CONFORM TO PATTERN "C". LAYUP TAPES SO THEY ARE TANGENT TO 2.84 DIA. AND SO THEY DO NOT GAP OR OVERLAP AT 8.50 DIA.

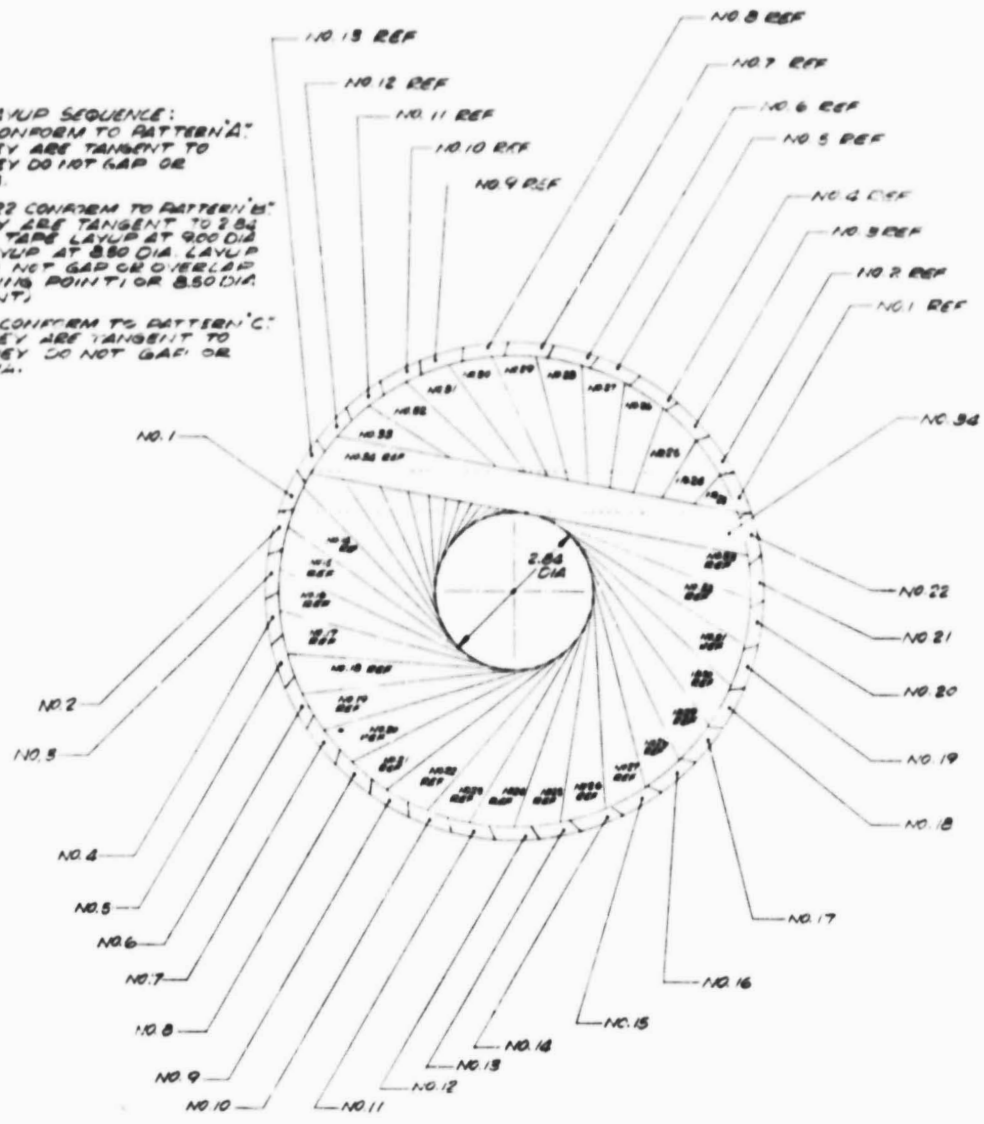

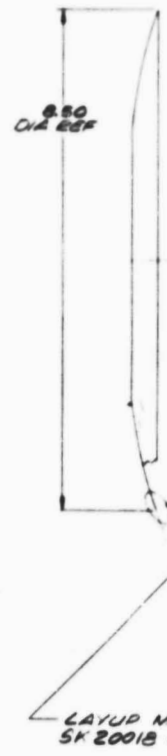

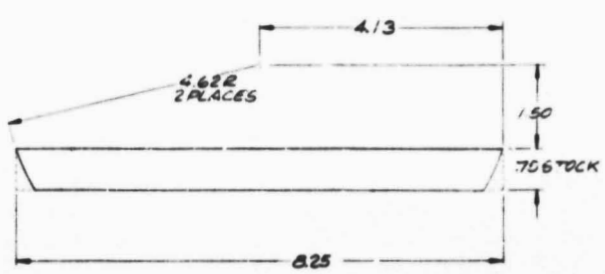

FLAT PATTERN A
TAPES NO. 1 THRU 13

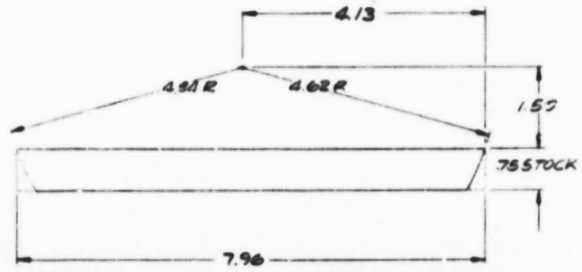

FLAT PATTERN B
TAPES NO. 14 THRU 22

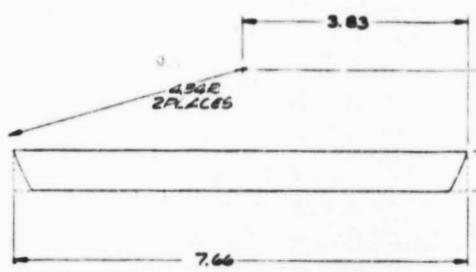

FLAT PATTERN C
TAPES 28 THRU 34

Head Reinforcement (Second), 18-in.-dia GFR Inconel X-750 (STA

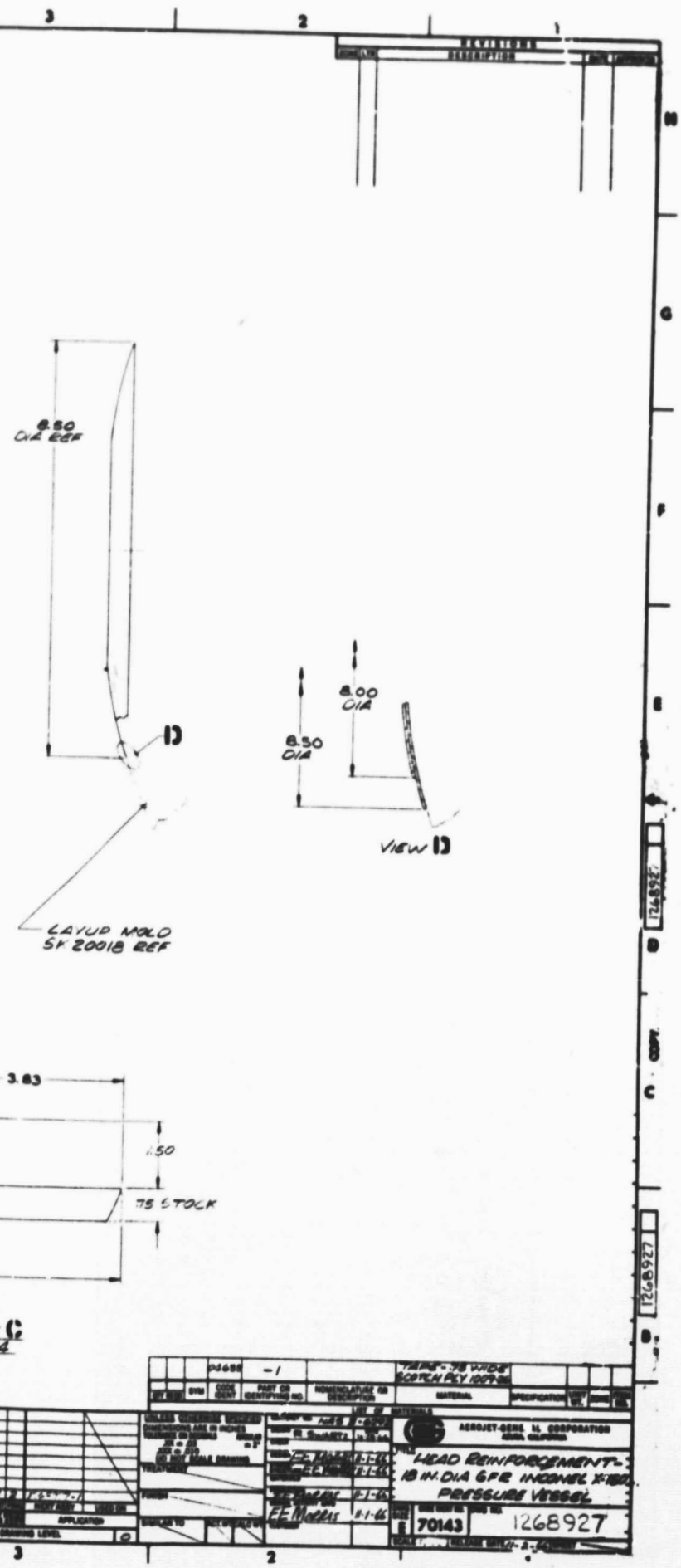

750 (STA) Tank

Figure 17, Sheet 2 of 2

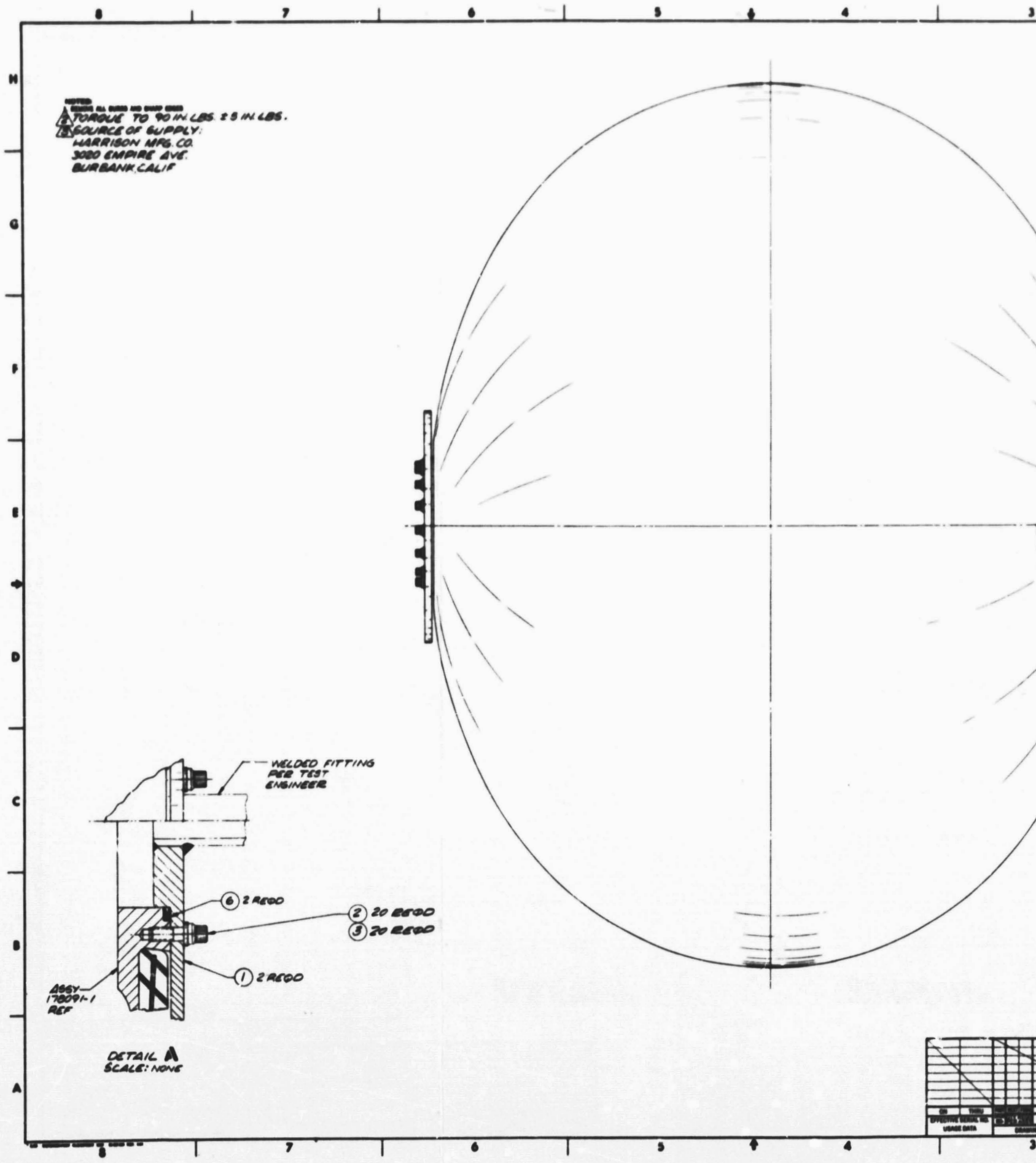

Test Assembly, 18-in.-dia CFR Inconel X-750 (STA) Ta

Figu

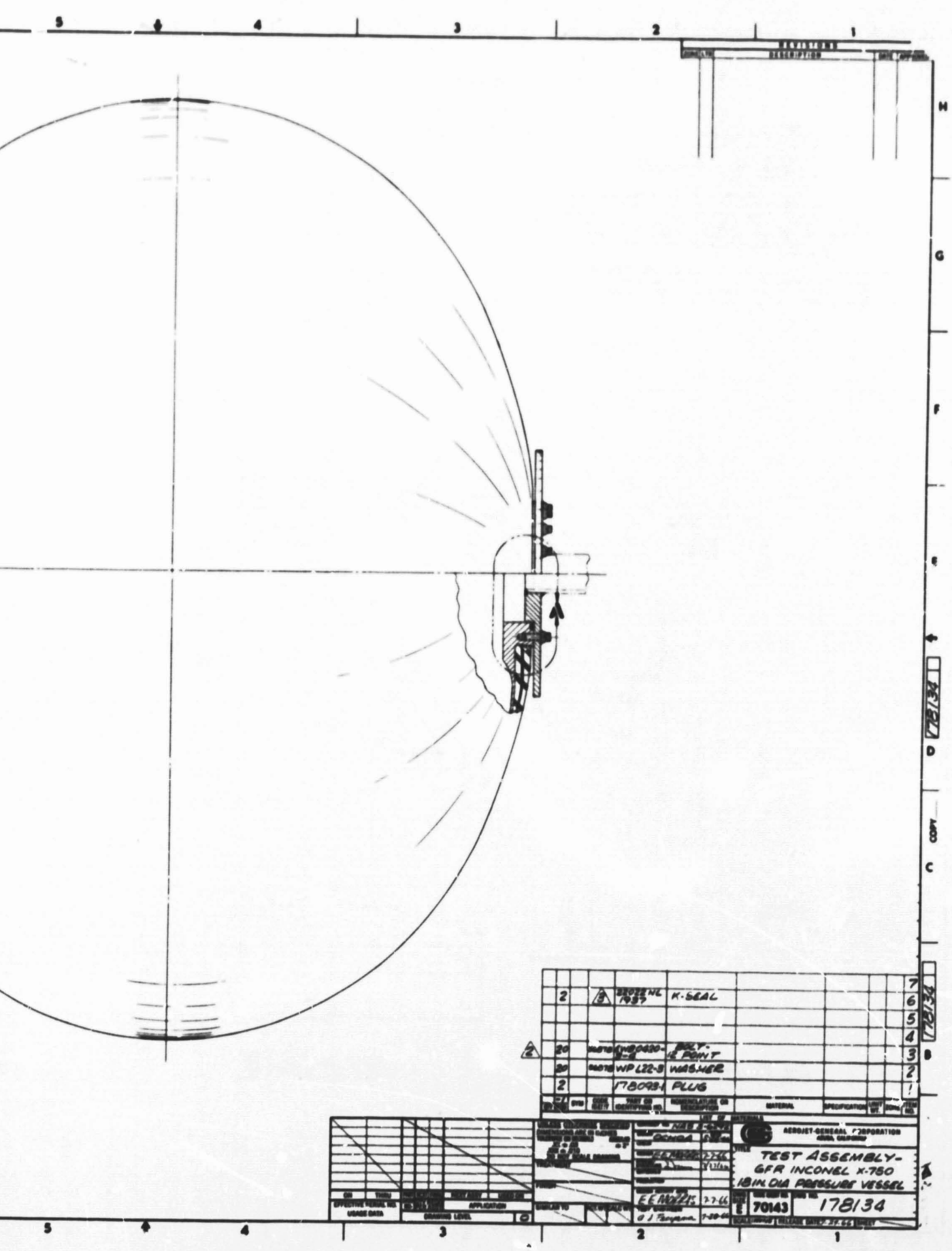

-in.-dia GFR Inconel X-750 (STA) Tank

Figure 18

EQUATOR OF HEADS AT Z = 1.0

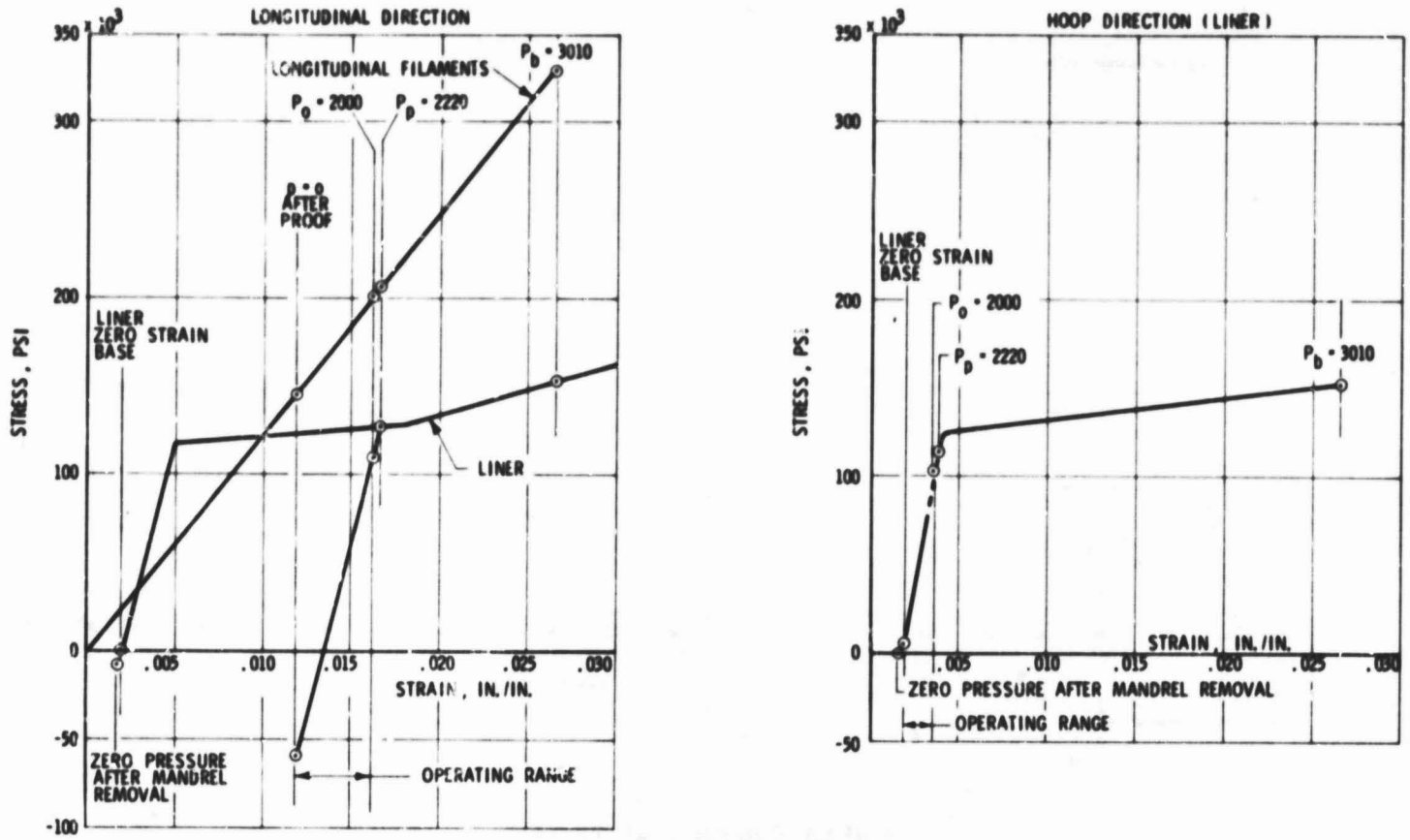

UP HEAD CONTOUR AT Z = 0.50

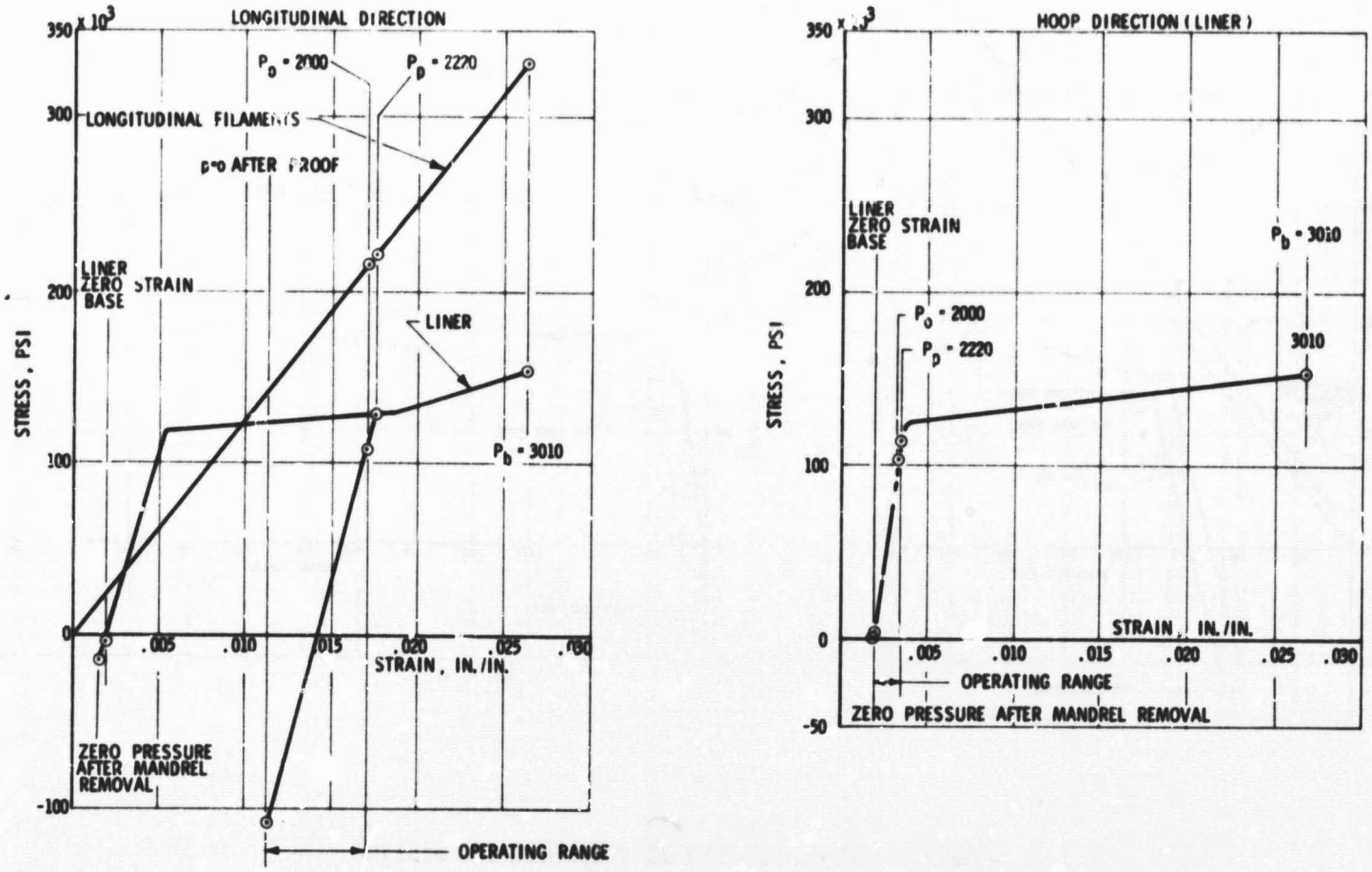

Room-Temperature Stress-Strain Relationships
(2220-psi Proof Pressure and 2000-psi Operating Pressure)

Figure 19

EQUATOR OF HEADS AT Z = 1.0

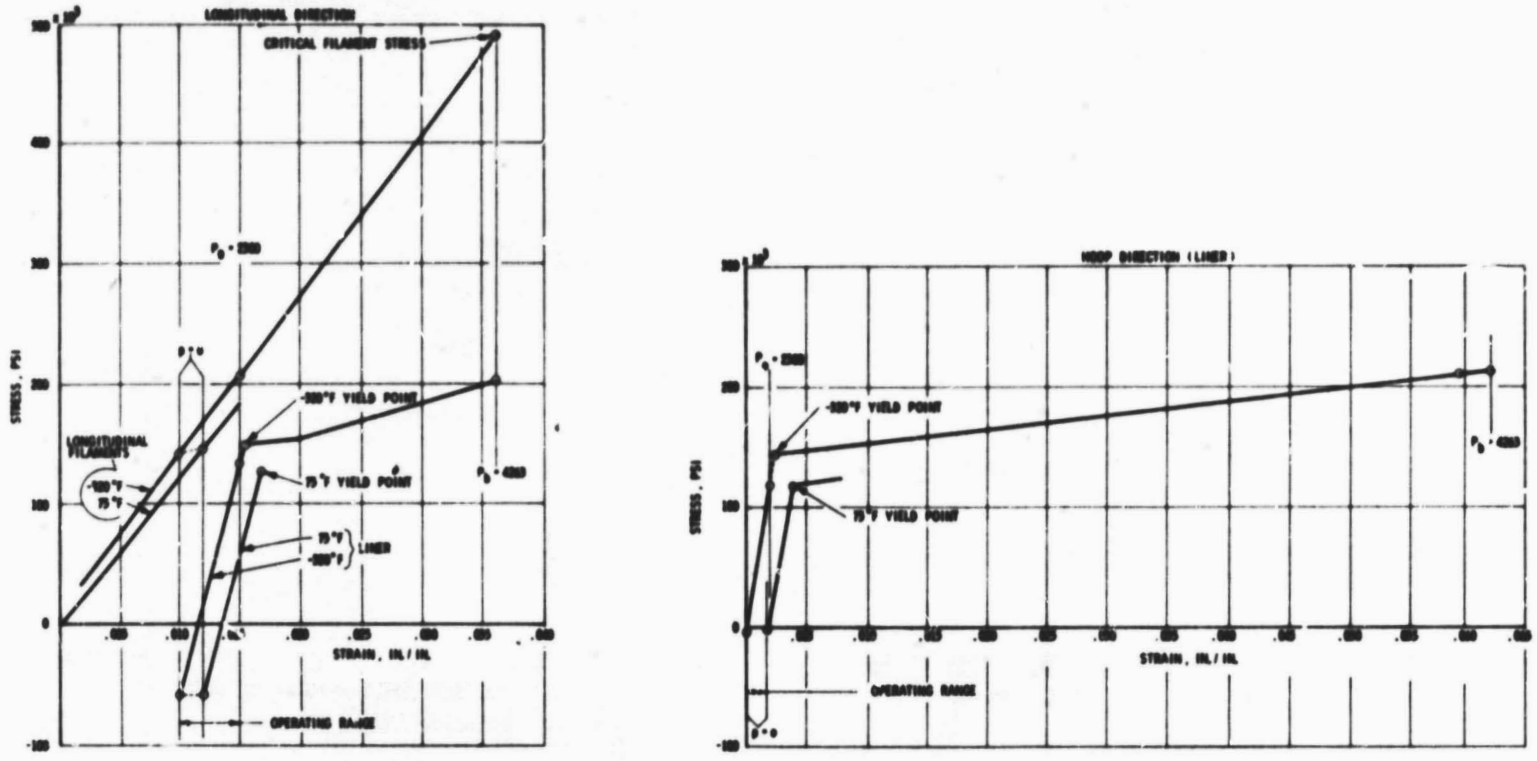

UP HEAD CONTOUR AT Z = 0.5

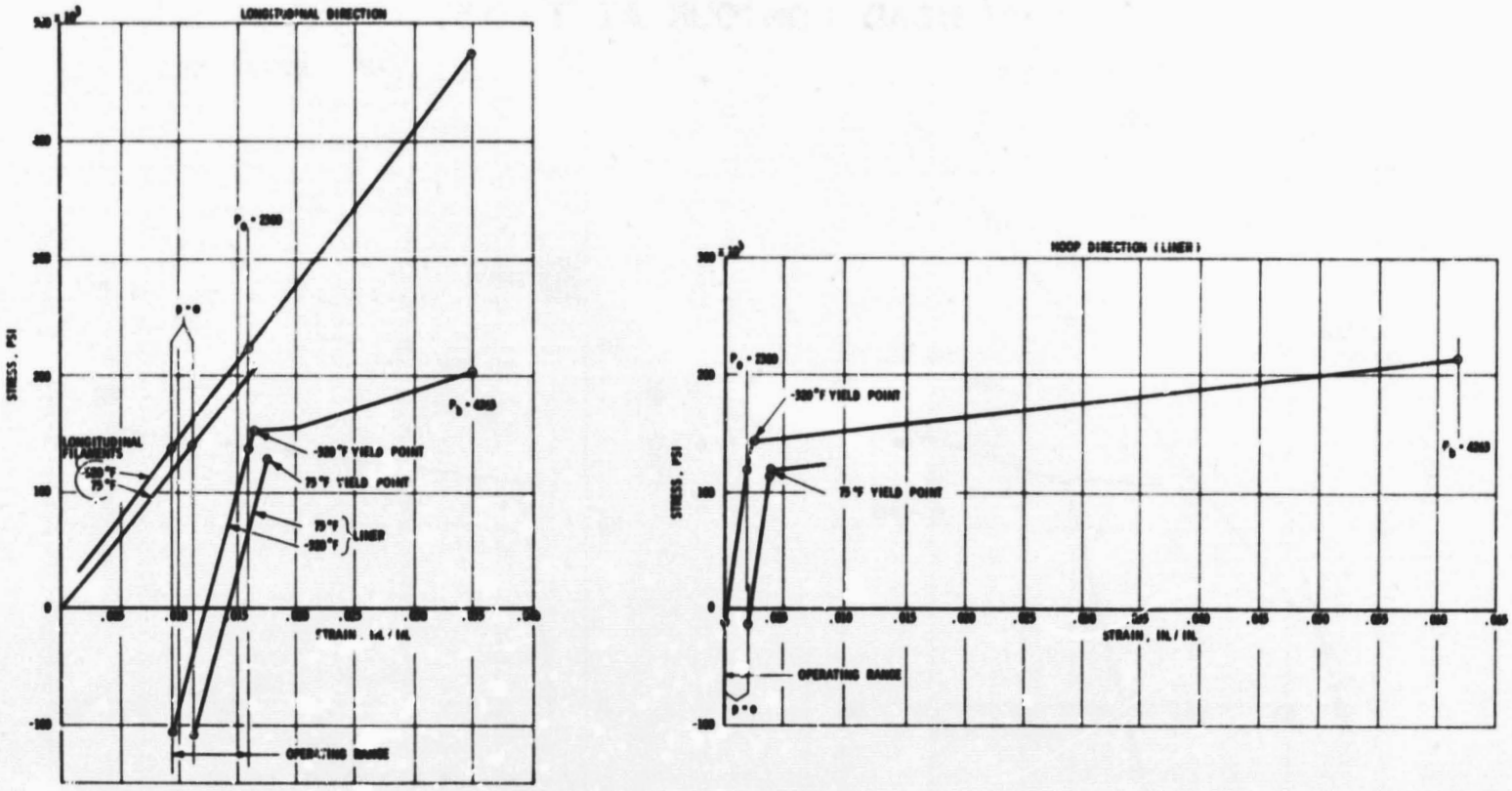

-320°F Stress-Strain Relationships
(2220-psi Proof Pressure at 75°F and 2300-psi Operating Pressure at -320°F)

Figure 20

EQUATOR OF HEADS AT Z = 1.0

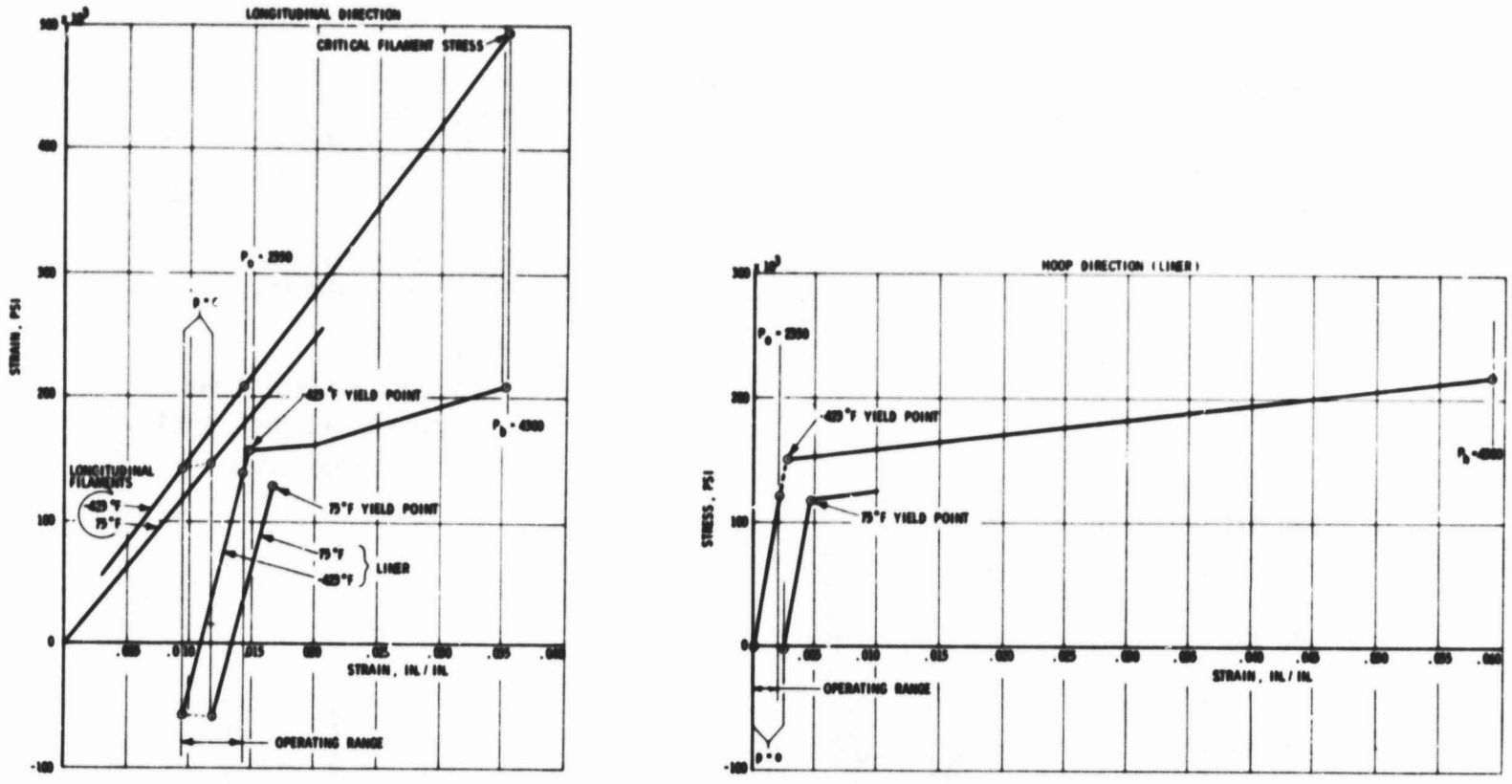

UP HEAD CONTOUR AT Z = 0.5

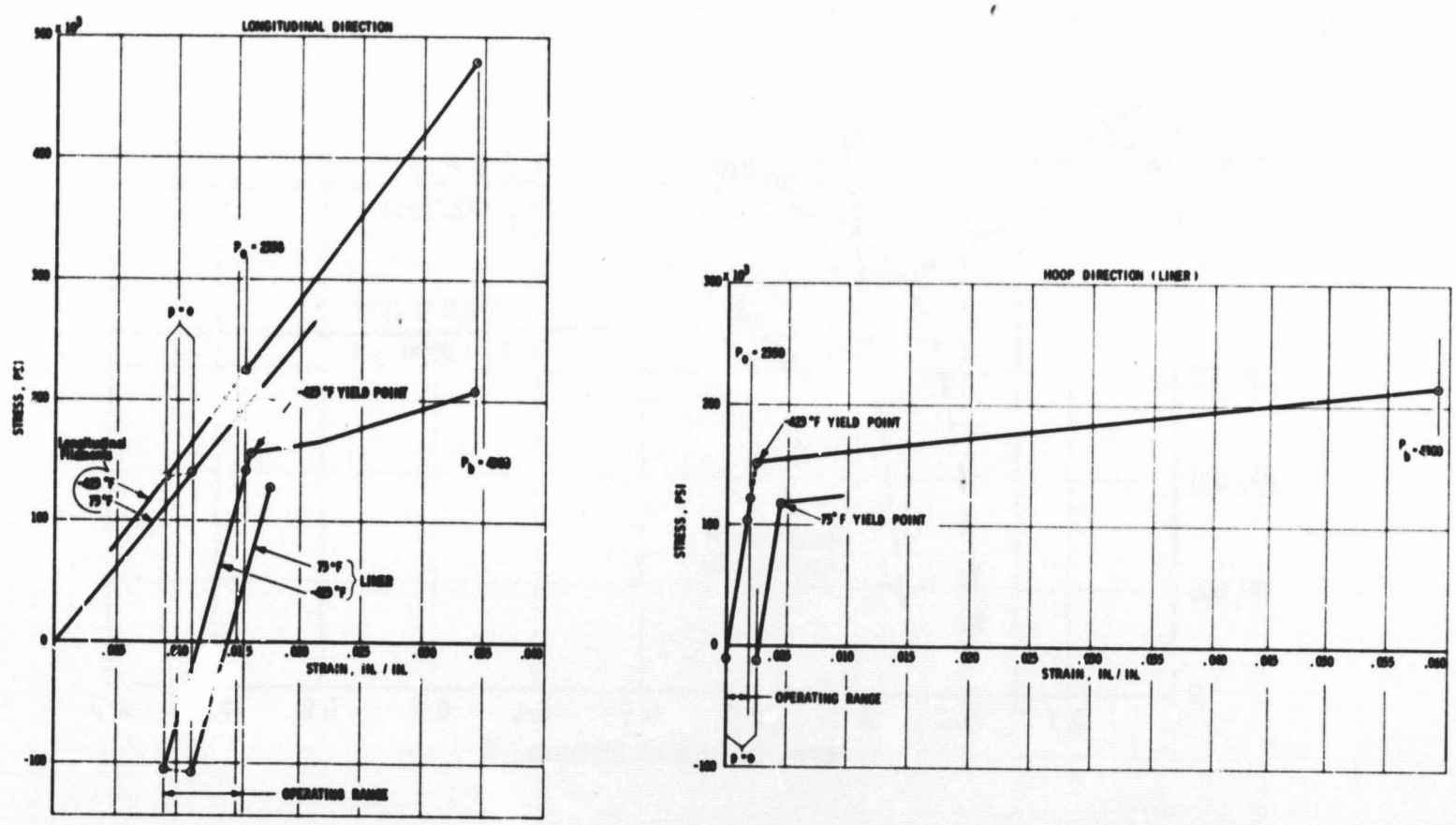

-423°F Stress-Strain Relationships
(2220-psi Proof Pressure at 75°F and 2350-psi Operating Pressure at -423°F)

Figure 21

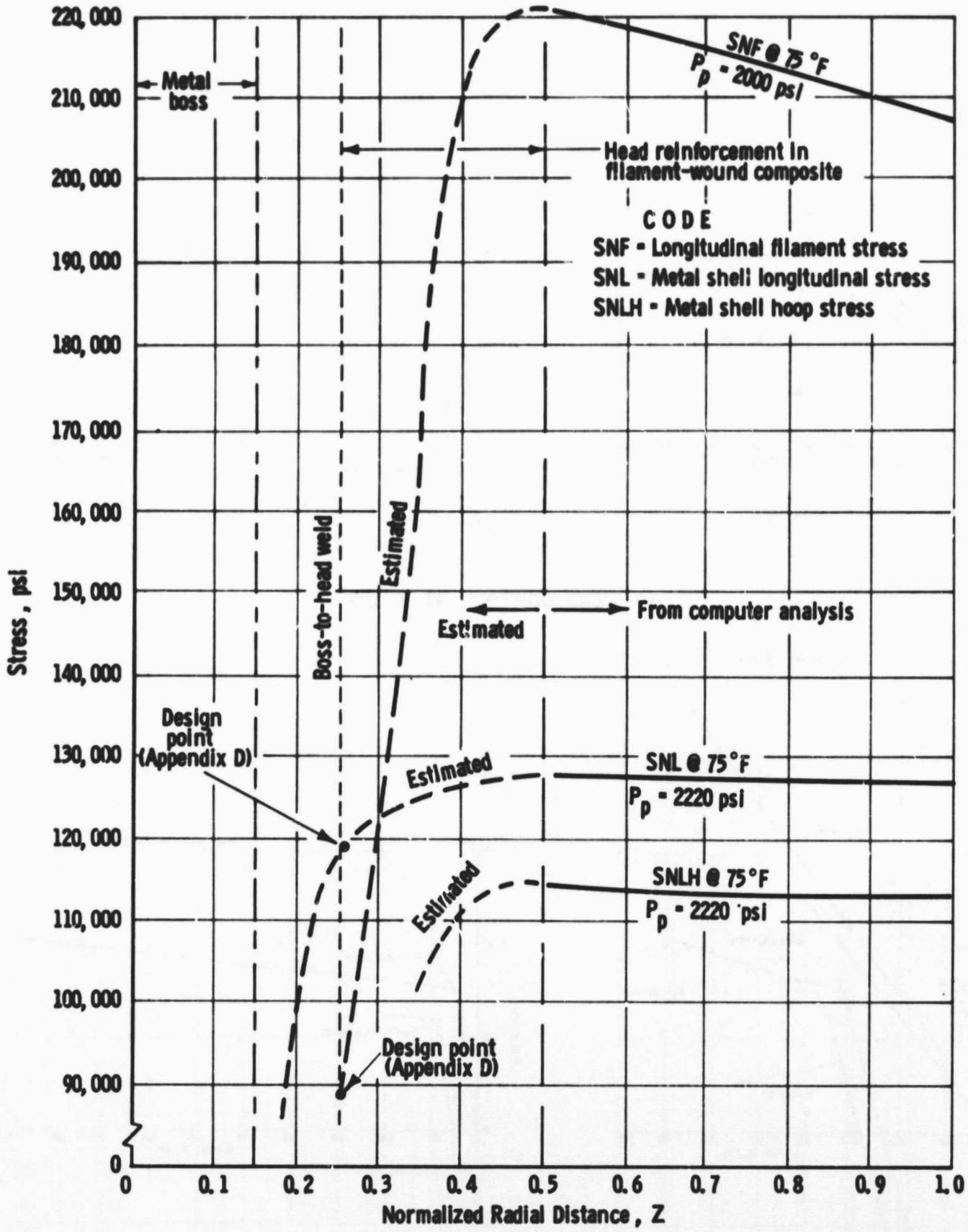

Head Stresses at 2220-psi Proof Pressure

Figure 22

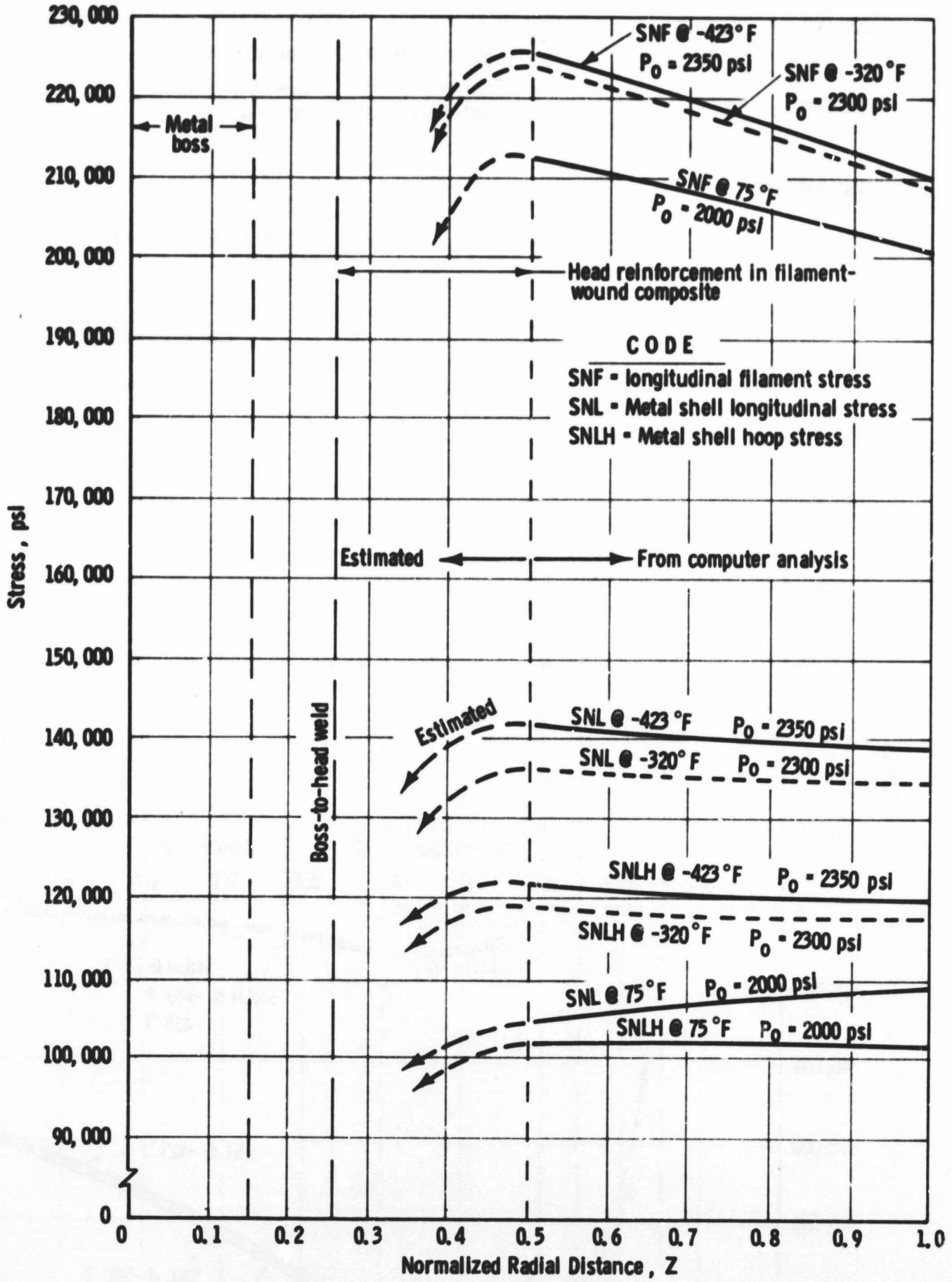

Head Stresses at Operating Pressure
(2220-psi Proof Pressure and 2000-psi Operating Pressure at 75°F)

Figure 23

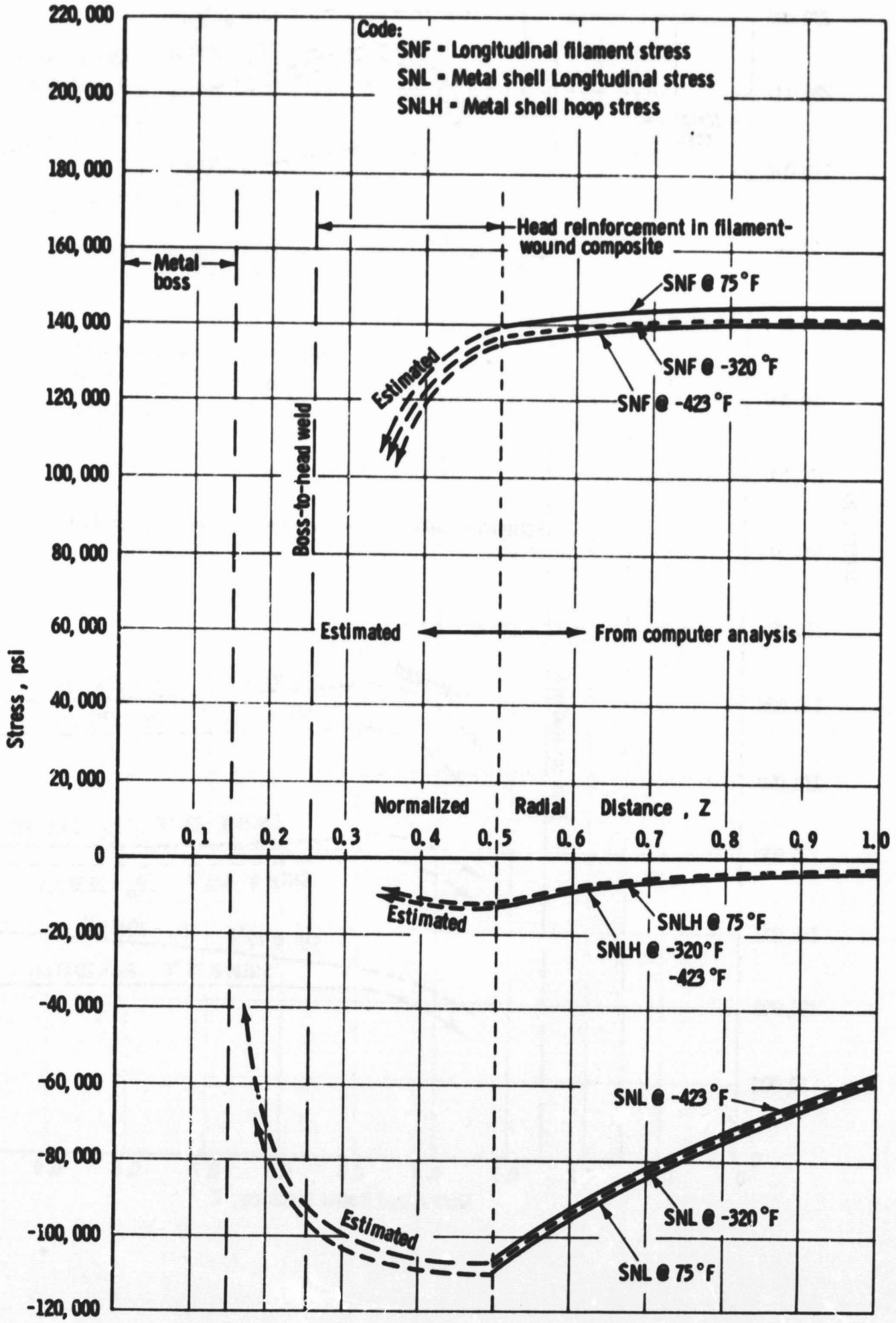

Head Stresses at Zero Pressure
(2220-psi Proof Pressure at 75°F)

Figure 24

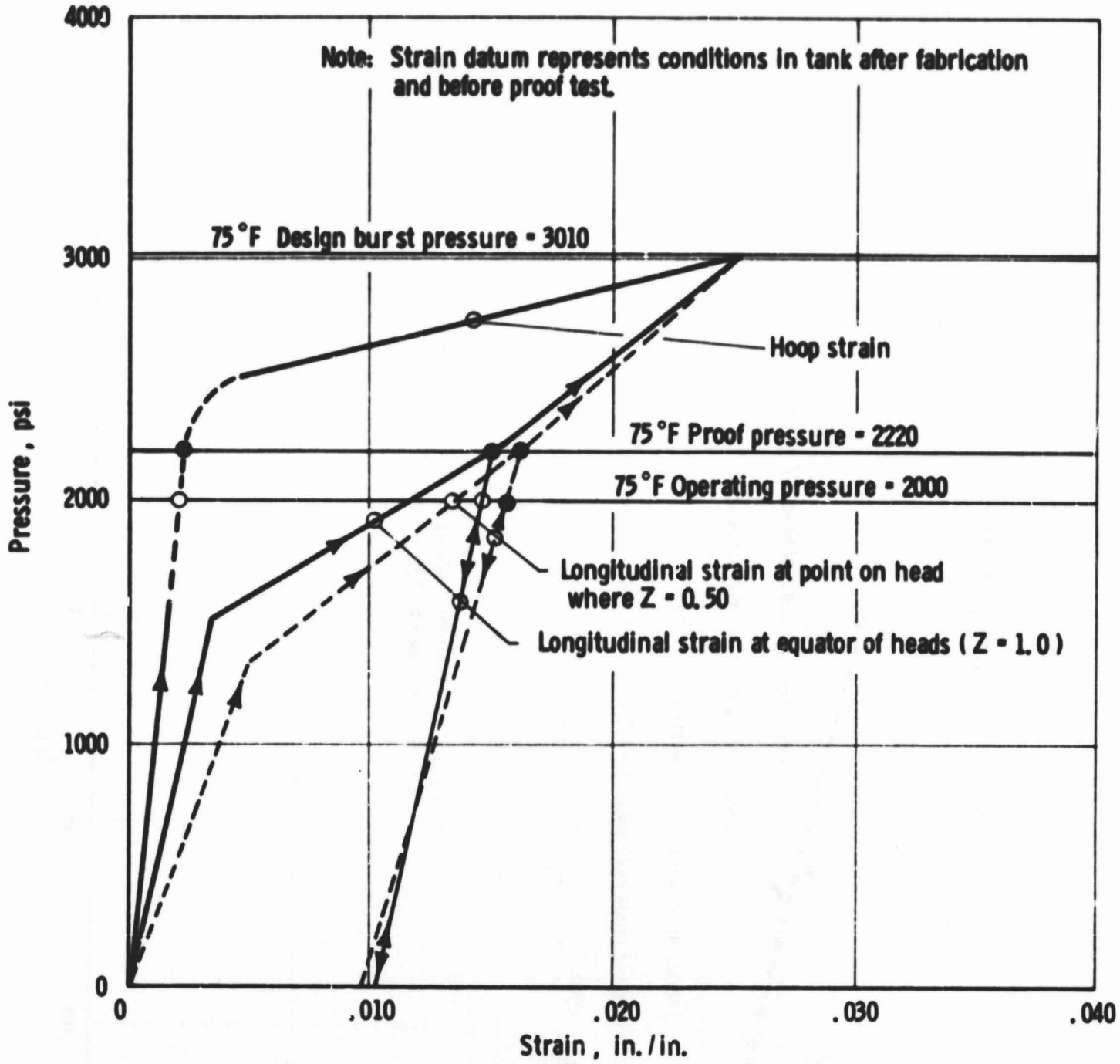

Tank Pressure vs Strain (75°F)

Figure 25

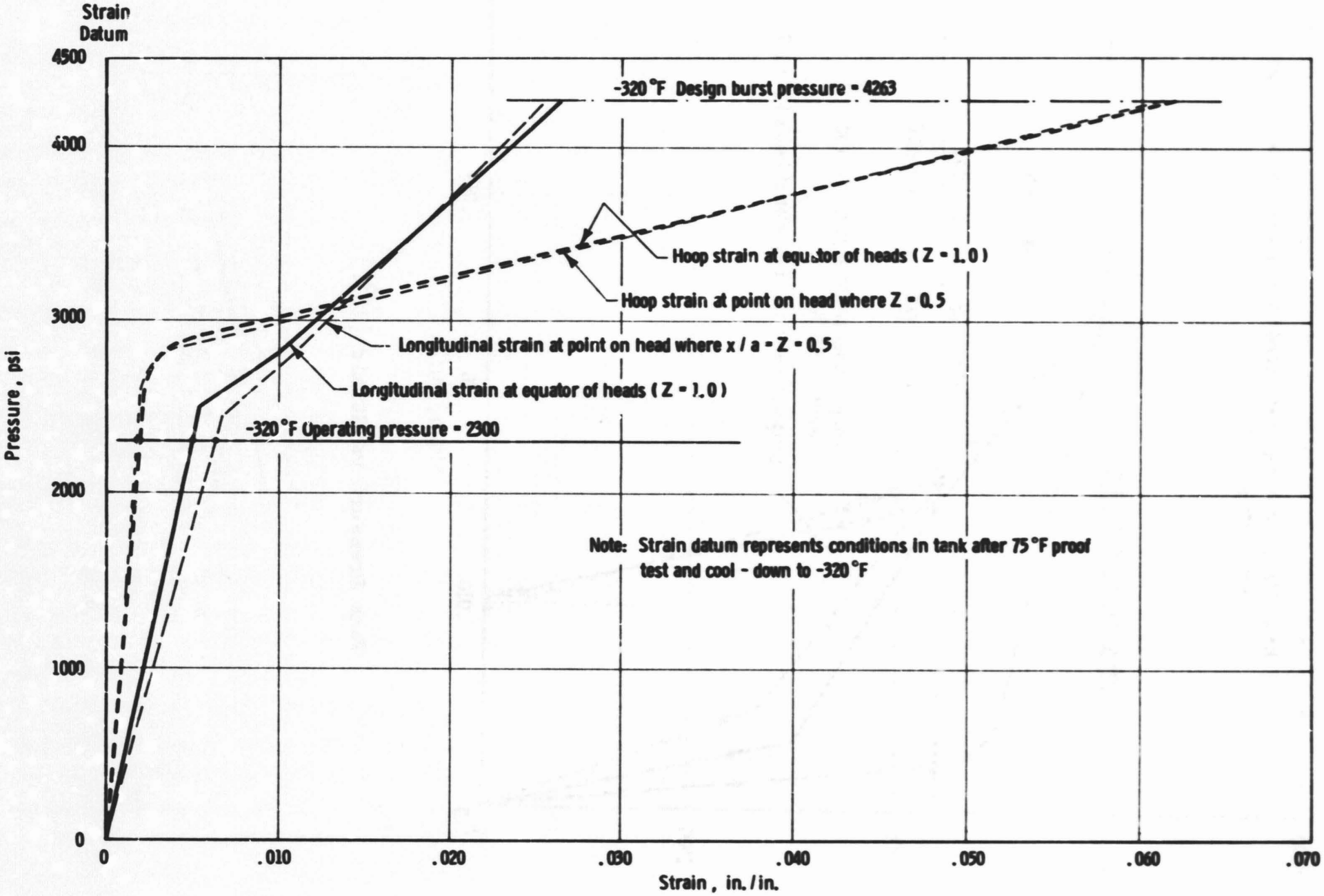

Tank Pressure vs Strain (-320°F)

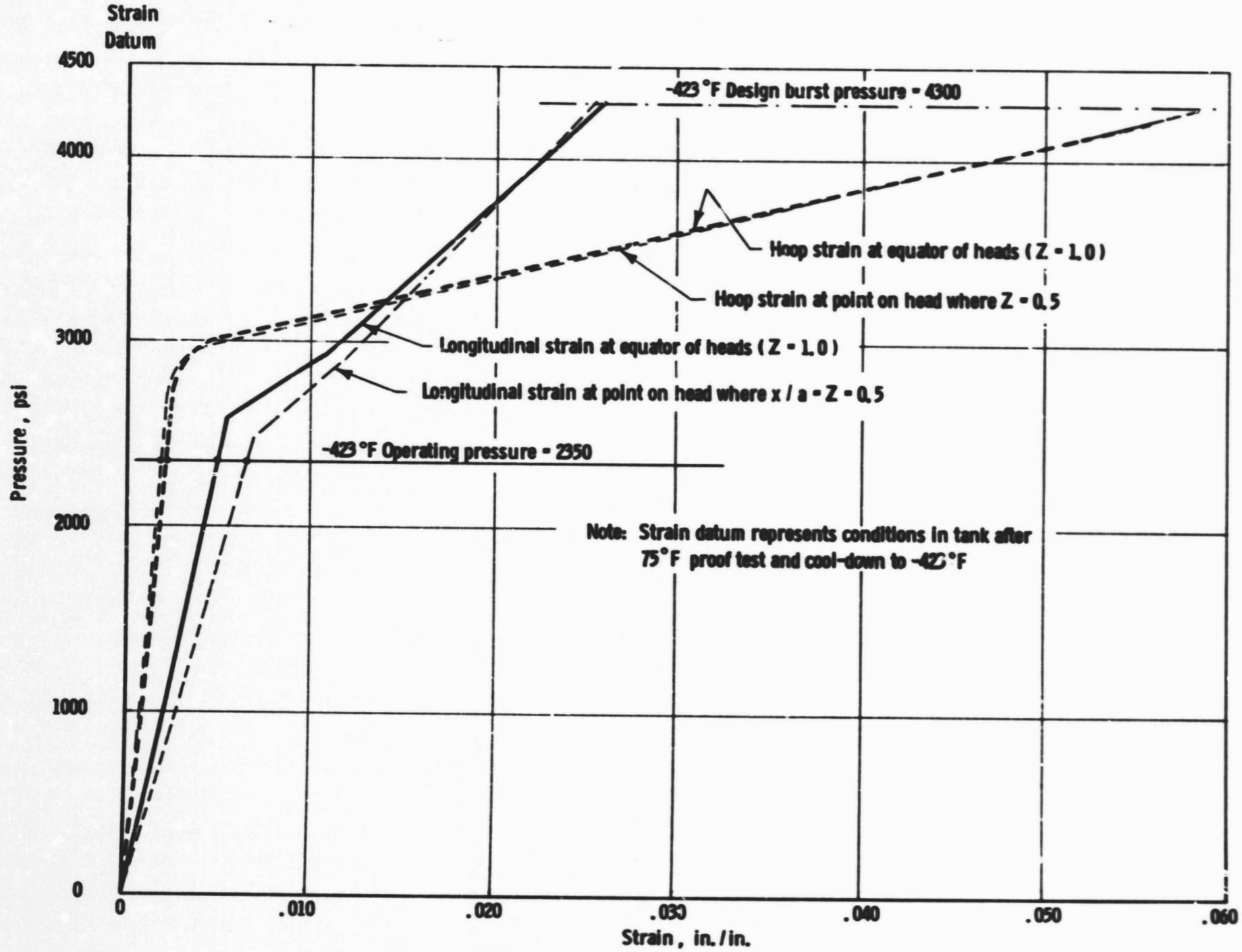

Figure 27

Tank Pressure vs Strain (-423°F)

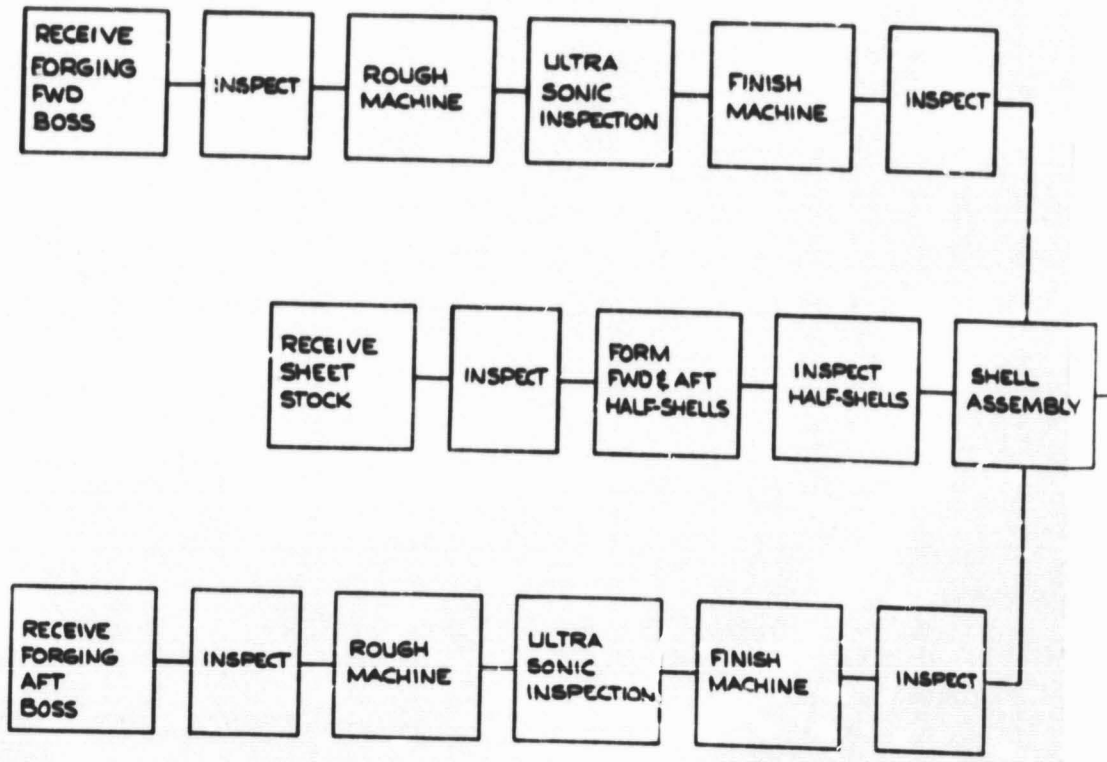
RECEIVE FORGING FWD BOSS
INSPECT
ROUGH MACHINE
ULTRA SONIC INSPECTION
FINISH MACHINE
INSPECT
RECEIVE SHEET STOCK
INSPECT
FORM FWD & AFT HALF-SHELLS
INSPECT HALF-SHELLS
SHELL ASSEMBLY
RECEIVE FORGING AFT BOSS
INSPECT
ROUGH MACHINE
ULTRA SONIC INSPECTION
FINISH MACHINE
INSPECT

Figure 28 - /

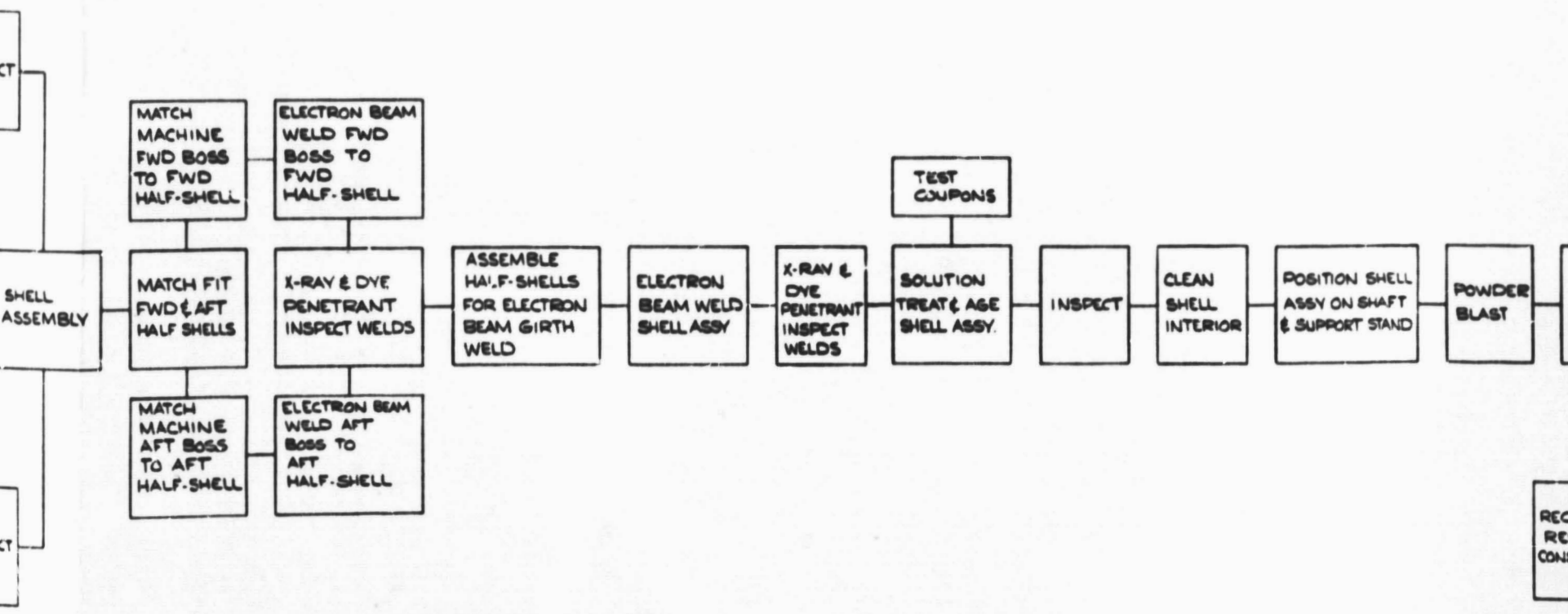

Manufacturing Flow Diagram for Tank

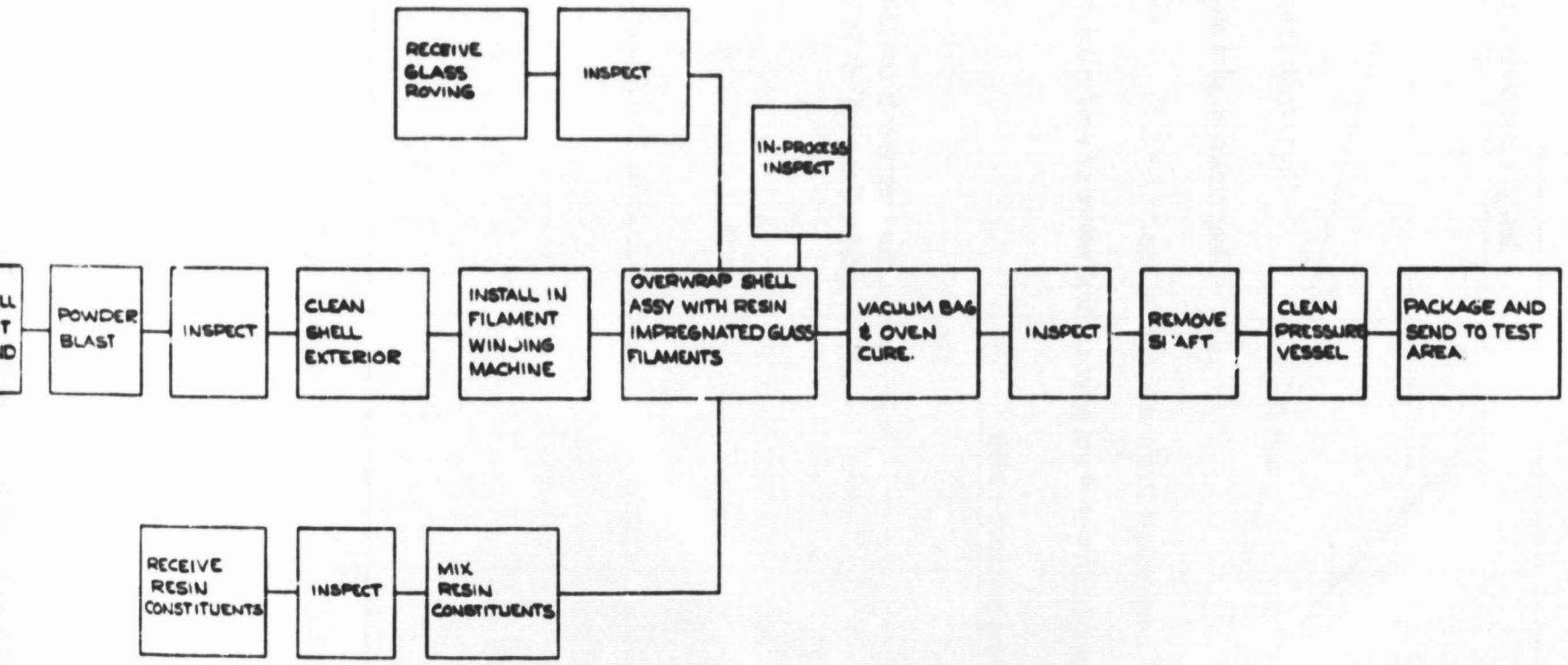
RECEIVE GLASS ROVING
INSPECT
IN-PROCESS INSPECT
POWDER BLAST
INSPECT
CLEAN SHELL EXTERIOR
INSTALL IN FILAMENT WINDING MACHINE
OVERWRAP SHELL ASSY WITH RESIN IMPREGNATED GLASS FILAMENTS
VACUUM BAG & OVEN CURE.
INSPECT
REMOVE SHAFT
CLEAN PRESSURE VESSEL
PACKAGE AND SEND TO TEST AREA
RECEIVE RESIN CONSTITUENTS
INSPECT
MIX RESIN CONSTITUENTS

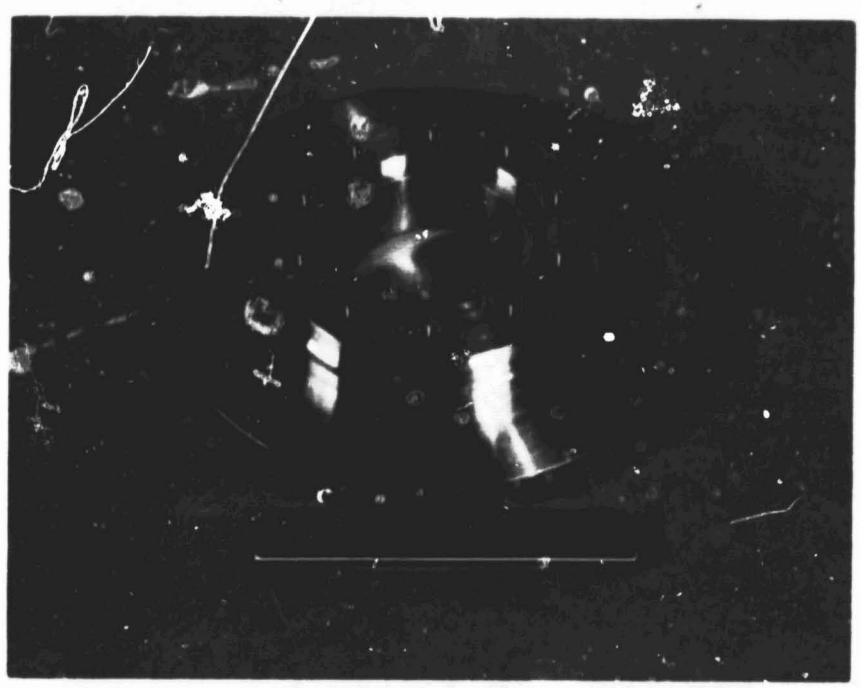

Fig. 29 Polar Boss

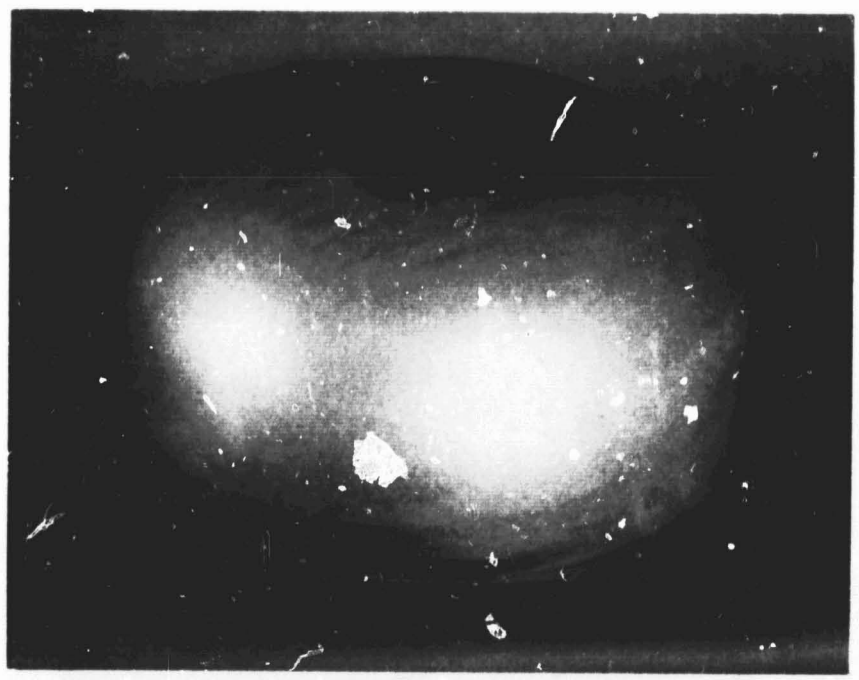

Fig. 30 18-in.-dia Formed Head

Figures 29 and 30

Fig. 31 Electron-Beam-Welding Machine

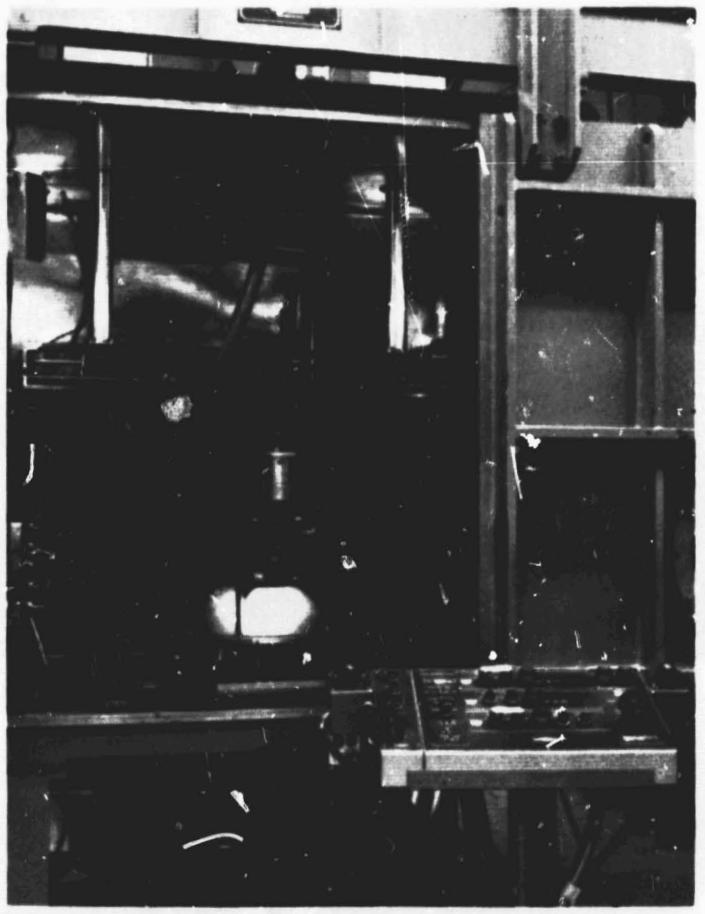

Fig. 32 Half Shell in Welding Chamber

Figures 31 and 32

Assembly of Formed Head and Polar Boss with Electron Gun in Position for Welding

Figure 33

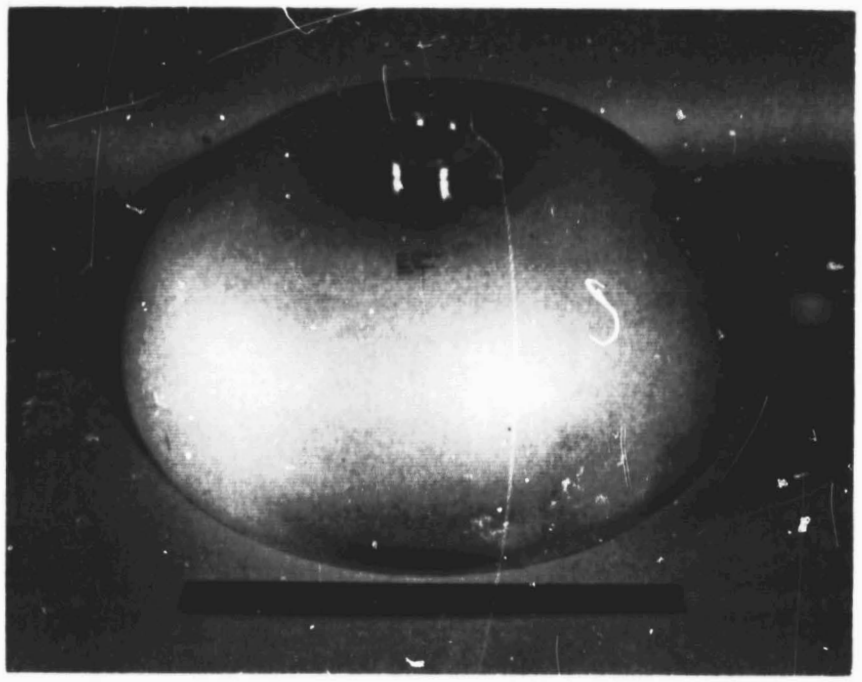

Fig. 34 Completed Half Shell, Exterior View

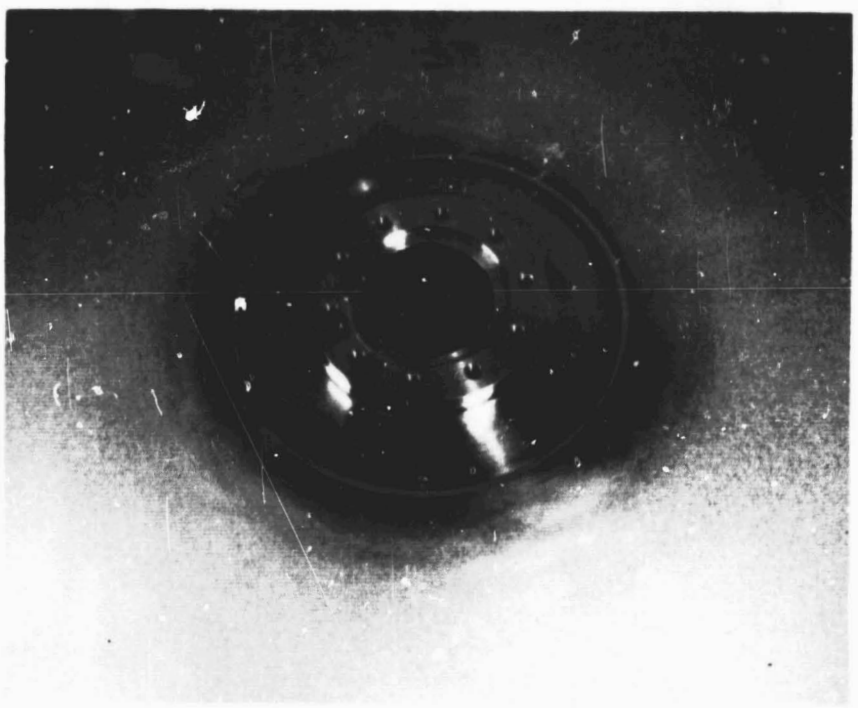

Fig. 35 Boss-to-Head Weld, Exterior View

Figures 34 and 35

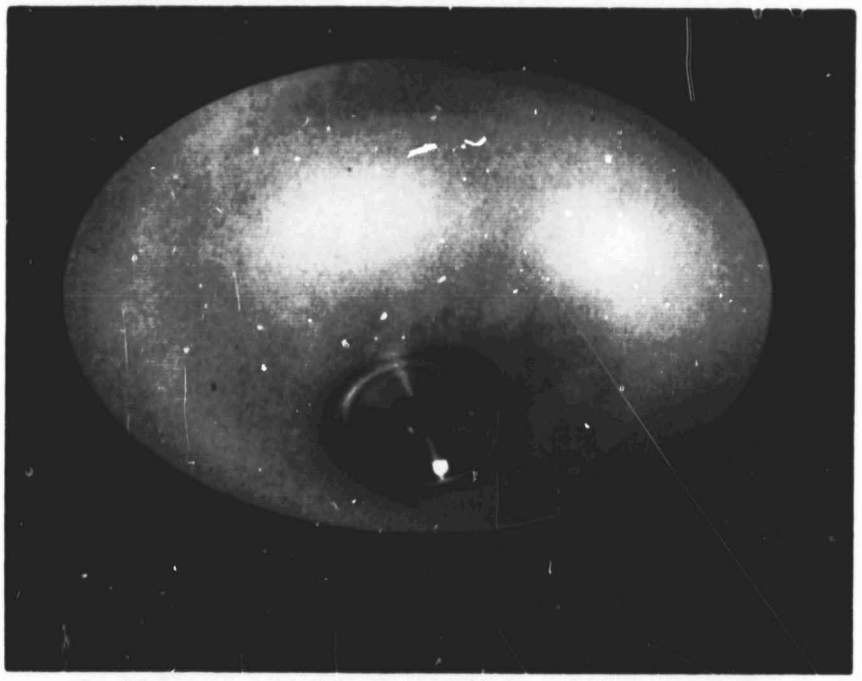

Fig. 36 Completed Half Shell, Interior View

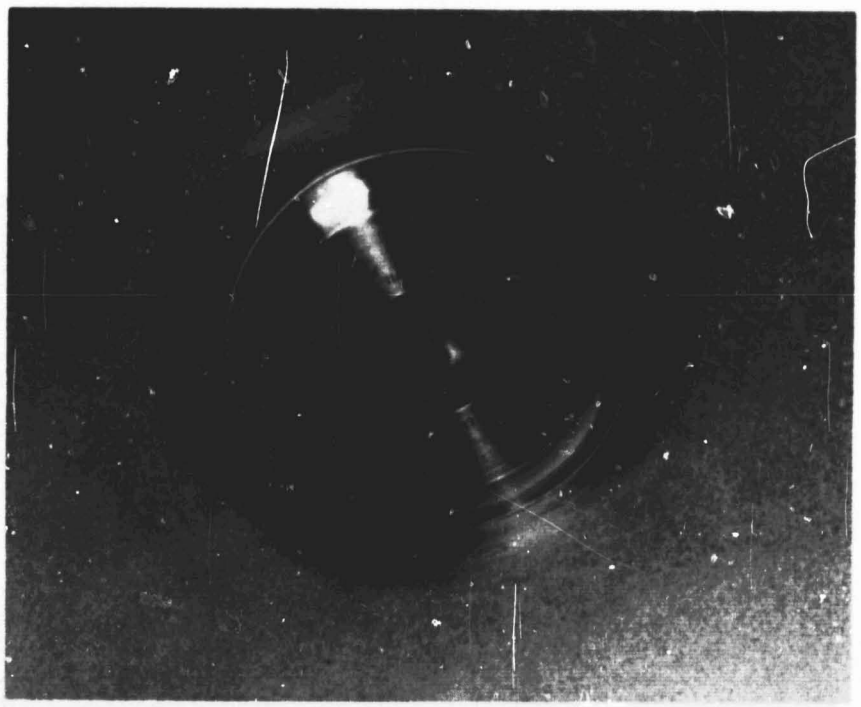

Fig. 37 Boss-to-Head Weld, Interior View

Figures 36 and 37

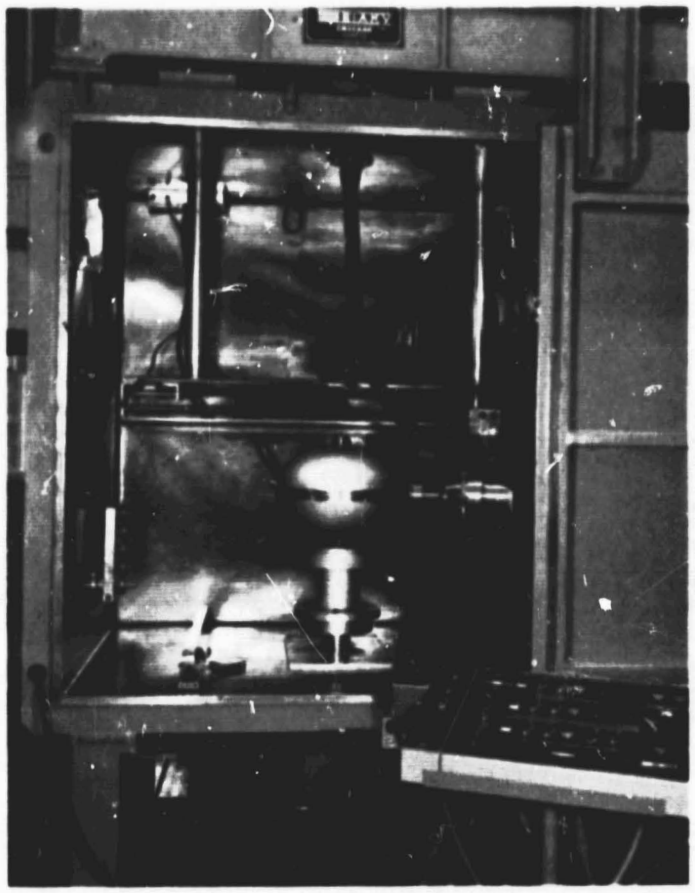

Fig. 38 Assembly of Two Half Sections in Welding Chamber with Electron Gun in Position for Welding

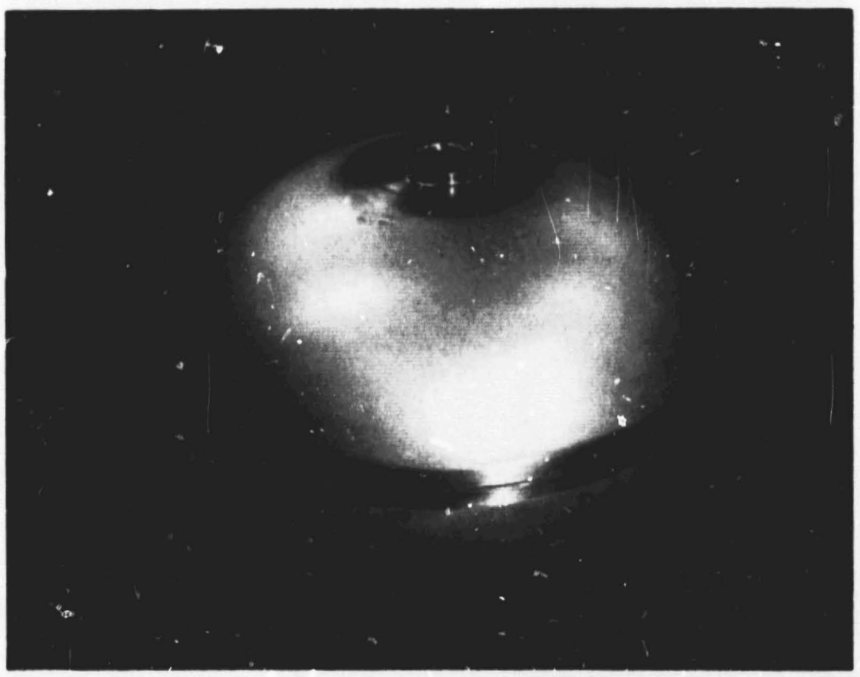

Fig. 39 Complete Metal-Shell Assembly

Figures 38 and 39

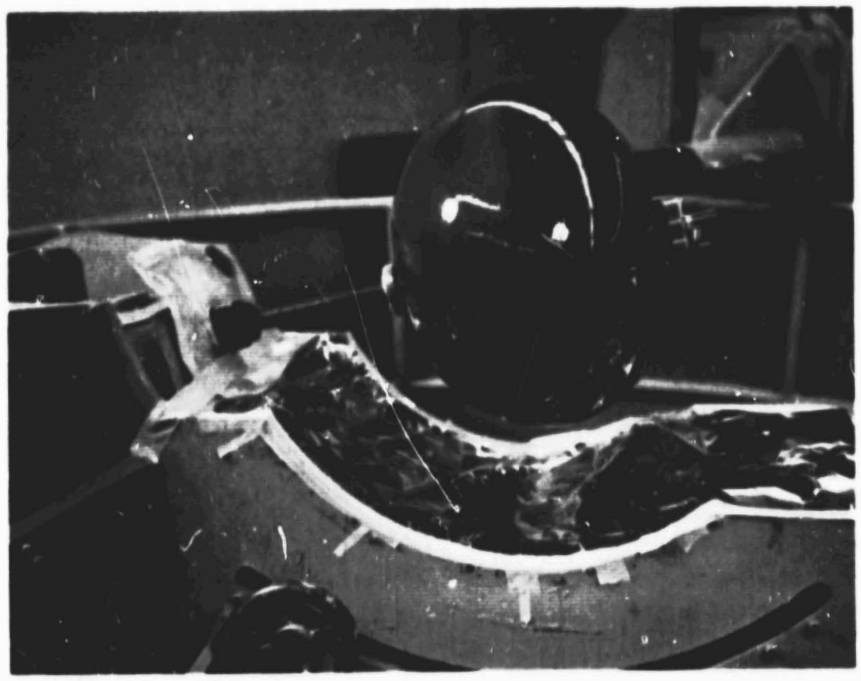

Fig. 40 Metal-Shell Assembly in Filament-Winding Machine

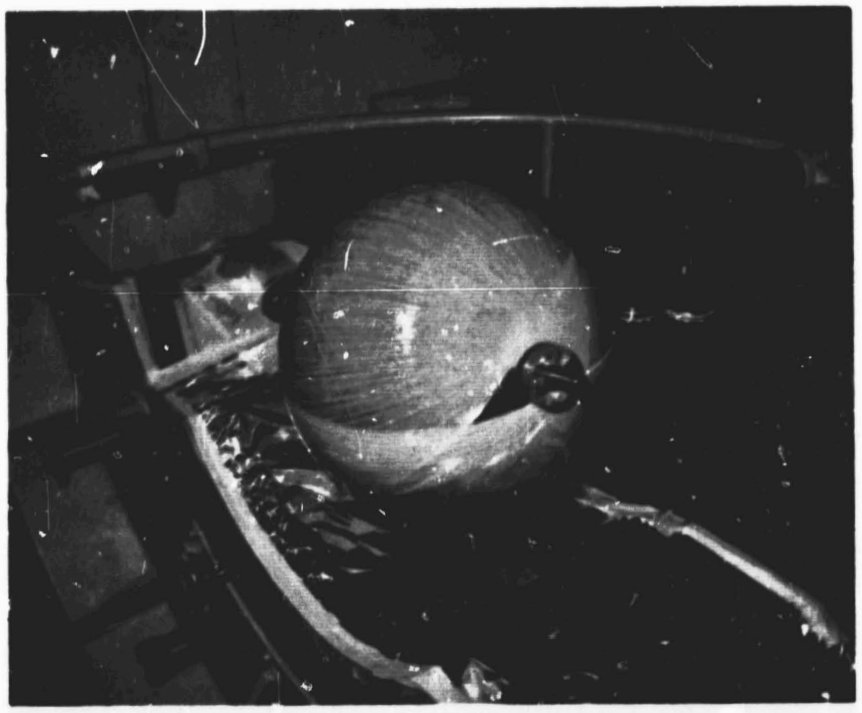

Fig. 41 Application of Longitudinal Filament Winding to Metal Shell

Figures 40 and 41

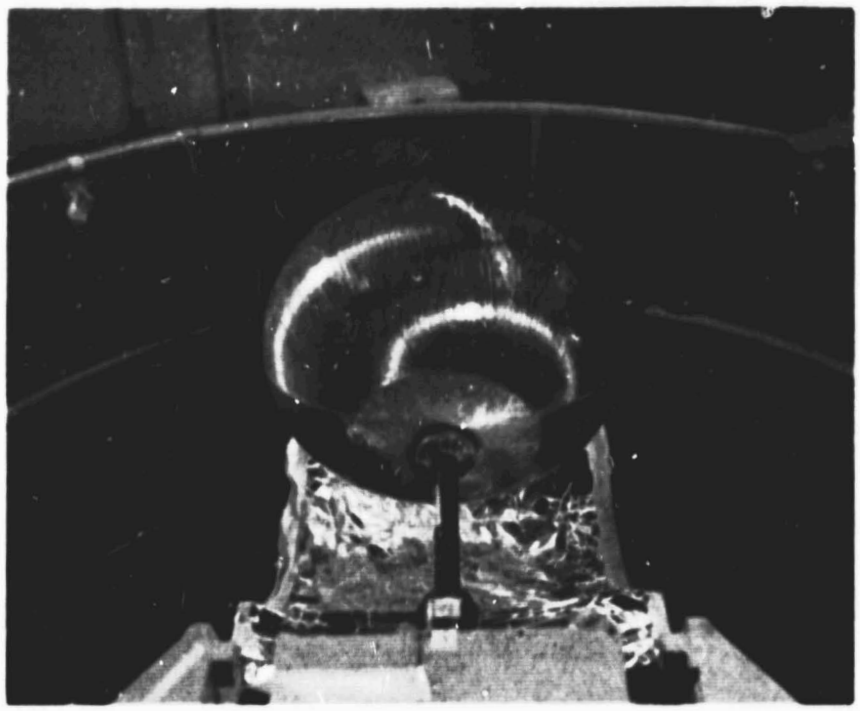

Fig. 42 Overwinding of Metal Shell
Showing Head Reinforcement

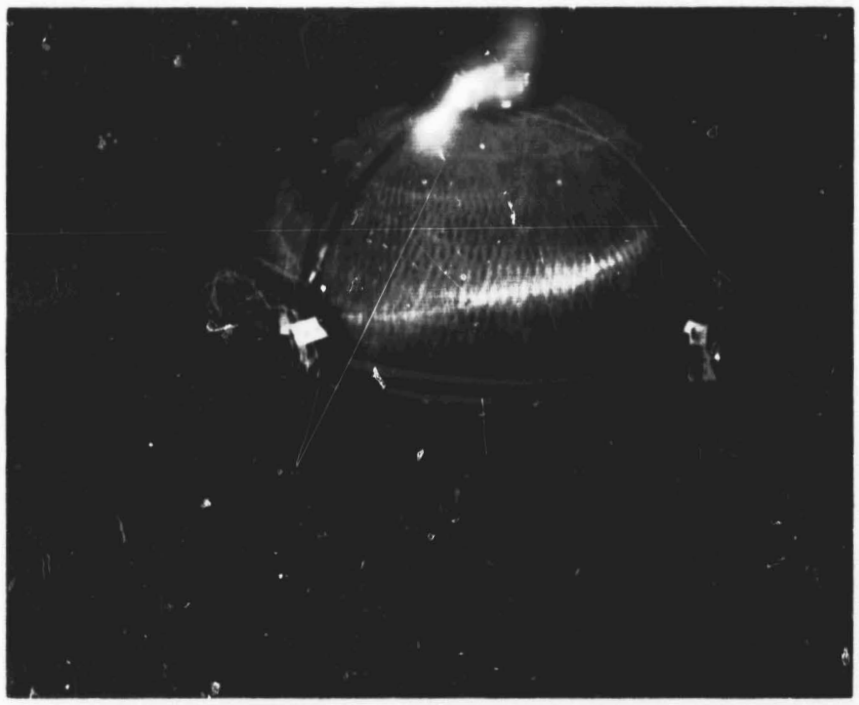

Fig. 43 Completed Tank Instrumented for Testing

Figures 42 and 43

Acceptable Girth Weld

Unacceptable Girth Weld (incomplete Penetration)

Acceptable Repair Weld of Above Area

X-Rays of Acceptable, Unacceptable, and Repaired Welds

Figure 44

Figure 45

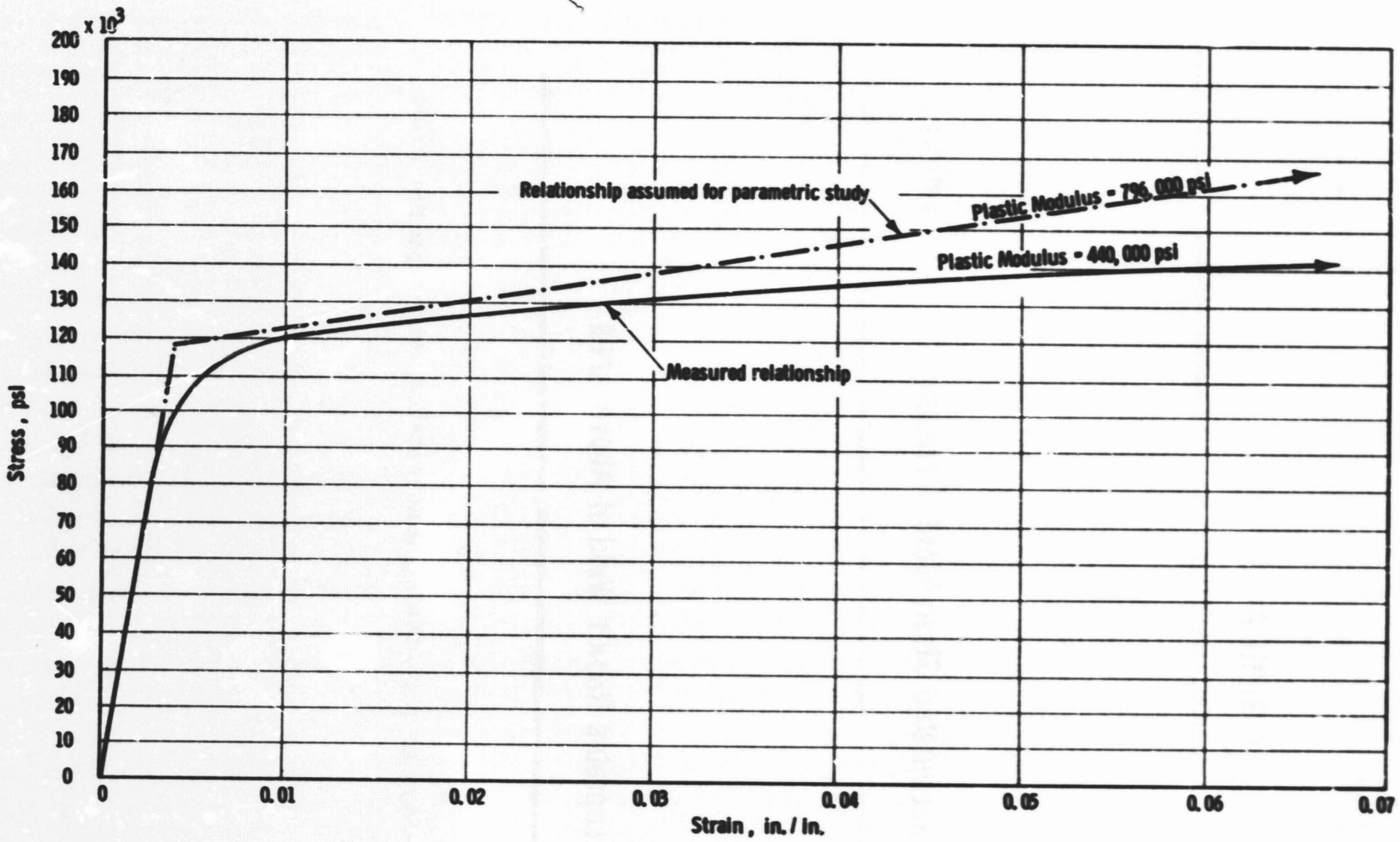

75°F Stress-Strain Curve for Inconel X-750 (STA)

Figure 46

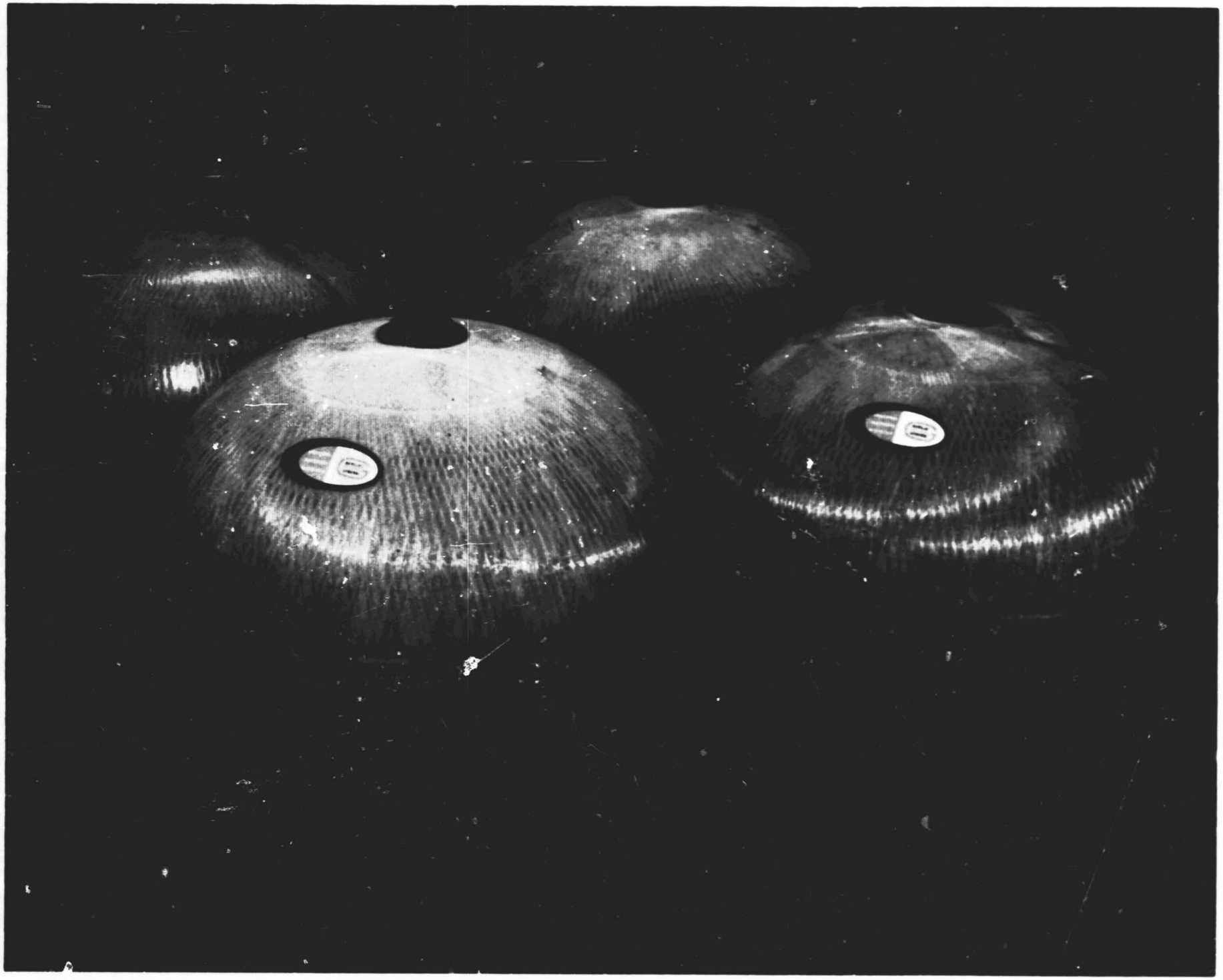

Group of Completed GFR Inconel X-750 Tanks

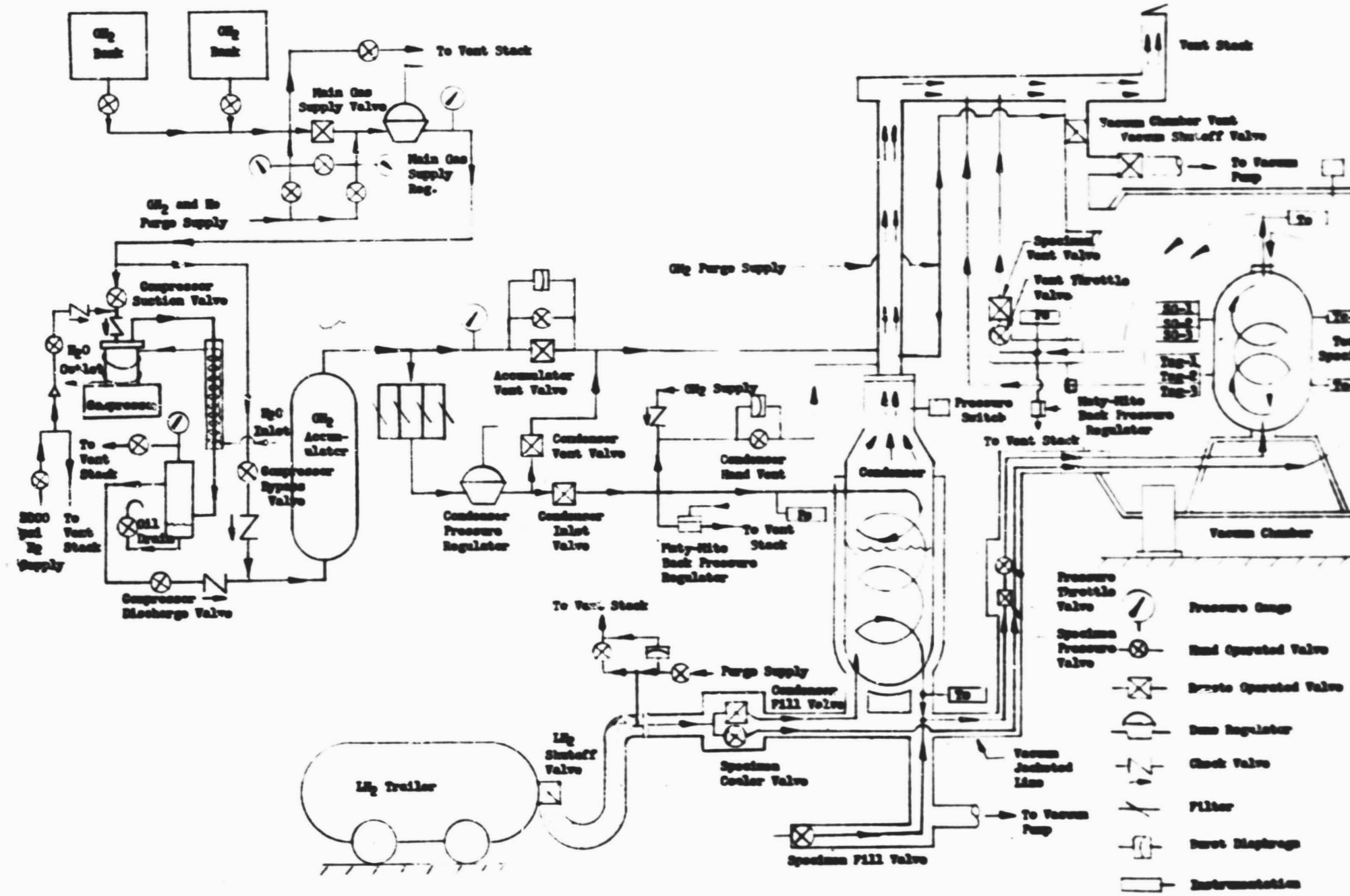

Figure 47

Liquid-Cryogen Pressurization System

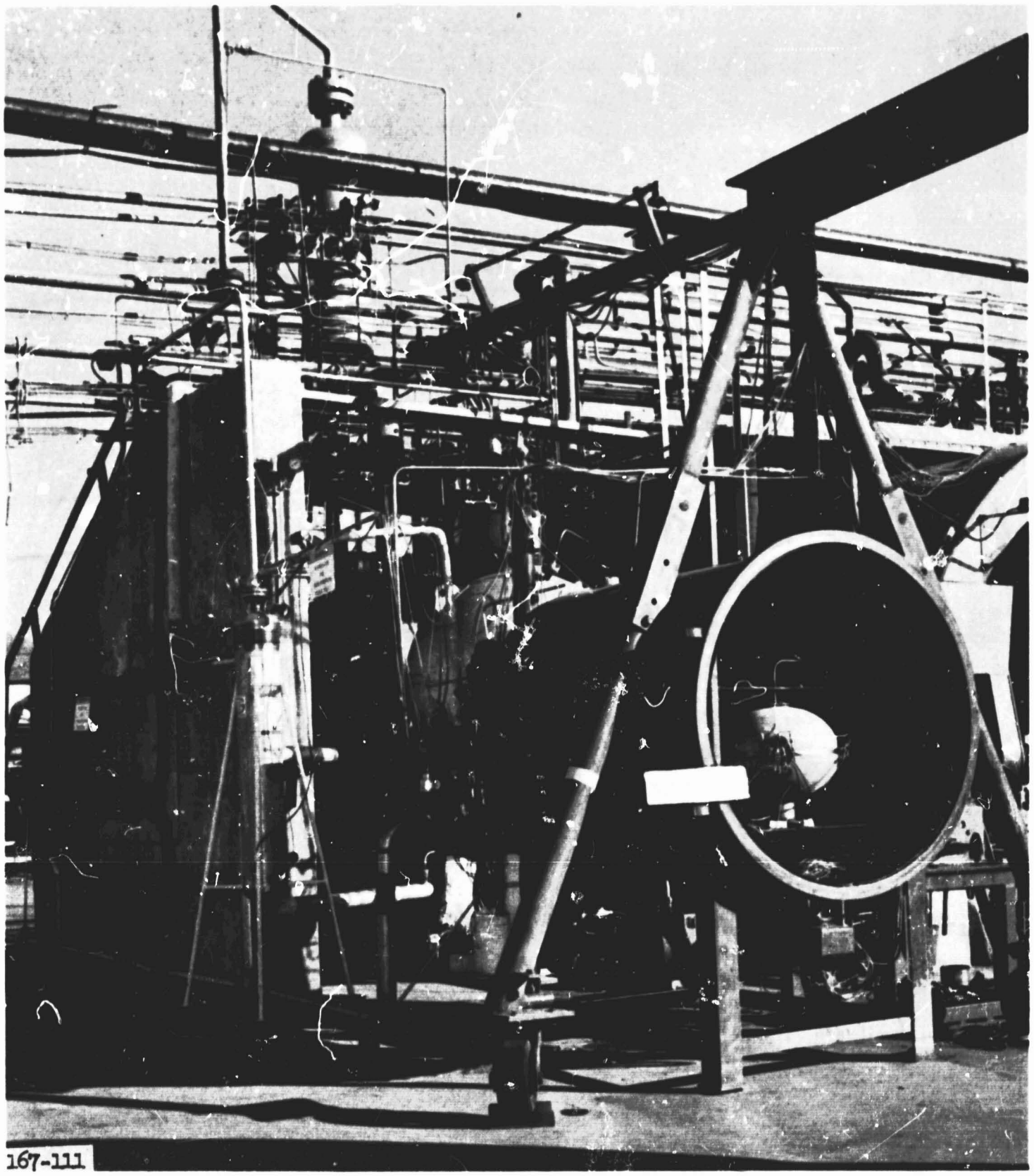

Cryogenic-Test Control Facility

Figure 48

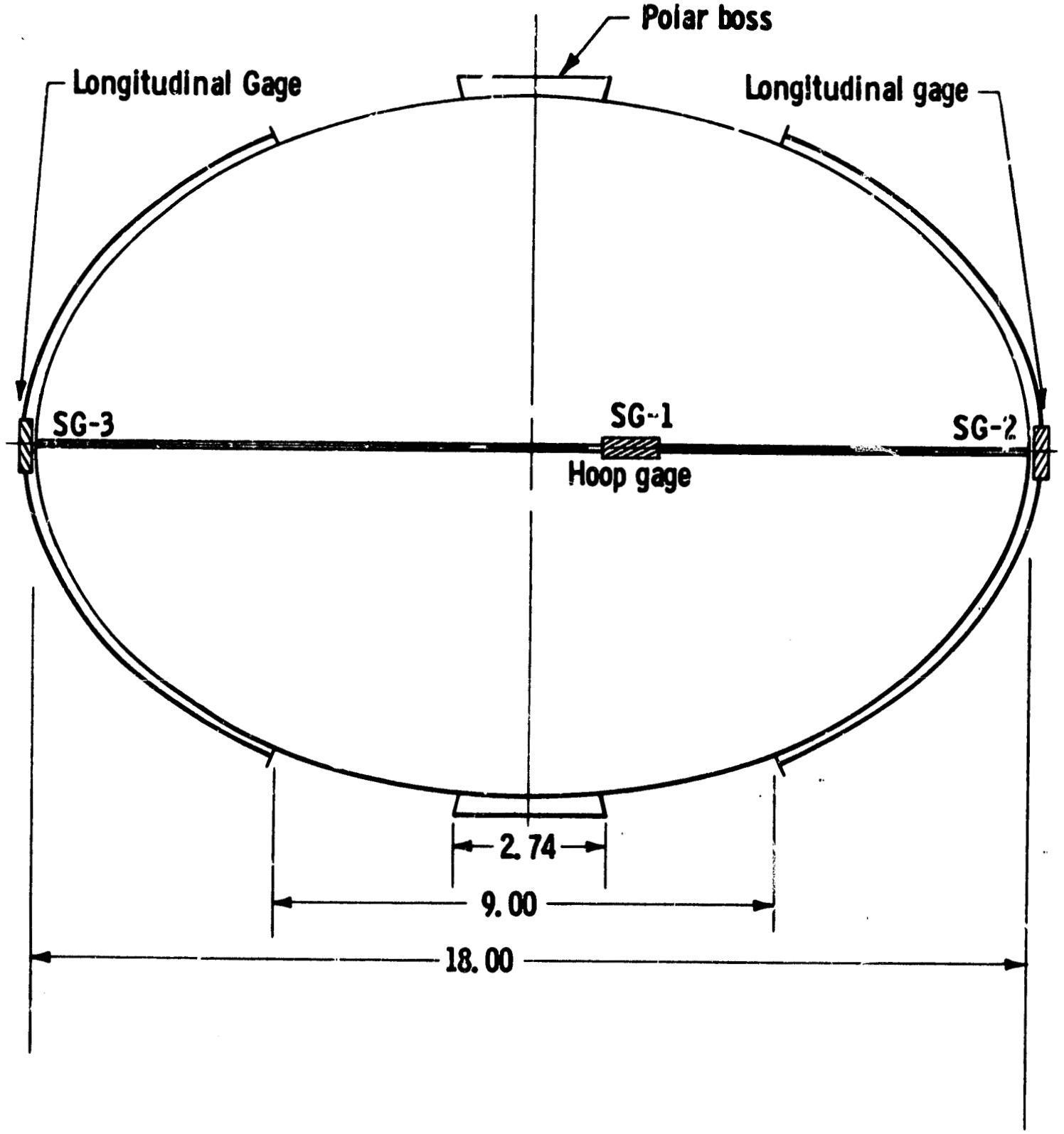

Extensometer Instrumentation

Figure 49

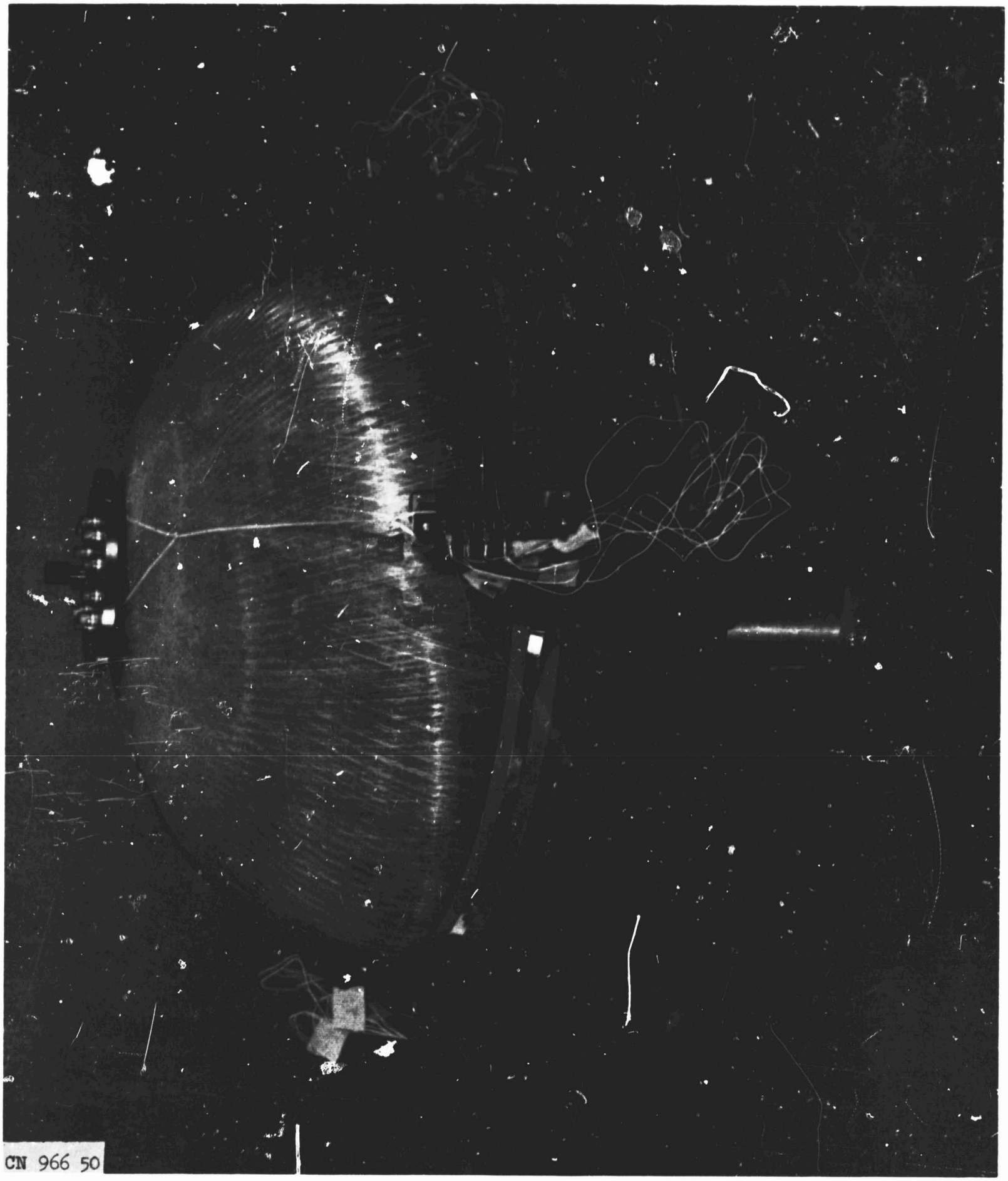

Bow-Tie Installation on Tank

Figure 30

Tank 2 After Test, Top View

Figure 51

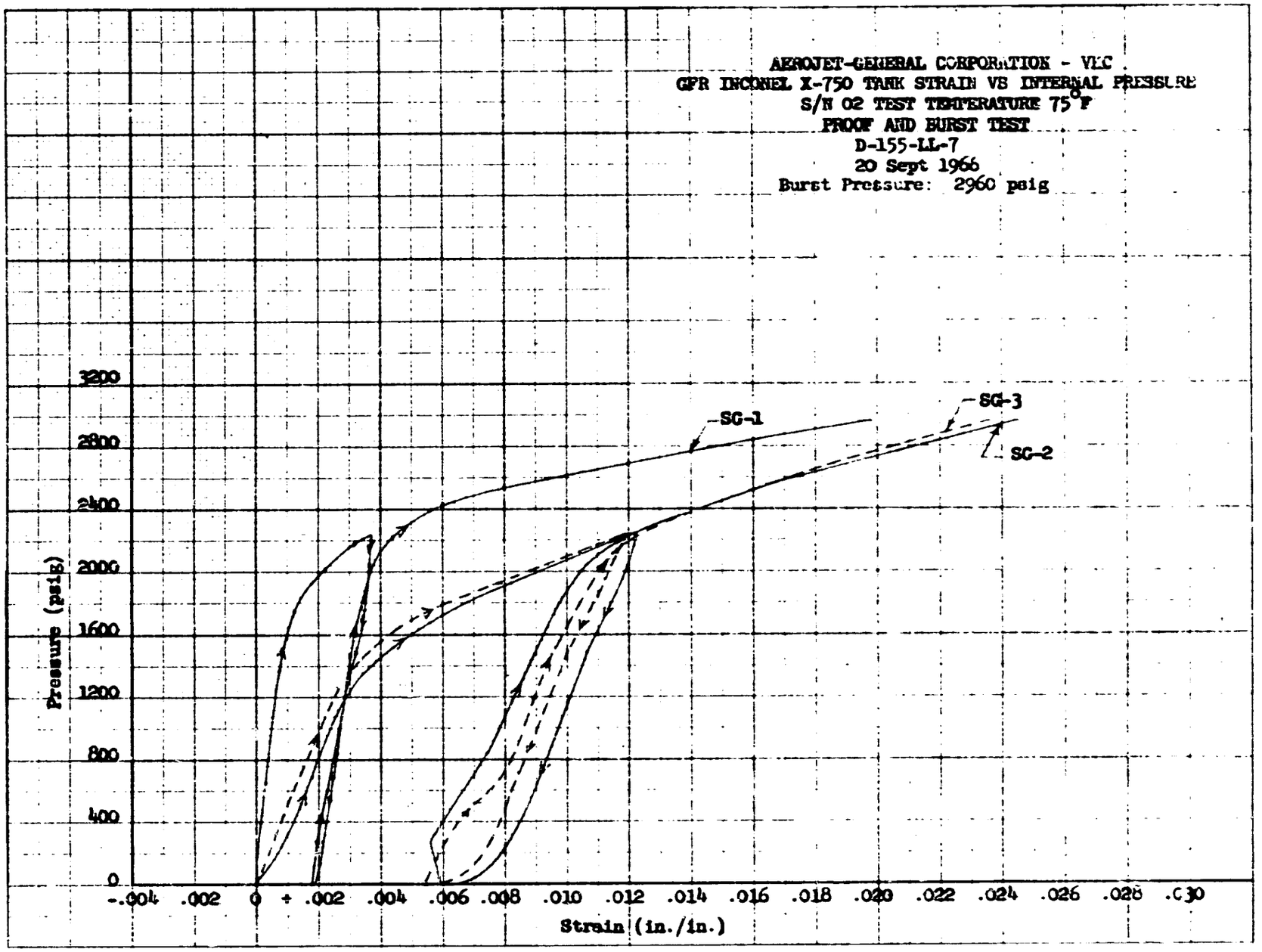

Figure 52

Tank 2 Pressure vs Strain for Proof and Burst-Test Phases at 75°F

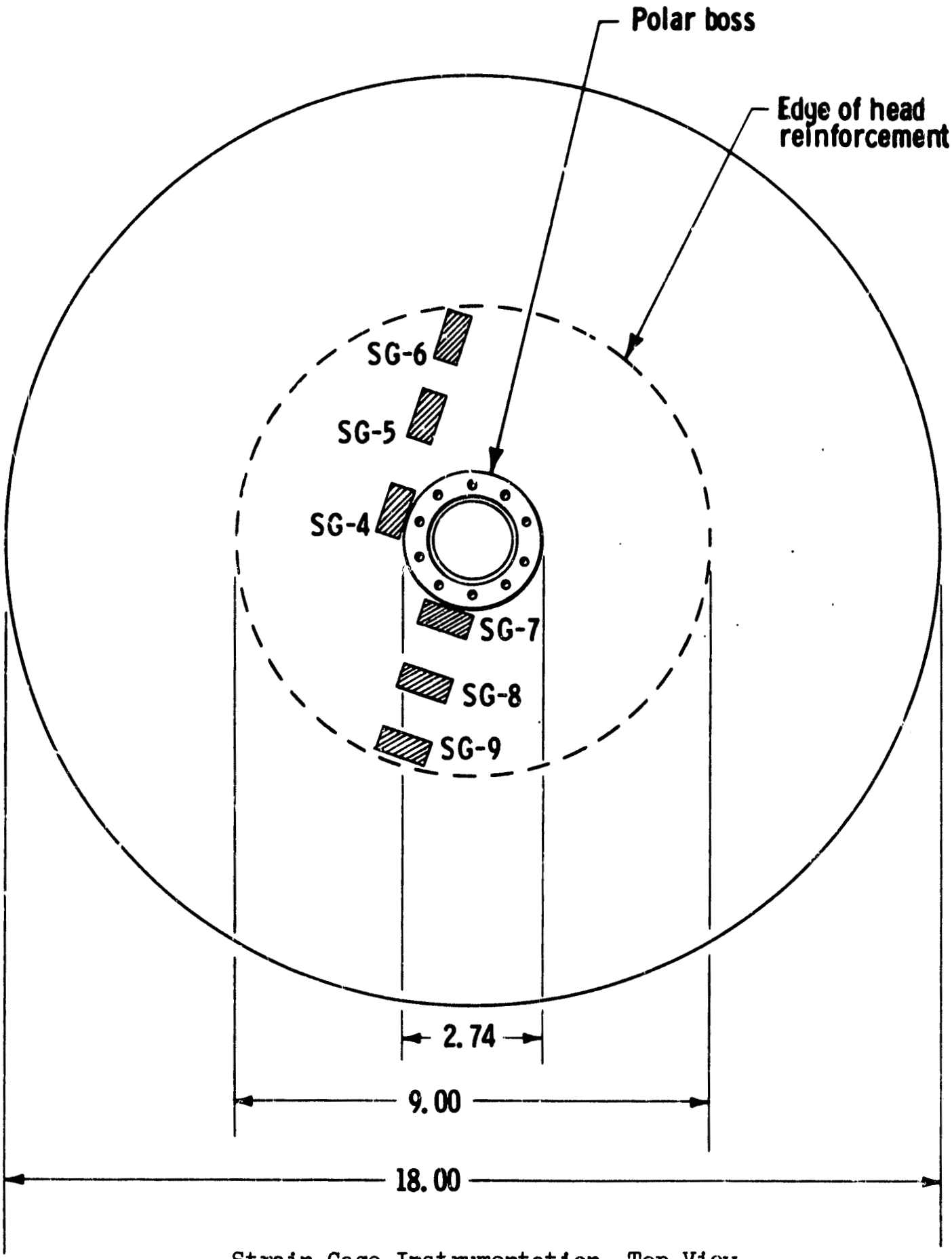

Strain-Gage Instrumentation, Top View

Figure 53

1066 019

Tank 3 After Test

Figure 54

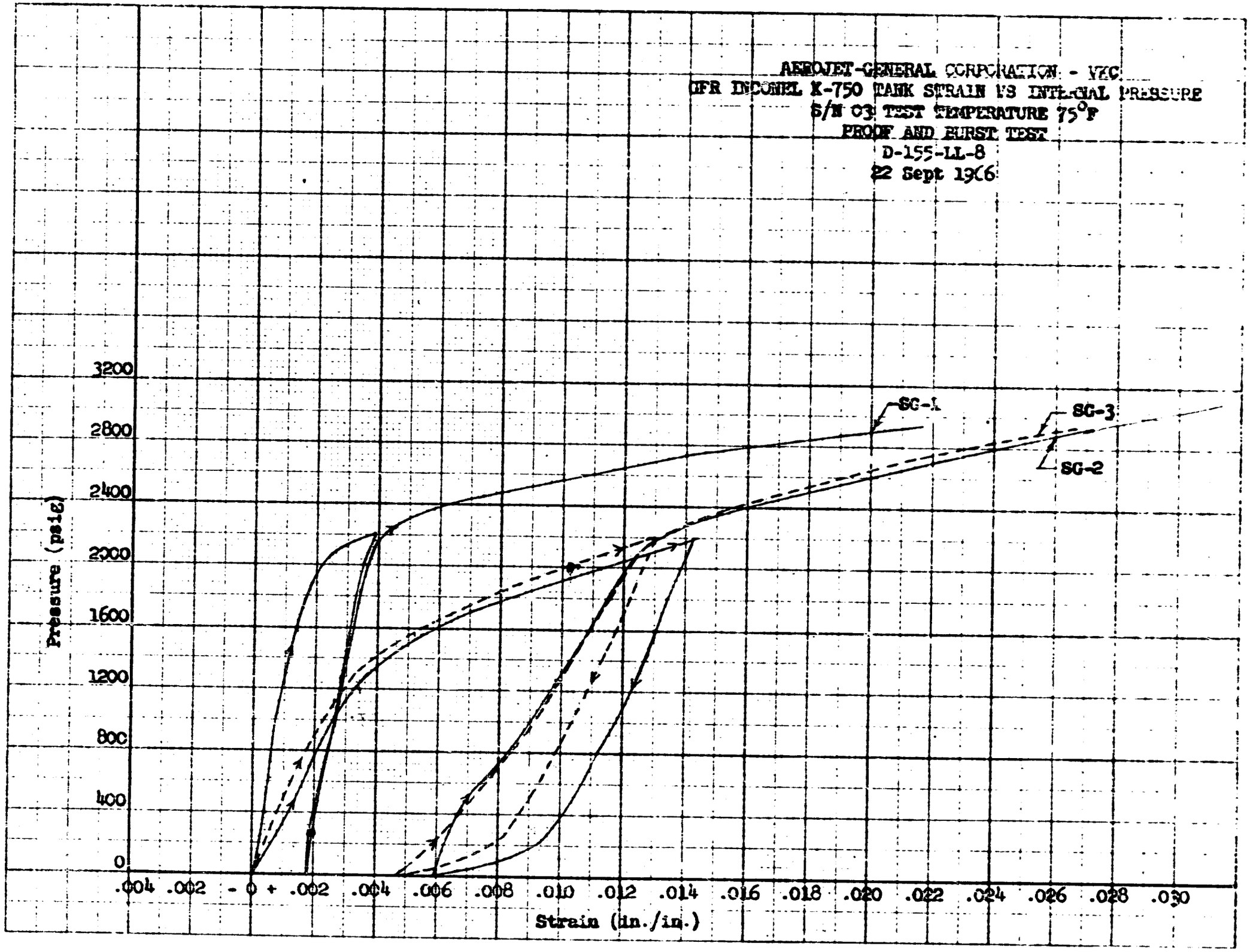

Figure 55

Tank 3 Pressure vs Strain for Proof and Burst-Test Phases at 75°F

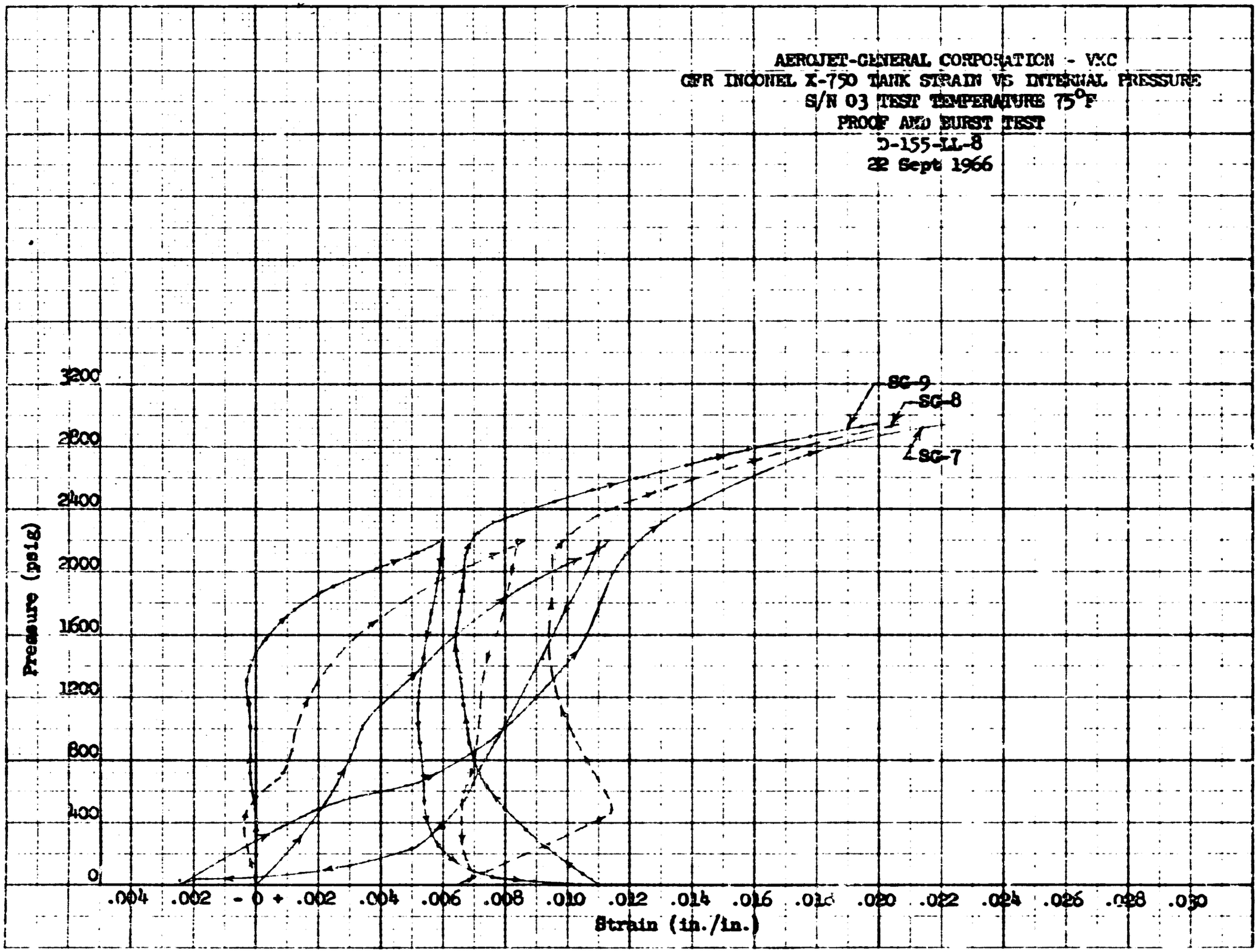

Tank 3 Hoop Strain Near Polar Boss for Proof and Burst-Test Phases at 75°F

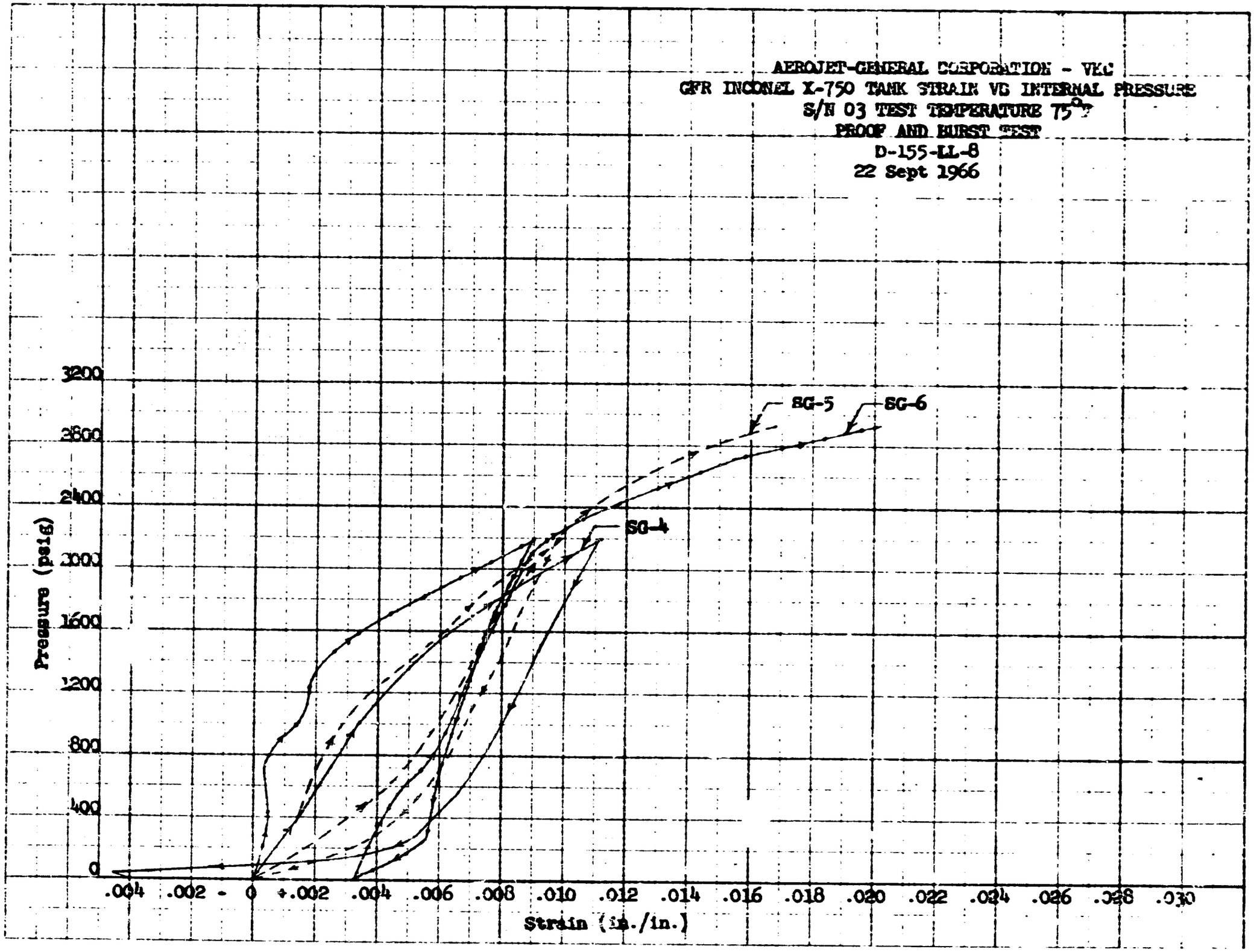

Figure 57

Tank 3 Longitudinal Strain Near Polar Boss for Proof and Burst-Test Phases at 75°F

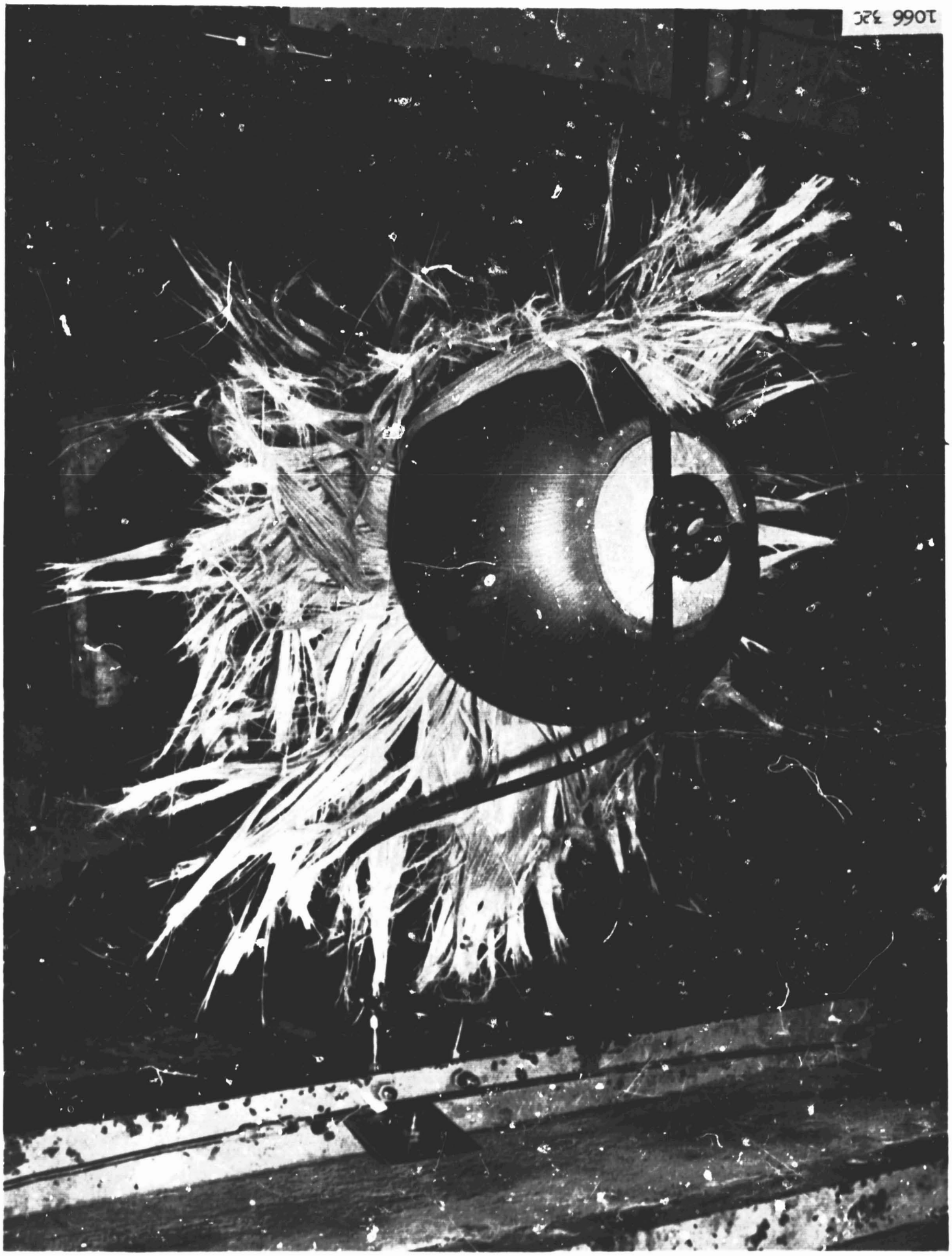

Tank 5 After Test

Figure 58

Figure 59

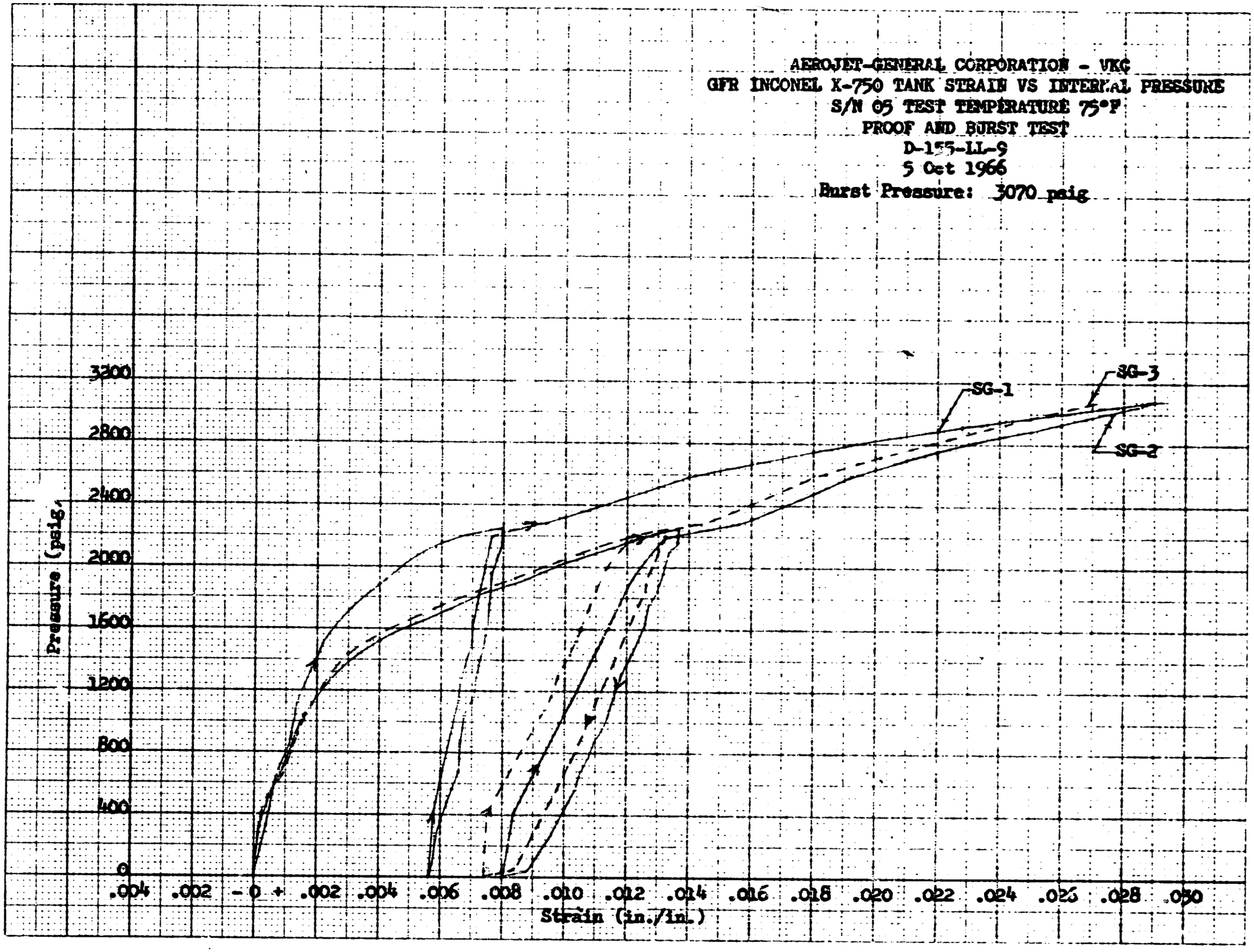

Tank 5 Pressure vs Strain for Proof and Burst-Test Phases at 75°F

Figure 60

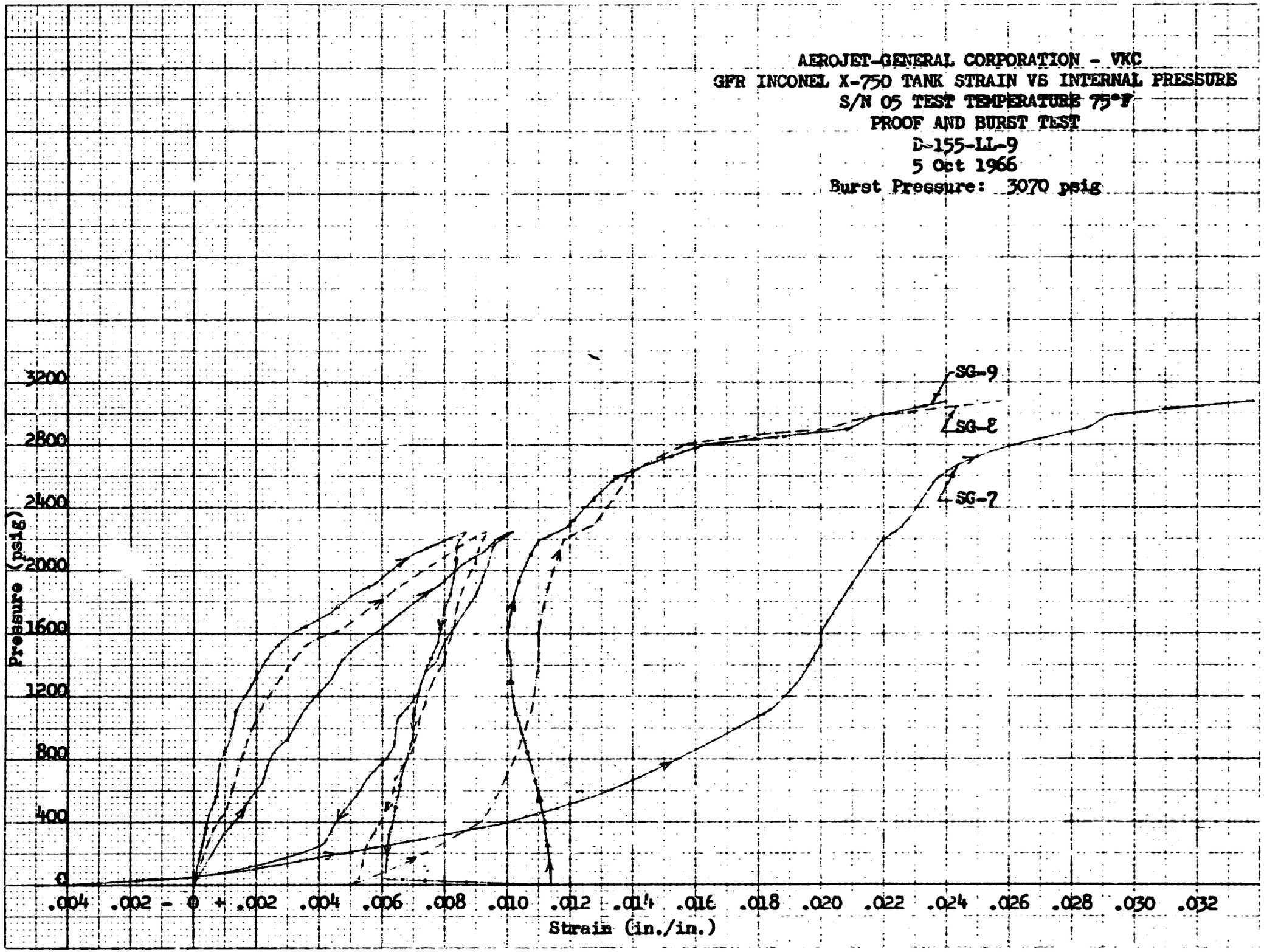

Tank 5 Hoop Strain Near Polar Boss for Proof
and Burst-Test Phases at 75°F

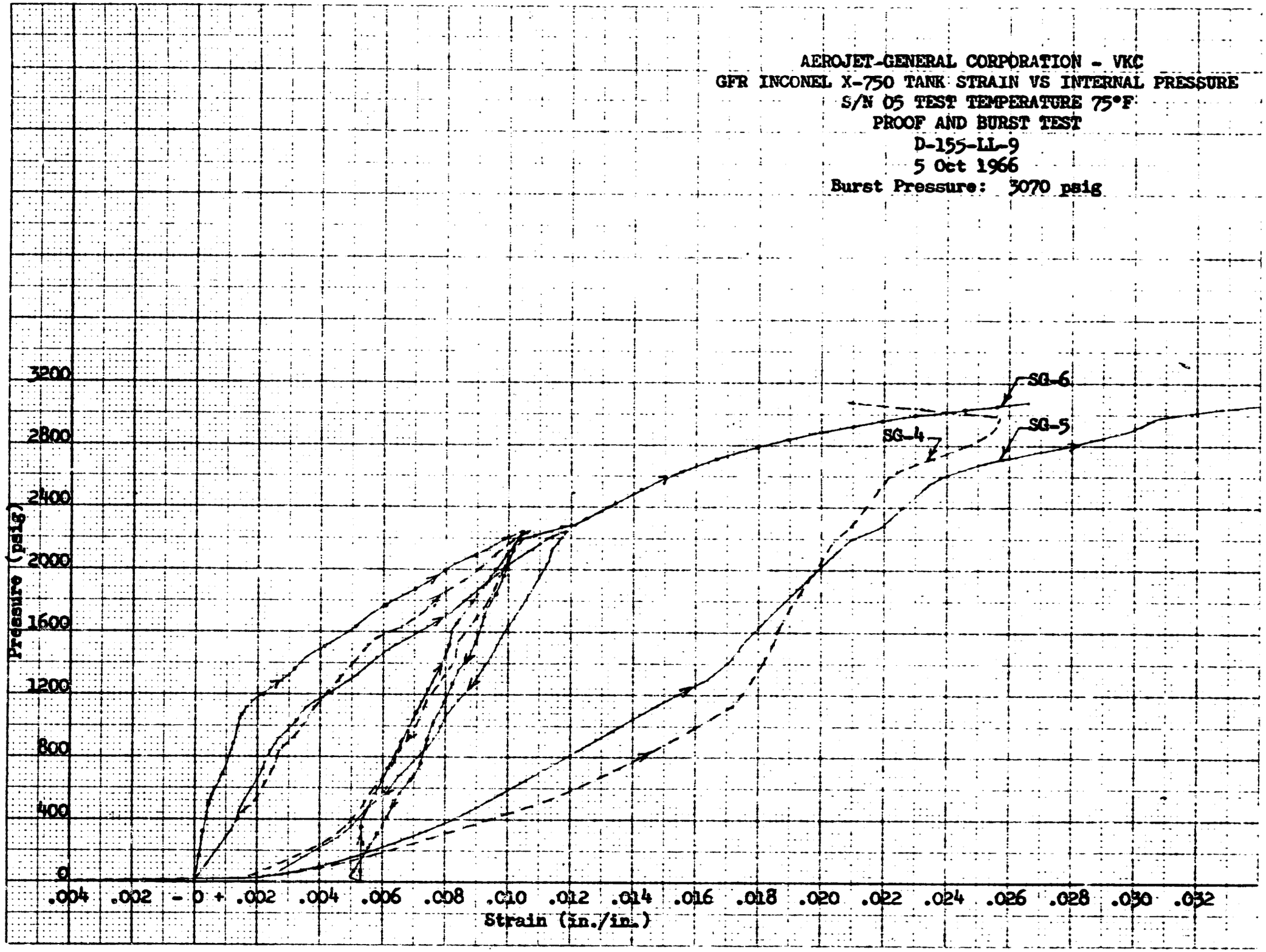

Figure 61

Tank 5 Longitudinal Strain Near Polar Boss
for Proof and Burst-Test Phases at 75°F

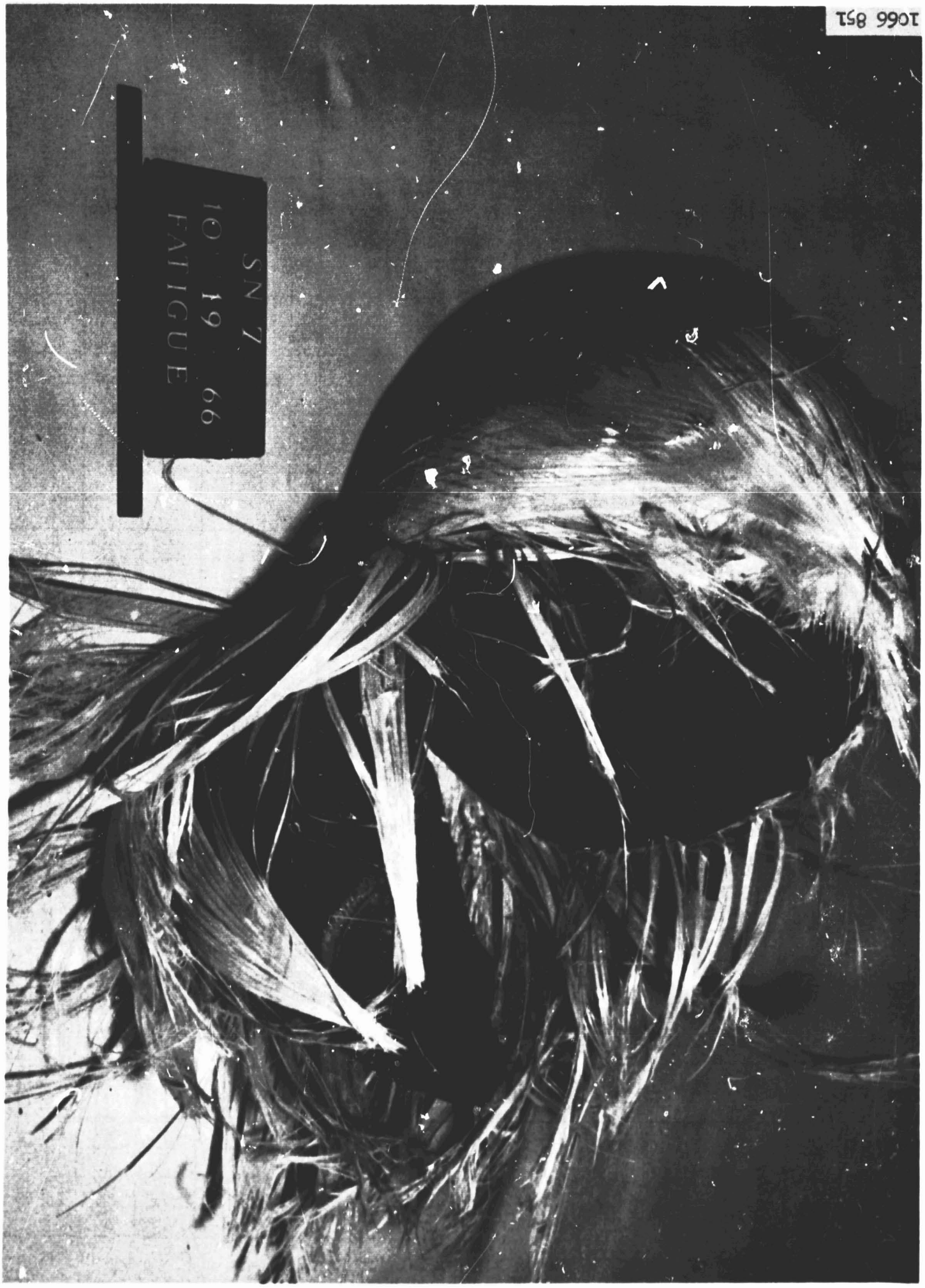

Figure 62

Tank 7 After Test

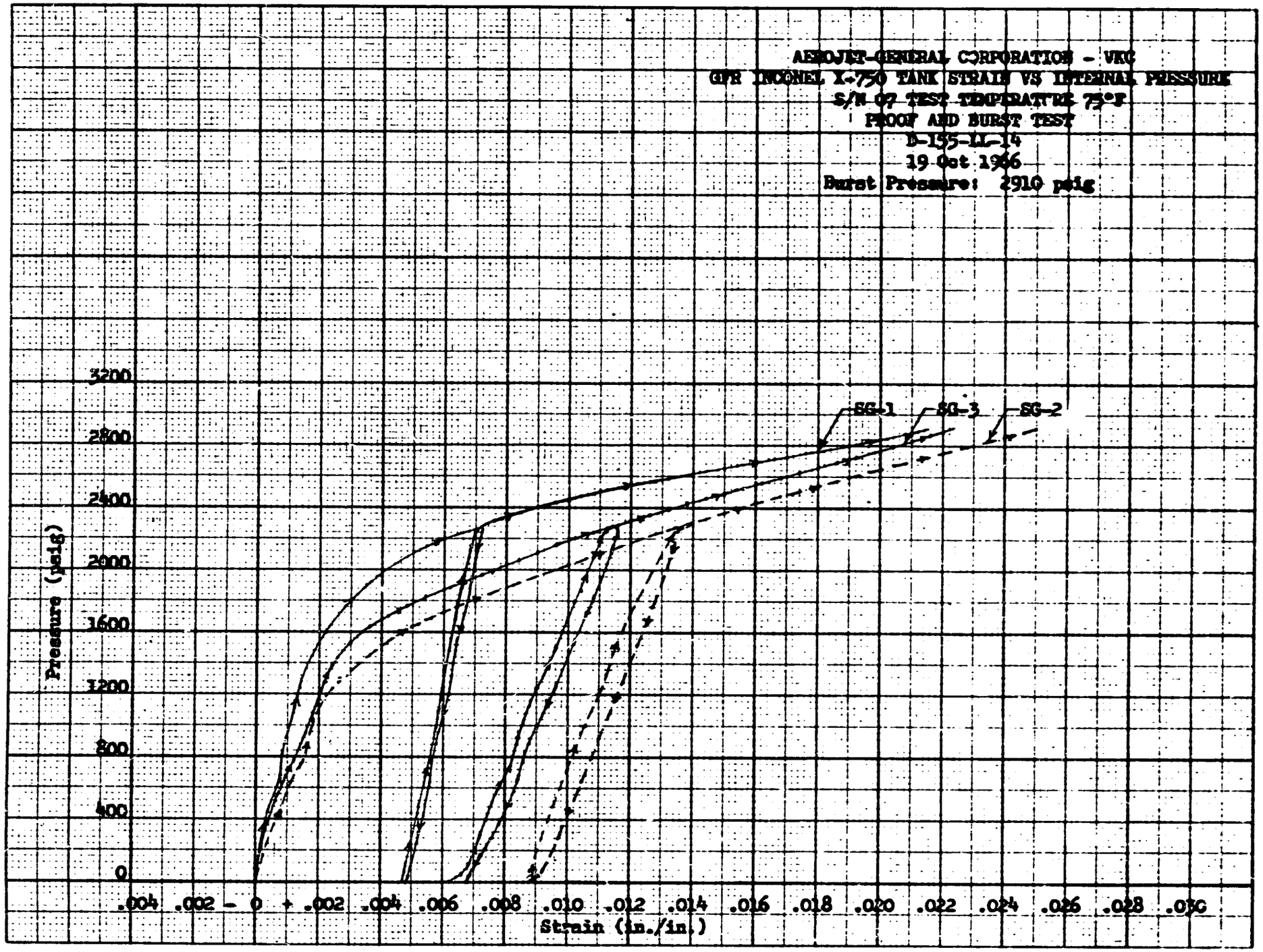

Figure 63 Tank 7 Pressure vs Strain for Proof and Burst-Test Phases at 75°F

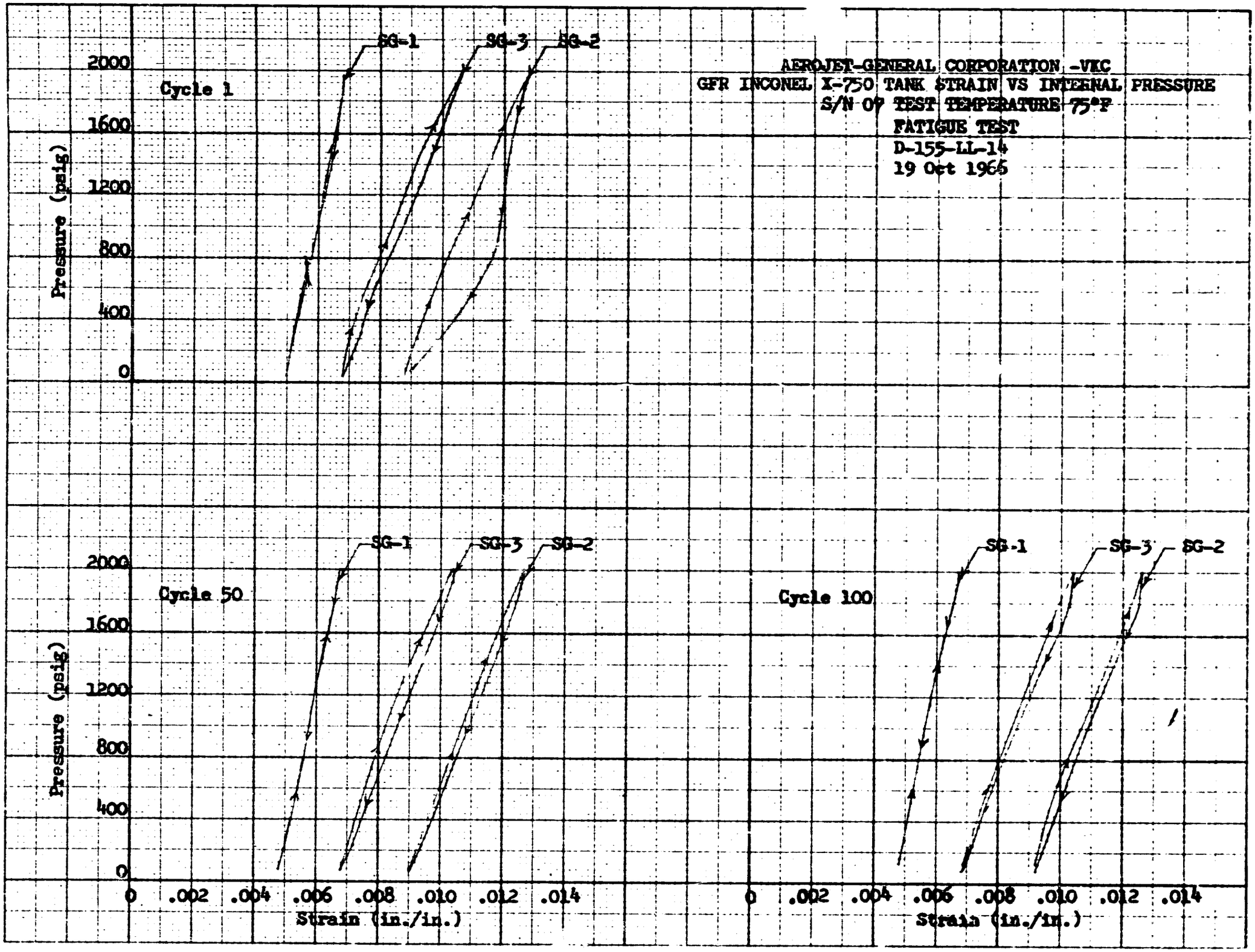

Tank 7 Pressure vs Strain During Pressure Cycling at 75°F

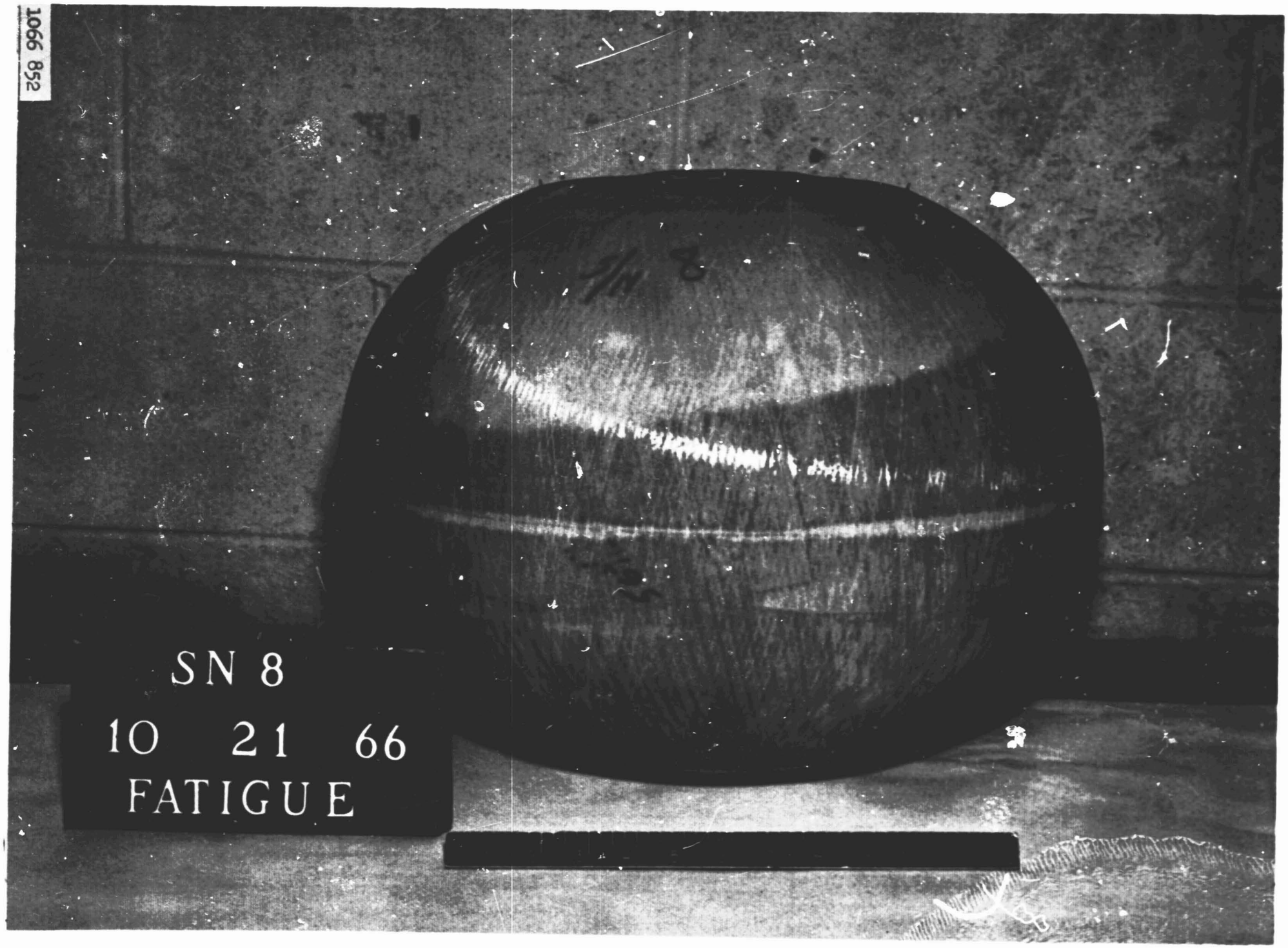

Tank 8 After Test

Figure 66

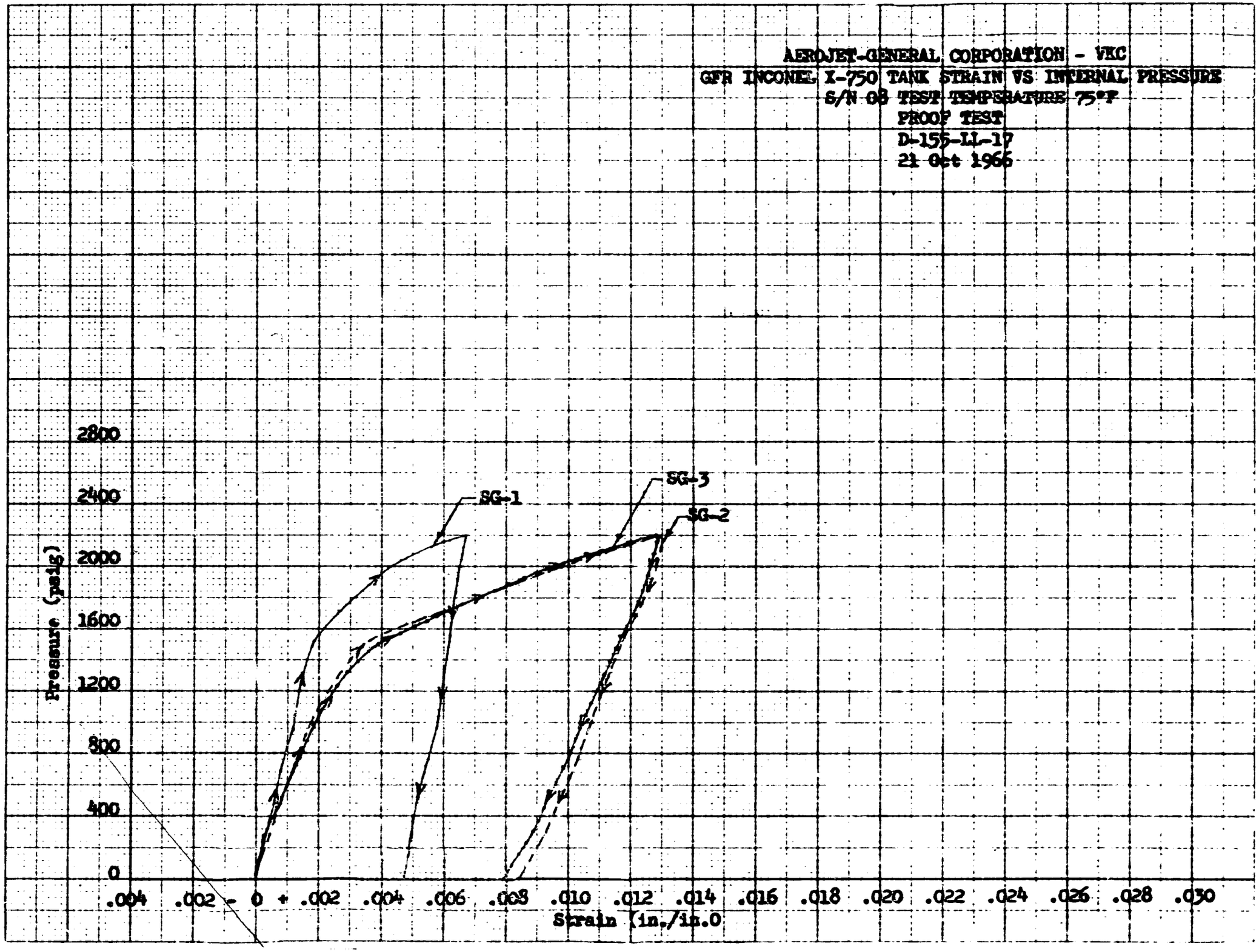

Tank 8 Pressure vs Strain for Proof-Test Phase at 75°F

Figure 67

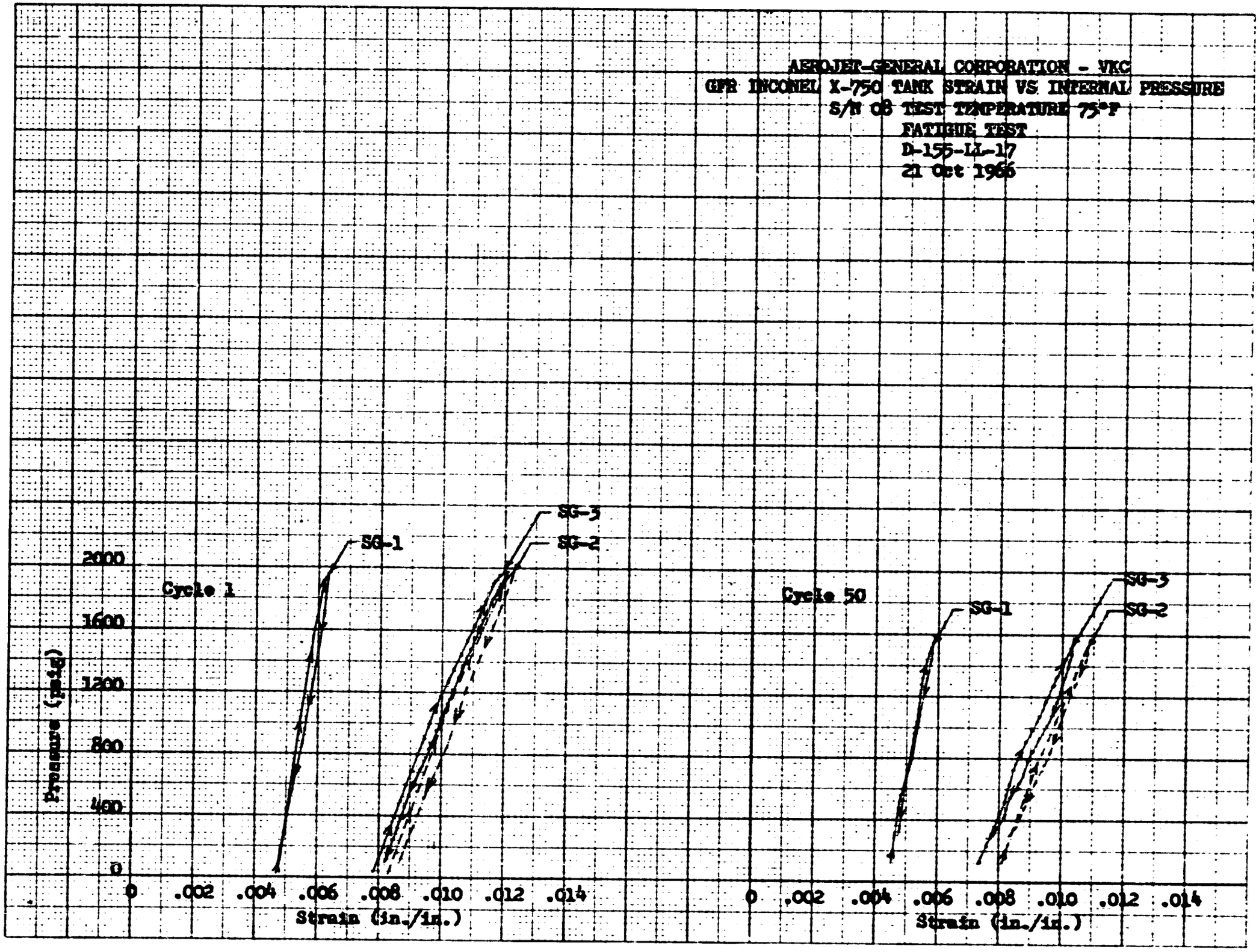

Tank 8 Pressure vs Strain During Pressure Cycling at 75°F

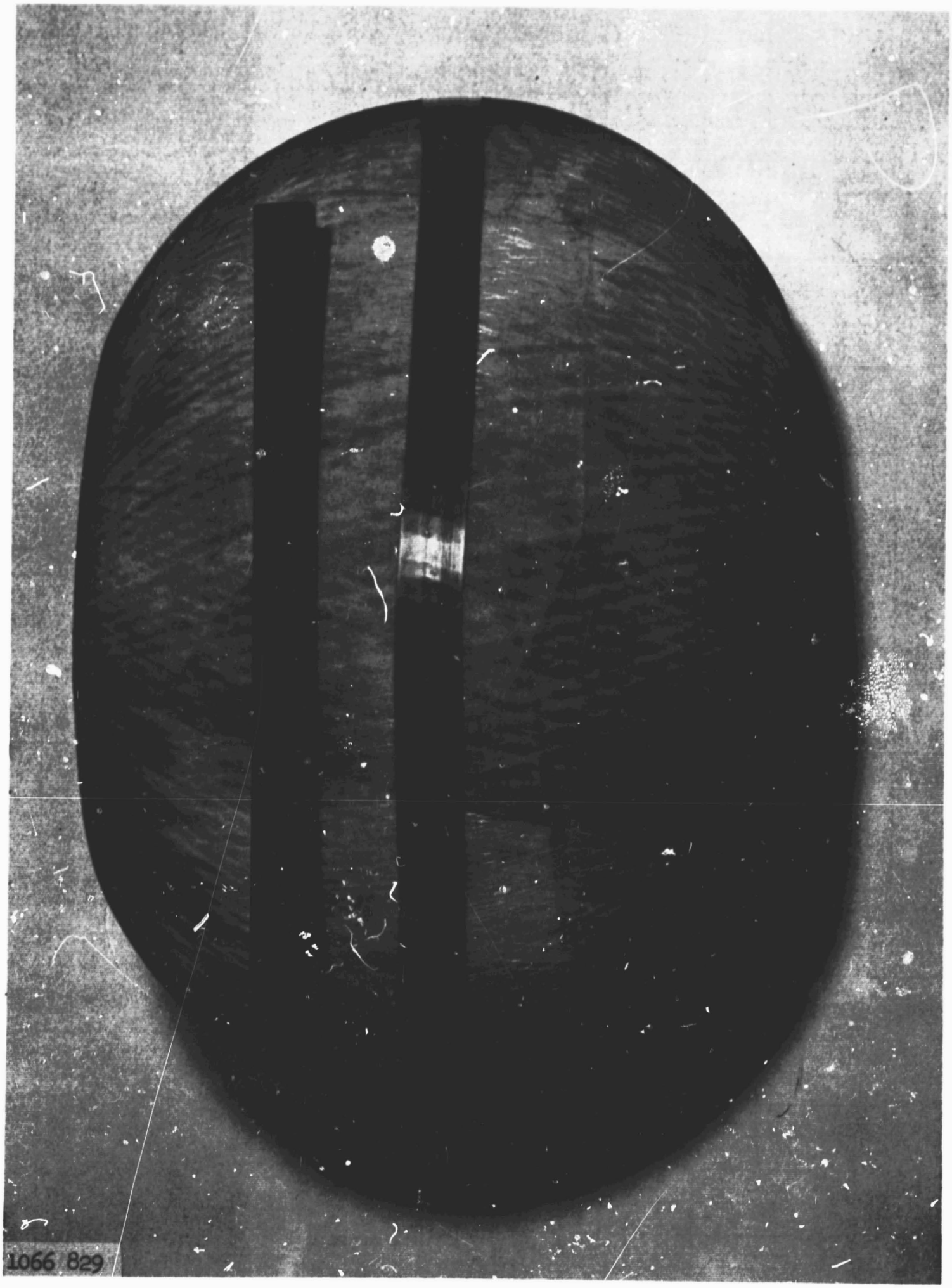

Tank 4 After Test

Figure 68

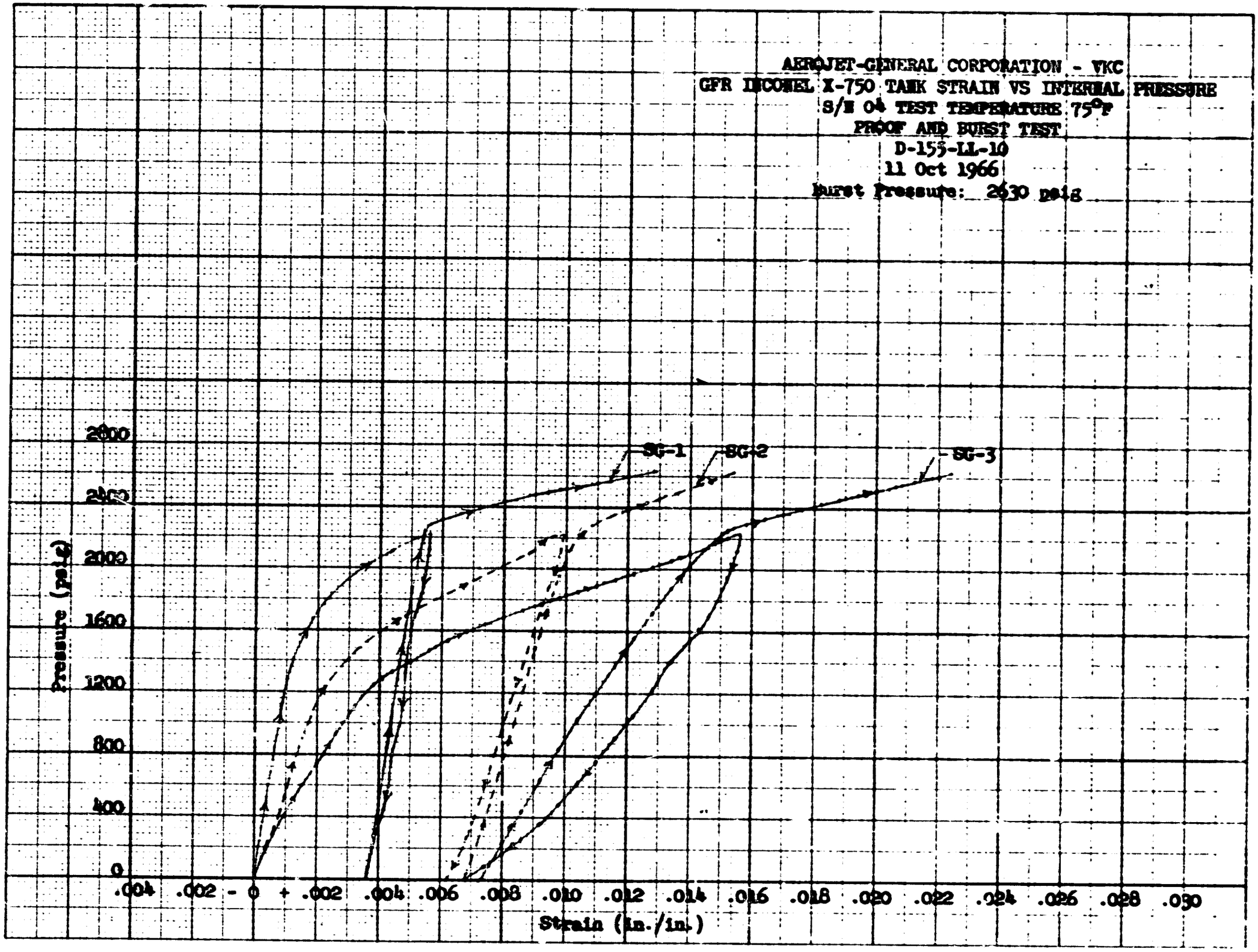

Tank 4 Pressure vs Strain for Proof and Burst-Test Phases at 75°F

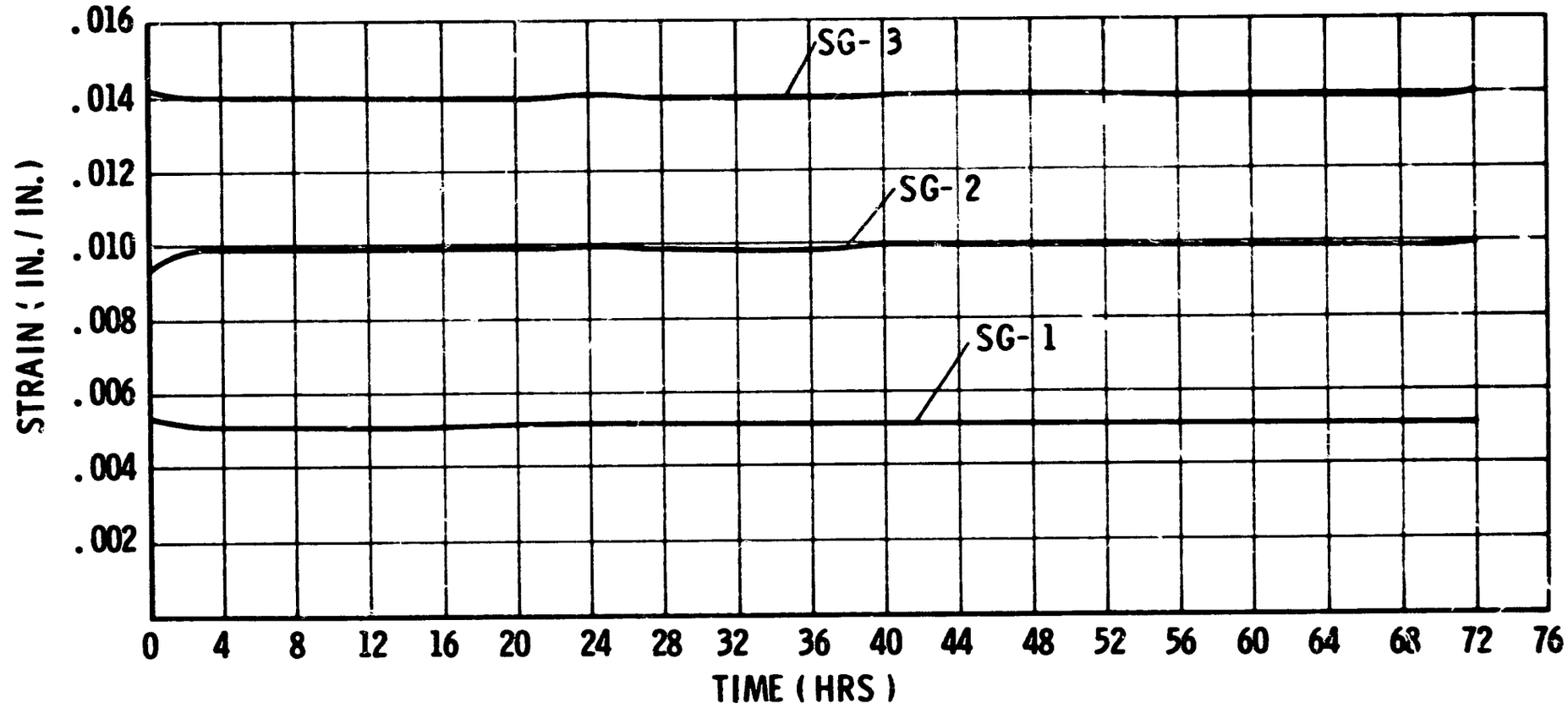

Tank 4 Strain During Creep Test at 75°F

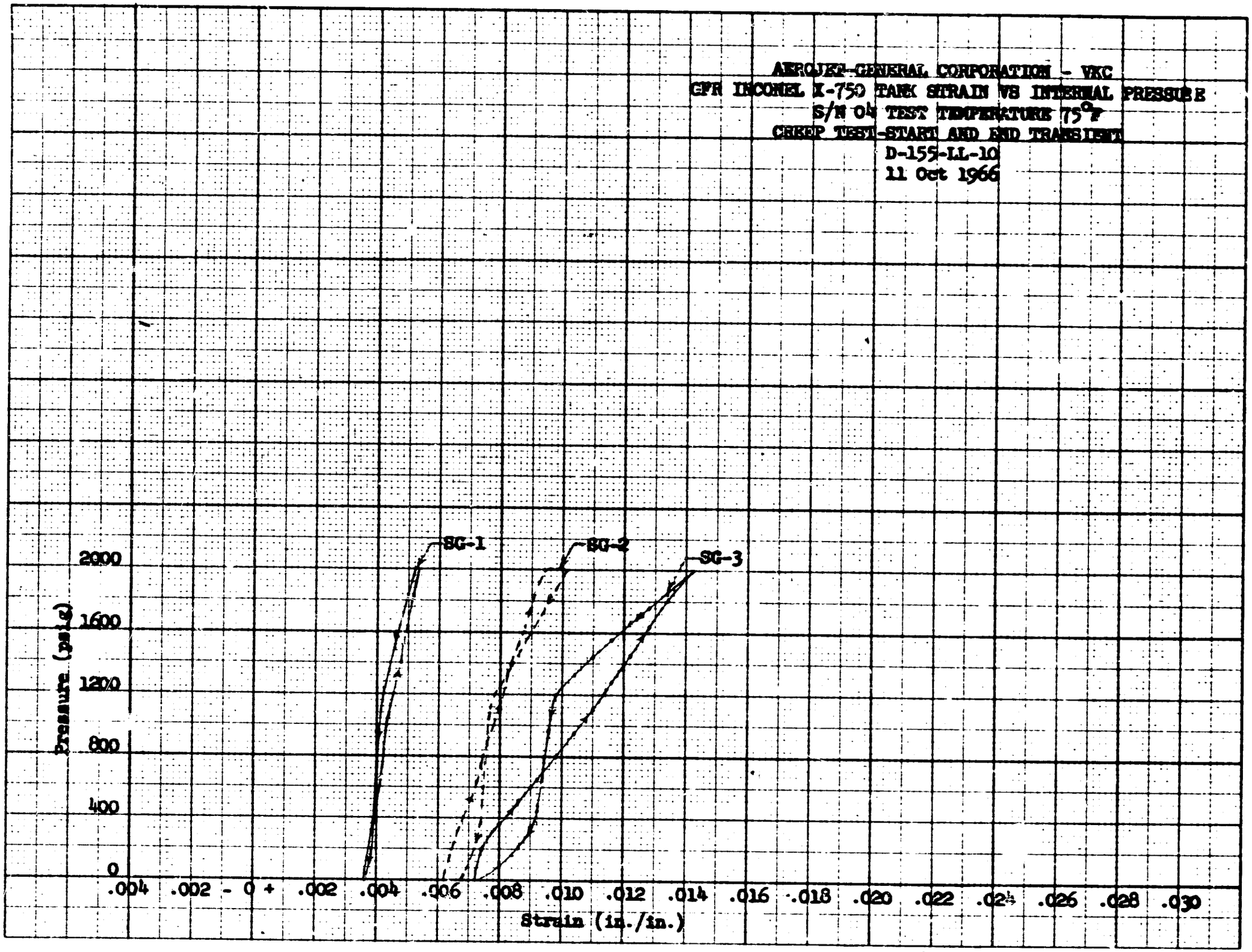

Figure 71

Tank 4 Creep Test, Start and End Transients at 75°F

Tank 6 After Test

Figure 72

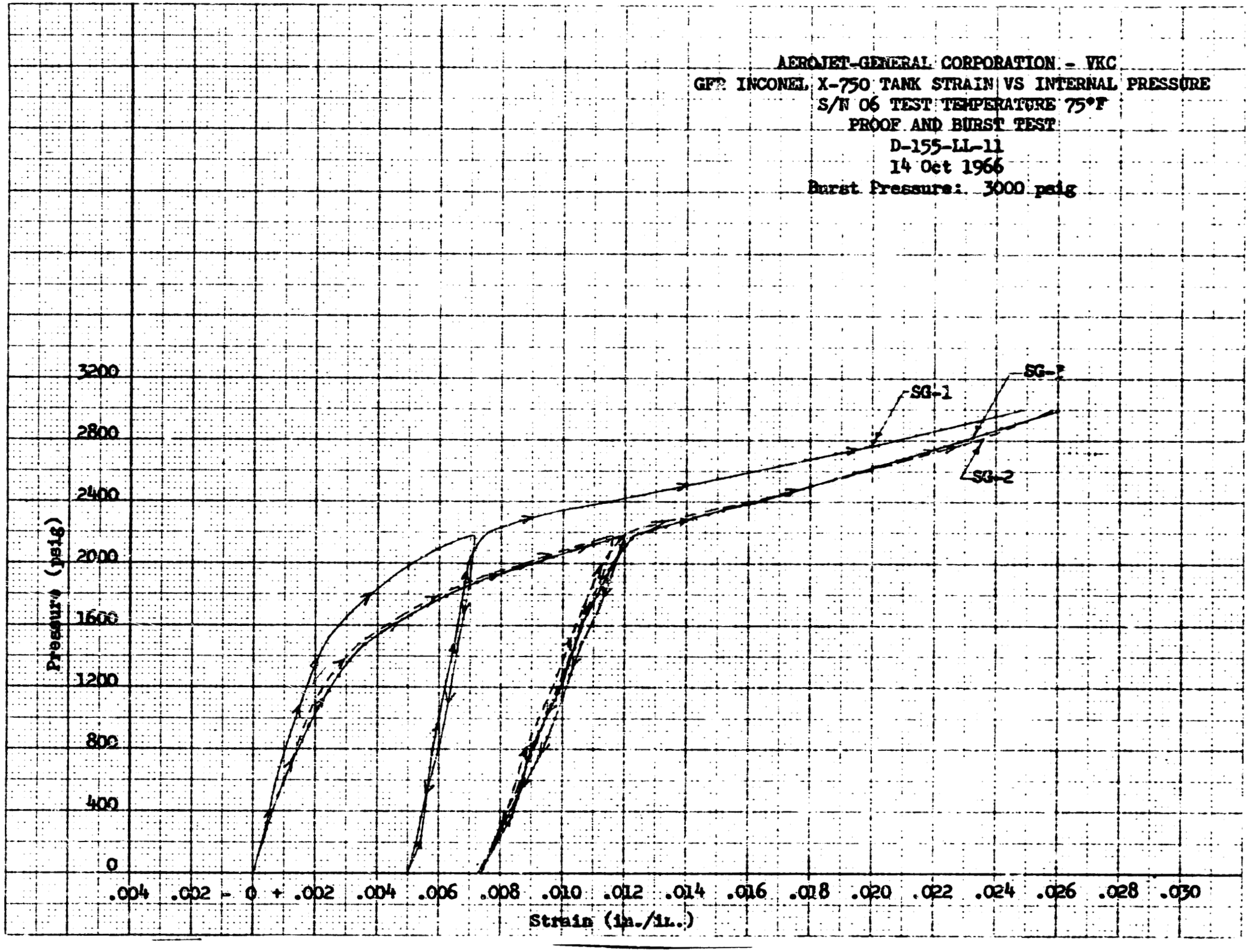

Figure 73 Tank 6 Pressure vs Strain for Proof and Burst-Test Phases at 75°F

AEROJET-GENERAL CORPORATION - VKC
GFR INCONEL X-750 TANK STRAIN VS INTERNAL PRESSURE
S/N 06 TEST TEMPERATURE 75°F
CREEP TEST
D-155-LL-11
14 Oct 1966

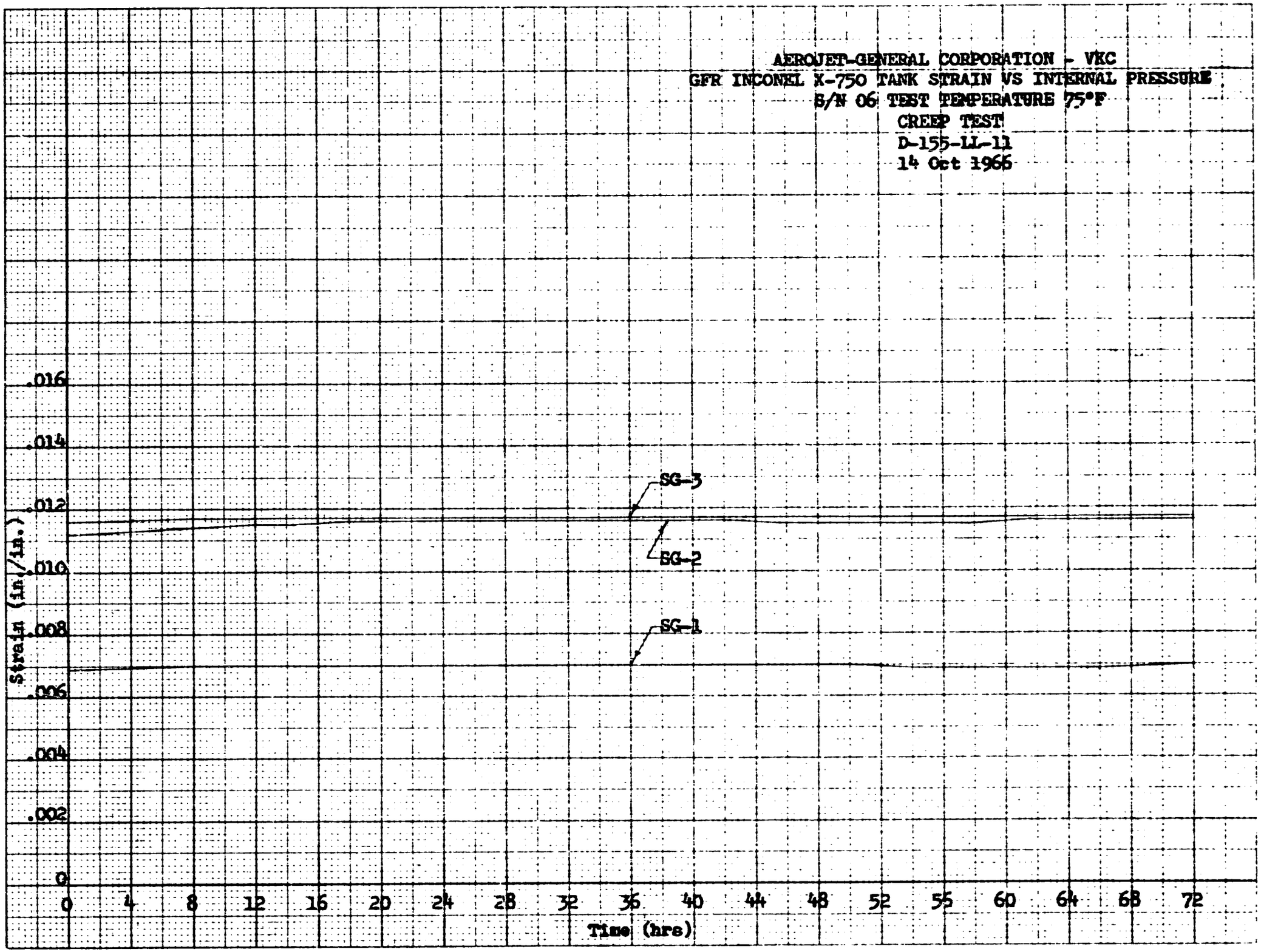

Figure 74 Tank 6 Strain During Creep Test at 75°F

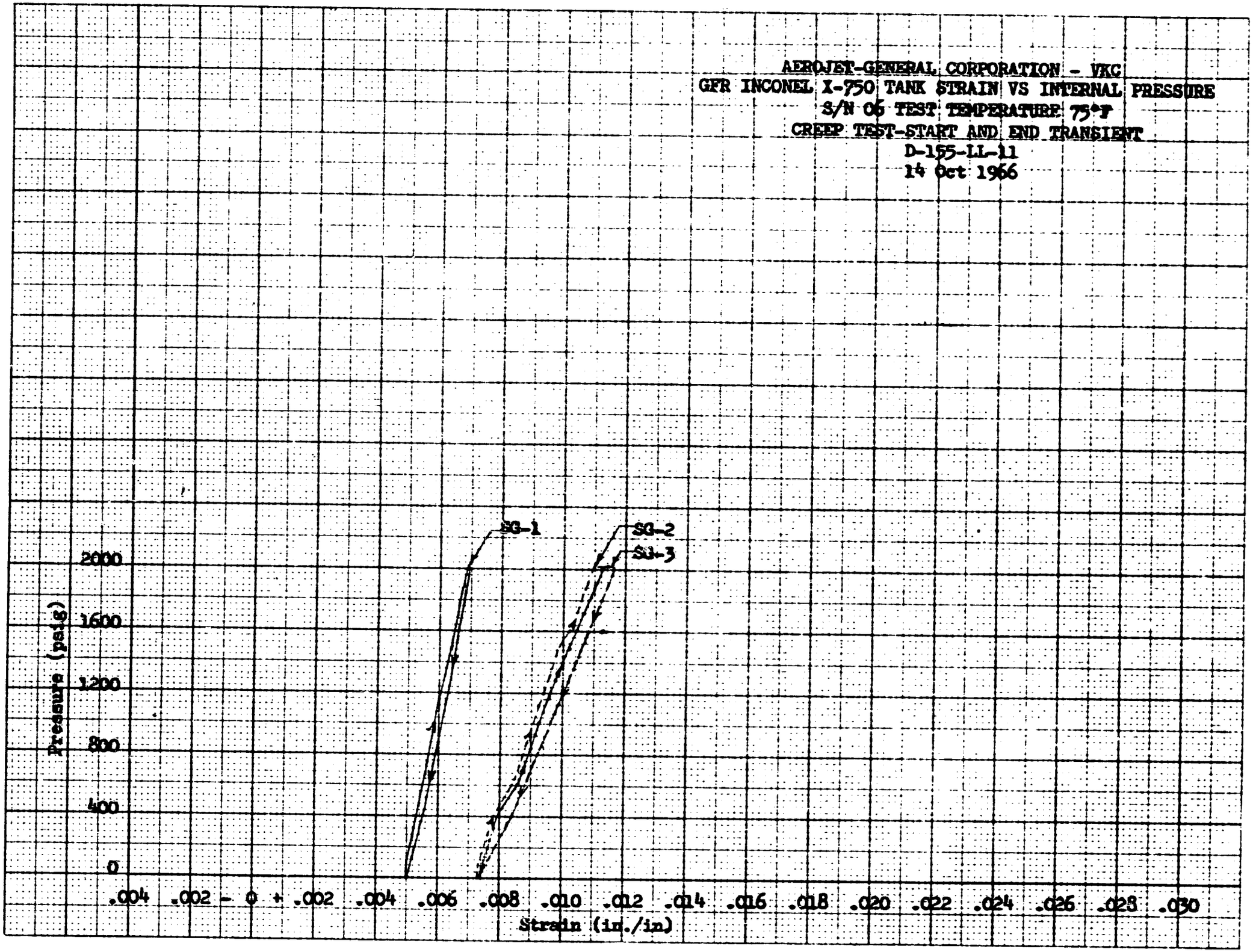

Figure 75 Tank 6 Creep Test, Start and End Transients at 75°F

Figure 76

Tank 13 After Test

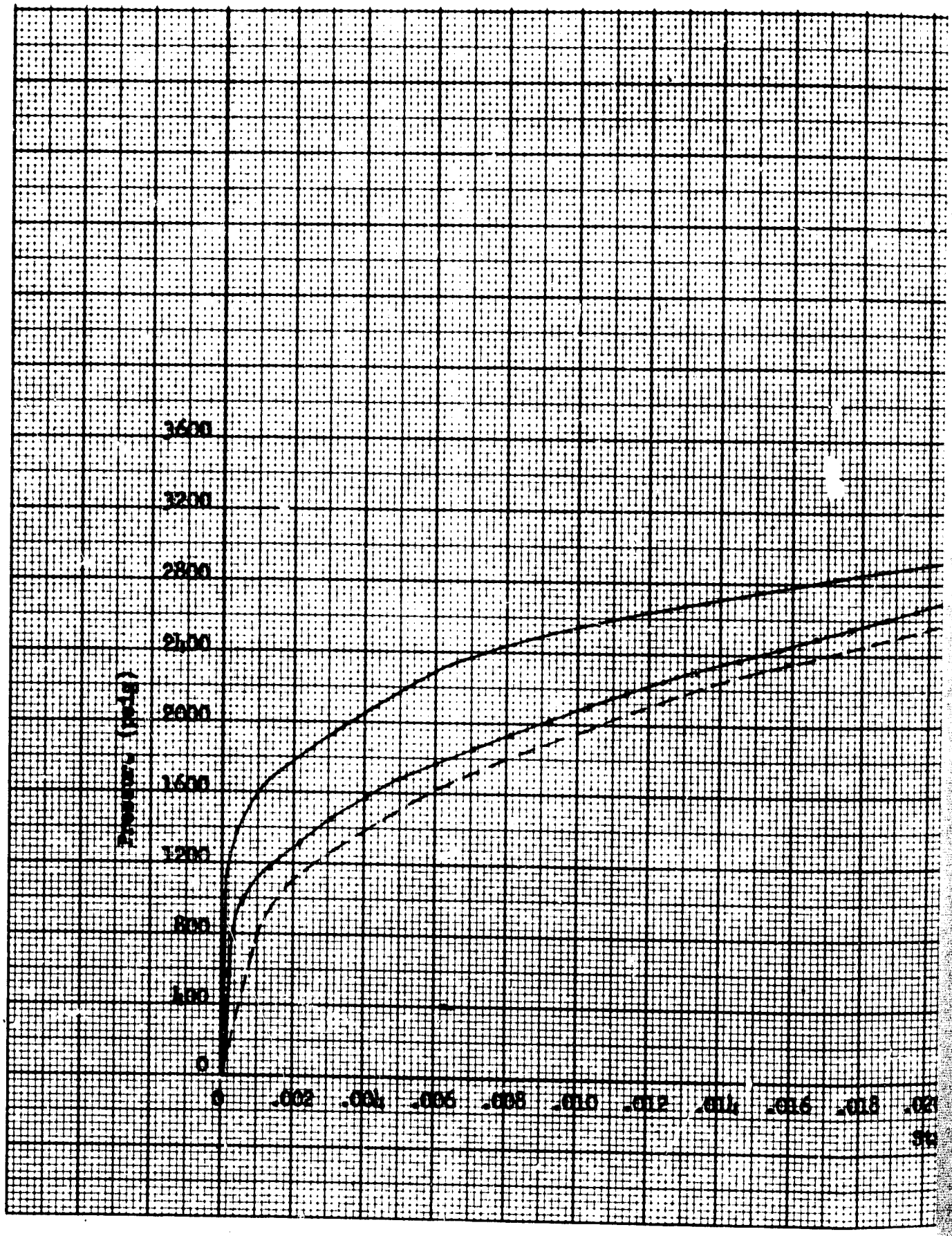

Tank 13 Press

Figure 77 - /

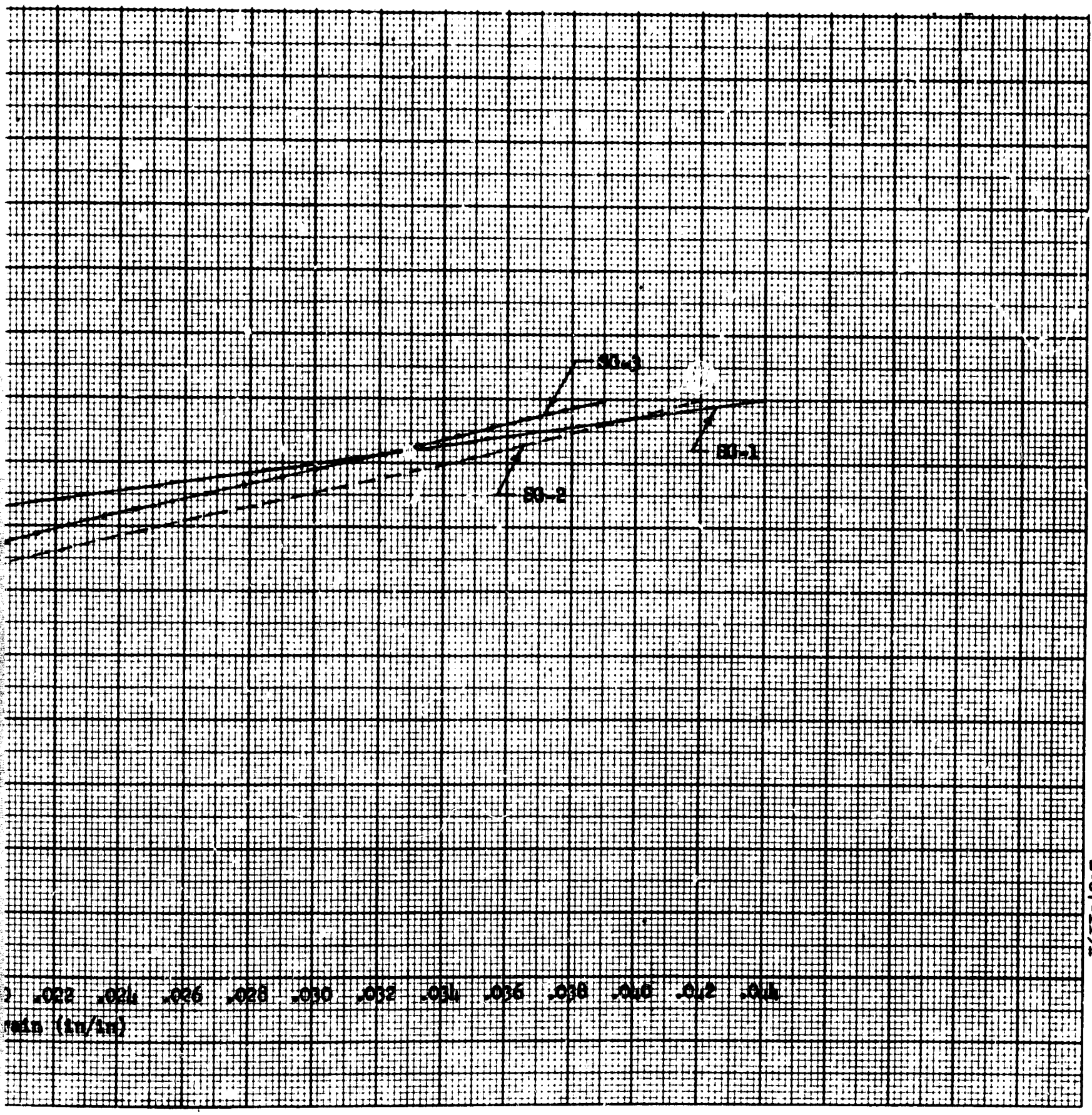

L-67-1197

ure vs Strain During Burst Test at -320°F

Figure 78

Tank 14 After Test

Figure 79

Tank 16 After Test

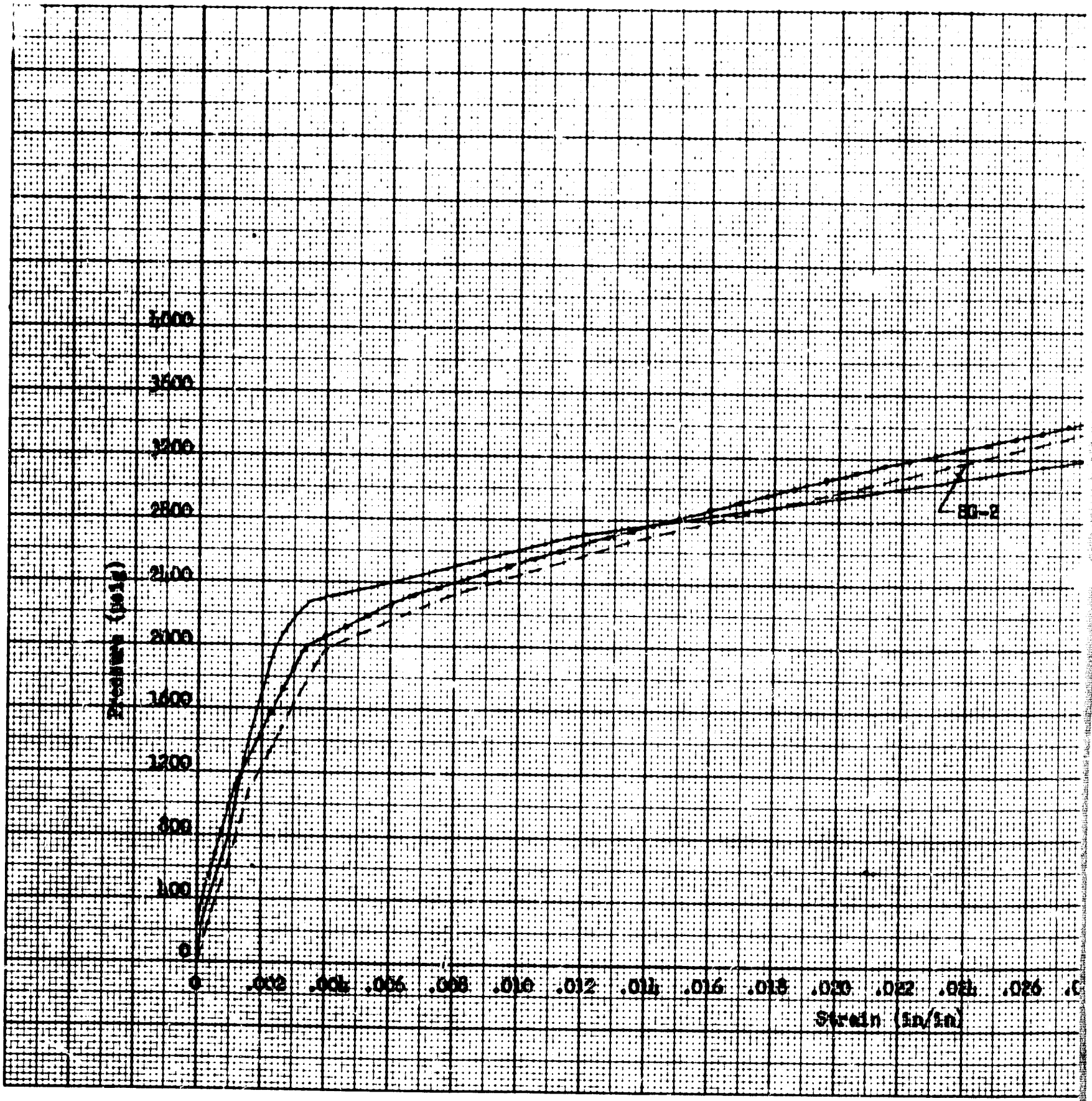

Tank 16 Pressure vs Strain During Burs

80 - 1

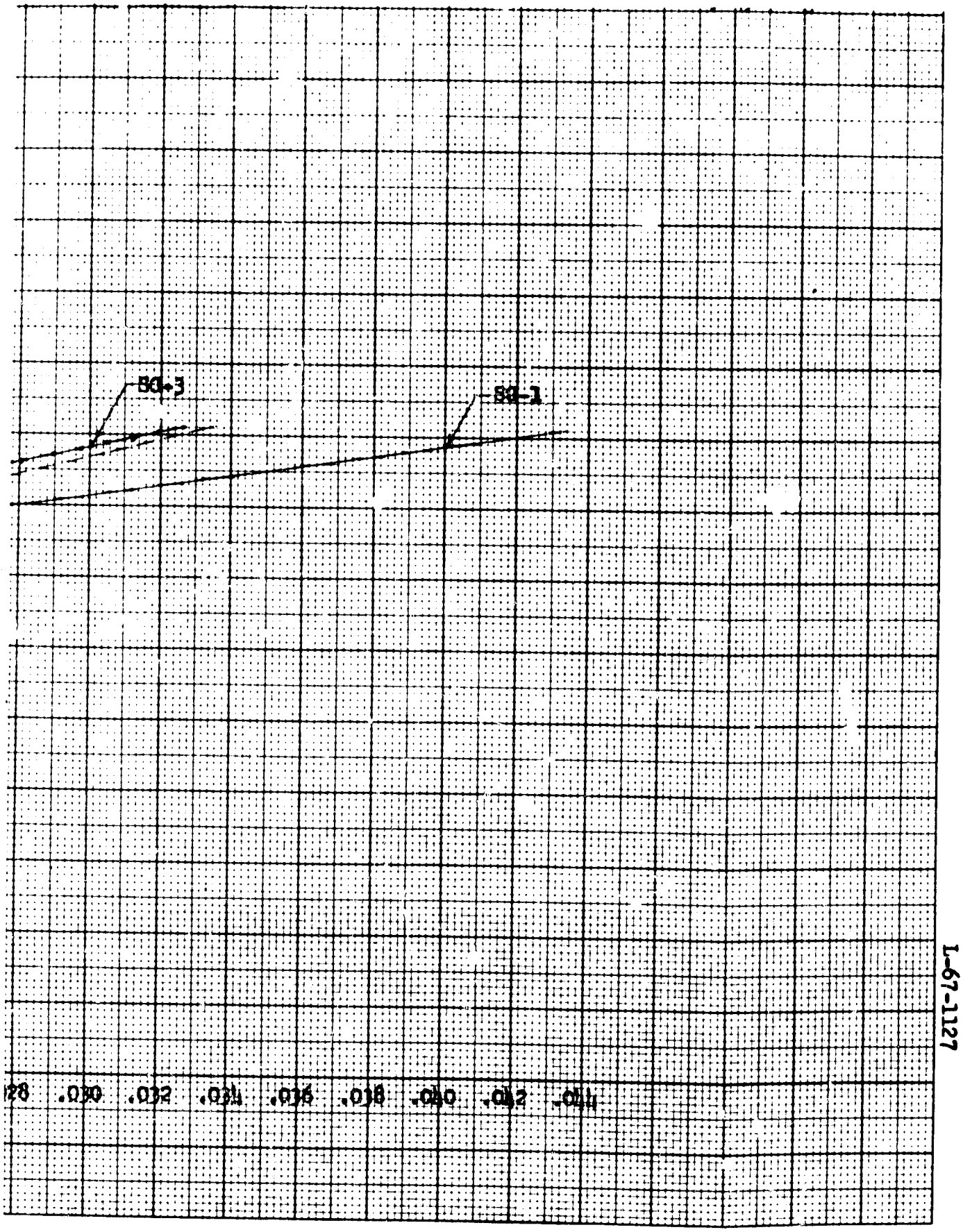

L-67-1127

st-Test Phase at -320°F

Figure 80 - 2

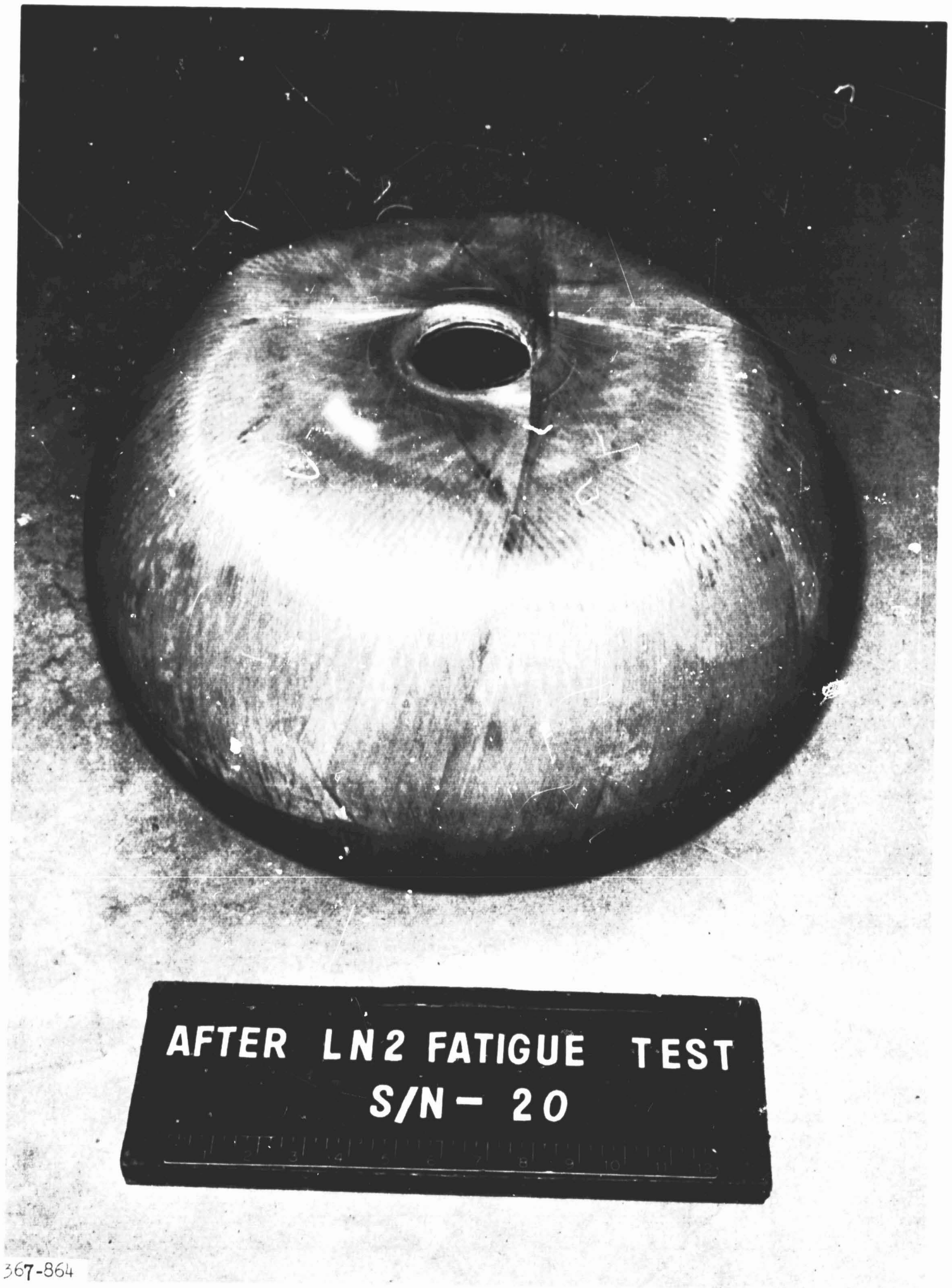

367-864

Tank 20 After Test

Figure 81

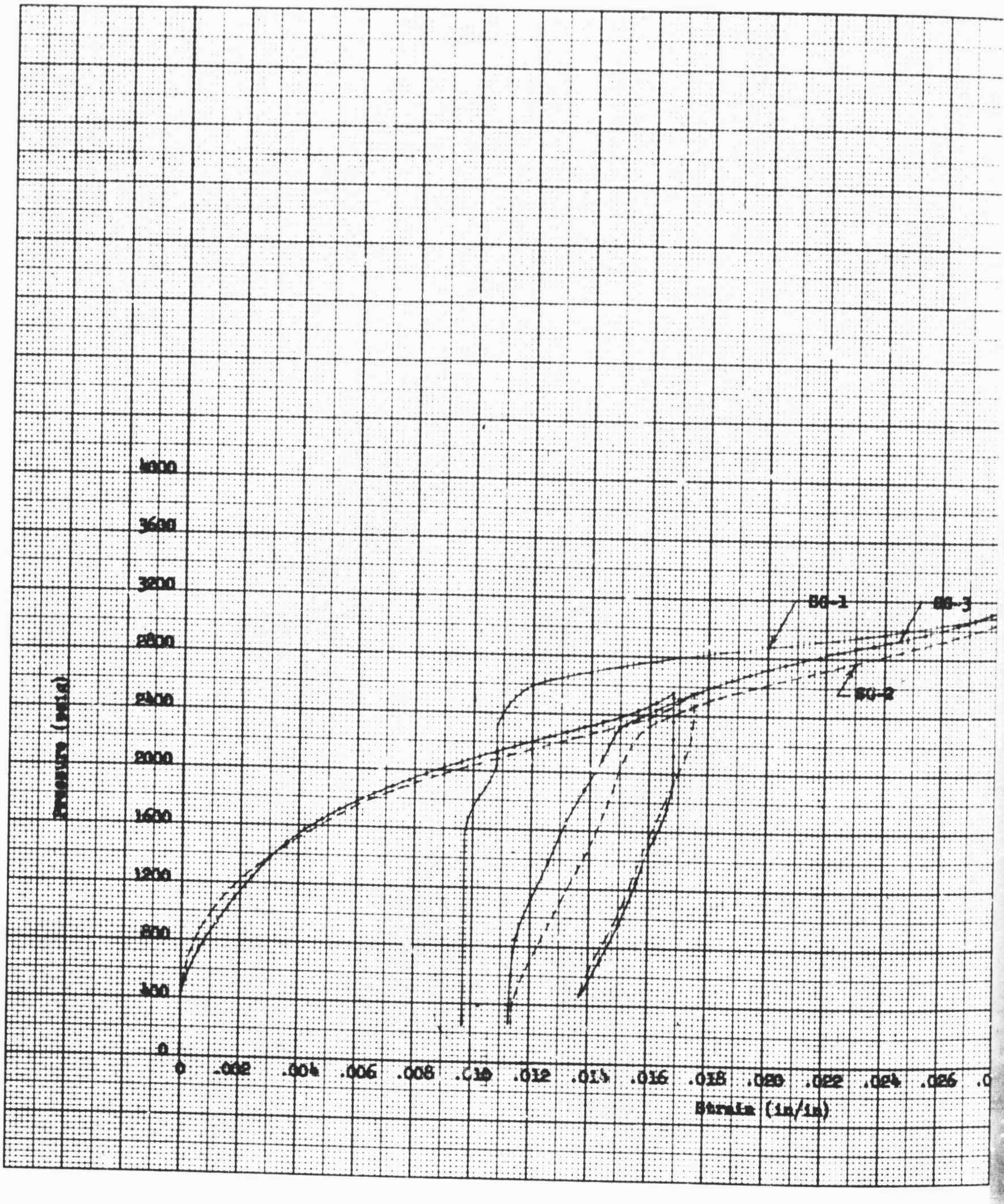

Tank 20 Pressure vs Strain for Initi
and Burst-Test Phases at

AEROJET-GENERAL CORPORATION - VKC
GFR INCONEL X-750 TANK STRAIN VS INTERNAL PRESSURE
S/N 20 TEST TEMPERATURE -295°F
FATIGUE CYCLE 1 AND BURST TEST
D-211-LT-11
16 Mar 1967
Burst Pressure: 3169 psig

Note:
Insufficient data
for 20-1, cycle 1

.028 .030 .032 .034 .036 .038 .040

1-67-1241

al-Pressurization
-320°F

Figure 82 - 1

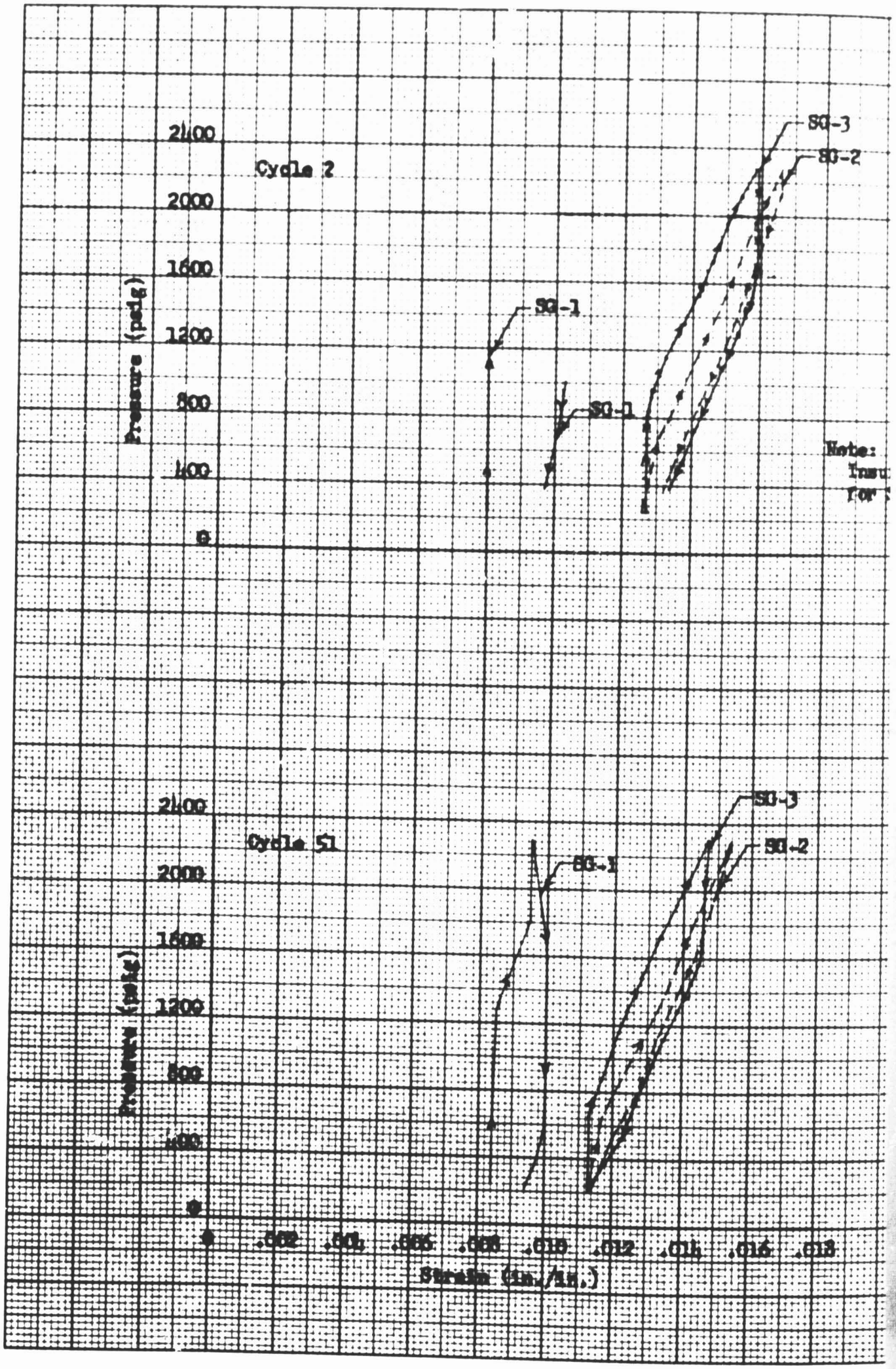

Tank 20 Pressure vs S

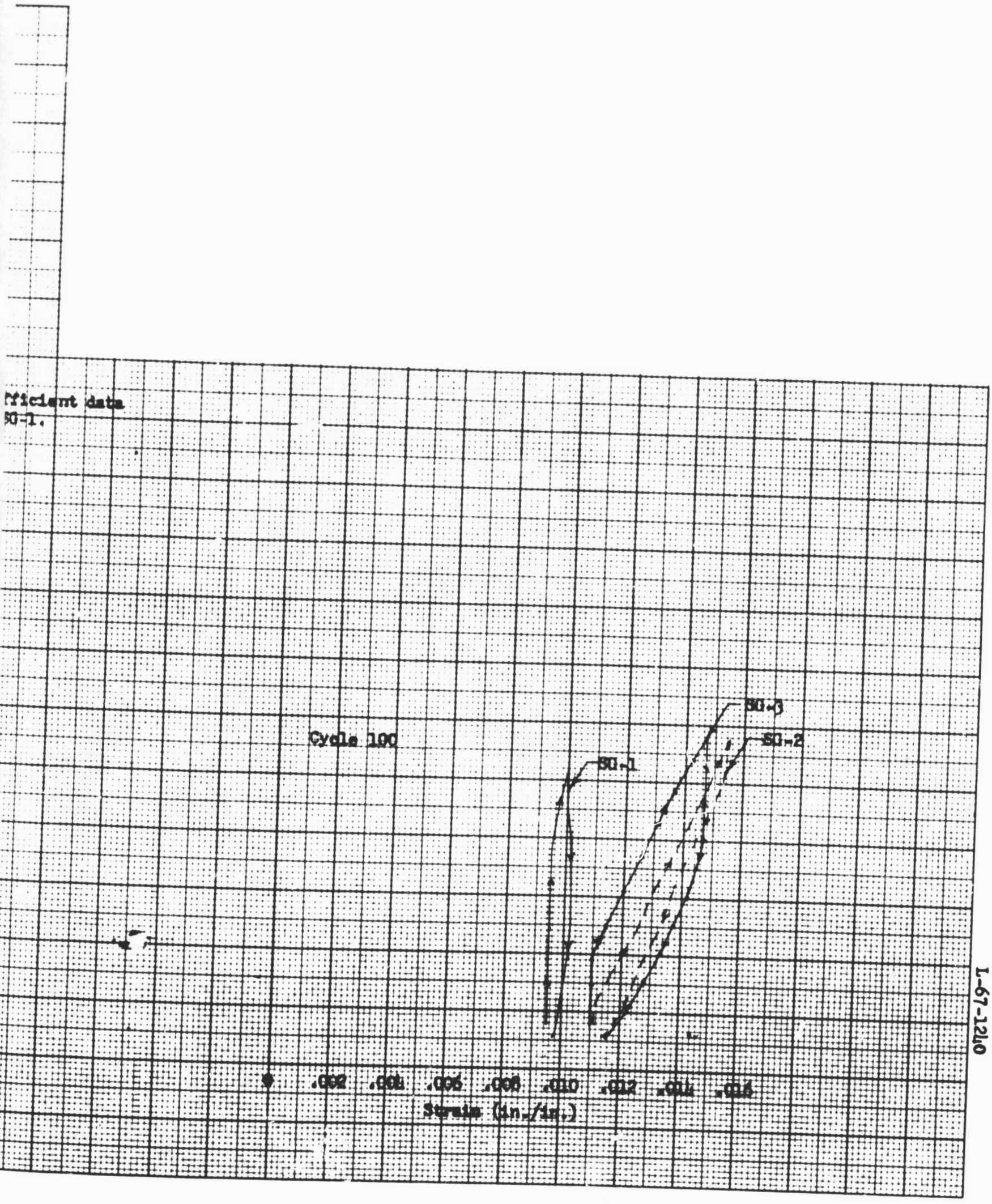

ain During Pressure Cycling at -320°F

Figure 83 – 2

Figure 84

Tank 21 After Test

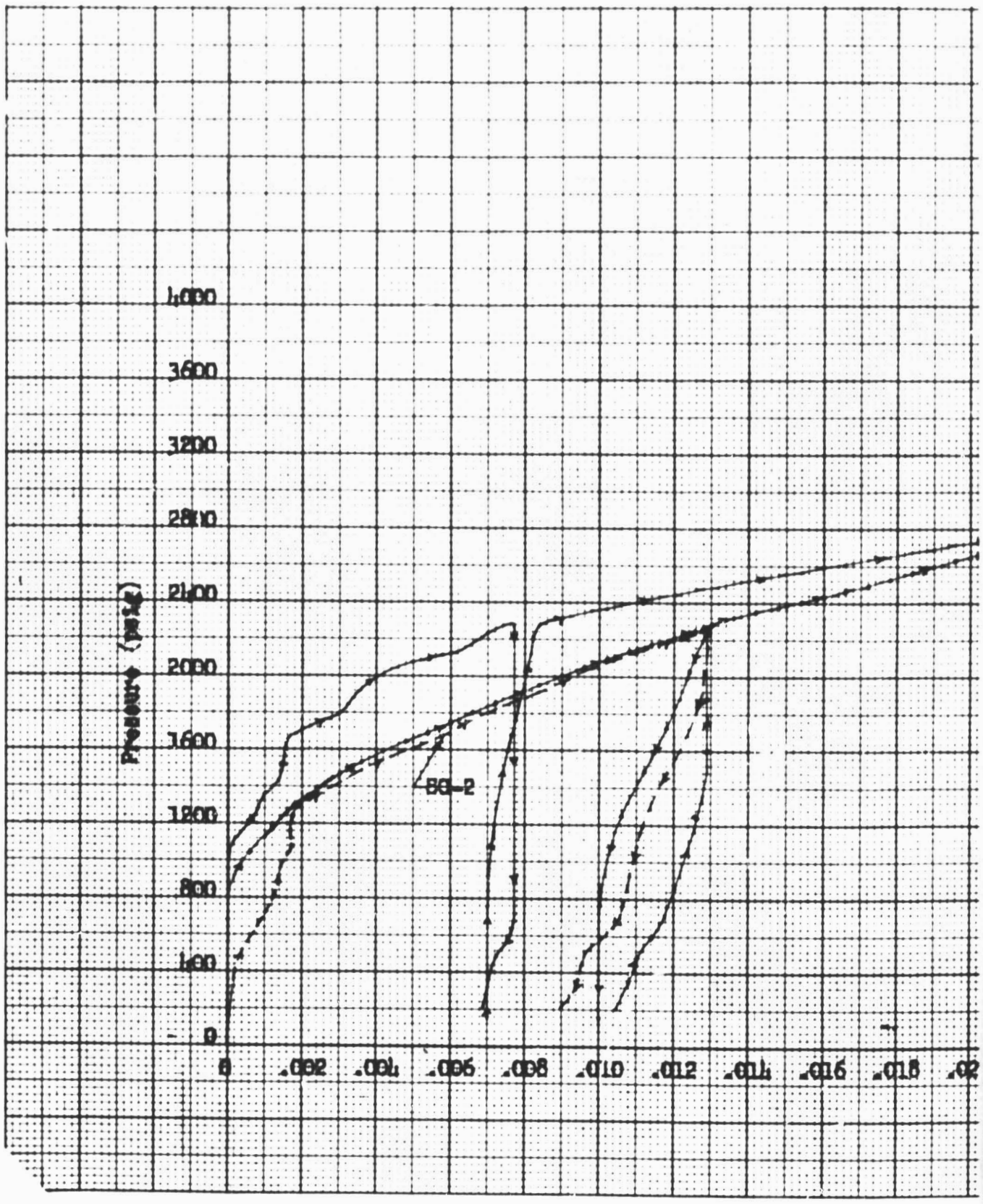

Tank 21 Pressure vs S
and Burst-

Figure 85-1

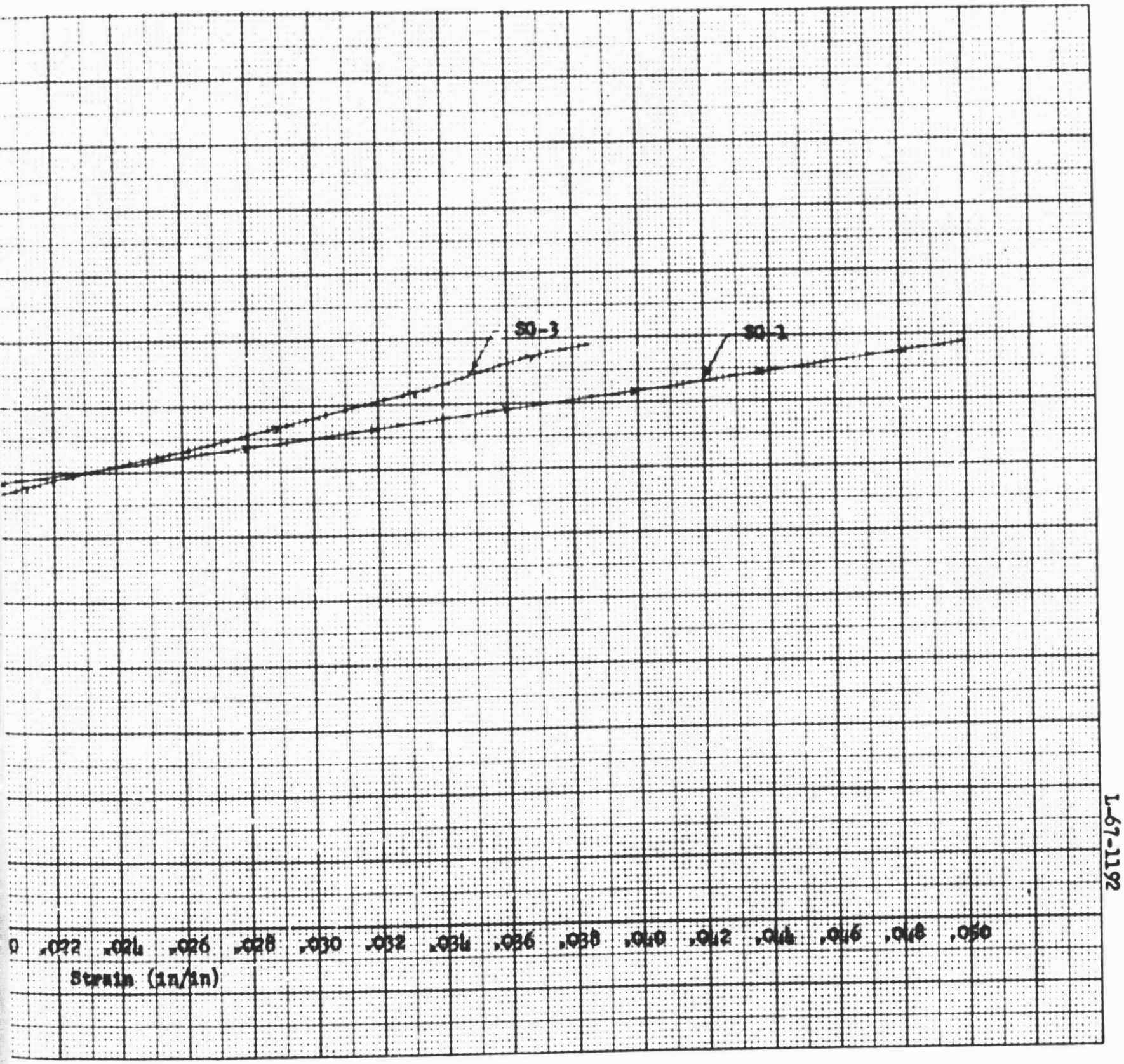

L-67-1192

Strain for Initial-Pressurization
Test Phases at -320°F

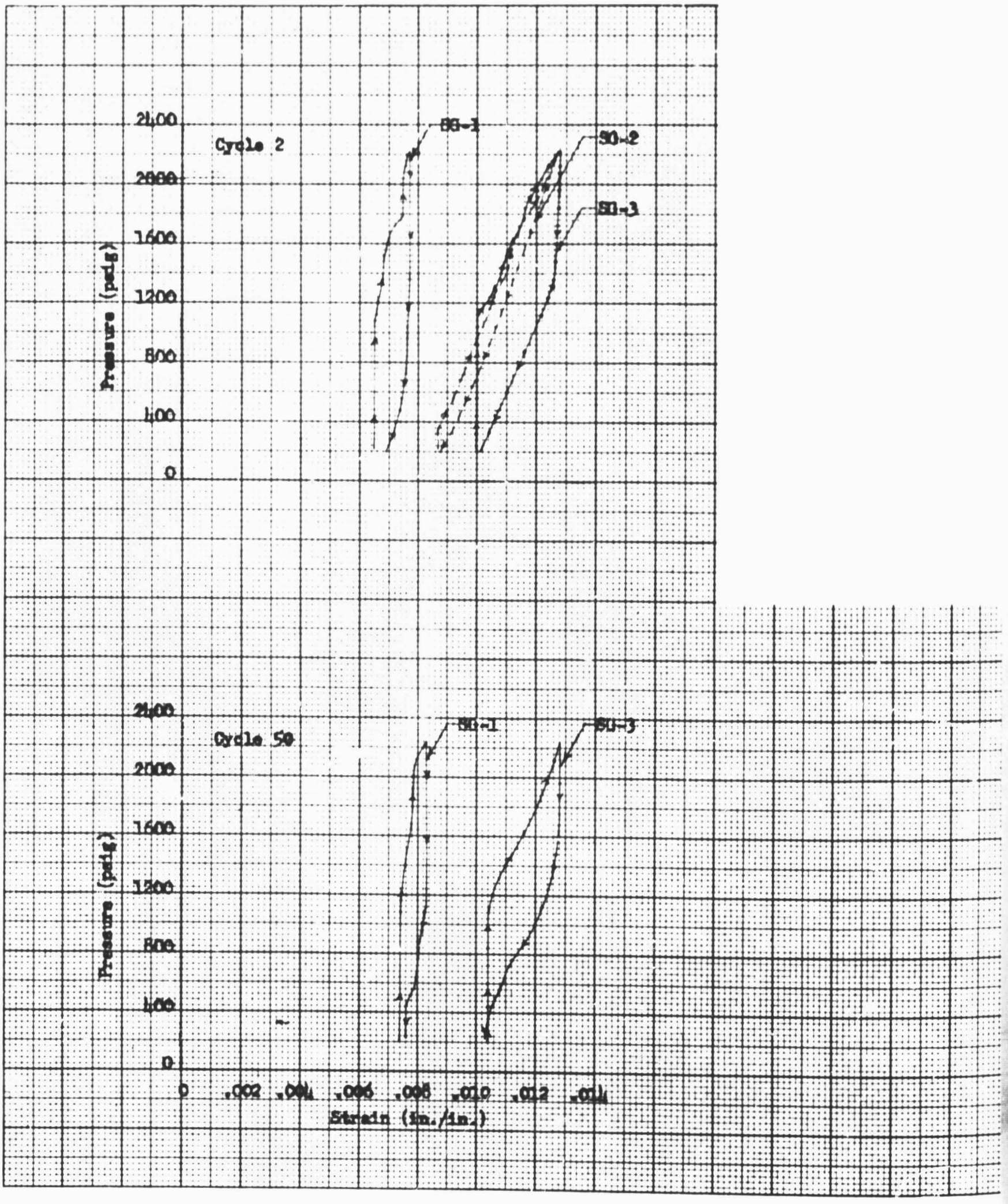

Figure 86-1

Tank 21 Pressure vs Strain During Press

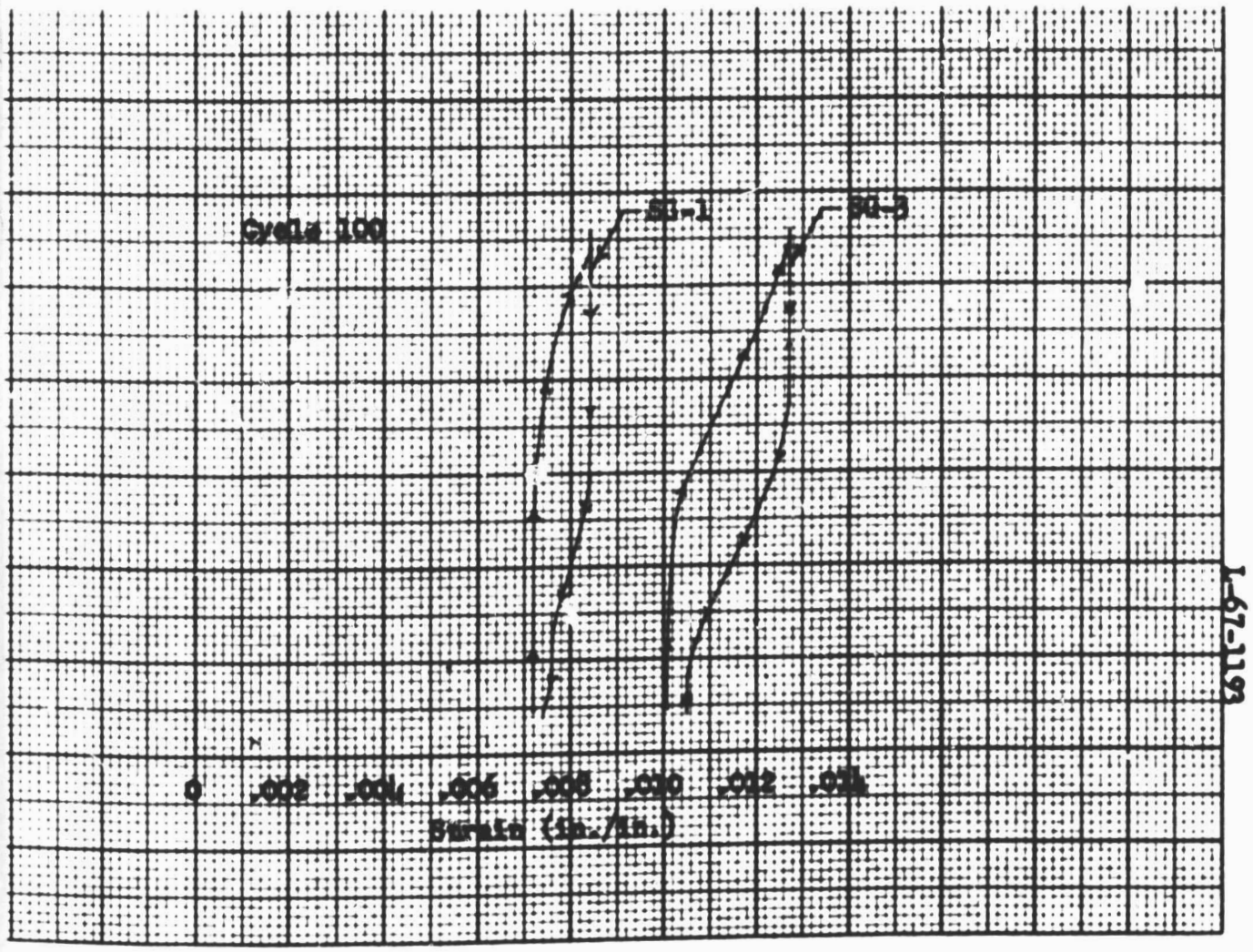

ure Cycling at -320°F

Figure 86 - 2.

Figure 87

Tank 15 After Test

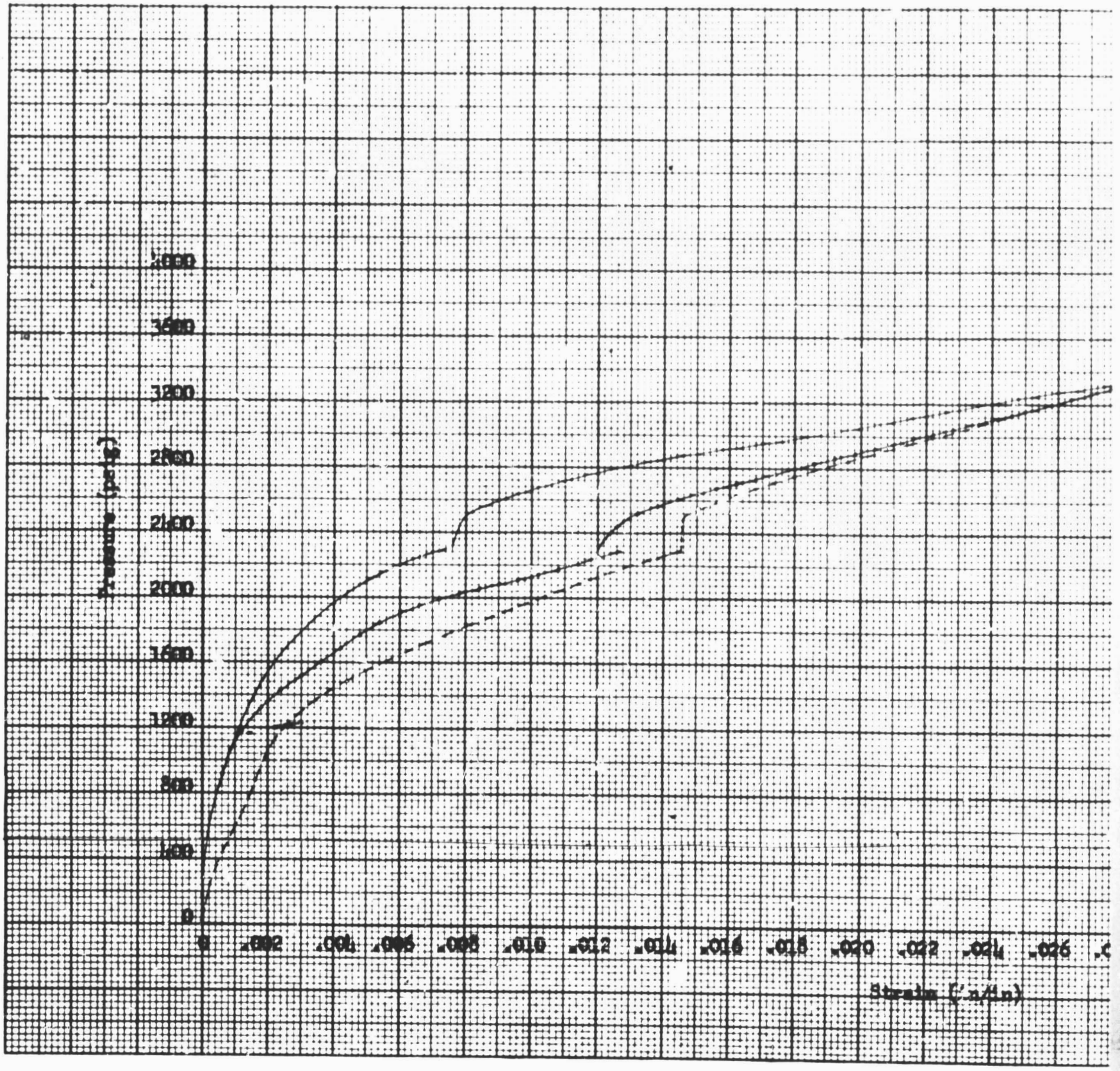

Tank 15 Pressure vs Strain for Initial
and Burst-Test Phases at -3

Figure 88-1

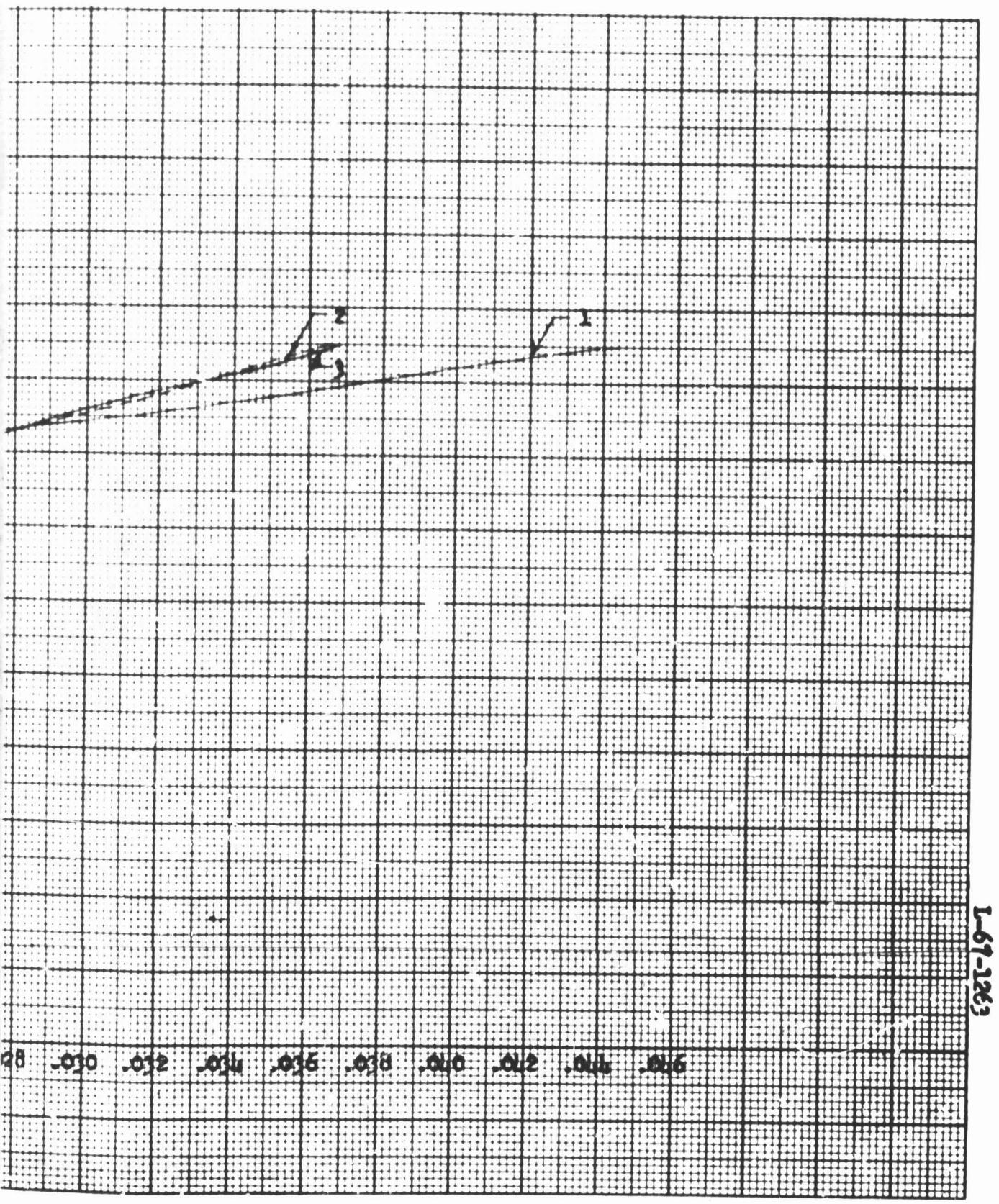

-Pressurization
20°F

Figure 88 - 2

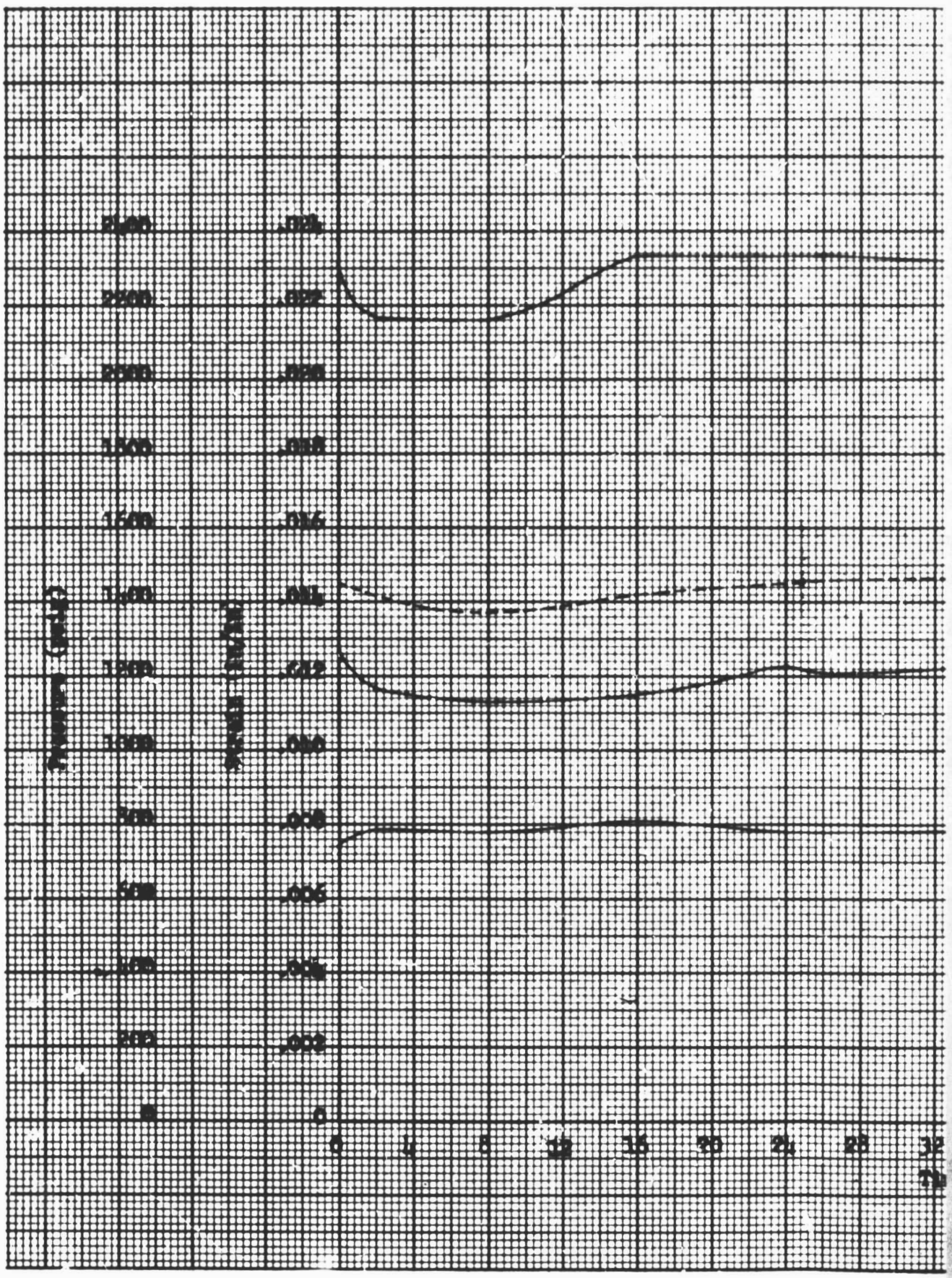
Tank 15 Pressure vs

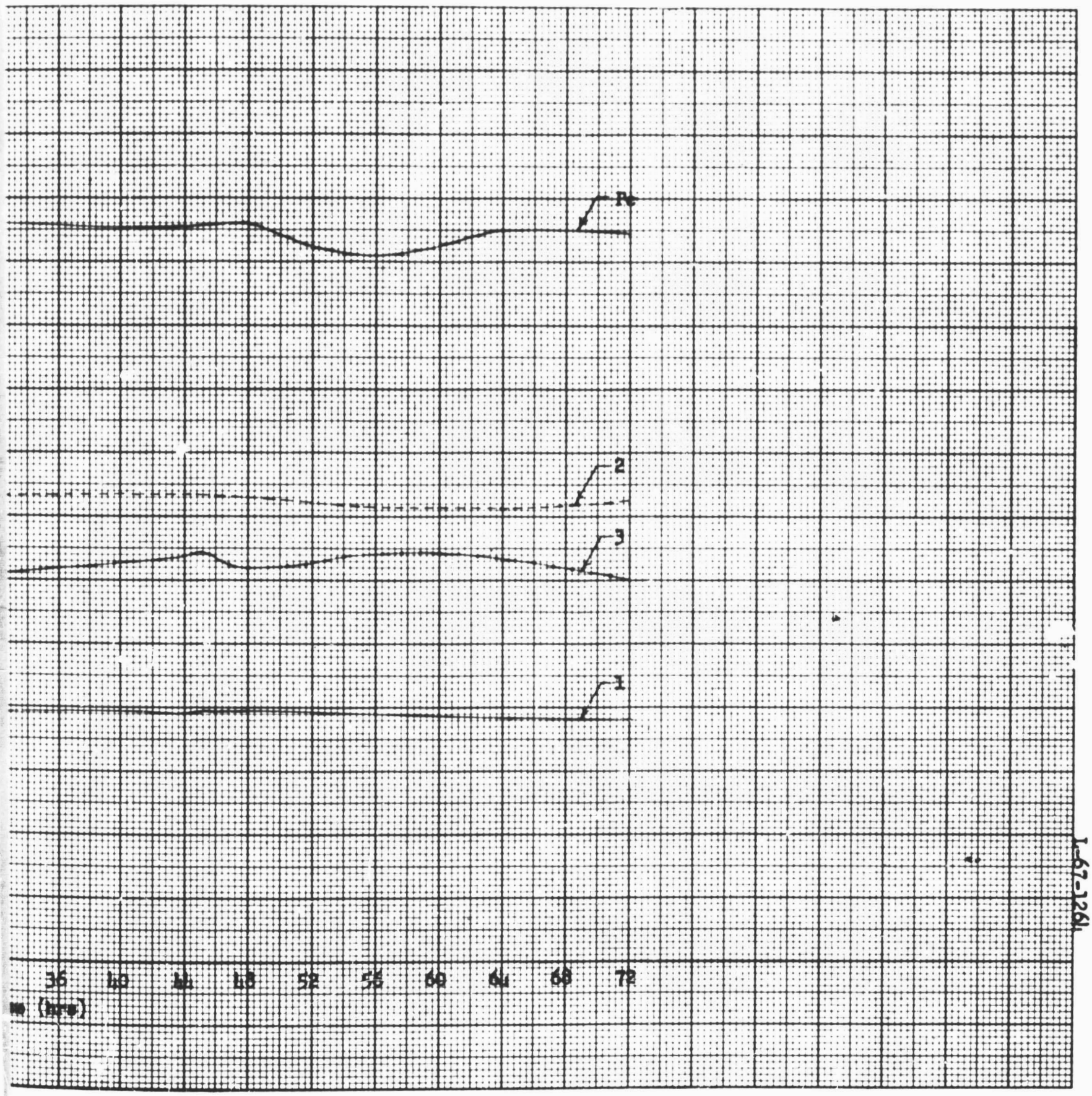

Strain During Creep Test at -320°F

Figure 89 - 2

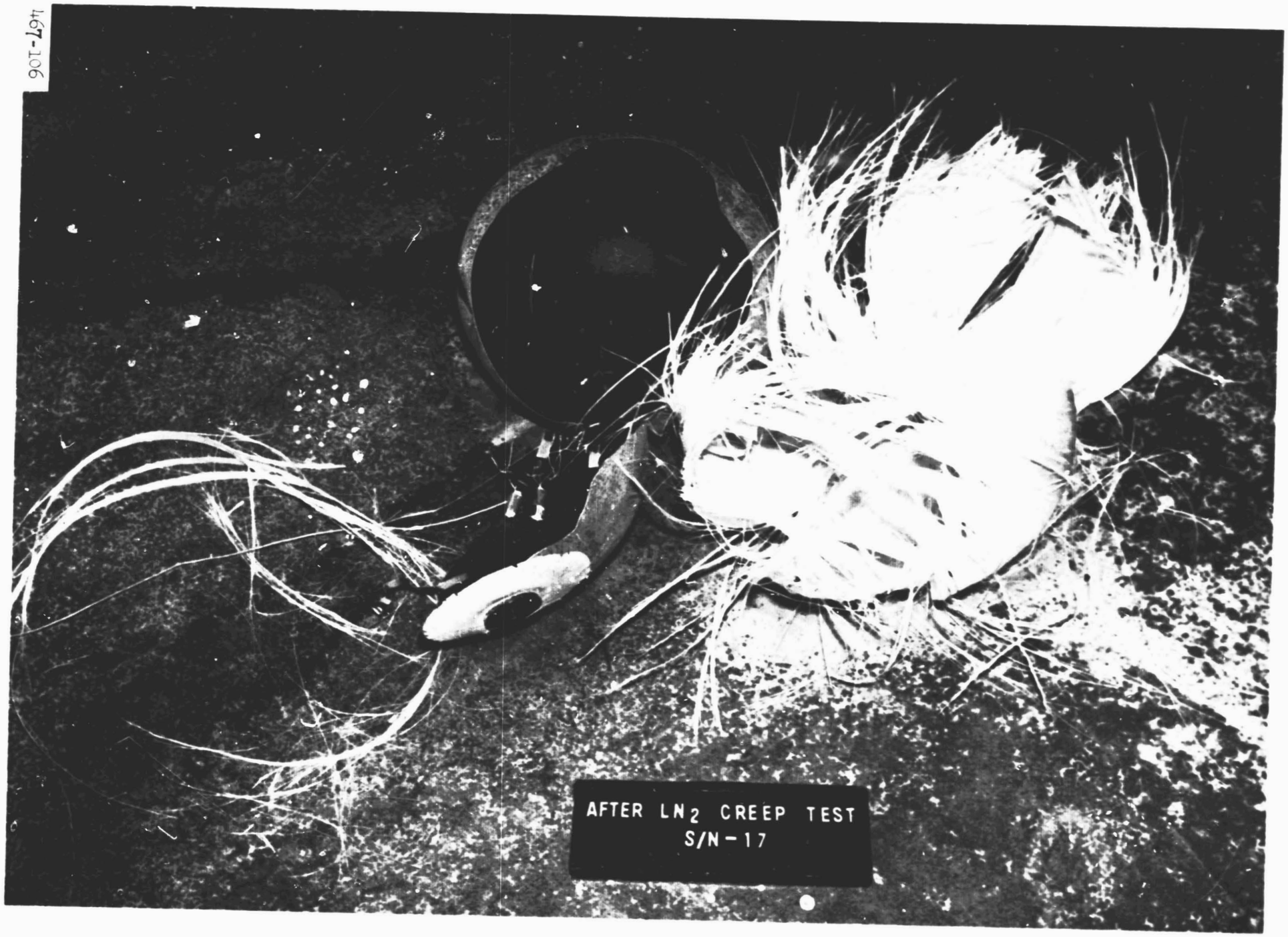

Figure 90

Tank 17 After Test

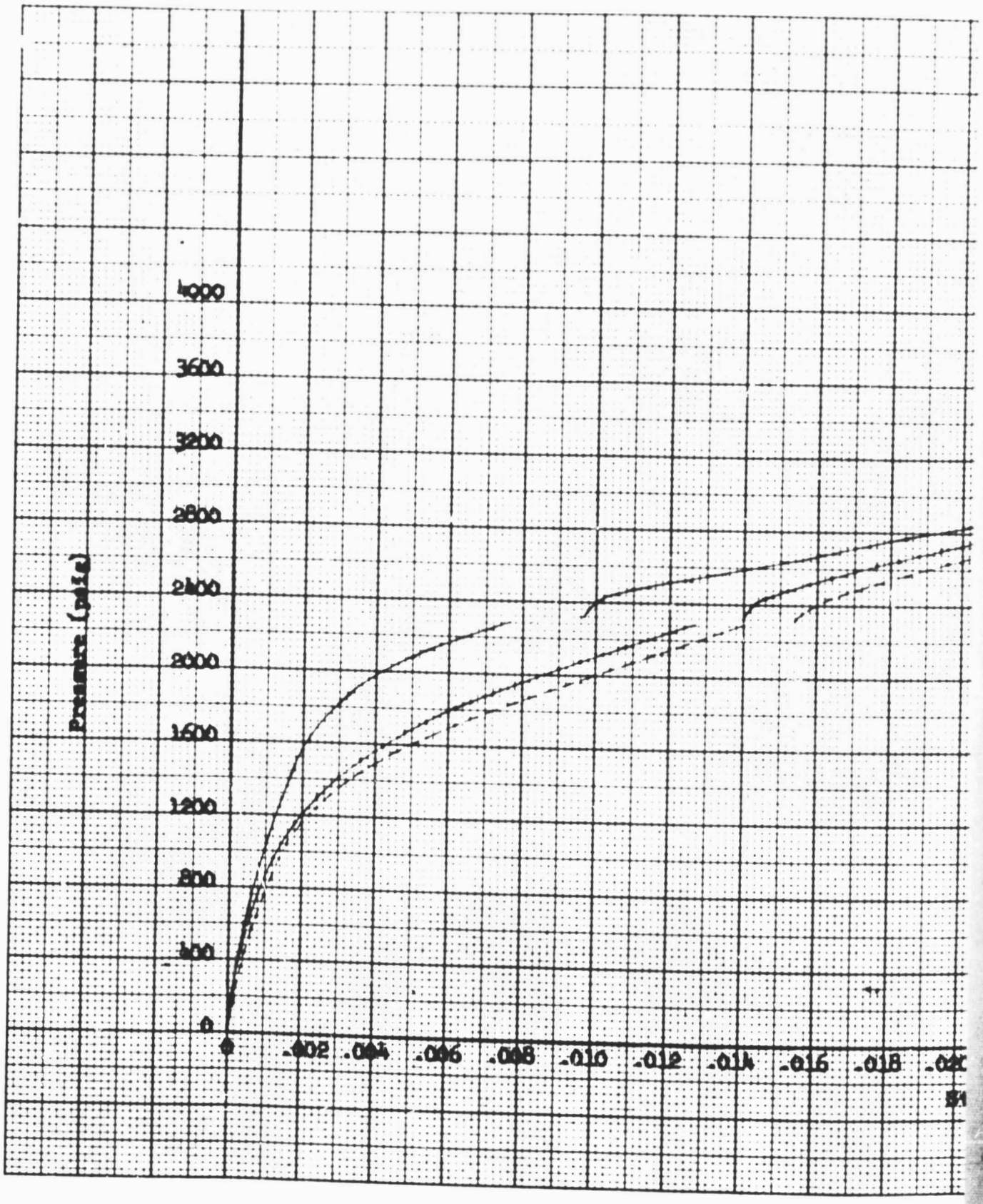

Tank 17 P

Figu e 91 - 1

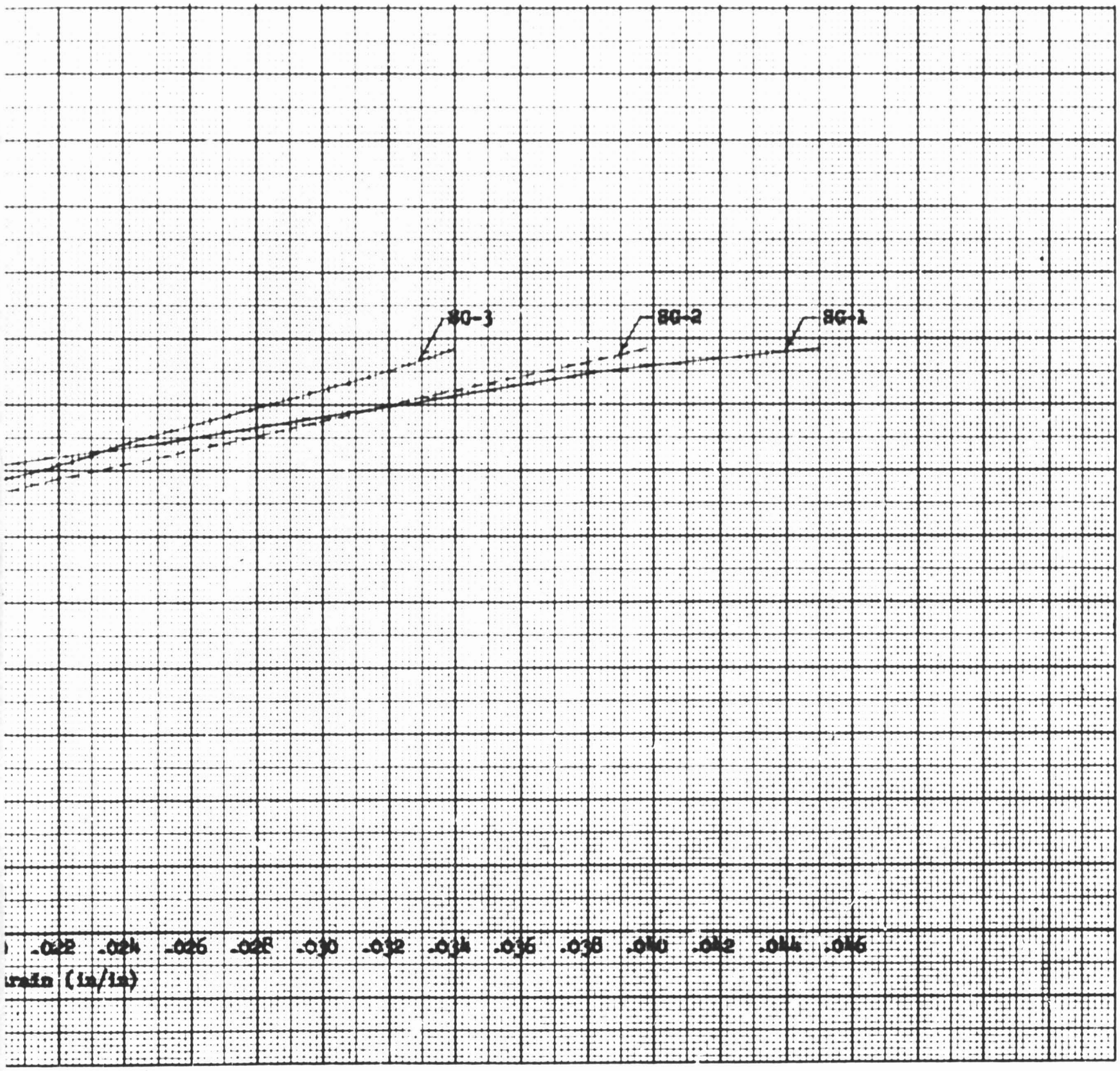

L-57-1265

ressure vs Strain for Initial Pressurization
and Burst-Test Phases at -320°F

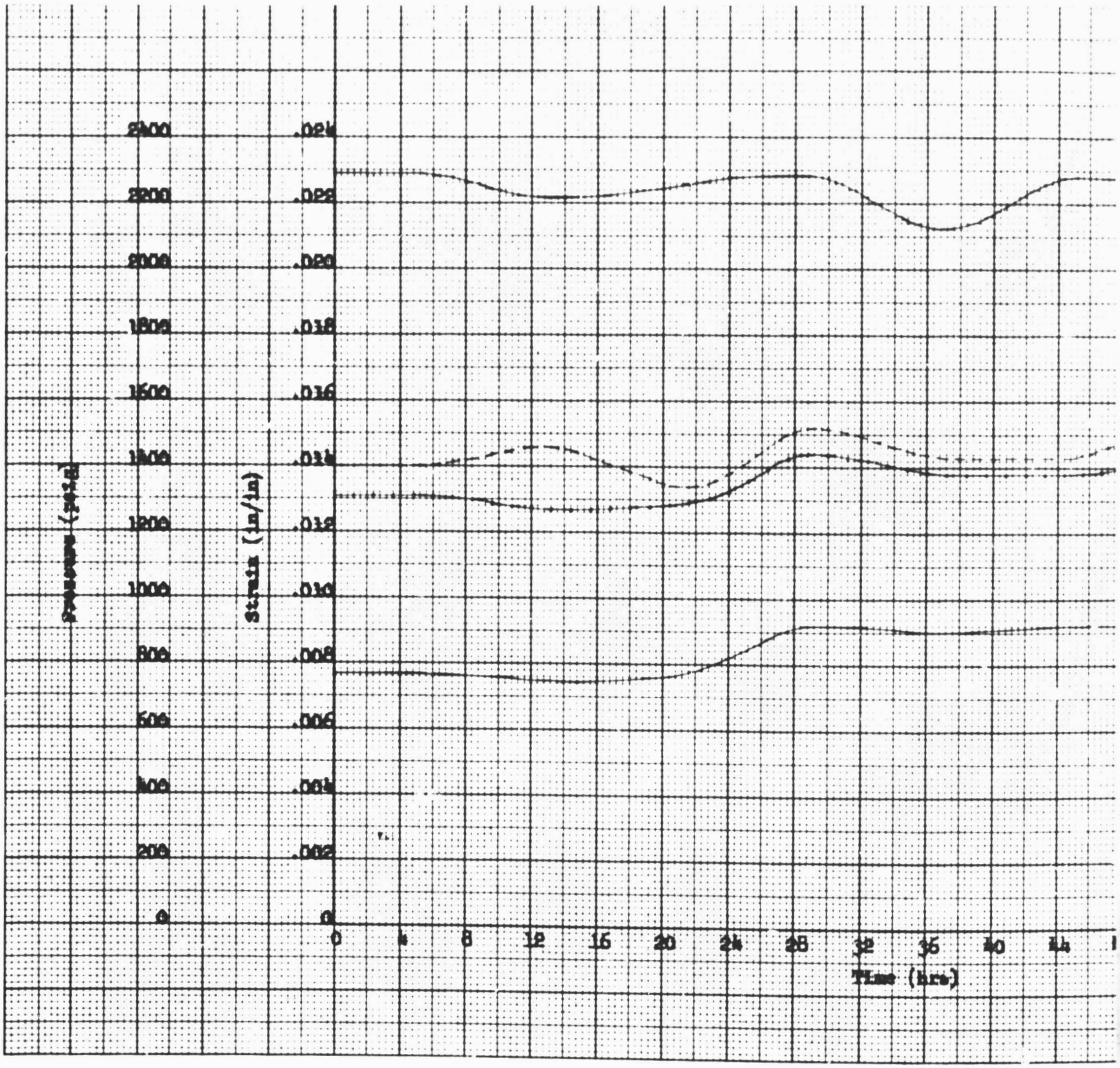

Tank 17 Pressure vs Strain During Creep

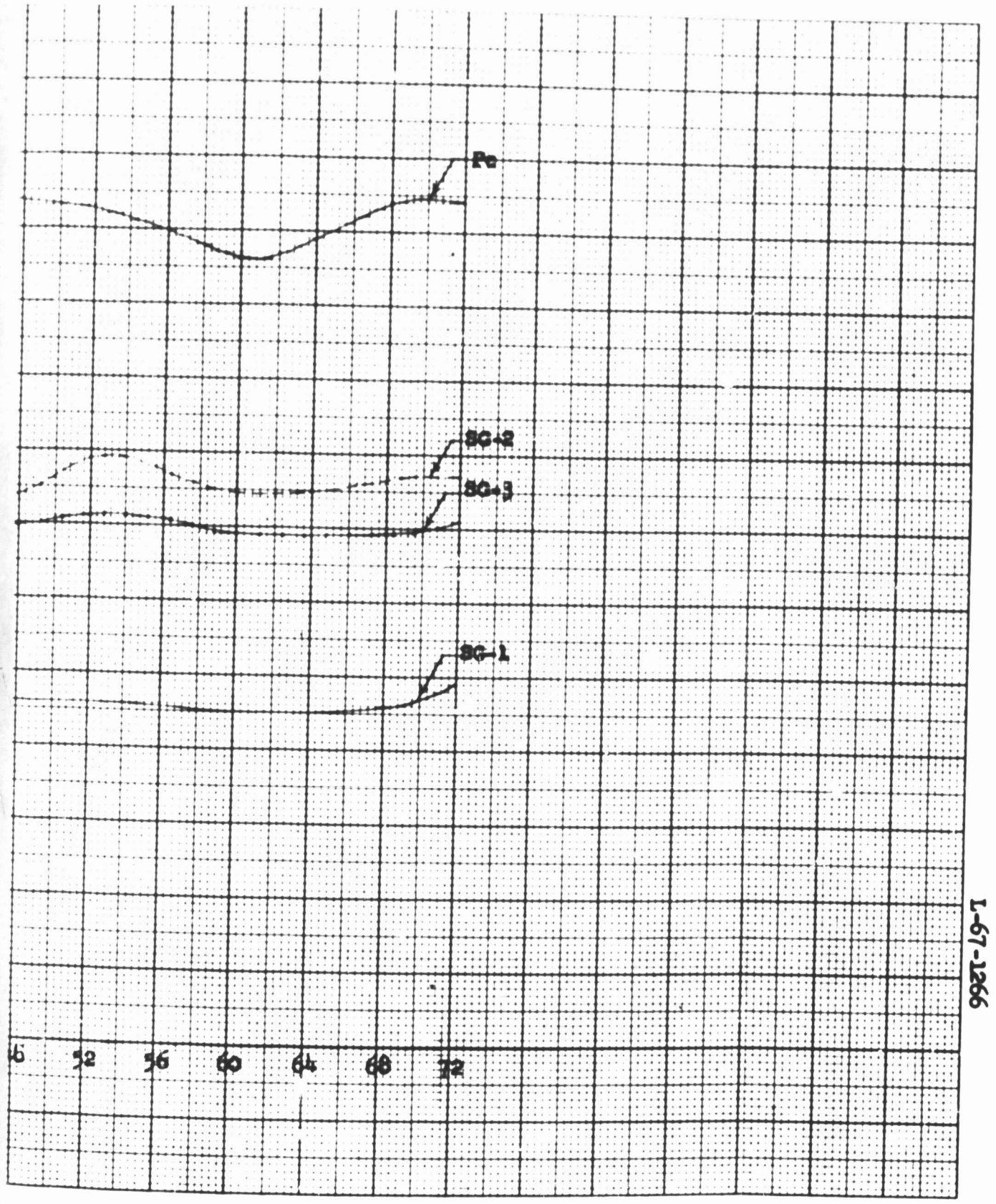

Test (-320°F)

Figure 92 - 2

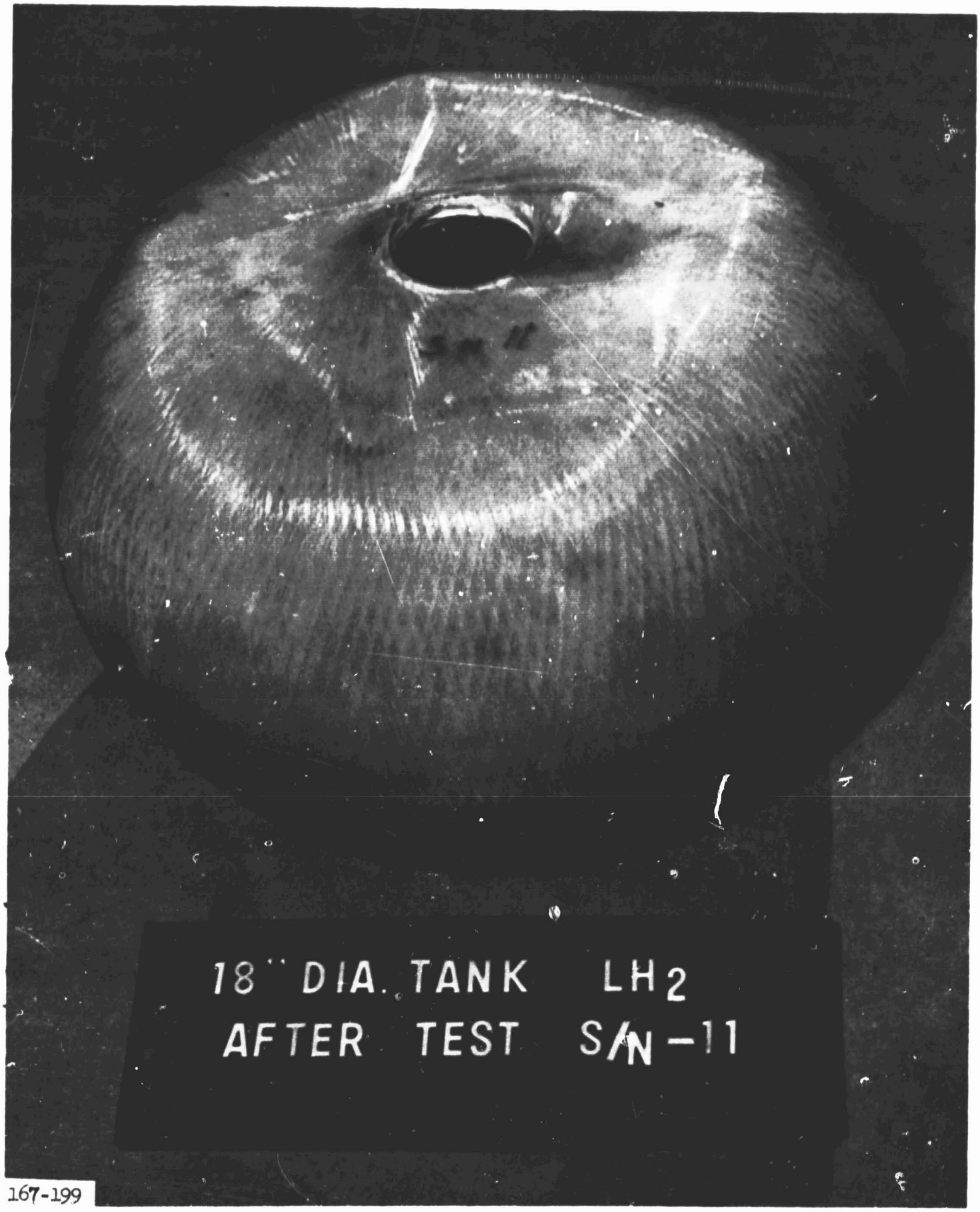

Tank 11 After Test

Figure 93

Figure 9

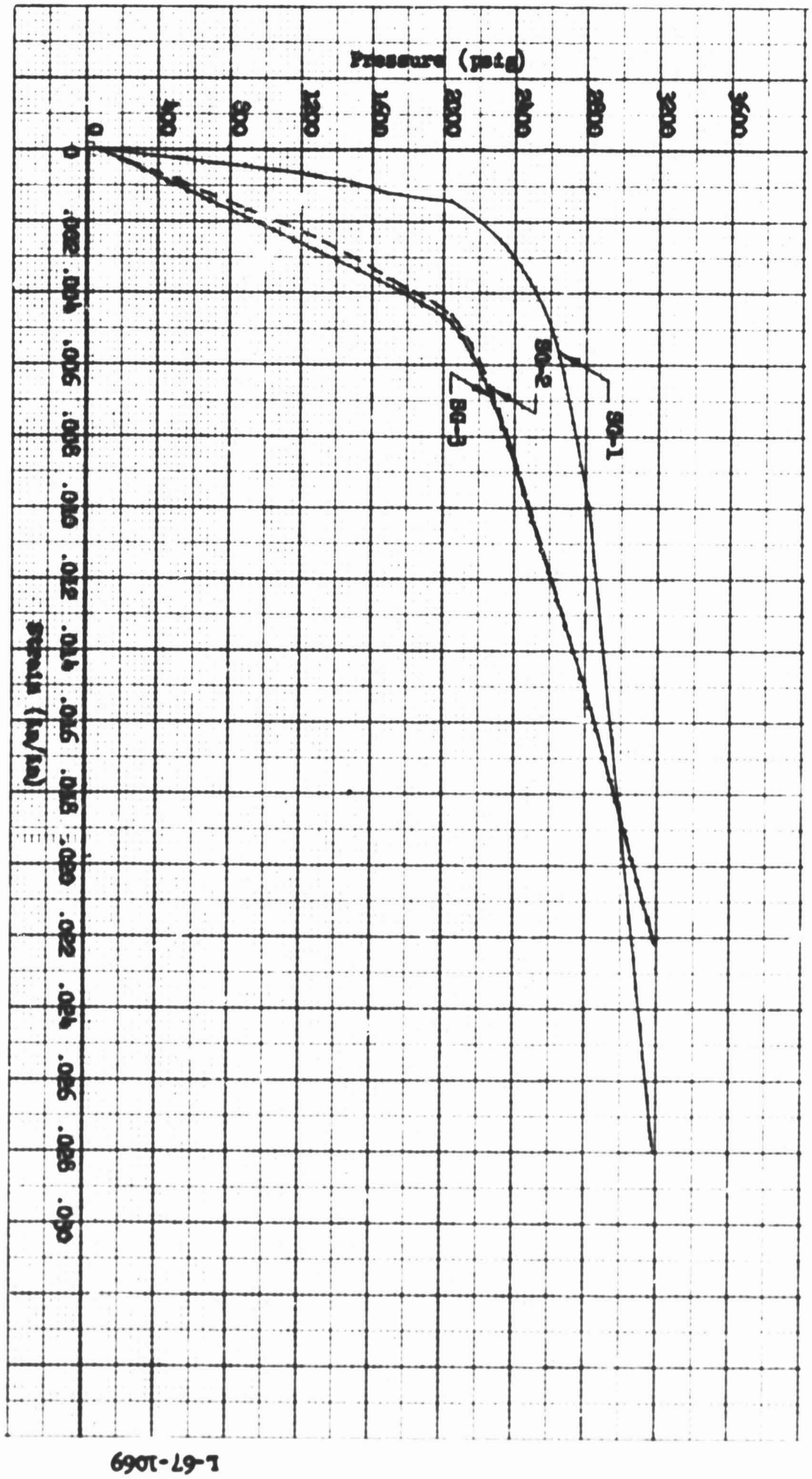

Tank 11 Pressure vs Strain for Burst Test at -423°F

Figure 95

Tank 19 After Test

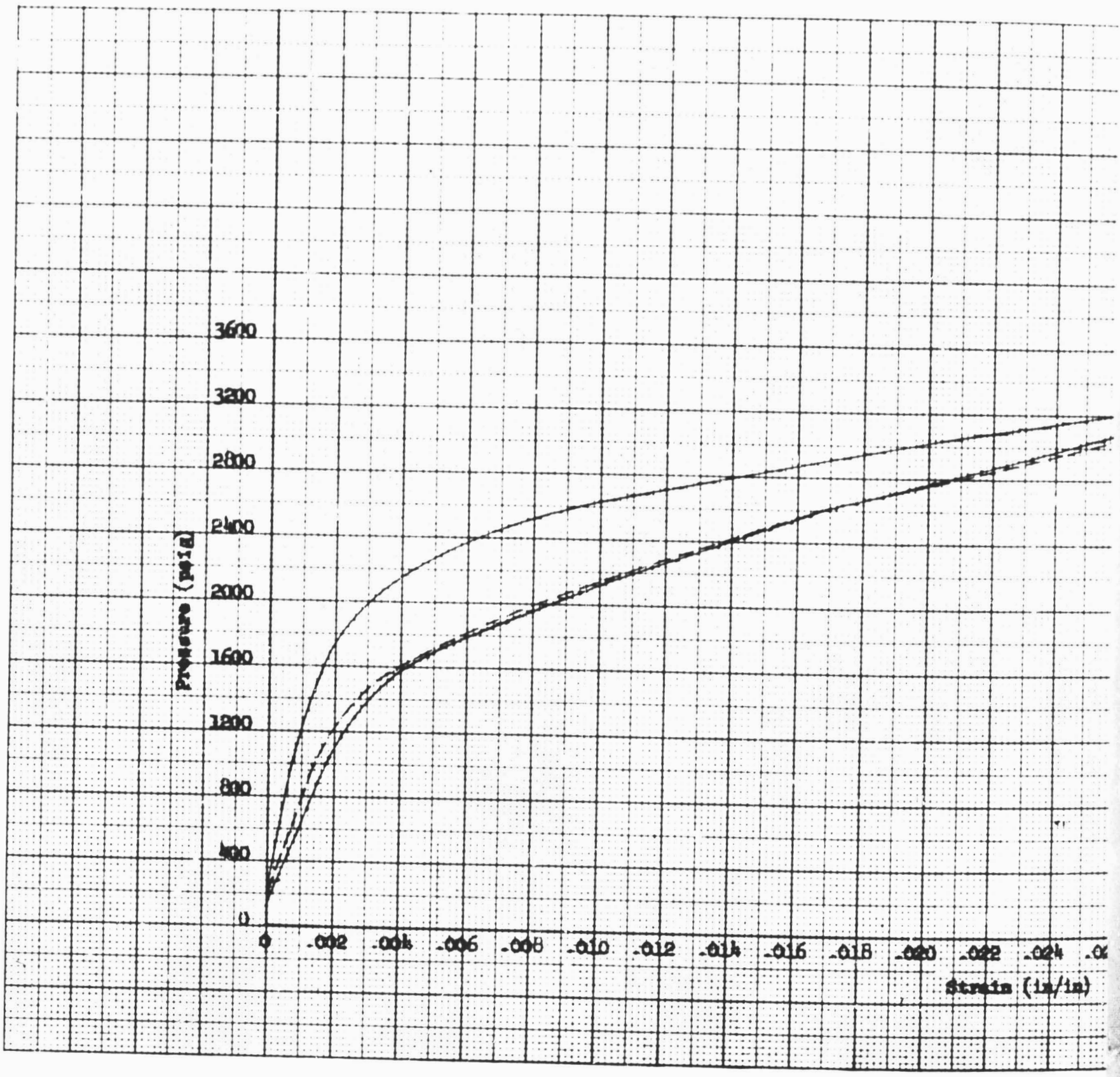

Tank 19 Pressure vs Strain for Burst Test

96-1

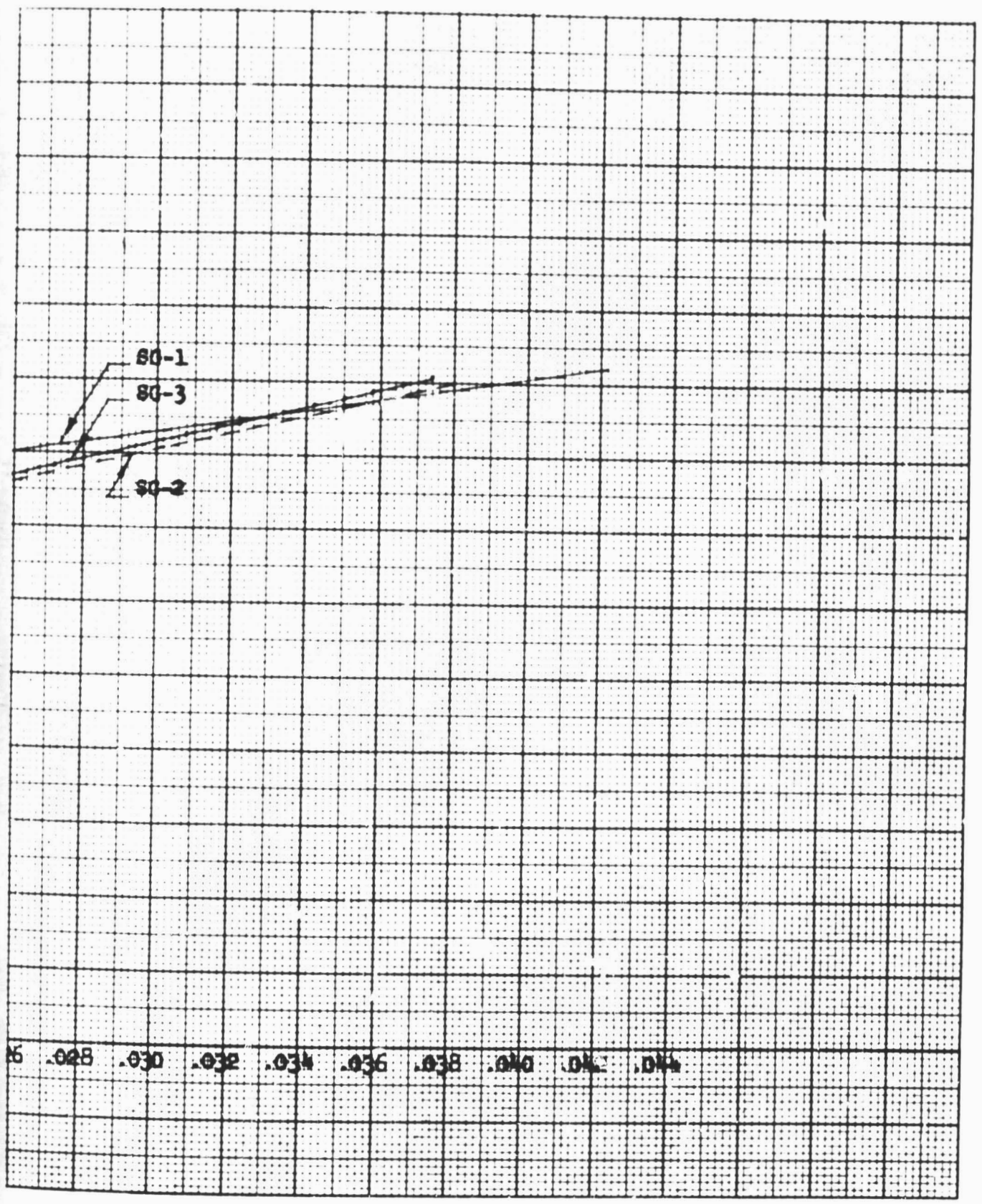

L-67-1067

; at -423°F

Figure 96 - 2

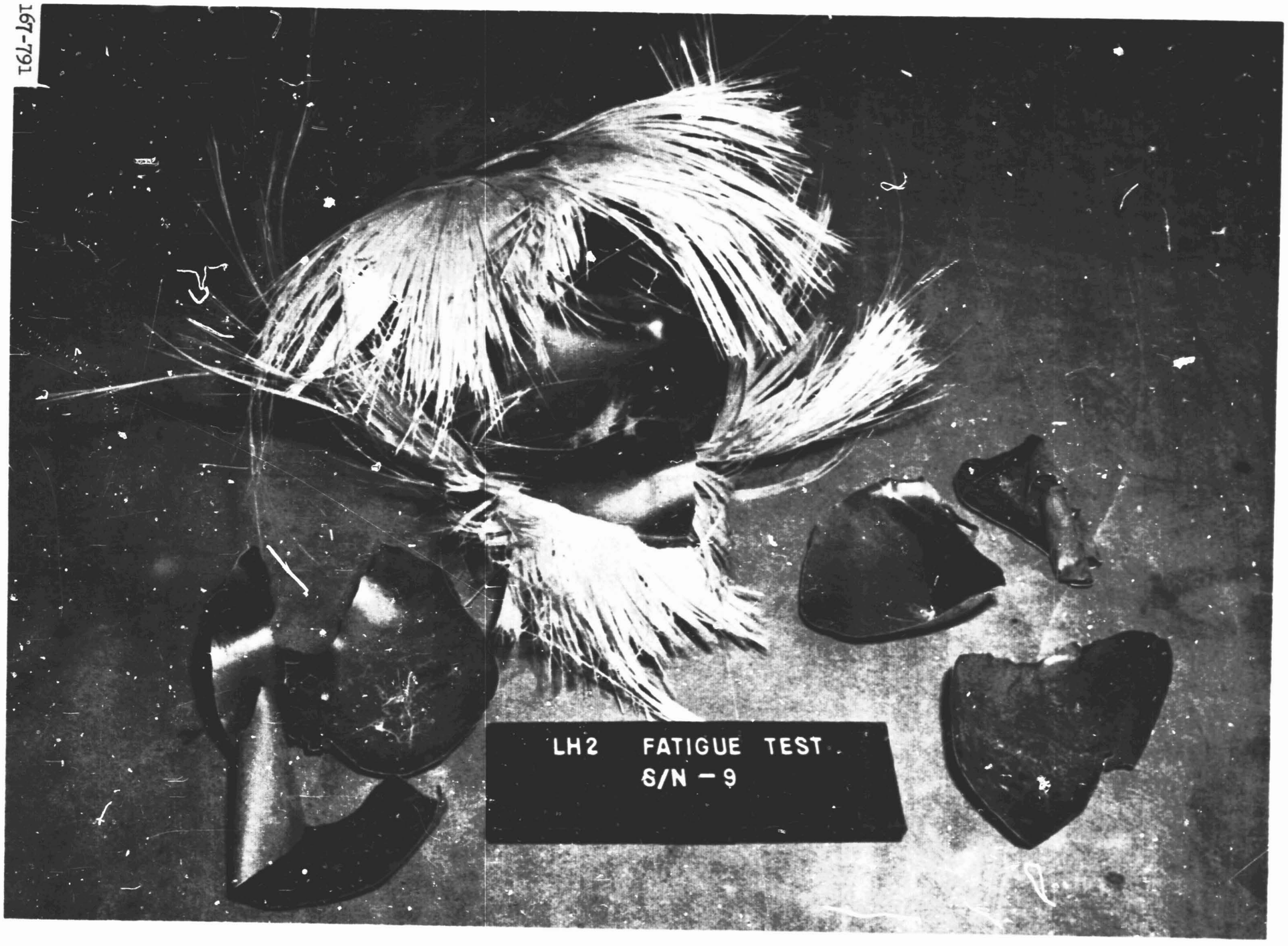

Tank 9 After Test

BEST AVAILABLE COPY CONTACT THE DOCUMENT ORIGINATOR.

L-67-1071

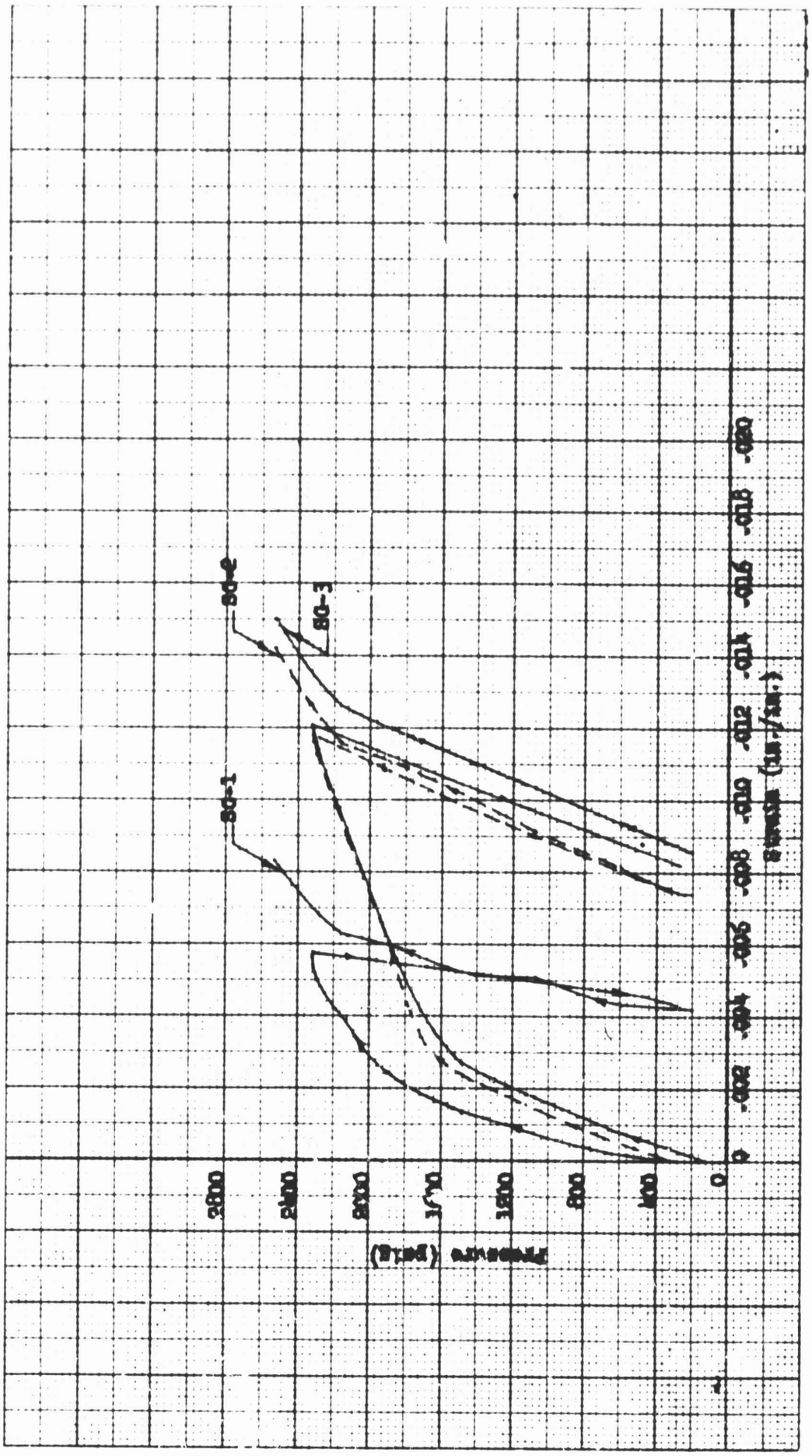

Tank 9 Pressure vs Strain for Initial-Pressurization and Burst-Test Phases at -423°F

Figure 98

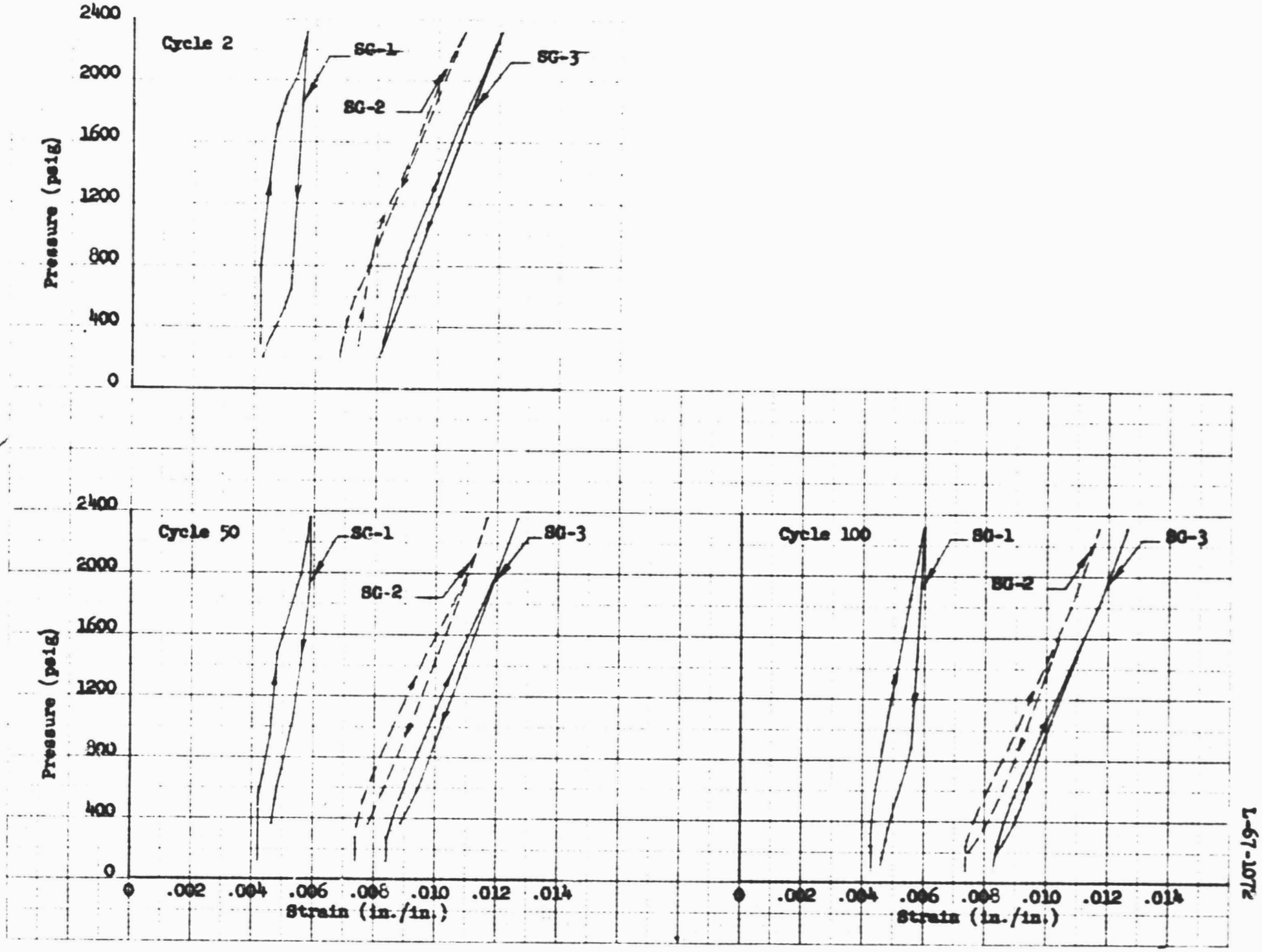

Figure 99

Tank 9 Pressure vs Strain During Pressure Cycling at -423°F

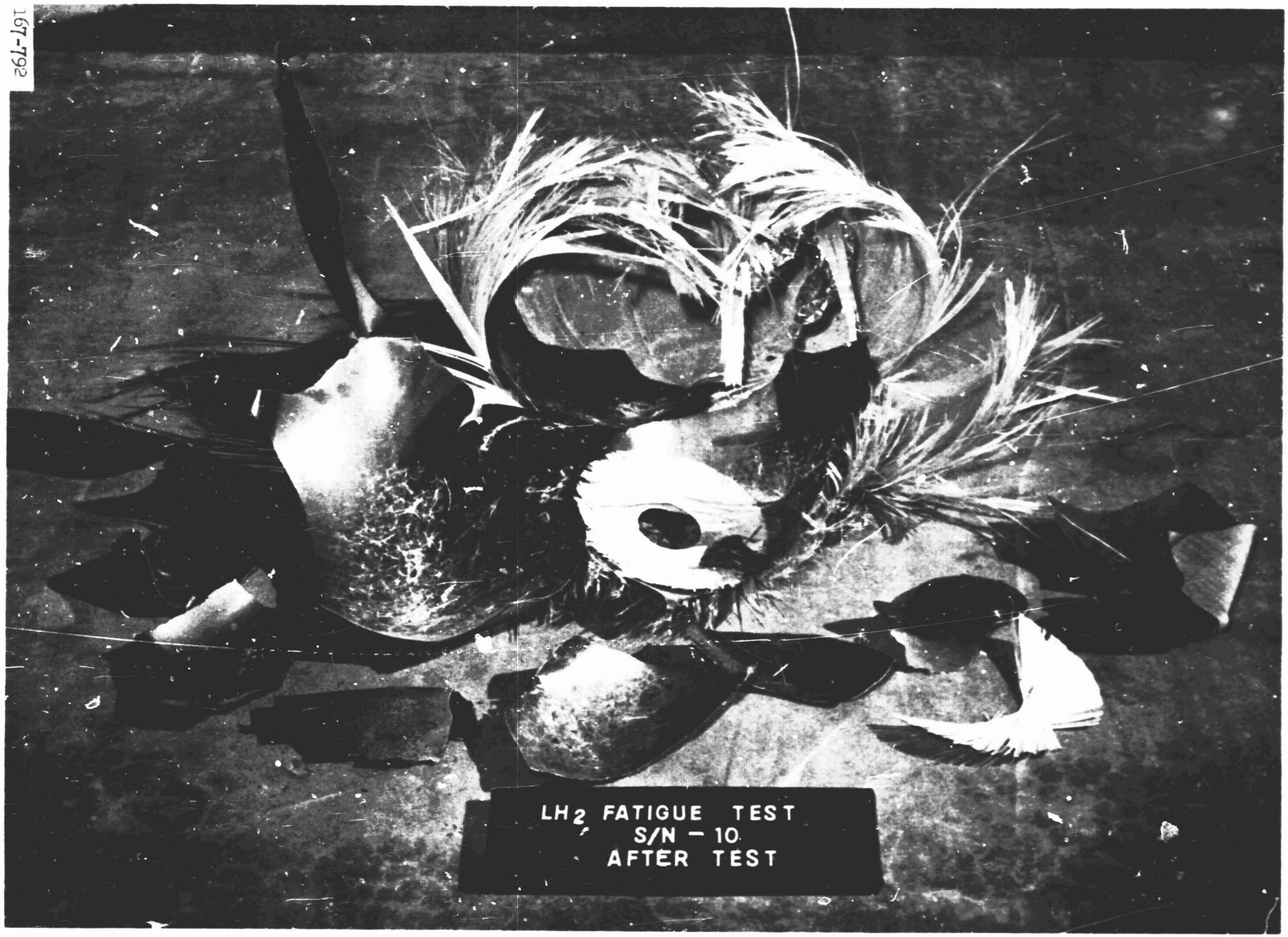

Figure 100 Tank 10 After Test

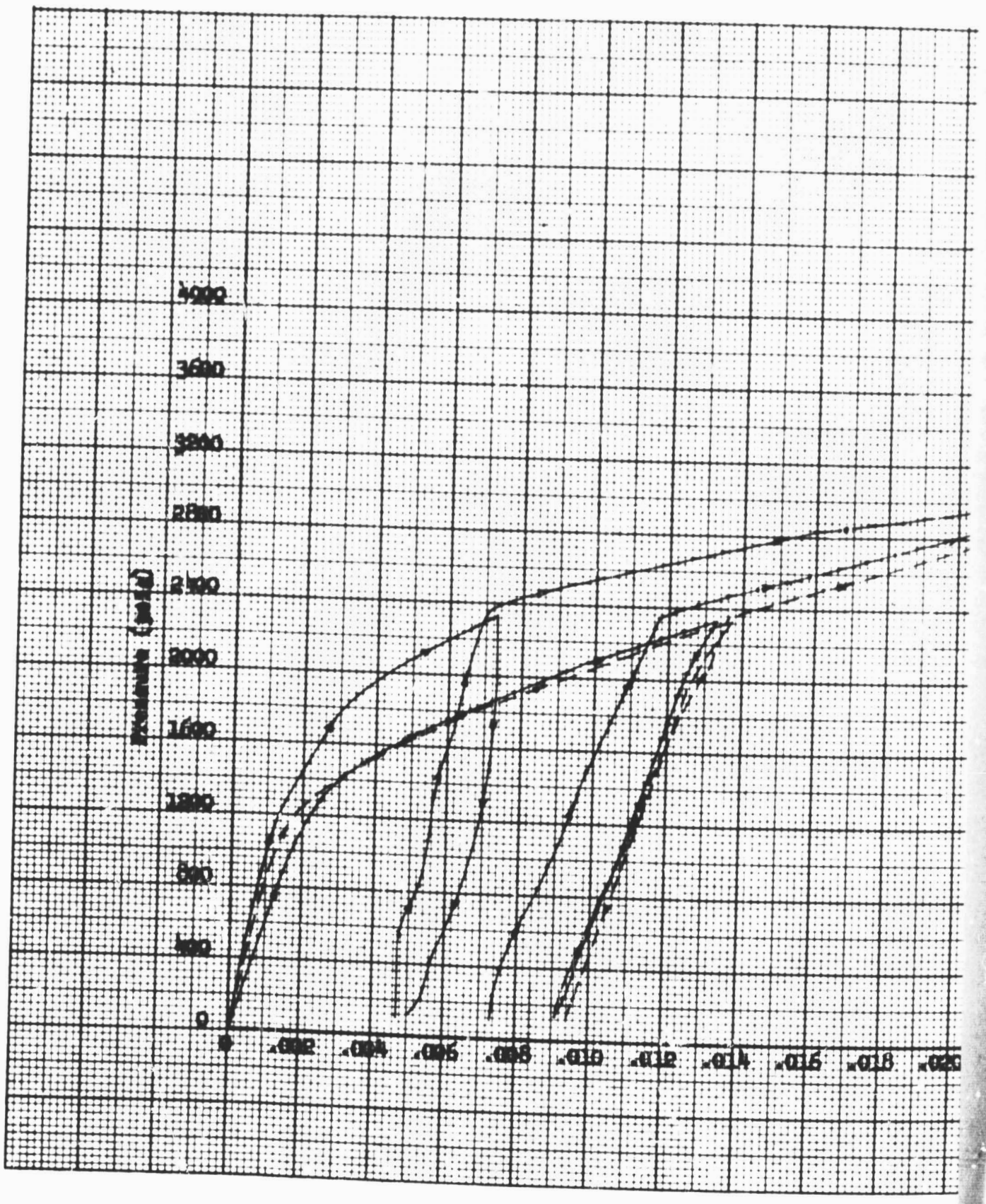

Tank 10 Pressure
and Bu

Figure 101-1

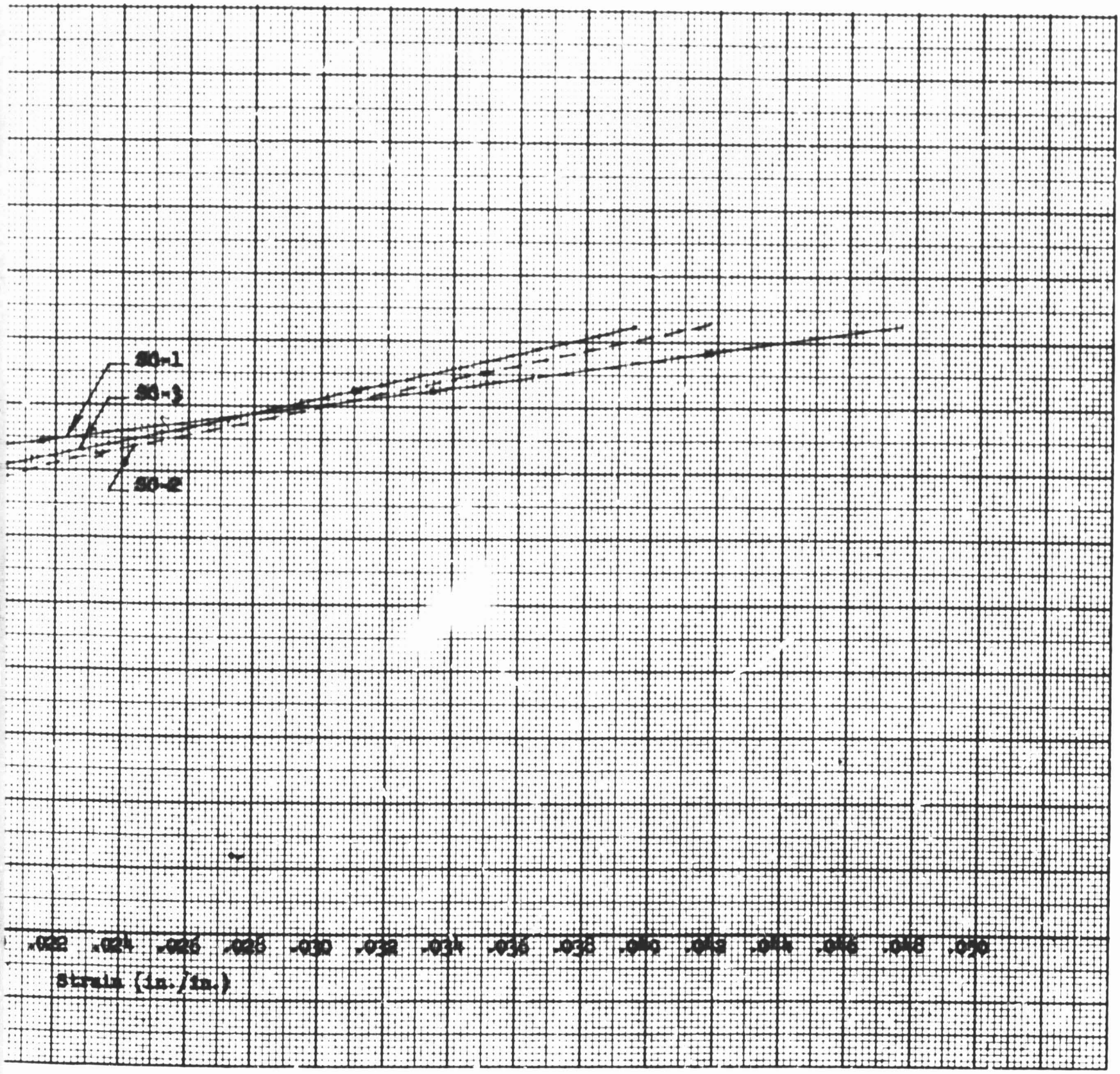

L-67-1073

vs Strain for Initial-Pressurization
rst-Test Phases at -423°F

101-2

FOR BETTER COPY CONTACT THE DOCUMENT ORIGINATOR

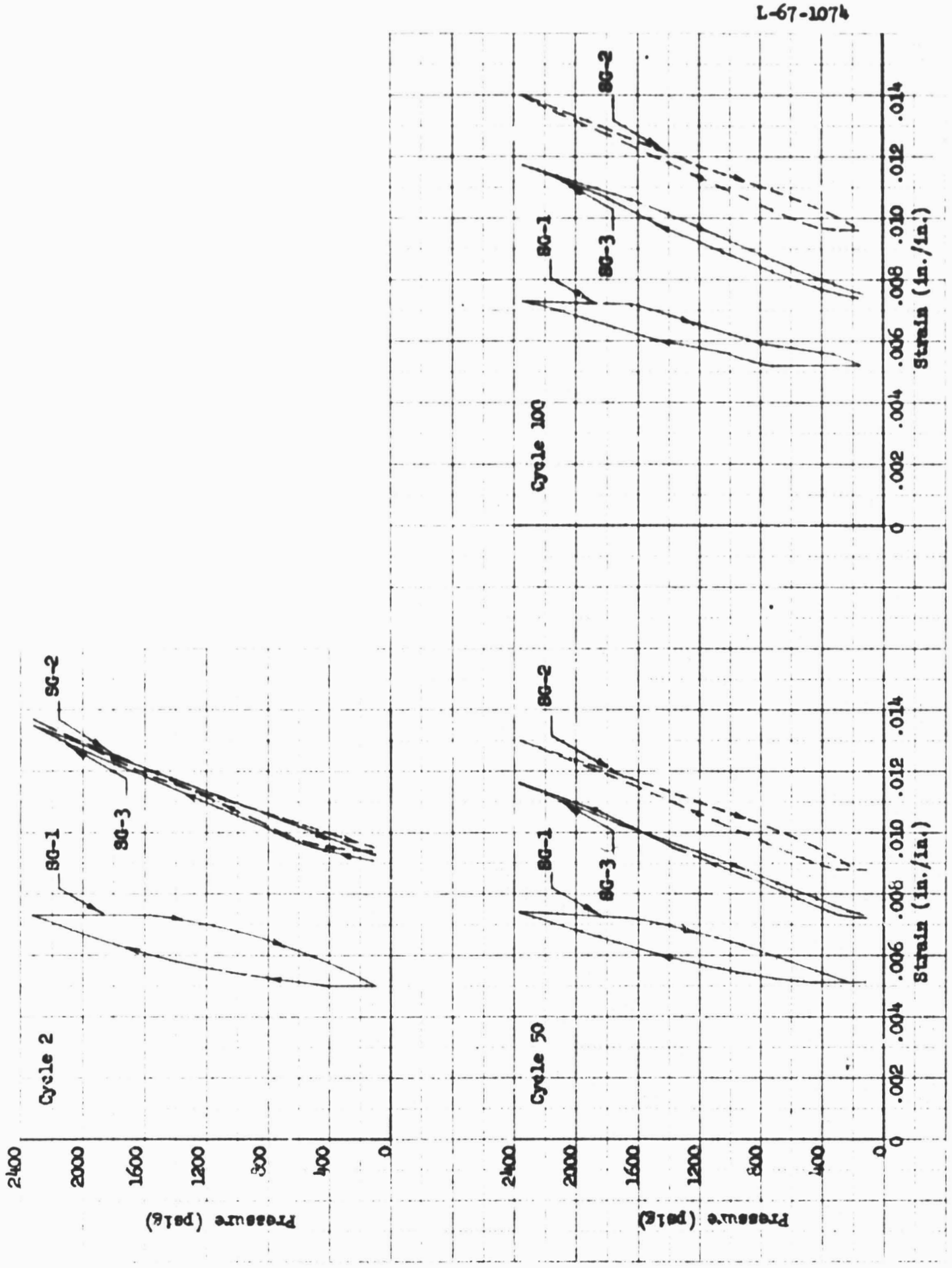

Tank 10 Pressure vs Strain During Pressure Cycling at -423°F

Figure 102

Figure 103

Tank 12 After Test

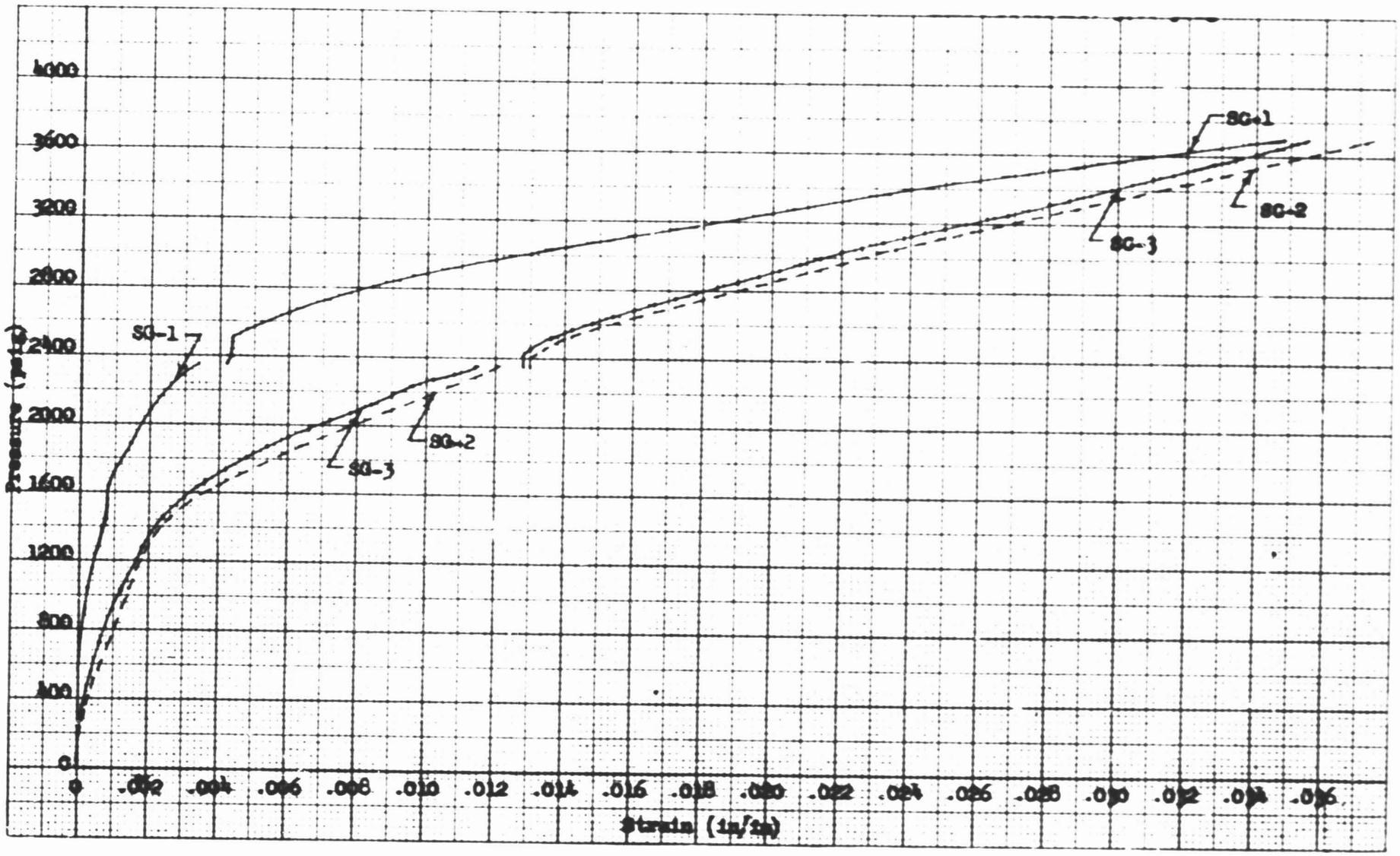

Tank 12 Pressure vs Strain for Initial-Pressurization and Burst-Test Phases at -423°F

Figure 104

BEST AVAILABLE COPY
FOR BETTER COPY CONTACT THE DOCUMENT ORIGINATOR

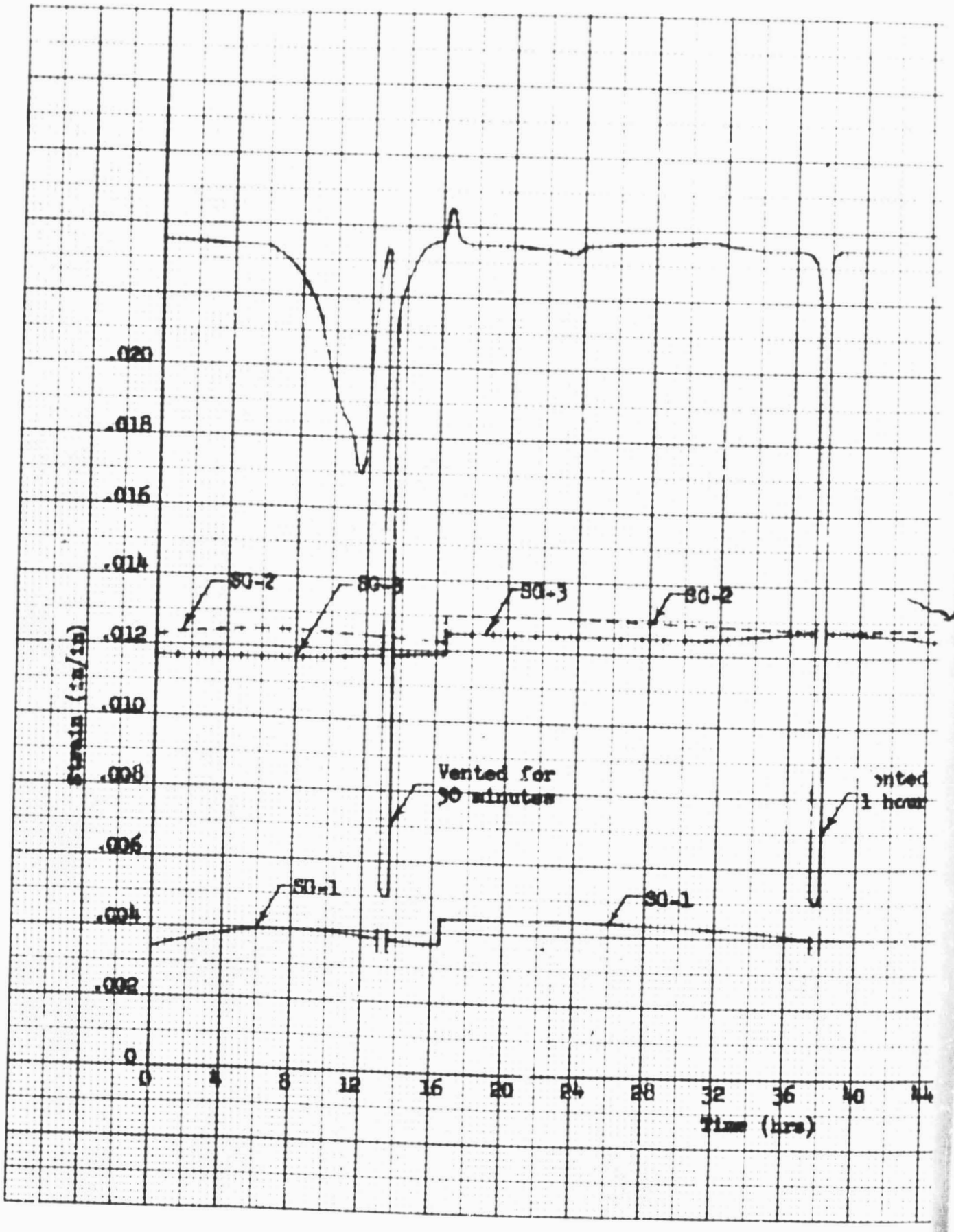

Tank 12 Pressure vs

Figure 105 - 1

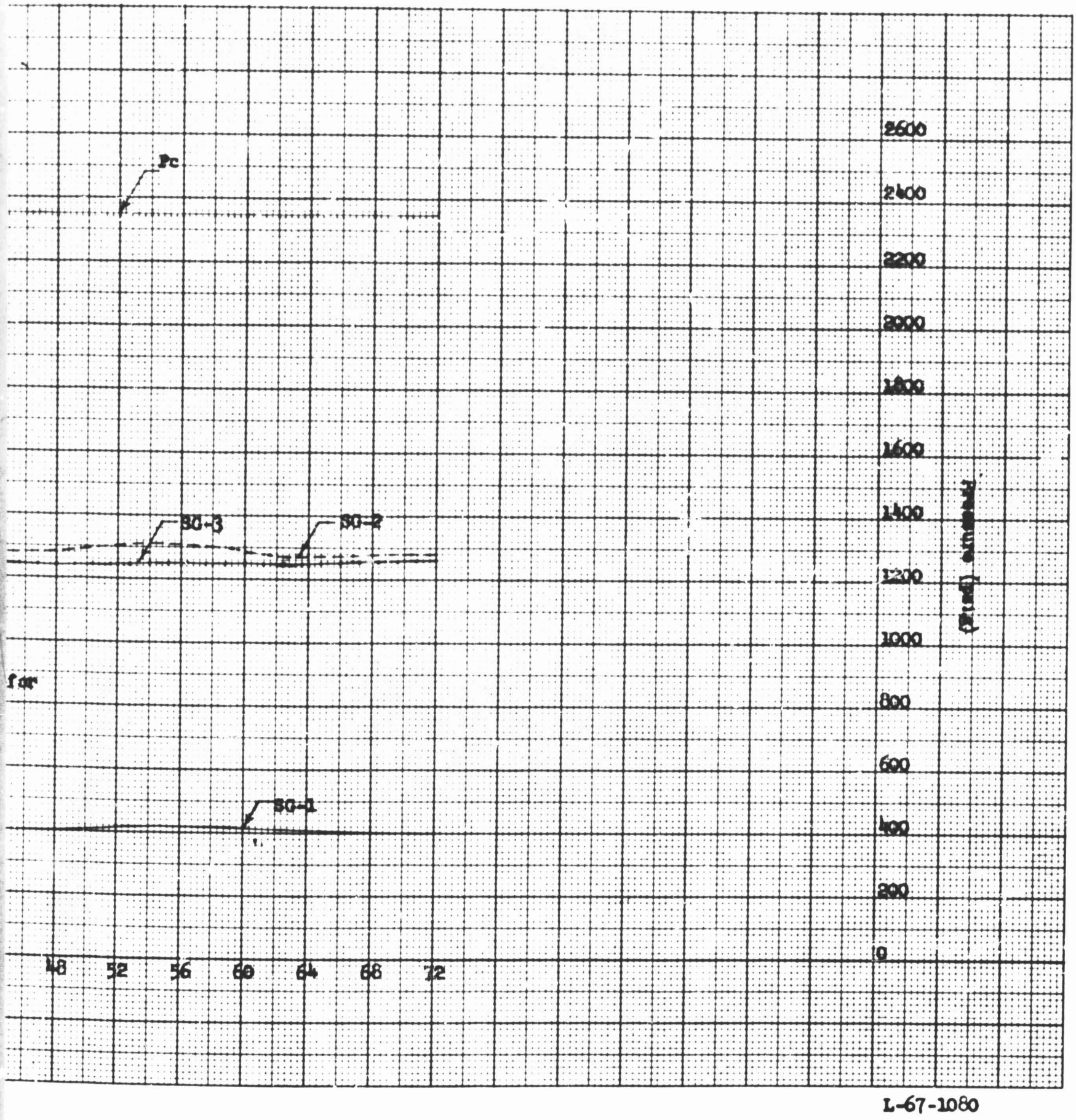

Strain During Creep Test at -423°F

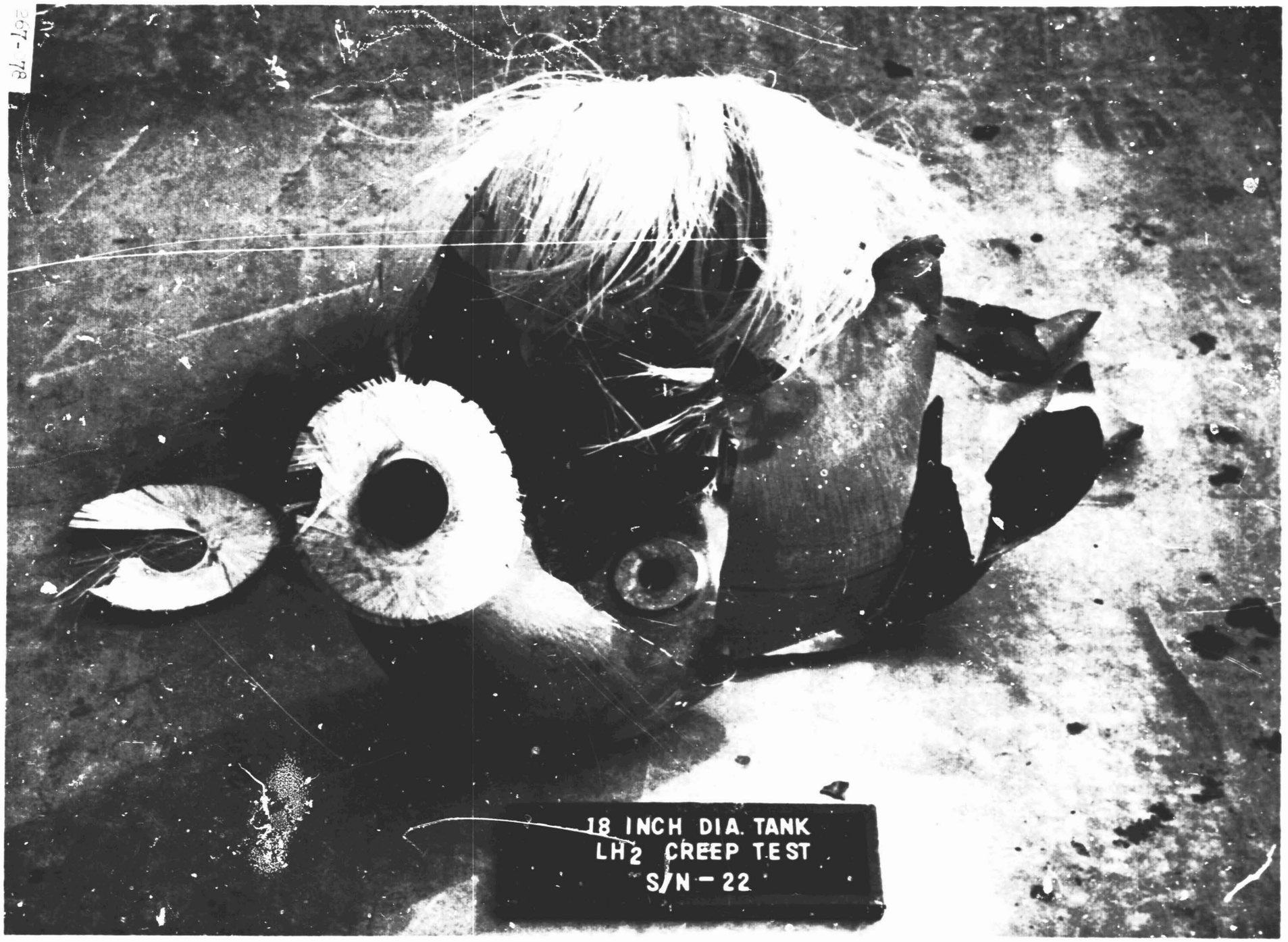

Figure 106

Tank 22 After Test

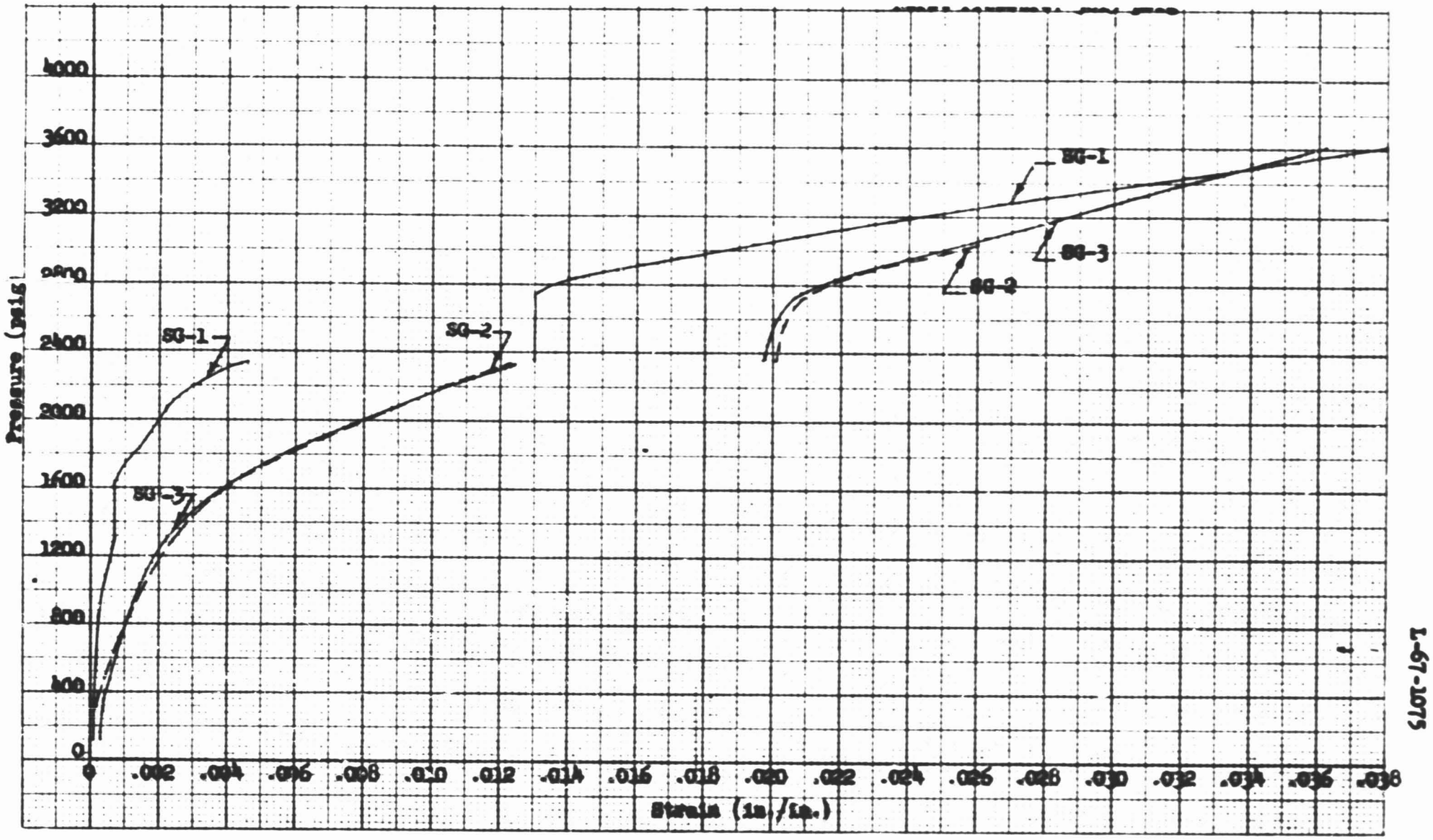

Figure 107

Tank 22 Pressure vs Strain for Initial-Pressurization and Burst-Test Phases at -423°F

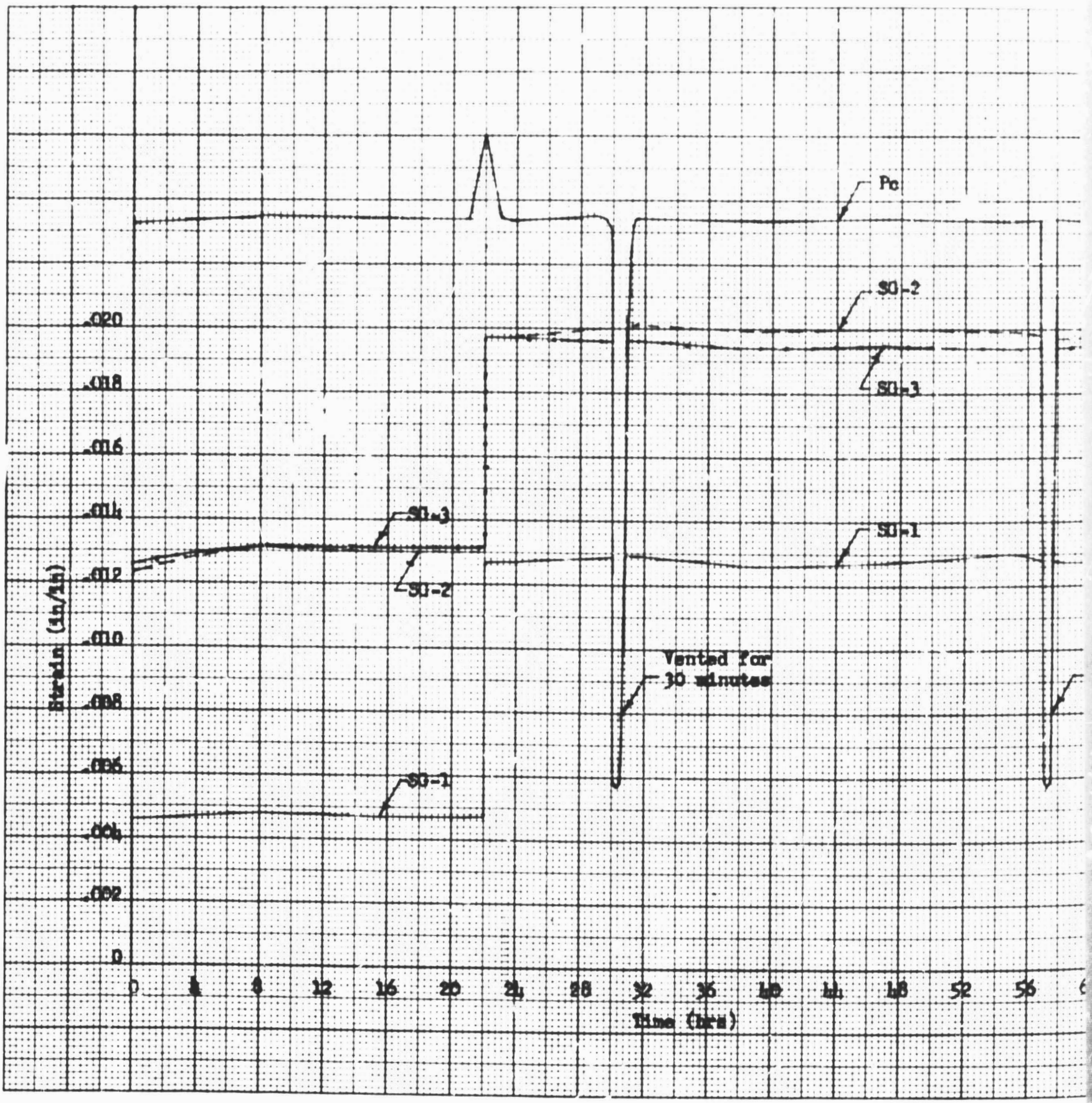

Tank 22 Pressure vs Strain During Creep

108-1

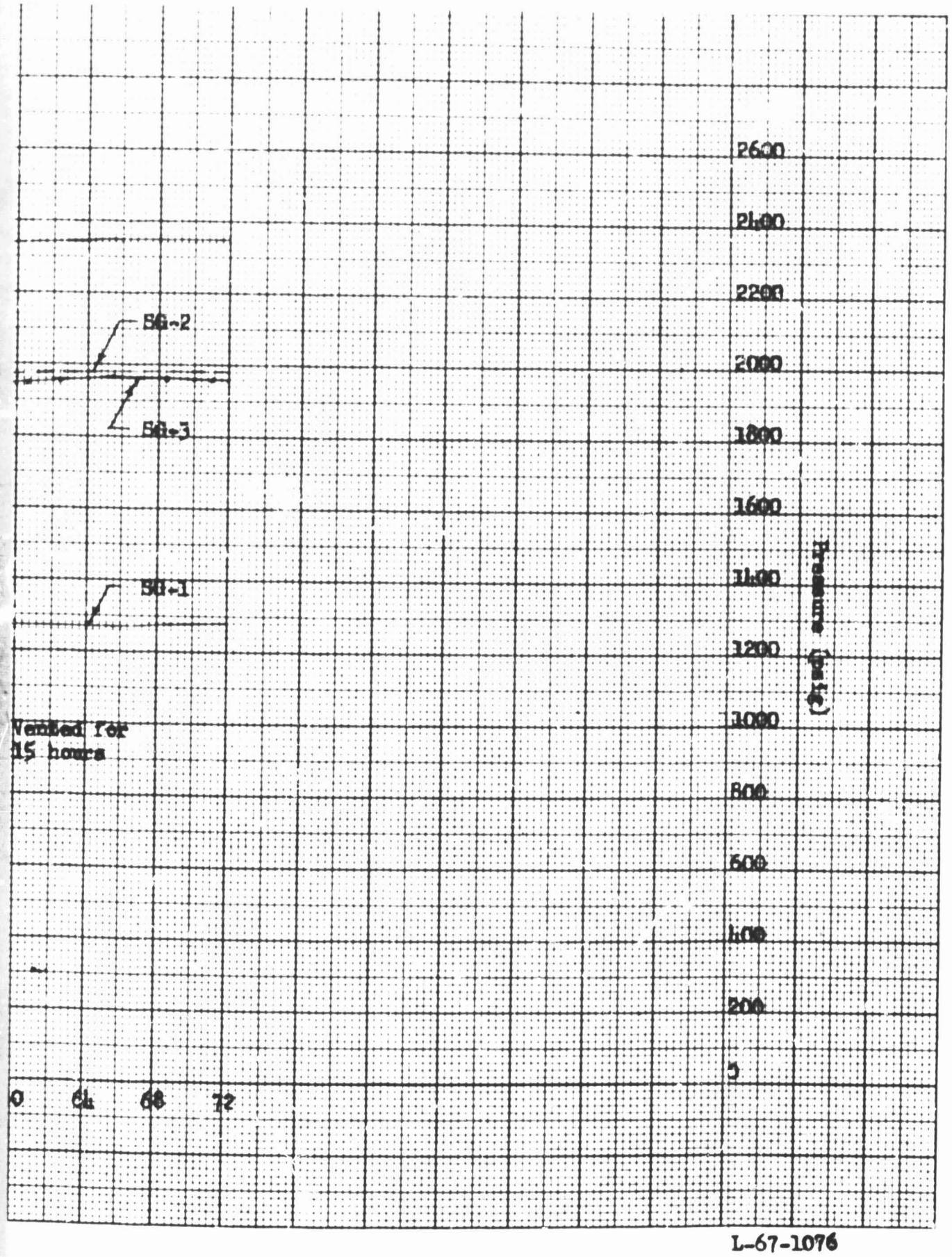

Test at -423°F

Figure 108 - 2

18" Dia Vessel, S/N E-1
LN_2 Temperature Evaluation Test
D-211-LT-15

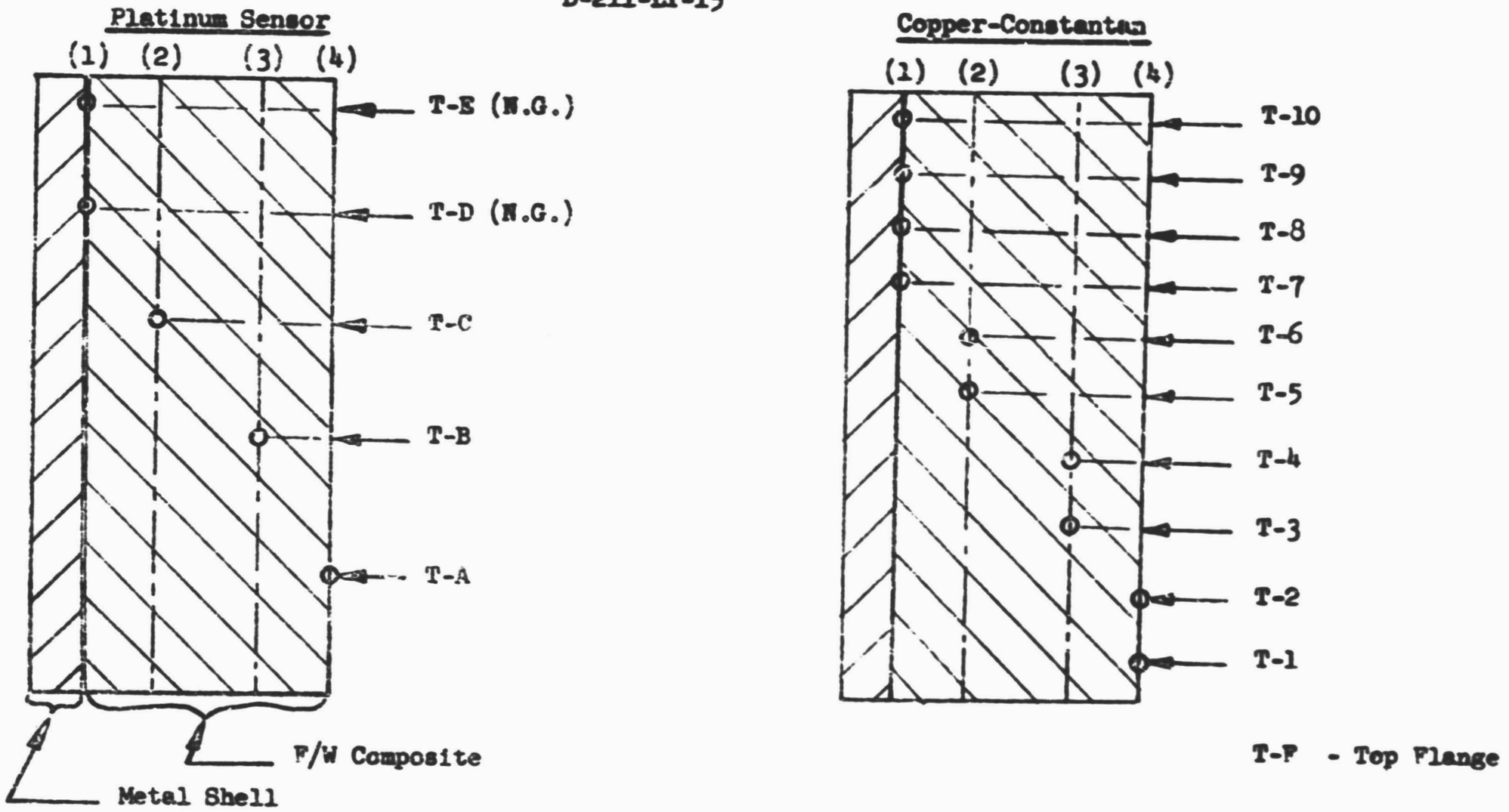

(1) Installed on metal shell surface.

(2) Installed on F/W composite after one revolution of windings.

(3) Installed during last layer of winding.

(4) Install on outer surface of F/W composite after resin cure.

Figure 109 Sensor Locations for Temperature-Evaluation Test

FOR BETTER COPY CONTACT THE DOCUMENT ORIGINATOR

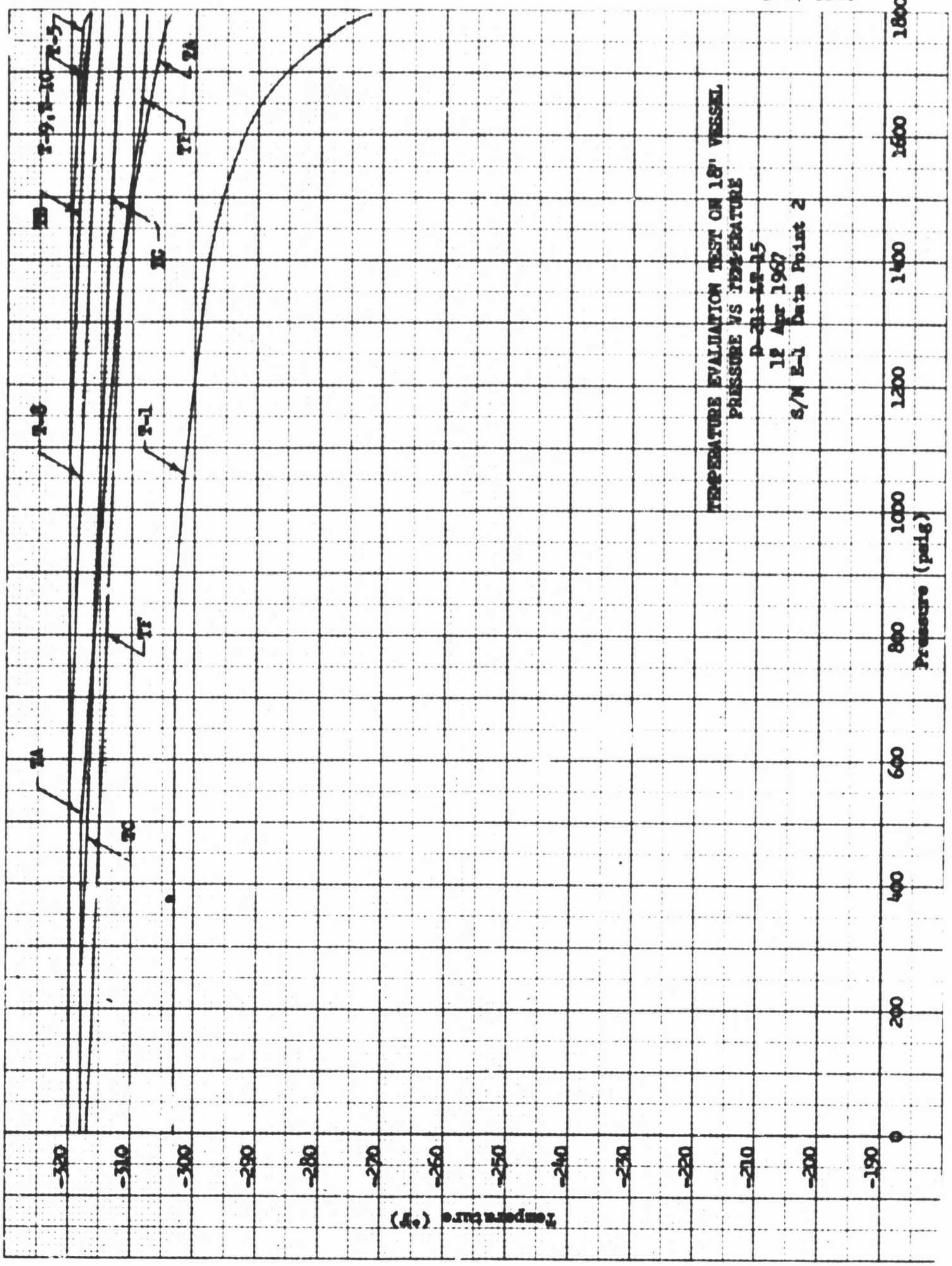

Pressure vs Temperature, Cycle 1

Figure 110

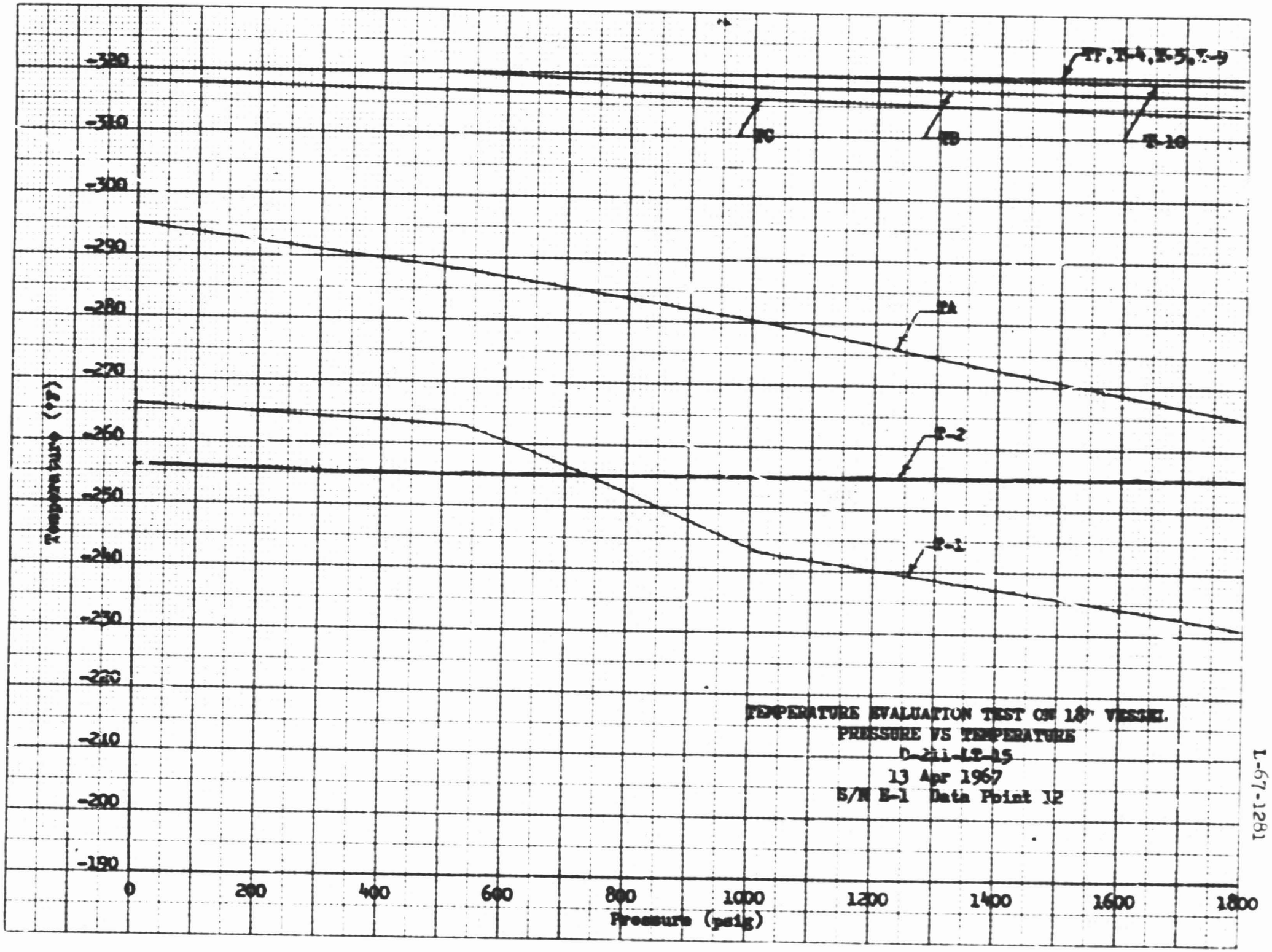

Figure 111

Pressure vs Temperature, Cycle 5

L-67-1282

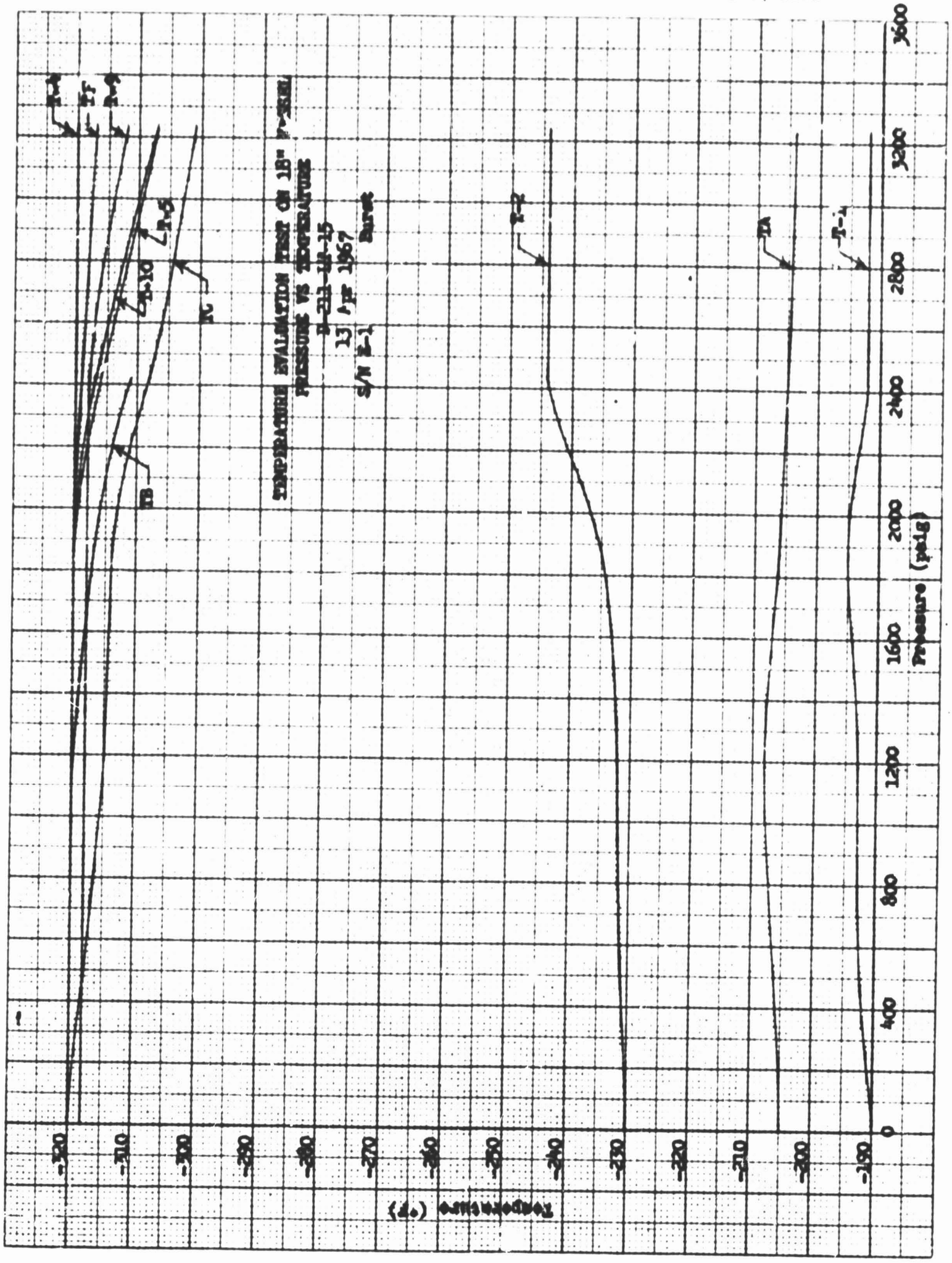

Pressure vs Temperature, Burst Cycle

Figure 112

Tank After Temperature-Evaluation Test

Figure 113

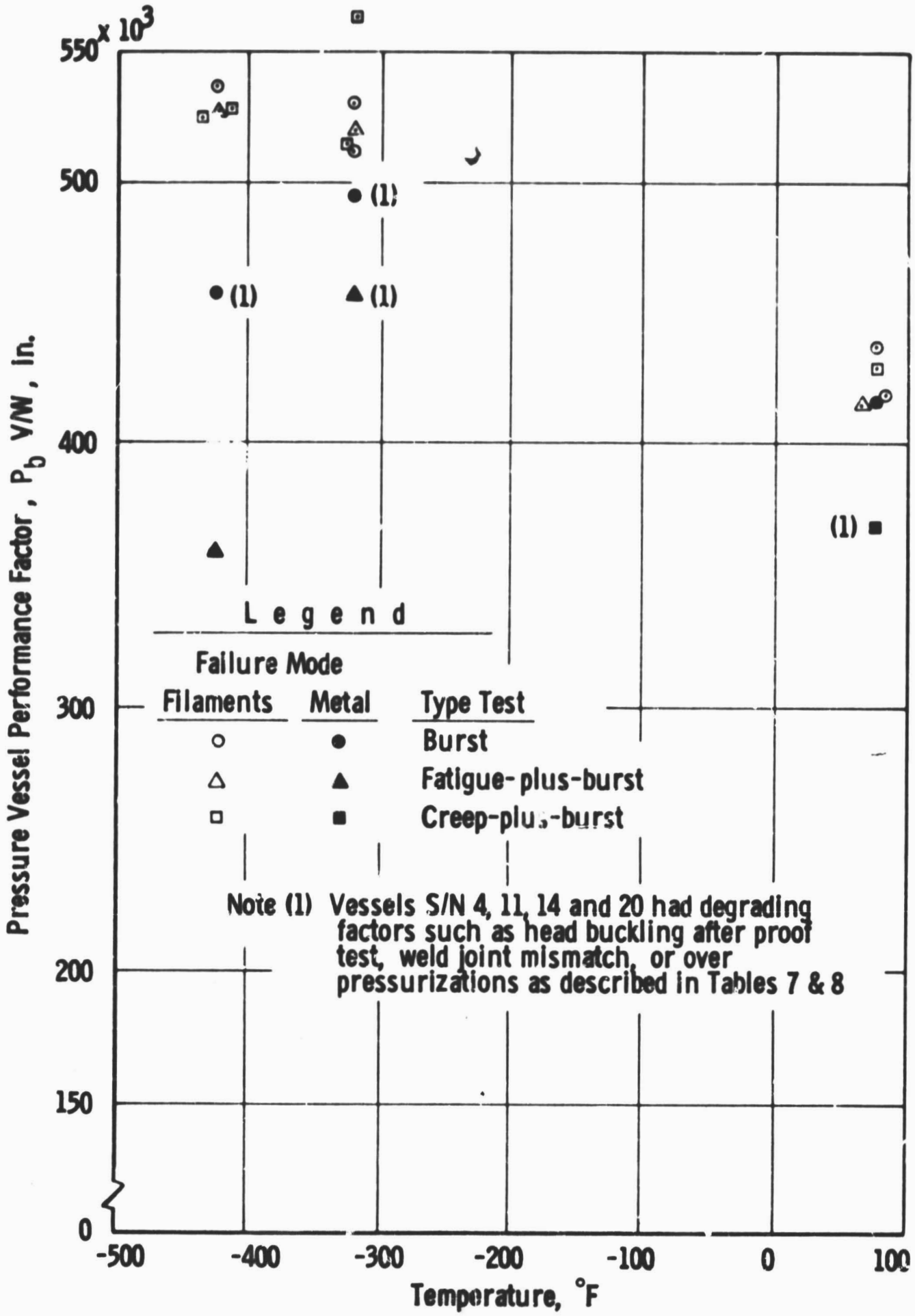

Pressure-Vessel Performance Factors for 18-in.-dia GFR Inconel X-750 (STA) Tanks

Figure 114

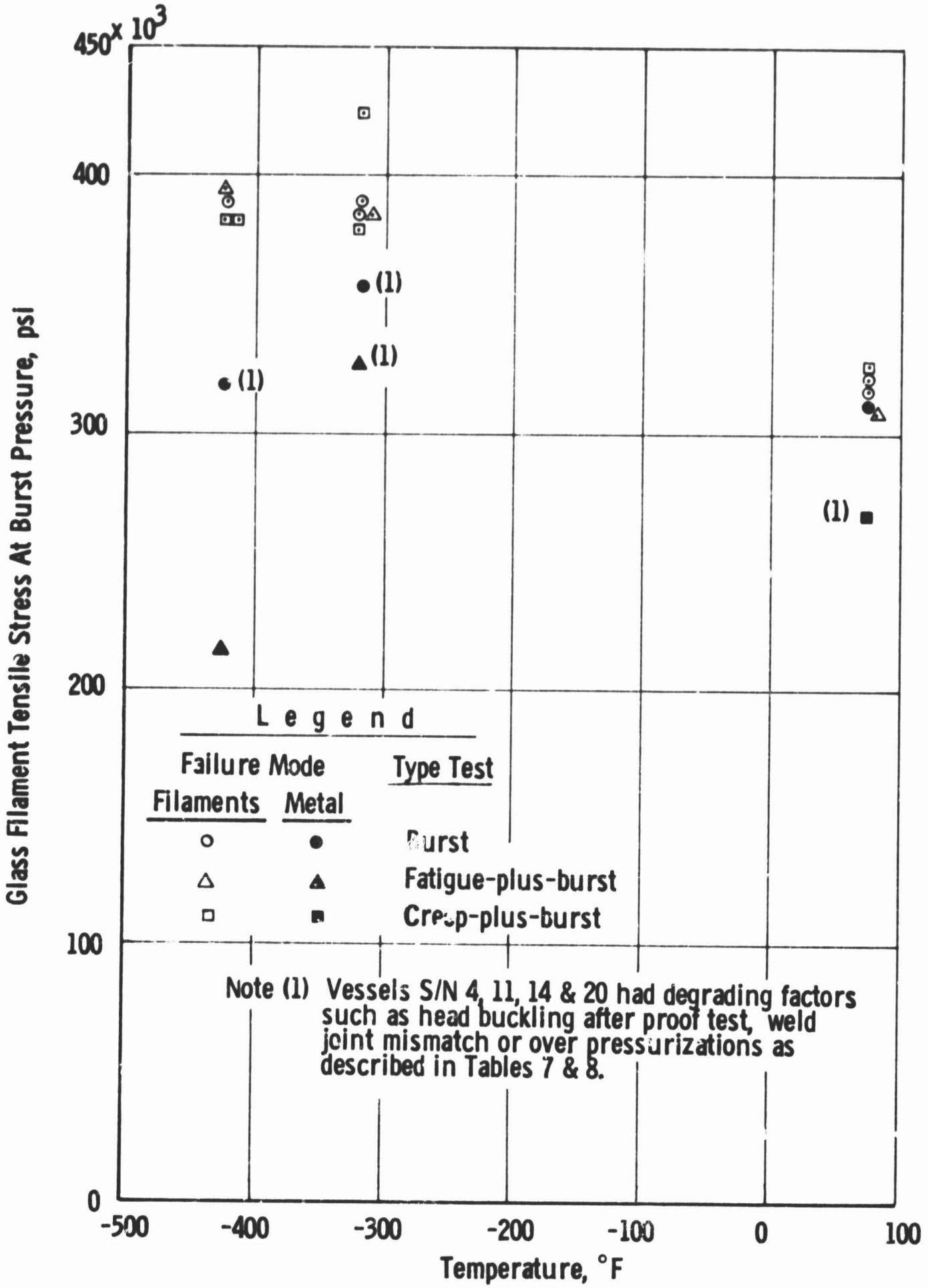

S-HTS Glass-Filament Tensile Stress at Burst Pressure for 18-in.-dia GFR Inconel 7-750 (STA) Tanks

Figure 115

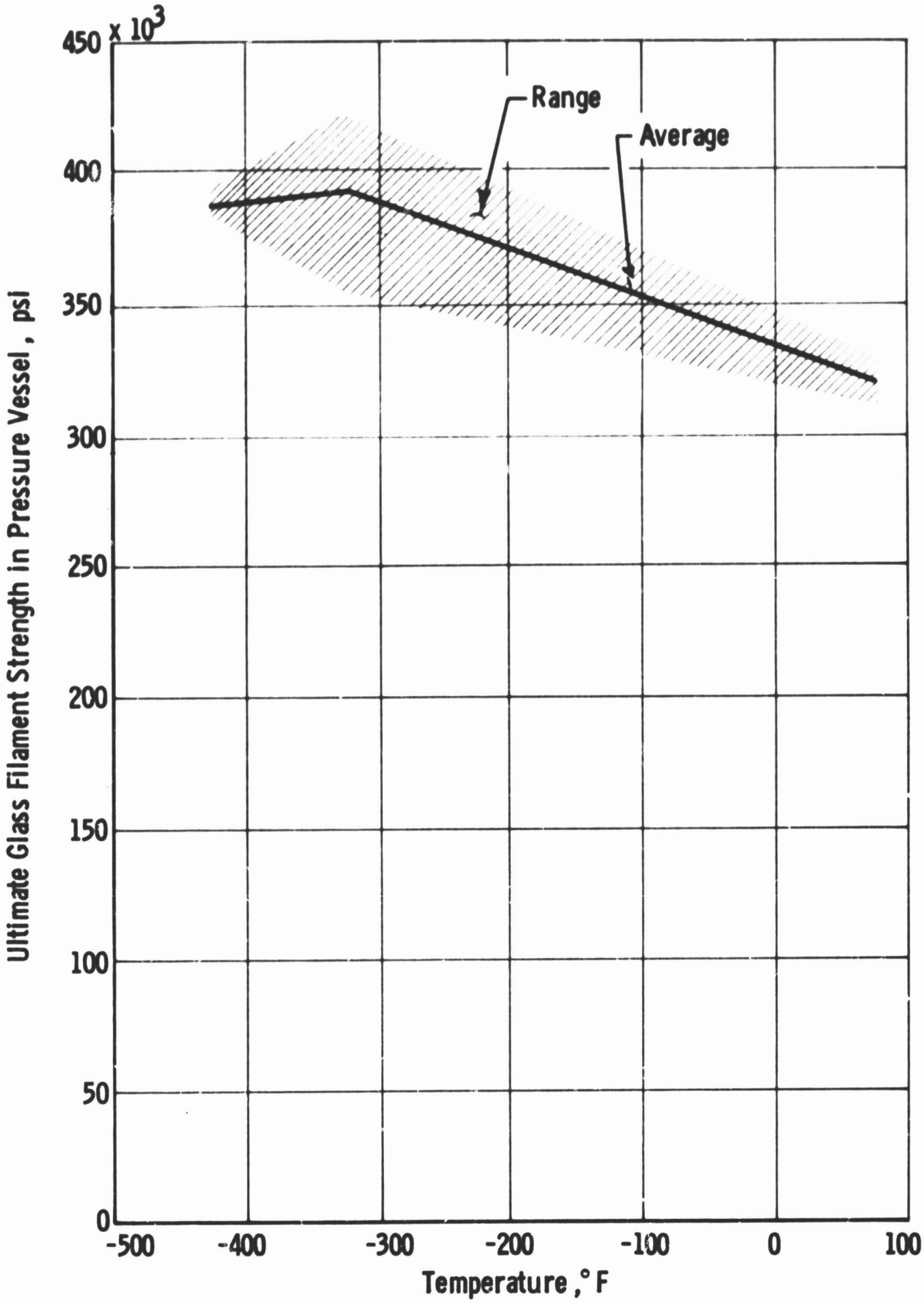

Ultimate S-HTS Glass-Filament Strength at Burst Pressure
in 18-in.-dia GFR Inconel X-750 (STA) Tanks

Figure 116

Figure 117

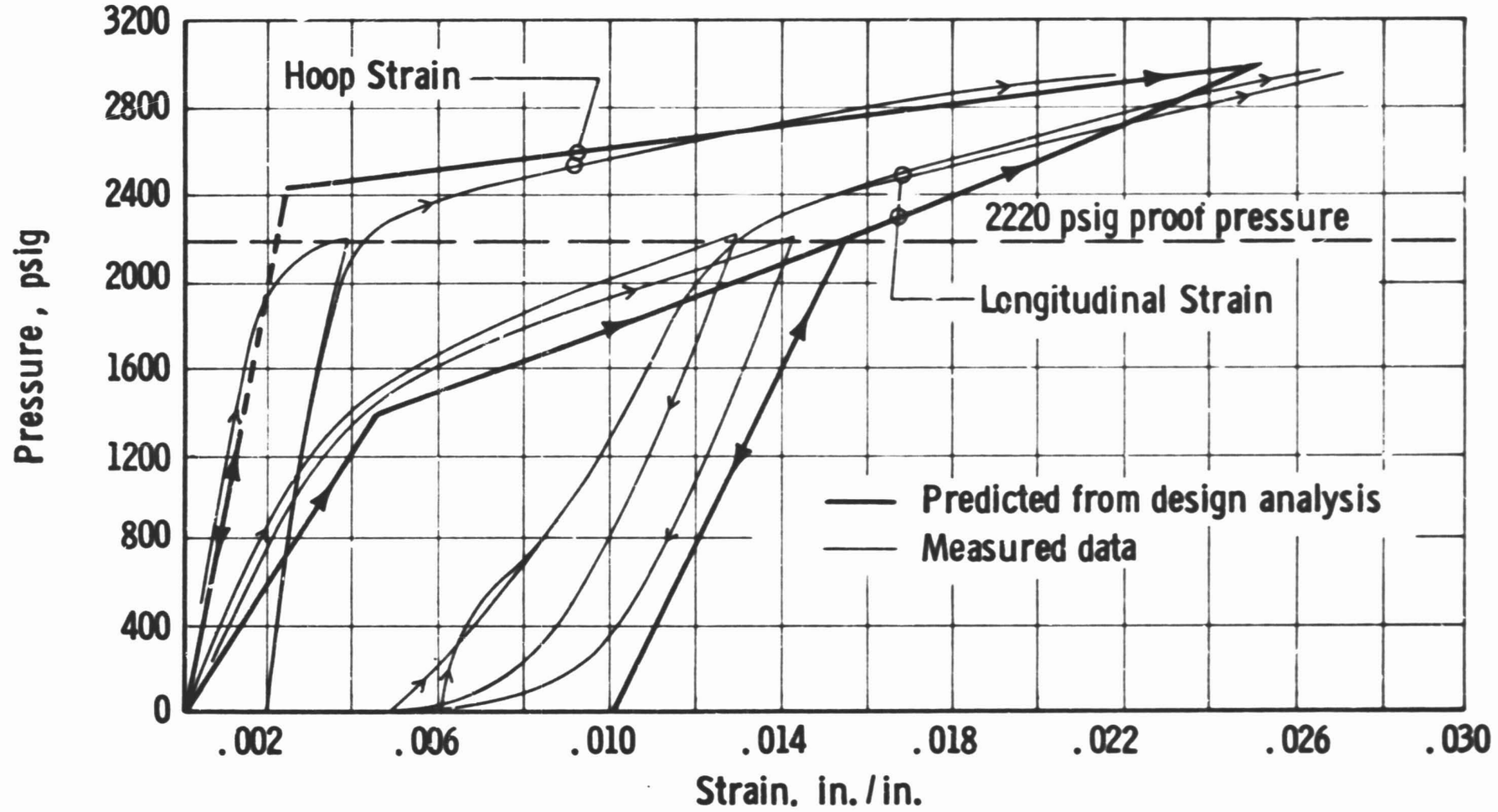

Predicted and Measured Pressure-vs-Strain Characteristics
75°F Proof and Burst Tests of 18-in.-dia GFR Inconel
X-750 Tank (Serial No. 3)

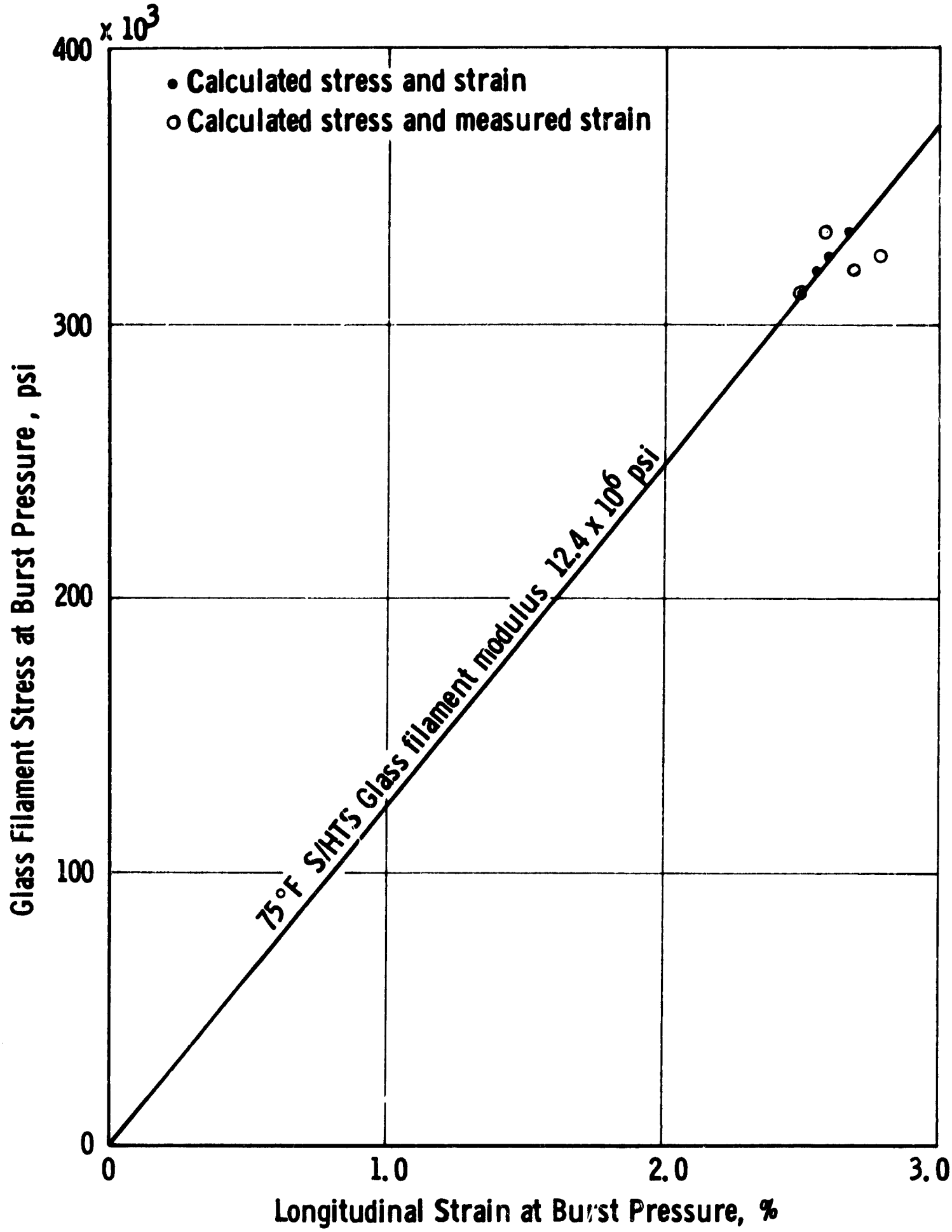

Comparison of Calculated and Measured Longitudinal-Filament Strains for 75°F Burst Tests of 18-in.-dia GFR Inconel X-750 (STA) Tanks

Figure 118

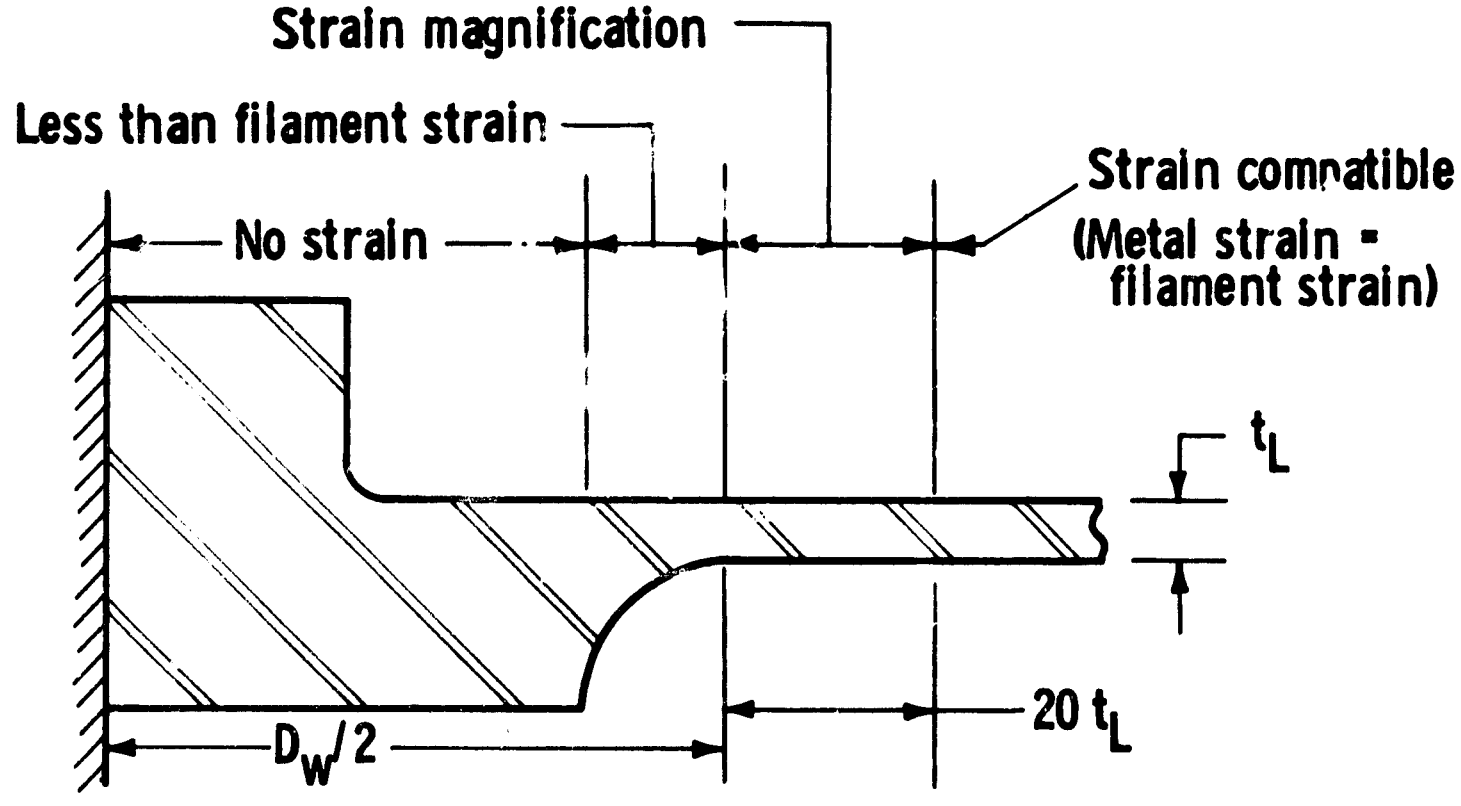

Strain Regions For a Typical Boss

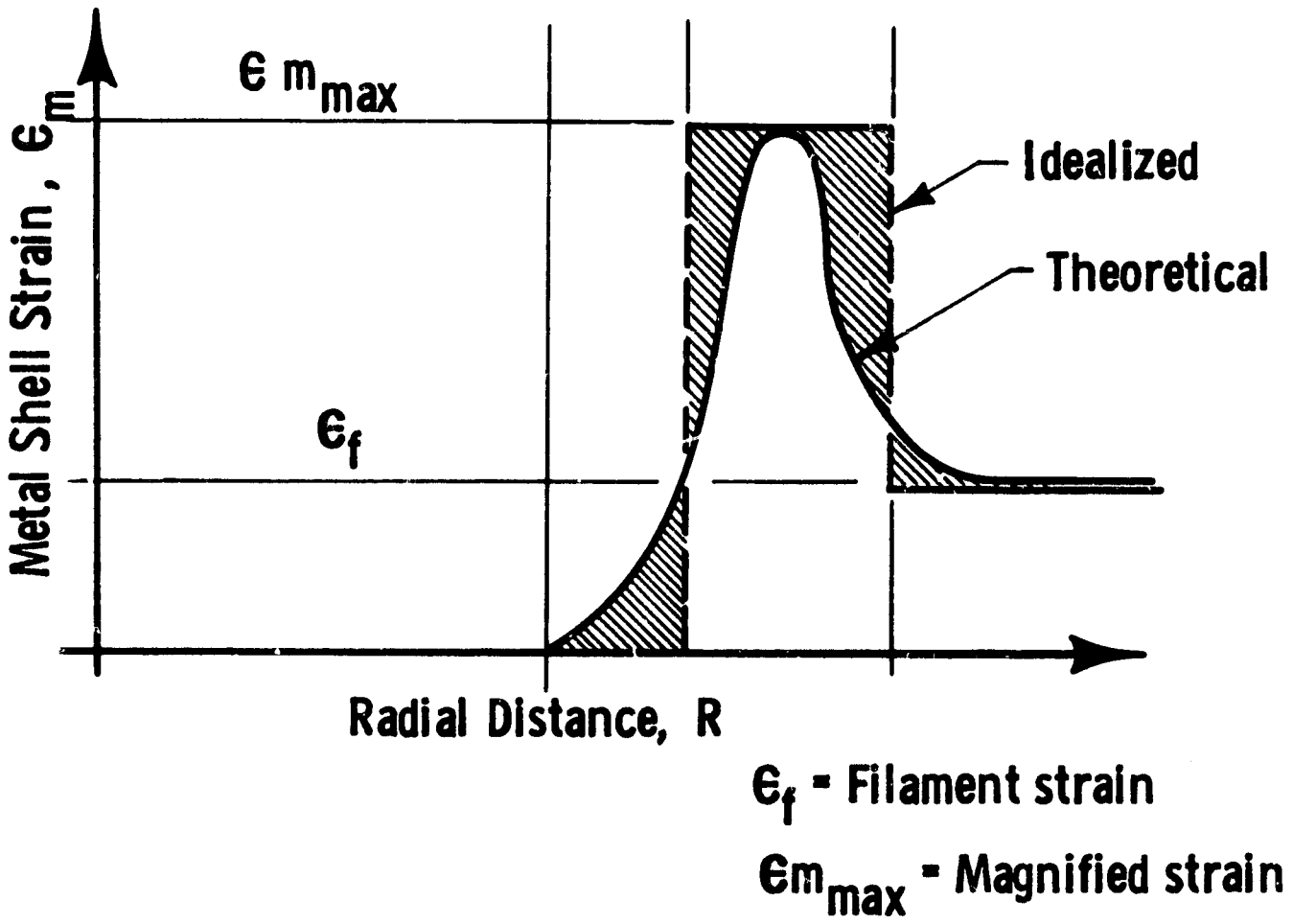

Strain Distribution in Metal Structure

Figure 119

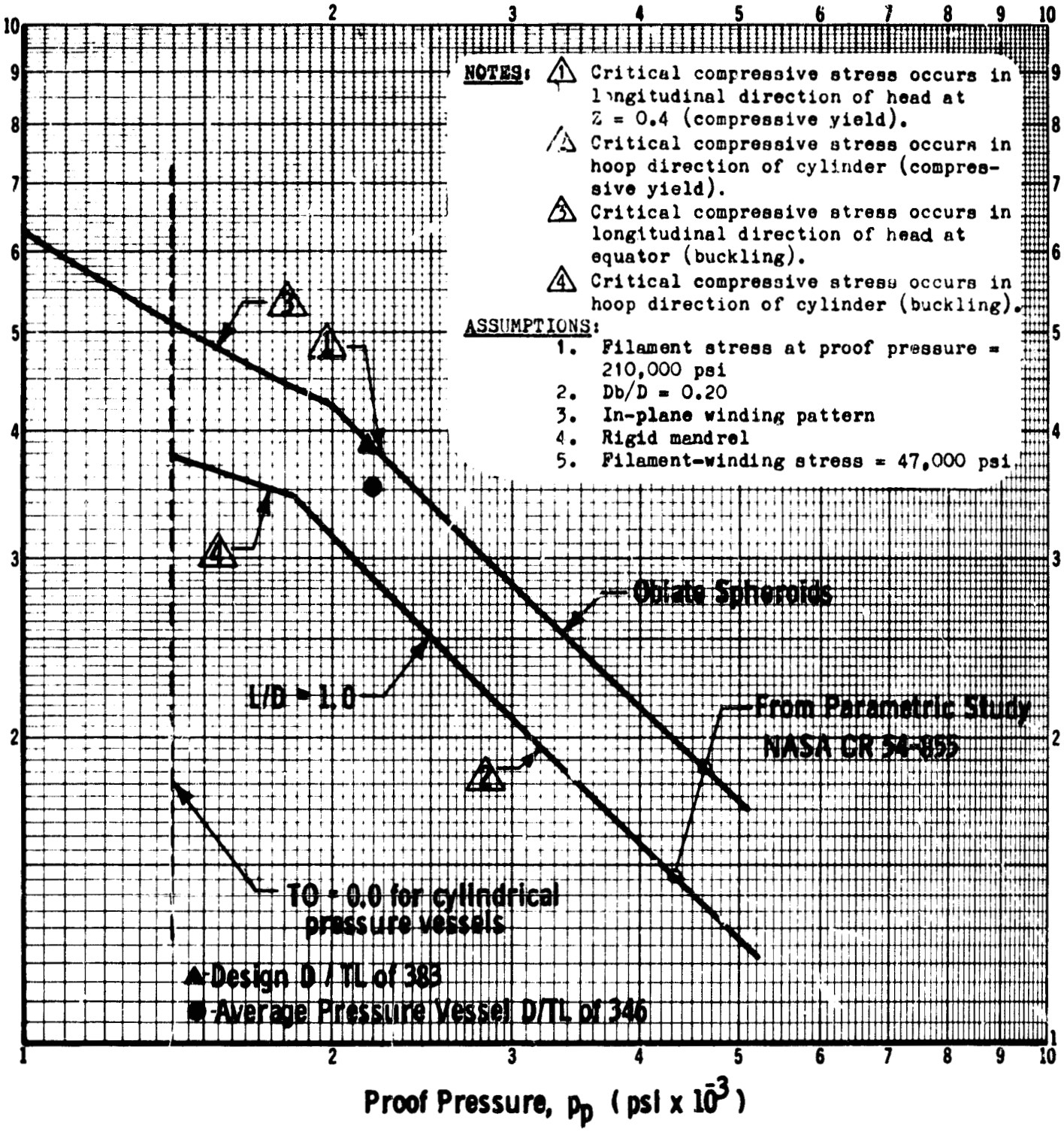

GFR Inconel X-750 (STA) Tanks, Optimum Diameter-to-Liner-Thickness Ratio

Figure 120

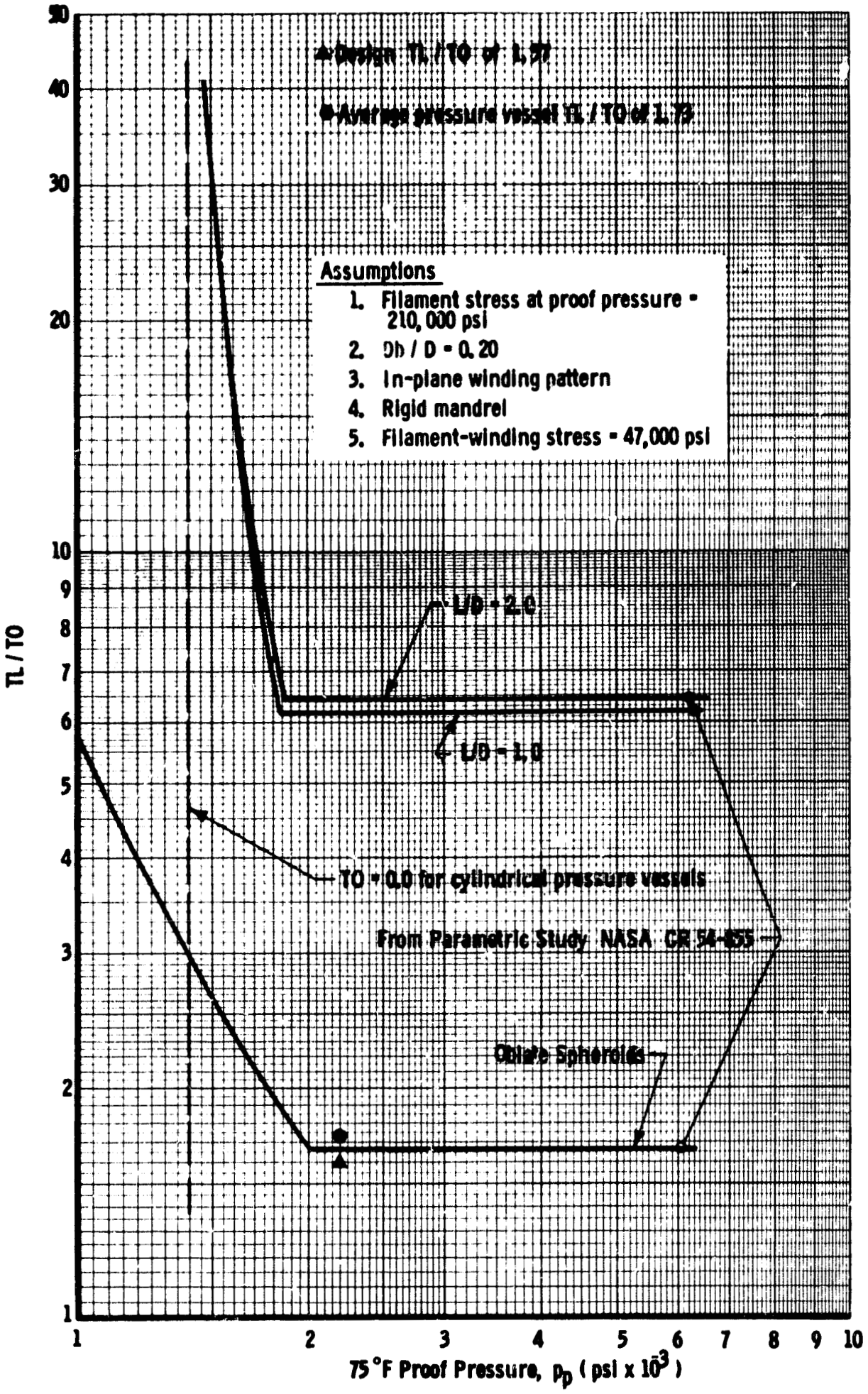

GFR Inconel X-750 (STA) Tanks, Optimum Liner-to-Longitudinal-Composite-Thickness Ratio

Figure 121

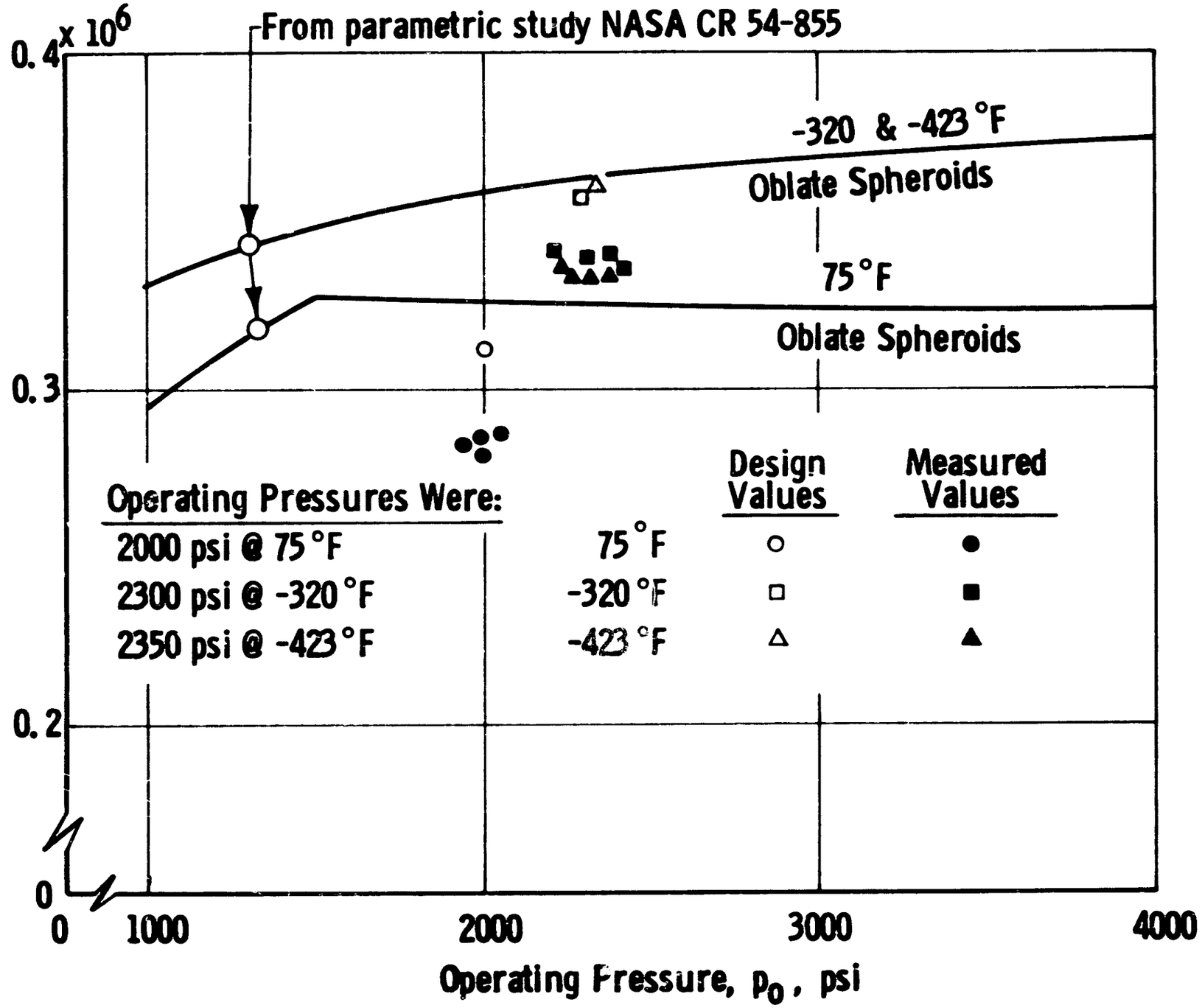

Figure 122

Operating-Pressure Performance Factors Demonstrated
by 18-in.-dia GFR Inconel X-750 (STA) Tanks

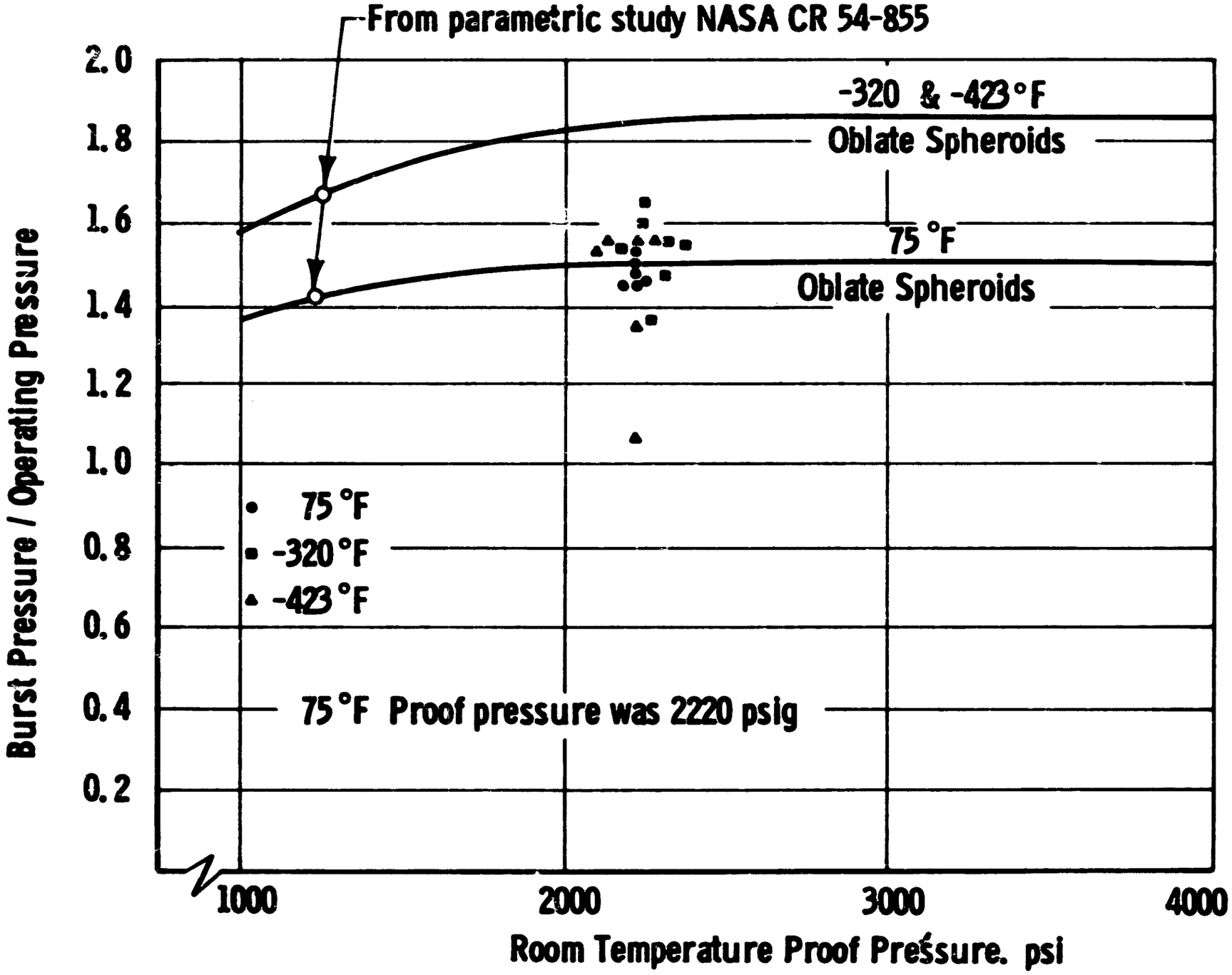

Figure 123

Factors of Safety Demonstrated by 18-in.-dia GFR Inconel X-750 (STA) Tanks

APPENDIX A

EXPERIMENTAL EVALUATION OF COMPRESSIVE-STRESS-STRAIN CHARACTERISTICS AND BUCKLING STRENGTH OF FILAMENT-OVERWRAPPED METAL CYLINDERS

Investigators are evaluating several metal-liner concepts for glass-FWC pressure-vessel structures. The concept studied in this program combines an overwrapped glass-filament shell with a load-bearing metal shell that is able to resist buckling from compressive stresses produced by the overwrapping when no bond exists between the two shells. In addition, when buckling will not occur before the compressive elastic limit of the metal shell is reached, the design must be such that this limit is not exceeded (to minimize hysteresis effects).

To design such a structure, it is necessary to establish the compressive-stress level at which (1) liner buckling occurs, and (2) the elastic limit of the liner is exceeded. In the past, however, buckling data have been scarce, and available analytical methods have not permitted the calculation of realistic compressive-buckling-stress design limits.

Experiments were conducted at 75°F to determine the compressive properties of open-ended metal cylinders overwrapped circumferentially with layers of tensioned filaments. Stress-strain curves and buckling-failure points were determined for three alloys: 2219-T62 aluminum, nickel-base Inconel X-750 (STA), and Ti-5Al-2.5Sn. The data were compared with other available data to provide a means for estimating compressive-stress limits as a function of the controlling parameters. The resulting information was compared with design criteria used for the parametric study of GFR metal tanks reported in Reference A-1.

I. CRITERIA FOR SELECTION OF METAL-CYLINDER DIAMETER-TO-THICKNESS RATIOS

R. H. Johns and A. Kaufman of the NASA Lewis Research Center have tested the buckling of metal cylinders overwrapped in the circumferential direction with layers of tensioned filaments. They conducted 29 tests on mild steel, stainless steel, nickel, and aluminum cylinders with diameter-to-thickness (D/t) ratios ranging from 175 to 3000, and obtained five other data points (with D/t ratios in the range from 320 to 600) from the literature.

Their results are presented in Reference A-2 and summarized in Figure 5 of the main text. They indicate that a straight-line correlation exists in logarithmic coordinates between D/t and σ_c/E_s, where σ_c is the critical hoop stress from overwrapping at buckling failure and E_s is the secant modulus at failure taken from the stress-strain curve. The parameter σ_c/E_s is the compressive hoop strain at buckling.

The analysis reported in Reference A-1 indicated that the compressive elastic limit of the metal shell was equal to or very near the optimum compressive-stress design point for many tanks having operating pressures in the range from 1000 to 4000 psi. The D/t ratio associated with buckling at the compressive elastic limit or yield point was therefore selected as the

single most important characteristic that should be determined for each of the three materials. Cylinder D/t ratios were chosen for the test program on the basis of the NASA data, which indicated the expected minimum buckling stresses were approximately equal to the compressive-yield strengths.

II. TEST SPECIMENS

A. DESIGN

1. Materials

Characterization analysis of candidate materials (Reference A-1) resulted in the selection of the 2219 aluminum alloy solution-heat-treated and aged to the T62 temper, Inconel X-750 (STA), and Ti-5Al-2.5Sn for the test specimens. Their compressive properties are summarized in Table A-1.

2. D/t Ratios

The following design D/t ratios were selected, on the basis of information in Figure 5 of the main text and Table A-1, to provide buckling stresses equal to the nominal values for compressive-yield strength:

Material	D/t Ratio
Ti-5Al-2.5Sn	265
2219-T62 aluminum	325
Inconel X-750 (STA)	325

3. Length-to-Diameter Ratio

The ranges of geometries used in analyzing buckling under external pressure included (a) short and transition-length cylinders, (b) long cylinders, and (c) very long cylinders, as shown in Figure A-1. The test cylinder was designed to be sufficiently long to ensure no restraint on deformation imposed by the radial rigidity of its end plates. The length-to-diameter ratio was chosen as 1.5, on the basis of information in Reference A-3 and Figure A-1, and an estimation of end effects due to rigid end plates.

4. Diameter, Length, and Thickness

A diameter of 12 in. and a length of 18 in. were selected for the test cylinders. Sheet material was purchased to the closest available thickness that would approximately permit the required D/t ratio at D = 12 in. After it was received, its thickness was accurately determined and cylinder diameters were chosen to yield the required D/t:

	Required D/t	Measured Thickness, in.	Required Cylinder Diameter, in.
2219 aluminum	325	0.040	13.00
Inconel X-750	325	0.041	13.32
Ti-5Al-2.5Sn	265	0.041	10.88

B. FABRICATION

Three cylinders of each material were fabricated. Constant-thickness sheet was used because these alloys have high welded-joint efficiencies [90 to 102% for Ti-5Al-2.5Sn, 100% for 2219-T62 aluminum (welded in the T31 condition and solution-treated and aged to T62) and 100 to 105% for Inconel X-750 (welded in the solution-treated condition and aged after welding)].

The sheet was roll-formed to the proper contour and the ends were joined to form the longitudinal weld joint. The rolled cylinder was supported by tooling during tungsten inert-gas (TIG) welding, and all weld beads were ground flush on the inner and outer surfaces.

The weldments were then subjected to 100% radiographic inspection. The propagating defects noted were ground out and repair-welded. After re-inspection, the cylinders were given the applicable heat treatment and were X-rayed again to ensure freedom from propagating defects.

Two cylinders of each material were selected for testing; their characteristics, including the heat treatment used, are summarized in Table A-2. The six cylinders are shown in Figure A-2.

III. TEST PLAN

A. INSTRUMENTATION

Uniaxial and biaxial strain measurements were made at four 90° intervals around the interior of the cylinder approximately at the longitudinal center, as indicated in Figure A-3. Two active longitudinal gages and four active circumferential gages, with an inactive counterpart for each, were used (a total of 12 per cylinder). The strain-gage measurements, together with one temperature measurement and one pressure measurement, were made through hermetic seals in the cylinder-support tooling. A slip ring was provided in the tooling so that these readings could be taken continuously or intermittently during filament winding and testing without breaking the electrical circuit.

Constantan foil-type gages on an epoxy carrier with an effective gage length of 0.5 in. were used [Baldwin Lima Hamilton FAB-50-35 S-6 and S-13]. They had temperature compensations of 6 and 13 ppm/°F for titanium, nickel, and aluminum. For good results in the low elastic range, an active-dummy half-bridge configuration was used to compensate for temperature changes. Figures A-4 and A-5 depict a typical installation of strain gages on a cylinder and of the cylinder on a portion of the support tooling.

Continuous-recording equipment was used to obtain strain, pressure, and temperature measurements during winding and testing.

B. EXPERIMENTAL PROCEDURE

Buckling studies had formerly been conducted by winding on a cylinder until collapse occurred. If the cylinder buckled before the elastic limit was reached, stresses could be determined from the measured strains and an assumed modulus-of-elasticity value. If the cylinder buckled above the elasti limit, external loads and the resultant stresses were estimated from the filame winding tension and the number of filaments applied. This approach has inherent inaccuracies because (1) the winding-tension measurement is not exact, and (2) the tension in already deposited layers decreases as the cylinder is compressed by additional layers.

The test procedure in this program employed a pressure mandrel for support during overwinding. The use of internal pressure to counterbalance the winding load made it possible to determine exactly the external force on the cylinder from the overwindings at the start by pressurizing until the metal strain was zero. This pressure was equal to the external pressure. Recordings of pressure decay vs compressive strain were then used to accurately determine compressive stresses vs strains.

After the cylinders were strain-gaged and assembled to the pressure-mandrel tooling, the unit was positioned in a winding machine and electrical connections were made to the slip ring as shown in Figure A-6. The test assembly was connected to a portable, self-contained, hydraulic, pressure-mandrel system and was filled with a liquid.

Zero readings were taken on all strain gages. Following the pressurized-mandrel concept, the internal pressure was increased to balance the applied compression loads as filament layers were applied under tension. Dacron filaments were used because (1) they could be wound at relatively high tension, and (2) the applied tension load would be relieved very slowly as the cylinder compressed because of the low modulus of elasticity of the filaments. After the winding of each layer, the internal pressure was increased to bring the circumferential-strain-gage readings back to the original, stress-free, reference point. Sufficient layers were applied to induce high compressive stresses if the internal pressure was removed.

The internal pressure was gradually reduced after a given number of layers were wound and after pressure adjustments to bring the strain-gage readings to the initial, stress-free, reference point. The strain and internal pressure were recorded continuously. Because there was concern that a positive pressure inside the cylinder would tend to retard buckling, the initial de-pressurization cycle was scheduled to occur before enough filaments had been applied to buckle the cylinder. If the cylinder did not buckle when zero pressure was reached, it was repressurized to the original reference point, and additional layers were applied. The cylinder was again depressurized, and this sequence was repeated until it buckled.

In the first test, the cylinder (Serial No. 3, aluminum) buckled on the first depressurization cycle. In all subsequent tests, from two to nine cycles were needed. Table A-3 summarizes the overwrap data for each cylinder tested, including the winding pattern, tension, number of layers, internal pressure, and maximum compressive stresses and strains.

IV. TEST RESULTS

The buckling characteristics in all cases were in excellent agreement with the predicted behavior, as determined from the correlation established by NASA [compressive hoop strain (σ_c/E_s) vs D/t ratio] and shown in Figure 5 of the main text. This agreement is shown in Figure 6 of the main text, where data from these cylinders are compared with other available data.

All the cylinders buckled in the longitudinal seam weld at high stress levels (see Figure A-7). All were cusp-buckling failures. No metal fracture occurred in the Inconel cylinders, but metal fracture occurred along the weld seam in the titanium and aluminum cylinders after snap-through of the cusp buckle. This failure was usually accompanied by leakage inside the cylinder, followed by additional liner collapse and tearing due to the action of the highly tensioned, low-modulus, Dacron filaments (shown in Figure A-8). Figures A-9 to A-14 show the buckled cylinders.

A. PRESSURE-STRAIN DATA

Figures A-15 to A-20 plot cylinder-mandrel pressure vs average hoop and longitudinal strains. Compressive strains in the hoop direction were accompanied by tensile strains in the longitudinal direction, as was expected from the Poisson's-ratio effect (longitudinal extension resulting from circumferential compression). For the titanium cylinders (Figures A-19 and A-20), the longitudinal tensile strains reverse and go into compression as high compressive stresses are developed in the hoop direction. A possible explanation is that the axial restraint on cylinder extension imposed by the tooling caused the longitudinal compressive strains.

B. STRESS-STRAIN DATA

Hoop stress-strain curves were developed from the pressure-strain data. They are shown in Figures A-21 to A-25, along with estimated stress-strain curves. Incomplete data precluded a stress-strain diagram for the Serial No. 2 titanium cylinder. The curves were determined by calculating the stress at various internal-pressure levels, using load and strain compatibility equations. The only assumptions required were (1) a value for the elastic modulus of the metal, and (2) elastic behavior of the filaments from winding to buckling. Provision was thus made for load relaxation in the tensioned filaments as the cylinder compressed. The computed metal stresses were checked in the elastic region by the principal stress equations:

$$\sigma_1 = \frac{E}{1-m^2} (\epsilon_1 + m \epsilon_2)$$

and

$$\sigma_2 = \frac{E}{1-m^2} (\epsilon_2 + m \epsilon_1)$$

where

σ_1, σ_2 = principal stresses

ϵ_1, ϵ_2 = principal strains, from pressure-strain curves

m = Poisson's ratio

E = modulus of elasticity

The stresses computed by the two methods agreed well.

REFERENCES

A-1. Parametric Study of Glass-Filament-Reinforced Metal Pressure Vessels, NASA CR 54-855 (Aerojet-General report prepared under Contract NAS 3-6292), April 1966.

A-2. R. H. Johns and A. Kaufman, Filament-Overwrapped Metallic Cylindrical Pressure Vessels, NASA TMX-52171, Lewis Research Center, 1966.

A-3. G. Gerard and H. Becker, Handbook of Structural Stability - Part III - Buckling of Curved Plates and Shells, NACA TN 3783, August 1957.

TABLE A-1

COMPRESSIVE PROPERTIES FOR METAL CYLINDER MATERIALS

Alloy	Nominal Value, psi, at 75°F		
	Proportional Limit	Yield Strength	Modulus of Elasticity
Ti-5Al-2.5Sn			
Normal grade	92,000	120,000	15.5×10^6
ELI grade	90,000	105,000	15.5×10^6
2219-T62 aluminum	36,000	44,000	10.3×10^6
Inconel X-750 (STA)	108,000	120,000	31.0×10^6

TABLE A-2

DESCRIPTION OF METAL CYLINDER

Cylinder Material	Heat Treatment After Welding	Serial No.	Outside Diameter (D_o), in.		Thickness (t), in.		D_o/t Ratio		Remarks
			Design	Average Measured	Design	Average Measured	Design	Measured	
Aluminum Alloy 2219-0 (MIL-A-8920)	T62 condition per MIL-H-6088 (water-quenched, 150°F)	2	13.080	13.048	0.040	0.041	327	318	Satisfactory weld quality
		3	13.080	13.043	0.040	0.040	327	326	
Inconel X-750, cool-rolled and annealed (MIL-N-7786)	Stress-equalized in air 4 hours at 1625 ±25°F, air-cooled, aged in air at 1300°F for 20 hours, and air-cooled	1	13.402	13.337	0.041	0.041	327	325	Same
		2	13.402	13.352	0.041	0.041	327	325	Same
Ti-5Al-2.5Sn (MIL-T-9046, Type II, Composition A)	Stress-relieved in air 2 hours at 1100°F and air-cooled	1	10.960	10.923	0.041	0.041	267	267	Same, except for one 0.018-in. porosity
		2	10.960	10.919	0.041	0.040	267	273	Same as Serial No. 1

Table A-2

TABLE A-3

DATA ON OVERWRAPPED METAL CYLINDERS*

Cylinder Material	Serial No.	Filament Overwinding	Winding Tension lb/ strand	Overwrap Layers	Internal Pressure** psig	Buckling Compression Stress psi	Buckling Compression Strain in./in.	Remarks
2219-T62 aluminum	2	Dacron type 52 yarn 1100 denier	6	9	505	43,500	0.0050	Depressurization Cycle 1 at 6 layers and 310 psig; Cycle 2 at 7 layers and 370 psig; Cycle 3 at 8 layers and 425 psig; Cycle 4 at 9 layers and 505 psig. Buckled when pressure decreased to zero.
	3	Same	8	7	460	35,200	0.0048	Cycle 1 at 7 layers and 460 psig. Buckled when pressure decreased to 25 psig.
Inconel X-750 (STA)	1	Same	6	16	830	99,000	0.0032	Cycle 1 at 14 layers and 722 psig; Cycle 2 at 16 layers and 830 psig. Buckled when pressure decreased to zero.
	2	Same	6	22	1120	139,000	0.0039	Cycle 1 at 15 layers and 742 psig; Cycle 2 at 16 layers and 805 psig; Cycle 3 at 17 layers and 860 psig; Cycle 4 at 18 layers and 900 psig; Cycle 5 at 20 layers and 980 psig; Cycle 6 at 22 layers and 1120 psig. Buckled when pressure decreased to 15 psig.
Ti-5Al-2.5Sn	1	Same	-	19	1720	103,000	0.0080	Cycle 1 at 11 layers and 1100 psig; Cycle 2 at 13 layers and 1150 psig; Cycle 3 at 15 layers and 1345 psig; Cycle 4 at 17 layers and 1500 psig; Cycle 5 at 19 layers and 1720 psig; Cycle 6 at 21 layers. Buckled when pressure decreased to zero.
	2	Same, plus E-glass roving (20-end count)	-	42	2000	-	0.0112	Dacron used for winding first 28 layers, then glass roving. Nine depressurization cycles - at overwrap layers 15, 18, 23, 25, 28, 33, 36, 41, and 42 - before cylinder buckling.

*Circumferential-winding pattern = 60 strands per inch per layer.

**Required to counterbalance total overwrap.

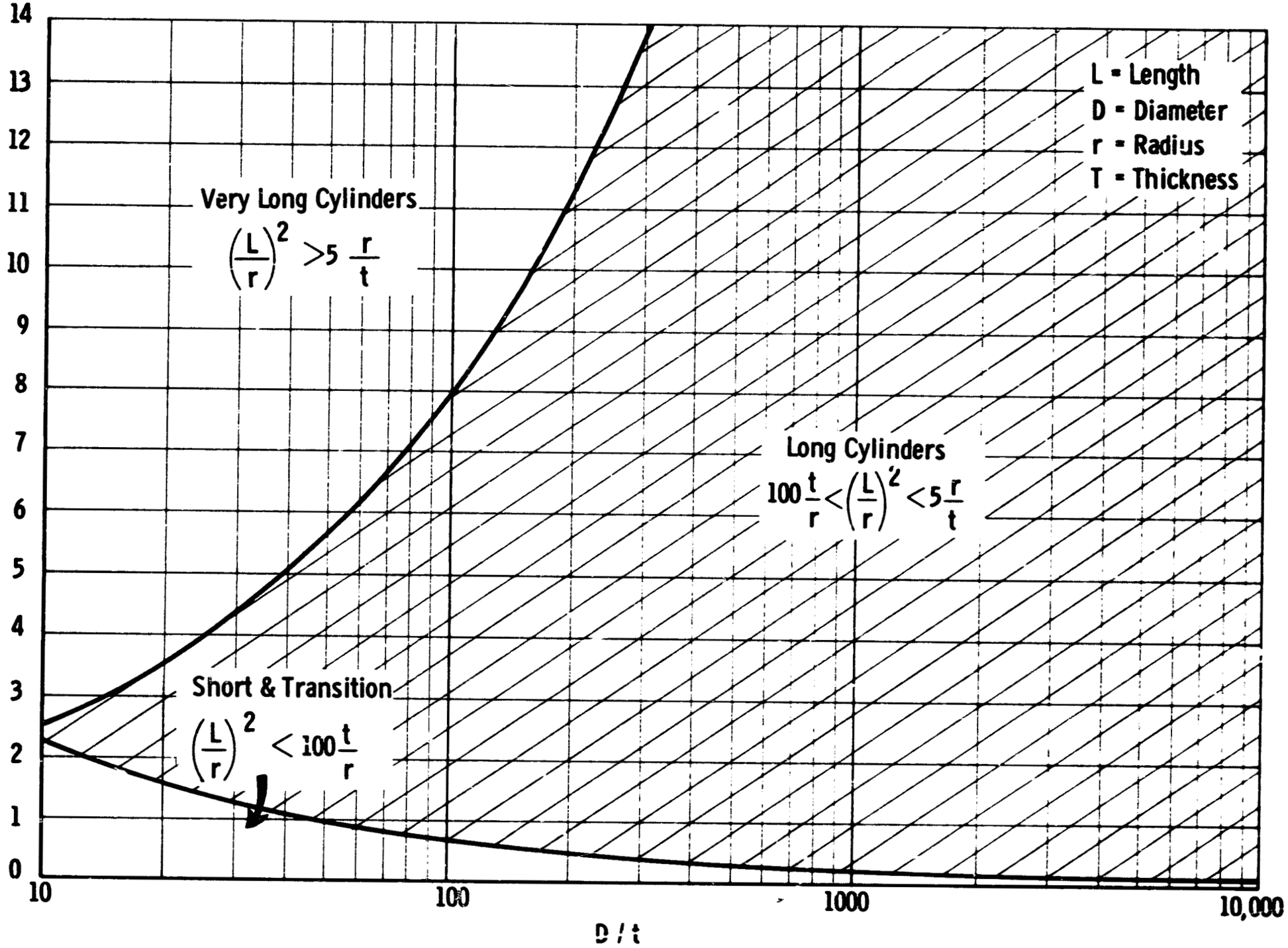

Figure A-1

Range of Cylinder Geometries Used in Calculation
of Buckling of Circular Cylinders Under External Pressure

Figure A-2

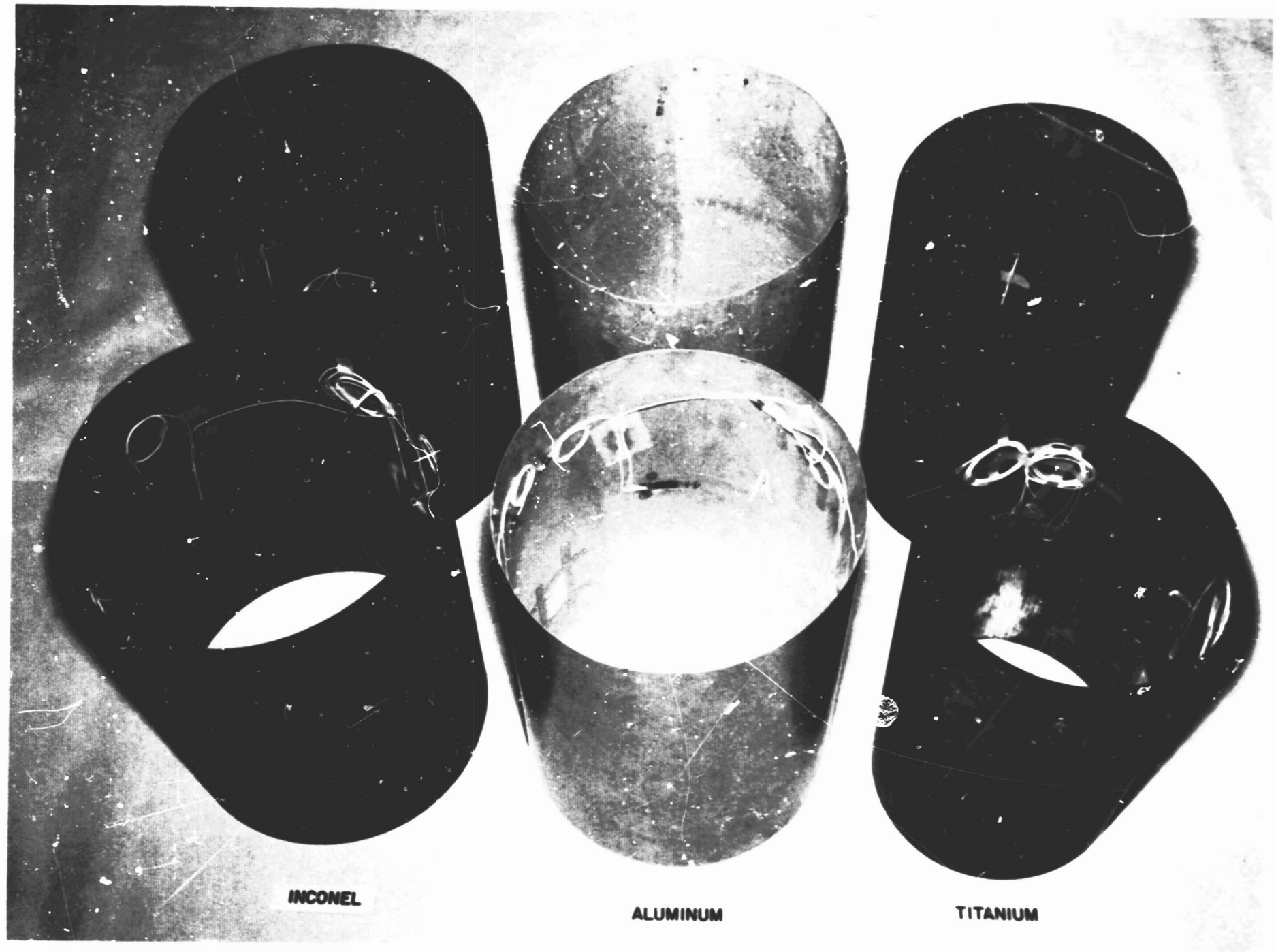

366-603

Cylinders for Buckling Study

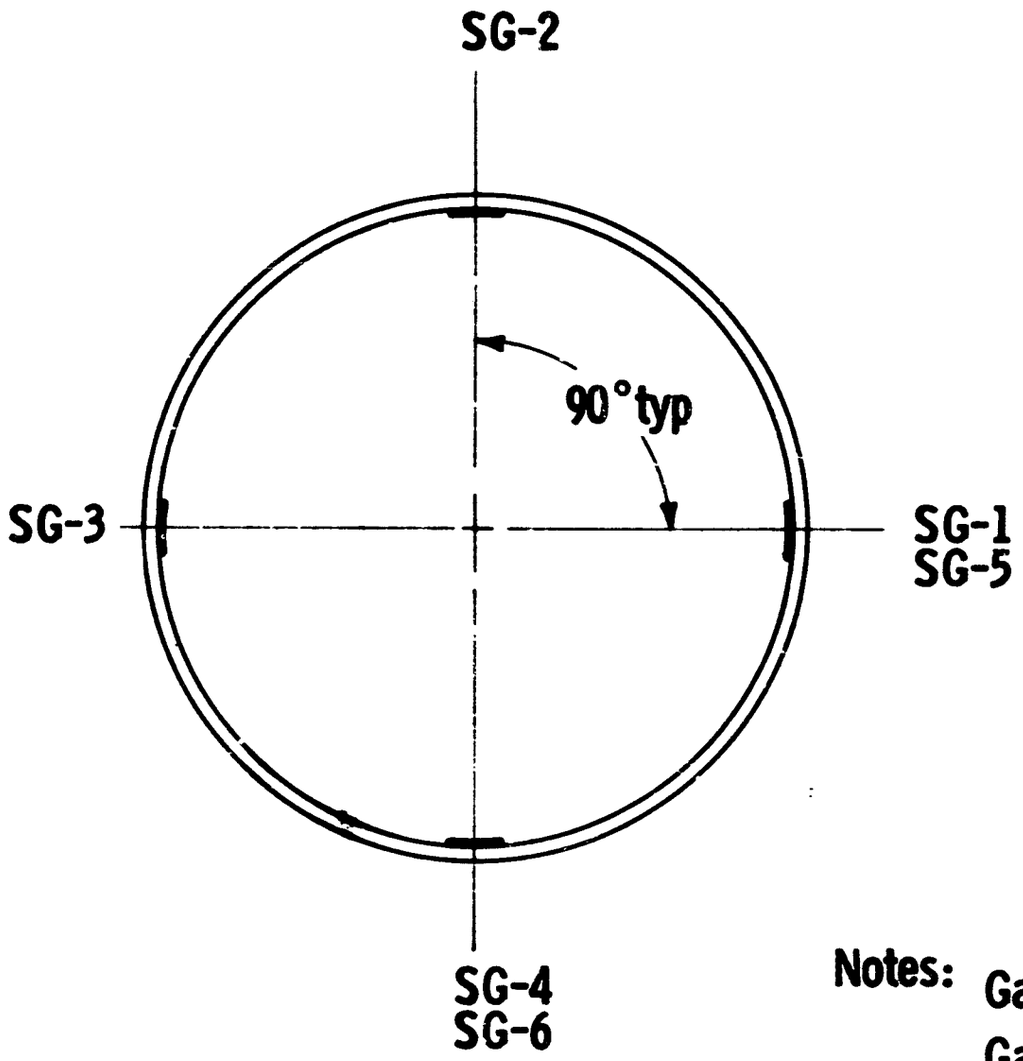

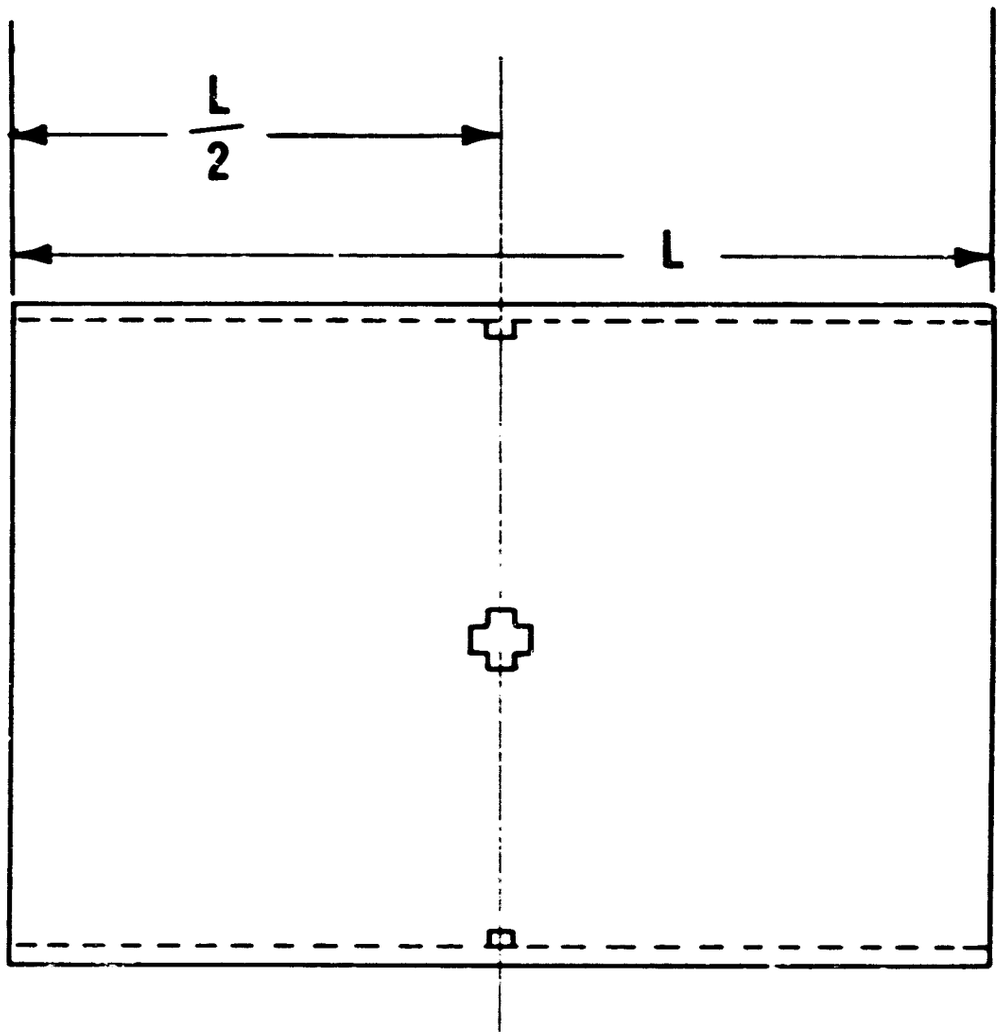

Notes: Gages SG-1 to SG-4 measure hoop strain
Gages SG-5 to SG-6 measure longitudinal strain

Figure A-3 Strain-Gage Locations

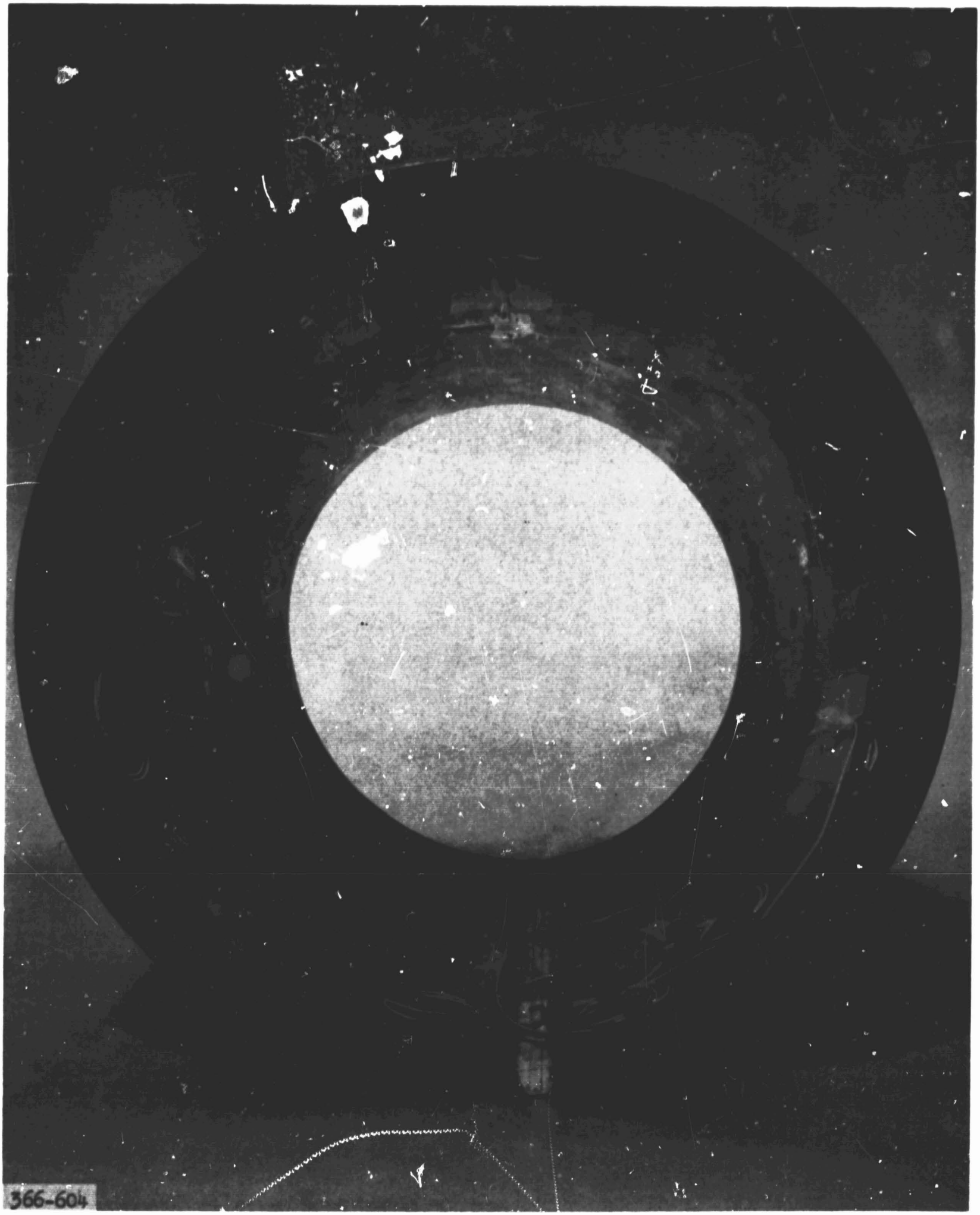

Strain-Gage Instrumentation

Figure A-4

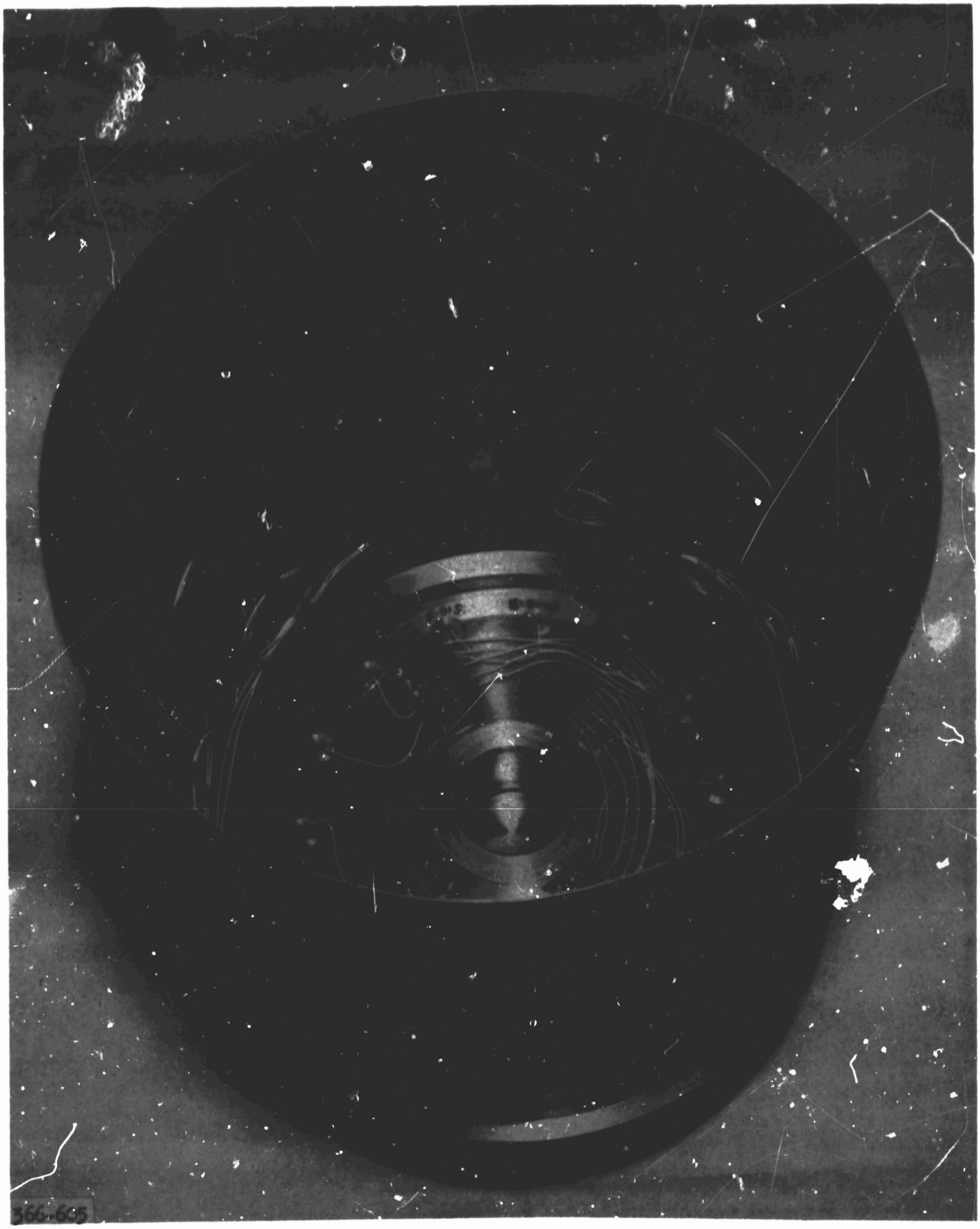

Cylinder Assembly to End Plate

Figure A-5

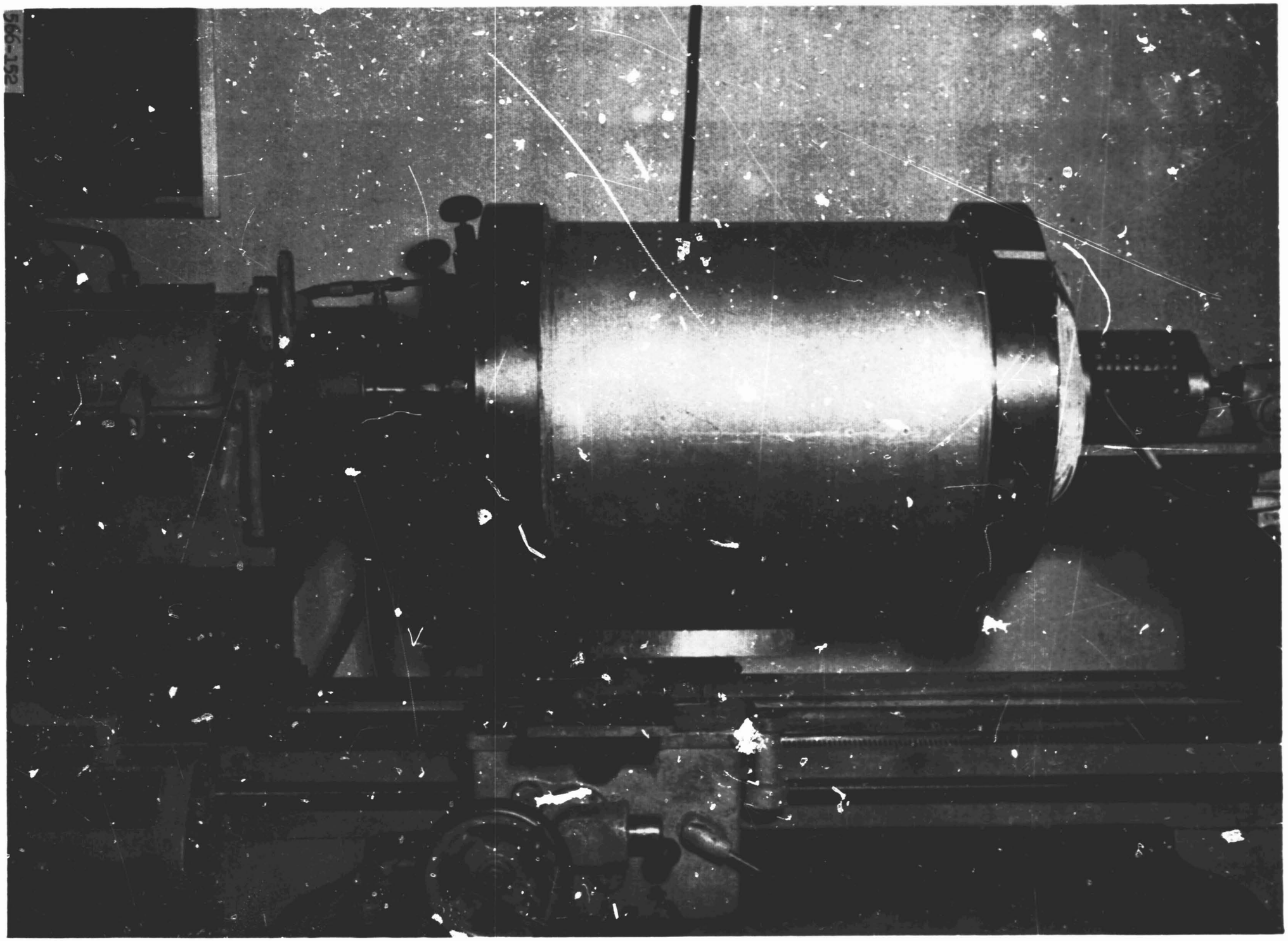

Cylinder and Tooling Assembly in Winding Machine

Figure A-7

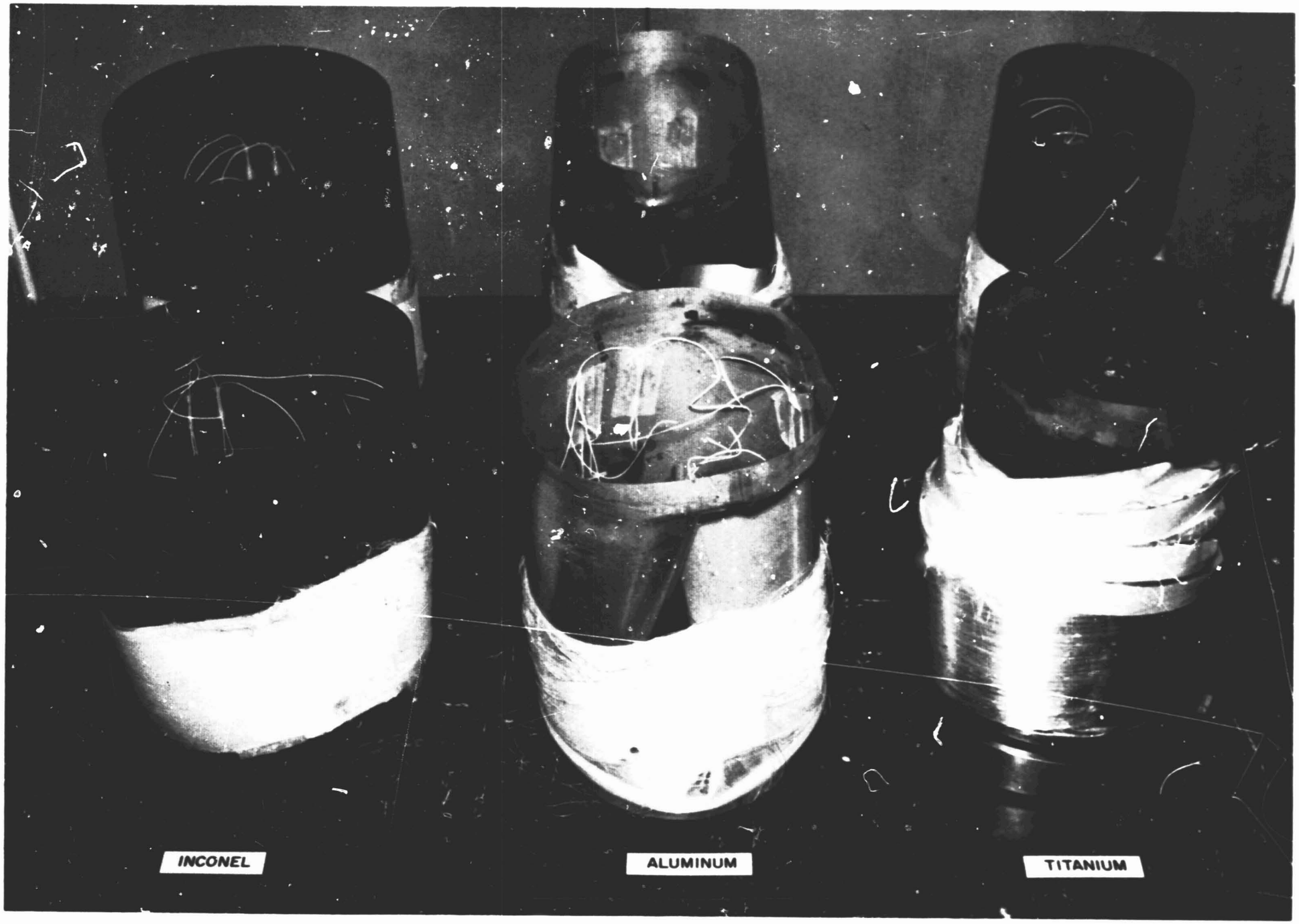

566-156

Buckled Cylinders

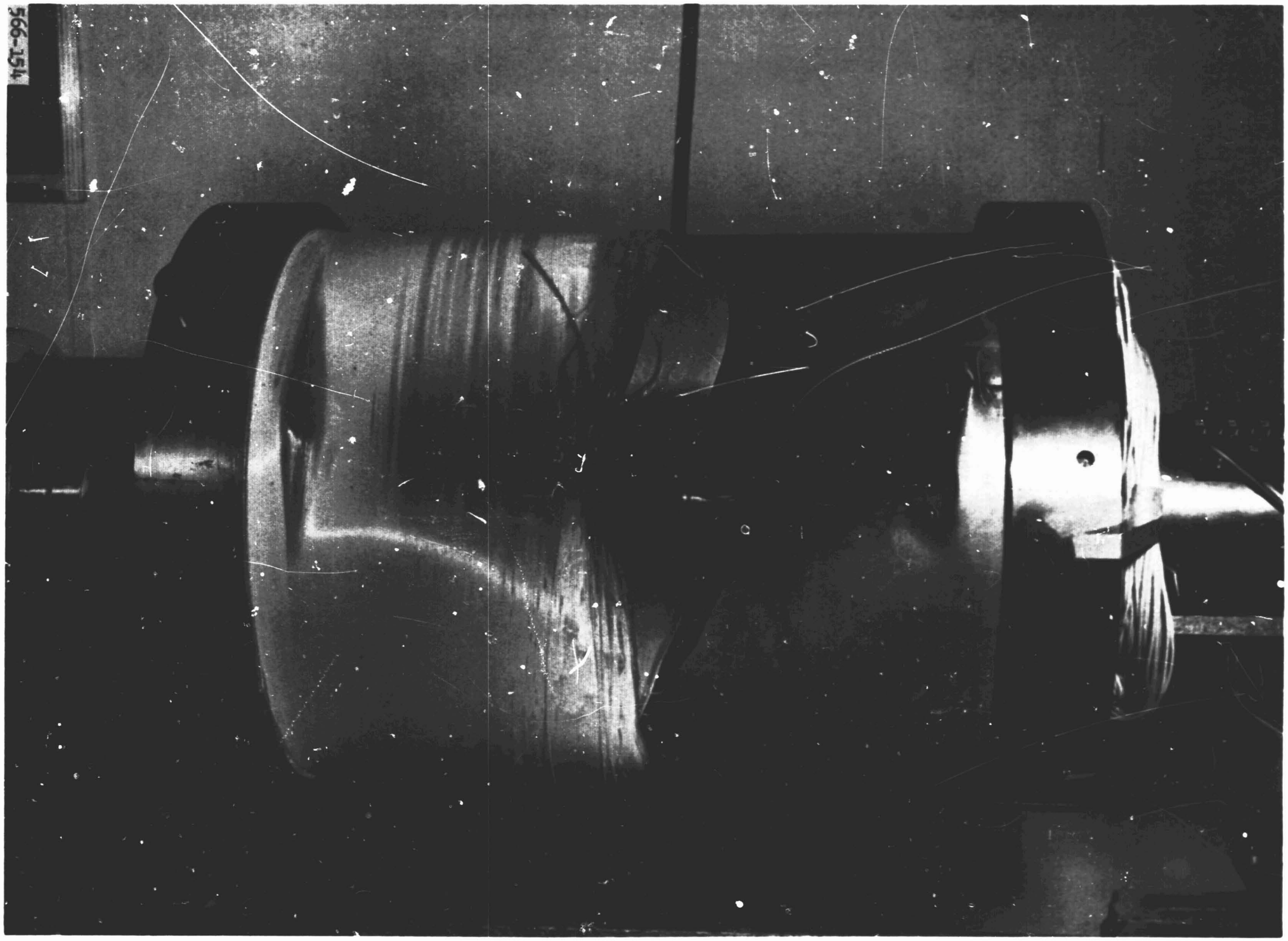

Buckled Cylinder with Portion of Windings Removed

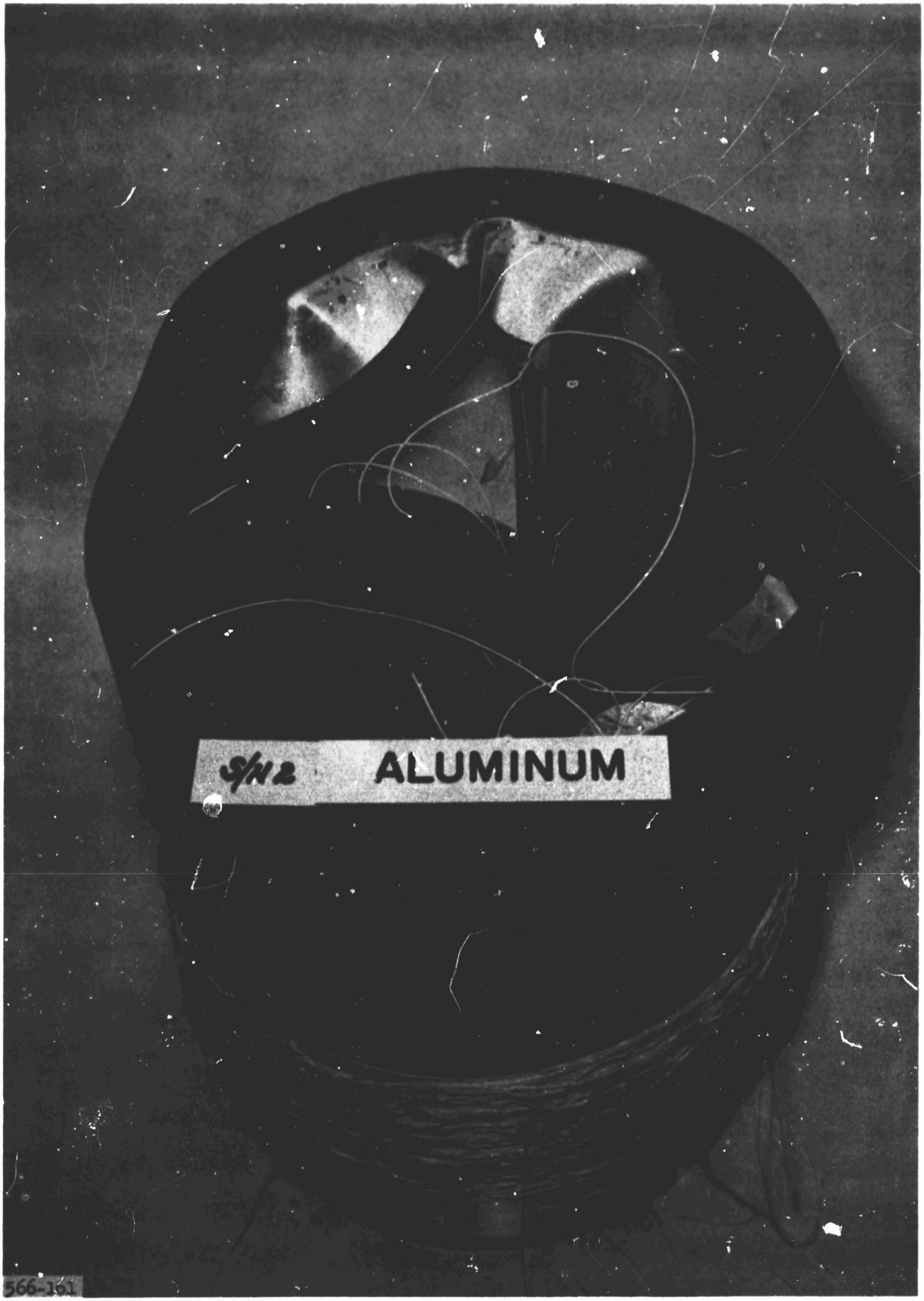

Aluminum Cylinder 2

Figure A-9

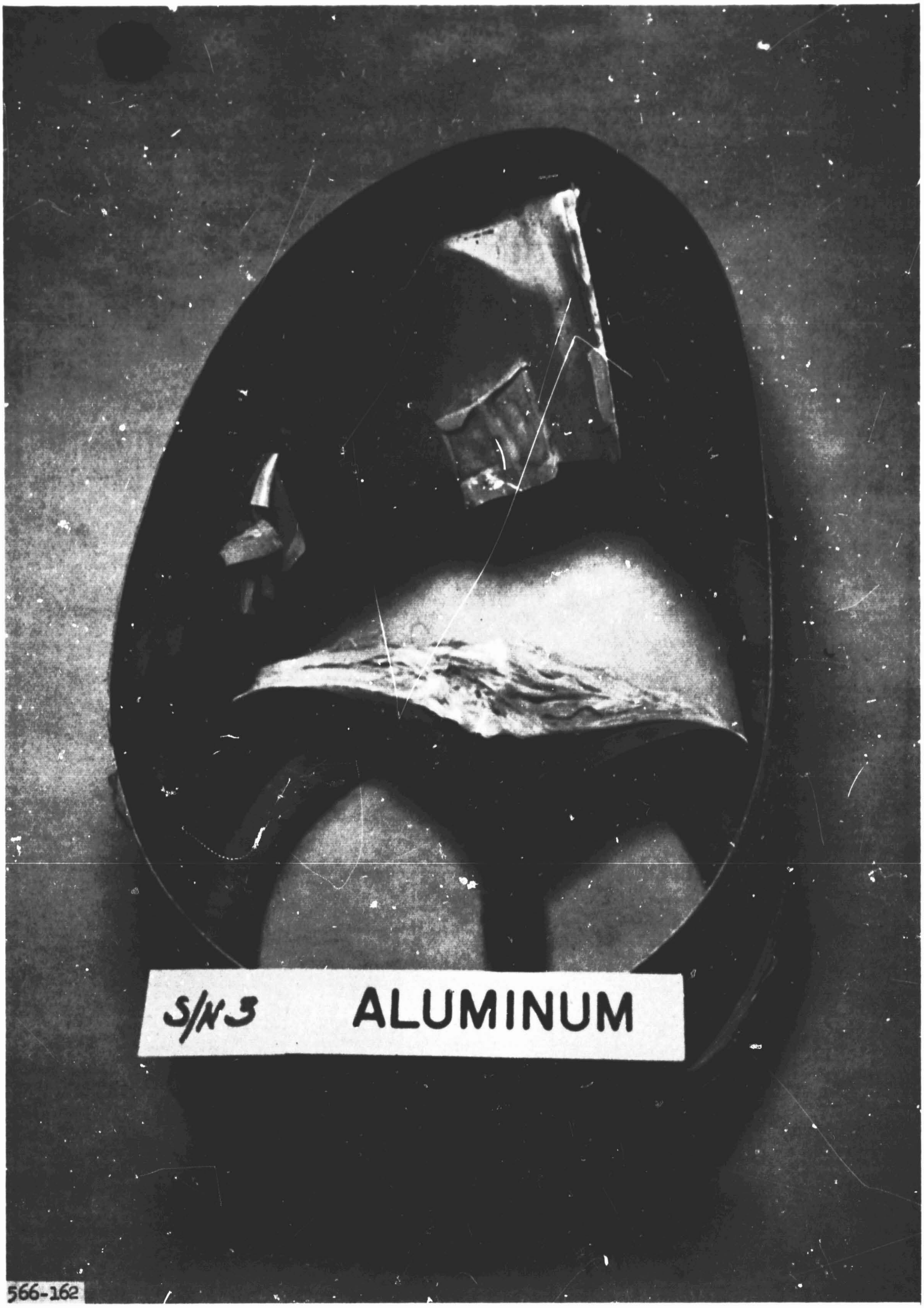

Aluminum Cylinder 3

Figure A-10

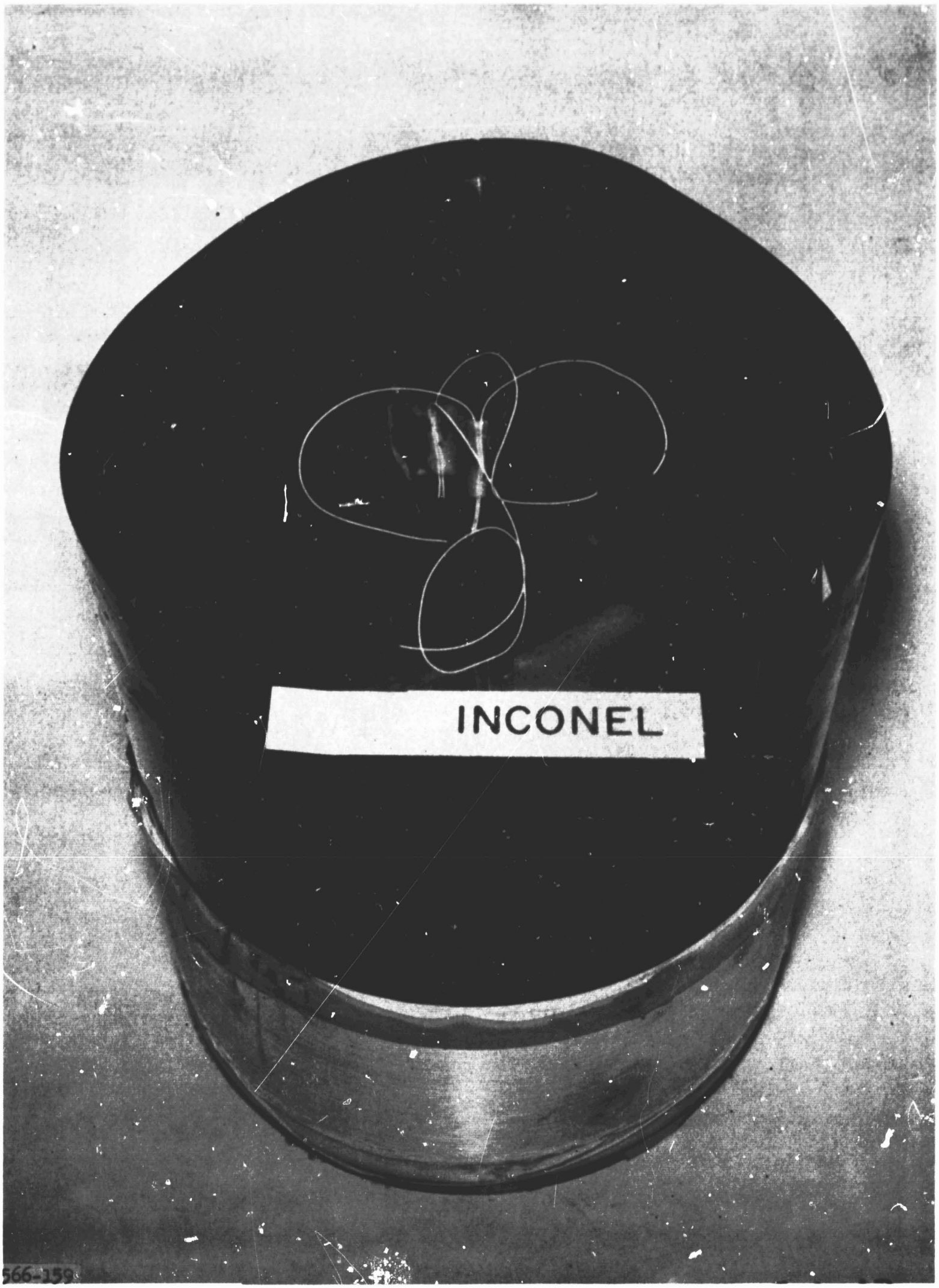

Inconel Cylinder 1

Figure A-11

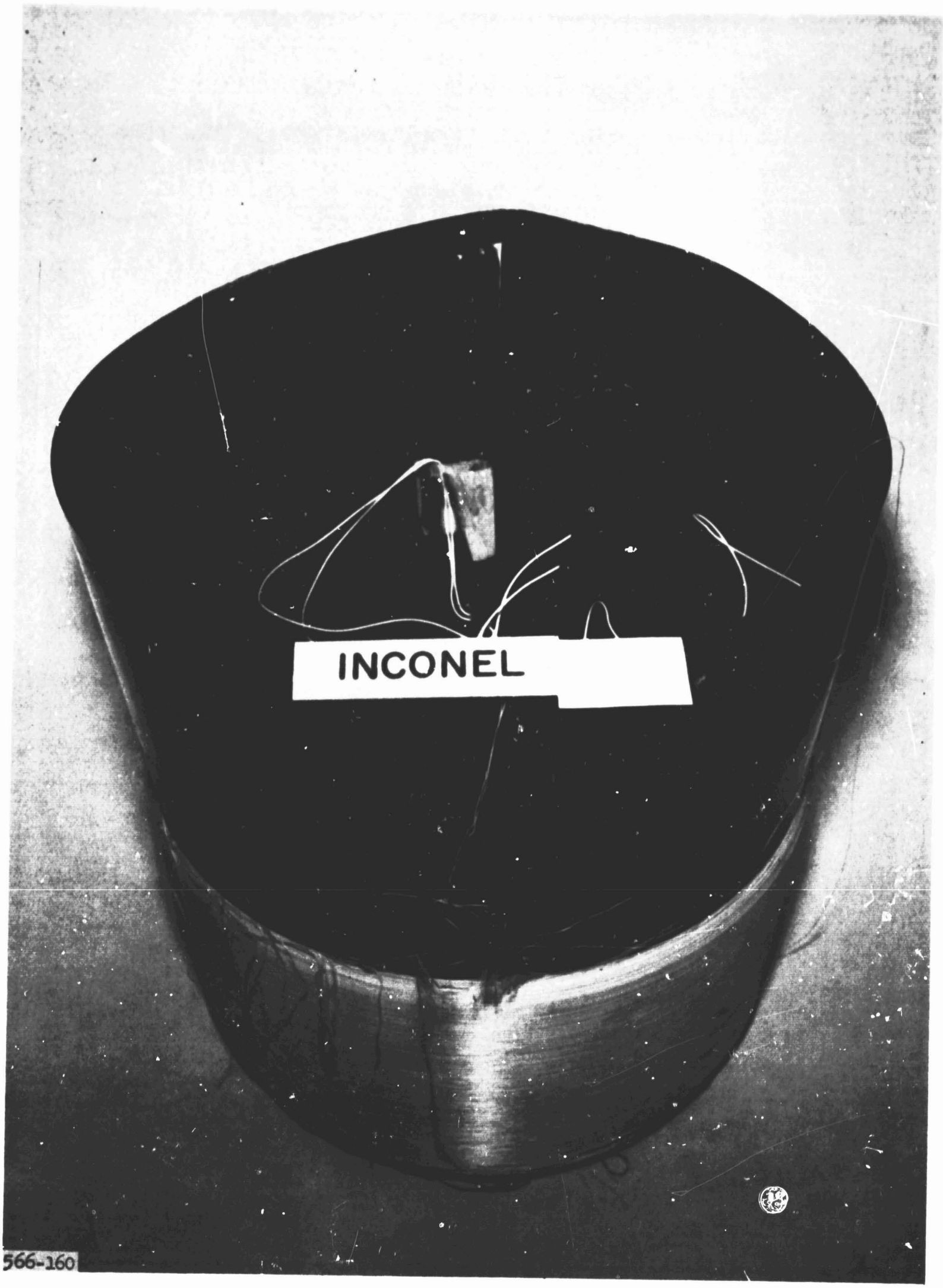

Inconel Cylinder 2

Figure A-12

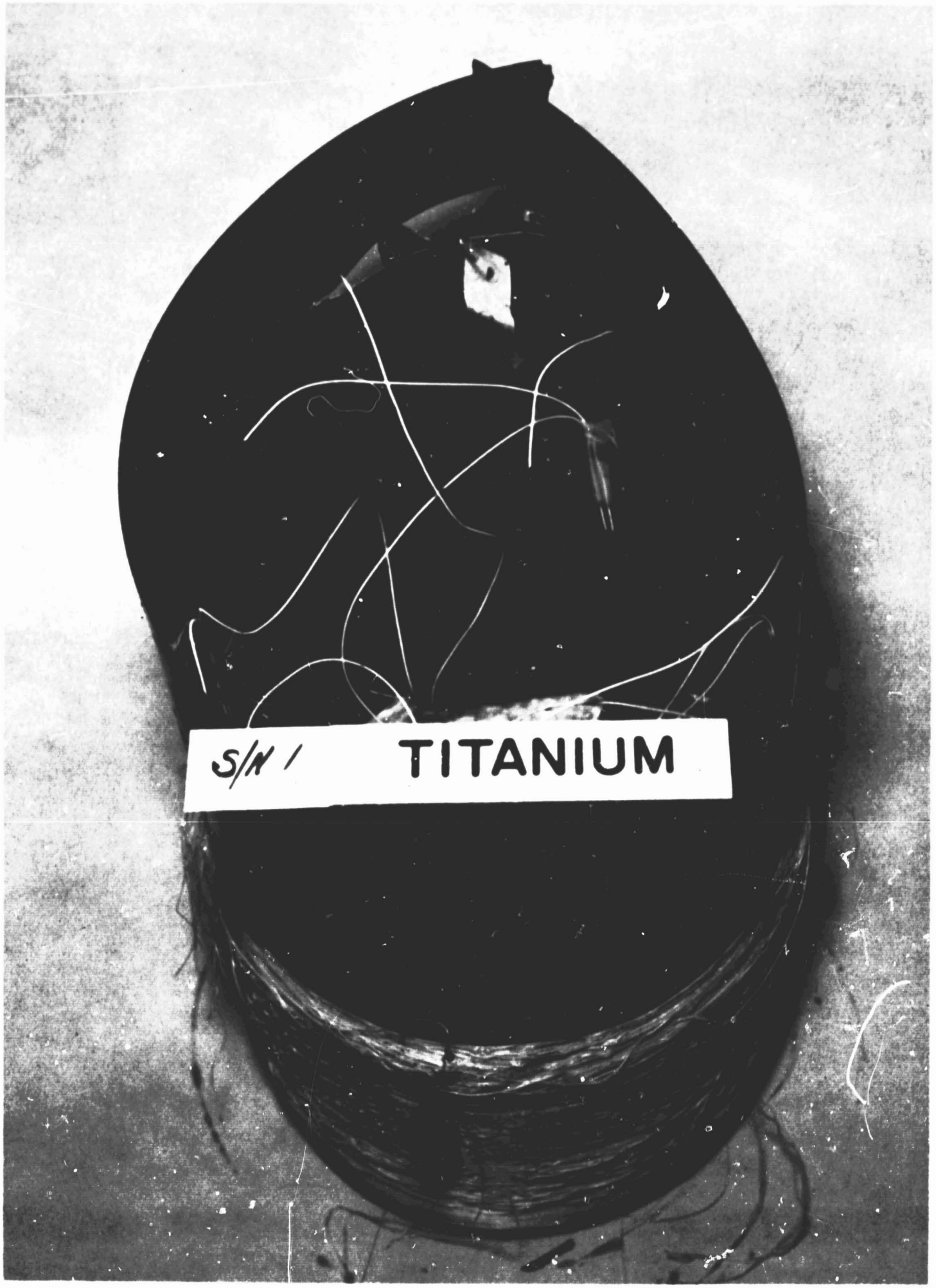

566-157

Titanium Cylinder 1

Figure A-13

Titanium Cylinder 2

Figure A-14

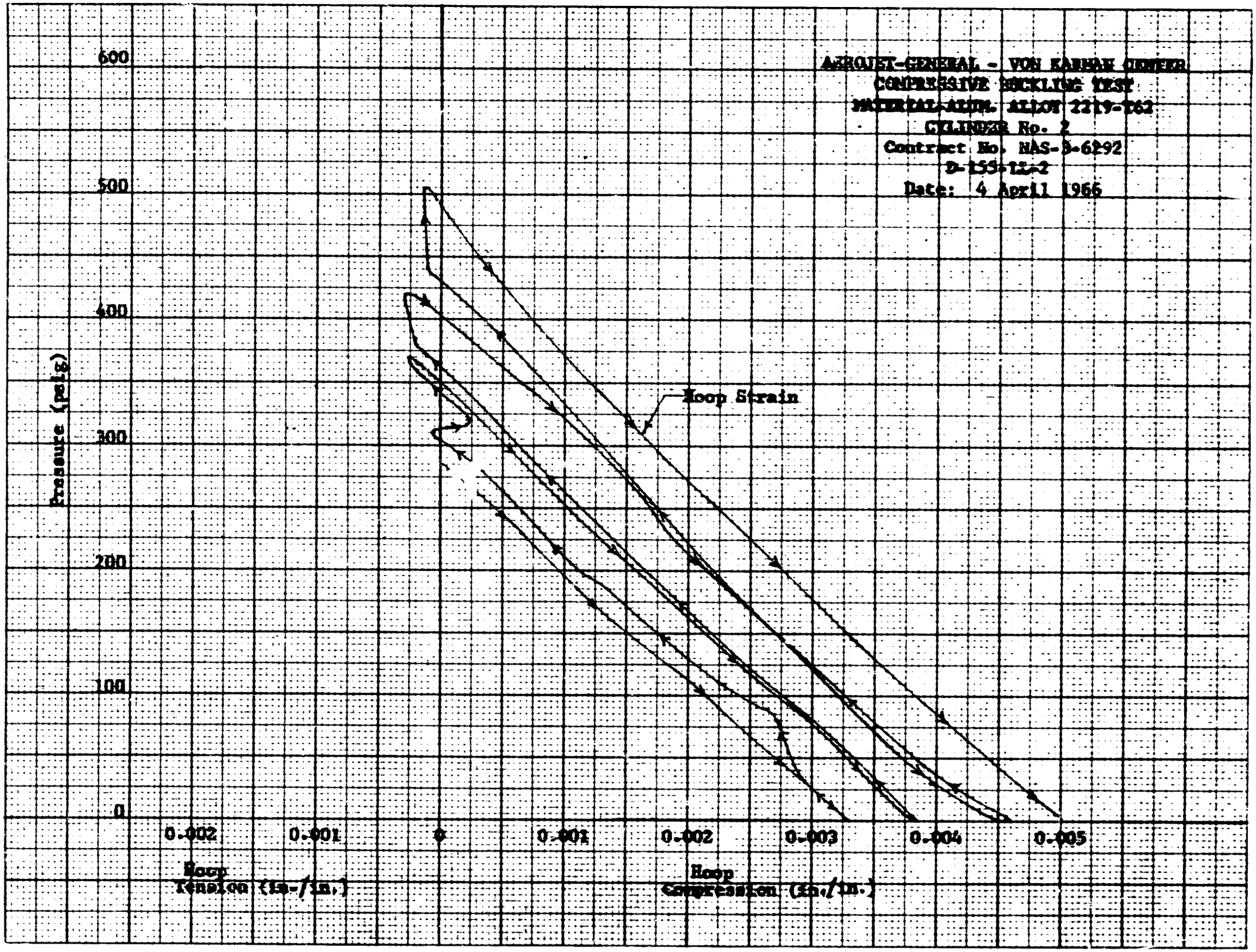

Aluminum Cylinder 2, Hoop Compression vs Pressure

Figure A-15, Sheet 1 of 2

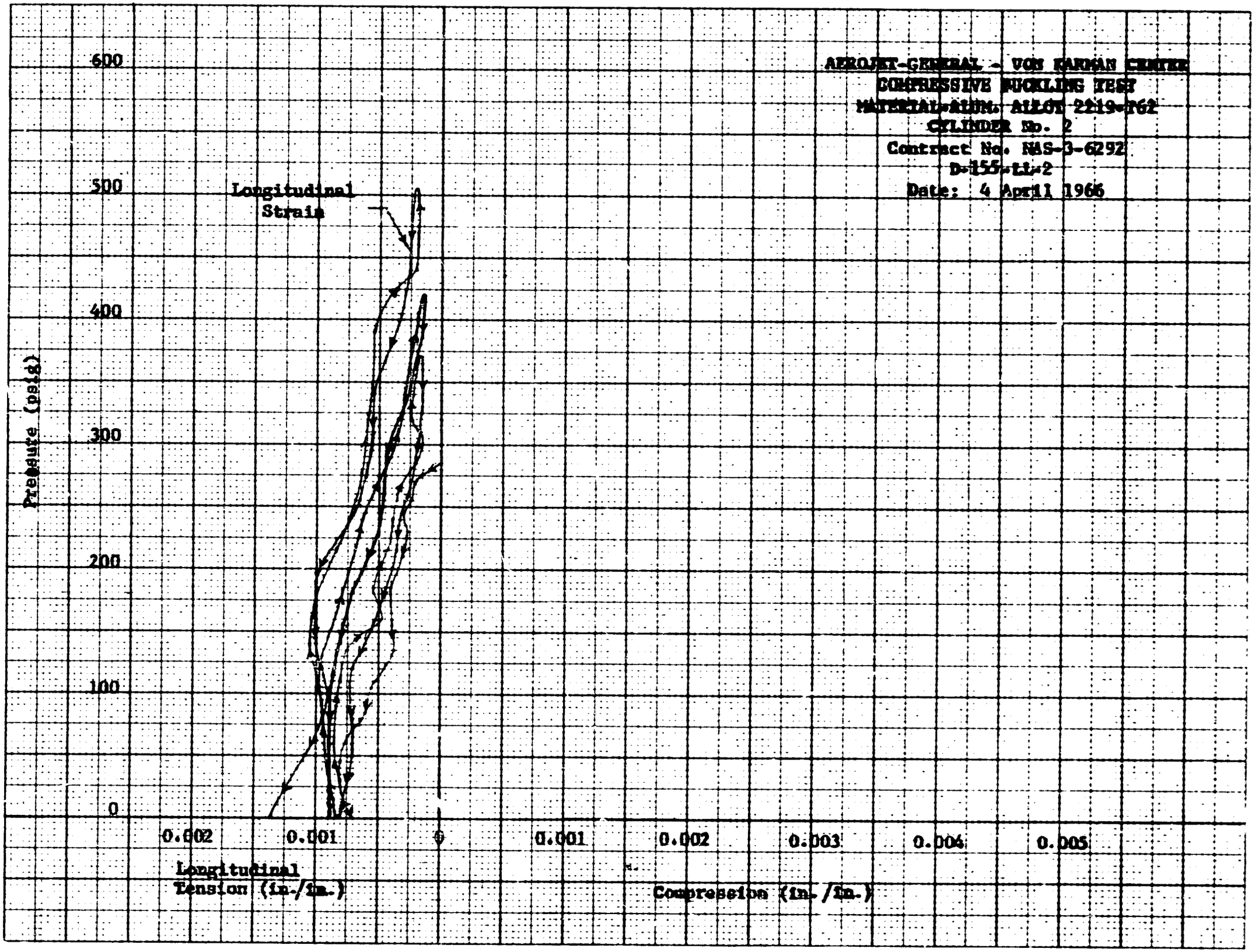

Aluminum Cylinder 2, Longitudinal Tension vs Pressure

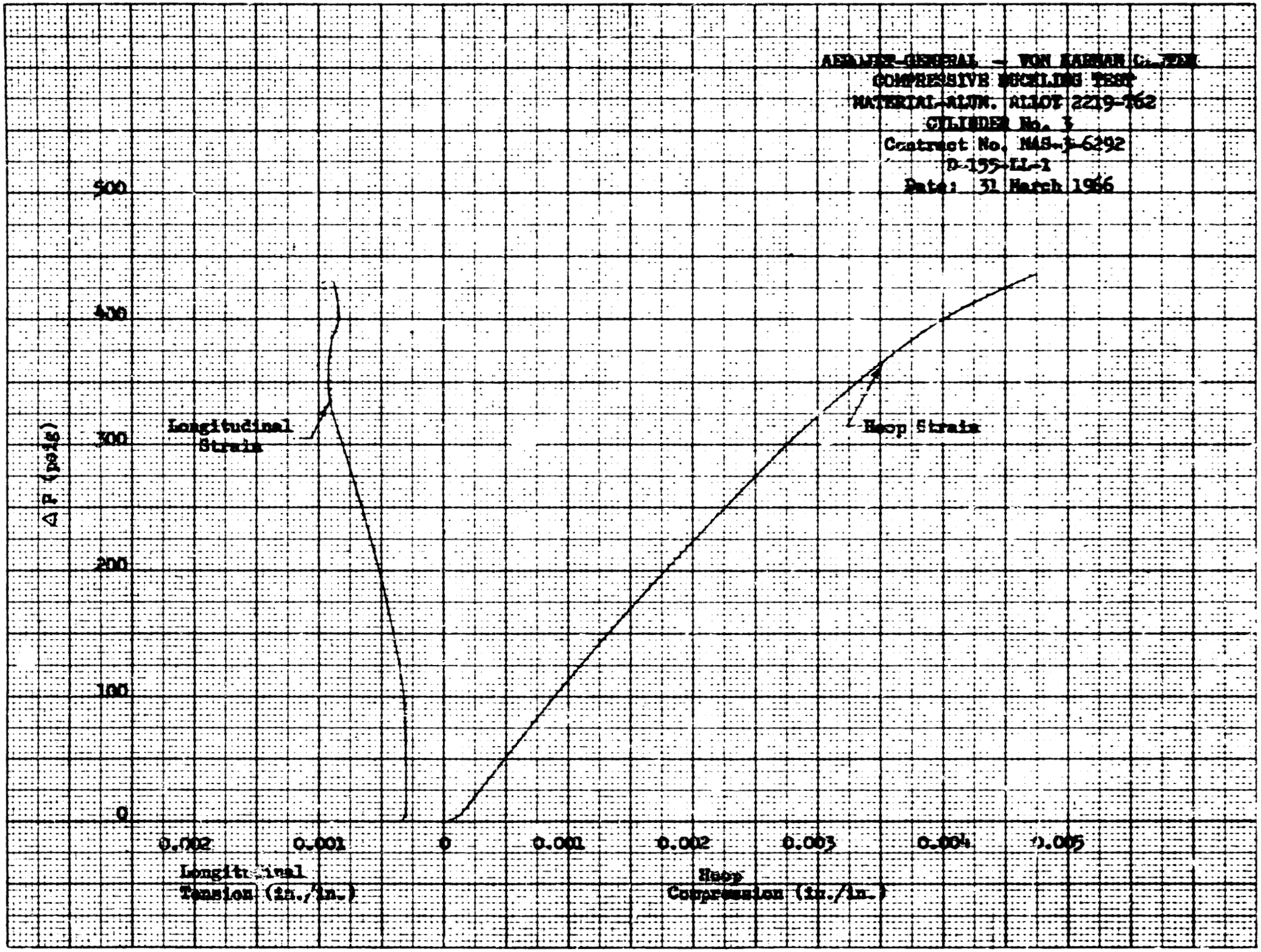

Aluminum Cylinder 3, Compression vs Pressure

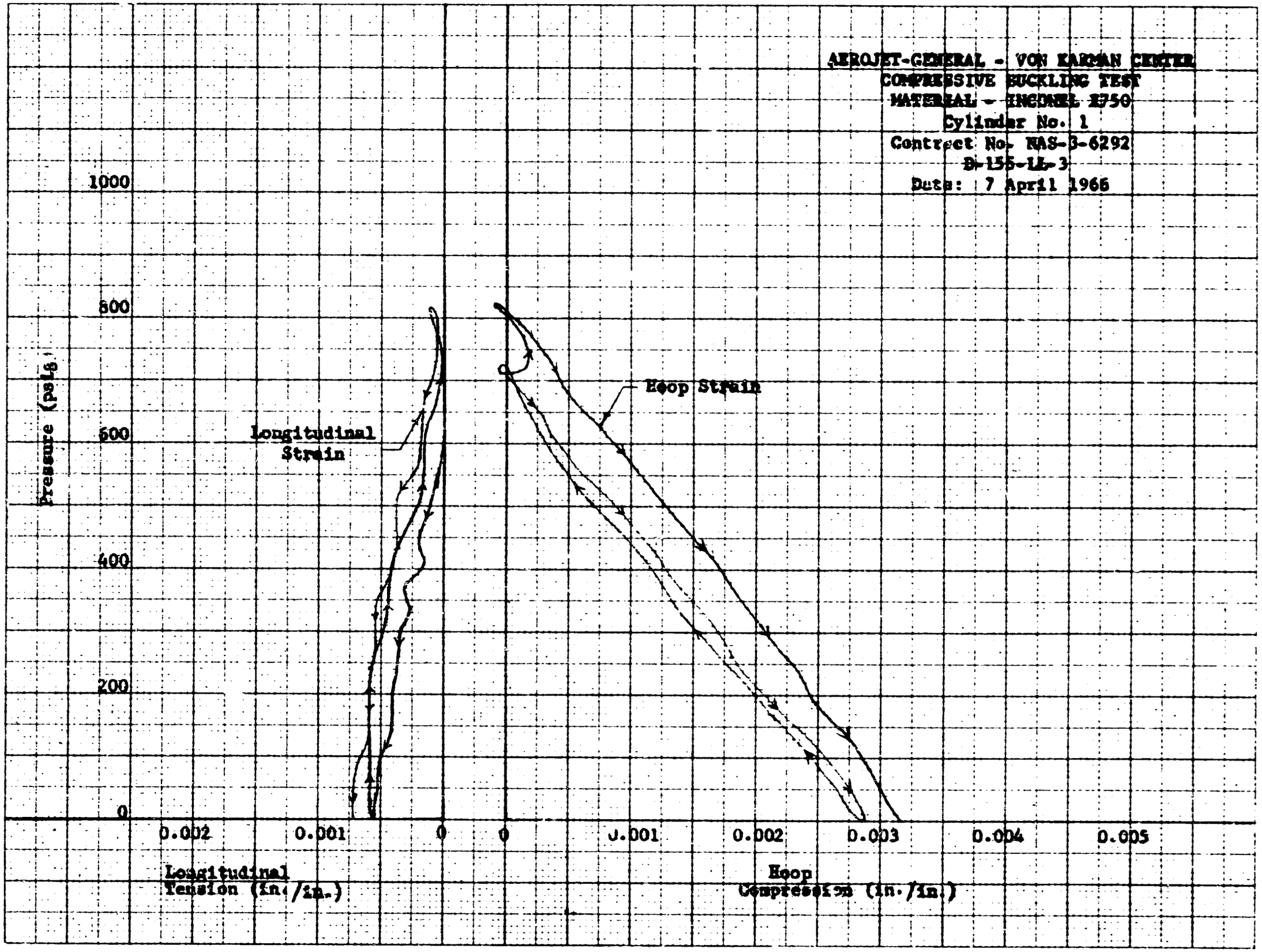

Figure A-17

Inconel Cylinder 1, Compression vs Pressure

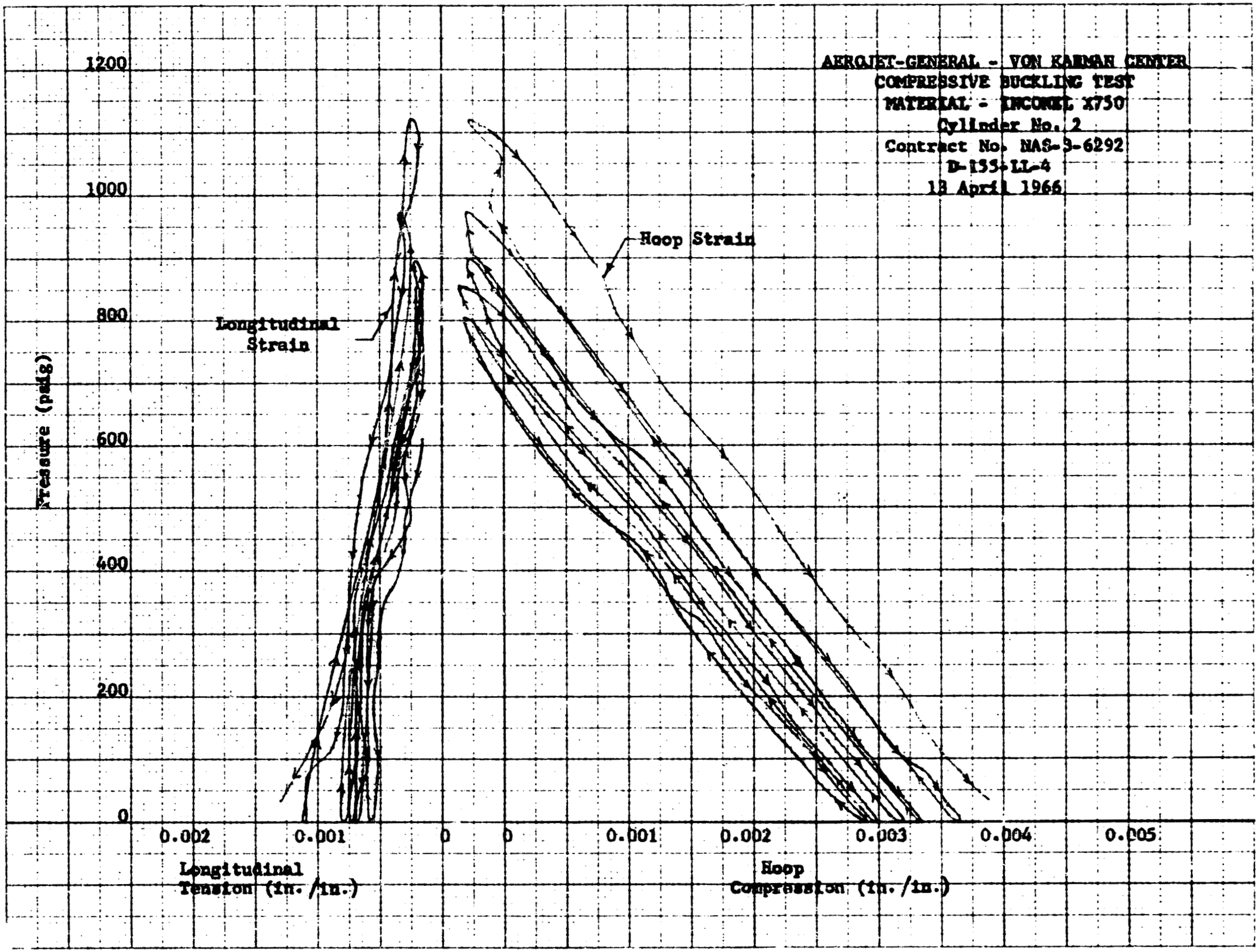

Inconel Cylinder 2, Compression vs Pressure

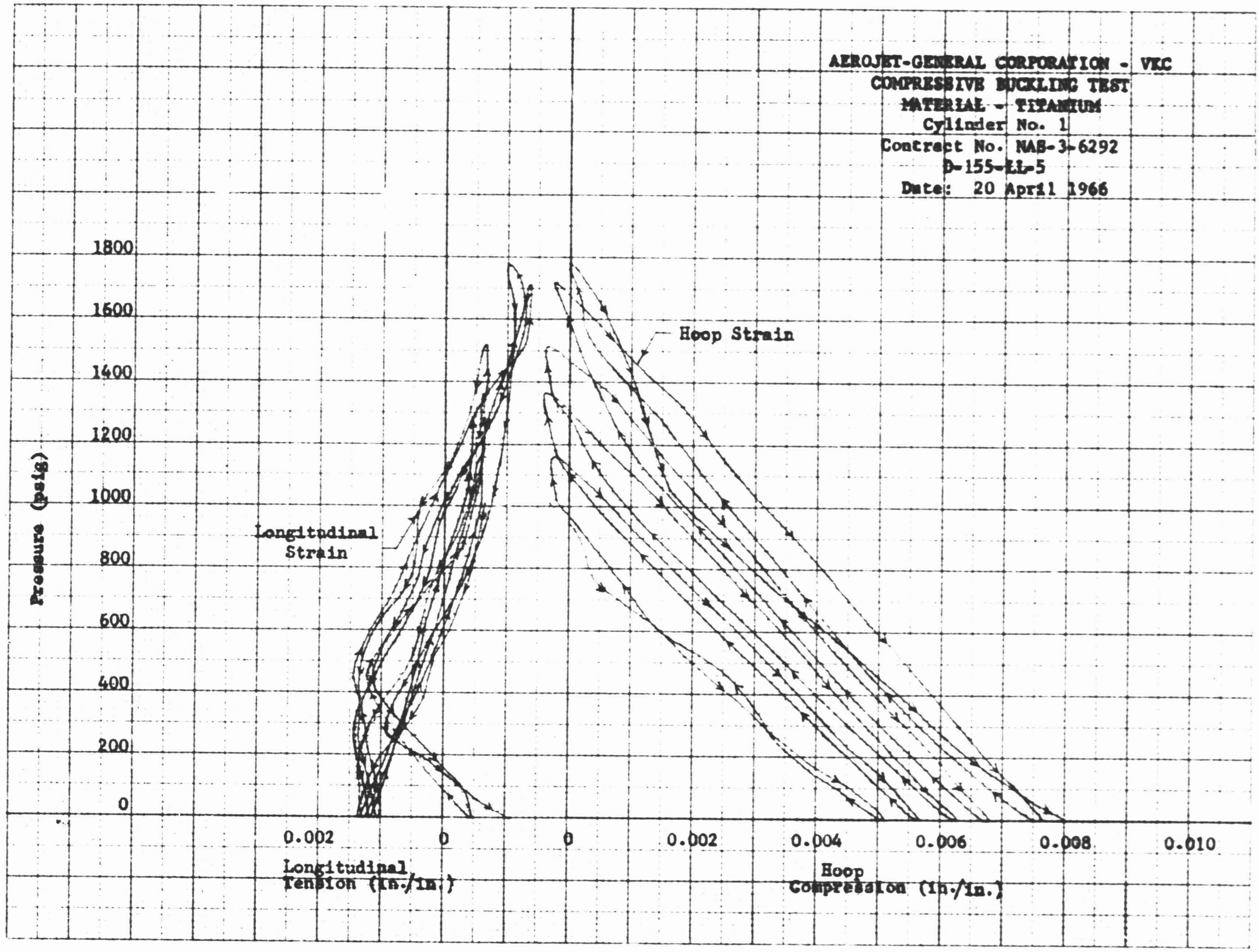

Titanium Cylinder 1, Compression vs Pressure

REPRODUCIBILITY OF THE ORIGINAL PAGE IS POOR.
FOR BETTER COPY CONTACT THE DOCUMENT ORIGINATOR.

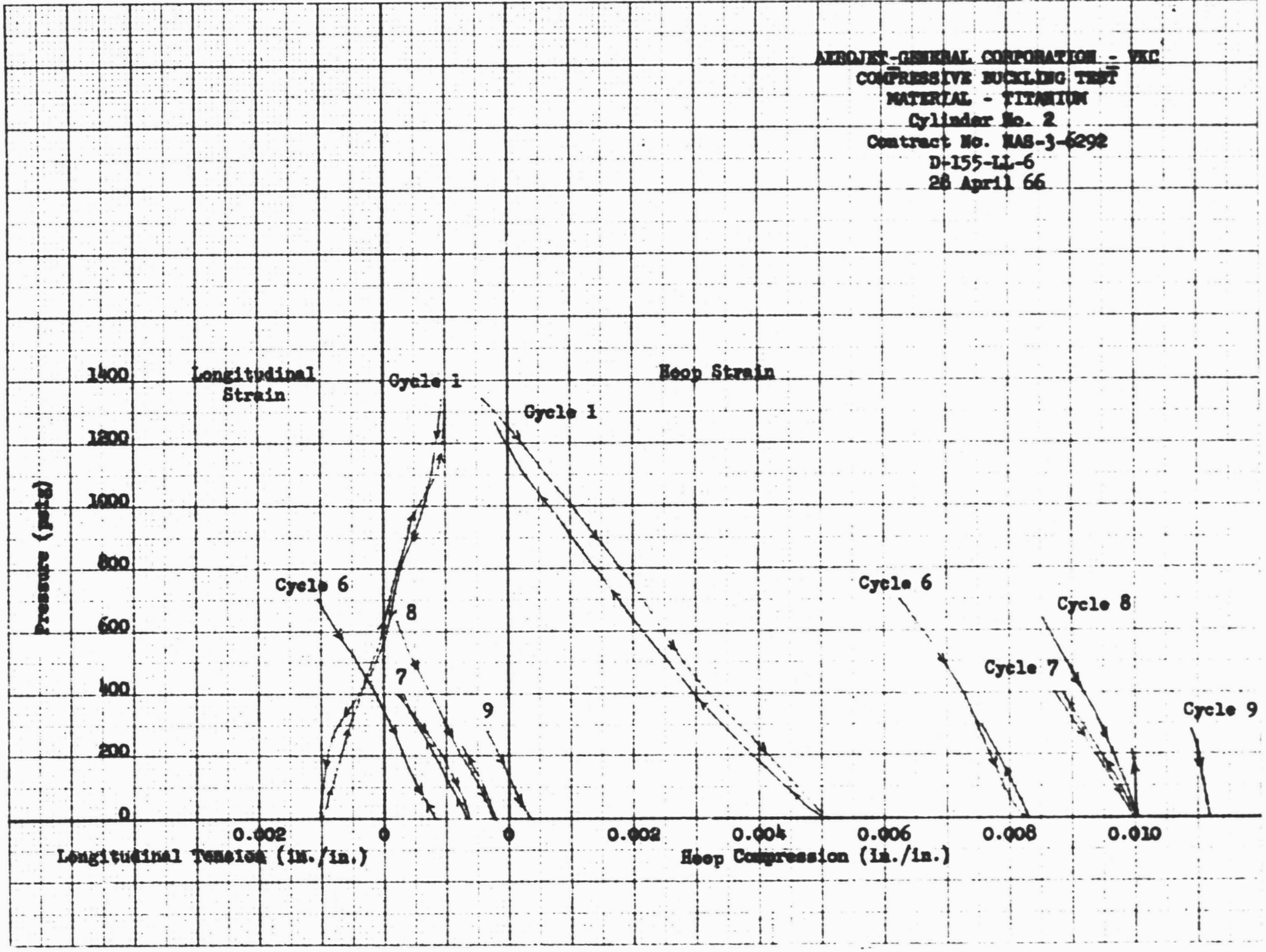

Figure A-20

Titanium Cylinder 2, Compression vs Pressure

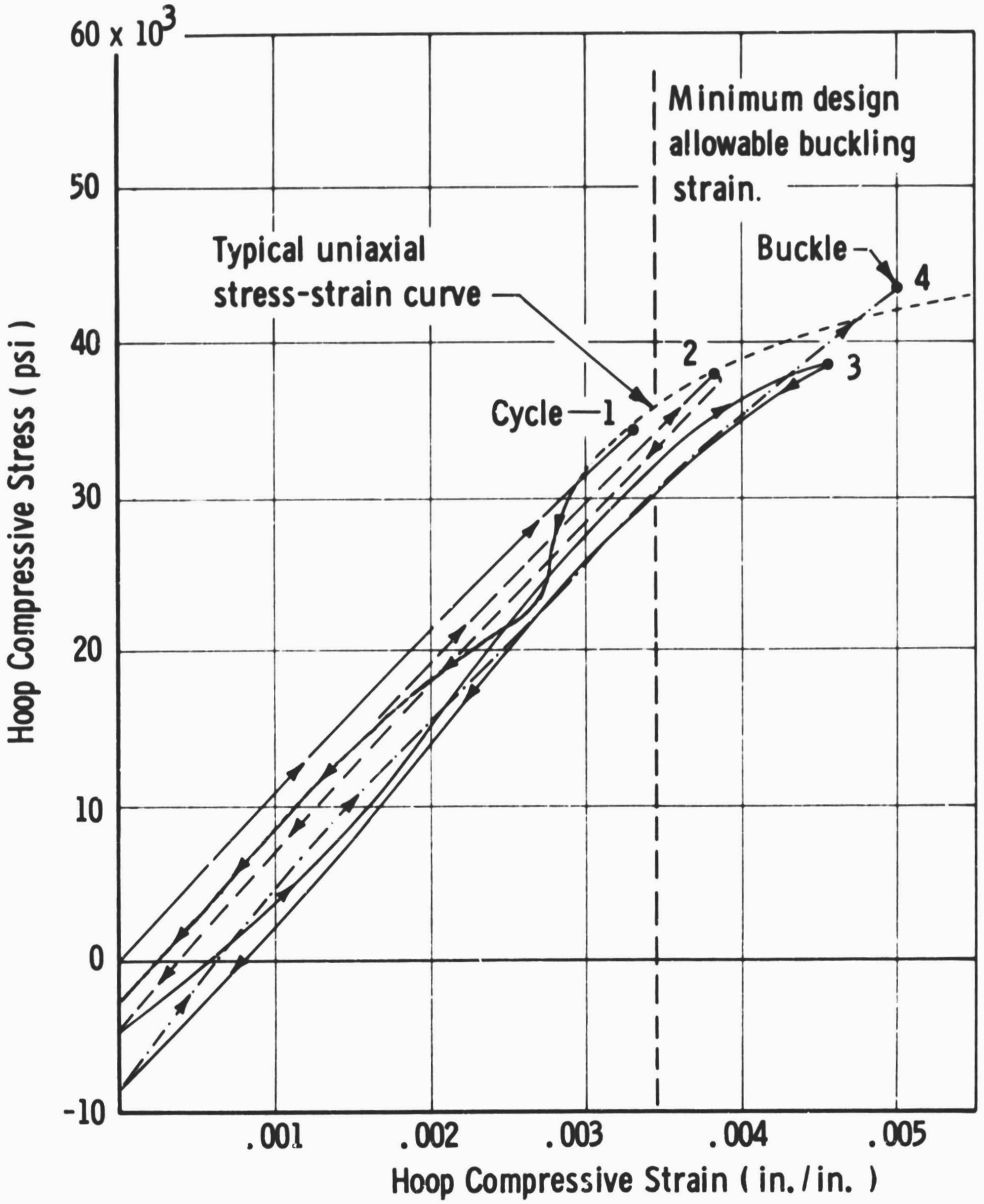

Compressive Stress-Strain Curve for Aluminum Cylinder 2, Buckling Test

Figure A-21

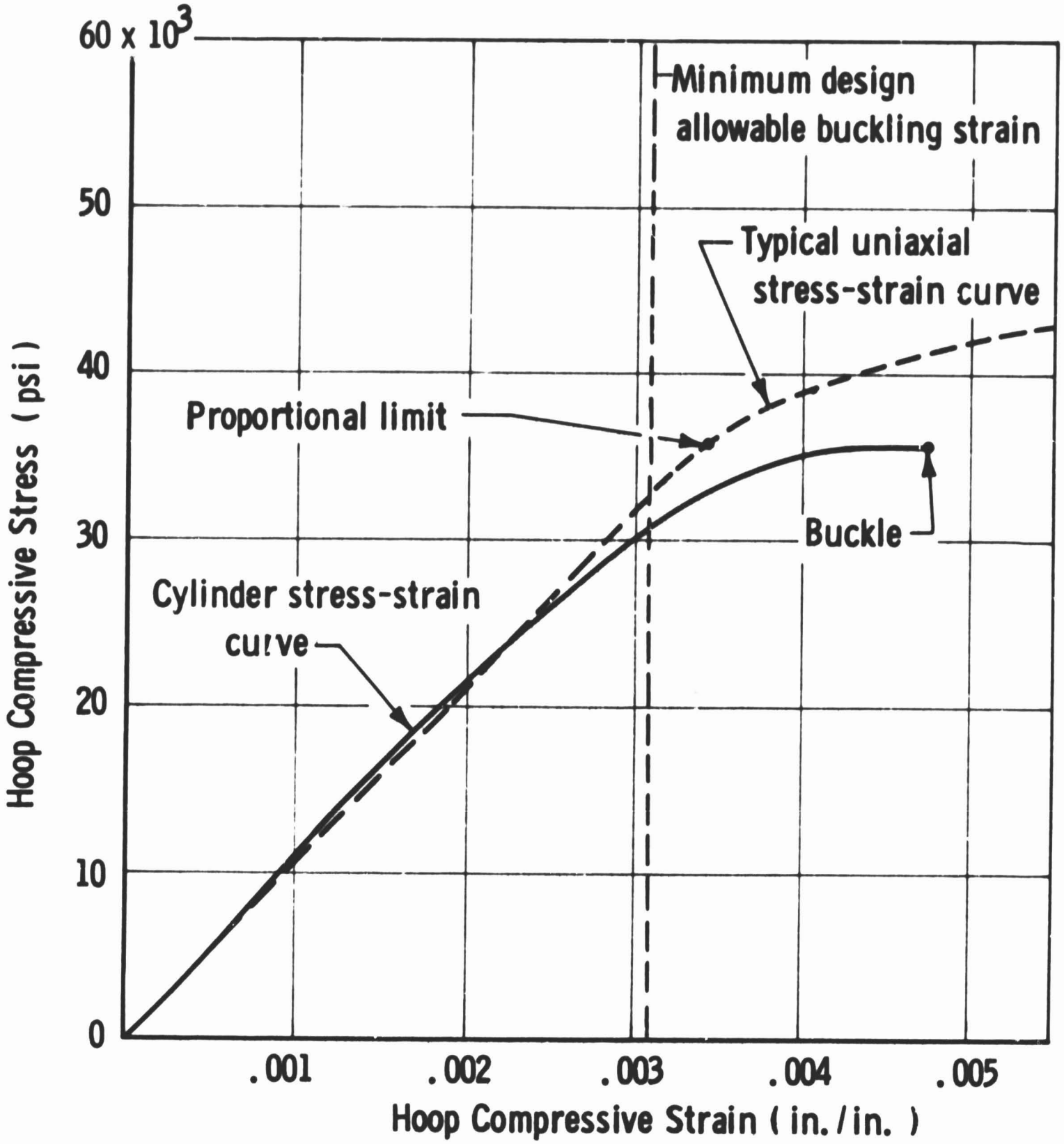

Compressive Stress-Strain Curve for Aluminum Cylinder 3, Buckling Test

Figure A-22

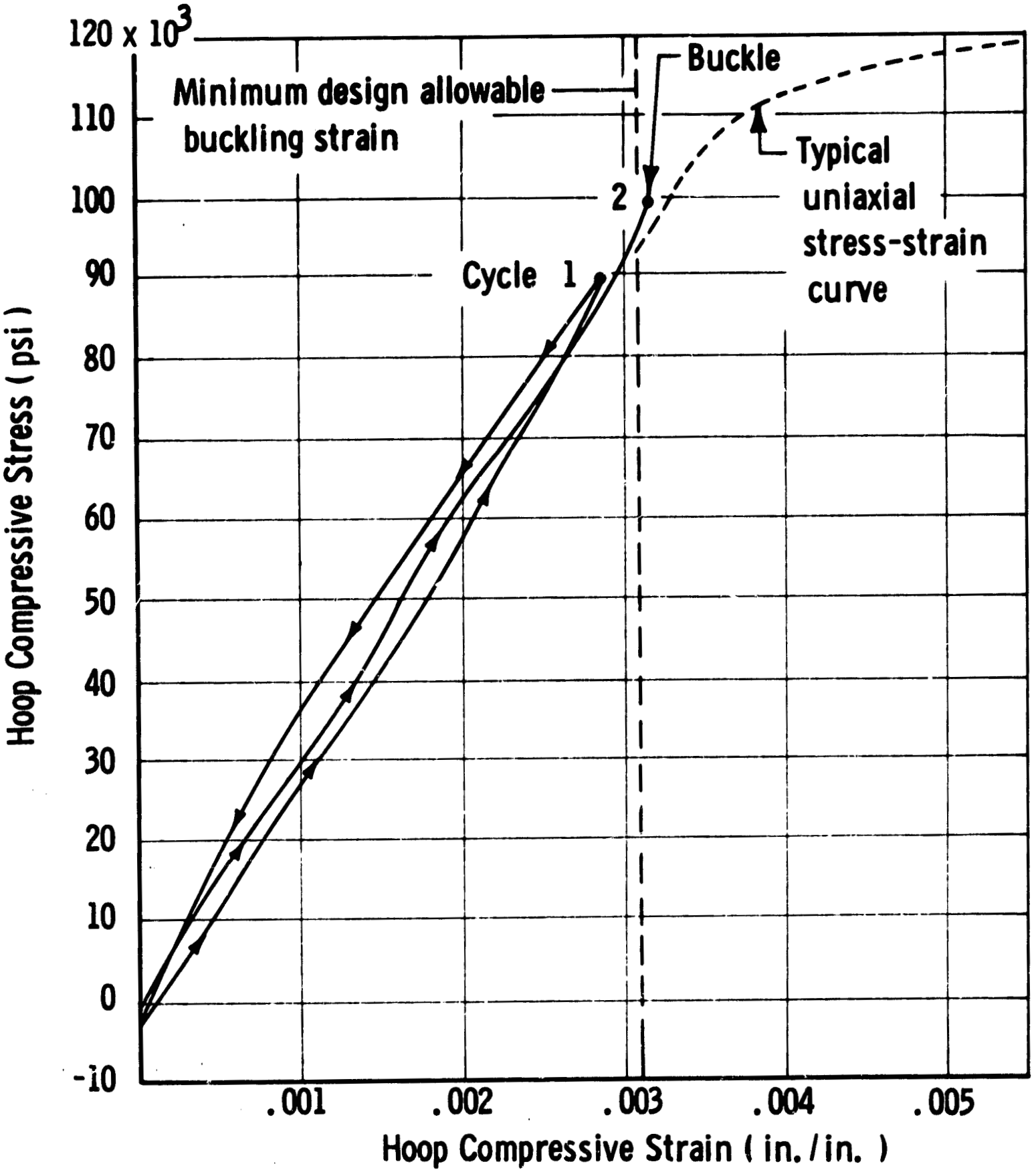

Compressive Stress-Strain Curve for Inconel Cylinder 1, Buckling Test

Figure A-23

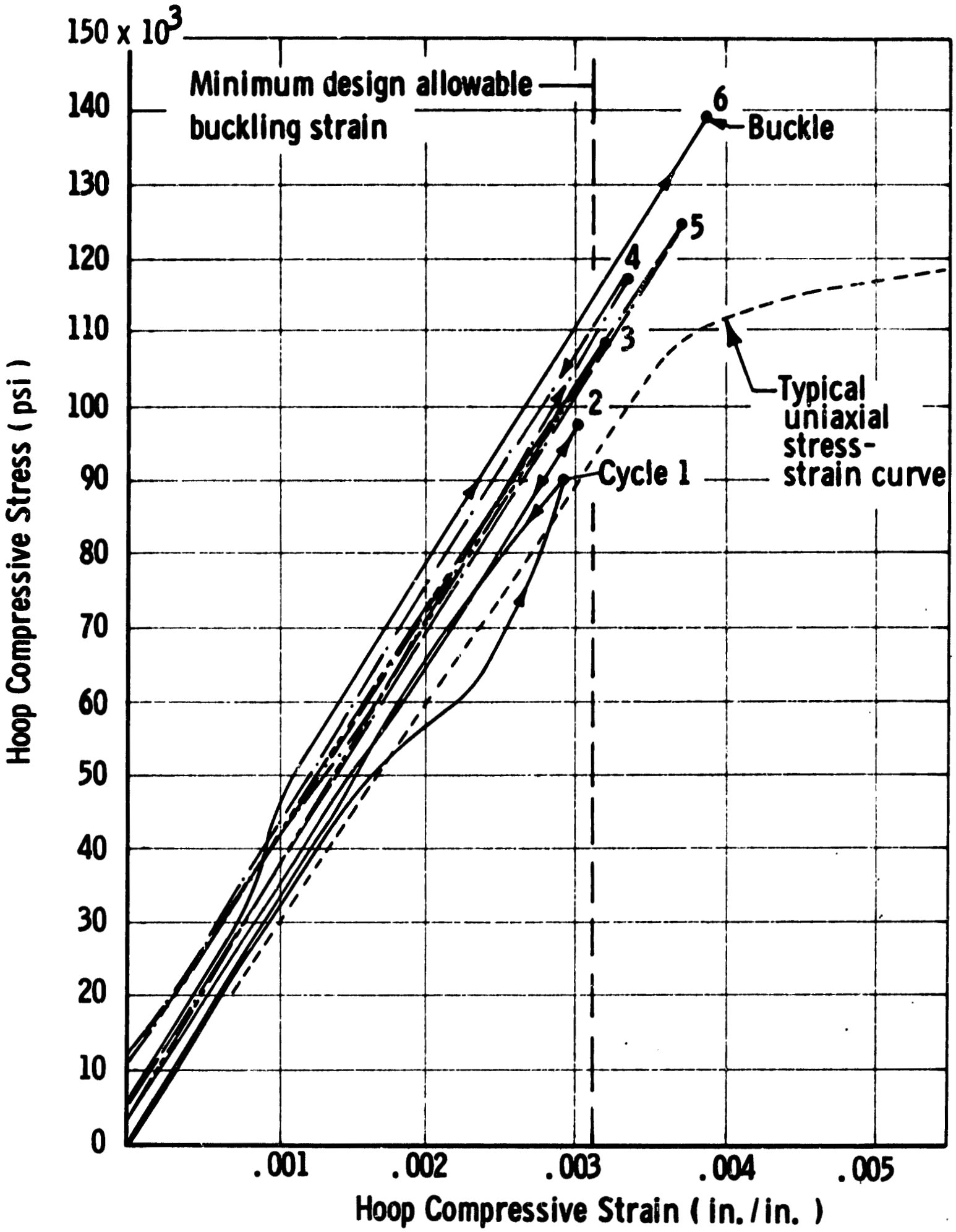

Compressive Stress-Strain Curve for Inconel Cylinder 2, Buckling Test

Figure A-24

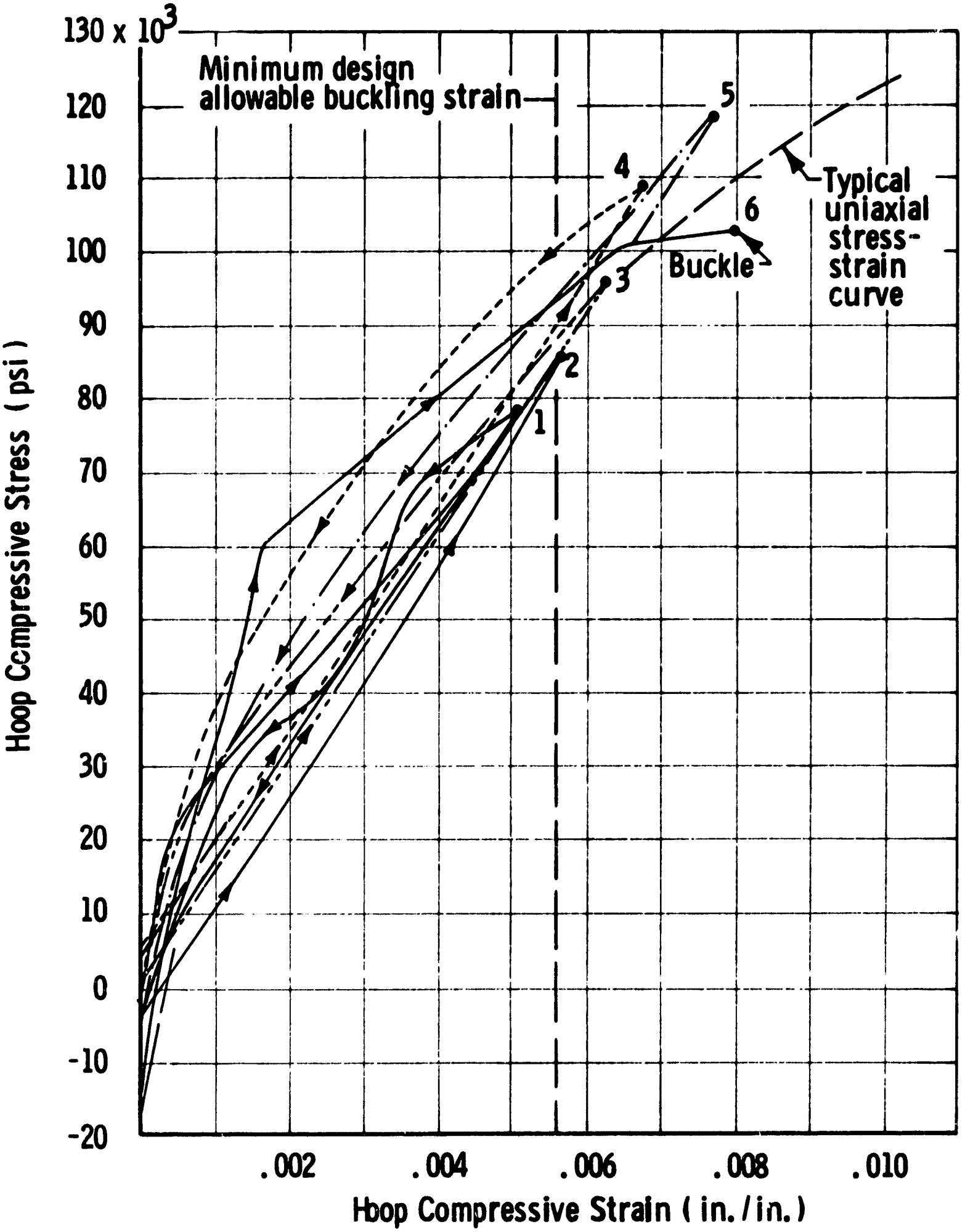

Compressive Stress-Strain Curves for Titanium Cylinder 1, Buckling Test

Figure A-25

APPENDIX B

COMPUTER PROGRAM FOR ANALYSIS OF FILAMENT-REINFORCED METAL-SHELL PRESSURE VESSELS

This program analyzes and designs complete metal-lined tanks filament-wound with either geodesic (helical) or in-plane patterns along the cylinder and over the end domes and complemented by circumferential windings in the cylinder.

It establishes the optimum head contours at both ends, computes the filament and metal-liner stresses and strains at zero and design pressures, establishes the hoop-wrap thickness required for the cylindrical portion, and computes the weight, volume, and filament-path length of the components and complete vessel. It also determines the stresses and strains in the filament and metal shells throughout service cycling on the basis of a series of pressure, composite-temperature, and metal-liner-temperature inputs.

I. ANALYTICAL APPROACH

The analysis is based on assumptions that

A. The filament stresses are constant along their length.

B. The metal-liner stresses are constant in the meridional direction.

C. Equal strains are produced in the hoop and meridional directions at the equator of the head and in the cylinder with increases from the winding pressure to the design pressure.

D. The liner thickness is constant to permit ease of fabrication.

E. The effect of the resin matrix is negligible (a netting analysis can be used).

F. Filament rotation is negligible with increases or decreases from the winding pressure.

G. The head-contour radii of curvature differ negligibly between the unpressurized and pressurized conditions.

H. The stress-strain relationships of the metal liner can be represented by two straight lines (i.e., primary and secondary moduli).

I. The stress-strain relationships of filaments can be represented by a straight line.

J. Poisson's effect is negligible in a filament-wound composite.

K. Poisson's ratio = 1/2 in the plastic range of the metal-liner stress-strain curve.

L. The metal-liner biaxial-yield stress equals the uniaxial-yield stress in a 1-to-1 stress field.

The filament shell is subjected to a netting analysis that assumes constant stresses along the filament length; both geodesic and planar winding paths are analyzed. The structural contribution of the resin matrix in the filament shell is ignored. That shell and the metal shell are considered in combination by equating strains in the meridional and hoop directions and adjusting the radii of curvature to match the combined material strengths at the design pressure. The heads are designed first, and the cylinder is designed to complement them.

Once the vessel design is fixed, another analysis is used to determine stresses and strains at any temperature and pressure condition. Temperature-variation effects are accounted for by inputs of thermal coefficients of contraction and changes in various physical properties of the shells. For this analysis, the end conditions are the primary concern and it is assumed that the physical-property changes are directly proportional to the temperature.

In general, the metal-shell compressive hoop force imposed on the head at a zero internal pressure by the composite cannot approach the liner's meridional compressive stress because of filament-shell strength components. The difference in relative rigidities in the hoop and meridional directions is most noticeable at the equator of the head at a zero pressure. The hoop force applied there by the filament shell is extremely small in comparison with the meridional force, because the wrap angle (α) is small and the hoop force is equal to the meridional force times $\tan^2\alpha$.

The forces in the filament shell have to balance those in the metal shell, and it is impossible to induce equal compressive stresses in the liner in all directions except when $\alpha = 45^\circ$ or when the wrapping tension and pressures are zero. Consequently, the analysis does not require that the head stresses be equal in the hoop and meridional directions, but does require that the strain changes be equal in those directions at the equator of the head with increases from the winding pressure to the design pressure. When the liner has rigid mandrel support during overwrapping, equal strains (and hence equal stresses) are produced in the hoop and meridional directions at the equator of the head and up the meridian of the head. and in the hoop and longitudinal directions of the cylinder.

II. PROGRAM

The program includes four functional parts for use in pressure-vessel-design and service-cycle-history analyses.

A. VESSEL DESIGN

The first three parts of the computer program analyze and design complete pressure vessels, wound with either geodesic (helical) or in-plane patterns along the cylinder and over the end domes and complemented by circumferential windings in the cylinder.

The program includes as input material properties and various geometric parameters, metal-shell and filament-shell material properties, filament and longitudinal-metal-shell stresses at the winding condition, and design conditions of temperature. It also has the following seven optional variables, of which four must be input: (1) the tensile hoop strain in the metal shell at the design pressure, (2) the tensile longitudinal strain in the metal shell at the design pressure, (3) the filament stress at the design pressure, (4) the design pressure, (5) the metal-shell thickness, (6) the filament-shell thickness at the equator, and (7) the metal-shell hoop stress at the winding condition.

The program establishes the optimum head contours at both ends; computes contour coordinates of the vessel's neutral axis, and inner and outer surfaces; computes the filament- and metal-shell stresses and strains at the winding and relaxed conditions and at the design pressure and operating-temperature conditions; establishes the metal- and filament-shell thicknesses; and computes the filament-path length for the components and complete vessel. The tank may be designed to a specific condition of pressure and of metal-shell and composite temperatures, and stress and strain calculations for the design will be as established by these conditions. All information at a zero internal pressure assumes room temperature; should zero-pressure information be required for other temperatures, the pressurization-history analysis noted below may be used.

In addition, the program (1) optimizes the overall vessel by designing the cylinder section to complement the head design, and (2) calculates the weights of the metal shell, filament shell, and entire vessel; the surface area and contained volume; and the vessel performance factor, pV/W.

B. SERVICE-CYCLE HISTORY

The fourth part of the program permits analysis of the stresses and strains in the filament and metal shells during the operating history of the vessel through the input of a series of pressures, composite temperatures, and metal-shell temperatures. It permits analysis of pressure and temperature cycles on the vessel, taking into account previous strains and loads.

APPENDIX C

METAL-BOSS ANALYSIS

The metal boss (Part No. 178089) is fabricated from nickel-base alloy Inconel X-750, which is solution-treated and aged after being welded to the metal shell. The significant dimensions of the boss for this analysis are given below (only one side of symmetrical boss shown).

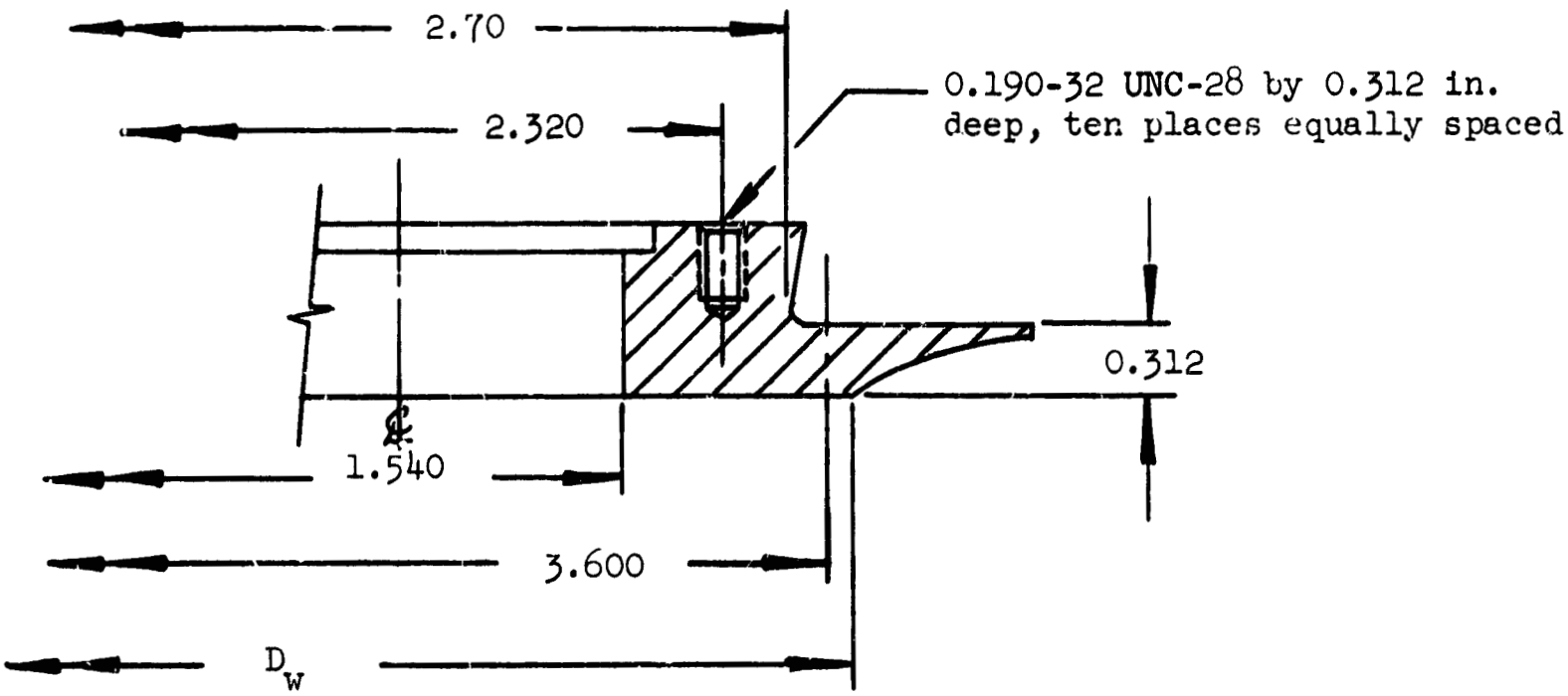

I. MATERIAL PROPERTIES

Inconel X-750 (STA) has the following strength properties:

	Strength, psi		
	75°F	-320°F	-423°F
Ultimate, F_{tu}	165,000	210,000	225,000
Yield, F_{ty}	105,000	128,000	130,000
Shear, F_{su}	105,000	128,000	130,000

II DESIGN CRITERIA

The metal boss is to be capable of sustaining the design burst pressure of the GFR Inconel X-750 tank (Part No. 178091) at 75, -320, and -423°F service temperatures. The design burst pressures (p_b) are 3010 psi at 75°F, 4263 psi at -320°F, and 4300 psi at -423°F.

The required margins of safety for the boss design are 0.25 for flange shear and bending, and 0.50 for bolts and bolt threads.

III. ANALYSIS

Only the most critical section of the boss, located at the base of the flange, was analyzed. Stresses there were determined by using the conservative assumption that the flange is a flat plate with a concentrated annular load and a fixed inner edge (the body).

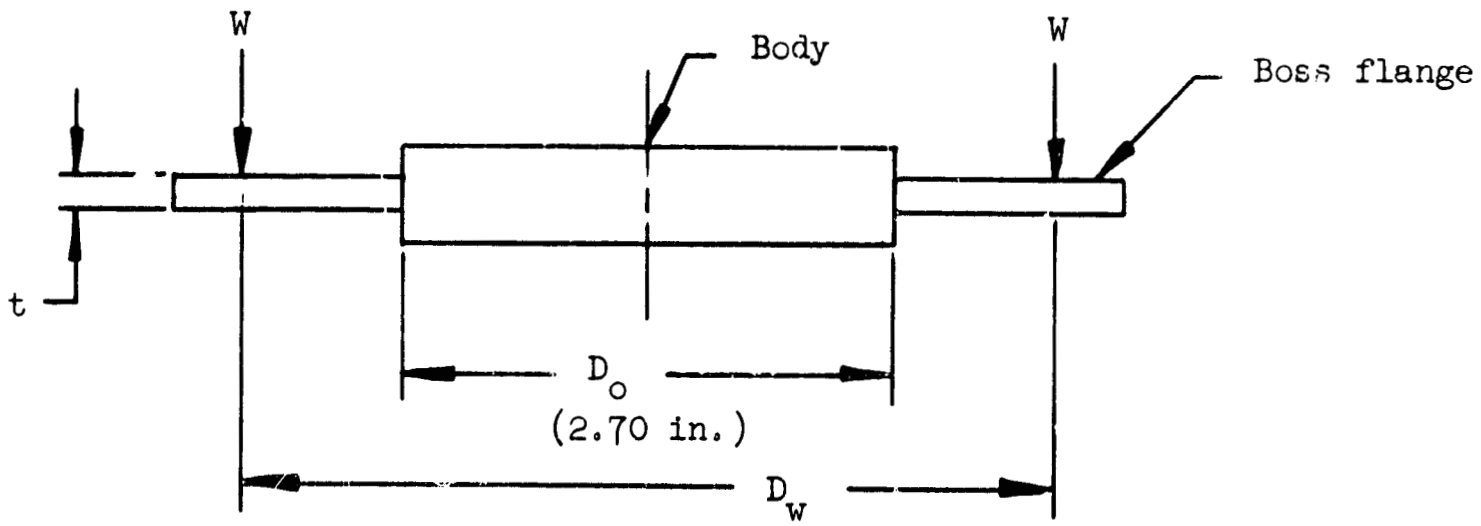

The end-for-end wrap pattern of the longitudinal filaments produces a rigid band around the boss that supports the flange. The load applied (W) is the reaction of the boss flange bearing against the composite structure. The total load is therefore equivalent to the pressure acting over the area within the reaction circle. The diameter at which the load is assumed to act (D_w) is (from Reference C-1)

$$D_w = (1 + \varepsilon_{f,1})\ D_o + 2.5\ W_L$$

where

$\varepsilon_{f,1} = \dfrac{\sigma_{f,1}}{E_f}$ = filament strain at ultimate stress, in./in.

$\sigma_{f,1}$ = ultimate filament strength, psi = 330,000 psi at 75°F, and 495,000 psi at -320 and -423°F

E_f = filament modulus, psi = 12.4×10^6 psi at 75°F, and 13.6×10^6 psi at -320 and -423°F

W_L = filament-winding-tape width (= 0.333 in. from Figure 16 of the main text)

A. FLANGE BENDING

The bending stress at the juncture of the flange and boss (σ_b) is calculated in accordance with formulas for loading on a flat plate (Reference C-2, Case 22, p. 201):

$$\sigma_b = \frac{\beta_{22} W}{t^2}$$

where

$$W = \frac{\pi p_b D_w^2}{4}$$

$$\beta_{22} \simeq \frac{D_w}{D_o} - 1$$

t = flange thickness, in. = 0.312 in.

Solving the relationships for conditions at 75, -320, and -423°F,

$$\epsilon_{f,1}\Big|_{75^\circ F} = \frac{\sigma_{f,1}}{E_f}\Big|_{75^\circ F} = \frac{330{,}000 \text{ psi}}{12.4 \times 10^6 \text{ psi}} = 2.68 \times 10^{-2} \text{ in./in.}$$

$$\epsilon_{f,1}\Big|_{\substack{-320\ \&\\ -423^\circ F}} = \frac{495{,}000 \text{ psi}}{13.6 \times 10^6 \text{ psi}} = 3.64 \times 10^{-2} \text{ in./in.}$$

$$D_w\Big|_{75^\circ F} = (1 + 0.0268)\ (2.70) + 2.5\ (0.333) = 3.602 \text{ in.}$$

$$D_w\Big|_{\substack{-320\ \&\\ -423^\circ F}} = (1 + 0.0364)\ (2.70) + 2.5\ (0.333) = 3.632 \text{ in.}$$

$$\beta_{22}\Big|_{75^\circ F} \simeq \frac{L_w}{D_o}\Big|_{75^\circ F} - 1 = \frac{3.602}{2.700} - 1 = 0.335$$

$$\beta_{22}\Big|_{\substack{-320\ \&\\ -423^\circ F}} \simeq \frac{D_w}{D_o}\Big|_{\substack{-320\ \&\\ -423^\circ F}} - 1 = \frac{3.632}{2.700} - 1 = 0.343$$

$$W\Big|_{75^\circ F} = \frac{\pi p_b D_w^2}{4}\Big|_{75^\circ F} = \frac{\pi\ (3010)\ (3.602)^2}{4} = 30{,}600 \text{ lb}$$

$$W\Big|_{-320^\circ F} = \frac{\pi\,(4263)\,(3.632)^2}{4} = 44{,}100 \text{ lb}$$

$$W\Big|_{-423^\circ F} = \frac{\pi\,(4300)\,(3.632)^2}{4} = 44{,}400 \text{ lb}$$

$$\sigma_b\Big|_{75^\circ F} = \frac{\beta_{22}\,W}{t^2}\Big|_{75^\circ F} = \frac{(0.335)\,(30{,}600)}{(0.312)^2} = 105{,}000 \text{ psi}$$

The margin of safety (M.S.) is given by

$$\text{M.S.} = \frac{F_{tu}}{\sigma_b} - 1$$

Thus,

$$\text{M.S.}\Big|_{75^\circ F} = \frac{165{,}000}{105{,}000} - 1 = \underline{+0.570}$$

$$\sigma_b\Big|_{-320^\circ F} = \frac{(0.343)\,(44{,}100)}{(0.312)^2} = 156{,}000 \text{ psi}$$

$$\text{M.S.}\Big|_{-320^\circ F} = \frac{210{,}000}{156{,}000} - 1 = \underline{+0.345}$$

$$\sigma_b\Big|_{-423^\circ F} = \frac{(0.343)\,(44{,}400)}{(0.312)^2} = 156{,}000 \text{ psi}$$

$$\text{M.S.}\Big|_{-423^\circ F} = \frac{220{,}000}{156{,}000} - 1 = \underline{+0.410}$$

B. FLANGE SHEAR

The shear stress in the boss flange is given by

$$\sigma_s = \frac{p\,D_w}{4t}$$

Thus,

$$\sigma_s\Big|_{75^\circ F} = \frac{(3010)\ (3.602)}{(4)\ (0.312)} = 8{,}675 \text{ psi}$$

From

$$\text{M.S.} = \frac{F_{su}}{\sigma_s} - 1$$

$$\text{M.S.}\Big|_{75^\circ F} = \frac{105{,}000}{8{,}675} - 1 = \underline{\text{+ HIGH}}$$

$$\sigma_s\Big|_{-320^\circ F} = \frac{(4263)\ (3.632)}{(4)\ (0.312)} = 12{,}400 \text{ psi}$$

$$\text{M.S.}\Big|_{-320^\circ F} = \frac{128{,}000}{12{,}400} - 1 = \underline{\text{+ HIGH}}$$

$$\sigma_s\Big|_{-423^\circ F} = \frac{(4300)\ (3.632)}{(4)\ (0.312)} = 12{,}500 \text{ psi}$$

$$\text{M.S.}\Big|_{-423^\circ F} = \frac{130{,}000}{12{,}500} - 1 = \underline{\text{+ HIGH}}$$

C. FLANGE THREADS

The shear stress in the threads (σ_{st}) was determined from

$$\sigma_{st} = \frac{p_b\ D_{bc}^{\ 2}\ \pi}{4\ N\ \pi\ D_b\ \ell\ (0.5)}$$

where

D_{bc} = bolt-circle diameter = 2.32 in.

N = number of bolts = 10

D_b = bolt diameter = 0.190 in.

ℓ = thread grip length = 0.285 in.

Thus,

$$\sigma_{st}\Big|_{75^\circ F} = \frac{(3010)\ (2.32)^2\ \pi}{4\ (10)\ (\pi)\ (0.190)\ (0.285)\ (0.5)} = 15{,}000 \text{ psi}$$

From

$$\text{M.S.} = \frac{F_{su}}{\sigma_{st}} - 1$$

$$\text{M.S.}\Big|_{75^\circ F} = \frac{105{,}000}{15{,}000} - 1 = \underline{+6.00}$$

$$\sigma_{st}\Big|_{-320^\circ F} = \frac{4263}{3010}\ (15{,}000) = 21{,}300 \text{ psi}$$

$$\text{M.S.}\Big|_{-320^\circ F} = \frac{128{,}000}{21{,}300} - 1 = \underline{+5.00}$$

$$\sigma_{st}\Big|_{-423^\circ F} = \frac{4300}{3010}\ (15{,}000) = 21{,}400 \text{ psi}$$

$$\text{M.S.}\Big|_{-423^\circ F} = \frac{130{,}000}{21{,}400} - 1 = \underline{+5.07}$$

D. BOLT STRENGTH

The load per bolt (L) was calculated from

$$L = \frac{p_b\ D_{bc}^{\ 2}\ \pi}{4\ N}$$

For SPS-B-186 No. 10-32 bolts with a tensile strength of 200,000 psi at ambient temperature, the ultimate tensile load per bolt (L_{tu}) is 4000 lb at 75°F and 4400 lb at -320 and -423°F.

Thus,

$$L\Big|_{75^\circ F} = \frac{(3010)\ (2.32)^2\ \pi}{(4)\ (10)} = 1270 \text{ lb}$$

From

$$\text{M.S.} = \frac{L_{tu}}{L} - 1$$

$$\text{M.S.}\Big|_{75^\circ F} = \frac{4000}{1270} - 1 = \underline{+2.15}$$

$$L\Big|_{-320^\circ F} = \frac{4263}{3010}\ (1270) = 1800 \text{ lb}$$

$$\text{M.S.}\Big|_{-320^\circ F} = \frac{4400}{1800} - 1 = \underline{+1.44}$$

$$L\Big|_{-423^\circ F} = \frac{4300}{3010}\ (1270) = 1820 \text{ lb}$$

$$\text{M.S.}\Big|_{-423^\circ F} = \frac{4400}{1820} - 1 = \underline{1.42}$$

E. BOLT SPACING

The bolt spacing (S) is given by

$$S = \frac{\pi\ D_{bc}}{N_b\ D_b} = \frac{\pi\ (2.32)}{(10)\ (0.190)} = 3.83 \text{ bolt diameters}$$

REFERENCES

C-1. Aerojet-General Corporation, Structural Materials Handbook, February 1964.

C-2. J. J. Roark, Formulas for Stress and Strain, New York, McGraw-Hill, 1954.

APPENDIX D

FILAMENT-WINDING PATTERN AND HEAD-REINFORCEMENT DESIGN

I. DETERMINATION OF FILAMENT-WINDING-PATTERN PARAMETERS

A single winding pattern is applied to the metal shell in fabricating the filament shell. Filaments oriented side by side are applied longitudinally in a plane over the shell and adjacent to the polar bosses.

The pattern for a pressure vessel requires a specific quantity of glass roving to obtain the necessary strength. As described in Section IV,E,2 of the body of this report, the required longitudinal FWC thickness at the equator of the heads (T_O) is 0.030 in., based on a filament content of 67.3 vol%. The pattern is analyzed here on the basis of actual winding data and laboratory tests of glass roving and composite specimens, which have shown that a cured single layer of 20-end roving created by a side-by-side orientation has a thickness ($t_{s,1}$) of 0.0075 in.

The required number of layers of winding (L_1) is given by

$$L_1 = \frac{T_O}{t_{s,1}} = \frac{0.030}{0.0075} = 4$$

Two layers are formed for each revolution of the winding mandrel. The number of revolutions required (N_1) is therefore

$$N_1 = \frac{L_1}{2} = \frac{4}{2} = 2$$

The winding-tape width (W_L) is given by

$$W_L = \frac{N_2 A}{t_{s,1} P_{vg}}$$

where

N_2 = number of 20-end roving strands per tape, selected as 4

A = cross section of 20-end roving = 420×10^{-6} in.^{2}

P_{vg} = glass-filament fraction in composite = 0.673

Thus,

$$W_L = \frac{(4)\ (420 \times 10^{-6})}{(0.0075)\ (0.673)} = 0.333 \text{ in.}$$

The number of turns per revolution (N_3) must be an integer, and is given by

$$N_3 = \frac{\pi\ D_c \cos \alpha}{W_L + \epsilon} \qquad \text{to the nearest integer}$$

where

D_c = vessel diameter = 18.00 in.

α = longitudinal in-plane winding angle = $11^{\circ}17'$

ϵ = space between tapes (which should equal zero)

Therefore,

$$N_3 = \frac{\pi\ (18.00)\ (0.981)}{0.333} \cong 166 \text{ turns per revolution}$$

II. ANALYSIS OF HEAD REINFORCEMENT

The head section of the GFR Inconel X-750 tank must be reinforced in the vicinity of the rigid polar boss to reduce FWC deflection there so that the filament-shell strains are equated to the metal-shell strains. The reinforcement will also limit plastic deformation of the liner during proof-pressure application to the level required to keep the springback stress above the compressive proportional limit when the pressure is reduced from the proof value to zero.

Although glass fabric can be employed, a more efficient approach to the addition of local rigidity is the use of a prefabricated cap-type doily made of unidirectional glass-filament tapes laid tangentially to the circle described by the outside diameter of the polar bosses.

Head reinforcements are made by laying strips of resin-coated glass filaments over a form of the same contour and dimensions as the metal-shell heads. Because two revolutions of the winding mandrel are needed to achieve the four filament layers required, the head reinforcement should be placed between the second and third layers (i.e., between the first and second mandrel revolutions).

The head-reinforcement design calculations are based on division of the load carried by the wound filaments, the metal shell, and the reinforcement to match the desired strain level in the vicinity of the reinforcement.

A. DESIGN CRITERIA

Sufficient reinforcement must be added to limit the plastic deformation of the metal shell at the proof pressure so that the compressive stress does not exceed the proportional limit when the pressure is reduced to zero. Computer design analysis shows that the tank without the head

reinforcement springs back into longitudinal compression after proof testing at 2220 psig to stresses greater than the compressive proportional limit, at points where the normalized radial distance (Z) is less than 0.50.

Head reinforcement is also added because the local rigidity of the polar boss requires reduction in the glass-FWC strains near the boss to ensure strain compatibility at the boss-to-head weld.

The tank geometry is shown in Figure D-1. The longitudinal stress-strain curve is presented in Figure D-2 for points on the head ranging from the equator (Z = 1.0) to the boss-to-head weld (Z = 0.264). The critical portion of the structure for reinforcement design (maximum metal-shell compression) is at the boss-to-shell weld.

B. LOAD-CARRYING CAPACITY AT BOSS-TO-HEAD WELD

Figure D-2 shows that the filament strain at the proof pressure without the head reinforcement must be limited to 0.013 in./in. at the boss-to-head weld (Z = 0.264) if the longitudinal springback stress is not to exceed -108,000 psi, the compressive proportional limit of Inconel X-750 (STA). The rigidity of the polar boss, however, makes it advisable to keep filament- and metal-shell strains at an even lower level at the boss-to-shell weld.

Preliminary analysis indicated that - if the strain of the basic windings could be limited to 0.007 in./in. at the boss-to-shell weld at the proof pressure - (1) an acceptable head-reinforcement design could be developed, (2) the compressive springback stress could be maintained well above the compressive proportional limit, and (3) strains at the boss-to-shell weld could be reduced to an acceptable level.

1. Total Load (P_t)

Figure D-3 depicts a pressure-vessel membrane and the meridional loads (N_ϕ) produced at diameter D_b by pressure p. If a reinforcement system is to carry meridional loads (P_t) around the opening described by D_b, the values for each side of the reinforcement are given by

$$P_t = \frac{p\, r_2}{2} \frac{D_b}{2} = \frac{p\, r_2}{4} D_b$$

where

p = pressure, psi

r_2 = hoop radius of curvature, in.

D_b = diameter at point under consideration, in.

At the boss-to-shell weld, at proof pressure,

$Z = 0.264$

$p = 2220$ psi

$r_2 = 17.78$ in.

$D_b = 4.720$ in.

and

$$P_t = \frac{(2220)\ (17.78)\ (4.720)}{4} = 46{,}500 \text{ lb}$$

This load is shared by the vessel components in accordance with

$$P_t = P_g + P_l + P_r$$

where

P_g = load carried by filament windings, lb

P_l = load carried in metal shell, lb

P_r = load carried by head reinforcement, lb

These loads are evaluated below.

2. Load Carried by Windings (P_g)

The load P_g is found by methods described in Appendix V of Reference D-1. A rough approximation of the angle (ψ) between sequential windings is obtained by dividing the number of degrees in a circle by the number of wraps of winding per mandrel revolution. In this case, the winding pattern is 166 turns/revolution. Therefore,

$$\psi = \frac{360}{166} = 2.16^\circ$$

From Figure 8 of Reference D-1, the value of the factor for determination of the reinforcement strength is $K_R = 53$ at $\psi = 2.16^\circ$.

The winding in the vicinity of the boss can be assumed to consist of tangentially placed material oriented uniformly around the opening. From a given point on the edge of the boss opening, the strength component of each tape that crosses a radially directed line through the point is considered. The total strength is the sum of all the individual strengths and is determined by calculating an effective area (A_e) (see p. 40, Reference D-1):

$$A_e = A_f K N \sum_{n\psi = -90^\circ}^{n\psi = 90^\circ} \cos n\psi$$

where

A_f = cross section of a single tape

K = strength-reduction factor employed to include the effect of a widely distributed area (assumed to be 1.0 in the present calculations)

N = number of layers of longitudinal winding

$\sum_{n\psi = -90^\circ}^{n\psi = 90^\circ}$ $\cos n\psi = K_R = 53$ (as determined above)

ψ = angle between adjacent tapes

n = all integers between limits of $-90/\psi$ and $90/\psi$

The cross-sectional area of 20-end roving is 420×10^{-6} in.^{2}. Each tape consists of four 20-end rovings, and A_f for the tape is therefore

$$A_f = (4)\ (420 \times 10^{-6}) = 1680 \times 10^{-6} \text{ in.}^2$$

Then,

$$A_e = (1680 \times 10^{-6})\ (1.0)\ (4)\ (53) = 35.6 \times 10^{-2} \text{ in.}^2$$

The load carried by the glass of the basic windings is given by

$$P_g = A_e E \epsilon$$

where

E = glass-fiber tensile modulus = 12.4×10^6 psi for S-glass

ϵ = desired strain, assumed to be 0.007 in./in.

Thus,

$$P_g = (35.6 \times 10^{-2})\ (12.4 \times 10^{6})\ (0.007) = 31{,}000 \text{ lb}$$

3. Load Carried by Metal Shell (P_1)

The meridional load carried by the metal shell between the vessel axis and the boss-to-shell weld is given by

$$P_1 = \sigma_1\ t_1\ \frac{D_b}{2}$$

where

σ_1 = metal-shell stress at 0.007-in./in. strain in the basic windings = 120,000 psi (from Figure D-2)

t_1 = metal-shell thickness = 0.047 in.

Thus,

$$P_1 = (120{,}000)\ (0.047)\ \left(\frac{4.720}{2}\right) = 13{,}300 \text{ lb}$$

4. Load Carried by Head Reinforcement (P_r)

The load that must be carried by the head reinforcement to keep the proof-pressure strain at 0.007 in./in. is given by

$$P_r = P_t - P_1 - P_g$$

$$= 46{,}500 - 13{,}300 - 31{,}000 = 2200 \text{ lb}$$

C. HEAD-REINFORCEMENT DESIGN

The required angle between adjacent tapes of the head reinforcement can be obtained from Figure 8 of Reference D-1 when the required filament area (A_e) is known. As before,

$$A_e = A_f\ K\ N \sum_{n\psi = -90^\circ}^{n\psi = 90^\circ} \cos n\psi = A_f\ K\ N\ K_R$$

where in this case

N = number of plies of reinforcement (N = 1 selected for the design considered)

Let

$$A_e \geq \frac{P_r}{F_t}$$

where F_t is the filament stress in the tape at the desired strain. Then,

$$\frac{P_r}{F_t} = A_f K N K_R$$

and, because K = 1.0 and N = 1.0,

$$\frac{P_r}{F_t} = A_f K_R$$

At the desired strain of the basic windings, the head-reinforcement strain (e_{HR}) is given by

$$e_{HR} = e_{BW} - \frac{\sigma_w}{E}$$

where

e_{BW} = desired strain in basic windings = 0.007 in./in.

σ_w = basic-winding tension = 23,800 psi

Thus,

$$e_{HR} = 0.007 - \frac{23,800}{12.4 \times 10^6} = 0.007 - 0.002 = 0.005 \text{ in./in.}$$

The stress in the tape (F_t) at a strain of 0.005 in./in. is

$$F_t = e_{HR} E = (0.005)(12.4 \times 10^6) = 63,000 \text{ psi}$$

Thus,

$$A_e \geq \frac{P_r}{F_t} = \frac{2,200}{63,000} = 0.0350 \text{ in.}^2$$

The effective-area requirement computed above for Z = 0.264 can be assumed to be the same as at Z = 0.150 (at the boss), because the tape width will approximately equal the difference between Z = 0.264 and Z = 0.150 (0.94 in. for the 18-in.-dia tank). Therefore,

$$A_e \geq 0.035 = A_f K_R$$

and

$$A_f = \frac{0.035}{K_R}$$

For tapes of width W_t used in constructing the head reinforcement,

$$A_f = \left(A_{\text{one end}}\right) \text{ (number of ends/inch) } (W_t)$$

For 3M 1009-26S unidirectional tape, there are 200 ends/inch and

$$A_f = \left(\frac{420 \times 10^{-6}}{20}\right) (200) (W_t) = 0.0042\ W_t$$

Thus,

$$\frac{0.035}{K_R} = 0.0042\ W_t$$

and

$$K_R = \frac{0.035}{0.0042\ W_t} = \frac{8.35}{W_t}$$

The edge of the head reinforcement must extend to Z = 0.50, where the perimeter of the reinforcement = (2) (π) (0.5) (9 in.) = 28.2 in. If the requirement is imposed that the tapes be oriented so they butt up side-by-side at Z = 0.5, the space (s) available for each tape width at the head-reinforcement perimeter is

$$s = \frac{28.2}{360/\psi} = 0.07844\ \psi$$

Figure D-4 shows the geometry of the head-reinforcement layup pattern, from which the following parameters are computed:

$$a = \sqrt{c^2 - b^2} = \sqrt{(4.50)^2 - (1.42)^2} = 4.26 \text{ in.}$$

$$\sin \psi = \frac{W_t}{a}$$

$$W_t = 4.26 \sin \psi$$

and

$$K_R = \frac{8.35}{W_t} = \frac{8.35}{4.26 \sin \psi} = \frac{1.96}{\sin \psi}$$

K_R values determined by calculation and from Figure 8 of Reference D-1 are shown below for various values of ψ.

	K_R Value	
ψ, degrees	From $1.96/\sin \psi$	From Fig. 8, Ref. D-1
15	7.57	8.0
14	8.10	8.8
12	9.42	9.5
10	11.3	11.0
8	14.1	13.5

A value of $\psi = 10^\circ$ was selected for head-reinforcement design. The number of tapes required in each head reinforcement is 360/10 = 36. The required tape width is

$$W_t = 4.26 \sin \psi = (4.26)\ (0.1737) = 0.74 \text{ in.}$$

D. SPRINGBACK STRESS IN METAL SHELL

At zero pressure after the proof test,

$$\frac{D_b}{2} \frac{p\ r_2}{2} = 0 = \sigma_1\ t_1 \frac{D_b}{2} + (A_e\ \sigma_f)_{BW} + (A_e\ \sigma_f)_{HR}$$

$$0 = (0.047)\ \sigma_1 \left(\frac{4.720}{2}\right) + 0.356\ (\sigma_f)_{BW} + 0.035\ (\sigma_f)_{HR}$$

Figure D-5 presents a stress-strain diagram for springback at Z = 0.264. Trial-and-error solution of the above equation established that the metal-shell springback stress (σ_1) at zero pressure was -72,000 psi in the longitudinal direction.

REFERENCE

D-1. F. J. Darms, R. Molho, and B. E. Chester, Improved Filament-Wound Construction for Cylindrical Pressure Vessels, Volume II - Design Procedures, ML-TDR-64-43, Vol. II (Air Force Materials Laboratory technical documentary report prepared by Aerojet-General under Contract AF 33(616)-8442), March 1964.

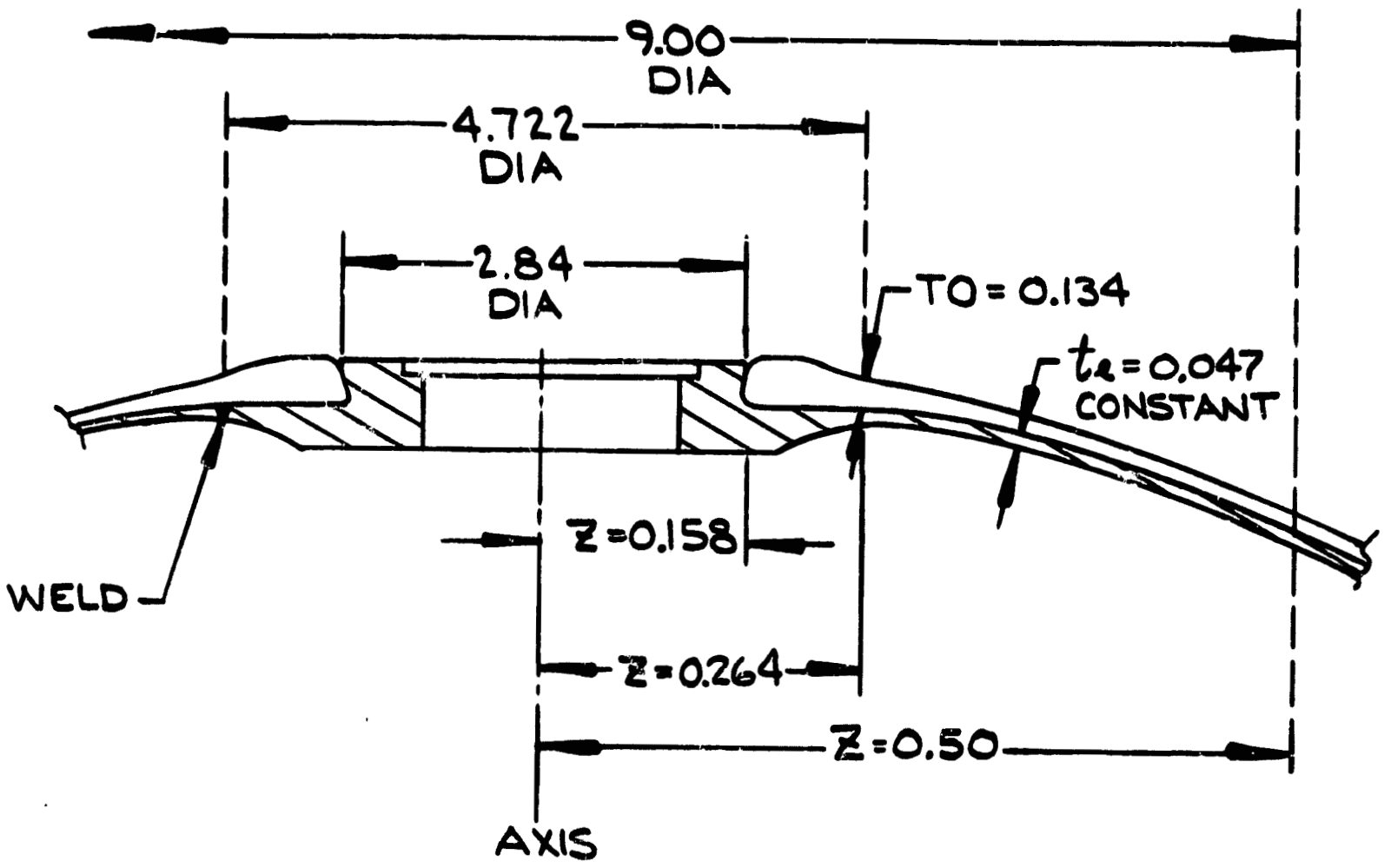

Tank Geometry

Figure D-1

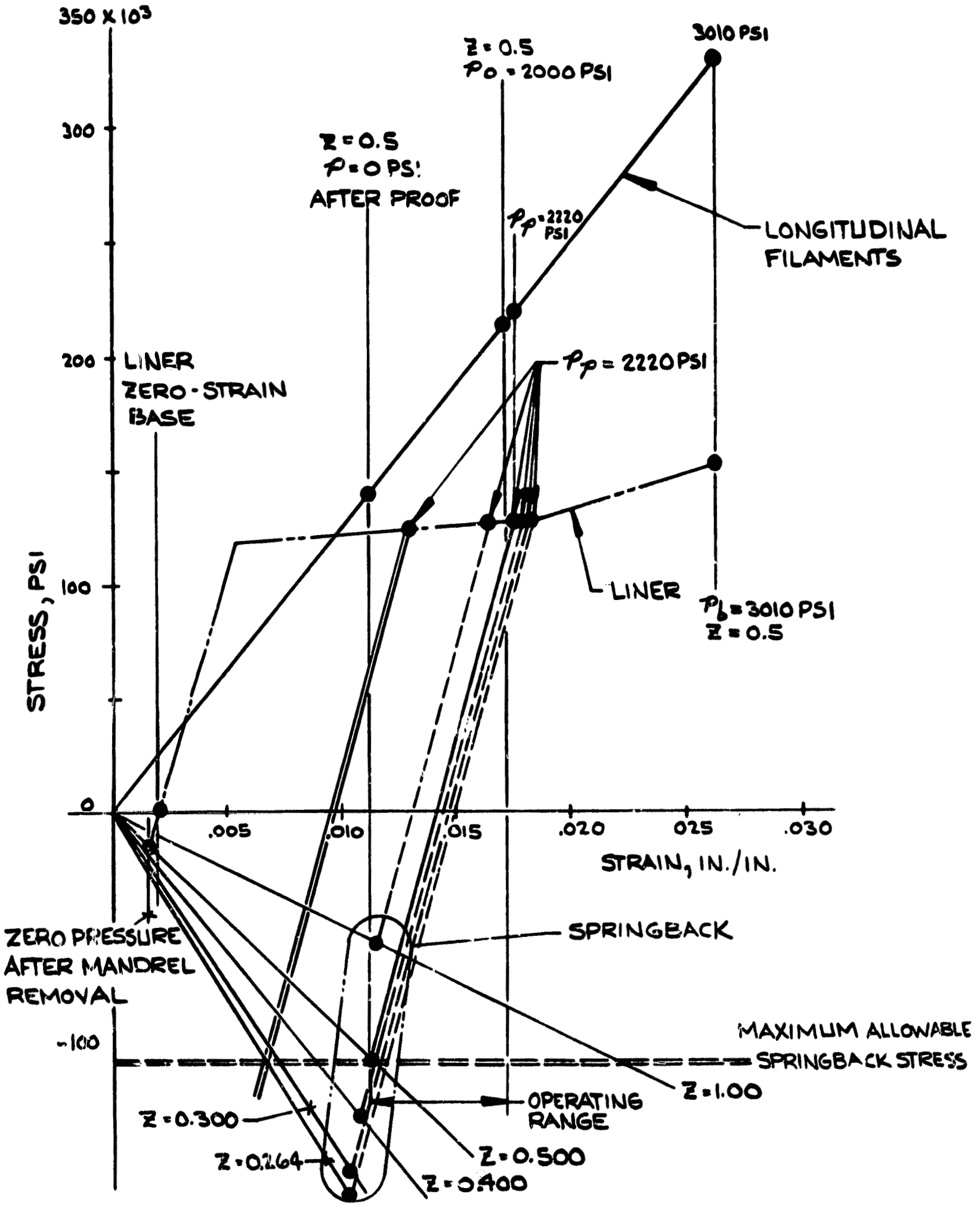

Stress-Strain Diagram for Various Points on Head
(Design Without Head Reinforcement)

Figure D-2

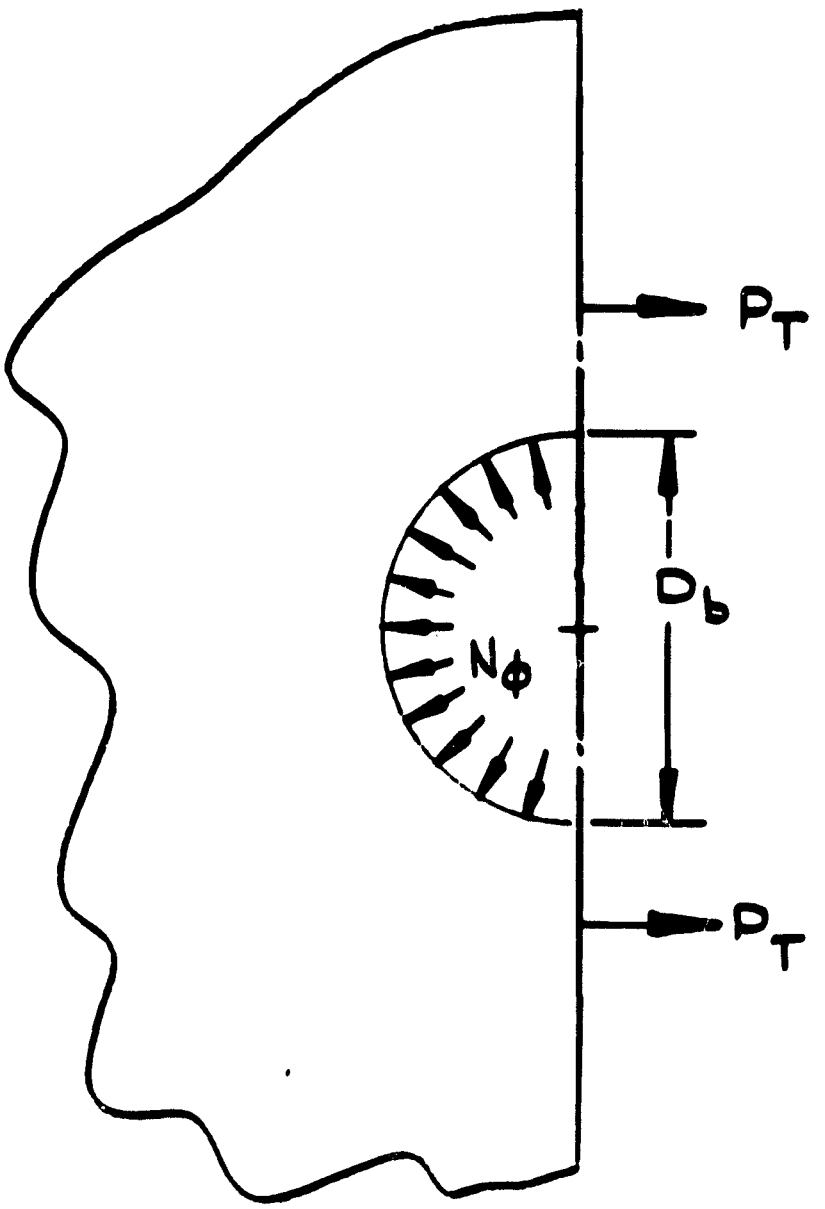

$$2P_T = N_\phi D_B$$

$$N_\phi = \frac{Pr^2}{2}$$

$$P_T = \frac{Pr^2 D_B}{4}$$

Pressure-Vessel Membrane and Meridional Loads

Figure D-3

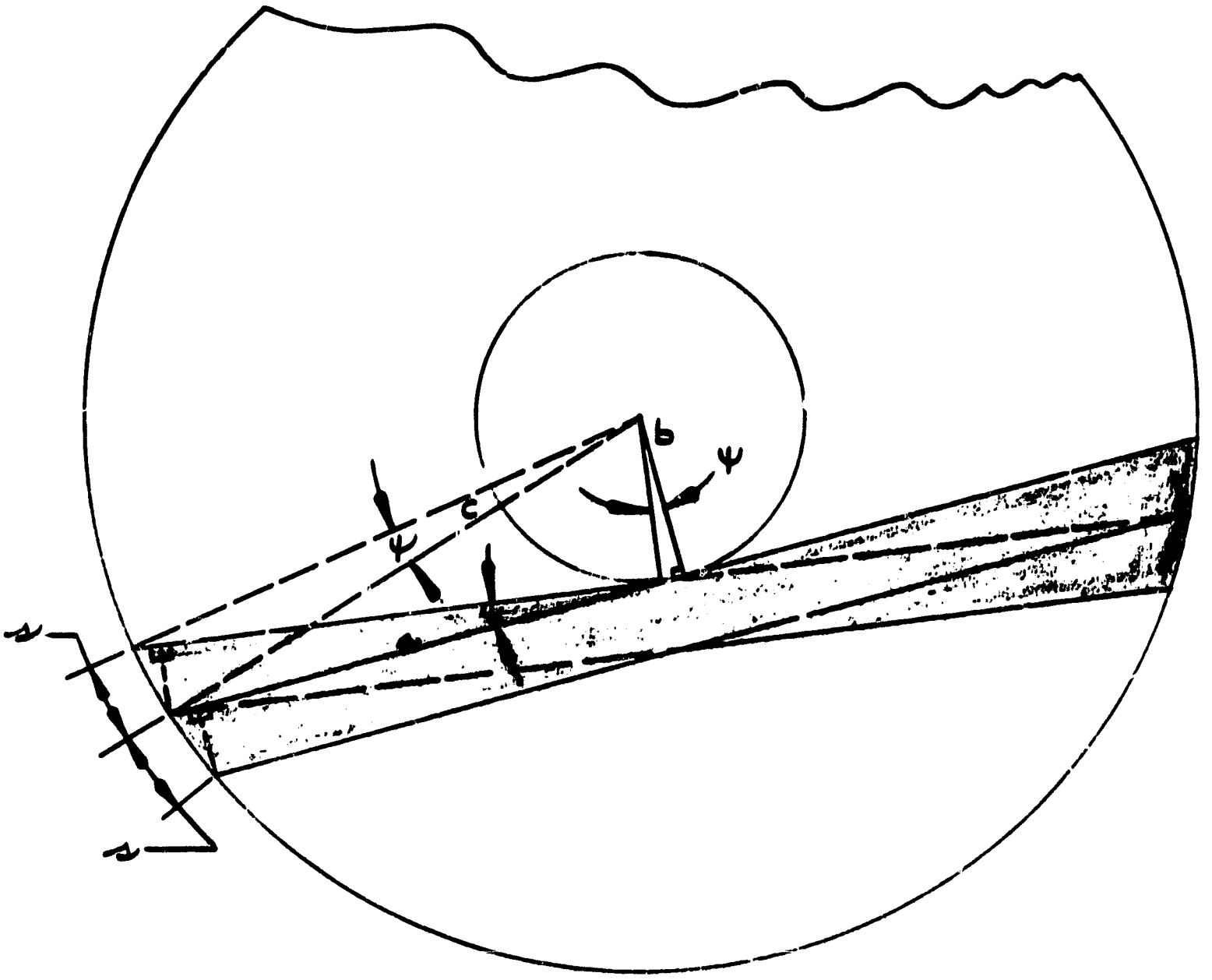

C = 4.50 IN.
b = 1.42 IN.

Geometry of Head Reinforcement

Figure D-4

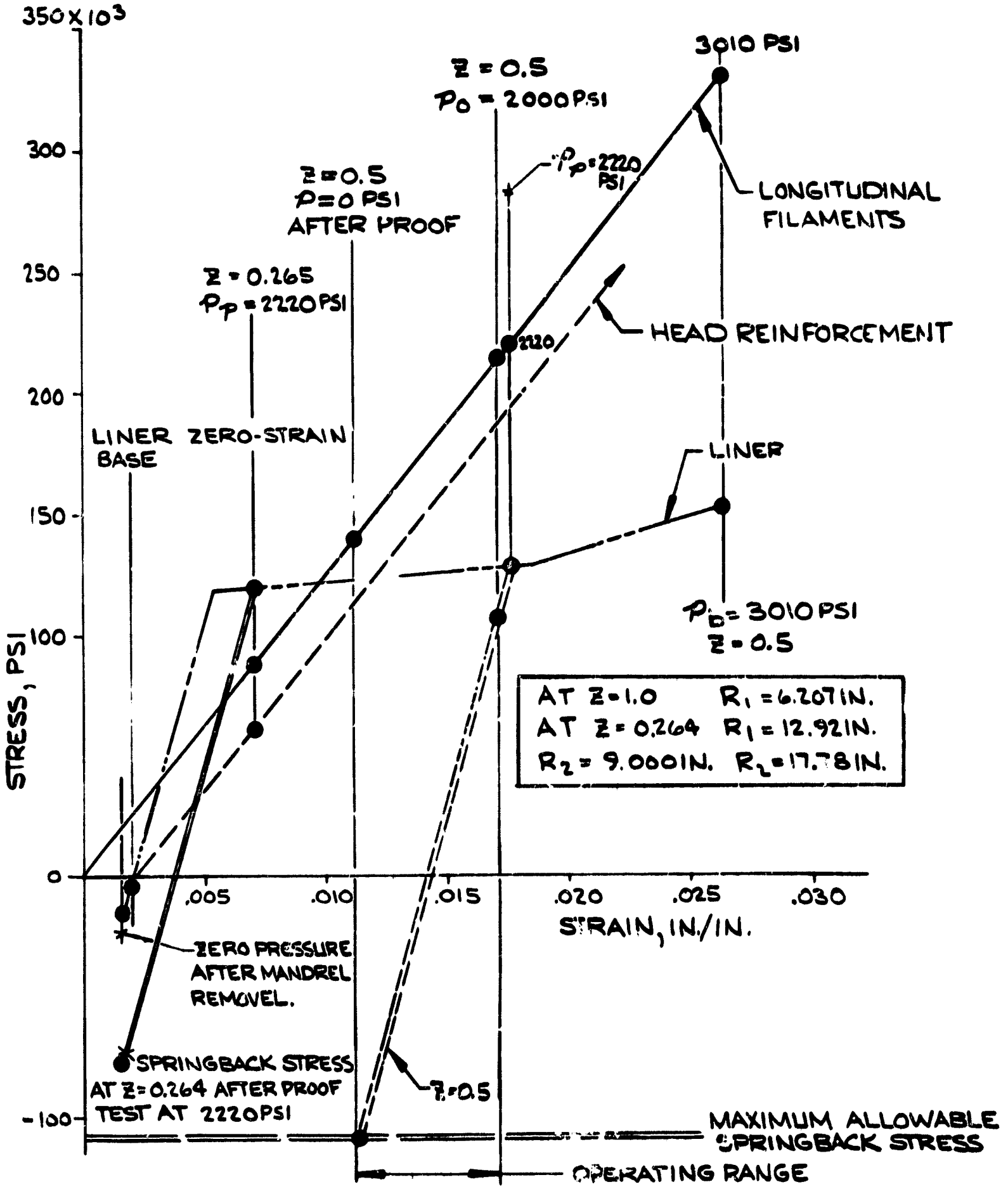

Stress-Strain Diagram for Z = 0.264
for Tank with Head Reinforcement

Figure D-5

APPENDIX E

METAL-SHELL ASSEMBLY SPECIFICATION

The provisions of Aerojet-General Specification No. AGC-10508A presented below were used to control the fabrication, inspection, and acceptance of Inconel X-750 shell assemblies - Part No. 178087 (26-in. diameter) or Part No. 178090 (18-in. diameter) - employed in the construction of GFR metal tanks in this program.

1. SCOPE

1.1 This specification establishes the requirements for the fabrication of the Metal Shell Assembly (Inconel X-750 Alloy), Drawing 178087 or 178090, for GFR metallic tanks for cryogenic service. Fabrication, inspection, and testing procedures are included.

2. APPLICABLE DOCUMENTS

2.1 Government Documents.- Unless otherwise specified, the following standard, of the issue in effect on the date of invitation for bids, shall form a part of this specification to the extent specified herein:

STANDARDS

Federal

Fed. Test Method Std. No. 151 Metals; Test Methods

2.2 Other Documents.- Unless otherwise specified, the following documents, of the issue in effect on the date of invitation for bids, shall form a part of this specification to the extent specified herein:

PUBLICATIONS

Aerospace Materials Specifications

AMS 5542	Alloy Sheet, Strip, and Plate, Corrosion and Heat Resistant, Nickel Base - 15.5 Cr - 2.5Ti-1 (Cb + Ta)-0.7 Al-7Fe
AMS 5667	Alloy, Corrosion and Heat Resistant, Nickel Base - 15.5 Cr - 7Fe-2.5Ti-1(Cb + Ta)-0.7Al
AMS 5778	Alloy Wire, Corrosion and Heat Resistant, Nickel Base - 15.5 Cr - 2.4Ti-1(Cb + Ta)-0.7Al-7Fe

2.3 Aerojet-General Documents.- Unless otherwise specified, the following specifications, standard, and drawings, of the issue in effect on the date of invitation for bids, form a part of this specification to the extent specified herein:

SPECIFICATIONS

AGC-13859	Inspection, Radiographic, All Metals, Procedures for
AGC-13860	Radiographic Quality Levels, Fusion Weldments
AGC-13884	Acceptance Level, Ultrasonic, Components of Liquid Propellant Rocket Propulsion System
AGC-13937	Ultrasonic Inspection Requirements and Procedures
AGC-13972	Inspection, Dye Penetrant, Metal Parts

STANDARD

AGC-STD-1194	Welding, Fusion

DRAWINGS

0-178086	Boss-GFR-Inconel X-750 Pressure Vessel
0-178087	Metal Shell - 26-in. Dia. GFR Inconel X-750 Pressure Vessel
0-178089	Boss-GFR-Inconel X-750 Pressure Vessel
0-178090	Metal Shell - 18-in. Dia. GFR Inconel X-750 Pressure Vessel

3. REQUIREMENTS

3.1 Materials.- Fabrication of the metal shell assembly shall be governed by the following material requirements:

3.1.1 Component Parts.- All oblate spheroidal heads, P/N 178087-3 or P/N 178090-3, shall be formed using cold-rolled, annealed and pickled Inconel X-750 nickel-base alloy in accordance with Specification AMS 5542. All bosses, P/N 178086 or P/N 178089, shall be closed die pancake forgings of Inconel X-750 nickel-base alloy in accordance with Specification AMS 5667 or, as an alternate, machined from plate of Inconel X-750 nickel-base alloy in accordance with Specification AMS 5542.

3.1.2 Material and Component Identification

3.1.2.1 Heads.- Each sheet of blank material shall be assigned a serial number (1, 2, 3, etc.), which shall be painted near one of the corners of the sheet. The mill heat number for the sheet material shall also be painted in the same corner as the sheet serial number. Each head that is fabricated shall be identified by its part number, part serial number (H1, H2, H3, etc.), mill heat number, and serial number of sheet from which the part was made. Care shall be used to assure that the mill heat number, part serial number, and

sheet serial number do not become disassociated from the part at any stage of shell assembly. To retain identity of heads during the forming and annealing operations, the mill heat number, part serial number, and sheet serial number shall be stamped on an area that will be subsequently trimmed.

3.1.2.2 Bosses.- Each boss that is fabricated shall be assigned a serial number (B1, B2, B3, etc.) and be identified by its part number, serial number, and mill heat number of the forging stock or plate from which it was fabricated. Care shall be used to assure that part serial number and mill heat number do not become disassociated from the part during any stage of assembly.

3.1.2.3 Marking Components and Maintaining Records.- Prior to assembly, the head serial number and boss serial number shall be metal-stamped on the boss in the location indicated on Aerojet Drawing 178086 or 178089 as applicable. Written records identifying these serial numbers with the shell assembly (see 3.8) and the information specified in 3.1.2.1 and 3.1.2.2 shall be maintained and delivered to Aerojet with the shell assembly and test coupons.

3.1.3 Components, Heat Treatment

3.1.3.1 Annealing Heads.- A process anneal at 1900°F ±25 in an atmosphere of completely dissociated ammonia with a dew point of -70 to -100°F shall be performed on all shell heads between successive forming operations and after the final forming operation. Parts shall be charged into a furnace preheated to 1900°F, held at temperature for 30 ±5 minutes, and then rapidly air-cooled to room temperature.

3.1.3.2 Annealing Forged Bosses.- Prior to machining, all boss pancake forgings shall be process-annealed in the same manner as specified for spun heads in 3.1.3.1 except they shall be water-quenched from the annealing temperature.

3.1.4 Ultrasonic Inspection of Boss Pancake Forgings.- Prior to machining, all boss pancake forgings shall be ultrasonic-inspected both before and after process annealing (see 4.2.1).

3.1.5 Test Coupons

3.1.5.1 Heads.- Four tensile-test-coupon blanks 3/4 in. wide x 8 in. long shall be cut longitudinal to the direction of rolling from each sheet and metal-stamped on one end with the mill heat number and sheet serial number. Two of these test coupons shall be selected to represent each of the two heads fabricated from the sheet from which the coupons were cut. The serial number of the head they represent shall be metal-stamped on the other end. The trimmed scrap from blank sheet material used for spherical heads shall be metal-stamped with the mill heat number and sheet serial number, and sent to the Aerojet Project Engineer.

3.1.5.2 Bosses

3.1.5.2.1 Forged.- Three tensile-test coupons 1 in. x 1 in. x 6 in. long representing each mill heat of forging stock used for bosses shall be forged and metal-stamped on one end with the mill heat number. To be representative of the bosses, the forged test coupons shall have the same reduction as the forged bosses and be annealed (see 3.1.3.2) with the forgings.

3.1.5.2.2 Machined from Plate.- Three tensile-test coupons 1 in. wide x 8 in. long x plate thickness representing each mill heat of plate used for bosses shall be cut both longitudinal and transverse to the direction of rolling and metal-stamped on one end with the mill heat number.

3.1.5.3 Test-Coupon Disposition.- When the shell assembly is ready for the final heat-treatment operation (see 3.7), the four tensile-test coupons representing the heads and the coupons representing the bosses shall accompany the tank assembly to the heat-treating plant. The coupons shall be hung by wires on the heat-treat fixture and accompany the tank assembly through the heat-treating operation. When all bosses are fabricated from forging stock or plate from the same mill heat, test coupons representing bosses need only accompany the first shell assembly.

3.1.5.4 Post-Heat-Treat Disposition of Test Coupons.- Upon completion of the heat-treatment operation, the test coupons shall remain with the shell assembly they represent and accompany that assembly on its delivery to Aerojet. When tensile specimens are machined from the coupons and tested in accordance with Fed. Test Method Std. No. 151 by Aerojet-General Corporation, the results of the tests shall comply with the following values:

3.1.5.4.1 Heads.-

Ultimate tensile strength, psi	165,000 min
Yield strength (0.2% offset), psi	105,000 min
Elongation in 2 in., percent	20 min

3.1.5.4.2 Forged Bosses.-

Ultimate tensile strength, psi	165,000 min
Yield strength (0.2% offset), psi	105,000 min
Elongation in 4D,* percent	20 min
Reduction of area, percent	25 min

3.1.5.4.3 Bosses Machined from Plate.-

Ultimate tensile strength, psi	155,000 min
Yield strength (0.2% offset), psi	100,000 min
Elongation in 2 in., percent	20 min

*The test-section gage length is four times the section diameter (D).

3.2 Handling.- All handling of the shell assembly or its components in the uncrated condition shall be performed using maximum care because of the susceptibility of the material to damage during all stages of fabrication. Components or assemblies damaged from handling shall be subject to rejection. Components shall be kept in suitable crates or on pallets except when they are being worked.

3.3 Machining.- Machining of the shell-assembly components shall conform to the requirements of Aerojet Drawings 178086 and 178089. After final machining, a cleaning method shall be employed to guarantee the shell interior complete freedom from machining residue, shavings, and cuttings. After cleaning, shell openings shall remain sealed at all times, except when removal of seals is necessary for final fabrication or testing. Cutting tools shall be maintained at proper sharpness to prevent burnishing of the metal surface.

3.4 Assembly Procedures.- The shell shall be assembled in accordance with Aerojet Drawing 178087 or 178090 as applicable.

3.5 Welding Requirements.- All components and subassemblies shall be TIG or Electron Beam welded in accordance with AGC-STD-1194 and the detail requirements of this specification in lieu of paragraph 1.2.2 of AGC-STD-1194. Certification of welding operators and qualification of procedures in accordance with AGC-STD-1194 is required prior to the welding of production parts.

3.5.1 Filler Wire.- When required, filler wire shall be Inconel 69 alloy in accordance with Specification AMS 5778.

3.5.2 Inert Gas.- All TIG welding operations shall be performed with gas backup. Inert gas used shall be either pure helium or a 75 percent helium and 25 percent argon mixture.

3.5.3 Inert Gas Purge for TIG Welding.- Prior to welding of the final girth closure, the shell assembly shall be purged with a large volume flow of inert gas to exclude air. During welding, the gas flow rate shall be maintained at 3 to 5 cu ft per hour. If the gas flow is interrupted during TIG welding, the welding operation shall be discontinued. The shell assembly shall then be repurged prior to resuming the welding operation.

3.5.4 Preheat.- Preheat, in general, is not required. However, if the metal temperature should drop below 70°F, it is best to preheat the joint to 70°F for 6 in. on both sides of the weld joint.

3.5.5 Cleaning.- In addition to the cleaning requirements of AGC-STD-1194, interbead cleaning of multiple-pass TIG welds to remove the refractory oxide film shall be done by means of power wire brushing. The use of sandblasting is prohibited.

3.5.6 Weld Beads.-

3.5.6.1 Boss to Head Weld Joint.- Weld beads shall be ground flush both inside and outside in accordance with Aerojet Drawing 178087 or 178090 as applicable.

3.5.6.2 Circumferential Closure Weld.- Weld bead shall be ground flush on the outside. Drop-through shall be uniform and shall not exceed 0.010 inch.

3.5.7 Mismatch.- Mismatch in weld joints shall not be in excess of that shown in Aerojet Drawing 178077 or 178090 as applicable.

3.6 Weld Repairs.- Weld repairs shall be performed in accordance with AGC STD-1194 and the requirements of this specification.

3.6.1 Weld Repair Procedures.- Prior to any TIG welding repair work, the careful removal of the defect by grinding is necessary. A minimum amount of material shall be removed. Grinding equipment such as small Radiac or Rayflex (FP or F) grinding wheels and rotary files may be used to handle most repair work. Maximum groove width shall be approximately 1/8 inch. For Electron Beam weld repair, removal of defects is not required.

3.6.1.1 Repair of TIG Weld Defects.- The following repair procedure shall be performed.

3.6.1.1.1 Defect Location.- Locate defect areas from the radiographic film or by dye-penetrant inspection.

3.6.1.1.2 Grinding Procedure.- If there is no surface indication of the defect, grind the weld bead in progressive stages of 1/64 inch in depth. Dye-penetrant-inspect the weld after each stage of grinding and proceed in this manner until the defect has been located and removed by grinding.

3.6.1.1.3 Cleaning.- Prior to repair welding, the groove and areas around and on both sides of the groove shall be cleaned by flushing with clean, uncontaminated isopropyl alcohol, or equivalent. This operation shall be followed by thorough brushing with a clean austenitic stainless steel wire brush. Do not wipe the cleaned area with cloth or similar material.

3.6.1.1.4 Repair Welding.- Manually TIG weld the ground-out area following the requirements of 3.5.

3.6.1.2 Repair of Electron Beam Welds.- The following repair procedure shall be performed:

3.6.1.2.1 Defect Location.- Locate defect areas from the radiographic film.

3.6.1.2.2 Cleaning.- Prior to repair welding, the weld and areas on both sides of the weld joint shall be cleaned with clean, uncontaminated isopropyl alcohol, or equivalent. This operation shall be followed by thorough brushing with a clean austenitic stainless steel wire brush.

3.6.1.2.3 Repair Welding.- Reweld the entire joint using the approved Electron Beam weld schedule meeting the requirements of 3.5.

3.6.2 Repair of Welds on Age-Hardened Material.- Weld repairs shall not be permitted on age-hardened material.

3.7 Welded Test Strips.- Two strips 4 in. wide by 36 in. long shall be cut across the width from each of three sheets of heat blank material and identified with the mill heat number and sheet serial number. Each pair of strips shall be welded in accordance with 3.5 and inspected in accordance with 4.2.2.

3.7.1 Disposition of Welded Test Strips.- The three welded test strips shall accompany the first shell assembly through the heat-treatment operations of 3.8 and its delivery to Aerojet to be retained for tensile and bend tests by Aerojet-General Corporation.

3.8 Heat-Treatment Operations.- The welded shell assembly shall be annealed and aged in accordance with the following procedure:

3.8.1 Annealing Heat Treatment.- Charge the shell assembly into a furnace previously preheated to 1900°F ±25; maintain at temperature for 30 minutes ±5 and then air-cool.

3.8.2 Age Hardening Heat Treatment.- After annealing, the shell assembly shall be age-hardened by heating to 1300°F ±25, holding at temperature for 20 hours, and air cooling.

3.8.3 Furnace Atmosphere.- To prevent excessive oxidation, heat-treatment operations shall be performed in an atmosphere of completely dissociated ammonia or dry hydrogen with a dew point of -70 to -100°F.

3.9 Identification of Shell Assembly.- The shell assembly shall be assigned serial numbers S1, S2, S3, etc., which shall be electrolytically etched in the location indicated on Aerojet Drawing 178087 or 178090 as applicable.

3.10 Workmanship.- The shell assembly, including all component parts, shall be fabricated, heat-treated, finished, and tested in a thoroughly workmanlike manner. Particular attention shall be given to neatness and thoroughness in the forming and welding of the component parts. Non-conformance can be cause for rejection.

4. QUALITY ASSURANCE PROVISIONS

4.1 Supplier's Responsibility.- The supplier shall be responsible for the fabrication, heat treatment, inspection, and tests of the shell assembly in accordance with all of the requirements and procedures of this specification. No deviation from fabrication, heat treatment, inspection and testing requirements, and procedures of this specification shall be allowed except in the form of an amendment to this specification or to the purchase order. Test data, letters of conformance, and other pertinent information affecting shell fabrication shall be forwarded without delay to the cognizant Aerojet-General project engineer and Aerojet-General inspection department.

4.1.1 Acceptance Criteria.- Acceptance of the shell assembly shall be based upon compliance with the requirements herein as verified by a series of in-process acceptance tests (see 4.2) and final inspection (see 4.3) of the finished product. Detailed inspection records shall be maintained to insure that all requirements of this specification have been met.

4.1.2 Cognizant Aerojet-General Personnel.- As required, Aerojet-General personnel, such as the project engineer, welding engineer, metallurgical engineer, stress engineer, inspector, etc., shall be permitted to observe those phases of work as is necessary.

4.2 In-Process Acceptance Inspection.- All requirements of this specification shall be assured through inspection. Inspection tests shall be performed in accordance with the requirements specified herein.

4.2.1 Ultrasonic Inspection.- All boss forgings shall be ultrasonic-inspected in accordance with Specification AGC-13937.

4.2.1.1 Basis for Rejection.- All forgings shall meet the requirements of Specification AGC-13884 as applicable to 410 stainless steel bar stock.

4.2.2 Inspection During Assembly.-

4.2.2.1 Weld Inspection.- All joints shall be visually inspected for compliance with the requirements of 3.5 and the applicable drawings, and shall be inspected in accordance with the following:

4.2.2.1.1 Dye-Penetrant Inspection.- Dye-penetrant inspection in accordance with Specification AGC-13972 shall be performed on all welds. After inspection, welds shall be cleaned thoroughly and the welded surfaces and adjacent areas brushed with a stainless steel wire brush.

4.2.2.1.1.1 Basis for Rejection.- Each weld shall be free of external cracks or propagating defects.

4.2.2.1.2 Radiographic Inspection.- Radiographic inspection shall be performed on all welds in accordance with Specification AGC-13859. Radiographs shall be subject to the interpretation and acceptance of designated Aerojet-General quality control and project representatives. Radiographic film shall be numbered to coincide with the identification markings of the shell assembly. China-marking lead shall be used for marking weld identifications so that the exact location of weld areas with corresponding radiographs may be easily identified. All radiographic film shall become the property of Aerojet.

4.2.2.1.2.1 Basis for Rejection.- All welds shall meet the requirements of Specification AGC-13860, Class 11 (eleven).

4.2.3 Inspection of Shell Assembly Prior to Heat Treatment.- The shell assembly shall be free of oil, grease, paper, or any type of carbonaceous material prior to heat treatment.

4.2.4 Inspection of Shell Assembly After Heat Treatment.-

4.2.4.1 Test Coupons.- After heat treatment of the shell assembly, the test coupons may be tested by Aerojet-General Corporation to verify compliance with 3.1.5.4 of this specification.

4.2.4.1.1 Basis for Rejection.- Failure to meet the tensile-test requirements of 3.1.5.4 shall be the basis for rejection.

4.3 Final Inspection.- The completed shell assembly shall be subjected to surface inspection, with visual examination for imperfections and finish. The surface shall be such that the removal of scratches or other surface imperfections shall not reduce the thickness of the metal below the minimum specified on the drawing. Inspection of workmanship shall conform to 3.9. Measurements of dimensions (with attention to Aerojet drawing tolerances) shall be included in this inspection.

5. PREPARATION FOR DELIVERY

5.1 Packing.- The shell assembly shall be crated and firmly supported to avoid damage during shipping.

6. NOTES

6.1 Intended Use.- This metal shell assembly will be used for glass-filament-reinforced metallic tankage for the storage of cryogenic fluids.

APPENDIX F

FABRICATION PROCEDURE FOR GLASS-FWC SHELL

Instructions given for the fabrication of the glass-FWC shell are listed below.

I. INSPECTION OF METAL-SHELL ASSEMBLY

A. Wear clean white cotton gloves while handling the metal shell.

B. Remove the shell from its protective plastic bag.

C. Measure its length, diameter, and weight and record them on Figure F-1.

D. Replace the shell in the plastic bag.

II. ASSEMBLY OF WINDING SHAFT

A. Wear clean white cotton gloves while handling the metal shell.

B. Remove the shell from its plastic bag, and place it on a foam pad covered with clean, lint-free cheesecloth.

C. Obtain a winding shaft and install it in the shell until the fixed collar rests against the boss face.

D. Align the five holes of the fixed collar with the boss holes. Install 10-32 UNF by 7/8-in.-long socket-head cap screws, and finger-tighten. Cross-torque all screws to 5 in.-lb.

E. Position the floating collar on the other end of the shaft. Align the five holes of the floating collar with the boss holes. Install 10-32 UNF by 7/8-in.-long socket-head cap screws and finger-tighten. Cross-torque all screws to 5 in.-lb.

F. To protect the boss face, K-seal groove, and bolt holes from resin spillage, apply Teflon tape to cover the side of the boss and the shaft collar so resin will not migrate to the boss-face area.

G. Cover the metal-shell/winding-shaft assembly with a plastic bag if the next operation will not be performed immediately.

III. WINDING-MACHINE SETUP AND CALIBRATION

A. Install four rolls of 20-end roving in the tension devices.

B. Install the roving-guide rollers.

C. Install the resin-impregnation pot.

D. Crank the machine mount for the winding shaft to a vertical position.

E. Secure the metal-shell/shaft assembly in the threaded mount. Thread the shaft into the mount until the shaft flange rests against the mount.

F. Crank the winding-shaft mount to the setting that provides approximately the required longitudinal-winding angle.

G. Tighten the bolt on the back of the winding-machine mount to securely lock the winding shaft into position.

H. Dry-run the winding arm (without paying off roving) and adjust the machine settings to obtain the required 166 $\pm$5 winding-arm turns per mandrel revolution of 360°. Record the machine setting on Table F-1 once the turns are obtained.

I. Thread the four dry 20-end rovings through the guide rollers and the payoff roller. Secure the roving ends and set the tension at approximately 10 lb per 20 ends.

J. Adjust the rollers as required to assure a uniform-thickness, 0.333-in.-wide tape.

K. Ensure that the 0.333-in.-wide tape passes tangent to each boss, with a maximum permissible distance between the boss and tape edge of 0.020 in., by making a few winding-arm turns. Adjust the winding-shaft-mount setting as required to provide the proper winding angle.

L. Calibrate the tension devices to provide a dynamic tension of 10 $\pm$1 lb per 20-end roving at the roving payoff. Calibrate the tension devices statically and then dynamically. Record on Table F-1 the static tension needed to provide the required dynamic tension. Also record there the tension-device settings.

IV. POSITIONING OF METAL SHELL IN WINDING MACHINE

Prior to this operation, establish machine settings for the winding pattern, winding angle, payoff-roller adjustments, resin-impregnation-pot adjustments, etc. as described in Section III, above.

A. Wear clean white cotton gloves while handling the metal shell.

B. Crank the machine mount for the winding shaft to a vertical position.

C. Select four prefabricated head reinforcements and weigh each. Record their weights on Table F-1.

D. Place two prefabricated head reinforcements, completely covered with protective plastic sheet and top side down, over the machine mount for the winding shaft. Secure them in place with tape if required.

E. Carry the metal shell to the winding machine and secure the shaft in the threaded mount. Thread the shaft into the mount until the shaft flange rests against the mount.

F. Crank the winding-shaft mount to the predetermined setting that provides the required longitudinal winding angle.

G. Tighten the bolt on the back of the winding-shaft mount to securely lock the winding shaft into position.

H. Protect the shell with plastic sheet if it is not to be overwrapped with filaments immediately.

V. GENERAL INSTRUCTIONS FOR HANDLING OF GLASS ROVING

A. Keep each roll of 20-end glass-filament roving in its protective plastic bag with end plates in place in its individual box in cold storage at 32°F or lower, except when it is being used to overwind one or more metal shells on a given day.

B. Weigh each spool of roving before initiating winding. For subsequent weighing, plastic-bag any scrap obtained during winding.

C. At the completion of winding on each day, immediately remove each roll of roving from the tension devices, repackage it with end plates in its plastic bag and box, and return it to cold storage (32°F or lower).

VI. RESIN PREPARATION

A. Obtain the Epon 828, DSA, Empol 1040, and BDMA resin constituents.

B. Measure out the following quantities of each constituent for each of two batches:

	Quantity, g
Epon 828	200 ±0.5
DSA	231 ±0.5
Empol 1040	40 ±0.5
BDMA	2 ±0.0

C. Mix and warm the Epon 828 and Empol 1040 to 212°F. Cool the mixture to room temperature and add the DSA and BDMA. Thoroughly mix the constituents. Heat the mixed resin to 85 to 100°F.

VII. OVERWRAPPING OF METAL SHELL

A. General Notes - (1) Stop overwrapping, remove the windings, and restart the process if any of the following should occur: (a) filament breakage, (b) loss of end or ends on guide roller, (c) loss of roving tension, (d) lack of resin impregnation in roving, (e) winding-pattern gapping, or (f) excessive variation of filament-tape width; and (2) retain in a plastic bag all excessive roving not used in winding but included in the initially recorded roving-spool weights; weigh it and record the weight on Table F-1.

B. Obtain four rolls of 20-end roving and weigh each roll. Record the weight on Table F-1, and place the rolls on tension-device spindles. Record on Table F-1 the number of the spindle on which each roll is mounted.

C. Thread the roving through the guide rollers and payoff head tangent to the metal-shell boss and secure it in place.

D. Pour the mixed resin (see Section VI) in the impregnation pot. Brush-impregnate the roving between the impregnation pot and the metal shell. Maintain the resin temperature at 85 to 100°F.

E. Set the machine-turn counter to zero.

F. Identify the starting position of the winding-shaft mount in relation to the stationary point on the machine immediately adjacent to the mount.

G. Position one head reinforcement against each end of the metal shell, and press them securely in place.

H. Start the longitudinal filament winding. If required, brush on extra resin or remove excess resin on filaments.

I. Stop winding at the completion of the first mandrel revolution (should be 166 ±5 turns). Maintain the tension on the roving. Enter the number of turns required to complete one revolution on Table F-1.

J. Position the head reinforcement over the boss on each end of the tank and press it securely in place. Squeeze the external surface of the head reinforcement to compact it against continuous windings.

K. Locate the instrument terminals at the edge of the head reinforcement in accordance with instructions from the cognizant engineer.

L. Continue the longitudinal filament winding until the second mandrel revolution is completed (should be 332 ±10 turns). Secure the end of the tape, and then cut it.

M. Record on Table F-1 the total number of turns applied.

N. Remove the four spools of roving from the tension devices, weigh them, and record their weights on Table F-1.

O. Weigh the scrap roving, and enter this weight on Table F-1. Compute the total weight of roving used.

VIII. PREPARATION FOR CURING

A. In vacuum-bagging the wound tank shell for the cure, use one layer of 2353 Dacron cloth for release/bleeder cloth.

B. Bag the shell with 6-mil polyvinylacetate (PVA) sheet tailored to avoid excess wrinkles.

C. Seal the bag with zinc chromate putty.

D. Install a vacuum valve over the Dacron padding on the head.

E. Evacuate the bag to 20 in. Hg or better, and check for leaks.

IX. CURE

A. Transfer the vacuum-bagged unit to the curing oven.

B. Mount the winding shaft on the support fixtures in the oven.

C. Check the vacuum for 20 in. Hg or better.

D. Cure at 150°F for 2 hours and at 300°F for 4 hours. Keep a record of the cure on the continuous recording chart.

E. Reduce the oven temperature to 100°F at a rate not to exceed 100°F/hour.

X. FINAL INSPECTION

A. Remove the cured tank from the oven, and strip off the vacuum bag.

B. Remove the winding shaft.

C. Measure the wound-tank length, diameter, and weight and record them on Figure F-1.

D. Place the wound tank in the storage box.

TABLE F-1

WINDING DATA (FORM)

Winding Tension

Winding speed _____ turns/minute

Static tension at payoff required for dynamic tension of 10 ±1 lb/20-end roving at payoff:

Tension-Device Spindle No.	Static Tension, lb	Tension-Device Setting
A	_____	_____
B	_____	_____
C	_____	_____
D	_____	_____

Head-Reinforcement Weight

Reinforcement A _____ g. Reinforcement B _____ g.

Reinforcement C _____ g. Reinforcement D _____ g.

Roll No.	Tension-Device Spindle No.	Weight, g		
		Starting	Final	Roving
____	_____	_____	____	_____
____	_____	_____	____	_____
____	_____	_____	____	_____
____	_____	_____	____	_____
			Total	_____
			Less scrap weight (subtract)	_____
			Total roving on tank	_____

Winding Pattern

Revolution No.	Winding-Arm Turns	
	Design	Actual
1	166 ±5	_____
2	332 ±10	_____

Time winding started _____

Time winding completed ____

Table F-1

INSPECTION OF METAL-SHELL ASSEMBLY (FORM)

Serial No. _____

Before-winding data: Date _____ Signature _____

After-winding data: Date _____ Signature _____

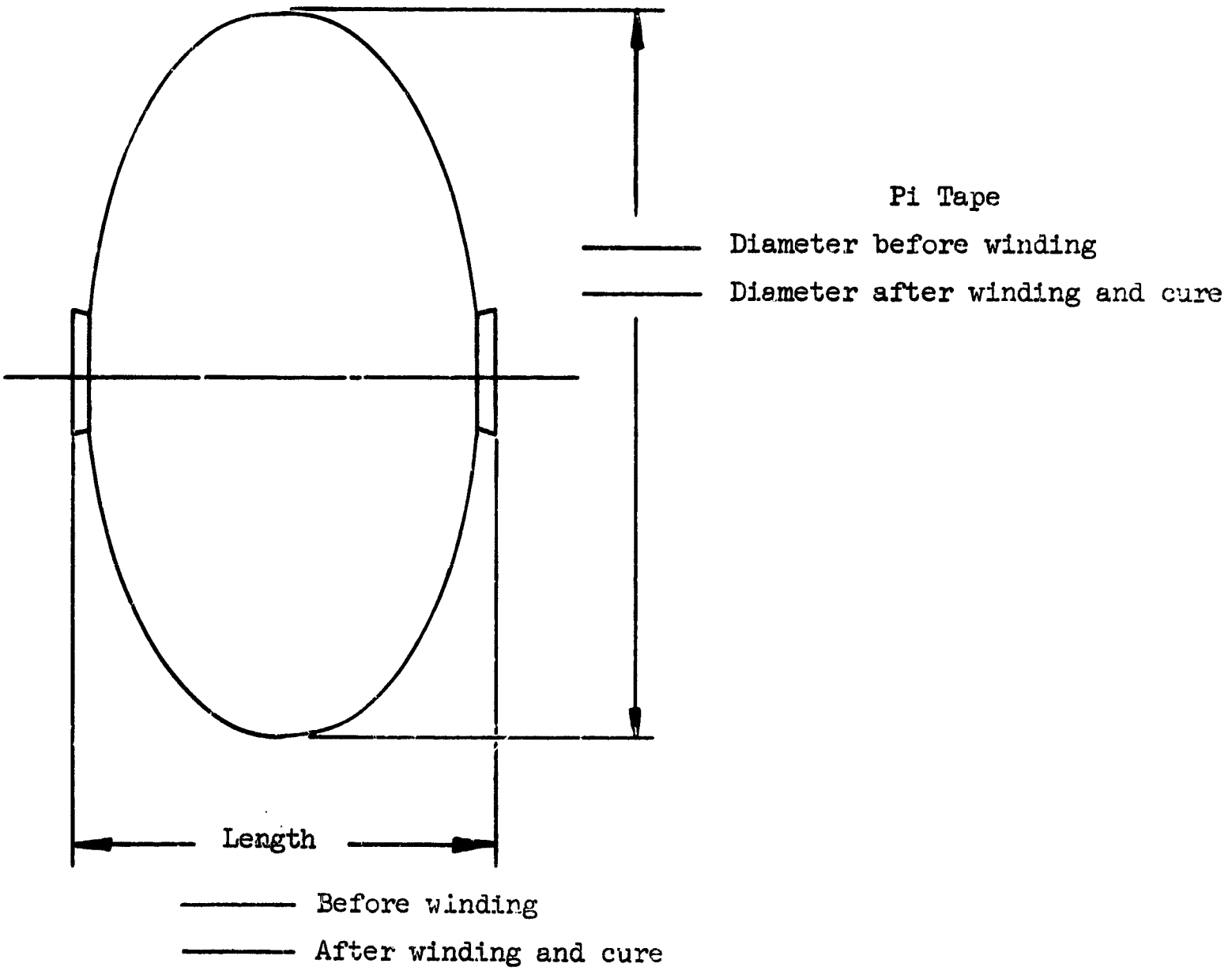

Weight of metal shell before winding _____ g

Weight of metal shell after winding and cure _____ g

Figure F-1

APPENDIX G

CALIBRATION OF BOW-TIE, STRAIN-GAGE, DISPLACEMENT TRANSDUCERS

A single-step, end-to-end calibration was performed on each bow-tie, strain-gage, displacement transducer used in testing. Each pressure-vessel test required three transducers, two for longitudinal displacement and one for hoop. The transducers were calibrated in place on the vessel, with all instruments installed and connected to the data-acquisition equipment (a continuous-strip-chart recorder for each transducer).

Laboratory conditions (ambient temperature) were employed, because the strain gages were maintained within the gage-compensation temperature range ($70 \pm 20^{\circ}F$) during cryogenic testing by manual adjustment of current through bifilar heater windings. The test temperature was monitored by means of a thermocouple very close to but not directly on the strain gage; the beryllium-copper reed of the bow tie provided an excellent conductive path to the gage. Additional details on instrumentation are presented in Section VI,A,3 of the body of this report.

For use in calibration, a single washer was spot-welded at the end of each metal-foil band attached to the longitudinal transducers. Two calibration tools were inserted between each attachment tack and the inner surface of the washer, and the signal-conditioning system was adjusted for a zero output reading on the recorder. The distance between the upper and lower attachment posts was accurately measured and recorded. Rotation of the calibration tools produced a displacement of 0.250 in. for each band, with a total displacement of 0.500 in. The strain was then calculated from

$$\text{Strain} = \frac{\Delta L}{L}$$

where

ΔL = total displacement between centers of washers = 0.500 in.
L = distance between centers of attachment tacks, in.

A sample longitudinal-strain transducer-calibration calculation for a typical vessel follows. For the longitudinal transducer, L = 17.187 in. and

$$\text{Strain} = \frac{0.500}{17.187} = 0.0291 \text{ in./in.}$$

The span control of the signal-conditioning equipment was adjusted so that the instrument would record 29.1% of full scale (based on the foregoing value), to permit strain to be read directly on each strip chart during the pressurization test. This procedure was repeated to ensure reliability.

The procedure used to calibrate the girth (hoop) transducer on each vessel was similar to that described above. The center of the girth band was displaced a predetermined distance on each side of the transducer (total

amount, 2.000 in.). The calculations, and the zero and span adjustments, were performed as indicated above, except that values appropriate for girth measurements were used. A sample hoop-strain calculation, where

ΔL = total hoop-band displacement = 2.000 in.
L = pressure-vessel circumference = 56.688 in.

yields

$$\text{Strain} = \frac{2.000}{56.688} = 0.0353 \text{ in./in.}$$

Single-point strain-calibration data were obtained for all longitudinal and girth transducers on all vessels before the vessel-burst tests were initiated.

Detailed laboratory calibrations were performed under ambient conditions to determine the degree of transducer linearity and reproducibility. Various displacements were set with the aid of a vernier caliper (reading accuracy, 0.001 in.), and transducer outputs for these displacements were measured with a recording potentiometer. The results for a longitudinal transducer are shown in Figure G-1.

The curves for displacement vs recorder output as a percentage of chart scale were based on several data points for each configuration. All the data points repeatedly fell within the width of the plot line. Because all the transducers were linear and reproducible to 0.5% within a displacement range from 0.06 to 2.00 in., it was not necessary to perform multiple-point calibrations for the individual transducers used in each test setup.

Vessel contraction during cryogenic conditioning before testing did not affect the accuracy of the strain data, because the transducer responses were linear and reproducible. As installed for testing, the transducers were preloaded for a displacement of approximately 1.50 in.

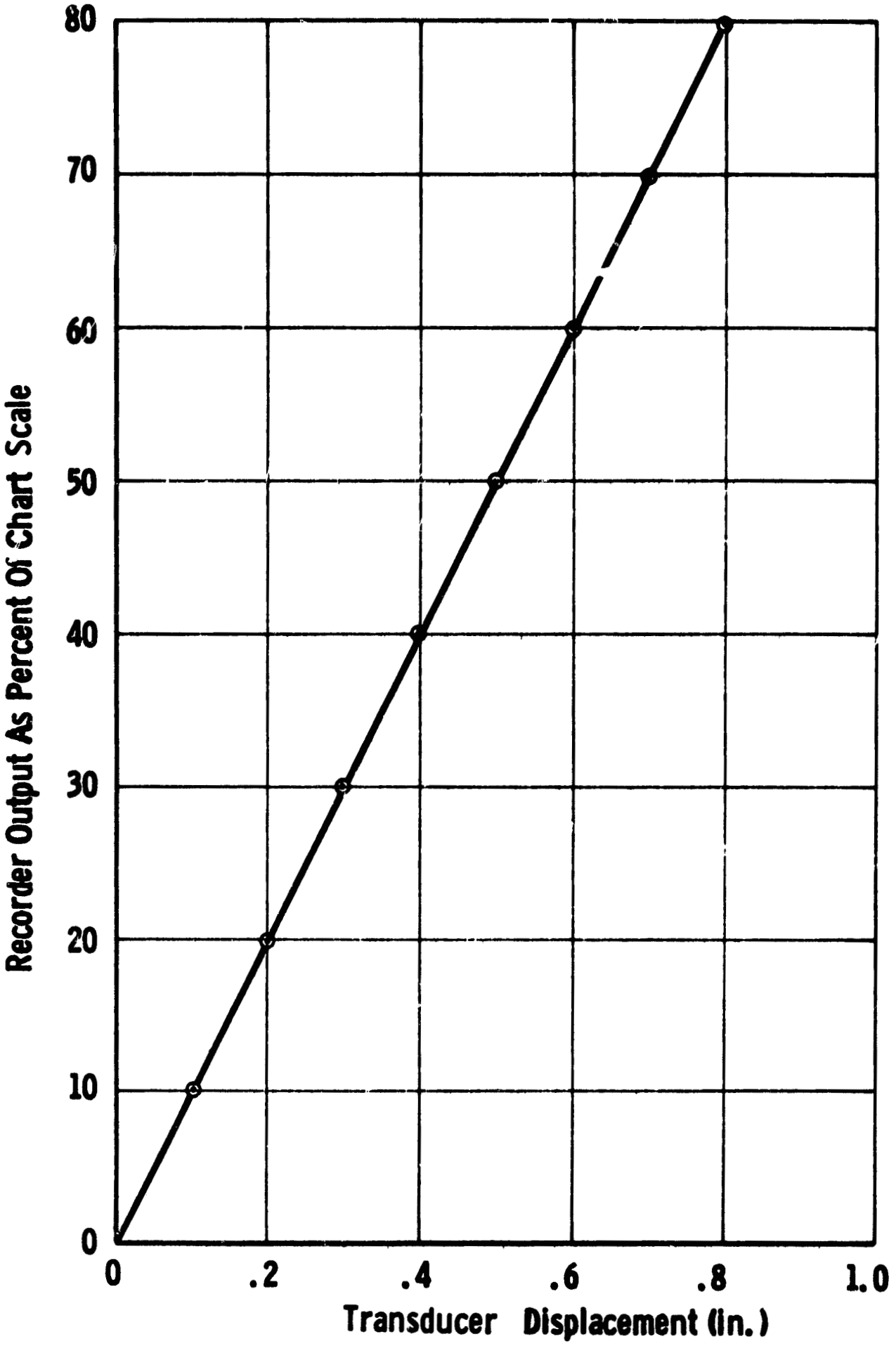

Calibration-Test Data to Demonstrate Linearity
of Strain-Gage Displacement Transducers

Figure G-1

APPENDIX H

METALLURGICAL ANALYSIS OF INCONEL X-750 TANK LINER

An 18-in.-dia, GFR, Inconel X-750 tank (Part No. 178091, Serial No. 2) was proof-tested at 2220 psig for 1 min prior to the burst test. During the burst-test cycle at room temperature, pressure was increased at 1200 psig/min until failure occurred at 2960 psig, in the metal liner at the weld joint between the boss and the formed head.

Tensile tests were performed to evaluate the welding schedule and the parent material in the tank with the tensile properties used in the design of the tanks. The metallurgical analysis included one of the tensile specimens that failed prematurely.

I. DISCUSSION

The fracture that occurred in the tank liner is shown in Figure H-1. Much of the fracture area could not be examined because the two surfaces rubbed together, producing a galled or disturbed metal surface.

The Y-shaped weld nugget was produced with a two-step welding schedule. The depth of penetration and breadth of beam are shown in Figure H-2.

Figure H-3 shows the microstructure of the weld adjacent to the fracture. The grains in the weld are relatively coarse and have directional orientation. The directionality develops during the first welding pass because the tank liner and boss act as a heat sink. This forces directional solidification from the outer edges to the center of the weld nugget. The grains produced in the second pass are also directional, but are radially oriented, about the center line of the nugget produced in the first pass. Radial orientation occurs because the heat sinks include that nugget as well as the liner and boss.

The grains in the narrow heat-affected zone are coarser than in the parent metal away from the weld (see Figures H-3 to H-5). Figures H-4 and H-5 show the location of the fracture in relation to the weld.

Figure H-6 is a macrophotographic view of the fracture surface of a longitudinally welded tensile specimen (No. L-6). The ductility was approximately 5 to 6% less than that exhibited by a similar sample. During examination of the fracture surface, a gas hole in the weld nugget was found (see Figure H-6).

Figure H-7 illustrates the microstructure along the length of the weld and the depth of the gas hole, which is approximately 0.005 in. in diameter and 0.004 in. deep.

The highly directional orientation of the weld grains is clearly evident in Figure H-7. The lower portion of each microphotograph shows the

structure that developed during the first weld pass and the upper portion the second weld pass.

II. CONCLUSIONS

A. Fracture in the Inconel X-750 tank occurred at the interface between the heat-affected zone of the liner and the weld nugget joining the liner to the boss.

B. No defects were found, but the possibility of a localized weld undercut could not be fully evaluated because of plastic deformation.

C. Based on the microstructure and normal conditions (e.g., equal cross section and lack of defects), the probable cause of failure was the abrupt change in microstructure at the interface between the parent-metal heat-affected zone and the weld.

D. Grain refinement in the heat-affected zone and weld would force random failures to occur in the liner, but can be accomplished only by working the areas.

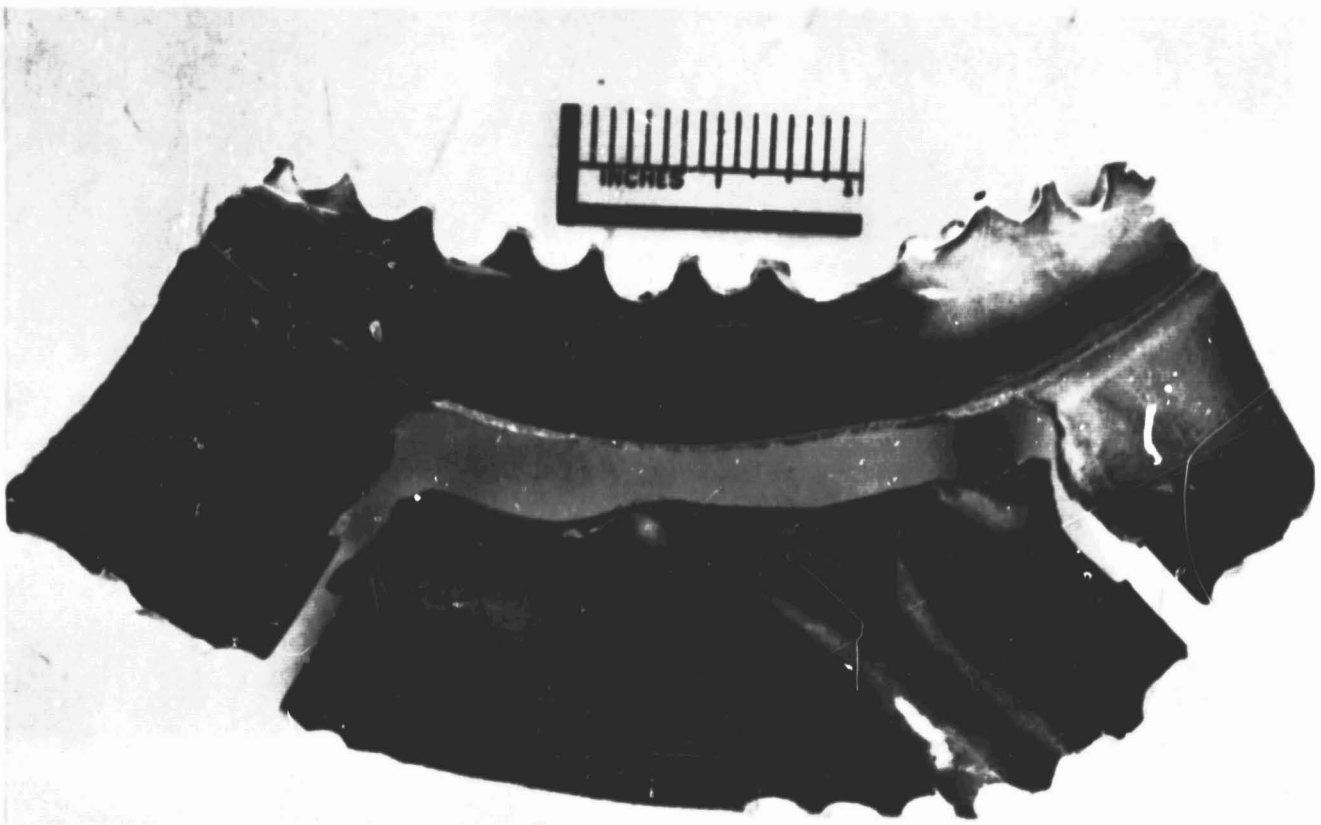

Figure H-1. Fracture Surface Between Boss and Tank Liner
(Note: Straight cut edges in liner are saw cuts.)

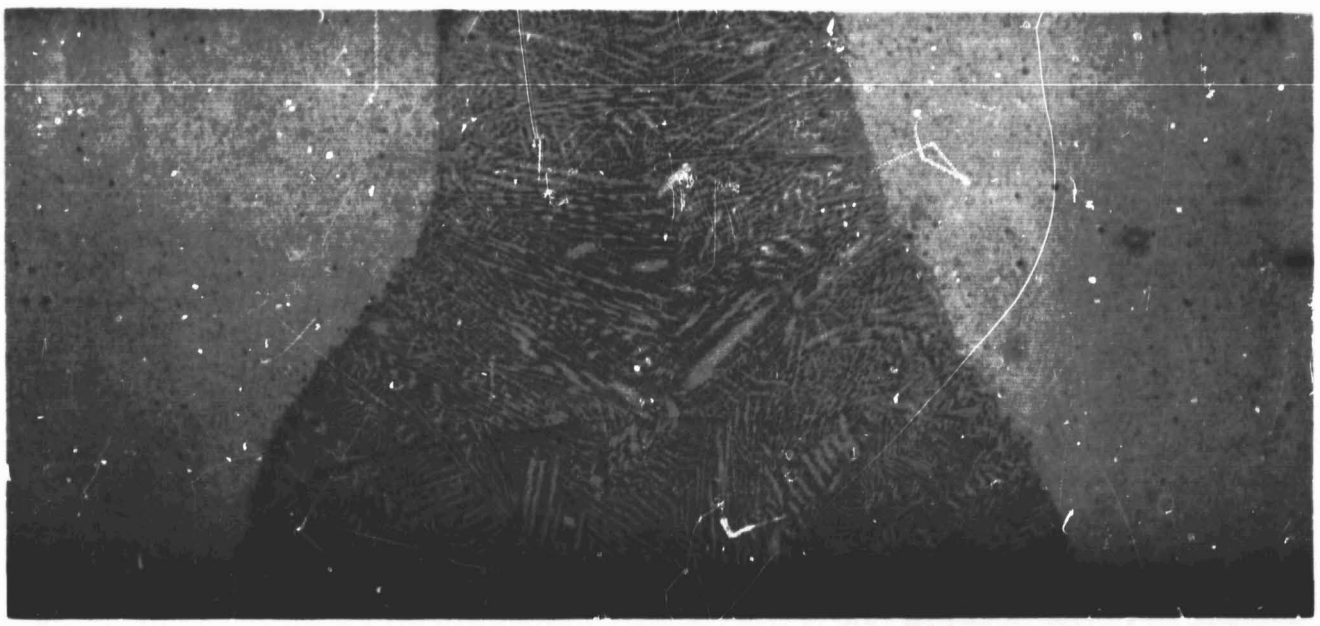

Etchant: 10% oxalic acid 50X

Figure H-2. Microstructure of Boss-to-Liner Weld

Figures H-1 and H-2

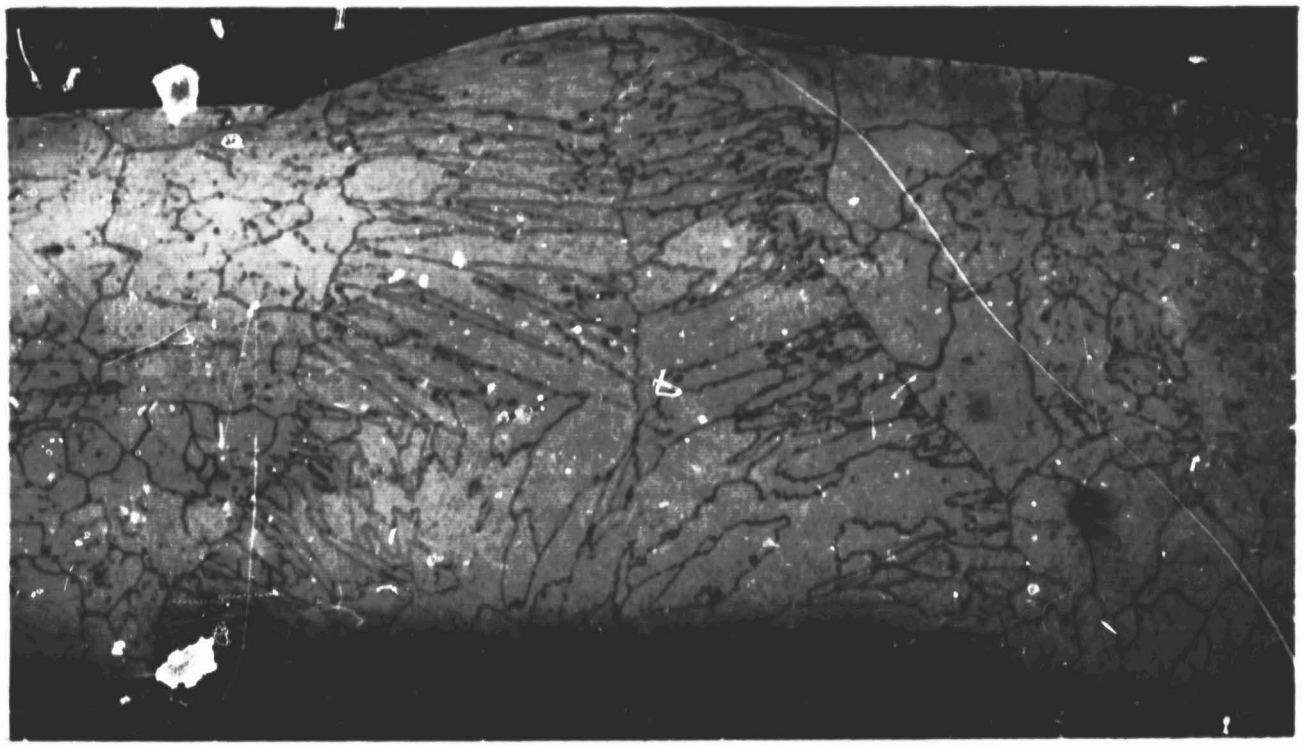

Etchant: 10% oxalic acid 50X

Figure H-3. Microstructure of Tank Weld Adjacent to Fracture (Liner material at left, weld nugget center, and boss right. Note the coarse grain structure in the heat-affected zone and the directional grain orientation in the weld nugget.)

Etchant: 10% oxalic acid 50X

Figure H-4. Microstructure of Weld Nugget and Location of Fracture in Tank (Fracture occurred along interface between metal liner and weld nugget.)

Figures H-3 and H-4

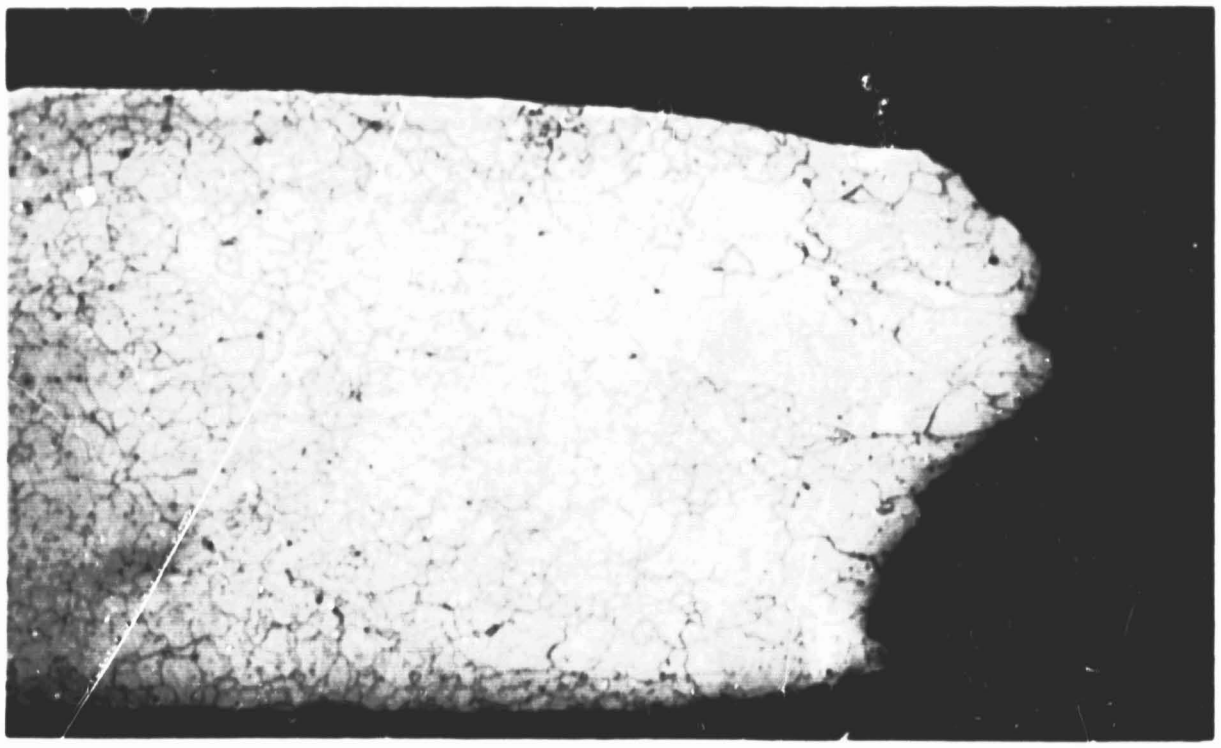

Etchant: 10% oxalic acid 50X

Figure H-5. Microstructure of Metal Liner
(Note that the heat-affected-zone grain structure is coarser than the rest of the parent material.)

Figure H-6. Macrophotographs of Tensile Specimen L-6
(Note: Near left edge of each piece, in weld nugget, is a gas hole, photographed as a black circle.)

Figures H-5 and H-6

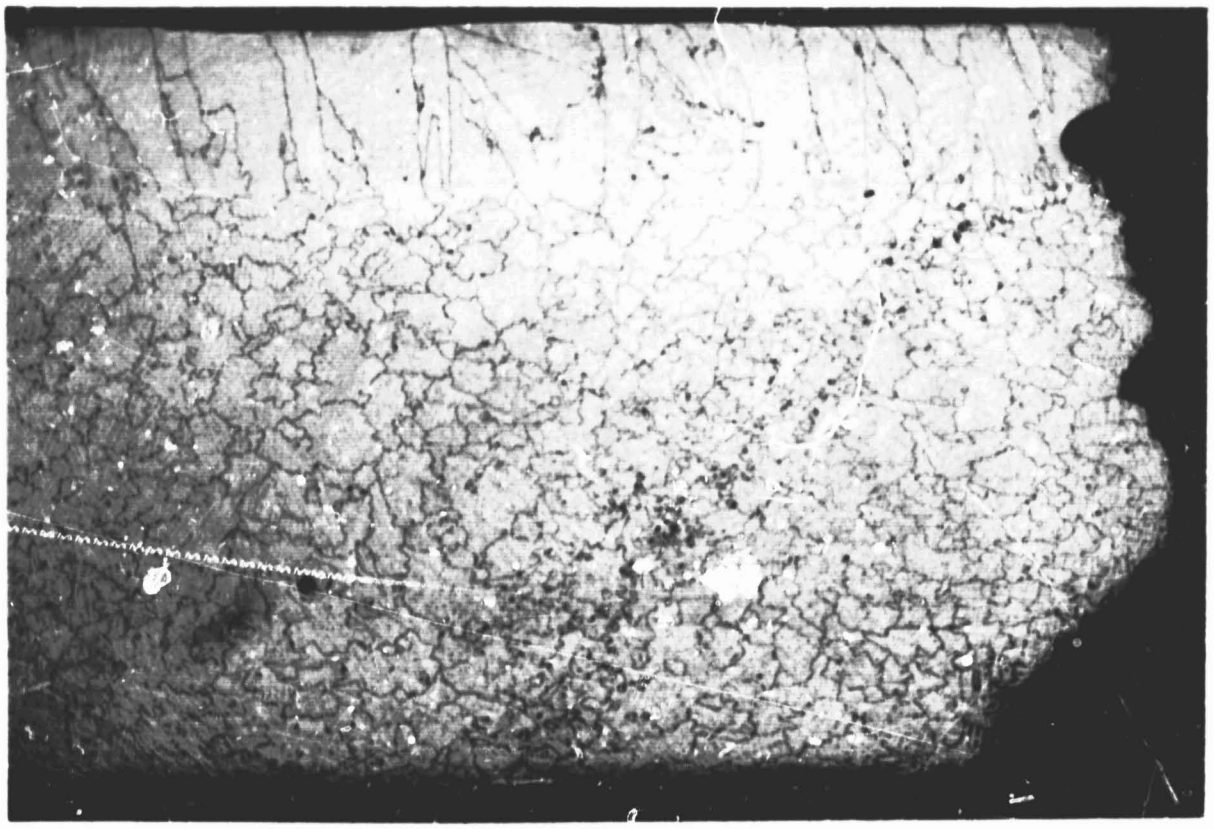

Etchant: 10% oxalic acid 50X

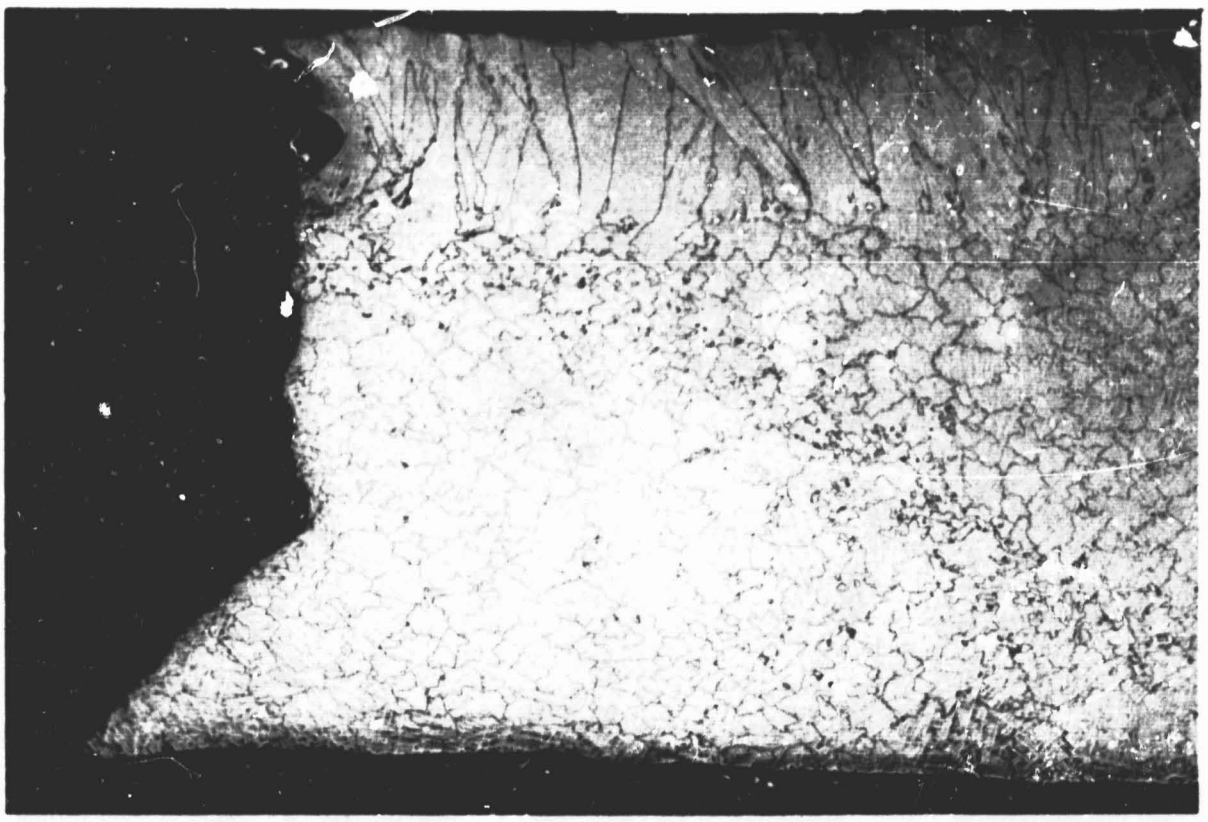

Etchant: 10% oxalic acid 50X

Microstructure Along Length of Weld

Figure H-7